

**DEVELOPMENT AND PERFORMANCE OF
SELF-HEALING AND SELF-IMMUNE
SOIL-CEMENT SYSTEMS
SUBJECTED TO FREEZE-THAW CYCLES**



Jingtao Chen

Department of Engineering

University of Cambridge

This thesis is submitted for the Degree of

Doctor of Philosophy

Hughes Hall College

October 2019

Dedicated To My Country and

My Loving Parents...

Jinming Chen and Qinglin Liao

DECLARATION

I hereby declare that, this thesis is the result of my own work and includes nothing which is the outcome of work done in collaboration except as declared in the Preface and specified in the text. It is not substantially the same as any that I have submitted, or, is being concurrently submitted for a degree or diploma or other qualification at the University of Cambridge or any other University or similar institution except as declared in the Preface and specified in the text. I further state that no substantial part of my thesis has already been submitted, or, is being concurrently submitted for any such degree, diploma or other qualification at the University of Cambridge or any other University or similar institution except as declared in the Preface and specified in the text. It does not exceed the prescribed word limit for the relevant Degree Committee

This thesis contains less than 65,000 words, inclusive of appendices, footnotes, tables and equations, and does not contain more than 150 figures.

ABSTRACT

DEVELOPMENT AND PERFORMANCE OF SELF-HEALING AND SELF-IMMUNE SOIL-CEMENT SYSTEMS SUBJECTED TO FREEZE-THAW CYCLES

Jingtao Chen

Soil-cement systems are used in a wide variety of engineering projects. However, soil-cement systems are vulnerable to cyclic freeze-thaw deterioration. The engineering properties of soil-cement systems, such as strength and permeability, can be substantially degraded under the action of freeze-thaw cycles. This durability problem substantially impairs the sustainability of soil-cement systems and raises their maintenance and repair costs. Thus, when subjected to freeze-thaw cycles, civil infrastructure projects that use soil-cement systems can suffer from decreased reliability. Although extensive research has been carried out to improve the freeze-thaw durability of soil-cement systems, no method associated with significant improvement has been developed thus far.

Biological systems have recently provided inspiration for scholarly attempts to develop smart materials that comprise sustainable and resilient systems, which similarly can continually adapt and respond to their environment. Most of these efforts so far have focused on self-healing properties in polymers and concrete, and many of them have shown promising results. However, to date there has been very little work reported on the development of effective smart systems for geotechnical applications and there is very little literature focusing on the specific damage scenario caused by freeze-thaw cycles. Those systems (and their geotechnical applications) pose challenging problems that are distinct from those of, for instance, concrete. For this reason, they require a complete reimagining of how such smart systems ought to be designed. Therefore, the focus of this PhD project is on the development and performance of self-healing and self-immune soil-cement systems that can respond and adapt to freeze-thaw cycles.

Two different materials, microcapsules (produced by Lambson, UK) and LUVOMAG MgO pellets (produced by Lehmann & Voss, Germany), were used to develop self-healing soil-cement systems, and their self-healing capability was investigated. It was found that the addition of Lambson microcapsules improved the self-healing capability of soil-cement systems considerably in terms of unconfined compressive strength (UCS). The addition of MgO pellets not only substantially improved the self-healing capability of soil-cement

systems in UCS, but also showed great potential in terms of crack sealing. The microstructure investigations revealed that brucite and different types of hydrated magnesium carbonates, such as hydromagnesite and dypingite, were produced in the self-healed MgO pellet-embedded soil-cement samples after freeze-thaw cycles.

Biological systems, provided insights that aided the development of a self-immune soil-cement system. This is a system that can protect itself from cyclic freeze-thaw action before damage is initiated, thus preventing the occurrence of the damage, partially or entirely. A special admixture, SikaAer[®] Solid air entraining microcapsules was introduced to develop such systems. These uniformly distributed small compressible microcapsules can serve as pressure vessels by buffering the excess pressure generated during water freezing. Although initial dry density and strength properties generally decreased with the addition of the microcapsules, the final results demonstrate that the freeze-thaw resistance of soil-cement systems was substantially improved. Based on the results of the physical properties of soil-cement systems after freeze-thaw cycles, the microscopic analysis and the high resolution X-ray computed microtomography, the self-immune mechanism of soil-cement with SikaAer[®] Solid microcapsules and its behaviour during freeze-thaw action was revealed.

A superabsorbent polymer (BASF SAP A) was also used to develop self-immune soil-cement systems. Compared to SikaAer[®] Solid microcapsules, the addition of SAPs had little effect on the initial dry density, strength properties, and permeability of the soil-cement mixes, and the self-immune mechanism was slightly different. SAPs can absorb water during the mixing of soil-cement and they have the ability to release the absorbed water during the hydration and hardening processes. As a result, small cavities are created in the soil-cement system as the water within SAPs is donated for cement hydration. These uniformly distributed small pores can serve as small reservoirs and pressure vessels for water to enter and expand within the soil-cement matrix during the freeze-thaw process. This quality is captured in the results of the experiments, which demonstrated that the freeze-thaw resistance can be substantially improved by the addition of SAPs.

Overall, the self-healing and self-immune systems developed in this study showed promising results in terms of improving the self-healing and self-immune capability of soil-cement systems subjected to freeze-thaw cycles. More broadly, these smart systems contribute to attempts to build more resilient and sustainable soil-cement systems that may undergo freeze-thaw deterioration in the engineering practice.

ACKNOWLEDGMENTS

First and foremost, I would like to express my heartfelt gratitude to my supervisor, Prof. Abir Al-Tabbaa, for her excellent guidance, immense patience and continuous support throughout my Ph.D.

Many thanks go to Dr. Rod Lynch and Dr. Michael Harbottle for their advice and valuable opinions in reviewing this thesis. I would also like to thank my advisor Prof. Gopal Santana Phani Madabhushi for his advice and support during my review meetings.

I must acknowledge my home country and the China Scholarship Council for providing me with a full scholarship to pursue my Ph.D.

My sincere appreciation goes to Chris Knight for his help with technical issues during my experimental work.

I would like to thank Dr. Fei Jin, Dr. Chrysoula Litina, Dr. L íia Ribeiro de Souza, Dr. Petros Giannaros, and Dr. Rami Jasser Alghamri, for their support and all the discussions we shared.

Many thanks go to all my colleagues in the geotechnical research office, in particular Benyi, Cheng, Fang, Heba, Ningjun, Wenting, Xuanyu, Yuk, Yunhui, Yiyun, Zhengtao, Zijing, for their company and support in my study and life at Cambridge. Special thanks go to Shenzhi, Xiwen, Qianchen, Jinlong, and Charlie for their much valued friendship and support in my life at Cambridge.

Above all, I would like to give special thanks to my father Jinming, my mother Qinglin, and my other half Yishu, for their love and support on my life and study. Despite of the long distance, your love and encouragement mean a lot to me. Without your love and support, I would never go this far.

Table of Contents

DECLARATION	i
ABSTRACT.....	iii
ACKNOWLEDGMENTS	v
Table of Contents	vii
List of Figures	xv
List of Tables	xxvii
List of Abbreviations	xxix
Chapter 1 Introduction	1
1.1 Background and motivation.....	1
1.1.1 Soil-cement systems.....	1
1.1.2 Sustainability and durability challenges of soil-cement systems subjected to freeze-thaw cycles	5
1.1.3 New approaches to develop durable and sustainable soil-cement systems subjected to freeze-thaw cycles.....	7
1.2 Aims and objectives	8
1.3 Thesis outline	9
Chapter 2 Literature Review	11
2.1 Degradation of soil-cement system subjected to freeze-thaw cycles.....	11
2.1.1 Overview of freeze-thaw degradation	11
2.1.2 Effects of freeze-thaw cycles on the properties of soil-cement systems.....	14
2.1.2.1 Strength.....	14
2.1.2.2 Permeability.....	16
2.1.2.3 Volume and water content.....	17
2.1.3 Factors that affect the freeze-thaw resistance of soil-cement systems.....	20
2.1.3.1 Cement content of soil-cement systems	20

2.1.3.2	Water content.....	22
2.1.3.3	Intensity of freeze-thaw exposure.....	23
2.1.3.4	Curing time.....	25
2.1.4	Microscopic analysis of soil-cement systems subjected to freeze-thaw cycles.....	25
2.1.5	Additives used to improve freeze-thaw resistance of soil-cement.....	27
2.1.5.1	Bassanite and fly ash.....	27
2.1.5.2	Silica fume.....	28
2.1.5.3	Autogenic healing in soil-cement systems.....	29
2.2	Air entrainment in concrete.....	30
2.2.1	Mechanisms of air entrainment to protect against freezing.....	30
2.2.2	Critical saturation ratio.....	33
2.3	Self-healing in cementitious materials.....	34
2.3.1	Introduction.....	34
2.3.2	Autogenic healing.....	35
2.3.3	Autonomic healing.....	36
2.3.3.1	Capsule-based chemical self-healing.....	37
2.3.3.2	Mineral admixture and additives.....	47
2.3.3.3	Pellet-based self-healing.....	52
2.4	SAPs in cementitious materials.....	54
2.4.1	Introduction.....	54
2.4.1.1	Water sorption ability of SAPs.....	54
2.4.1.2	Application of SAPs.....	56
2.4.2	Characteristics of SAPs.....	56
2.4.2.1	Particle size of SAPs.....	56
2.4.2.2	Swelling characteristics of SAP.....	57
2.4.2.3	SAP absorption and desorption.....	58

2.4.3	Self-healing applications of SAPs.....	61
2.4.4	SAPs used for improving freeze-thaw resistance	64
2.4.5	Effect of SAP addition on the engineering properties of cementitious materials.....	68
2.5	Concluding remarks	71
Chapter 3	Materials and Experimental Methods.....	73
3.1	Materials	73
3.1.1	Soil-cement systems	73
3.1.2	Additives and admixtures	75
3.1.2.1	Lambson microcapsules	75
3.1.2.2	LUVOMAG MgO Pellets.....	76
3.1.2.3	SikaAer [®] Solid Microcapsules.....	77
3.1.2.4	Super absorbent polymer (SAP)	78
3.1.3	Chemical reactivity of the MgO pellets	79
3.1.4	The tea bag method for the sorptivity of the SAP	79
3.1.5	Preparation of cement pore solution	79
3.2	Preparation of test specimens	80
3.3	Curing conditions for sample preparation, freeze-thaw exposure and self-healing.....	82
3.4	Fresh properties of soil-cement.....	84
3.4.1	Isothermal calorimetry	84
3.4.2	Workability.....	86
3.5	Experimental methods to verify self-healing and self-immune performance and mechanisms of soil-cement systems subjected to freeze-thaw cycles.....	87
3.5.1	Volume, water content and dry density.....	90
3.5.2	Porosity test	91
3.5.3	Strength properties	94
3.5.3.1	Uniaxial compressive strength (UCS) test	94

3.5.3.2	Splitting tensile strength test.....	94
3.5.4	Hydraulic conductivity k	95
3.5.5	Gas permeability test.....	98
3.5.6	Optical microscopy and image analysis	99
3.5.7	Microstructural analysis	100
3.5.7.1	Preparation of samples	100
3.5.7.2	Scanning electron microscopy (SEM) and energy dispersive X-ray spectroscopy (EDX)	101
3.5.7.3	Thermogravimetric analysis (TGA).....	101
3.5.8	High-resolution X-ray computed microtomography (μ CT).....	102

Chapter 4 Development and Performance of Self-healing Soil-cement Systems using Microcapsules and Pellets subjected to Freeze-thaw

Cycles.....	105	
4.1	Introduction..... 105	
4.2	Materials and mix proportions	105
4.3	Effect of freeze-thaw cycles on the physical and mechanical properties of soil-cement systems.....	108
4.3.1	Effect of freeze-thaw cycles on the UCS of soil-cement systems	108
4.3.2	Mechanisms behind the behaviour of soil-cement systems subject to freeze-thaw cycles.....	110
4.4	Development and performance of self-healing soil-cement systems subject to freeze-thaw cycles using Lambson microcapsules	112
4.4.1	Survivability of the Lambson microcapsules	112
4.4.2	SEM.....	113
4.4.3	Effect of the microcapsules on the mechanical properties of soil-cement systems.....	114
4.4.4	Self-healing performance of soil-cement systems embedded with Lambson microcapsules after freeze-thaw cycles	116

4.4.5	Image analysis.....	121
4.4.6	Summary of the performance of self-healing soil-cement systems using Lambson microcapsules	122
4.5	Autonomic self-healing performance of soil-cement systems with LUVOMAG MgO pellets after freeze-thaw cycles	122
4.5.1	Influence of LUVOMAG MgO pellets on the properties of soil-cement systems.....	123
4.5.1.1	Distribution of MgO pellets embedded within a soil-cement matrix.....	123
4.5.1.2	Effect of the MgO pellets on cement hydration.....	125
4.5.1.3	Flowability.....	126
4.5.1.4	Water content.....	128
4.5.1.5	Unconfined compressive strength.....	130
4.5.1.6	Unconfined compressive strength development	132
4.5.2	Crack sealing efficiency	133
4.5.3	Permeability.....	137
4.5.3.1	Water permeability.....	137
4.5.3.2	Gas permeability	139
4.5.4	Recovery of mechanical properties	141
4.5.4.1	UCS and Young's modulus	141
4.5.4.2	Tensile strength.....	145
4.5.5	Characterisation of the healing products	147
4.5.5.1	Thermogravimetric analysis of the healing products	147
4.5.5.2	SEM/EDX.....	150
4.6	Mechanisms of the self-healing processes	152
4.7	Concluding remarks	156
Chapter 5 Optimisation of Self-immune Soil-cement Systems Subjected to Freeze-thaw Cycles Using SikaAer® Solid Microcapsules.....		159
5.1	Introduction.....	159

5.2	Mix design of the soil-cements	160
5.3	Influence of SikaAer [®] Solid microcapsules on the properties of soil-cement systems.....	162
5.3.1	Survivability and distribution of SikaAer [®] Solid microcapsules within soil-cement matrices.....	162
5.3.2	Fresh properties of the SikaAer [®] soil-cement mixes.....	164
5.3.2.1	Calorimetry	164
5.3.2.2	Flowability	165
5.3.3	Physical properties	166
5.3.3.1	Water content.....	166
5.3.3.2	Dry density	167
5.3.4	UCS and Young's modulus	168
5.3.5	Unconfined compressive strength development	171
5.4	Evaluation of the self-immune capability of SikaAer [®] Solid microcapsules embedded soil-cement systems subjected to freeze-thaw cycles.....	172
5.4.1	Physical properties	172
5.4.1.1	Surface crack characterisation	172
5.4.1.2	Porosity, degree of saturation (Sr) and air content.....	175
5.4.1.3	Water content.....	179
5.4.1.4	Volume	180
5.4.1.5	Dry density	182
5.4.2	Mechanical properties	183
5.4.2.1	Unconfined compressive strength and Young's modulus	183
5.4.2.2	Tensile strength.....	187
5.4.3	Permeability.....	188
5.5	Mechanisms of self-immune soil-cement systems using SikaAer [®] Solid microcapsules under freeze-thaw conditions	190
5.5.1	Validation of temperature-responsive behaviour.....	190

5.5.2	Air content and freeze-thaw resistance	192
5.5.3	Critical degree of saturation.....	193
5.5.4	High resolution X-ray computed microtomography (μ CT)	194
5.5.5	Summary of principles underlying the development of soil-cement systems self-immune to freeze-thaw cycles using SikaAer [®] Solid microcapsules.....	196
5.5.6	Overview of the self-immunity mechanism	197
5.6	Concluding remarks	199
Chapter 6 Development and Performance of Self-immune Soil-cement Systems Subjected to Freeze-thaw Cycles with a Superabsorbent Polymer (SAP).....		201
6.1	Overview	201
6.2	Materials and mix proportions	202
6.3	Sorptivity of the BASF SAP A	203
6.3.1	Absorption kinetics	204
6.3.2	Desorption and resorption kinetics	207
6.4	Influence of the BASF SAP A on the fresh, physical, and strength properties of the soil-cement systems.....	209
6.4.1	Fresh properties of the SAP-containing soil-cement mixes	209
6.4.1.1	Calorimetry.....	209
6.4.1.2	Flowability of the fresh mixes	211
6.4.2	Physical properties	212
6.4.3	Unconfined compressive strength.....	215
6.5	Development and behaviour of self-immune soil-cement systems under freeze-thaw cycles using BASF SAP A	217
6.5.1	Physical properties	217
6.5.1.1	Porosity, degree of saturation and air content	219
6.5.1.2	Water content.....	222
6.5.1.3	Volumetric change	223

6.5.1.4	Dry density	225
6.5.2	Unconfined compressive strength.....	226
6.5.3	Permeability.....	228
6.5.4	Surface crack characterisation	230
6.5.5	Summary and recommended dosage of SAP addition for building self-immune soil-cement system.....	234
6.6	Mechanisms of self-immunity in soil-cement systems under freeze-thaw cycles using SAPs	234
6.6.1	Air content and freeze-thaw resistance	234
6.6.2	Critical degree of saturation.....	236
6.6.3	Scanning electron microscopy	236
6.6.4	High resolution X-ray computed microtomography (μ CT)	237
6.6.4.1	Microstructure of soil-cement samples containing the BASF SAP A	237
6.6.4.2	Development process of self-immune soil-cement system using SAPs ...	240
6.6.4.3	Behaviour of self-immune soil-cement systems during the freeze-thaw cyclic action	242
6.6.5	Summary of principles of the development and mechanisms of self-immune soil-cement system under freeze-thaw cycles using BASF SAP A	246
6.6.5.1	Development of self-immune soil-cement system using SAPs.....	246
6.6.5.2	Overview of the self-immune mechanism under freeze-thaw cycles	246
6.7	Comparison between the different self-immune soil-cement systems under freeze-thaw cycles	248
6.8	Concluding remarks	254
Chapter 7	Conclusions and Recommendations	257
7.1	Conclusions.....	257
7.2	Recommendations for practice and future research.....	261
	References.....	265

List of Figures

Figure 1.1 Cement stabilisation in (a) pavement construction, (b) solidification/stabilisation of industrial contaminants, (c) foundation construction of a school in Florida, US, and (d) cut-off wall construction (courtesy of Hayward Baker). 3

Figure 1.2 Effects of several variables on the strength of soil-cement systems: (a) soil type (Taki and Yang, 1991), (b) cement content (Uddin et al., 1997), and (c) curing period (Endo, 1976), and (d) variation of permeability with cement content (Porbaha et al., 2000)...... 4

Figure 2.1 (a) Formation process of pothole (Rabine Toolbox, 2014) and (b) pothole formed in pavement after freeze-thaw cycles (waynetimes.com)...... 13

Figure 2.2 Hydraulic conductivity of soil-cement samples after freeze-thaw cycles (Jamshidi et al., 2011)...... 17

Figure 2.3 Void ratio of soil versus the number of freeze-thaw cycles in loose and dense states (Viklander, 1998)...... 18

Figure 2.4 (a) $R (\Delta H/H_0)$ and (b) $T (\Delta w/w_0)$ vs. the number of freeze-thaw cycles (Liu et al., 2010). ΔH and Δw are the changes in height and water content obtained in thawed soil after n cycles, respectively. H_0 and w_0 are the initial height and water content of the samples, respectively. 19

Figure 2.5 Critical dynamic stress of cement-modified clay vs. number of freeze-thaw cycles (confining pressure is 20 kPa) (Liu et al., 2010)...... 21

Figure 2.6 Reduction in 7-day UCS of specimens via freeze-thaw action (Mardani-Aghabaglou et al., 2015). The abbreviations C, PC, Mg, and W indicate the percentage of cement, ordinary Portland cement, magnesium sulphate solution, and water environment, respectively...... 21

Figure 2.7 Summary of permeability results for different exposure scenarios and mix designs (Jamshidi et al., 2015a). “04” and “12” refer to the number of freeze-thaw cycles, and “-2”, “-10”, and “-20” refer to freezing temperatures; “20%” and “LWS” refer to 20% cement content and “lower water to solids ratio” conditions. 23

Figure 2.8 Changes of two properties subjected to various number of freeze-thaw cycles (Jamshidi et al., 2015a): (a) UCS ratios and (b) hydraulic conductivity ratios.	24
Figure 2.9 SEM images showing rubber powder particles (a) changing the direction of a micro-crack's path and (b) preventing micro-crack expansion (Wang et al., 2019).	26
Figure 2.10 Thin section images of ice lens formation in soil-cement (3% cement and 14% water) after exposure to 3 cycles of freeze-thaw (Lake et al., 2016).	26
Figure 2.11 Effects of repeated freeze-thaw (F-T) cycles on unconfined compressive strength and at various bassanite/soil (B/S) ratios for: (a) specimens without coal ash, (b) specimens with 10% coal ash content, and (c) specimens with 20% coal ash content (Shibi and Kamei, 2014).	28
Figure 2.12 Hydraulic conductivity recovery of freeze-thaw exposed specimens after over 120 days of post-exposure healing period (Jamshidi and Lake, 2014).	30
Figure 2.13 Schematic illustration of the effect of air pores during the freezing of concrete (Eriksson et al., 2018; Zeng et al., 2016). Upper pressure distribution refers to the case where the air pore solely acts as a reservoir for the expelled water, while the lower distribution refers to the case where it also acts as a cryo-pump. .	32
Figure 2.14 Air content vs. freeze-thaw durability of concrete (Cordon, 1967).	33
Figure 2.15 Air content of concrete vs. compressive strength (Mohammed and Pandey, 2015).	33
Figure 2.16 Schematic representation of the mechanisms of (a) autogenic self-healing (de Rooij et al., 2013) and (b) autonomic self-healing (Souza, 2017).	37
Figure 2.17 The concept of autonomic healing using microcapsules (White et al., 2001).	38
Figure 2.18 Microcapsule-based self-healing approaches. Reaction of spherical or cylindrical encapsulated agent while contact with: (A,B) moisture, or air, or due to heating; (C,D) the cementitious matrix itself; (E,F) a second component present in the matrix (small, light-coloured inclusions) or (G,H) a second component delivered by additional capsules (big, light-coloured inclusions) (Van Tittelboom and De Belie, 2013).	39

Figure 2.19 Recovery of mechanical properties for sodium silicate-embedded self-healing cement paste (Huang and Ye, 2011).	43
Figure 2.20 Representative images from a prism with sodium silicate-containing capsules: (a) crack area on the day of cracking and (b) crack filled after 28 days of healing (note: the hashed band corresponds to 500 μm) (Kanellopoulos et al., 2015).	44
Figure 2.21 Relative volumes of major compounds during cement hydration (Baquerizo Ibarra, 2015; Tennis and Jennings, 2000).	45
Figure 2.22 Mechanical behaviours of specimens with and without microcapsules (Huang and Ye, 2011).	45
Figure 2.23 Diagram of the self-healing capsules developed at University of Cambridge (Al-Tabbaa and Kanellopoulos, 2014).	46
Figure 2.24 Self-healing process of concrete containing expansive agents, geo-materials, and crystalline additives (Ahn and Kishi, 2010).	50
Figure 2.25 Permeability measurements of cracked, healed, and un-cracked control discs' (Qureshi and Al-Tabbaa, 2016) (a) sorptivity coefficient and (b) gas permeability coefficients. M and N denote two types of MgO and the number that follow indicates the percentages of each type used in the mixtures.	51
Figure 2.26 Mechanisms of the formation of balls (Srb and Ruzickova, 1988).	52
Figure 2.27 Schematic illustration for the pelletisation process using the fluid bed technique (Glatt GmbH Binzen, 2005).	53
Figure 2.28 Chemical structure of a synthetic polyacrylamide with potassium salt base superabsorbent polymer and its reaction with water (Mao et al., 2011).	54
Figure 2.29 Illustration of a typical acrylic-based anionic SAP material and a schematic presentation of SAP swelling (Zohuriaan-Mehr and Kabiri, 2008).	55
Figure 2.30 SEM images of bulk-polymerised SAP A and SAP B used in (Snoeck et al., 2015). The scale bar amounts 100 μm.	57
Figure 2.31 Changes in the average size of an SAP added to different types of solutions over time (Hong and Choi, 2017).	58

Figure 2.32 Absorption of SAPs in (a) distilled water and (b) an extracted cement pore solution, where SAP1, SAP3, and SAP4 are made of sodium salts of a crosslinked polyacrylic acid, and SAP2 is a potassium salt of a crosslinked polyacrylic acid-polyacrylamide copolymer (Farzanian et al., 2016).	60
Figure 2.33 SAP absorption for a range of pH levels (Craeye et al., 2018).	61
Figure 2.34 Desorption kinetics of SAPs (Yun et al., 2017).	61
Figure 2.35 Schematic representation of a potential healing mechanism using SAPs (Lee et al., 2010).	62
Figure 2.36 Images of crack before and after 28 wet-dry cycles (Gruyaert et al., 2016).	63
Figure 2.37 Water permeability results for mortars with and without addition of SAPs (Mignon et al., 2015). Length values between brackets show the range of crack widths.	64
Figure 2.38 Air content in fresh concrete (Mechtcherine et al., 2017).	67
Figure 2.39 Images (BSE) of 5-day-old cement pastes at 0.36 water/cement ratio containing 1% of 3 types of SAPs. Micrographs highlight the size, shape, and distribution of (1) SAP voids, (2) collapsed SAP particles, and (3) entrapped air, as well as the microstructure of the SAP/cement paste interface (Lee et al., 2010).	67
Figure 3.1 The particle size distribution curve of the sand used.	74
Figure 3.2 Image of the (a) sand, (b) clay, and (c) cement used.	74
Figure 3.3 Images of the Lambson microcapsules used (a) as observed by a Leica DM2700 optical microscope and (b) as observed by the naked eye; and (c) Leica DM 2700 upright optical microscope used.	76
Figure 3.4 LUVOMAG MgO pellets used in the study.	77
Figure 3.5 Images of the SikaAer[®] Solid microcapsules used in this work (a) an optical microscopic image and (b) a SEM image.	78
Figure 3.6 Images of the BASF SAP A used in this study (a) observed under an optical microscope and (b) an SEM image.	78
Figure 3.7 Production of cement pore solution.	80

Figure 3.8 (a) The automatic mixer, (b) samples vibrated on a vibrating table, (c) a plastic mould for the soil-cement samples, and (d) a silica gel mould for the disc samples.....	82
Figure 3.9 (a) The curing tank with 97% ($\pm 3\%$) RH, (b) the freezer used in the experiments, and (c) samples in a thawing tank.....	84
Figure 3.10 (a) the Calmetrix I-Cal 2000 HPC High Precision Isothermal Calorimeter used, (b) a laptop connected for data logging, and (c) typical relationship between thermal power and time for cement hydration samples (Nelson, 1990).	85
Figure 3.11 The flow table equipment used.....	86
Figure 3.12 Dimension measurements.....	90
Figure 3.13 Water content measurements using (a) electronic balance for weight measurements, and (b) oven for drying the samples.	91
Figure 3.14 (a) Mortar and pestle and, (b) boiling the soil-cement slurry on a thermometric device.	93
Figure 3.15 Sample tested by Uniframe 70-T0108/E Control Machine.	94
Figure 3.16 Splitting tensile test setup.....	95
Figure 3.17 Permeability testing: (a) the permeameters, peristaltic pumps, pressure transducers and data loggers used, and (b) a schematic set-up for permeability test (courtesy of Controls Group).	97
Figure 3.18 The gas permeability tests: (a) a schematic illustration of the experimental setup for the gas permeability test (Yang et al., 2011), and (b) the gas permeability test set-up used.....	98
Figure 3.19 The Leica LED2000 optical microscope used to measure and monitor cracks.	100
Figure 3.20 The Phenom Pro X Desktop scanning electron microscope (SEM) used. .	101
Figure 3.21 The Perkin Elmer STA 6000 thermogravimetric analysis system used.....	102
Figure 3.22 Nikon XT H 225 ST industrial CT scanning apparatus used.	103
Figure 4.1 7-day UCS values for soil-cement samples with different cement contents.	109

Figure 4.2 UCS values for soil-cement samples with 10%, 15%, and 20% cement content after varying numbers of freeze-thaw cycles.....	109
Figure 4.3 Correlations between (a) water content and volumetric change, (b) degree of saturation, (c) porosity, and (d) air content of C15 for increasing numbers of freeze-thaw cycles.	111
Figure 4.4 Lambson microcapsules within soil-cement mix samples (a) before freeze-thaw and (b) after 5 freeze-thaw cycles.	112
Figure 4.5 Lambson microcapsules in the soil-cement mixes before setting.....	113
Figure 4.6 SEM images of broken Lambson microcapsules within the soil-cement matrix.....	114
Figure 4.7 Effects of Lambson microcapsules on the 7-day UCS of soil-cement mixes.	115
Figure 4.8 UCS of the Lambson microcapsule-containing soil-cement samples after different numbers of freeze-thaw cycles and 7 days of healing for cement contents of (a) 20%, (b) 15%, and (c) 10%.	119
Figure 4.9 Water content of the Lambson microcapsule-containing soil-cement samples after different numbers of freeze-thaw cycles and 7 days of healing.....	120
Figure 4.10 E_{50} of the C20L5 and control mixes after different numbers of freeze-thaw cycles and a 7-day healing period.	120
Figure 4.11 Microscopic images of C20L5 samples that were damaged by 10 freeze-thaw cycles and self-healed afterward for (a) 0 days, (b) 7 days, (c) 28 days, and (d) 60 days.	121
Figure 4.12 Image of soil-cement specimens with and without the MgO pellets. Microscopic observation reveals the (a) distribution and (b) embedment of MgO pellets inside the soil-cement samples and the lack thereof within control samples (c).....	124
Figure 4.13 Effects of replacing 10% of sand with MgO pellets on the isothermal (23°C) power and energy production of soil-cement mixes.	126
Figure 4.14 Flow values of different soil-cement mixes with embedded MgO pellets. .	128

Figure 4.15 The 7-day water content of different soil-cement samples with MgO pellets.	129
Figure 4.16 The water content of the soil-cement mixes containing MgO pellets subjected to different number of freeze-thaw cycles.	129
Figure 4.17 The strength behaviour of soil-cement mixes with MgO pellets at different numbers of freeze-thaw cycles: (a) actual UCS values and (b) normalised UCS values.	131
Figure 4.18 The UCS of soil-cement samples containing MgO pellets over time.	133
Figure 4.19 Typical optical microscopic images of the crack-sealing patterns of control samples (a-b): (a) damaged by 7 freeze-thaw cycles and (b) self-healed for 60 days; and soil-cement samples containing MgO pellets (c-d): (c) damaged by 7 freeze- thaw cycles and (d) self-healed for 60 days.	135
Figure 4.20 Typical optical microscopic images showing the development of crack sealing on the surface of C15P10 samples over healing time.	136
Figure 4.21 Crack sealing efficiency of soil-cement samples, including controls and samples embedded with MgO pellets, both subjected to 7 freeze-thaw cycles, over healing time.	137
Figure 4.22 Evolution of the permeability values of a soil-cement mix containing MgO pellets and a control sample after 10 freeze-thaw cycles for several healing periods.	138
Figure 4.23 Average permeability ratios for several healing periods.	139
Figure 4.24 Gas permeability coefficient ratios over time for un-cracked and self-healed soil-cement samples after 7 freeze-thaw cycles.	140
Figure 4.25 Results for C15P10 samples over time following 10 freeze-thaw cycles in terms of (a) UCS values and (b) UCS recovery (ratio between the increased value after healing and the uncracked 7-day UCS value).	143
Figure 4.26 E_{50} of C15P10 samples over time following 10 freeze-thaw cycles in terms of (a) E_{50} value and (b) E_{50} recovery (ratio between the increased value after healing and the uncracked 7-day E_{50} value).	144

Figure 4.27 Tensile strength over time for C15P10 samples after 10 freeze-thaw cycles in terms of (a) tensile strength values and (b) tensile strength recovery (ratio between the increased value after healing and the uncracked 7-day tensile strength value).	146
Figure 4.28 Thermogravimetric analysis results for samples containing MgO pellets and controls at various healing times in terms of (a) TGA and (b) DTG curves.	149
Figure 4.29 SEM images of C15P10 samples subjected to 10 freeze-thaw cycles and self-healed for 28 days.	151
Figure 4.30 Examples of cracks induced by freeze-thaw cycles hitting an MgO pellet in soil-cement specimens.	153
Figure 4.31 Schematic representation of the hypothesised self-healing mechanism associated with Lambson microcapsules during (a) the initial triggering process and (b) after freeze-thaw damage has been healed.	154
Figure 4.32 Schematic representation of the hypothesised self-healing mechanism associated with the use of MgO pellets during (a) the initial triggering process and (b) after freeze-thaw damage has been healed.	155
Figure 5.1 Microscopic images and SEM images of SikaAer[®] Solid microcapsules within the soil-cement matrix. Images depict microcapsules before freeze-thaw cycles (a and c) and after 10 freeze-thaw cycles (b and d).	163
Figure 5.2 Effects of SikaAer[®] Solid addition on isothermal (23°C) power and energy production of soil-cement mixes.	165
Figure 5.3 Flow table values for soil-cement mixes with different dosages of SikaAer[®] Solid microcapsules compared to the control mix.	166
Figure 5.4 Water content of soil-cement mixes with different dosages of SikaAer[®] Solid.	167
Figure 5.5 (a) Dry density and (b) normalised dry density for soil-cement mixes with different dosages of SikaAer[®] Solid.	168

Figure 5.6 Mechanical properties of soil-cement samples containing varying dosages of SikaAer[®] Solid microcapsules: (a) 7-day UCS, (b) Young’s modulus, and (c) stress-strain curves.	170
Figure 5.7 UCS of soil-cement samples containing different proportions of SikaAer[®] Solid microcapsules over time.	171
Figure 5.8 Typical microscopic images of cracking patterns in (a) control samples and self-immune samples embedded with (b) 1.67% and (c) 3.33% microcapsule dosages after repeated freeze-thaw cycles.	175
Figure 5.9 (a) Porosity, (b) degree of saturation, and (c) air content of SikaAer microcapsule-embedded soil-cement systems over repeated freeze-thaw cycles... 	178
Figure 5.10 Water content of soil-cement samples containing different dosages of SikaAer[®] Solid microcapsules subjected to repeated freeze-thaw cycles.	180
Figure 5.11 Volumetric change of soil-cement samples embedded with different dosages of SikaAer[®] Solid microcapsules over repeated freeze-thaw cycles.	181
Figure 5.12 Dry density of soil-cement systems embedded with SikaAer[®] Solid subjected to repeated freeze-thaw cycles.....	182
Figure 5.13 Strength behaviour of soil-cement mixes with various dosages of SikaAer[®] Solid microcapsules over repeated freeze-thaw cycles in terms of (a) actual UCS values and (b) normalised UCS values.....	184
Figure 5.14 E₅₀ values for soil-cement samples over repeated freeze-thaw cycles.	185
Figure 5.15 Stress-strain behaviour after repeated freeze-thaw cycles for (a) control mix C15, (b) mix C15S0.67, (c) mix C15S1.67, (d) mix C15S3.33, and (e) mix C15S6.67.	186
Figure 5.16 Tensile strength of soil-cement samples with different dosages of SikaAer[®] Solid microcapsules over repeated freeze-thaw cycles.....	187
Figure 5.17 Evolution of the permeability values of SikaAer[®] soil-cement samples over repeated freeze-thaw cycles.....	189
Figure 5.18 Representative microscope images of SikaAer[®] Solid microcapsules in soil-cement in frozen and thawed states with area measurements.	191

Figure 5.19 Air content and porosity of soil-cement systems with different dosages of SikaAer® Solid microcapsules.	193
Figure 5.20 Representative μCT cross-section images of (a) C15 specimens and (b) C15S3.33 specimens with SS microcapsules.	195
Figure 5.21 3D reconstruction of a typical 7-day C15S3.33 sample using X-ray μCT.	197
Figure 5.22 Representation of the theorised self-immune mechanism conferred by the use of SikaAer® Solid microcapsules in a soil-cement matrix (a) before freezing and (b) during freezing.	198
Figure 6.1 Hypothesis of a self-immune soil-cement system during freeze-thaw action.	202
Figure 6.2 Microscopic images showing the (a) dried SAPs and (b) soaked SAPs in the revisable process of the SAP absorption and desorption.	203
Figure 6.3 Absorption kinetics of SAP A in different types of solutions.	205
Figure 6.4 Absorption capacity of SAP A in different (a) pH values and (b) ionic concentration.	206
Figure 6.5 Changes in volume of SAP A in deionised water, tap water, and cement pore solution.	207
Figure 6.6 Desorption and resorption kinetics of the BASF SAP A in 50% ($\pm 10\%$) and 95% ($\pm 2\%$) RH environment.	208
Figure 6.7 The effect of the BASF SAP A addition on the isothermal (23°C) power and energy production of the soil-cement mixes.	210
Figure 6.8 Flow values of different soil-cement mixes with different dosages of the BASF SAP A.	212
Figure 6.9 Effects of the BASF SAP A on the (a) water content, and (b) the degree of saturation of the soil-cement mixes tested.	213
Figure 6.10 Effects of the addition of the BASF SAP A on the dry density of soil-cement mixes tested.	214

Figure 6.11 Effects of the BASF SAP A on the 7-day UCS of the soil-cement mixes used.	216
Figure 6.12 The UCS of the SAP-containing soil-cement mixes at different curing times.	217
Figure 6.13 Photo of the soil-cement specimens after ten freeze-thaw cycles with highlighted cracks and spalling.	218
Figure 6.14 Properties of the soil-cement mixes with different percentages of SAP additions against the number of freeze-thaw cycles in terms of (a) porosity, (b) degree of saturation, and (c) air content.	221
Figure 6.15 The water content of the soil-cement mixes containing different dosages of the BASF SAP A subjected to a number of freeze-thaw cycles.	223
Figure 6.16 The volumetric change of the soil-cement mixes embedded with different dosage of the BASF SAP A under freeze-thaw cycles.	224
Figure 6.17 The correlation between water content and volumetric change of the soil-cement mixes embedded with different dosage of the BASF SAP A over repeated freeze-thaw cycles.	225
Figure 6.18 The dry density of the SAP-embedded soil-cement systems over repeated freeze-thaw cycles.	226
Figure 6.19 The USC of the soil-cement mixes with different dosages of the SAP over repeated freeze-thaw cycles.	227
Figure 6.20 The strength behaviour of the soil-cement mixes with two different w/c ratios that are both embedded with 2% SAP over repeated freeze-thaw cycles...	228
Figure 6.21 The evolution of the permeability values of the SAP-containing soil-cement mixes over repeated freeze-thaw cycles.	229
Figure 6.22 Surface crack identification of mixes C15 (a-c) and C15SAP2 (d-f): (a) C15 with no freeze-thaw cycles, (b) C15 after 5 freeze-thaw cycles and (c) C15 after 8 freeze-thaw cycles, (d) C15SAP2 with no freeze-thaw cycles, (e) C15SAP2 after 5 freeze-thaw cycles, and (f) C15SAP2 after 20 freeze-thaw cycles.	233

Figure 6.23 Air content and porosity of the soil-cement systems with different dosage of the BASF SAP A.....	235
Figure 6.24 SEM images of C15SAP2 soil-cement samples containing SAPs. The scale bars in (a) and (b) are 80 and 50 μm, respectively.	237
Figure 6.25 The BASF SAP particles identified in the soil-cement matrix using μCT.	238
Figure 6.26 Representative μCT cross-section images of (a) the C15 control mix specimens and (b) C15SAP2 specimens with 2% SAP content.....	239
Figure 6.27 Representative μCT cross-section images of mix C15SAP2 specimens, highlighting the SAP particles, at the curing age of (a) 20 hours, (b) 36 hours, and (c) 60 hours.	242
Figure 6.28 Representative μCT cross-section images of (a) frozen C15 control sample, (b) frozen C15SAP2 sample, and (c) partially thawed C15SAP2 sample. The micrographs highlight the SAP voids (1), SAP particles (2), and soil-cement matrix (3).	245
Figure 6.29 A schematic representation of the hypothesised self-immune mechanism taking place based on the use of the BASF SAP A in a soil-cement matrix (a) during mixing, (b) during cement hydration, (c) at room temperature and (d) during freezing.	247
Figure 6.30 3D reconstruction of a representative 7-day C15SAP2 sample before freeze-thaw cycles using μCT.....	248
Figure 6.31 Comparison between self-immune systems embedded with SikaAer[®] Solid and BASF SAP A in terms of (a) degree of saturation, (b) air content, (c) water content, (d) volumetric change, (e) UCS, (f) dry density, and (g) permeability. ...	254

List of Tables

Table 2.1 Summary of reduction of strength properties of soils stabilised with different amounts of cement and subjected to various numbers of freeze-thaw cycles.	15
Table 2.2 Overview of the healing agents that have been reported in literature (adapted from Van Tittelboom and De Belie, 2013).	40
Table 2.3 Categories of mineral additives used for self-healing cementitious materials.	47
Table 2.4 (a) SAP concrete mix proportions and (b) bubble counter data (Riyazi et al., 2017).	66
Table 2.5 Changes in strength properties and air content of cementitious materials with different dosages of SAPs.	69
Table 3.1 Soil classification chart (ASTM: D2487-17, 2017).	75
Table 3.2 Chemical composition and properties of LUVOMAG MgO pellets.	77
Table 3.3 The compositions of soil-cement mixes prepared.	81
Table 3.4 Experimental programme for investigating the self-healing performance of soil-cement specimens.	88
Table 3.5 Experimental programme for investigating the self-immunity performance of soil-cement specimens.	89
Table 4.1 Mix composition of soil-cement samples containing Lambson microcapsules.	107
Table 4.2 Mix composition of soil-cement samples containing MgO pellets.	107
Table 4.3 Initial setting time and peak power values for soil-cement samples with and without MgO pellets.	126
Table 4.4 Thermal decomposition of the samples collected from all mixes.	148
Table 5.1 Mix composition of soil-cement samples containing SikaAer[®] Solid microcapsules.	161
Table 5.2 Initial setting time and peak power values for soil-cement mixes containing different dosage of SikaAer[®] Solid microcapsules compared to the control.	165

Table 6.1 Mix composition of soil-cement samples containing SAPs.	203
Table 6.2 Initial setting time and peak power values for soil-cement mixes containing different dosage of SAP.	210
Table 6.3 Comparison of key properties among C15, C15S3.33, and C15SAP2.	250

List of Abbreviations

Ø	Diameter
µCT	X-ray computed microtomography
ρ _d	Dry density
A	Air content
ASTM	American Society for Testing and Materials
CA	Cyanoacrylate
Ca(OH) ₂	Calcium hydroxide (portlandite)
CaCO ₃	Calcium carbonate
CaO	Calcium oxide, lime
CO ₂	Carbon dioxide
CH	Clay of high plasticity, fat clay
CL	Clay of low plasticity, lean clay
CMS	Cement-modified soils
CSA	Calcium sulfoaluminate
C-S-H	Calcium silicate hydrate
CSE	Crack sealing efficiency
CTB	Cement-treated base
DTG	Differential thermogravimetry
e	Void ratio
e ^{res}	Residual void ratio
E ₅₀	Secant modulus
EA	Ethyl acrylate
EDX	Energy-dispersive x-ray spectrometry

EPSRC	Engineering and Physical Sciences Research Council
EVA	Ethylene vinyl acetate
G_s	Specific gravity
GP	Gas permeability
H ₂ O	Water
HC	Hydraulic conductivity test
HMC	Hydrated magnesium carbonate
k	Hydraulic conductivity
LOI	Loss on ignition
LWS	Lower water to solids ratio
m_f	Mass fraction
MgO	Magnesium oxide, magnesia
MA	Microstructure analysis of extracted samples
MMA	Methyl methacrylate
n	Porosity
Na ₂ SiO ₃	Sodium silicate
OECD	The Organisation for Economic Co-operation and Development
OM	Optical microscopic analysis
PC	Portland cement
PCA	Portland Cement Association
PP	Polypropylene
PU	Polyurethane
PVA	Polyvinyl alcohol
SAP	Superabsorbent polymer

SDI	Strength development index
SEM	Scanning electron microscope
SS	SikaAer [®] Solid
Sr.	Degree of saturation
S _{cr}	Critical degree of saturation
ST	Splitting tensile test
TGA	Thermogravimetric analysis
UCS	Unconfined compressive strength
UF	Urea formaldehyde
USEPA	United States Environmental Protection Agency
USCS	Unified Soil Classification System
USGS	United States Geological Survey
<i>R</i>	Gas permeability coefficient ratio
RH	Relative humidity
RILEM	International Union of Laboratories and Experts in Construction Material, Systems and Structures
RM4L	Resilient Materials for Life
V	Volume
<i>v_f</i>	Volume fraction
w	Water content

Chapter 1 Introduction

1.1 Background and motivation

1.1.1 Soil-cement systems

Soil-cement was first used in 1935 to improve the roadbed for State Highway 41 near Johnsonville, South Carolina (PCA, 2005). Since then, Portland cement (PC) has been used to stabilise soils and aggregates for thousands of miles of pavement applications all over the world (PCA, 2005). Today, as shown in **Figure 1.1**, the applications of soil-cement systems have been expanded to include geotechnical and infrastructure projects. For example, soil-cement systems are used in pavement stabilisation, grouting applications, cut-off walls, foundations, slopes, embankments, environmental remediation projects (e.g. soil stabilisation/solidification), and other projects. In various geotechnical applications, adding cement to soil to form a soil-cement system is an effective and economical technique to improve the engineering properties of soils that are unsatisfactory for construction in their natural state. The addition of cement can substantially improve the engineering properties of soft or contaminated soil that would be unsatisfactory for construction in its natural state. Cement can fortify soil by increasing its strength, decreasing its permeability, or limiting its deformation (Nicholson, 2015; Porbaha et al., 1998). Soil-cement systems also have historically been used for volume stability, settlement reduction, increased durability to dynamic/repeated loads, and dust control. For example, cement stabilisation techniques have been adopted in the stabilisation of ice-rich frozen soils in China for the construction of subgrade (Chai et al., 2017). This study's authors reported the unconfined compressive strength (UCS) of 15% cement-stabilised soil increased from 0.65 MPa to 1.2 MPa compared to unstabilised soil.

The soil-cement system has several important advantages over potential alternatives. First, mixing cement with soil is a quick operational technique associated with rapid solidification, and thus it can help lower construction times. For example, the application of cement can significantly reduce the time required for soil's consolidation settlement. Secondly, soil can be stabilised by either mixing with cement *in situ* or mixing ex-situ in a production plant. Furthermore, the cement can be applied *in situ* by a variety of means, including shallow mixing, deep mixing, grouting, and injection. Thus, engineering properties like strength, stiffness, and permeability can be dramatically enhanced in a wide range of contexts.

Moreover, in most cases, these improvements are permanent (Nicholson, 2015). The strength of soil-cement systems can be changed by adjusting the ratio of cement to soil in order to meet, for instance, the requirement of loading, soil type, and desired serviceability (Porbaha, 1998). Additional advantages of soil-cement systems include their relatively low environmental impact and the low amount of noise and vibration produced during their construction (compared to comparable alternatives) (Porbaha, 1998).

Figure 1.2a shows the effect of cement addition on several different types of soils. Generally, the quantity of cement required increases with the clay content of the soil. **Figure 1.2b** presents the effects of increasing cement content on the strength development index (SDI) of a soft clay. SDI is defined as the UCS ratio of the treated and untreated samples. It is conceivable that the SDI increase with the addition of cement. In addition, as with concrete, the strength of cement-treated soil tends to increase with time (**Figure 1.2c**). In terms of permeability, **Figure 1.2d** shows that the permeability of soil-cement reduces significantly as their cement content increases.

The soil-cement systems adopted in infrastructural and geotechnical practices are generally expected to maintain their engineering properties for decades. For example, cement-treated bases in pavement construction are required to retain a UCS of over 2.1 MPa over their service life (Garber et al., 2011). In addition, a low permeability value, which has been used in the UK for in-ground barriers of $<10^{-9}$ m/s (Al-Tabbaa and Evans, 1998) and in the US of $<10^{-8}$ m/s (USEPA, 1997) is also required for the solidification/stabilisation mix. However, soil-cement systems can deteriorate over time due to external effects such as freeze-thaw cycles, wet-dry exposure, and excessive loading. For this reason, Examinations on the durability including wet-dry and freeze-thaw exposure tests have been routinely conducted [e.g., (ASTM D559/D559M-15, 2015) and (ASTM D560/D560M-16, 2016)]. Among all, freeze-thaw action is considered to be one of the most destructive actions that can induce significant damage to soil-cement systems (Al-Tabbaa and Evans, 1998; Kamei et al., 2012; Khoury and Zaman, 2007; Shihata and Baghdadi, 2001; Wang et al., 2016). Consequently, the sustainability and durability of soil-cement systems subjected to freeze-thaw cycles are a matter of both scholarly and practical concern.



(a)



(b)



(c)



(d)

Figure 1.1 Cement stabilisation in (a) pavement construction, (b) solidification/stabilisation of industrial contaminants, (c) foundation construction of a school in Florida, US, and (d) cut-off wall construction (courtesy of Hayward Baker).

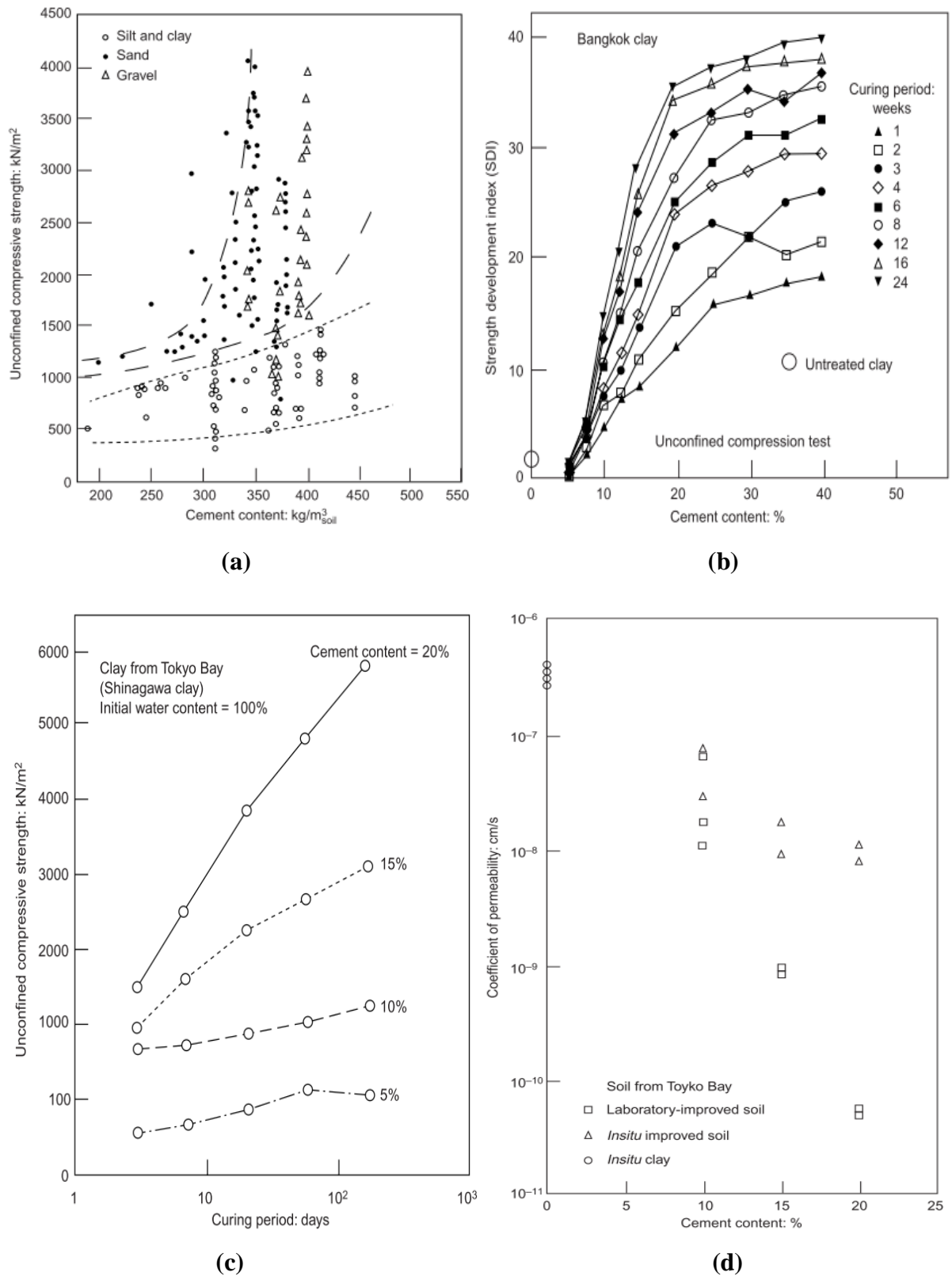


Figure 1.2 Effects of several variables on the strength of soil-cement systems: (a) soil type (Taki and Yang, 1991), (b) cement content (Uddin et al., 1997), and (c) curing period (Endo, 1976), and (d) variation of permeability with cement content (Porbaha et al., 2000).

1.1.2 Sustainability and durability challenges of soil-cement systems subjected to freeze-thaw cycles

Offering an early definition for sustainable development, the World Commission on Environment and Development argued in 1983 that “humanity has the ability to ensure that it meets the needs of the present without compromising the ability of future generations to meet their own needs” (World Commission on Environment and Development, 1983). Cement is the most widely used man-made construction material on earth, with 4.1 billion metric tons produced globally in 2017. Global cement production is expected to increase to almost 5 billion tonnes by 2030 (USGS, 2019). Portland cement (PC) is currently the most common binder material used in the construction of essential civil infrastructure around the world, to meet the basic needs of the development of humanity (e.g. buildings, bridges, roads, etc.). However, the production of cement emits a substantial amount of CO₂, accounting for 8–10% of global anthropogenic CO₂ emissions (Suhendro, 2014). As such, cement production is believed to contribute heavily to global climate change. Thus, in recent decades, the cement industry has been subjected to tremendous pressure in the form of carbon reduction initiatives (Anderson et al., 2008; Quadrelli and Peterson, 2007).

Durability, which is defined as the ability of a material or system to retain stability and integrity over years of exposure to destructive forces and weathering, is a crucial quality of most construction materials (Dempsey and Thompson, 1968). In cold regions, freeze-thaw durability is crucial for geotechnical infrastructure, as many of them undergo at least one freeze-thaw cycle annually, and many experience extensive repeated cycling. Deterioration due to freeze-thaw cycles result in civil infrastructures being out of service unpredictably.

In cold regions, freeze-thaw deterioration poses a serious threat to geotechnical infrastructure projects, as many undergo at least one freeze-thaw cycle annually, with others experiencing repeated cycling. A soil-cement system is naturally much more vulnerable to degradation and weathering than concrete due to these freeze-thaw cycles, as its volume fraction and the interspace of its internal voids are much larger. Water freezing inside pores usually contributes to an initial increase in volume of 9%, which can enlarge micro-cracks and generate internal pressure within the soil-cement system (thus producing bigger cracks). Physical properties of soil-cement systems, such as void ratio, water content and density, and permeability deteriorate with increasing numbers of freeze-thaw cycles, along with mechanical properties like strength and stiffness. For example, the UCS of 10% cement-

stabilised soil can be reduced by up to 95% after 12 freeze-thaw cycles (Jamshidi et al., 2015a).

Many studies have addressed the freeze-thaw cycle problem, but its underlying mechanisms are still unclear and no method for significantly improving freeze-thaw durability has been proposed. As the damage induced by freeze-thaw cycles usually manifests inside soil-cement systems, mitigation and repair are often unfeasible. After several freeze-thaw cycles, degradation can be severe, which can mean that the only responsible option available is to rebuild the entire structure, which is costly. Currently, such issue is addressed either through initial overdesign, implementation of maintenance programs, or both (Harbottle et al., 2014). However, these measures are uneconomical and time-consuming. In the past, to minimise the damage of freeze-thaw cycle, stabilised soils were sometimes covered by protection layers to protect the system from frost penetration. However, the US Federal Highway Administration performed frost penetration analysis for 41 sites and reported that maximum frost depth varied from about 0.37 m to 2.42 m (Selezneva et al., 2008). This deep frost penetration makes the construction of protection layers costly and inconvenient, and in many cases, the protection layer itself can even be susceptible to freeze-thaw exposure (Guthrie and Lay, 2007).

Consequently, the associated cost of maintenance, repair, and reconstruction of civil infrastructures is tremendous. Approximately £200 billion (in 2010 pounds) is needed for the maintenance and renewal of transportation networks alone in the UK from 2011 to 2030 (Mills et al., 2011). Roughly \$10 billion is spent each year on the maintenance and repair of railway bridges and tunnels in Japan (Ahn and Kishi, 2010). \$320 billion is needed each year in the US to maintain the country's infrastructure (Natale, 2010). In 28 OECD countries, the share of public maintenance funds dedicated to road expenditures was between 25%–35% in 2011 (OECD/ITF, 2013). Moreover, indirect costs due to traffic jams and the associated productivity loss indicated by comprehensive life cycle analyses can be 10 times the direct cost of maintenance and repair (Breugel, 2007). Besides the tremendous expenditure, the large amounts of Portland cement used for the maintenance, repair, and reconstruction of civil infrastructure result in enormous CO₂ emissions. Thus, it is imperative to the well-being of the planet (and of humanity itself) for researchers to develop more durable and sustainable soil-cement systems.

1.1.3 New approaches to develop durable and sustainable soil-cement systems subjected to freeze-thaw cycles

Historically, construction materials have been designed to meet fixed specifications, and material degradation has been viewed as inevitable. However, recently, inspiration from biological systems has fuelled research in the built environment to develop sustainable and resilient systems. These imagined systems comprise materials and structures that, like biological systems, can continually adapt and respond to their environment. This fundamental change in material design philosophy has led to the introduction of a host of “smart” materials. Self-healing materials count among the ranks of “smart” materials, which are defined by RILEM in terms of “any process by the material itself involving the recovery and hence improvement of a performance after an earlier action that had reduced the performance of the material” (de Rooij et al., 2013). Currently, most literature focuses on self-healing in polymers or concrete, and many studies have shown promising results (Ahn and Kishi, 2010; Dry et al., 2003; Joseph et al., 2010; Kanellopoulos et al., 2015; Li et al., 1998; Qureshi et al., 2016; White et al., 2001; etc.). However, to date, there has been very little work on the development of effective smart systems for geotechnical applications, and there is very little literature focusing on the damage caused specifically by freeze-thaw cycles. Fortunately, an EPSRC-funded Resilient Materials for Life (RM4L) project was carried out in collaboration between the Universities of Cardiff, Cambridge, Bath and Bradford along with more than 20 international industrial partners to develop innovative construction materials. The concept of applying smart materials to soil-cement systems in geotechnical applications emerged as part of this collaboration (Al-Tabbaa and Harbottle, 2015). A self-healing soil-cement system is a “smart” material that is able to detect, adjust, and repair its damage automatically and without any external intervention after being damaged. Self-healing materials can heal damage that manifests deep within the material as well, which is particularly helpful when damage is not externally visible or accessible. Furthermore, self-healing mechanisms are only triggered when damage occurs. For instance, microcapsules, once embedded in concrete, will remain stable before being triggered. Thus, the healing agent will only be released when triggered by damage. These qualities make self-healing mechanisms particularly auspicious candidates for addressing the freeze-thaw deterioration of soil-cement systems. Lambson microcapsules and LUVOMAG MgO pellets were used to develop such self-healing soil-cement systems.

The concept of self-immunity is also key to this research. In biological systems, an immune system is a system comprising many structures and processes within an organism that

protects against disease. Inspiration from biological systems, especially the immune system of the human body, provides insights into how a “self-immune” soil-cement system might be developed. Such a system would be able to respond and adapt to freeze-thaw cyclic action before damage is initiated, thus preventing the occurrence of the damage either partially or entirely. The self-immune soil-cement system resisting freeze-thaw cycle is then designed according to the properties of soil-cement systems as well as the damaging mechanism of freeze-thaw cycles. This study represents the first attempt to apply the concept of self-immunity to soil-cement systems undergoing freeze-thaw cycles and investigate this application via a detailed experimental framework. In this study, SikaAer[®] Solid air entraining microcapsules and superabsorbent polymers (SAP) were used to develop self-immune soil-cement systems by providing pressure vessels or reservoirs to accommodate the excess pressure generated during freezing.

In sum, this research applies the concepts of self-healing and self-immunity to soil-cement systems and investigates their performance under freeze-thaw conditions. The successful development of such nature-inspired self-healing, and self-immune soil-cement systems has the potential to yield substantial repair and maintenance savings and to enhance the durability, serviceability, sustainability, and safety of geotechnical applications subjected to freeze-thaw cycles.

1.2 Aims and objectives

The aim of this research is to improve the freeze-thaw durability of soil-cement systems by improving their self-healing and self-immune capabilities through the use of microcapsules, pellets, and SAP. As it is inspired by and intended to build on prior research, the objectives of this study are:

1. To develop self-healing soil-cement systems using suitable healing agents and embedding methods, and to investigate their self-healing performance subjected to freeze-thaw cycles.
2. To optimise the self-immune soil-cement systems subjected to freeze-thaw cycles using SikaAer[®] Solid microcapsules.
3. To investigate the development and performance of self-immune soil-cement systems subjected to freeze-thaw cycles by using SAP.
4. To reveal the mechanism and behaviour of the developed self-healing and self-immune soil-cement systems subjected to freeze-thaw cycles.

Ultimately, this research aims to promote the development of “smart” self-healing and self-immune soil-cement systems to resist freeze-thaw deterioration and provide insight on their performance and mechanisms.

1.3 Thesis outline

This thesis consists of seven chapters. **Chapter 1** introduces the background of the problem, the purpose of this thesis, and the study’s aims and objectives. **Chapter 2** presents an in-depth critical literature review discussing the state-of-the-art work done by others on soil-cement systems subjected to freeze-thaw cycles and self-healing materials. The mechanism of the freeze-thaw process, the air-entraining technique, the applications of the self-healing concept, and the applications of SAP in cementitious materials are explored. **Chapter 3** characterises the materials and experimental techniques used in the subsequent study. **Chapter 4** covers the development and performance of self-healing soil-cement systems subjected to freeze-thaw cycles using Lambson microcapsules and LUVOMAG MgO pellets. The optimisation and performance of self-immune soil-cement systems subjected to freeze-thaw cycles using two different agents, SikaAer[®] Solid microcapsules and BASF SAP A, are presented in **Chapter 5** and **Chapter 6**, respectively. Finally, **Chapter 7** concludes the thesis by summarising the main findings of this research and offers recommendations for future work.

Chapter 2 Literature Review

This chapter critically reviews various literature relevant to the topic of this research. It starts with the degradation of soil-cement systems subjected to freeze-thaw cycles and the factors that may influence the freeze-thaw durability of soil-cement systems are reviewed in detail. However, until now, there is no satisfactory solution to tackle these challenges in soil-cement systems. It then elucidates the application and mechanism of the air entraining, as a technique that is adopted in concrete to improve the freeze-thaw durability. The latter part introduces the concept of self-healing and covers the mechanisms and applications of self-healing in cementitious materials, as a possible solution to the challenges stated. Finally, as a potential agent for developing self-healing and self-immune soil-cement system, the perspective of the application of superabsorbent polymers (SAPs) in cementitious materials is introduced and illustrated. The chapter concludes by summarising the research gaps and the rationale behind the PhD work.

2.1 Degradation of soil-cement system subjected to freeze-thaw cycles

2.1.1 Overview of freeze-thaw degradation

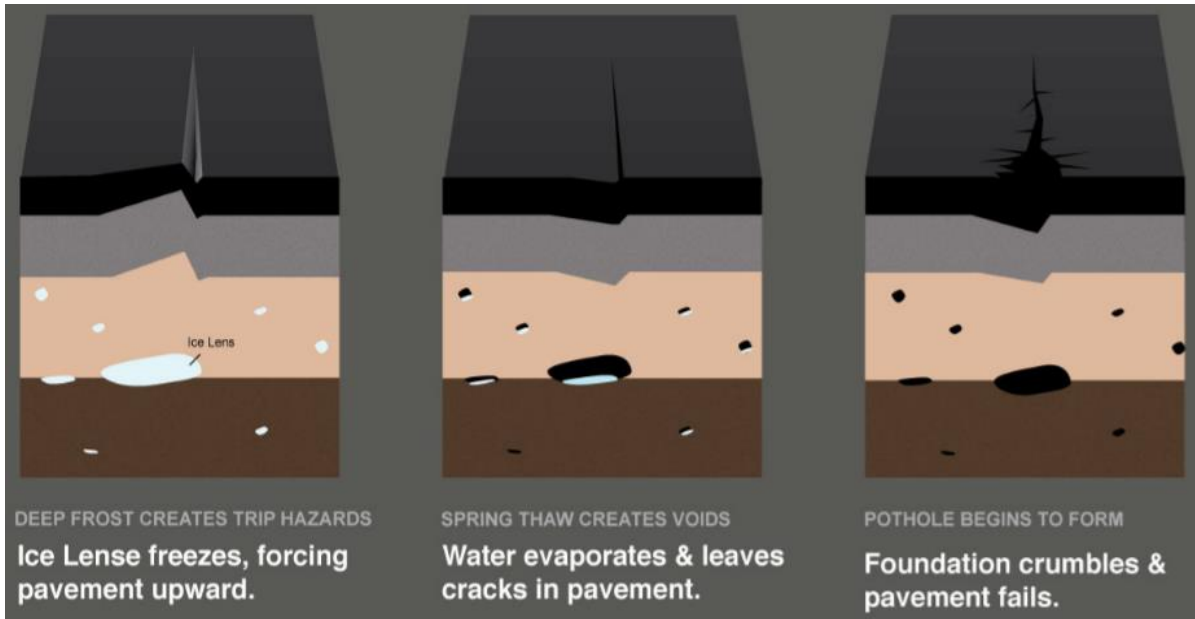
Geotechnical materials located in the upper ground in seasonal frost regions suffer from freeze-thaw cycles, which leads inevitably to the deterioration of any associated structures. In large areas of Asia, northern Europe, Alaska, Canada, and about a third of the continental US, cement-stabilised shallow ground is frequently subjected to freezing and frost heaving in the winter, and thaw settlement and weakening during spring. Frost heaving is the upward swelling of soil during freezing conditions due to the ingress of subsurface water and the 9% volume expansion of that water within the soil as it turns into ice.

The uptake of water from warmer underlying soil into the frost front is due to two main mechanisms. Generally, the controlling mechanism is capillary rise (Guthrie and Lay, 2007; Peppin and Style, 2013). The formation of ice and the ensuing reduction of water pressure in the freezing front cause a dramatic increase in capillary suction. Thus, liquid water migrates from warmer to colder regions within the system (Dash et al., 2006). The transportation of water through the soil matrix can be a controlling parameter for the growth of ice lenses. The other mechanism is caused by the vapour in frozen soil condensing into liquid water and ultimately crystallising into ice. When this occurs, the vapour flows towards the cold front, as the vapour pressure in the warmer underlying ground is greater than in the cooler ground

(Guthrie et al., 2006). However, it should be noted that much of the existing literature has not considered the effect of water ingress in their experiments therefore may lead to distinct freeze-thaw degradation results.

After freeze-thaw cycles, the engineering properties of soil (including its strength and permeability) can substantially deteriorate (Guthrie and Lay, 2007; Jamshidi and Lake, 2014). Craeye et al. (2018) argued that freeze-thaw deterioration is one of the most destructive actions for subgrade damage and the impact of freeze-thaw cycles usually defines the bounds of the environmental impact on the performance of the pavement. A typical example of the formation of a pothole after several freeze-thaw cycles is presented in **Figure 2.1**. Zhang et al. (2016) reported that the upper 0.3 m of pavement materials can be subjected to 10–50 freeze-thaw cycles annually in Iowa, US. However, many soil-cement systems survive fewer than 3 freeze-thaw cycles (Al-Tabbaa and Evans, 1998). Therefore, for construction projects involving soils exposed to cyclic freeze-thaw, care must be taken to improve freeze-thaw resistance. For instance, as reported in Eigenbrod(1996), in the Canadian province of Quebec, it is common practice for newly constructed highways to be left unpaved for several years. This practice is to allow the settlement caused by freeze-thaw action to occur before the grading and application of the final road surface so as to reduce the possibility of reconstruction. However, this practice is time-consuming and inefficient for obvious reasons.

Many studies have suggested that soil-cement systems are more resistant to freeze-thaw weakening than unstabilised soils (Altun et al., 2009; Liu et al., 2010; Shibi and Kamei, 2014). However, many studies have suggested that although soil-cement systems are more resistant to freeze-thaw cycles than unstabilised soils, they still suffer significant degradation (Altun et al., 2009; Davis et al., 2007; Jamshidi and Lake, 2014; Janoo et al., 1999; Qi et al., 2008; Shibi and Kamei, 2014; Wang et al., 2007). In addition, how (and to what extent) the engineering properties of soil-cement systems are affected is a matter that is still under investigation, as are the factors that influence freeze-thaw durability.



(a)



(b)

Figure 2.1 (a) Formation process of pothole (Rabine Toolbox, 2014) and (b) pothole formed in pavement after freeze-thaw cycles (waynetimes.com).

2.1.2 Effects of freeze-thaw cycles on the properties of soil-cement systems

2.1.2.1 Strength

Strength is a crucial parameter for the serviceability, stability, and durability of most soil-cement systems adopted in engineering practice (Eskişar et al., 2015; Jamshidi and Lake, 2014; Liu et al., 2010; Mardani-Aghabaglou et al., 2015; Portland Cement Association, 2001). Shihata and Baghdadi (2001) stated that UCS is among the most informative of the factors used to evaluate the freeze-thaw durability of soil-cement systems. A number of studies show that the UCS of cemented soils inevitably decreases with an increase in the number of freeze-thaw cycles (Eskişar et al., 2015; Jamshidi et al., 2015b; Kamei et al., 2012; Mardani-Aghabaglou et al., 2015). **Table 2.1** summarises strength losses for different types of soils stabilised with different amounts of cement and subjected to various numbers of freeze-thaw cycles (as reported in the literature). Generally, the strength of cement-stabilised soil deteriorates dramatically after freeze-thaw cycles. For example, a field test on a subgrade stabilised with 3.5% Portland cement was conducted by Janoo et al. (1999), revealing that UCS losses of up to 50% were caused by freeze-thaw cycles during the winter of 1996–1997 in Stratford, Connecticut, US. Jamshidi et al. (2015a) reported that the UCS of 10% cement-stabilised soil was reduced by up to 95% after 12 freeze-thaw cycles. Wang et al. (2016) also found that 6% cement-stabilised loess specimens showed obvious cracking after 7 freeze-thaw cycles and were destroyed after 9 freeze-thaw cycles.

Table 2.1 Summary of reduction of strength properties of soils stabilised with different amounts of cement and subjected to various numbers of freeze-thaw cycles.

Soil type	Cement content (%)	Number of freeze-thaw cycles	Reduction in strength (%)	Reference
On-site soil	3.5	a winter	50	(Janoo et al., 1999)
Soft clay	5	2 and 5	48–50	(Shibi and Kamei, 2014)
Clay soil	6	10	27	(Liu et al., 2010)
Silty sand	3	3	20–40	(Lake et al., 2016)
	6	3	10–20	
	10	12	52–95	(Jamshidi et al., 2015a; Jamshidi and Lake, 2014)
Kaolin	5	6	15	(Mardani-Aghabaglou et al., 2015)
	10	6	14	
	15	6	5	
	5	12	27	
	10	12	23	
	15	12	13	
Recycled base materials	4	3–6	50	(Ebrahimi et al., 2012)
Fat clay	5	5	50	(Eskişar et al., 2015)
Lean clay				
Fat clay	10		42	
Lean clay			37	
Note: the definition of fat clay (CH) and lean clay (CL) is presented in Table 3.1.				

2.1.2.2 Permeability

The permeability of soil/cemented soil can increase considerably when subjected to freeze-thaw cycles (Jamshidi and Lake, 2014; Lake et al., 2016; Mardani-Aghabaglou et al., 2015), and the first cycle generally exerts the greatest influence (Jamshidi et al., 2011; Othman and Benson, 1993; Viklander, 1998). Jamshidi et al. (2011) indicated that an increase of up to two orders of magnitude in the permeability of cemented soil can be observed after 4 freeze-thaw cycles (as shown in **Figure 2.2**). Jamshidi and Lake (2014) reported that both minor reductions and increases of up to 5250 times were observed in the permeability of soil-cement systems after freeze-thaw cycles and suggested that the reduction in permeability may be due to the continued hydration of the cement. Lake et al. (2016) reported that the permeability of 3–6% cement-stabilised soil increased less than an order of magnitude after 3 freeze-thaw cycles. The least damage was recorded in soil-cement compacted at dry of optimum water content. This indicates that increased water content may increase permeability damage for soil-cement systems exposed to freeze-thaw cycles. Wong and Haug (1991) reported that the permeability of soft fine-grained soils can be increased by 1–2 orders as a result of the fissures and joints induced by up to 5 freeze-thaw cycles. Many studies show similar findings with regards to the magnitude of the increase in permeability (Chamberlain et al. 1990; Pamukcu et al., 1994; Jamshidi et al., 2011). Othman and Benson (1993) reported that the change in permeability of soil after freeze-thaw cycles can be reduced by isotropic loading during thawing, and a 70 kPa pressure was sufficient to prevent the increase in hydraulic conductivity. However, Viklander (1998) argued that the effect of this isotropic loading was largely depended on temperature gradient, water content, and test configuration.

Chamberlain et al. (1990) argued that the increase in permeability after freeze-thaw cycles is caused by the enlargement of pores within soils as micro-fissures are enlarged by freezing ice and drainage of water as well as fine particles moving out of large pore space during thawing. The freezing of water inside pores contributes to an initial increase in volume, which can generate an internal pressure within the soil-cement matrix and induce cracks. Moreover, when the ice inside the soil-cement system thaws, the swelled system is unable to constrict or compress, and more cracks can thus be produced due to external forces or gravity. The cracks propagate in the soil matrix, leading to an increase in permeability. However, some researchers found that increased permeability can be observed while the soil is densified by freeze-thaw cycles (Chamberlain and Gow, 1979; Kim and Daniel, 1992). They reported that freezing and thawing reduce the void ratio but increase the vertical permeability of four fine-

grained soils. It appears that freeze-thaw cycles do not necessarily increase the void ratio of soil, and an increase in permeability after freeze-thaw exposure is possibly due to changes in soil structure and the interconnection of a network of micro-cracks that enable the flow of fluids.

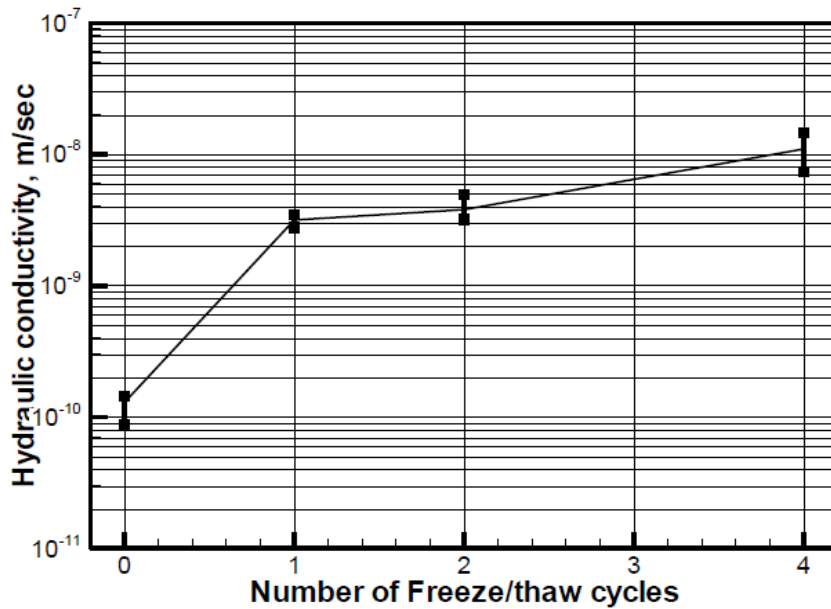


Figure 2.2 Hydraulic conductivity of soil-cement samples after freeze-thaw cycles (Jamshidi et al., 2011).

2.1.2.3 Volume and water content

It has been reported that soft fine-grained soils can experience maximum volume changes of up to 10–30% after cyclic freeze-thaw (Chamberlain et al. 1990). The factors that affect the variation in this change include initial moisture content, the plasticity of the clay, and the rate and mode of freezing (Eigenbrod K.D., 1996; Wong and Haug, 1991). Li et al. (2017) reported that the volume increase of densely compacted loess samples exposed to 7–8 one-dimensional freeze-thaw cycles was 16%. The researchers also found that a volume decrease of 2% was observed for loose samples after 31 freeze-thaw cycles. This result is in line with Viklander's (1998) position that loose soils tend to compact after freeze-thaw cycles, while dense soils tend to expand. As shown in **Figure 2.3**, Viklander's (1998) proposed a residual void ratio e^{res} for freeze-thaw action, meaning that both loose and dense soils may approach a similar void ratio after a sufficient number of freeze-thaw cycles for a specific kind of soil. Wang et al. (2007) conducted lab tests on subgrade fill material from the Nagqu Logistics Center Yard along the Qinghai-Tibet Railway and also obtained similar findings. The study demonstrated that there was a critical compactness level for the soil samples after repeated

freeze-thaw cycles. Since the density of soil is usually increased by adding cement, it is anticipated that the volume of soil-cement systems will generally increase after freeze-thaw cycles.

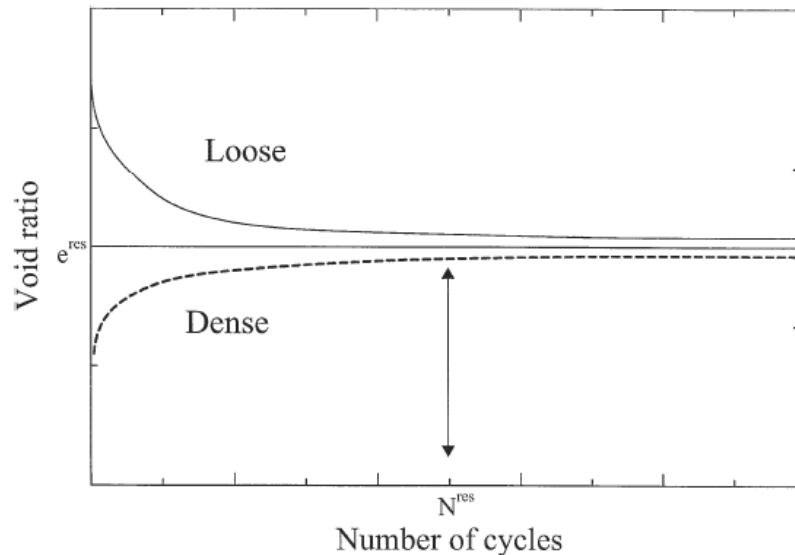
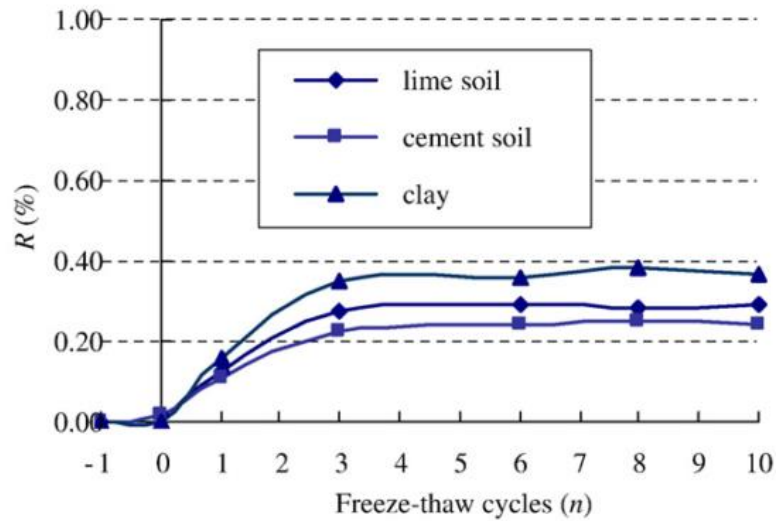


Figure 2.3 Void ratio of soil versus the number of freeze-thaw cycles in loose and dense states (Viklander, 1998).

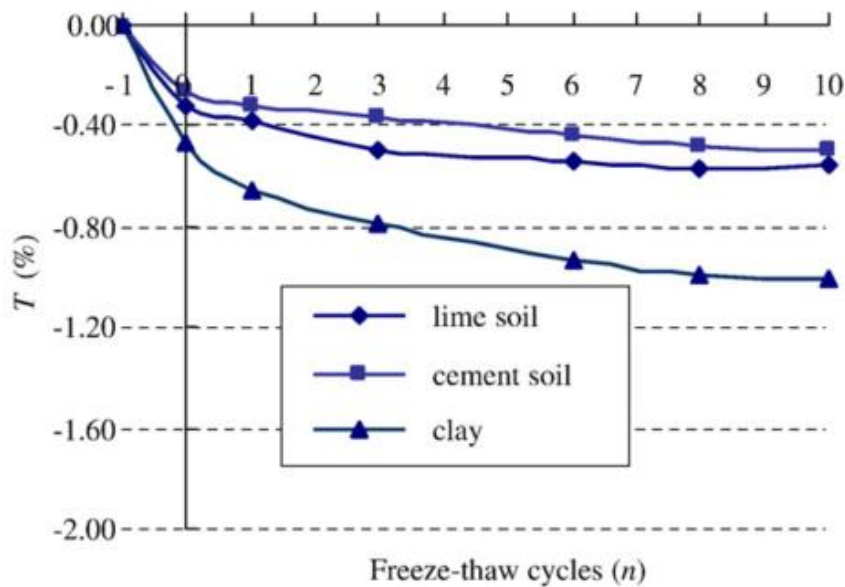
Shibi and Kamei (2014) reported that the volume of cement-stabilised very soft clay increased slightly with increasing numbers of freeze-thaw cycles. Liu et al. (2010) measured the height of cemented clay samples before and after being subjected to freeze-thaw cycles, finding that the height of the sample increased slightly but became steady after 3 cycles (as shown in **Figure 2.4a**). A cement content of 6% and a water content of approximately 18.4% were used in the study. The researchers also suggested that the height change in cement-modified samples was about 40% less than in untreated clay samples as a result of the larger bond force. Davis et al. (2007) carried out a study on the effect of fines content on four cement-treated aggregates and found that fines content appeared to confer a protective effect on the durability of the specimens subjected to freeze-thaw cycles. Their study implies that a reduction in porosity may exert a positive effect on the resistance of soil-cement systems to freeze-thaw cycles. In addition, it should be noted that expansion and rupture may deteriorate after several freeze-thaw cycles due to water ingress in the cracks.

Liu et al. (2010) assessed the water content changes of cemented clays after freeze-thaw cycles and suggested that the water content decreased with an increasing number of freeze-thaw cycles, stabilising gradually after 8 cycles (as shown in **Figure 2.4b**). However, Shibi and Kamei (2014) reported that freeze-thaw action had little influence on the water content of

cement-stabilised clay containing bassanite and coal ash. It should be noted that in the studies performed by Shibi and Kamei (2014) and Liu et al. (2010), the freeze-thaw cycles were conducted under closed systems, which means no external water source was accessible during the freeze-thaw process. However, a closed system fails to account for the water ingress common to freeze-thaw cycles in natural environments.



(a)



(b)

Figure 2.4 (a) R ($\Delta H/H_0$) and (b) T ($\Delta w/w_0$) vs. the number of freeze-thaw cycles (Liu et al., 2010). ΔH and Δw are the changes in height and water content obtained in thawed soil after n cycles, respectively. H_0 and w_0 are the initial height and water content of the samples, respectively.

2.1.3 Factors that affect the freeze-thaw resistance of soil-cement systems

The degree to which the engineering properties of soil-cement systems are altered by freeze-thaw cycles depends on a number of factors including the soil type, cement content, initial permeability, void ratio, water content, and the intensity of the freeze-thaw cycles. In this section, the effects of some of important factors are reviewed.

2.1.3.1 Cement content of soil-cement systems

Cement content is a crucial factor that can affect the freeze-thaw resistance of soil-cement systems, and it has thus been the subject of many studies (Eskişar et al., 2015; Jamshidi et al., 2015a; Liu et al., 2010). A cement content of 3–6% was used by Davis et al. (2007) and they found that the freeze-thaw resistance of cement-treated aggregate increased as the cement content increased. Liu et al. (2010) also reported that the freeze-thaw resistance of cemented clay increased considerably with increases in cement content, as shown in **Figure 2.5**. They reported that the critical dynamic stress attenuation coefficient for clayey soils stabilised with 0%, 3%, 6%, 9%, and 12% cement subjected to up to 10 freeze-thaw cycles were 0.35, 0.58, 0.73, 0.80, and 0.82, respectively. Zhang et al. (2016) reported that for the recycled subbase, frost heave rates decreased as the cement content was increased to 5% and 10%, while there was little improvement at 2.5% cement content. Mardani-Aghabaglou et al. (2015) investigated the effects of freeze-thaw action on the UCS of kaolin stabilised with different amounts of cement. The results of this study are presented in **Figure 2.6**. They demonstrate that the freeze-thaw resistance of cemented clay (i.e., the UCS) increased as the cement content increased for both a magnesium sulphate solution and a water environment. Examining permeability, Jamshidi et al. (2015) suggested that the freeze-thaw durability of cemented silty sand improved as the cement content increased. Lake et al. (2016) also reported that less permeability damage was recorded in 6% cement content samples when compared to 3% cement content samples. However, the amount of cement added to a given soil should not be selected arbitrarily. Guthrie and Lay (2007) performed laboratory tests on a silty subgrade soil treated with cement contents of 2.0, 3.5 and 5.0 percent. The results suggested that too much cement may cause shrinkage cracking while too little cement may cause worse frost heave behaviour than that observed in untreated specimens. Similar results indicating little improvement on freeze-thaw resistance for 2.5% cement stabilised soil were reported by Zhang et al. (2016). To sum up, most research to date has suggested that the freeze-thaw durability of soil-cement systems improves with an increase in cement content,

though some reported that the freeze-thaw durability of soil-cement can be reduced if cement content is relatively low (e.g. <3%).

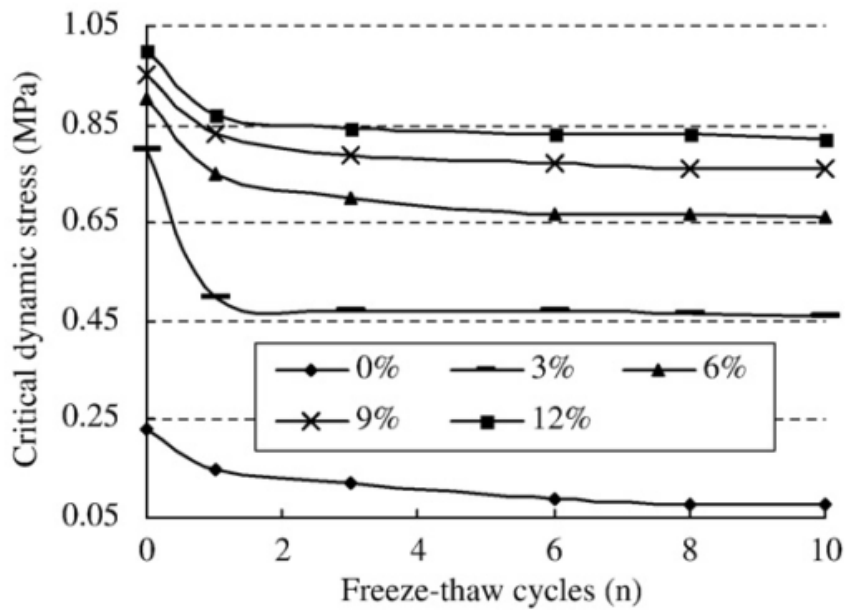


Figure 2.5 Critical dynamic stress of cement-modified clay vs. number of freeze-thaw cycles (confining pressure is 20 kPa) (Liu et al., 2010).

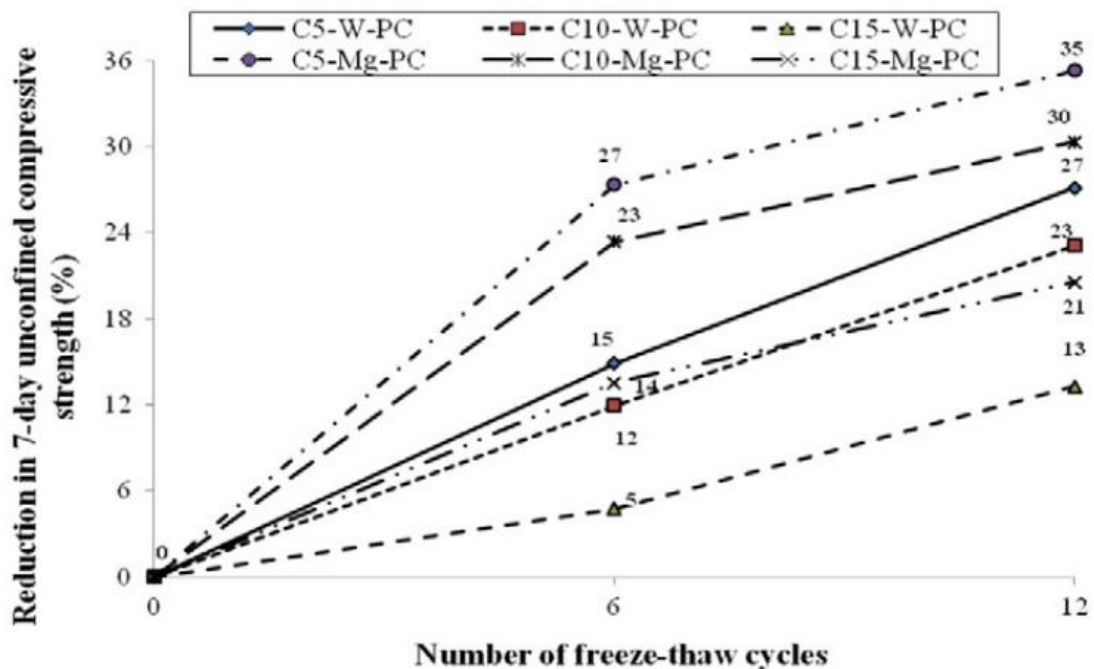


Figure 2.6 Reduction in 7-day UCS of specimens via freeze-thaw action (Mardani-Aghabaglou et al., 2015). The abbreviations C, PC, Mg, and W indicate the percentage of cement, ordinary Portland cement, magnesium sulphate solution, and water environment, respectively.

2.1.3.2 Water content

Water content also plays an important role in the susceptibility of soil-cement systems to the effects of freeze-thaw cycles. Only a few studies examine the effects of water content on the freeze-thaw durability of soil-cement systems. Among these, some reported that higher water content led to inferior freeze-thaw durability (Jamshidi et al., 2016, 2015a; Jamshidi and Lake, 2014), while others argued that water content had little effect on the freeze-thaw durability of soil-cement systems (Eskişar et al., 2015). Kim and Daniel (1992) found that permeability can be increased by two orders of magnitude after freeze-thaw cycles if soil sample are compacted wet of optimum water content, but are increased by only two to six times if compacted dry of optimum. As shown in **Figure 2.7**, Jamshidi et al. (2015a) also reported that a soil-cement system was less susceptible to freeze-thaw cycles as water content decreased. It is also interesting to note that the permeability for samples with lower water to solids ratio (LWS) also may have even decreased after 12 freeze-thaw cycles compared to the permeability after 4 cycles. The decrease in permeability for samples with low water content is possibly due to the continuing hydration of the excess cement. However, Eskişar et al. (2015) carried out a study to assess the freeze-thaw performance of cement-treated clays at different water contents and reported that water content exerted little effect on freeze-thaw durability in terms of UCS. It also had little effect on permeability, although lower water content was associated with higher UCS for cement-treated clays. Therefore, it is hard to confirm the effect of water content on the freeze-thaw durability of soil-cement systems from the available literature. Thus, this effect should not be oversimplified. It appears that water content can be treated as a damaging factor that affects expansion inside the matrix, or a factor that affects the hydration of cement, or as a lubricant that affects the degree to which soil-cement systems are able to mix.

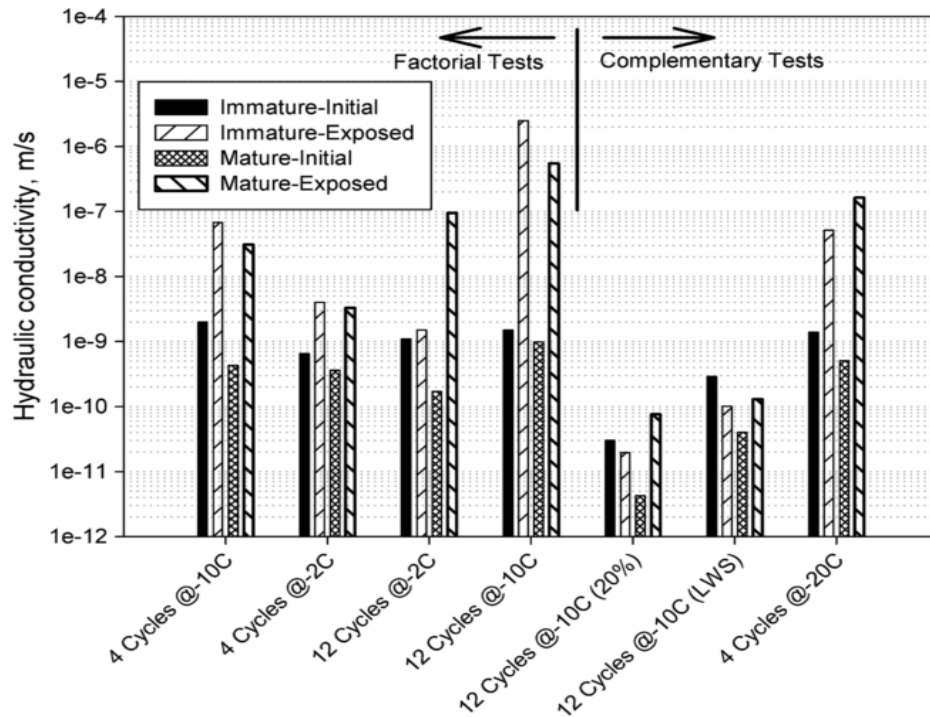


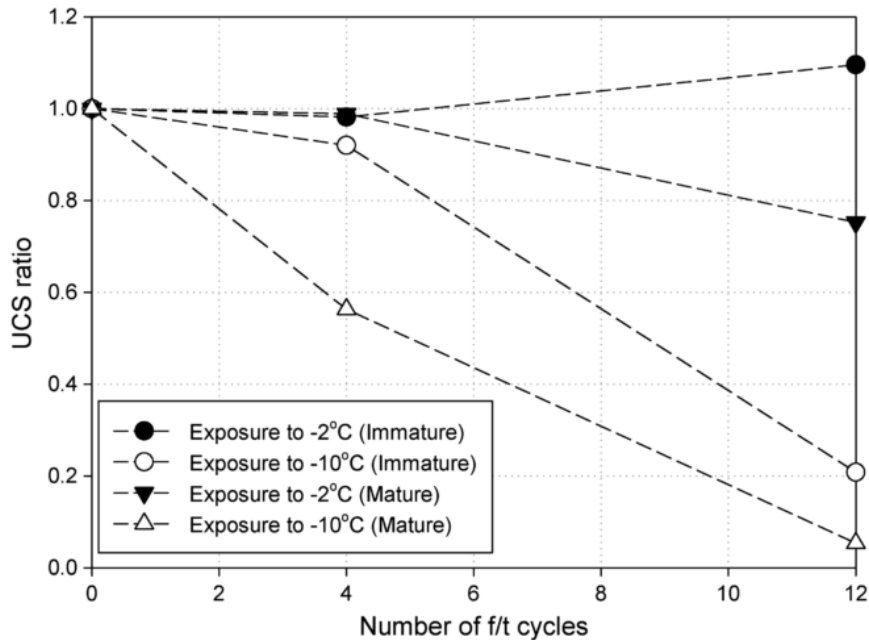
Figure 2.7 Summary of permeability results for different exposure scenarios and mix designs (Jamshidi et al., 2015a). “04” and “12” refer to the number of freeze-thaw cycles, and “-2”, “-10”, and “-20” refer to freezing temperatures; “20%” and “LWS” refer to 20% cement content and “lower water to solids ratio” conditions.

2.1.3.3 Intensity of freeze-thaw exposure

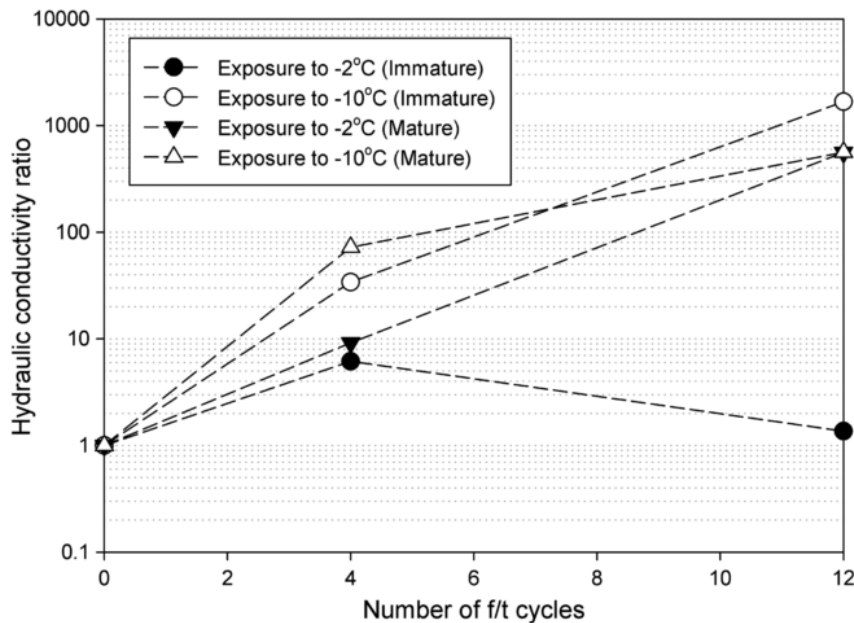
The degradation of soil-cement systems is highly related to the intensity of freeze-thaw exposure. The intensity of freeze-thaw exposure depends on the number of freeze-thaw cycles, freezing and thawing temperatures, duration of cycles, and other factors (Kamei et al., 2012).

It is commonly believed that soil-cement systems continually deteriorate with increased number of freeze-thaw cycles (Eskişar et al., 2015; Jamshidi et al., 2015; Shibi and Kamei, 2014). For the durability test suggested by ASTM: D560/D560M-15 (2015), specimens tested should be subjected to 12 freeze-thaw cycles. Previous research also indicates that 8 to 12 cycles of freeze-thaw can be considered adequate for investigating the effects of freeze-thaw cycles on various engineering parameters, including strength and hydraulic conductivity (Jamshidi et al., 2015a; Musharraf and Houry, 2003; Shihata and Baghdadi, 2001). Jamshidi et al. (2015b) reported that freezing temperature also posed an influence on the change of UCS (**Figure 2.8a**) and permeability (**Figure 2.8b**) for cemented soils subjected to freeze-thaw cycles. This trend suggests that the lower the freezing temperature, the more significant

the increase in permeability and the greater the reduction in UCS that can be observed. In general, increasing intensity of freeze-thaw exposure (that is, a greater number of freeze-thaw cycles, a lower freezing temperature, a higher thaw temperature, and longer freeze-thaw exposure) causes the deterioration of soil-cement systems to accelerate.



(a)



(b)

Figure 2.8 Changes of two properties subjected to various number of freeze-thaw cycles (Jamshidi et al., 2015a): (a) UCS ratios and (b) hydraulic conductivity ratios.

2.1.3.4 Curing time

In general, mature samples (that is, samples that have cured for longer) can be more vulnerable to freeze-thaw cycles than immature ones (Jamshidi et al., 2015a; Jamshidi and Lake, 2014). As shown in **Figure 2.8**, mature specimens (i.e., those cured for over 110 days) exhibited greater increases in permeability values and a greater UCS ratio reduction than immature specimens (cured for 16 days) after freeze-thaw cycles. There are two possible explanations for the vulnerability of mature soil-cement systems. Firstly, the brittleness of cemented soil increases as curing time increases. Therefore, mature samples could be more susceptible to deformations induced during freezing. Moreover, continuing hydration is less pronounced within the mature soil-cement systems than within the immature samples (Jamshidi and Lake, 2014).

2.1.4 Microscopic analysis of soil-cement systems subjected to freeze-thaw cycles

Microscopic techniques were used by Klich et al. (1999) to investigate how freeze-thaw cycles can cause cracking of cement-treated stabilisation/solidification materials. They posited several advantages for using microscopic analysis to evaluate the weathering of stabilisation/solidification wastes. First, microscopic analysis can observe the exact area of chemical analysis without disturbing the nature of the sample. Secondly, microscopic features like cracks and the relationships between minerals can be observed and analysed. Furthermore, material changes like the mode of alteration, alteration pathways, and secondary products of alteration under weathering conditions can be identified through microscopic and mineralogical analysis. As a result, the degradation of soil-cement systems subjected to freeze-thaw cycles can be better understood by microscopic analysis. Surface analyses of the morphology, shape, and size of cracks and materials can be conducted by using equipment like microscopy and scanning electron microscope (SEM).

Wang et al. (2019) used these techniques to investigate the effect of crumb rubber on the frost resistance of soil-cement. Using SEM, the authors found that rubber powder can prevent micro-crack generation and delay the development of existing cracks (**Figure 2.9**). Jamshidi et al. (2011) conducted crack analysis on cemented soil samples after freeze-thaw cycles and reported that the disruption of an extended longitudinal-crack network with a spacing of approximately 1.2 mm was observed in as little as one freeze-thaw cycle. They also reported that the crack network propagated further into the matrix with additional freeze-thaw cycles. Lake et al. (2016) conducted optical microscopy in thin sections and suggested that the

increased permeability was possibly due to the localised porosity increase after freeze-thaw cycles. **Figure 2.10** presents the ice lens (blue region) formation in a soil-cement system with 3% cement content after exposure to 3 cycles in their study.

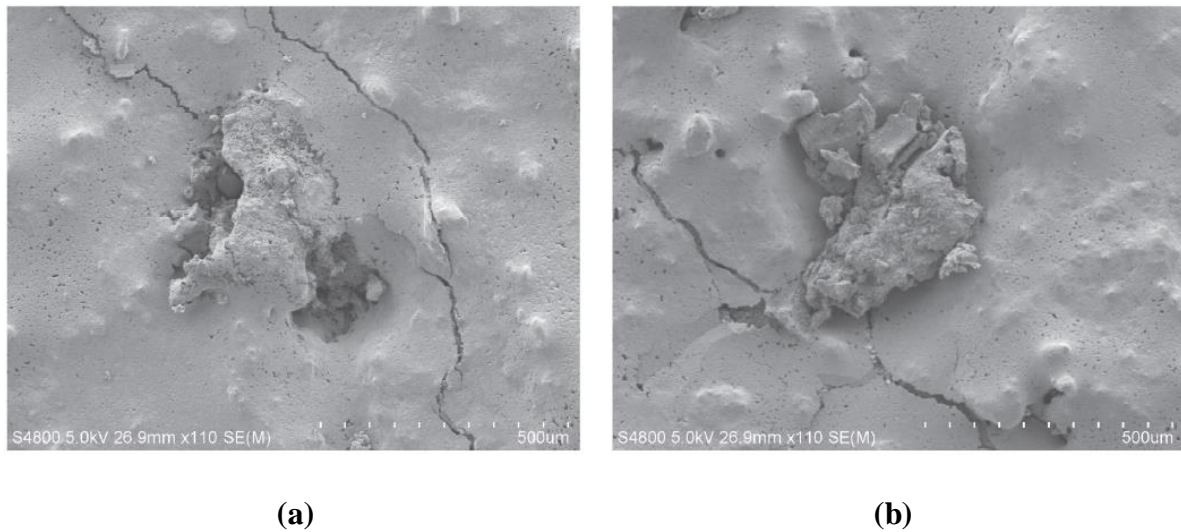


Figure 2.9 SEM images showing rubber powder particles (a) changing the direction of a micro-crack's path and (b) preventing micro-crack expansion (Wang et al., 2019).

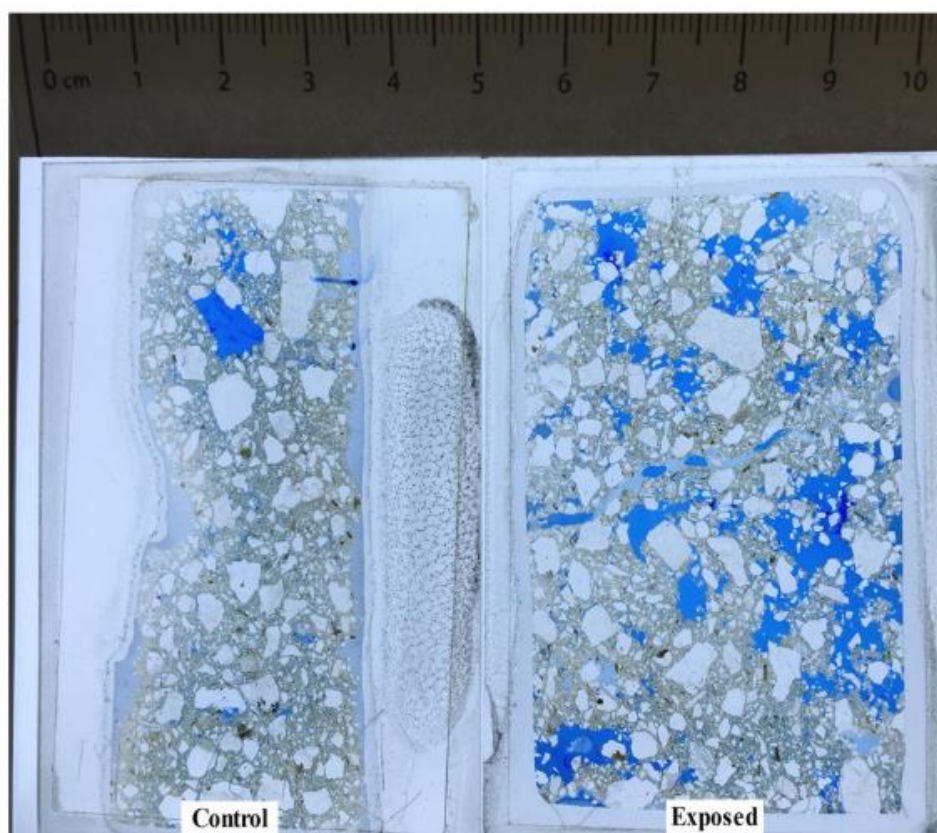


Figure 2.10 Thin section images of ice lens formation in soil-cement (3% cement and 14% water) after exposure to 3 cycles of freeze-thaw (Lake et al., 2016).

2.1.5 Additives used to improve freeze-thaw resistance of soil-cement

Although the freeze-thaw resistance of soils can be improved by the addition of cement, the performance of ordinary soil-cement systems is still inadequate for a sustainable design. Increasing the cement content could be considered as an approach to improve the freeze-thaw resistance of soil-cement systems. However, in a closed-system experiment, Mardani-Aghabaglou et al. (2015) increased cement content from 5% to 15% and found that the reduction in UCS after 12 freeze-thaw cycles only decreased from 27% to 13%. This indicates that, despite the benefits of the practice, adding excess cement into soil-cement systems is unlikely to be a cost-effective solution to freeze-thaw deterioration. There have also been attempts by some researchers to improve the freeze-thaw durability of soil-cement systems by adding extra minerals. Mineral additives such as bassanite (Kamei et al., 2012; Shibi and Kamei, 2014), fly ash (Bin-Shafique et al., 2010; Shibi and Kamei, 2014; Wei et al., 2015), and silica fume (Yarbaşı et al., 2007) have been employed to serve this purpose.

2.1.5.1 Bassanite and fly ash

Recycled bassanite ($2\text{CaSO}_4 \cdot \text{H}_2\text{O}$) is produced from gypsum waste material. It was first used in Japan as an additive in ground improvement projects (Ahmed et al., 2011; Kamei et al., 2012; Shibi and Kamei, 2014). Shibi and Kamei (2014) conducted tests on 5% cement-stabilised soft clay containing fly ash and bassanite subjected to freeze-thaw cycles and found that the UCS of the 5% cement-stabilised clay decreased approximately 50% after five freeze-thaw cycles. As shown in **Figure 2.11**, they found that UCS decreases 35–45% for samples stabilised by either recycled bassanite or fly ash. This number is only 15–35% for samples with both recycled bassanite and fly ash added. These results indicate that the addition of bassanite and fly ash can improve the freeze-thaw durability of soil-cement systems and that a combination of multiple additives may lead to still greater improvement. However, as shown in **Figure 2.11**, even when the soil-cement system incorporates 20% bassanite and fly ash, the UCS reduction after 5 freeze-thaw cycles is still in the range of 15–35%.

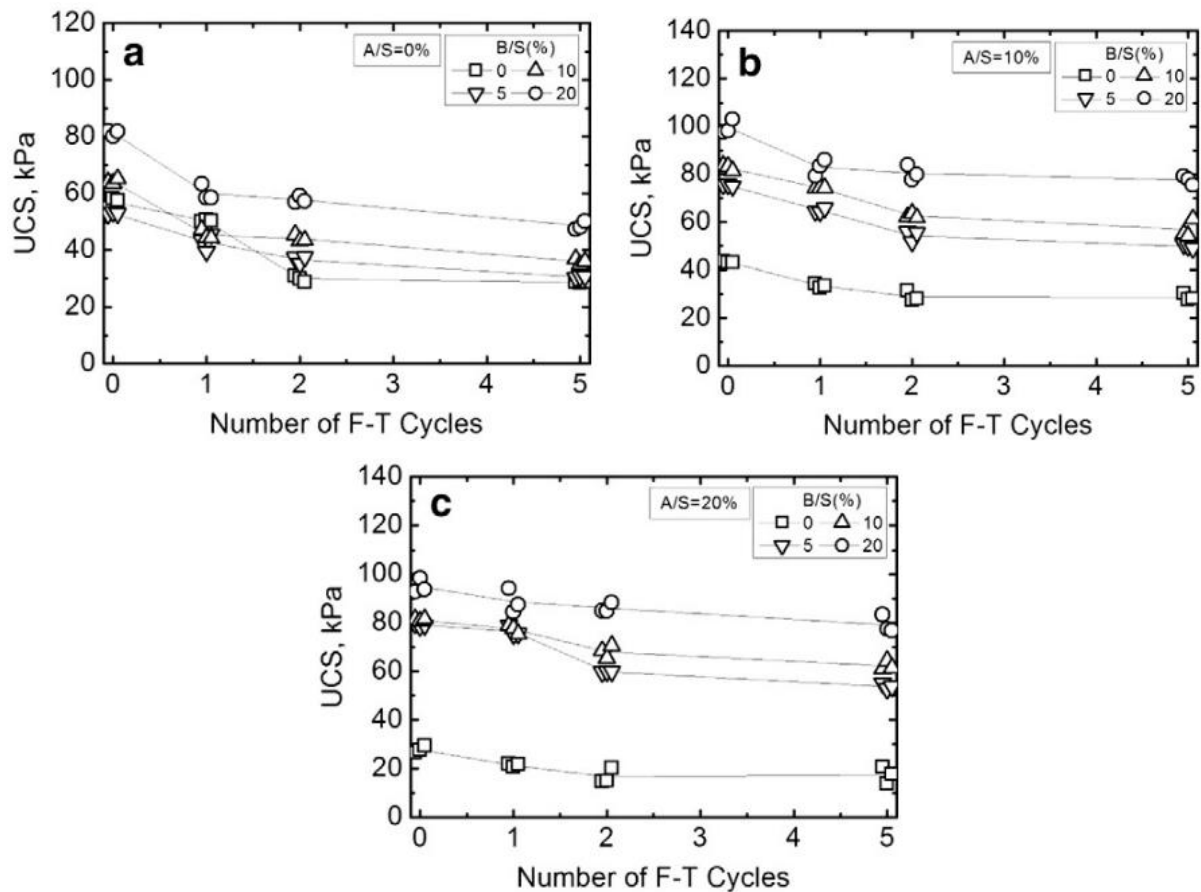


Figure 2.11 Effects of repeated freeze-thaw (F-T) cycles on unconfined compressive strength and at various bassanite/soil (B/S) ratios for: (a) specimens without coal ash, (b) specimens with 10% coal ash content, and (c) specimens with 20% coal ash content (Shibi and Kamei, 2014).

2.1.5.2 Silica fume

Silica fume, which is also known as microsilica, is a by-product of the manufacture of silicon or ferrosilicon alloys from high-purity quartz with coal in an electric arc furnace. It has been widely adopted for the production of high-strength concrete and it has recently been applied in soil-cement systems to improve their durability and engineering properties. Yarbaşı et al. (2007) conducted experiments on soils modified by red mud, lime, fly-ash, silica fume, and cement that were subjected to freeze-thaw cycles. The authors found that freeze-thaw durability was improved considerably in terms of UCS, California bearing ratio, ultrasonic pulse velocity, and damping ratio. They also suggested that a silica fume-lime mixture was the best stabiliser for granular soil that subjected to freeze-thaw cycles. However, their freeze-thaw tests were conducted in a closed system without access to additional water.

Despite this, a considerable reduction in California bearing ratio, UCS, ultrasonic pulse velocity, and damping ratio was recorded after 10–30 freeze-thaw cycles.

Although additives such as fly-ash, bassanite and silica fume have been applied in soil-cement systems to improve freeze-thaw performance, there are still many deficiencies and uncertainties regarding the capability and long-term performance of the mixtures. Moreover, even though some healing ability is implied by soil-cement systems containing additives, the self-healing concept is seldom mentioned. Very little literature incorporating the self-healing concept in studies of soil or soil-cement systems exists.

2.1.5.3 Autogenic healing in soil-cement systems

Some researchers believe that soil-cement systems possess a natural self-healing ability that derives from the cement itself. Jamshidi et al. (2015) reported that the permeability for soil-cement samples with low water content decreased after 12 freeze-thaw cycles when compared to the permeability after 4 cycles. As presented in **Figure 2.12**, Jamshidi and Lake (2014) allowed a post-exposure healing period of over 120 days for 10% cement-stabilised soil specimens damaged by 12 freeze-thaw cycles and observed some reduction in permeability. In addition, the healing phenomenon is more noticeable for immature specimens than mature specimens. The decrease in permeability for samples with low water content is possibly the result of continued hydration of the cement. However, the recovery of permeability is insignificant even for a healing period of over 120 days. Compared to other cementitious materials like concrete, mortar and cement paste, the cement content in soil-cement systems is relatively low, and their water content, void ratio, and pore space can be much higher. As a result, autogenic healing is unlikely to provide adequate self-healing capability for the aims of this study.

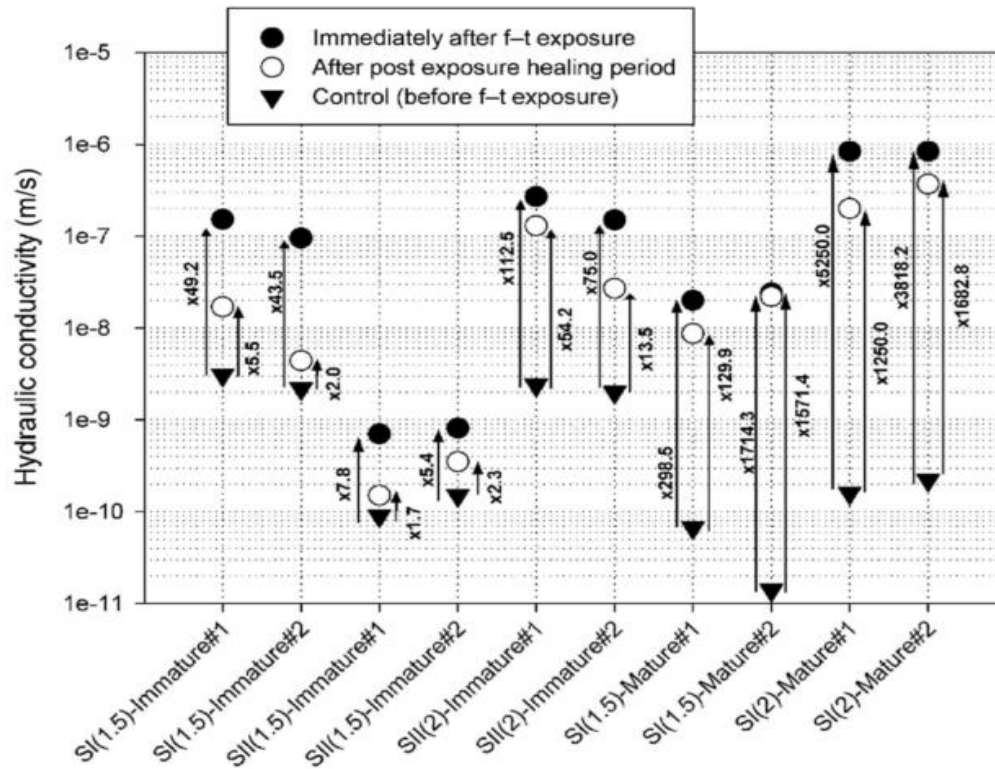


Figure 2.12 Hydraulic conductivity recovery of freeze-thaw exposed specimens after over 120 days of post-exposure healing period (Jamshidi and Lake, 2014).

2.2 Air entrainment in concrete

Air entrainment in concrete was discovered (by accident) in the 1930s (Du and Folliard, 2005). The idea of air entrainment is that creating tiny air bubbles in concrete mixes relieves the internal pressure generated by water expansion during freezing. The freeze-thaw durability of concrete can be significantly improved by air entraining (Gokce et al., 2004; Shang and Yi, 2013). For example, Shang and Yi (2013) reported that the relative dynamic modulus of elasticity only decreased to 94.35 and 98.75 percent for C25 and C30 air-entrained concrete after 100 cycles of freeze-thaw, while that of the plain concrete decreased to 64 percent. The mechanisms of air entrainment and the freeze-thaw process are still under investigation. The following sections, however, attempt to offer a critical review of the theory and hypothesis reported in the literature.

2.2.1 Mechanisms of air entrainment to protect against freezing

According to the hydraulic pressure theory proposed by Powers (1945), the formation of ice from liquid water, which experiences a 9% volume increase while freezing, produces an increase in hydraulic pressure. In concrete, this pressure expels free water into any

surrounding fissures or pore networks. In a fully saturated system without air entraining, the hydraulic pressure generated and the expanding pressure becomes high and causes cracking of capillary pores and expansion of fissures if the tensile stress reached the material strength. Powers (1945) suggested that the air pores in air-entrained concrete act as reservoirs that can receive water expelled from freezing sites and therefore relieve the pressure generated. This mechanism is presented in **Figure 2.13**, where the upper pressure distribution corresponds to the case wherein air pores act as reservoirs for the expelled water. The water that enters the air pores is subsequently depressurised and freezes instantaneously, as the air pressure inside the pores is approximately equal to atmospheric pressure.

Another mechanism (**Figure 2.13**, lower pressure distribution) suggested by other researchers is the theory of microscopic ice lens growth (Powers and Helmuth, 1953; Coussy, 2005; Eriksson et al., 2018; Zuber et al., 2000). These researchers have suggested that larger air pores also act as cryo-pumps due to the inequilibrium of chemical potential among ice, liquid water, and water vapor. The propagation of ice in the porous network was demonstrated theoretically by Scherer (1999, 1993) and has been observed in low-temperature calorimetry studies of ice formation in concrete (Zuber et al., 2000). These studies suggested that ice formed progressively in the porous network, starting with the largest water-filled pores during freezing and then propagating into smaller pores. The ice crystals in the larger pores then induced a negative liquid pressure in the vicinity of the confined ice crystals, creating a so called cryo-suction effect (Coussy, 2005; Eriksson et al., 2018; Penttala, 2009; Zeng et al., 2016). As a result, water was sucked into the bigger pores from surrounding capillary pores.

As a result of these two mechanisms, the excess hydraulic pressure in the freezing site is reduced. Consequently, the capillary pores and air pores do not suffer from breaking pressure as long as the excess water in the capillary pores can be expelled opportunely and the air pores have enough space to store the ice crystals. The building rate of excess hydraulic pressure therefore depends on the cooling rate compared to the capability of the pore network's ability to drain extra liquid to nearby voids (Coussy, 2005). Therefore, the effectiveness of the air pores and the pressure level depends on the distance from the freezing site to the air pores, the permeability of the material, and the rate of ice formation. In terms of distance, it is well established that appropriately spaced entrained air pores significantly increase the freeze-thaw durability of concrete (Powers, 1949; Penttala, 2009). Powers (1949) proposed a spacing factor equal to the longest distance between each pair of adjacent air pores to estimate the efficiency of an air pore system. Several other spacing factors have been

proposed in the literature as well. The suggested value is generally smaller than 0.35–0.45 mm (ASTM C457/C457M-16, 2016; Penttala, 2009). This spacing factor therefore requires air pores to be homogeneously distributed in the matrix.

The spacing factor and pore size distribution can be assessed optically from a thin section test (Penttala, 2009). Moreover, the spacing factor to some degree reflects the minimum volume fraction that should be adopted in an air-entrained system. The relationship between air content and the durability factor of concrete is presented in **Figure 2.14**. In the general practice, air entraining requires the air pores to account for 3–7% of the concrete volume (ASTM C457/C457M-16, 2016). Penttala (2009) also suggested that the air content measured in normal concrete should exceed 4.5% in fresh concrete. A sufficient average value should be 5.5% if the distribution of the spacing factors is taken into consideration. However, air voids tend to decrease the compressive strength of concrete, with about a 5% reduction for each 1% increase in the volume of air voids (as shown in **Figure 2.15**) (Popovics, 1998). In terms of the size of the air pores, Penttala (2009) argued that the optimal diameter can range from 0.02–0.1 mm. Medium-sized air pores provide enough air space for ice formation, which can also hinder the capillary flow of water in concrete. In addition, a reasonable size air pore can minimise the strength reduction that air-entrained concrete usually suffers.

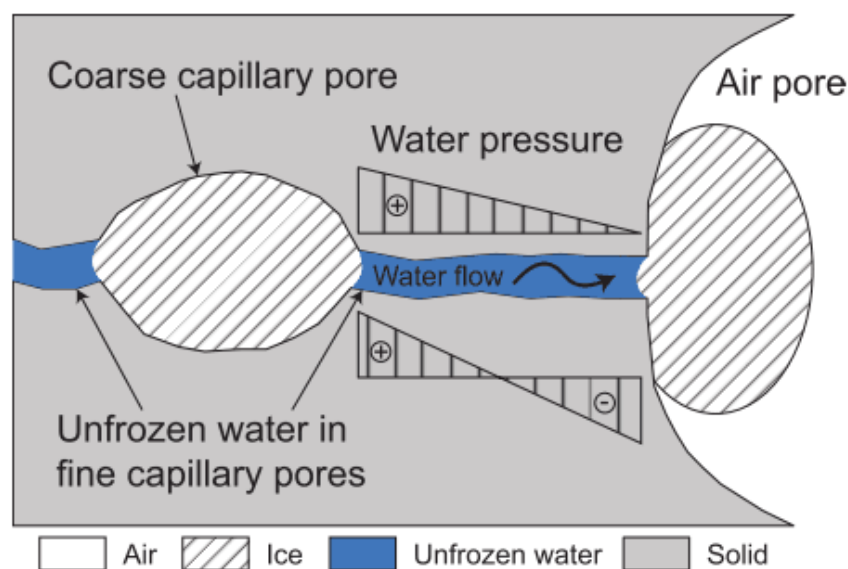


Figure 2.13 Schematic illustration of the effect of air pores during the freezing of concrete (Eriksson et al., 2018; Zeng et al., 2016). Upper pressure distribution refers to the case where the air pore solely acts as a reservoir for the expelled water, while the lower distribution refers to the case where it also acts as a cryo-pump.

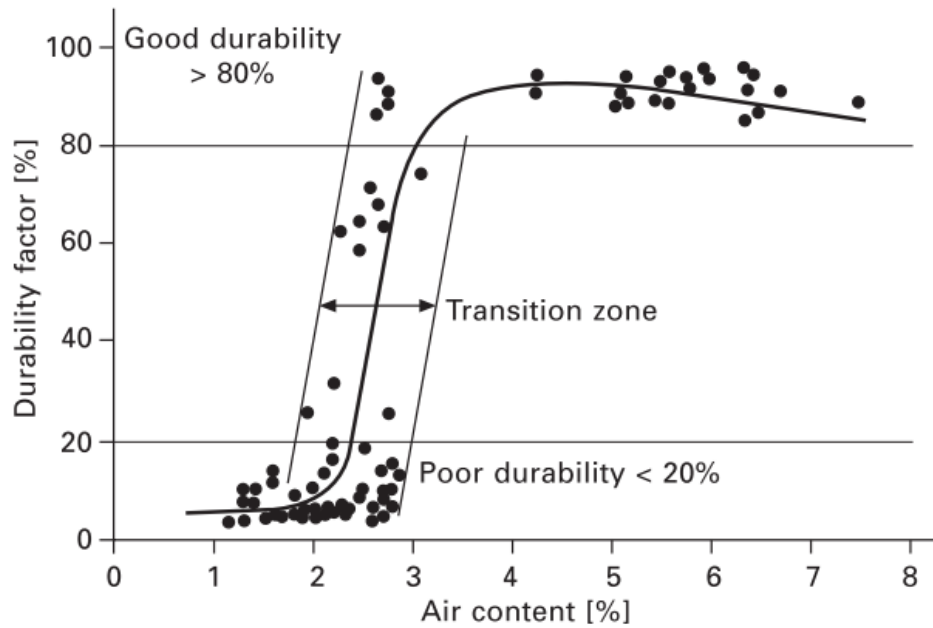


Figure 2.14 Air content vs. freeze-thaw durability of concrete (Cordon, 1967).

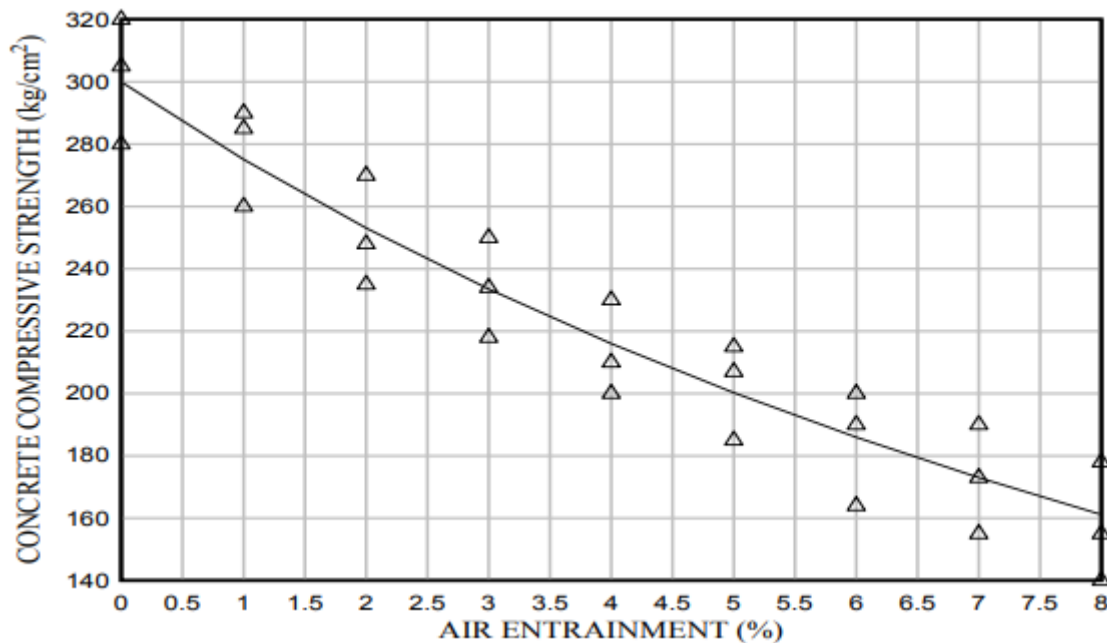


Figure 2.15 Air content of concrete vs. compressive strength (Mohammed and Pandey, 2015).

2.2.2 Critical saturation ratio

As is the case for the relationship between air content and the freeze-thaw durability of concrete, some researchers have suggested that the susceptibility of concrete to freeze-thaw damage is related to the degree of its saturation (Fagerlund, 1973; Li et al., 2012; Litvan, 1988). This claim is based on the fact that freeze-thaw damage is generally caused by water

expansion during freezing, and saturated pores are more vulnerable to the freeze-thaw damage. To define the level of saturation at which freeze-thaw damage begins to initiate, researchers have suggested a critical degree of saturation (S_{cr}). Once the degree of saturation exceeds S_{cr} , damage to the material will occur during freeze-thaw action (Fagerlund, 1977, 1973; Litvan, 1988). For soil-cement systems, S_{cr} appears to be a more predictive metric than the concrete's air content, as these systems are often exposed to an open freeze-thaw system where water or moisture can be absorbed into the soil-cement matrix. Li et al. (2012) suggested that the critical degree of saturation for concrete was 86-88%. In specimens that have a degree of saturation higher than 86–88%, damage can be observed after a few freeze-thaw cycles. Therefore, as discussed in **Section 2.2.1**, the freeze-thaw resistance of the system depends on the quality of air distribution and the volume of the air in the concrete. Theoretically, assuming the water is completely frozen during freezing and the excess volume of water can be fully accommodated by the air pores, the volume of protective pores should be not less than 9% of the volume of the water.

Although extensive research has been conducted on the air entrainment of concrete, no literature on the use of air entrainment in soil-cement systems exists. This lack of investigation may be due to the nature of soil-cement systems, which are considered to have relatively low strength and high initial porosity, and which are expected to endure more extreme environmental conditions than traditional above-ground concrete. As a result, the air entrainment of soil-cement system is more complex than for concrete, which necessitates that it be in a more controlled and smarter way. Nonetheless, the mechanisms and the successful application of air entrainment in concrete provide insights for the development of soil-cement systems with high freeze-thaw resistance.

2.3 Self-healing in cementitious materials

2.3.1 Introduction

Smart materials, are defined as the materials that have the instinctive capability to sense and respond to environmental conditions or stimuli. The development of smart materials has thrived in the past decades. Self-healing materials are man-made smart materials, which have the ability to repair themselves autogenously or with the minimal help of an external stimulus. The development of self-healing materials is inspired by the biological processes that commonly exist in nature. A typical example of the self-healing phenomenon is the damaged skins of living plants and animals, which can autonomously heal themselves (Wu et al., 2012).

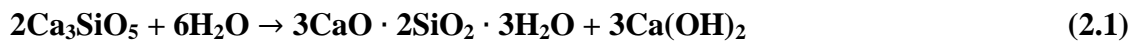
Self-healing as defined by RILEM is “any process by the material itself involving the recovery and hence improvement of a performance after an earlier action that had reduced the performance of the material” (de Rooij et al., 2013). Self-healing processes within cementitious materials can be generally divided into two categories: autogenic and autonomic.

2.3.2 Autogenic healing

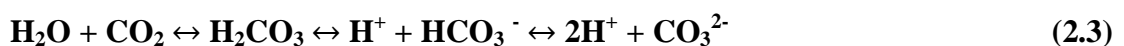
Autogenic self-healing is a recovery process wherein a material can heal its own cracks by virtue of inherent components that are not specifically designed for self-healing. The self-healing of cement-based materials is not a completely new concept. It was reported by the French Academy of Science as early as 1836, which documented self-healing in water retaining structures, culverts and pipes (de Rooij et al., 2013). Cement-based materials have a certain built-in capacity, termed autogenic healing, to fill and seal structural damage without any external operations and stimulus (Jacobsen et al., 1996; Ramm and Biscopig, 1998). As presented in **Figure 2.16a**, the causes of autogenic healing can be mainly divided into 3 categories (de Rooij et al., 2013): physical, chemical, and mechanical.

Physical healing is caused by the swelling of hydrated cement paste near the crack surface. However, the effect of the swelling is marginal. The effect typically only results in a fluid flow reduction of less than 10%.

Chemical causes can be attributed to two underlying mechanisms. Firstly, continuing hydration is the main driving force for autogenic healing at the early age. This is due to the relatively high content of unhydrated cement. The continued hydration of cement commonly occurs in cementitious materials due to lack of water. When new hydration products are formed, they grow into the free space of the cracks, as the hydration products occupy about twice the space of the original cement grain (de Rooij et al., 2013; Ramm and Biscopig, 1998). The most common hydration product is believed to be calcium silicate hydrate (C-S-H). The generalised equations for its formation are:



Over time, the dissolution and subsequent carbonation of $\text{Ca}(\text{OH})_2$ becomes dominant (Hearn and Morley, 1997; Ramm and Biscopig, 1998). The associated chemical reaction process for CaCO_3 is illustrated by **Eqs. 2.3-2.5** (Qureshi and Al-Tabbaa, 2014; Wu et al., 2012):

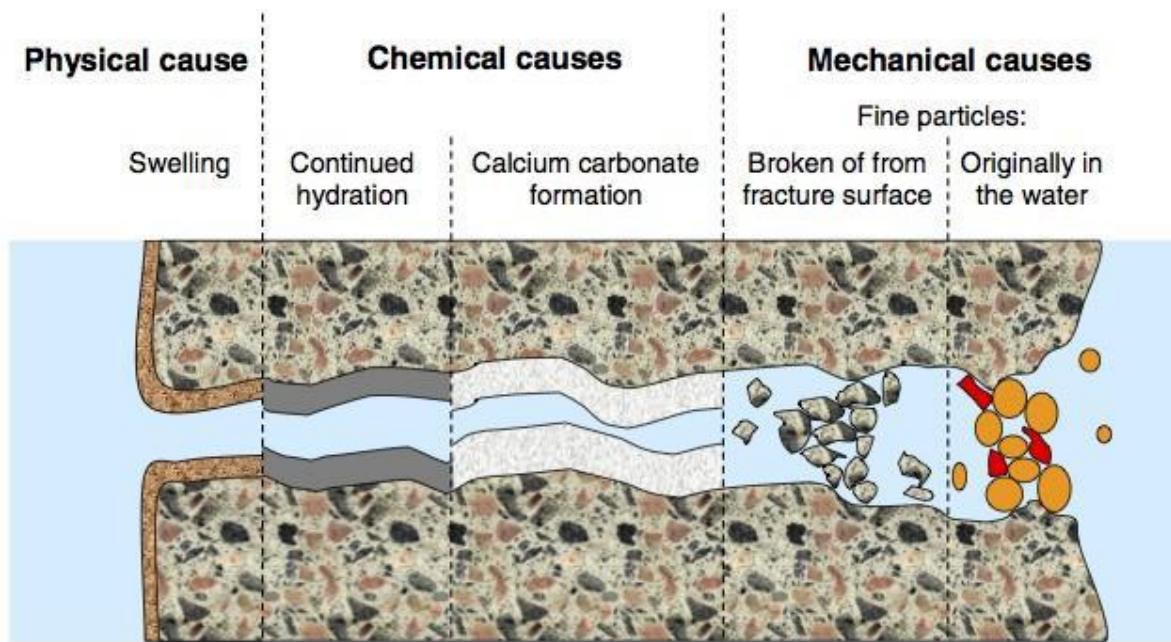




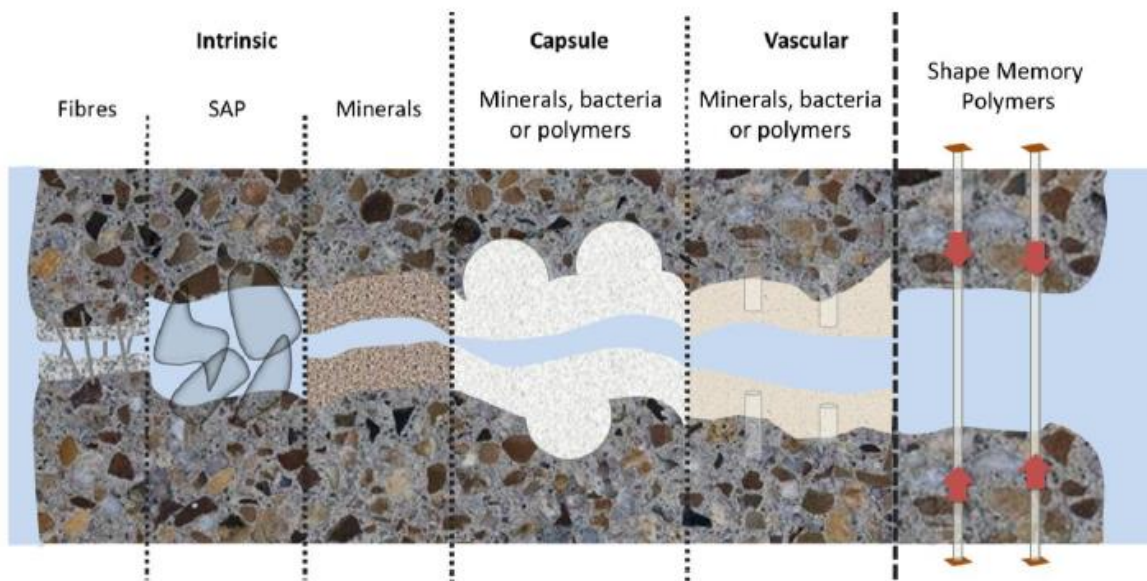
Besides these two chemical mechanisms, autogenic healing may also be induced by the swelling of the matrix and the filling of the crack due to debris or fine particles present in ingress water resulting from cracking. (Hua, 2010; Van Tittelboom and De Belie, 2013). Water is crucial for all autogenic self-healing because water is important for the all aforementioned processes (i.e., swelling, continued hydration, crystallisation of CaCO_3 , and transportation of fine particles). The overall degree of autogenic self-healing depends on the age of cementitious materials and the crack width. However, it has been widely documented that the regain of mechanical properties is slow and requires water-immersion for several weeks (Granger et al., 2007; Jacobsen and Sellevold, 1996). Moreover, it is rare for autonomic-healed specimens to fully regain their original mechanical properties. Therefore, the slow process and limited capacity of autogenic self-healing has led researchers to explore suitable engineered autonomic self-healing techniques.

2.3.3 Autonomic healing

As shown in **Figure 2.16b**, a recovery process that involves any engineered additions or measures intended to improve the self-healing capabilities of the materials is referred to as autonomic self-healing (Van Tittelboom and De Belie, 2013). For autonomic healing, any agent used to promote healing is engineered and cannot be found within the original materials. Currently, most literature in the field of civil and environmental engineering has focused on the self-healing of cementitious material. Many studies have shown promising results (Ahn and Kishi, 2010; Dry et al., 2003; Eigenbrod, 2003; Joseph et al., 2010; Kanellopoulos et al., 2015; Kessler et al., 2003; Li et al., 1998; Qureshi et al., 2016; etc.). Chemicals in hollow tubes, chemical encapsulation, bacterial encapsulation, and mineral admixtures are four common applications for autonomic healing (Li and Herbert, 2012). Chemicals in hollow tubes are unsuitable for soil-cement systems like highway pavement projects and other deep-mixing projects, so this application will not be considered in this study. Self-healing by bacterial encapsulation will also not be considered. Due to the nature of the freeze-thaw process, the survivability of bacterial in low temperature could be a problem. The other two categories, chemical encapsulation and mineral admixture and additives, are reviewed in the following sections.



(a)



(b)

Figure 2.16 Schematic representation of the mechanisms of (a) autogenic self-healing (de Rooij et al., 2013) and (b) autonomic self-healing (Souza, 2017).

2.3.3.1 Capsule-based chemical self-healing

In some studies, chemical healing agents are introduced to concrete via tiny microcapsules. An autonomic polymeric system embedded with microcapsules filled with healing agent and randomly dispersed catalyst was firstly proposed by (White et al., 2001). As shown in **Figure**

2.17, when damage (i.e. cracks) propagates in the self-healing system, the healing mechanism is triggered through the rupture of capsules and the release and reaction of healing agents in the damaged area. The behaviour of healing agents after release can be summarised via four categories (Van Tittelboom and De Belie, 2013): (1) The healing agents react upon contact with moisture or air or due to heating (**Figure 2.18A,B**); (2) the healing agents react upon contact with the cementitious matrix itself (**Figure 2.18C,D**); (3) the healing agents react when making contact with a second component present in the matrix (**Figure 2.18E,F**); (4) the healing agents react when making contact with a second component delivered by other capsules (**Figure 2.18G,H**).

Various kinds of healing agents have been used in microcapsule-based self-healing systems. The healing agents used most-commonly to date include cyanoacrylate (CA), polyurethane, methyl methacrylate (MMA), epoxy resin, silicone, foam, sodium silicate (Na_2SiO_3) solution, bacterial solution, and expansive minerals. In **Table 2.2**, an overview of the most relevant properties of a variety of healing agents used for cementitious materials is presented.

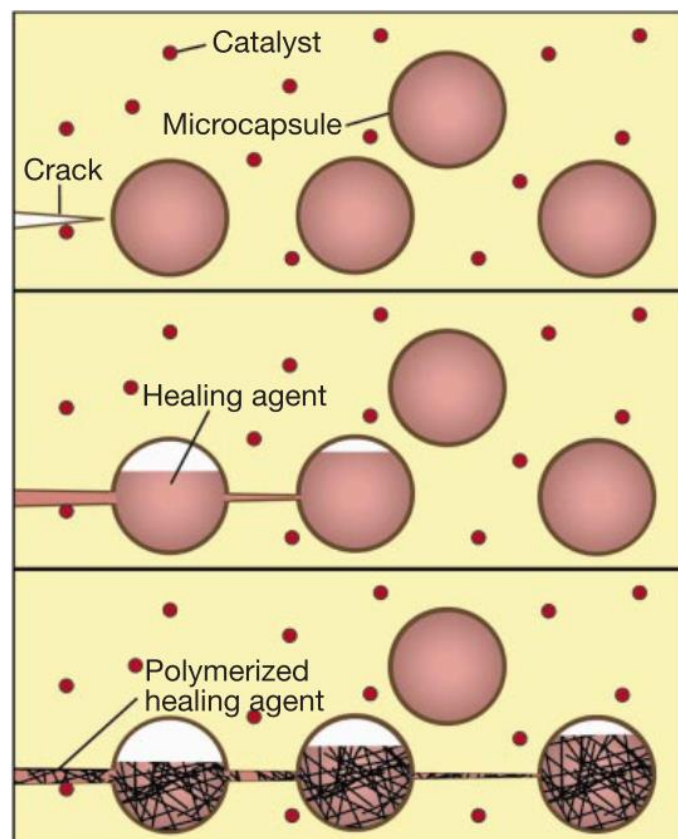


Figure 2.17 The concept of autonomic healing using microcapsules (White et al., 2001).

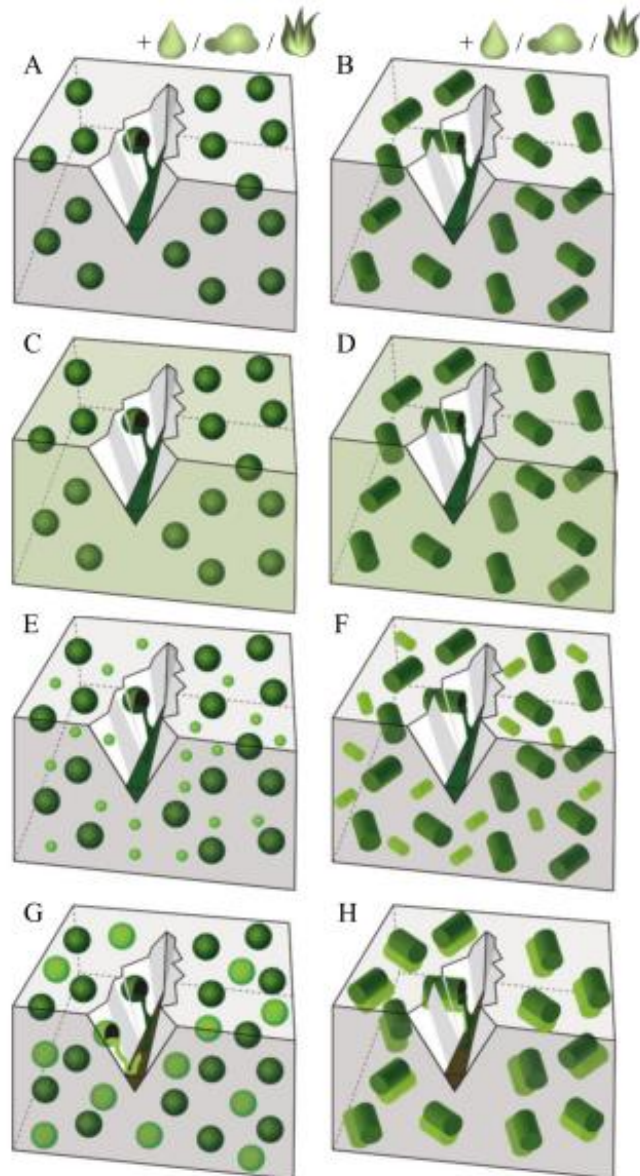


Figure 2.18 Microcapsule-based self-healing approaches. Reaction of spherical or cylindrical encapsulated agent while contact with: (A,B) moisture, or air, or due to heating; (C,D) the cementitious matrix itself; (E,F) a second component present in the matrix (small, light-coloured inclusions) or (G,H) a second component delivered by additional capsules (big, light-coloured inclusions) (Van Tittelboom and De Belie, 2013).

Table 2.2 Overview of the healing agents that have been reported in literature (adapted from Van Tittelboom and De Belie, 2013).

Agent	Number of components		Viscosity (mPas)	Way of curing	Curing time	Expansion		Strength (MPa)	References
	1	>2				Yes	No		
CA	√	–	<10	Moist	Seconds	–	√	20	(Li et al., 1998; Van Tittelboom and De Belie, 2010)
Epoxy	–	√	150	Contact component	30 min	–	√	5.1	(Van Tittelboom and De Belie, 2010)
	–	√	80	Contact component	30 min	–	√	4.2	
	–	√	360	Contact component	40 min	–	√	45	
	√	–	–	Contact component	3 days	–	√		(Wang et al., 2013)
MMA	–	√	±1	Contact component	–	–	√	–	(Yang et al., 2011)
	–	√	34	Contact component	1 h	–	√	50	(Van Tittelboom et al., 2011)
Polyacrylate	–	√	7	Contact component	40 s	–	√	–	(Van Tittelboom and De Belie, 2010)
Polyurethane	√	–	7200	Moist	40–180 min	√	–	–	(Van Tittelboom and De Belie, 2010)
	–	√	600	Contact component	50–300 s	√	–	–	(Van Tittelboom and De Belie, 2010)
Foam	√	–	–	–	–	√	–	–	(Dry et al., 2003)
Na ₂ SiO ₃ solution	√	–	–	Ca(OH) ₂ matrix, moist	Several days/weeks	–	√	–	(Giannaros et al., 2016; Huang and Ye, 2011; Kanellopoulos et al., 2015; Pelletier et al., 2010)
Silicone	√	–	–	Air	–	–	√	–	(Dry et al., 2003)

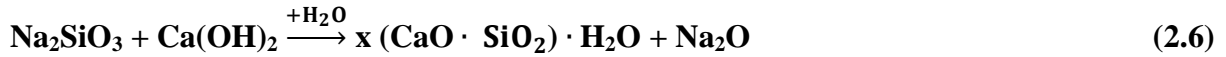
Colloidal silica	√	–	–	Ca(OH) ₂ matrix, moist	–	–	√	–	(Kanellopoulos et al., 2015; Litina, 2016)
Na ₂ SiO ₃ powder	√	–	–	Ca(OH) ₂ matrix, moist	Several days/weeks	–	√	–	(Mao, 2018)
Ca(NO ₃) ₂ solution	√	–	–	Matrix	–	–	√	–	(Dry and Corsaw, 1998)
Na ₂ FPO ₃ solution	√	–	–	Hydration and carbonation products	28 days	–	√	–	(Sisomphon et al., 2011)
Silica fume	√	–	–	Ca(OH) ₂ matrix, moist	–	–	√	–	(Litina, 2016)
MgO, bentonite, and quick lime	–	√	–	Hydration, swelling and carbonation products	28 days/ 56 days	–	√	–	(Qureshi et al., 2016)

Non-native organic healing agents like epoxy and MMA are less compatible with soil-cement matrices and may negatively affect hydration kinetics. Moreover, high water content and water ingress into soil-cement system during the freeze-thaw process may affect the functionality and durability of organic healing agents. In addition, organic healing agents can contaminate ground water sources if used in geotechnical applications. Therefore, more effective, durable healing can be expected in soil-cement systems with chemical agents like sodium silicate, as these healing products are more compatible with a cementitious matrix.

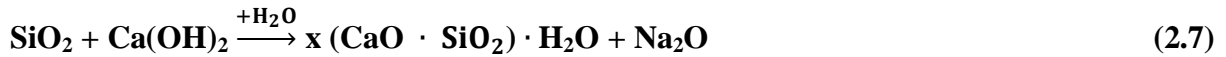
Sodium silicate has been used in cements to improve early strength and density. In recent years, encapsulated sodium silicate solutions have been used in cementitious materials. Many studies have found these applications to lead to crack closure and considerable recovery of the material's engineering properties (Giannaros et al., 2016; Huang and Ye, 2011; Kanellopoulos et al., 2015; Pelletier et al., 2010). Pelletier et al. (2010) encapsulated sodium silicate solution in PU microcapsules (40–800 μm) to concrete specimens and found that the 2% (by volume) microcapsule-containing specimen showed 10–12% higher flexural strength recovery than the control samples. In a study performed by Huang and Ye (2011), sodium silicate solution was encapsulated within wax shells and embedded in concrete. As shown in **Figure 2.19**, the specimens with capsules exhibited significant recovery in terms of deflection capacity, stiffness, and flexural strength, and recovery efficiency increased with increasing concentration of sodium silicate solution. In terms of durability, Giannaros et al. (2016) reported that a 4% volumetric fraction of Lambson microcapsules containing sodium silicate solution reduced sorptivity by 15% after 7 days of healing compared to control samples. However, he also found that microcapsule-containing samples absorbed slightly more water than control samples after 28 day of healing. This observation is important, as greater water ingress can be detrimental for soil-cement systems subjected to freeze-thaw cycles. Kanellopoulos et al. (2015) encapsulated three liquid (sodium silicate, colloidal silica and tetraethyl orthosilicate) and one powdered (magnesium oxide) minerals in thin-walled soda glass capsules for cement-based composites. The researchers reported that crack area closure ranged from 85% to 100% for all mineral-treated samples cured in water and the measured reduction in both sorptivity and intrinsic gas permeability varied from 18% to 69%, depending on the parameter measured and the mineral type. Images showing self-healing of a prism with sodium silicate-containing capsules are presented in **Figure 2.20**. The researchers also suggested that colloidal silica and sodium silicate were more efficient and consistent healing agents and can thus be used more readily than the alternatives. The chemical

reactions for the healing action associated with each mineral are demonstrated in Eqs. 2.6–2.9:

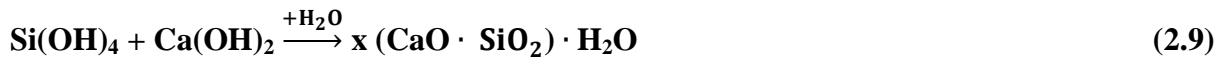
Sodium silicate



Colloidal silica



Ethyl silicates



Qureshi et al. (2016) encapsulated expansive mineral powders (magnesium oxide, bentonite, and quicklime) for self-healing in cement-based mortars. In the study, mortar samples containing concentric macrocapsules with different mineral combinations were cracked and healed under three different curing regimes: ambient conditions, high humidity exposure, and immersion in water. The optimum healing efficiency, with ~95% crack sealing and ~25% strength recovery in 28 days, was found for samples immersed in water.

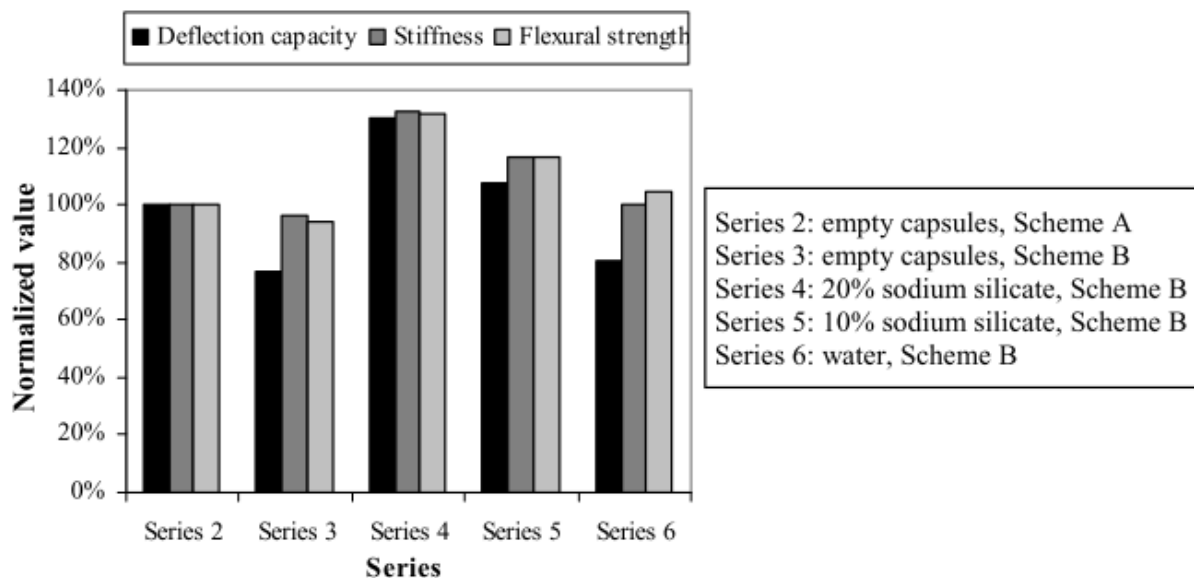


Figure 2.19 Recovery of mechanical properties for sodium silicate-embedded self-healing cement paste (Huang and Ye, 2011).

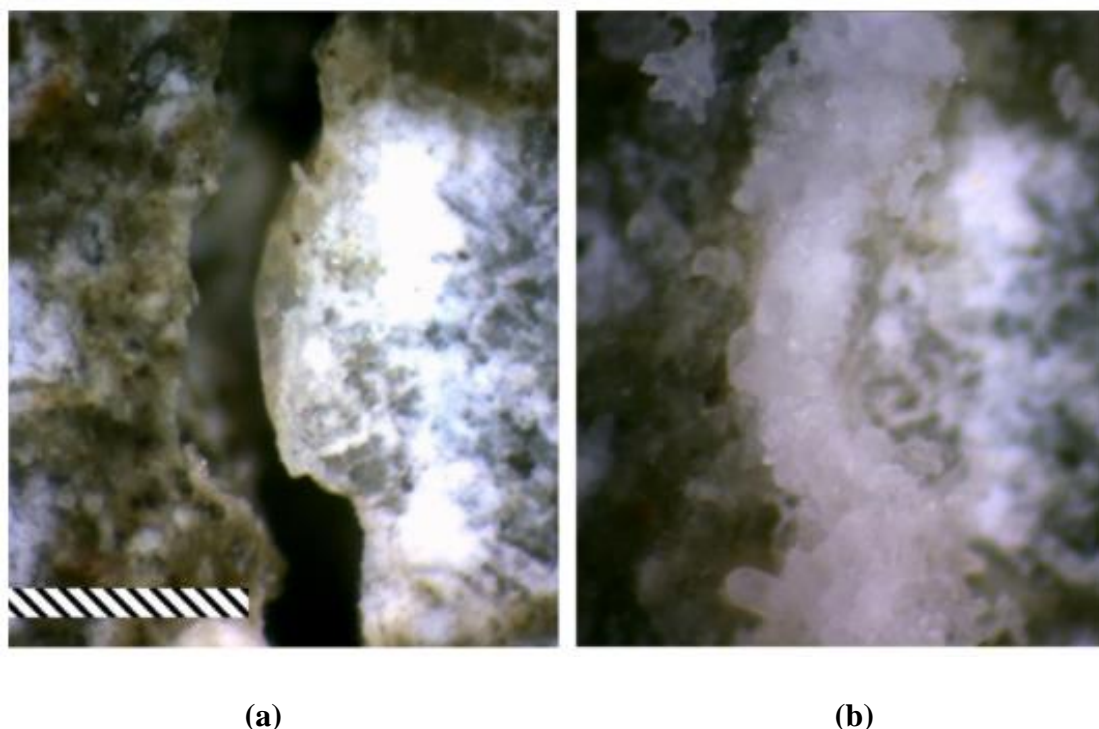


Figure 2.20 Representative images from a prism with sodium silicate-containing capsules: (a) crack area on the day of cracking and (b) crack filled after 28 days of healing (note: the hashed band corresponds to 500 μm) (Kanellopoulos et al., 2015).

The encapsulation of sodium silicate solution as a healing agent in cementitious materials is reported to be a very promising technique. The reaction of calcium cations with dissolved sodium silicate, which leads to the crystallisation of excess sodium silicate, promotes the main mechanism of self-healing (Huang and Ye, 2011; Litinia and Al-Tabbaa, 2013). Sodium silicate can also react with calcium hydroxide produced by cement hydration to produce more C-S-H gel (the main hydration product in cement). Therefore, cracks can be filled and the cementitious material's strength can be partially recovered (Huang and Ye, 2011; Pelletier et al., 2010). C-S-H gel is not only the main hydration product of cement, but also the main contributor to most of the engineering properties of cement paste. However, it should be noted that the C-S-H gel itself is not an intrinsically strong or stable material. It provides strength for cementitious materials by binding particles and forming continuous layers in the matrix (Thomas and Jennings, 2006). Calcium hydroxide is the by-product of cement hydration, which accounts for about 10% of the total volume of hydration products (**Figure 2.21**). However, soil-cement systems with a relatively low cement content can have only a limited amount of calcium hydroxide available. As a result, although sodium silicate can increase the strength of soil-cement as more C-S-H gel is produced, it may not have great

potential for sealing cracks, as the volume of calcium hydroxide is limited in soil-cement systems. In addition, it should be noted that mechanical behaviours such as flexural strength and deflection capacity may be reduced for samples with capsules, as presented in **Figure 2.22** (Huang and Ye, 2011). The authors reported that the flexural strength and deflection capacity of specimens with microcapsules were reduced by approximately 27% and 40%, respectively, compared to control specimens.

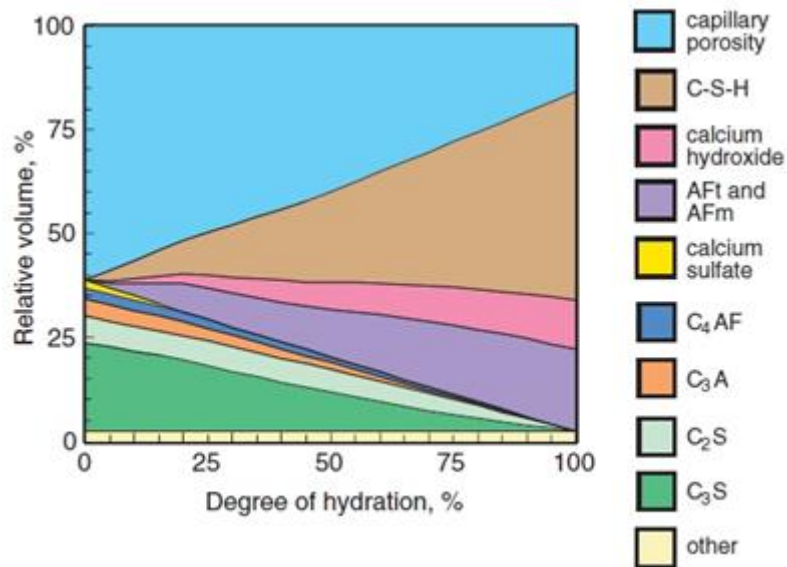


Figure 2.21 Relative volumes of major compounds during cement hydration (Baquerizo Ibarra, 2015; Tennis and Jennings, 2000).

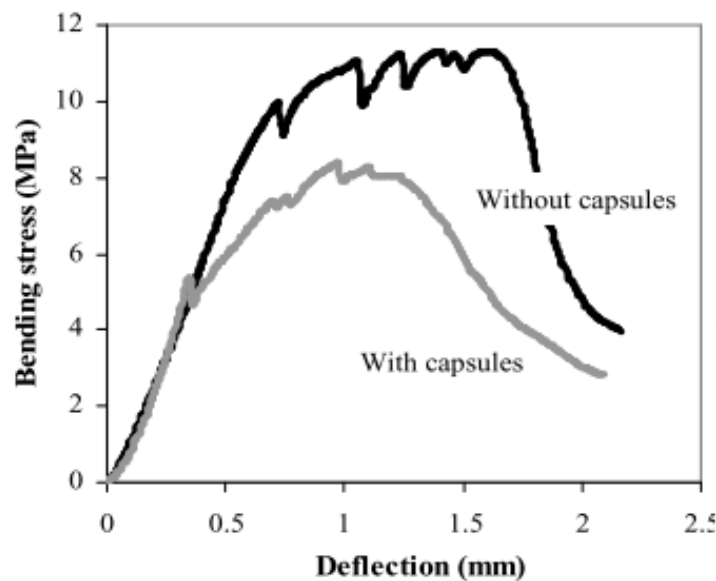


Figure 2.22 Mechanical behaviours of specimens with and without microcapsules (Huang and Ye, 2011).

The latest application of sodium silicate solution (Giannaros et al., 2016; Kanellopoulos et al., 2017, 2016, 2015) as a healing agent for cementitious material was developed by the research group I am part of at the University of Cambridge. A microcapsule developed at the University of Cambridge, which usually consists of an outer shell and inner cargo material, is shown in **Figure 2.23**. Litina (2016) and Litina et al. (2014) studied a range of microencapsulation techniques, including interfacial polymerisation and microfluidic and hydrogel processing during in the production of microcapsules. These techniques were tested with a range of shell and cargo materials to assess their applicability to cementitious materials. They suggested that shell materials must have a suitable thickness, strength, and stiffness for it to rupture when a crack develops in the cementitious matrix, but not to break during processing or mixing. Gelatine, which meets these requirements, can be used as a shell material to provide a controlled triggering mechanism, as it is flexible when saturated and brittle when dried (Kanellopoulos et al., 2017). Cargo materials such as methyl-methacrylate, sodium silicate, silica gel, and magnesia can be adopted in these gelatine capsules. The microcapsules then can be mixed with the cementitious mixture and uniformly distributed in the matrix without rupturing. Site-specific autonomic control of repair can then be achieved by a damage-induced triggering mechanism. When the cracks propagate, the healing agent is released and diffuses into the damaged area via either gravitational forces, capillary forces or both. Thus, a sodium silicate solution encapsulated in a gelatine shell appears to be a promising capsule-based healing material for soil-cement systems.

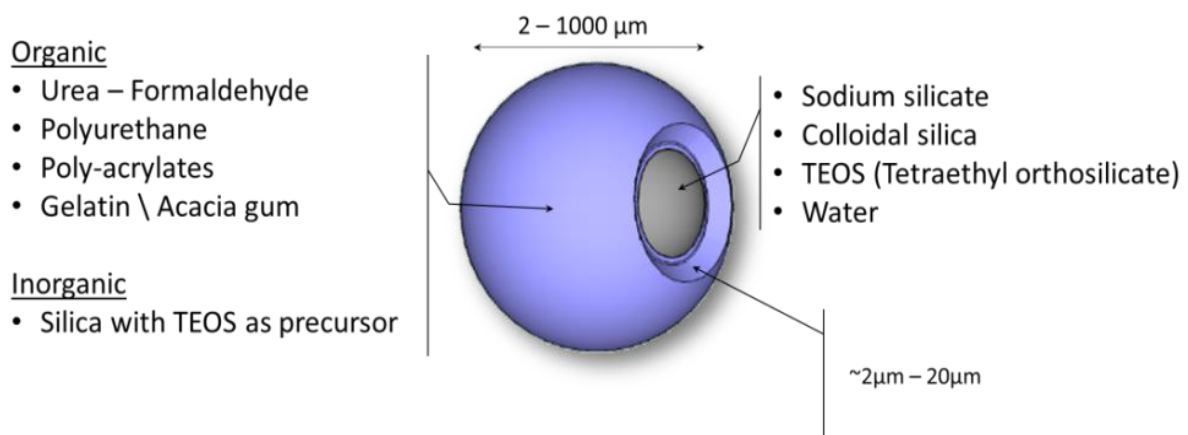


Figure 2.23 Diagram of the self-healing capsules developed at University of Cambridge (Al-Tabbaa and Kanellopoulos, 2014).

2.3.3.2 Mineral admixture and additives

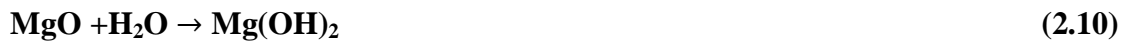
Mineral admixtures and additives are another type of self-healing technique used to improve the self-healing capabilities of cement-based composites. Researchers have added pozzolanic, expansive minerals, and latent hydraulic materials such as fly ash, bentonite, silica fume, blast furnace slag, and MgO to cement-based composites. These admixtures are added to the cement during mixing. When cracks propagate in the cement-based composite, the mineral admixtures at crack surfaces react with water to form healing products and fill the cracks. The mineral admixtures and additives studied in relevant literature can be generally categorised into four groups, as seen in **Table 2.3**: geo-materials, expansive additives, crystalline additives and silica-based additives.

Table 2.3 Categories of mineral additives used for self-healing cementitious materials.

Category	Healing material	Healing mechanism	References
Geo-materials	Bentonite	Swelling after water absorption	(Qureshi et al., 2016; Sivakumar Babu et al., 2001)
	Montmorillonite		(Ahn and Kishi, 2010)
Expansive additives	Free lime	React with water and the volume of the reaction products is larger than the admixture itself	(Ahn and Kishi, 2010; Jiang et al., 2015; Litinia and Al-Tabbaa, 2013; Qureshi et al., 2016)
	Calcium sulfoaluminate (CSA)		(Ahn and Kishi, 2010; Sisomphon et al., 2013, 2012)
	Reactive magnesium oxide		(Alghamri et al., 2018; Litinia and Al-Tabbaa, 2013; Mao, 2018; Qureshi et al., 2016; Qureshi and Al-Tabbaa, 2016)
Crystalline additives	NaHCO ₃ , Na ₂ CO ₃ and Li ₂ CO ₃ , etc.	Promote crystallization and sedimentation in the matrix of cement-based materials.	(Ahn and Kishi, 2010; Jiang et al., 2015; Sisomphon et al., 2013, 2012)
Silica-base additives	Silica fume	React with calcium hydrates and produce C-S-H gel	(Jiang et al., 2015; Litinia and Al-Tabbaa, 2013)

The self-healing capability of geo-materials such as bentonite has been documented in geosynthetic clay liners (Sivakumar Babu et al., 2001). However, for self-healing cement-based materials, geo-materials are usually added with other additives. Ahn and Kishi (2010) embedded geo-materials (mainly montmorillonite), expansive additives (CSA), and crystalline additives in concrete. The researchers argued that the best self-healing performance was induced by combining the swelling effect of geo-materials, the expansion effect of expansive additives, and the enhanced recrystallisation induced by crystalline additives within the cementitious matrix. They found that complete sealing of 0.15 mm cracks can be observed after a re-curing time of three days (**Figure 2.24**) for samples embedded with three additives while cracks were remained open after curing for 33 days if only geo-materials were incorporated.

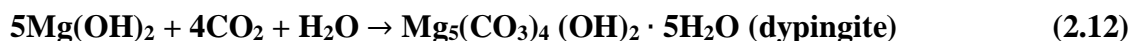
Recently, MgO has attracted attention as a potential self-healing material due to its expansive properties. When it reacts with water, MgO expands, giving it great potential to seal cracks, as shown in **Eq. 2.10**.



In the presence of moisture and CO₂, brucite can yield one or more hydrated magnesium carbonates (HMCs) (Al-Tabbaa, 2013), as shown in **Eqs. 2.11–2.13**. The volume of MgO increases by 117% when it turns into brucite, Mg(OH)₂, which is even higher than the equivalent volume increase for CaO (98%) (Mao, 2018). Moreover, the volume increase when brucite produces HMCs can be 80–210%, depending on the carbonate formed (Al-Tabbaa, 2013; Mo et al., 2010). Another important advantage of MgO is that its reactivity can be controlled, depending on the type of MgO. Therefore, it can be used to mitigate the shrinkage of concrete (Mo et al., 2010).



and/or



and/or



Most studies concerning the self-healing capability of MgO were conducted by previous researchers at the University of Cambridge (Alghamri, 2017; Alghamri et al., 2018; Litina and Al-Tabbaa, 2013; Qureshi et al., 2016; Qureshi and Al-Tabbaa, 2016).

In the study performed by Litina and Al-Tabbaa (2013), limestone, silica fume, and MgO were added as healing agents for cement paste, and considerable healing capability was reported. For example, 38% healing efficiency was observed for specimens with 10% MgO, and 80% healing efficiency was achieved for specimens with 30% limestone. Qureshi and Al-Tabbaa (2014) performed a study to compare the self-healing performance of cement pastes containing MgO and/or bentonite and found that the optimum combination of minerals for self-healing was 5% MgO with 5% of bentonite. Qureshi and Al-Tabbaa (2016) investigated the self-healing performance of drying shrinkage cracks of Portland cement embedded with expansive MgO. They reported that the crack area reduction was about 74%–99% after between 14 to 56 days of healing, which was much higher than the control samples' 43%–79% reduction for the same period. They also found that the addition of MgO improved the recovery of durability of PC in terms of gas permeability and sorptivity coefficients, as shown in **Figure 2.25**.

Mineral additives and admixtures have shown great potential as self-healing agents in cementitious materials. However, if mineral additives are added directly to the mix in powder form, they can react immediately, leading to consumption of the healing agent, and thus a decrease in the final material's self-healing efficiency. This may even cause further negative side-effects for the mechanical properties of cementitious composites (Ahn and Kishi, 2010; Qureshi and Al-Tabbaa, 2016). To tackle this problem, some researchers have recently suggested to granulate power active minerals and then further to encapsulate them via a coating process (Alghamri et al., 2018; Hung et al., 2013; Kishi, 2013; Lee and Ryou, 2016, 2014).

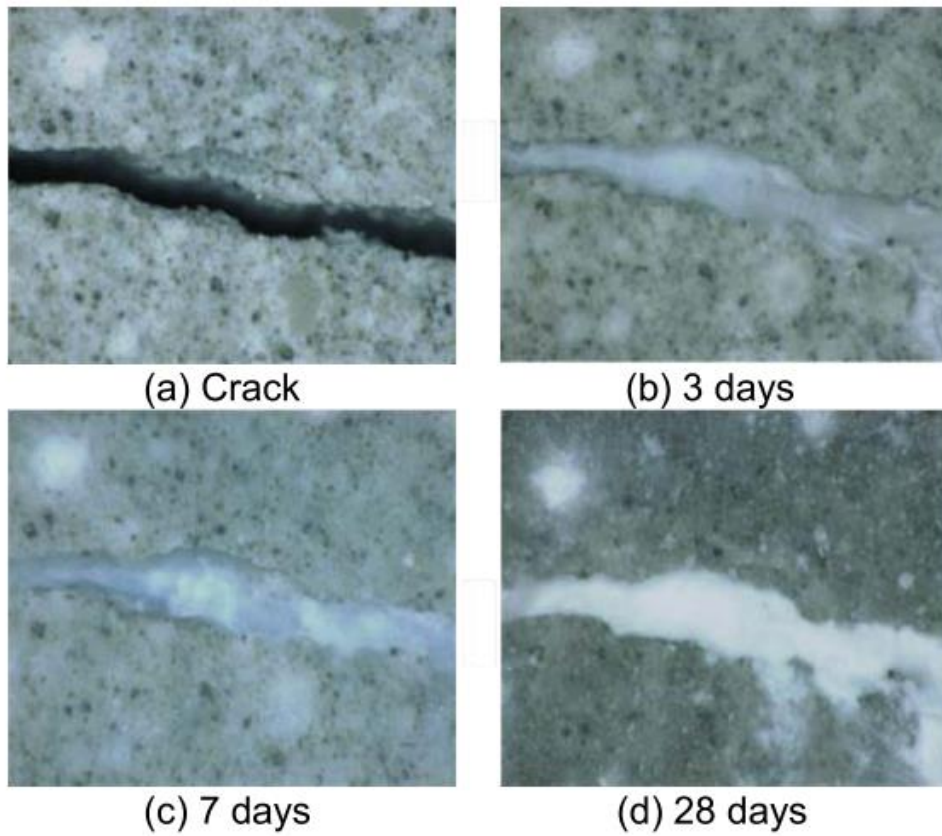
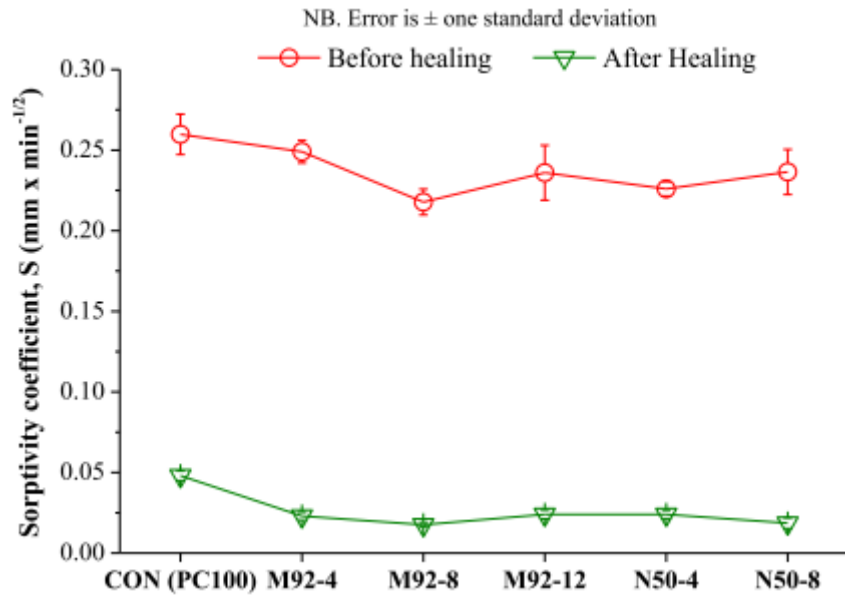
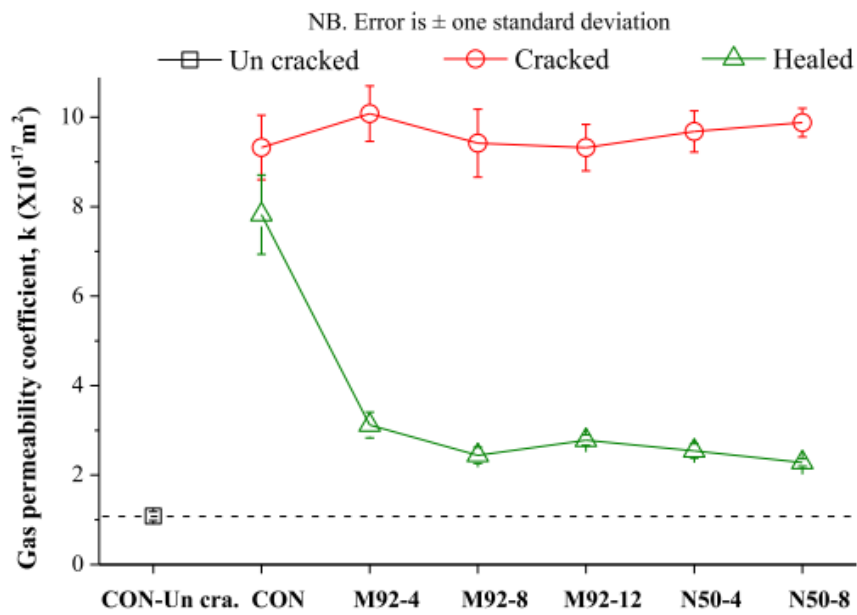


Figure 2.24 Self-healing process of concrete containing expansive agents, geo-materials, and crystalline additives (Ahn and Kishi, 2010).



(a)



(b)

Figure 2.25 Permeability measurements of cracked, healed, and un-cracked control discs' (Qureshi and Al-Tabbaa, 2016) (a) sorptivity coefficient and (b) gas permeability coefficients. M and N denote two types of MgO and the number that follow indicates the percentages of each type used in the mixtures.

2.3.3.3 Pellet-based self-healing

Pelletising is the process of agglomerating fine powders or particles into pellets. The pelletisation theory was developed in the 1940s and the mechanism of pellet formation is presented in **Figure 2.26**. **Figure 2.26a** displays the moisturisation of dry particles. In this process, the sprayed liquid can be either water or an organic solvent or another binder. When the particles are rotated in a balling drum or disc, the particles and the liquid are made to bond via the centrifugal and gravitational forces caused by the rotation, forming spherical structures (**Figure 2.26b-c**). With a carefully chosen rotation speed and liquid spray rate, uniform pellets can be produced. The size, size growth rate, and density of the pellets can be controlled via the feeding rate of the binder as well as the speed and angle of the centrifugal motion. **Figure 2.27** presents a schematic illustration of the pelletisation process using the fluid bed technique. The technique of pelletisation has been widely used for producing oral drugs (e.g., granules, pellets, tablets, and capsules) (Lavanya, 2011), as these types of pellets can lend drugs controlled-release properties.

Considering these advantages, the pelletisation technique has significant potential in the development of self-healing materials. Other applications of the technique include the agglomeration of fly ash, cement, and so on. Meissner et al. (1964) pelletised zinc oxide and found that for particles with a diameter of 0.25 or fewer microns, density and crushing strength could be markedly increased for pellets formed from loose powder. Baykal and Döven (2000) pelletised fly ash to improve its engineering performance and found that the pelletised fly ash was satisfactory for geotechnical applications.

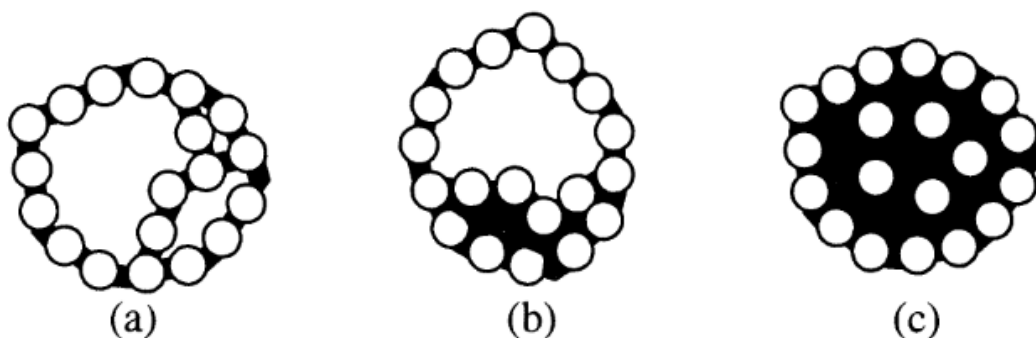


Figure 2.26 Mechanisms of the formation of balls (Srb and Ruzickova, 1988).

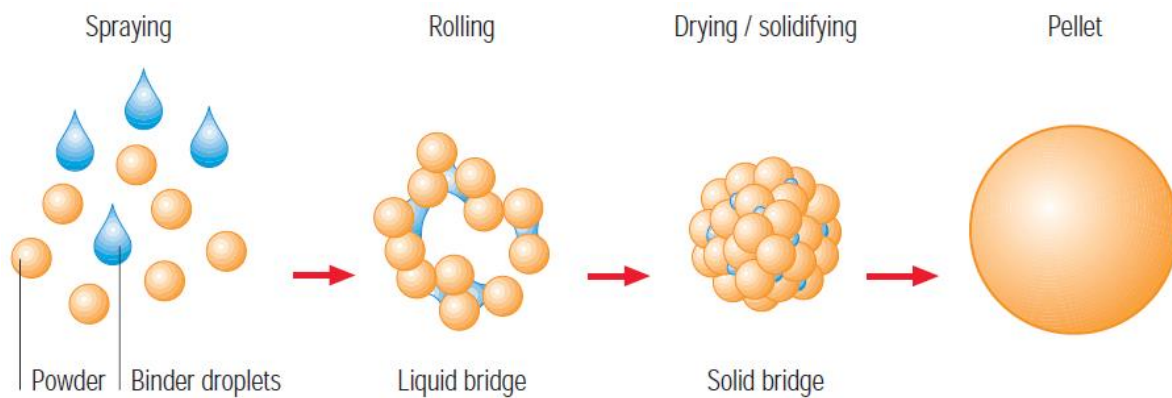


Figure 2.27 Schematic illustration for the pelletisation process using the fluid bed technique (Glatt GmbH Binzen, 2005).

Pellets containing healing agents such as reactive MgO, silica fume, and bentonite were used to lend self-healing properties to cement-based composites (Alghamri, 2017; Alghamri et al., 2018). In the study, the core materials were coated with a polyvinyl alcohol (PVA) film layer and were released when cracked. Promising self-healing performance for cement-based composites has been reported with this technique. Alghamri (2017) reported that 70–100% healing of 300 μm cracks in cement-based composites was obtained by utilising two types of commercial pellets and two types of prototype pellets containing reactive MgO. Complete crack closure was confirmed via microscopic inspection. In terms of water sorptivity, the inclusion of MgO pellets reduced the water capillary uptake by 30–65% with respect to the control sample. A considerable improved flexural strength regain of 9–23% was also reported by Alghamri (2017).

For healing agents in powder form, such as reactive MgO, Bentonite, lime (CaO), and cement, pellets represent an appropriate encapsulation technique. Pelletisation of cargo materials can be achieved by using a spray coating method. The thickness of the coating can be determined by the number of coating cycles the pellet is subjected to. Specific grading of pellets can be achieved by crushing pellets and sieving. Thus, the pellets can have dimensions comparable to grains of sand. This allows them to be easily mixed into cement grout and thus serve as a healing agent in soil-cement systems. Another advantage of pellets is that, as solid healing agents, they can release more healing materials into damaged matrix than encapsulated mineral solutions of similar size. In addition, pellets make it easier to ensure that healing agents are only released when triggered (e.g., by cracks or excess pressure induced by freeze-thaw cycles).

2.4 SAPs in cementitious materials

2.4.1 Introduction

Superabsorbent polymers (SAPs) are cross-linked polymers that can absorb and retain a large amount of water within a few minutes and swell to form a soft, insoluble gel (F. Buchholz and A. Graham, 1998; Hwang and Damodaran, 1996; Snoeck et al., 2015). When water molecules are drawn into the polymer network across a diffusion gradient, the polymer chains are not able to straighten, as they are cross-linked. As a result, water molecules begin to fill the empty spaces within the network, causing the particles to expand. **Figure 2.28** shows an example of the structure of a superabsorbent polymer and its reaction with water.

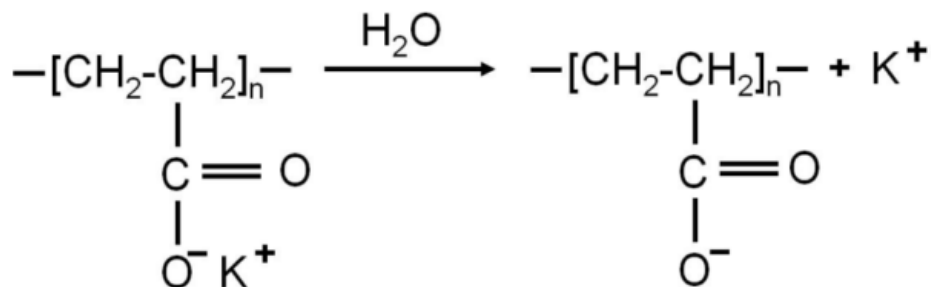


Figure 2.28 Chemical structure of a synthetic polyacrylamide with potassium salt base superabsorbent polymer and its reaction with water (Mao et al., 2011).

SAPs can generally be grouped into four categories based on the presence or absence of electrical charges located in the cross-linked chains (Zohuriaan-Mehr and Kabiri, 2008). The four groups of SAP include (i) Non-ionic, (ii) Ionic, which includes both anionic and cationic, (iii) Amphoteric electrolyte (ampholytic), containing both acidic and basic groups, and (iv) Zwitterionic (polybetaines), containing both anionic and cationic groups in each structural repeating unit. The majority of commercial SAP hydrogels are anionic.

2.4.1.1 Water sorption ability of SAPs

Water-absorbing ability varies for different types of SAPs. For a given SAP, water absorption depends on the properties of liquid, including its temperature, pressure, and ionic concentration of the aqueous solution. In deionised and distilled water, a SAP may absorb up to 1500 times its weight and can become up to 99.9% liquid. However, when added to a 0.9% saline solution, the SAP's absorbency can drop to approximately 50 times its weight (V. Mechtcherine, 2012). Lee et al. (2016) found that the absorption of SAPs in deionised water can be greater than 500 g/g, while this value drops to 10–20 g/g in a typical concrete pore

solution. **Figure 2.29** presents visual and schematic illustrations of acrylic-based anionic superabsorbent hydrogels in dry and water-logged states. The polymer chains are cross-linked and collapsed in the dry state, but when they encounter an aqueous medium, water molecules enter the polymer and the chains are forced to expand. However, the total absorbency and swelling capacity depend on the type and degree of cross-linked of the polymer and the properties of the water solution. Once water is absorbed by a SAP, it is held tightly in the polymer network via hydrogen bonding (Zohuriaan-Mehr et al., 2010).

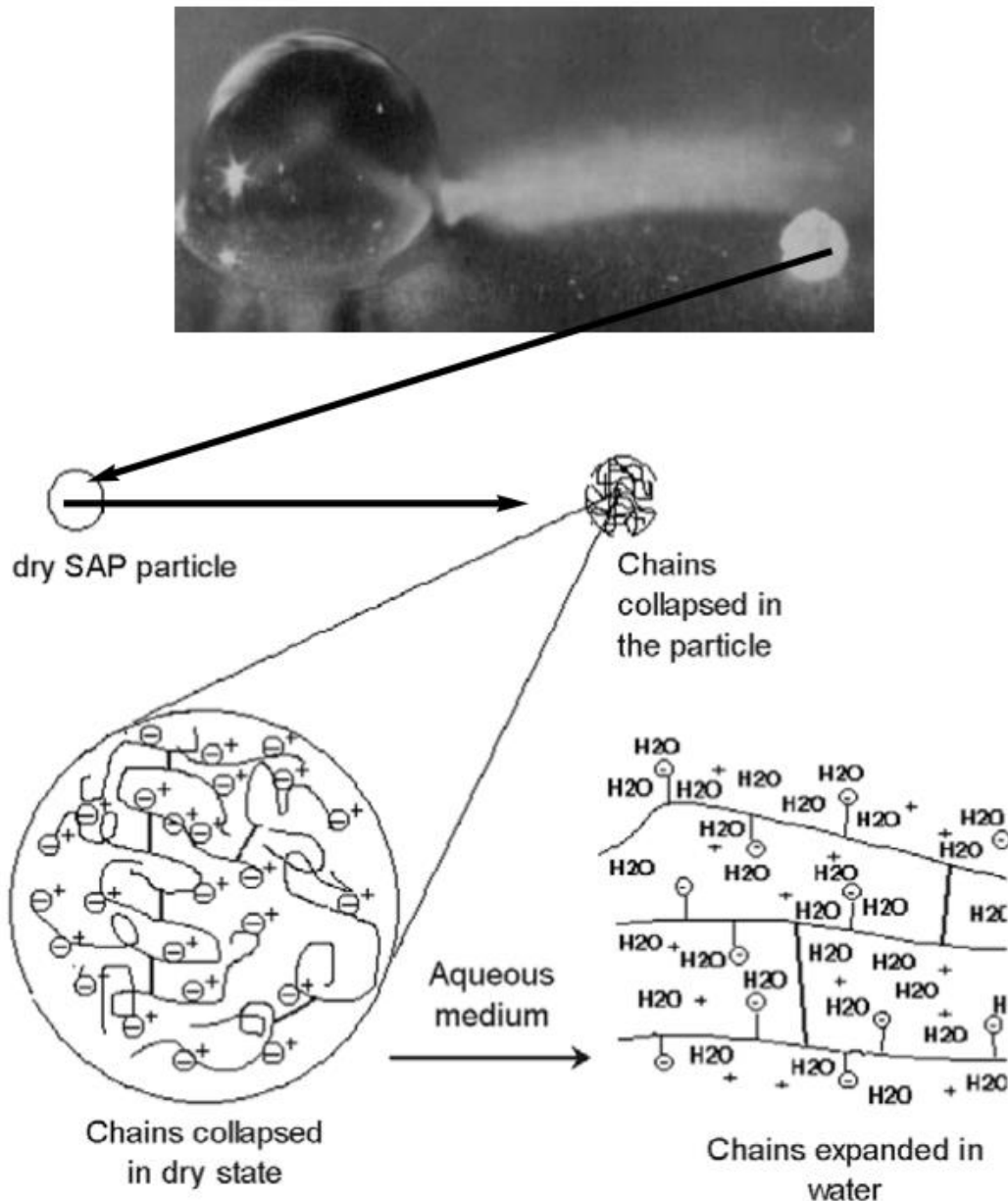


Figure 2.29 Illustration of a typical acrylic-based anionic SAP material and a schematic presentation of SAP swelling (Zohuriaan-Mehr and Kabiri, 2008).

2.4.1.2 Application of SAPs

SAPs were originally developed in the late 1930s, and they are now widely used in personal disposable hygiene products such as baby diapers. The global production of SAPs was estimated to be about 3.12 million tons in 2014, which was up 11.8% from the previous year (Research in China, 2015). Recently, research on SAPs has been conducted on applications such as agricultural (soil conditioning, water reservoirs, erosion control) (Lejcuś et al., 2018; Mao et al., 2011; Sayyari and Ghanbari, 2012) and waste solidification. Another important SAP application that has attracted attention recently is the use of SAPs in cementitious materials. The goals of SAP applications in mortar and concrete projects can include (i) enhancing strength and workability (Justs et al., 2015; Ma et al., 2017); (ii) preventing drying, shrinkage, cracking, and internal curing (Mignon et al., 2017; Shen et al., 2016; Snoeck et al., 2015); (iii) self-sealing and self-healing (Hong and Choi, 2017; Lee et al., 2010; Snoeck et al., 2014, 2012); and (iv) improving freeze-thaw resistance (Craeye et al., 2018, 2013; Hasholt et al., 2015; Mechtcherine et al., 2017).

2.4.2 Characteristics of SAPs

2.4.2.1 Particle size of SAPs

The size of SAPs can affect the microstructural properties of the cementitious materials they are added to. Four types of SAPs with median particle sizes of 197 μm , 59 μm , 140 μm , and 60 μm were used by Farzarian et al. (2016) in cement pastes. **Figure 2.30** presents the SEM images showing the morphology (irregular shape) of two kinds of SAPs used by Snoeck et al. (2015) with sizes of $100 \pm 21.5 \mu\text{m}$ and $477 \pm 53 \mu\text{m}$ respectively. Snoeck et al. (2014, 2012) added SAPs with irregular shapes and sizes of $477 \pm 53 \mu\text{m}$ to self-healing cementitious material. Some studies have found that SAPs with sizes of roughly 500 μm are ideal for promoting the self-healing and self-sealing of cementitious materials (Gruyaert et al., 2016; Snoeck et al., 2014, 2012).

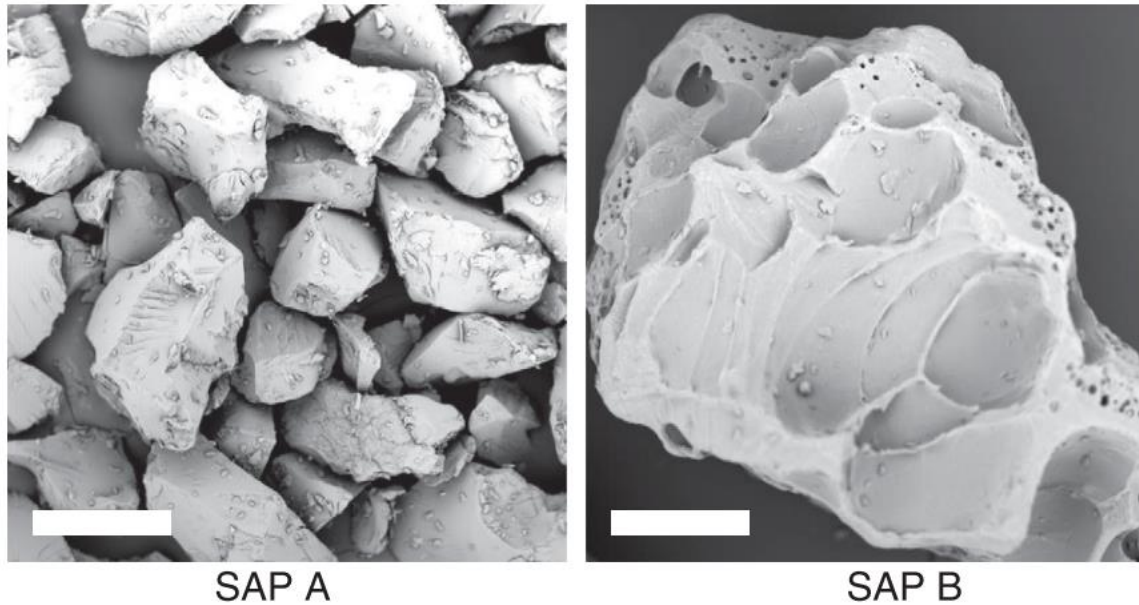


Figure 2.30 SEM images of bulk-polymerised SAP A and SAP B used in (Snoeck et al., 2015). The scale bar amounts 100 μm .

2.4.2.2 Swelling characteristics of SAP

The swelling ratio of an SAP depends on factors like the degree of cross-linking in the SAP, the chemical structure of the monomers constituting the SAP network, and the properties of the solution the SAP encounters, such as its pH, ionic concentration, and temperature (Peppas et al., 2000). The rate of swelling for SAP particles depends on the diffusion coefficient and diffusion path length of the polymer. It can range from less than one minute to several hours (F. Buchholz and A. Graham, 1998). Hong and Choi (2017) tested the swelling characteristics of SAP in a range of solutions that included distilled water, tap water, and a filtered cement pore solution. **Figure 2.31** plots the changes in particle size with time in different types of solutions and shows that the swelling ratio varies with the properties of the solution such as pH and ion concentration. The authors also found that the SAP swelled to its maximum size in approximately 5 minutes, regardless of the type of solution.

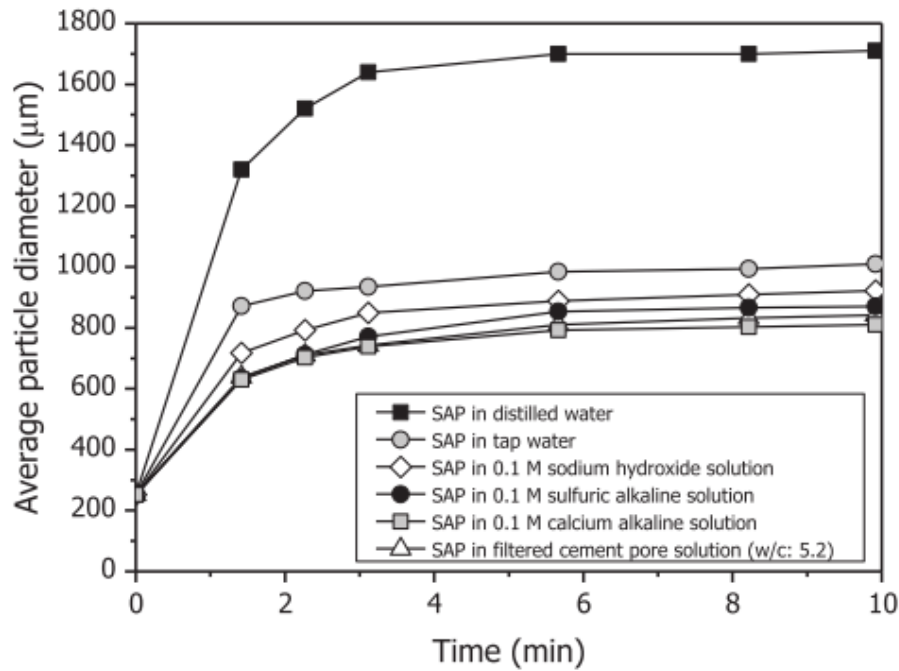


Figure 2.31 Changes in the average size of an SAP added to different types of solutions over time (Hong and Choi, 2017).

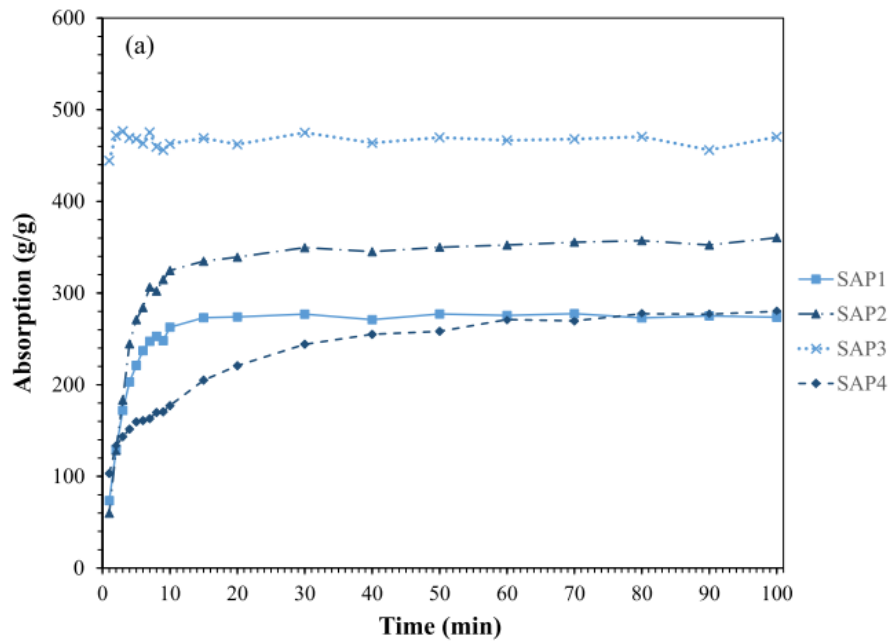
2.4.2.3 SAP absorption and desorption

Absorption is one of the key properties of SAPs (Zohuriaan-Mehr and Kabiri, 2008). SAPs can absorb up to 1500 times their dry mass in water (V. Mechtcherine, 2012), and this process can take from less than one minute to several hours (F. Buchholz and A. Graham, 1998). Similar to the SAP swelling ratio, SAP absorption depends on the type of SAP used and the ionic concentration of the aqueous solution (F. Buchholz and A. Graham, 1998; Kiatkamjornwong and Phunchareon, 1999). The typical absorption kinetics of SAPs exposed to distilled water and cement filtrate are presented in **Figure 2.32a** and **Figure 2.32b**, respectively. SAP absorption can be reduced by a factor of 25–50 by changing the solution from distilled water to an extracted cement pore solution (Craeye et al., 2018; Farzarian et al., 2016). Many researchers have reported that calcium ions within the cement pore solution limit the SAP’s absorption and swelling capacity (Huber, 1993; Rha et al., 1999; Schweins and Huber, 2001; Zohuriaan-Mehr and Kabiri, 2008). In any case, the absorption of SAP was found to generally have stabilised after about 20 minutes.

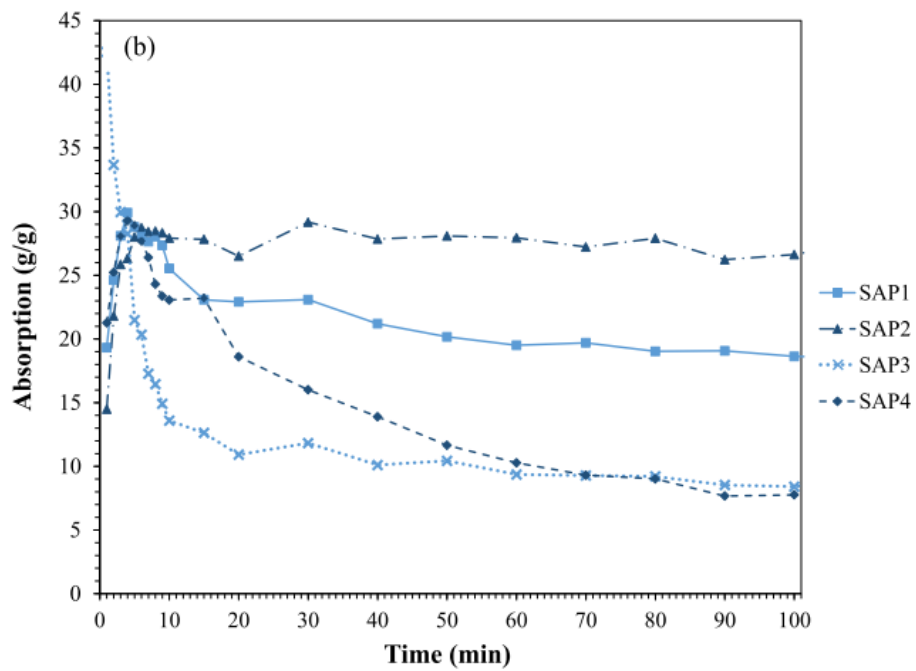
Many researchers have reported that the pH of the solution affects the absorption of SAPs, as shown in **Figure 2.33** (Craeye et al., 2018; Gruyaert et al., 2016). However, the reduction of SAP absorption in an acid or alkaline solution does not necessarily mean that SAP absorption

is determined entirely by the pH of the solution. Most research does not discount the effect of non-acid and non-alkaline ions. For example, in a NaOH solution, Na^+ ions can affect the absorption characteristics of SAPs in addition to (or instead of) OH^- ions. This notion is supported by Snoeck et al. (2014) as the authors reported that SAP absorption in solutions with similar pH values can differ greatly. For instance, the absorption value was found to be 305 g/g in deionised water (pH = 6.5) but only 30 g/g in artificial seawater (pH = 6.3). In addition, it has been found that the reaction between SAPs and water is reversible. For example, SAP absorption decreased from 105 g/g in deionised and distilled water to roughly 20 g/g when added to a 0.9% saline solution (Hwang and Damodaran, 1996). Lee et al. (2010) also reported that SAP absorption generally decreased with increasing saline concentration of the solution. Thus, for a given type of SAP, it is only certain that absorption depends on the ionic concentration of the solution and that absorption generally decreases with increasing ionic concentration. However, this effect may vary for different types of SAPs. According to the reaction presented in **Figure 2.28**, it is possible that the kinds of ion that limit SAP absorption depend on the electrical charge of the SAP (anionic or cationic). In this regard, this process is comparable to recrystallisation.

Another key feature of SAPs is that they can release absorbed water when dried. This process is called desorption. Typical desorption behaviour for SAPs is presented in **Figure 2.34**. Saturated SAPs exhibit almost linear weight loss for the first 100 minutes, but the rate of loss decreases noticeably thereafter. This is because the water near the surface of the SAP is held in place mainly by weak van der Waals forces, while the water closer to the core of the SAP held in place mainly by strong hydrogen bonds formed between the side chains of the polymer (Yun et al., 2017).



(a)



(b)

Figure 2.32 Absorption of SAPs in (a) distilled water and (b) an extracted cement pore solution, where SAP1, SAP3, and SAP4 are made of sodium salts of a crosslinked polyacrylic acid, and SAP2 is a potassium salt of a crosslinked polyacrylic acid-polyacrylamide copolymer (Farzanian et al., 2016).

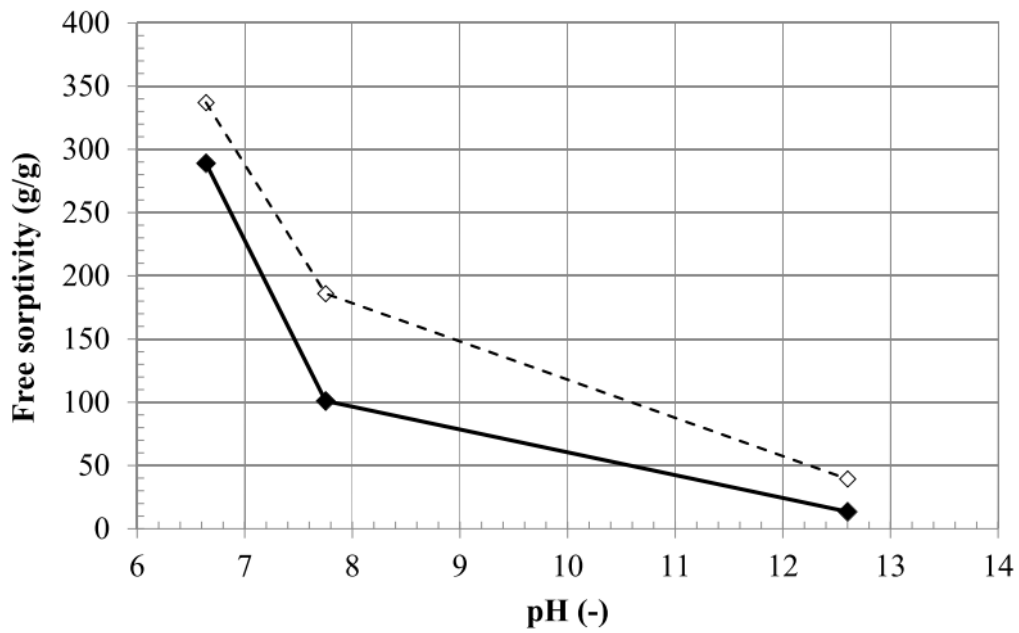


Figure 2.33 SAP absorption for a range of pH levels (Craeye et al., 2018).

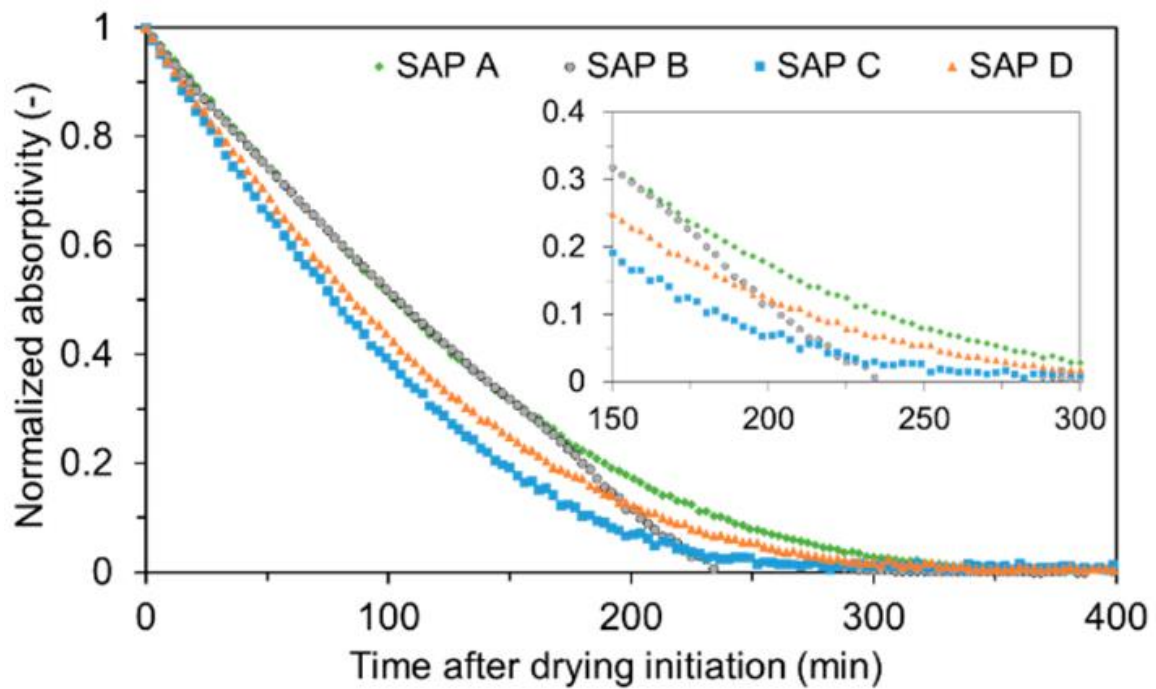


Figure 2.34 Desorption kinetics of SAPs (Yun et al., 2017).

2.4.3 Self-healing applications of SAPs

Due to their water absorption and swelling characteristics of SAPs, the polymers have shown potential for use in cementitious materials as self-healing agents and sealants (Gruyaert et al., 2016; Hong and Choi, 2017; Lee et al., 2010; Snoeck et al., 2016). In most applications, SAPs are added directly to the cementitious mixture. The healing mechanism of SAP-

embedded concrete was investigated by Lee et al. (2010) and is shown in **Figure 2.35**. The authors reported that the SAP swelled at a relatively small amount in a fresh cementitious mixture due to its highly alkaline environment. The water held within the SAPs was available for cement hydration later during the curing process. As the water was drawn out, the SAPs shrank and left behind voids near them (**Figure 2.35a**). When cracks propagated within the matrix, they tended to intersect the SAP particles and the voids nearby (**Figure 2.35b**). When the matrix was exposed to water, it penetrated the cracks and thus was absorbed by the SAPs. This caused the SAPs to expand, therefore clogging the crack (**Figure 2.35c**). This absorbed water was eventually released into the cementitious matrix for further hydration. The stored water therefore enhanced autogenic self-healing and had the potential to contribute to various other mechanisms of autonomic self-healing as well.

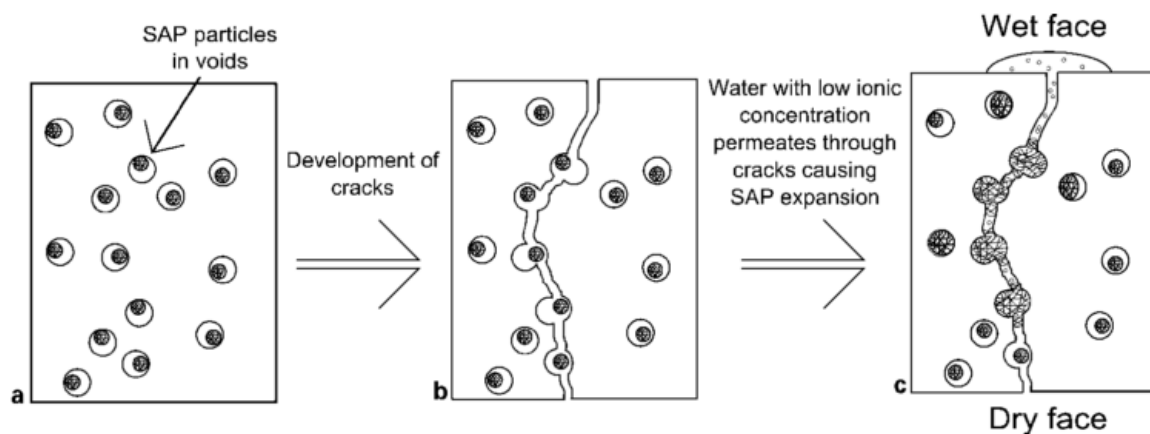
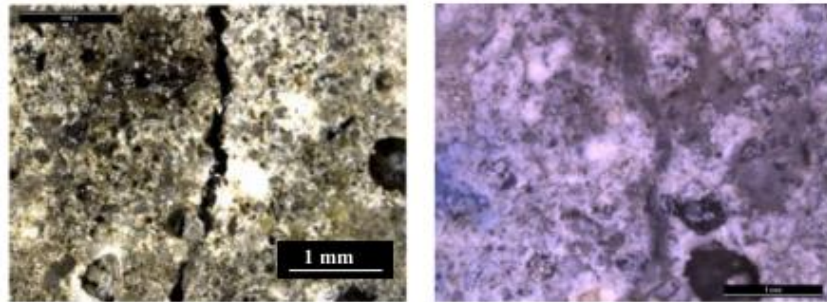


Figure 2.35 Schematic representation of a potential healing mechanism using SAPs (Lee et al., 2010).

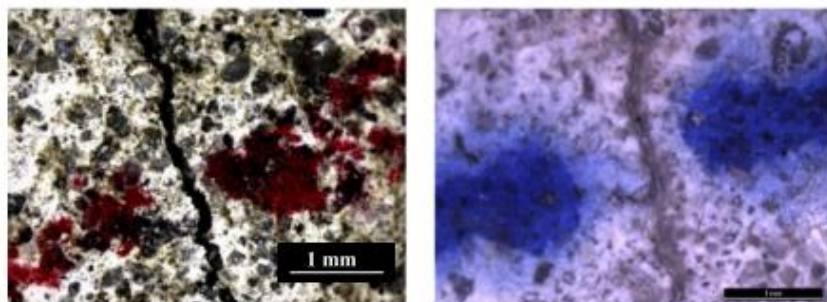
The crack sealing capability of SAPs offers great potential for structures whose water-tightness is of great importance. The typical self-sealing behaviour of a crack can be observed in **Figure 2.36**, which shows that cracks become water-tight after 28 wet-dry cycles. The crack sealing capability of SAPs embedded in cementitious materials depends on several factors such as the type, size, and dosage of SAPs. Hong and Choi (2017) reported that if SAPs are split by a crack, their swelling capacity is less than that of intact SAPs. Other factors such as curing condition and initial crack width also affect the crack sealing performance of concrete with SAPs. It has been found that the best healing is observed in samples subjected to wet-dry cycles (Hong and Choi, 2017; Snoeck et al., 2016, 2014). By using X-ray-computed microtomography, Snoeck et al. (2016) reported that the degree of healing increased in each sample according to the following order: REF (control) < (RH >

90%) < (SAP RH = 60%) < (SAP RH > 90%) < (REF wet/dry) < (SAP wet/dry). A reduction in water leakage/flow due to crack sealing has also been reported by many other researchers (Hong and Choi, 2017; Lee et al., 2016; Mignon et al., 2015). The typical reductions in water permeability for mortars embedded with SAPs are presented in **Figure 2.37**. Finally, it has been found that sealing efficiency reduces as crack width increases (Lee et al., 2016; Pelto et al., 2017).

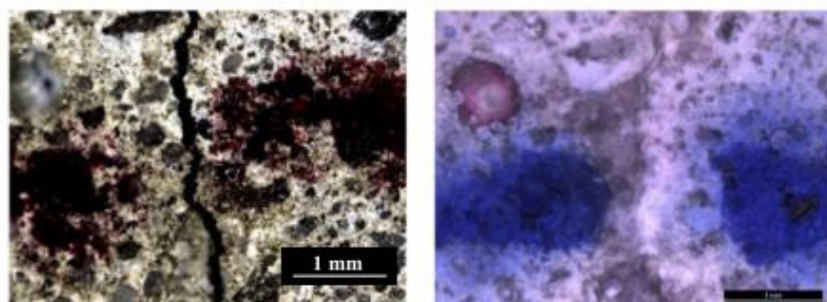
SAP 1 (0.5 wt.%)



SAP 2 a (0.5 wt.%)



SAP 2 b (0.5 wt.%)



SAP 2 c (0.5 wt.%)

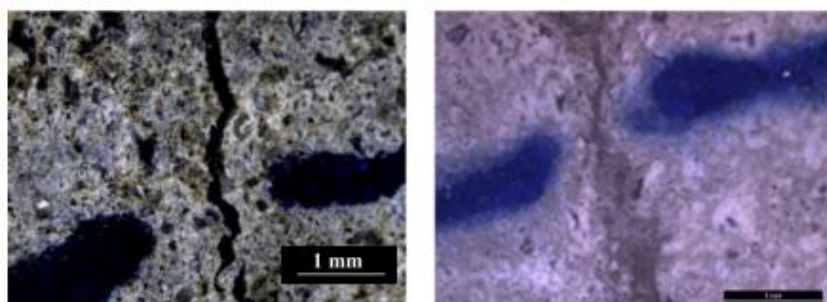


Figure 2.36 Images of crack before and after 28 wet-dry cycles (Gruyaert et al., 2016).

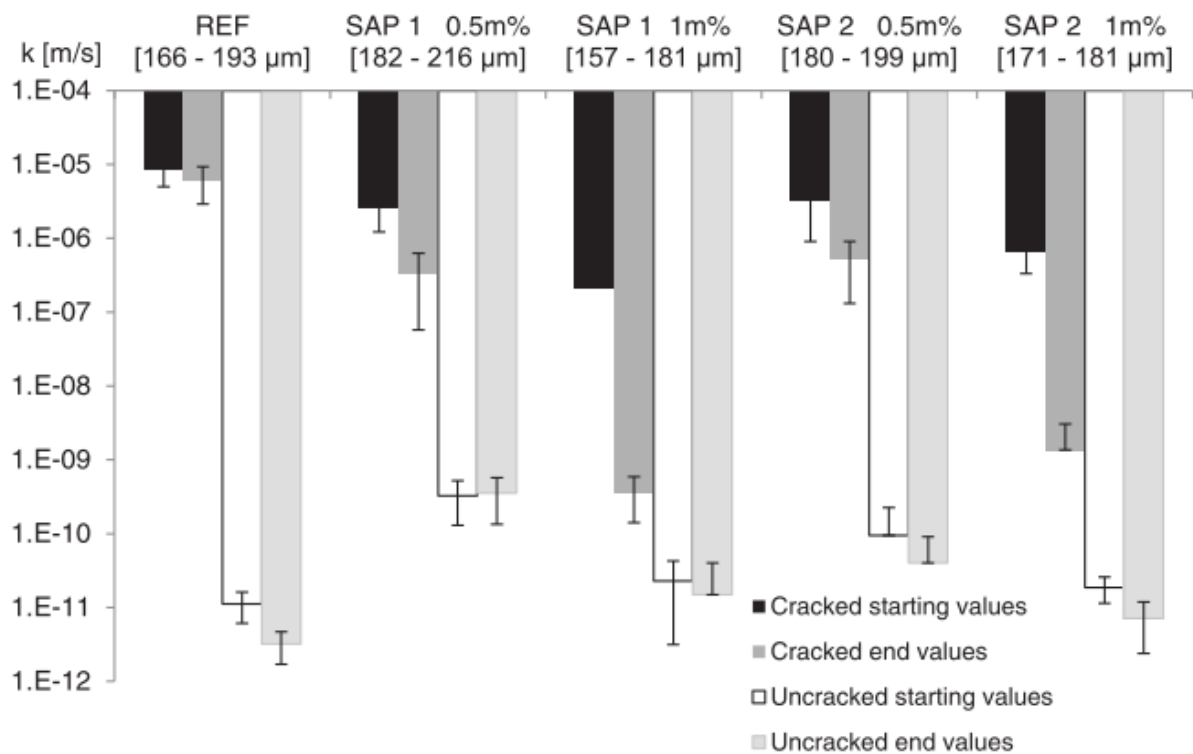


Figure 2.37 Water permeability results for mortars with and without addition of SAPs (Mignon et al., 2015). Length values between brackets show the range of crack widths.

2.4.4 SAPs used for improving freeze-thaw resistance

Research on the applications of SAPs for improving the freeze-thaw resistance of cementitious materials is relatively new. Most of the available literature has reported that adding SAPs in cementitious materials improves their freeze-thaw resistance (Craeye et al., 2018, 2013; Hasholt et al., 2015; Mechtcherine et al., 2017). However, some literature has found that SAPs can serve as alternatives for air entrainment agents (Craeye et al., 2018), while other studies have suggested that SAPs used in concrete do not provide sufficient freeze-thaw durability on their own (Jones and Weiss, 2014).

Regardless, the ability of SAPs to improve the freeze-thaw resistance of concrete can be attributed to three possible mechanisms. First, it is reported that the addition of SAPs may lead to an increase in the UCS of concrete (Craeye et al., 2018). If SAPs are added directly to concrete without additional water, they will absorb some water during mixing even though their ability to absorb water in an alkaline environment is limited. As a result, water/cement ratio is reduced, which could lead to higher freeze-thaw resistance.

Second, some studies have suggested that SAPs can act as air-entraining agents in concrete, as polymers can contain surfactant-like materials. **Figure 2.38** presents the results of air content measurements in fresh mixtures. Mechtcherine et al. (2017) summarised the works from 12 participants and posited that the addition of SAPs does not lead to additional air entrainment for fresh mixtures like the air-entraining agents. They suggested instead that the improved freeze-thaw resistance could be attributed solely to the continuous reaction of the SAPs at a later curing stage.

Finally, the polymers also have the ability to gradually release absorbed water during the concrete's hardening and hydration processes, thereby reducing the number of desiccation cracks in the concrete (Lee et al., 2016, 2010). In this process, the SAPs' volume decreases as water is released, and small pores are created. These pores therefore serve as pressure vessels like the air voids introduced by air entraining. This is considered to be a major cause for the improved freeze-thaw resistance SAP additives produce in cementitious materials (Craeye et al., 2018, 2013; Hasholt et al., 2015; Mechtcherine et al., 2017). **Figure 2.39** presents backscattered electron images of cement pastes containing 1% of 3 types of SAPs. The SAP voids can be easily differentiated from entrapped air voids, which are spherical and empty. Craeye et al. (2018) reported that small cavities in the concrete with diameters between 190 nm and 370 nm were created by the addition of SAPs. The size of the SAP voids ranged from 10 µm to over 500 µm, depending on the initial size of the dry SAP and the amount of swelling that occurred in the paste during mixing (Gruyaert et al., 2016; Lee et al., 2016, 2010). The effects of SAP on the air content of hardened concrete was investigated by Riyazi et al. (2017), whose results are summarised in **Table 2.4a-b**. The authors reported that a 0.5% addition of SAP resulted in an air content (6%) similar to that provided by a 0.07% addition of air-entraining agents.

It has been found that if SAP is added with additional water, the improvement in the freeze-thaw resistance of concrete is insignificant. However, when SAP is added directly without additional water, the concrete's performance subjected to freeze-thaw was improved to a level similar to that achieved by conventional air entrainment (Mechtcherine et al., 2017). At the same time, the reduction in strength due to the addition of SAP is less than that caused by conventional air entrainment. Moreover, it should be noted that during the freeze-thaw process, no water was made available for the concrete to absorb. However, a soil-cement system is very likely to absorb extra water during the freeze-thaw process. As a result, SAPs

in soil-cement systems not only provide air entrainment, but also can serve as sealing agents when water enters the cracks induced by freeze-thaw cycles.

Table 2.4 (a) SAP concrete mix proportions and (b) bubble counter data (Riyazi et al., 2017).

(a)

SAP concrete mix proportions.

Mixture notation	w/cm	Cement (kg/m ³)	Water (kg/m ³)	Fine aggregate (kg/m ³)	SAP (% of cement)	AEA (% of cement)
C1	0.48	571	281	1428	-	-
C2	0.48	571	281	1428	-	0.07
SAP1	0.48	571	281	1428	0.06	-
SAP2	0.48	571	281	1428	0.12	-
SAP4	0.48	571	281	1428	0.25	-
SAP8	0.48	571	281	1428	0.50	-
SAP16	0.48	571	281	1428	1.00	-
SAP32	0.48	571	281	1428	2.00	-
PSAP1	0.48	571	281	1428	0.06	-
PSAP2	0.48	571	281	1428	0.12	-
PSAP4	0.48	571	281	1428	0.25	-
PSAP8	0.48	571	281	1428	0.50	-
PSAP16	0.48	571	281	1428	1.00	-
PSAP32	0.48	571	281	1428	2.00	-
LW	0.48	571	281	980/450WSD	-	-

(b)

Bubble counter data.

Sample	Specific Surface		Spacing Factor (mm)		Air ≤ 1 mm		Total Air	
	(mm ⁻¹)	COV (%)	(mm)	COV (%)	(%)	COV (%)	(%)	COV (%)
C1	73.46	12.6	0.054	16.4	0.7	4.4	1.0	5.6
C2	33.42	8.1	0.043	12.9	4.4	2.7	6.1	1.3
LW	42.33	8.4	0.308	4.6	4.3	1.5	5.2	0.9
SAP1	27.15	5.4	0.097	2.6	3.7	2.6	5.0	1.2
SAP2	20.19	9.6	0.100	10.8	3.7	1.5	5.4	0.4
SAP4	28.57	6.1	0.081	10.9	3.9	1.7	5.5	2.0
SAP8	41.15	4.2	0.031	11.1	3.1	1.9	6.2	1.4
SAP16	33.34	10.0	0.039	10.2	3.4	1.5	7.8	1.9
SAP32	19.63	6.5	0.035	8.8	3.4	2.2	14.7	2.8
PSAP1	32.45	13.0	0.120	2.1	2.0	3.3	2.8	2.5
PSAP2	40.43	3.8	0.076	15.9	3.1	2.9	3.9	1.8
PSAP4	37.17	11.2	0.072	11.6	3.0	4.0	4.0	4.8
PSAP8	36.87	6.3	0.027	3.5	5.0	2.1	6.0	1.6
PSAP16	37.10	3.5	0.025	4.3	5.2	2.9	6.4	3.2
PSAP32	38.42	2.2	0.027	4.1	4.3	3.5	6.3	4.1

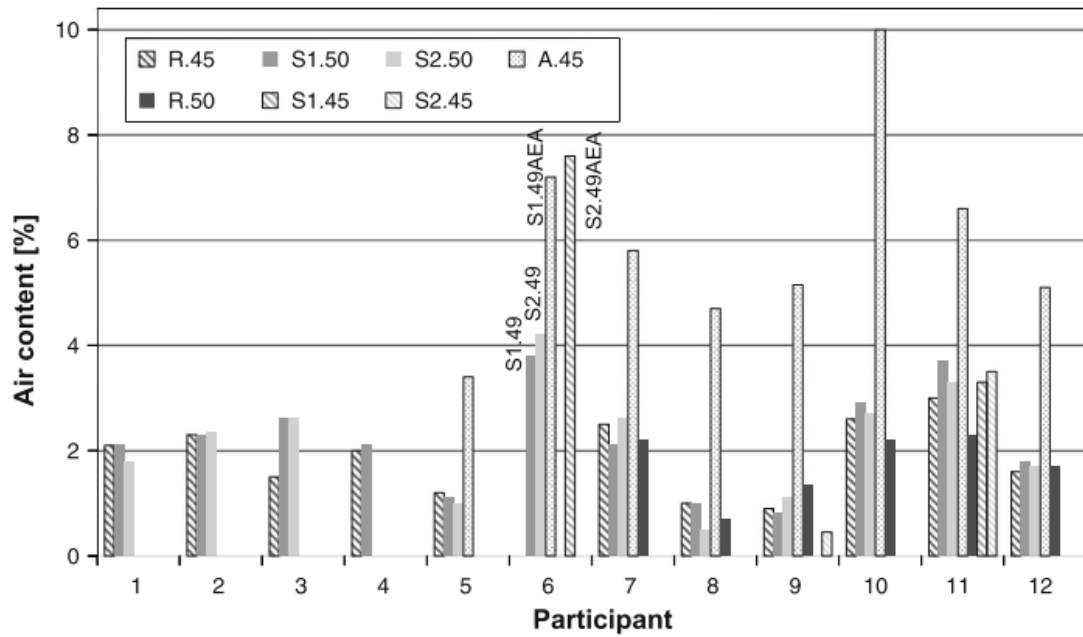


Figure 2.38 Air content in fresh concrete (Mechtcherine et al., 2017).

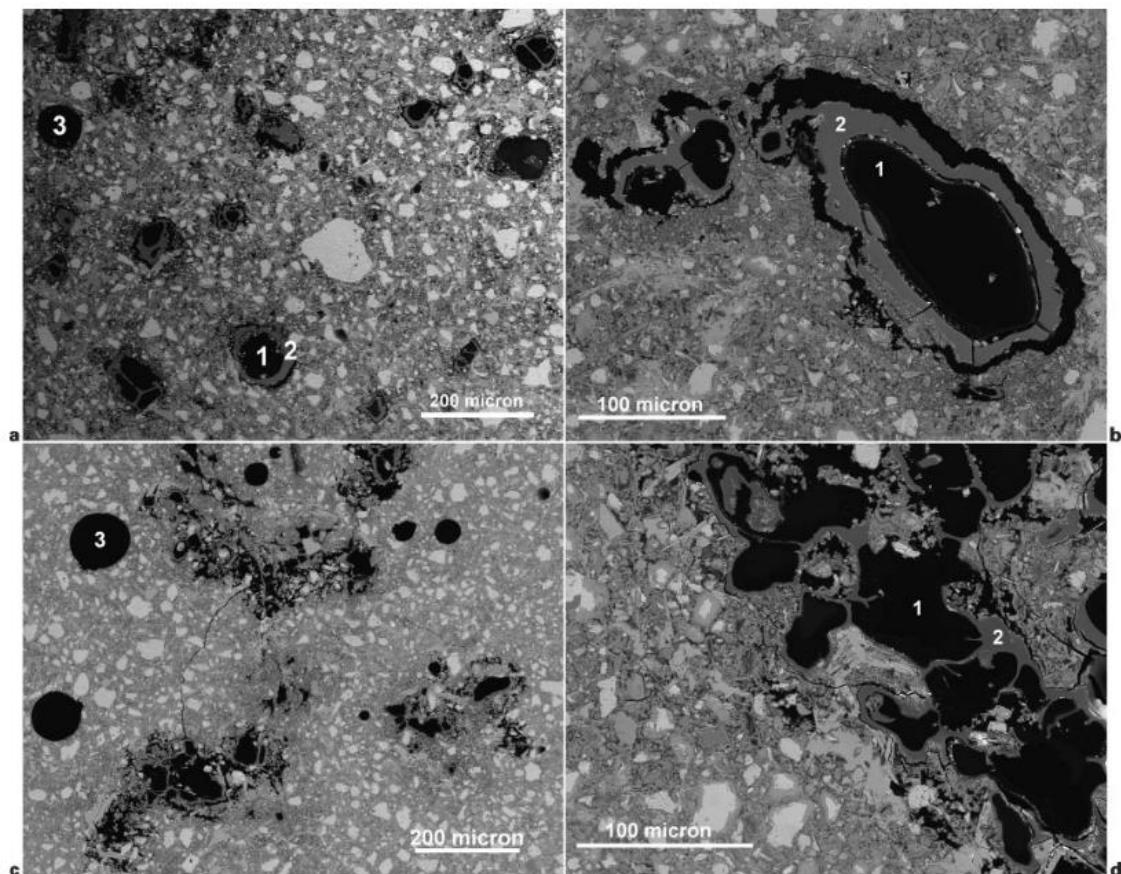


Figure 2.39 Images (BSE) of 5-day-old cement pastes at 0.36 water/cement ratio containing 1% of 3 types of SAPs. Micrographs highlight the size, shape, and distribution of (1) SAP voids, (2) collapsed SAP particles, and (3) entrapped air, as well as the microstructure of the SAP/cement paste interface (Lee et al., 2010).

2.4.5 Effect of SAP addition on the engineering properties of cementitious materials

The effect of SAPs on the engineering performance of cementitious materials depends on a variety of factors such as the type, dosage, and absorption/desorption behaviour of the SAPs, as well as the water/cement ratio of the mixture (Reinhardt et al., 2008; Sikora and Klemm, 2015). **Table 2.5** summarises the effects of different types and dosages of SAPs on the engineering properties of cementitious materials.

The main effect SAPs have on the engineering properties of cementitious materials relates to strength properties. As shown in **Table 2.5**, strength was generally reduced by the increased addition of SAPs for cementitious materials (Farzarian et al., 2016). In addition, the influence on the compressive strength of cement pastes was more noticeable at lower water/cement ratios than higher water/cement ratios (Farzarian et al., 2016; Mignon et al., 2015). However, it should be noted that in most of the studies reporting a strength reduction following SAP addition, additional water was added to the cementitious mixture to compensate for its decreasing workability. Thus, this reduction in strength may be due to the increased water/cement ratio of the mixture. Craeye et al. (2018) reported that if no additional water is added to soak the SAPs, the compressive strength of the concrete increases by 10% and 20% following the addition of 0.13% and 0.26% SAPs, respectively. If the SAP is added directly without additional water, the effect on strength is twofold. On one hand, SAPs can reduce autogenous shrinkage and improve hydration. This is achieved by releasing water into the surrounding area for hydration at later age. On the other hand, during the hydration of cement, water is released from swollen SAPs, causing a significant volume reduction and leaving macro/micro voids in the matrix, thereby reducing the strength of the concrete (Farzarian et al., 2016). In addition, the water absorbed by SAPs may not be completely released during hydration, which can affect the strength of cementitious materials. It should also be noted that if SAPs are added directly, the workability of the cementitious mixture can be considerably reduced, which can affect the degree of mixing (Craeye et al., 2018; Snoeck et al., 2016). Per **Table 2.5**, the amount of SAPs added to self-healing cementitious material falls generally in the range of 0.06% to 2%.

Table 2.5 Changes in strength properties and air content of cementitious materials with different dosages of SAPs.

Reference	Type of SAP	Dosage (%)	Additional water	Change of UCS (%)	Reduction of flexural strength	Change of air content (%)			
(Riyazi et al., 2017)	Partial sodium salt of cross-linked polypromancic acid	0.06	No	0.1	NA	+4			
		0.12		-10		+4.4			
		0.25		-17		+4.5			
		0.5		0.1		+5.2			
		1		-6.1		+6.8			
		2		-29		+13.7			
		0.06	YES	-0.1		+1.8			
		0.12		-0.1		+2.9			
		0.25		-10		+3			
		0.5		-21		+5			
		1		-32		+5.4			
		2		-34		+5.3			
		(Hong and Choi, 2017)	Spherical SAPs (polyacrylate-co-acrylamide)	0.5		Yes	-21	NA	NA
				1		Yes	-44	NA	NA
(Lee et al., 2016)	Sodium polyacrylate or potassium polyacrylate-co-acrylamide	5	Yes	-87.1	NA	NA			
		13	Yes	-87.4	NA	NA			

(Mignon et al., 2015)	In-house synthesized SAP	0.5	Yes	-26.3	-1.5	+ 4.0 to 6.6
			No	+0.5	+10.4	
		1	Yes	-52.0	-25.4	NA
			No	-10.3	+0.6	NA
(Farzarian et al., 2016)	Sodium salts of crosslinked polyacrylic acid	0.3	No	-23.0	+31.5	NA
		0.6	No	-45	+26.1	NA
(Craeye et al., 2018)	Bulk polymerized, covalently cross-linked acrylamide/acrylic acid copolymers	0.13	No	+10	NA	+0.5 (in fresh paste)
		0.26		+20		
(Gruyaert et al., 2016)	Cross-linked copolymer of acrylamide and acrylate	0.5	Yes	-25	2.5	NA
		1		-47	18	NA

Note: the dosage of SAPs is the ratio to the cement mass and the change of parameters is referenced that of the plain mix without SAP.

2.5 Concluding remarks

Soil-cement systems are widely used in infrastructure projects and many other engineering practices to improve the engineering properties of soils. However, the engineering properties of soil-cement systems can be substantially degraded by freeze-thaw cycles. This durability problem substantially impairs the sustainability of soil-cement systems and raises their maintenance and repair costs.

The behaviour of soil-cement systems subjected to freeze-thaw cycles was described in **Section 2.1**. Relevant literature documents show the freeze-thaw durability of soil-cement systems can be affected by factors such as cement content, water content, number of freeze-thaw cycles, freezing temperature, and curing conditions. However, even though the freeze-thaw durability of soil-cement systems is better than that of unstabilised soil, the degradation in engineering properties like strength, structure, and hydraulic conductivity is still significant. There is no widely accepted understanding of the mechanism of the behaviour of soil-cement systems subjected to freeze-thaw cycles. Moreover, although various methods have been used to improve the freeze-thaw resistance of soil-cement systems, no totally satisfactory technique has been proposed. As a result, more effective techniques for improving the freeze-thaw resistance of soil-cement system are necessary.

Air-entraining techniques for concrete have provided insights for improving the freeze-thaw resistance of soil-cement systems. However, the precise mechanisms underlying air entrainment and the freeze-thaw process are still the subject of investigation. **Section 2.2** presented a critical review of relevant theories and hypotheses reported in the literature. The entrained air pores act either as reservoirs that can receive the expelled water from the freezing sites or as cryo-pumps to suck water from capillary pores. By these two mechanisms, the excess hydraulic pressure created by the freezing of water can be relieved. As long as the air pores have enough space to store the ice crystals, the matrix will not suffer from breaking pressure. Therefore, the effectiveness of air entraining relies on having enough volume and a sufficiently homogeneous distribution of air pores. In addition, a critical saturation ratio has been proposed to determine the susceptibility of concrete to freeze-thaw damage. However, to date, there has been no literature written on the use of air entrainment in soil-cement systems. Due to the qualities that separate soil-cement systems from traditional concrete projects, a more carefully administered air-entraining system will likely be needed for soil-cement systems.

Section 2.3 reviews the research and applications on the nature-inspired concept of self-healing materials, with a specific focus on cementitious materials. Both autogenic and autonomic self-healing materials are able to heal themselves within their matrix, which is particularly helpful when damage is not visible or accessible. Another big advantage of self-healing mechanisms is that they can only be triggered when damage occurs. Various healing agents and self-healing techniques intended for cementitious materials, such as capsule-based self-healing, mineral admixtures and additives, and pellet-based self-healing were reviewed. Many researchers reported considerable recovery of mechanical properties and crack closure. Among all the possible options, capsule-based self-healing and pellet-based self-healing appear to be the most promising for soil-cement systems subject to freeze-thaw cycles. This is because their triggering mechanisms can be very carefully controlled. However, to date, there has been little work on self-healing applications for soil-cement systems. Those systems and relevant applications pose different, more challenging problems than typical concrete projects. This suggests that a successful marriage may require a complete rethink of how to design such smart (self-healing or self-immune) systems.

Finally, the properties of SAPs, their applications in self-healing and their suitability for improving the freeze-thaw resistance of cementitious materials were reviewed in **Section 2.4**. SAPs can absorb large amounts of water and swell when mixed with a cementitious mixture. The polymers also have the ability to gradually release the absorbed water during the hardening and hydration of cement. As a result, small pores are created, which can serve as pressure vessels similar to air voids created by air entraining. Moreover, when cracks propagate within the matrix, the SAP particles can swell in the presence of water, clogging the cracks. This water can eventually be released into the cementitious matrix to enhance autogenic self-healing and the reaction of various kinds of autonomic self-healing. However, SAPs have not yet been studied in soil-cement systems with regards to either to promote self-healing or to improve freeze-thaw resistance.

As a result, the following chapters aim to fill the gaps in the existing research by detailing the development of novel “smart” soil-cement systems that can withstand freeze-thaw cycles. Various agents, including Lambson microcapsules, LUVUMAG MgO pellets, SikaAer[®] Solid microcapsules, and SAPs are incorporated into soil-cement systems to serve this purpose.

Chapter 3 Materials and Experimental Methods

This chapter describes details of the raw materials, sample preparation and experimental methods and procedures adopted in this study.

3.1 Materials

3.1.1 Soil-cement systems

Several soil-cement systems with different cement contents were used in this study. Polwhite E China Clay and sand were used in producing the model soil-cement systems. The sand used is the fine sharp sand with a maximum particle size of 2 mm, D_{10} of 0.18 mm, D_{60} of 0.425, coefficient of uniformity of ~ 2.4 and coefficient of curvature of ~ 0.95 . The particle size distribution for the sand is presented in **Figure 3.1**. The sand can be classified as poorly graded clean sands (**Table 3.1**). Polwhite E China Clay used is a high quality medium particle size kaolin with specific gravity of 2.6 that produced from deposits in the south west of England (Richard Baker Harrison Ltd, 2011). All the clay particles passing the 300 mesh (0.045 mm aperture) and $>65\%$ of clay particles' diameter is smaller than 10 microns (Richard Baker Harrison Ltd, 2011). The model soil produced in this study composed of 85% sand and 15% clay by weight. According to the unified soil classification system (USCS) (ASTM: D2487-17, 2017), the soil used is classified as a clayey sand. As for the cement, high strength cement CEM-I 52.5N complying with BS EN 197-1, supplied by Hanson Limited, UK was used throughout this study. Images of the sand, clay, and cement used are shown in **Figure 3.2**.

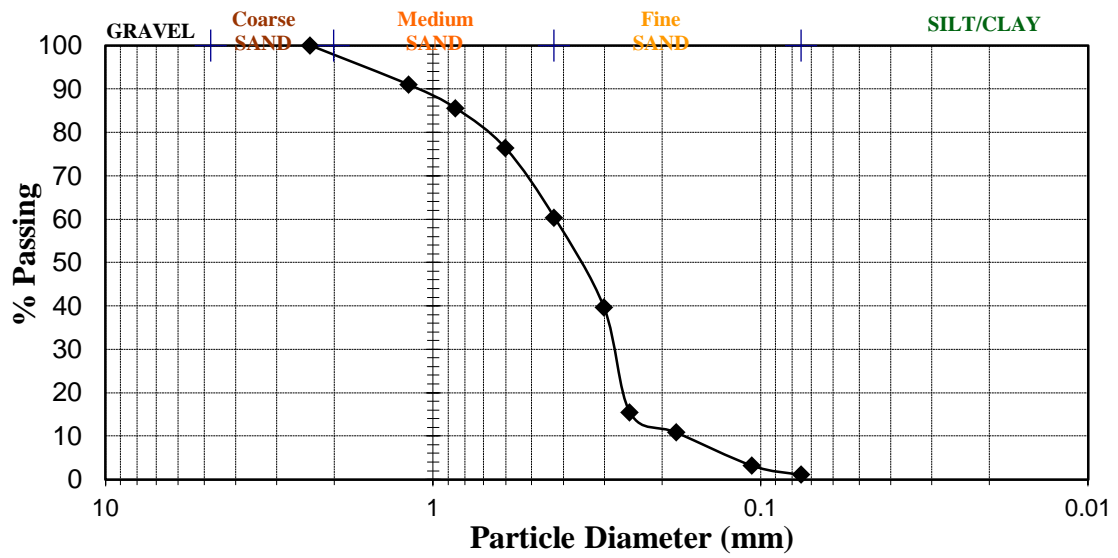


Figure 3.1 The particle size distribution curve of the sand used.



(a)

(b)



(c)

Figure 3.2 Image of the (a) sand, (b) clay, and (c) cement used.

Table 3.1 Soil classification chart (ASTM: D2487-17, 2017).

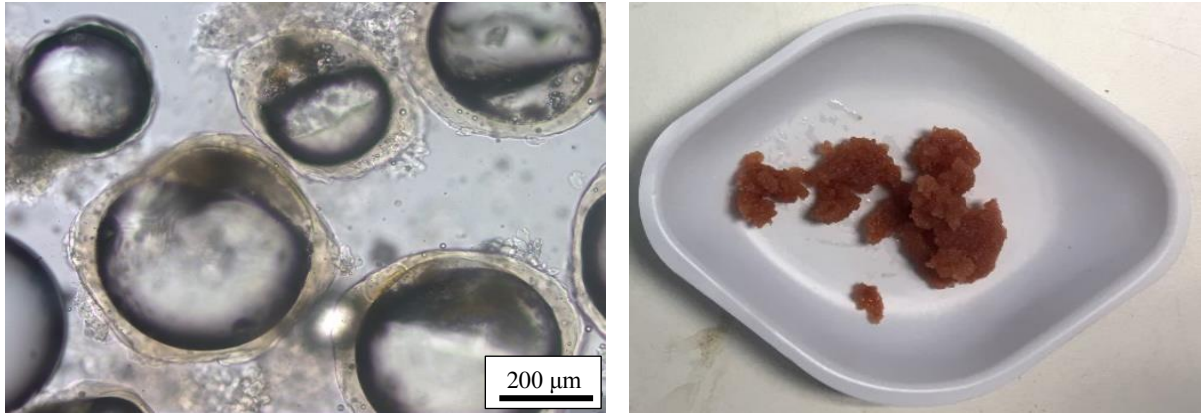
Criteria for Assigning Group Symbols and Group Names Using Laboratory Tests ^A				Soil Classification		
				Group Symbol	Group Name ^B	
COARSE-GRAINED SOILS	Gravels (More than 50 % of coarse fraction retained on No. 4 sieve)	Clean Gravels (Less than 5 % fines ^C)	Cu \geq 4.0 and 1 \leq Cc \leq 3.0 ^D	GW	Well-graded gravel ^E	
		Gravels with Fines (More than 12 % fines ^C)	Cu < 4.0 and/or [Cc < 1 or Cc > 3.0] ^D	GP	Poorly graded gravel ^E	
			Fines classify as ML or MH	GM	Silty gravel ^{E,F,G}	
	More than 50 % retained on No. 200 sieve	Sands (50 % or more of coarse fraction passes No. 4 sieve)	Clean Sands (Less than 5 % fines ^H)	Cu \geq 6.0 and 1.0 \leq Cc \leq 3.0 ^D	SW	Well-graded sand ^I
			Cu < 6.0 and/or [Cc < 1.0 or Cc > 3.0] ^D	SP	Poorly graded sand ^I	
		Sands with Fines (More than 12 % fines ^H)	Fines classify as ML or MH	SM	Silty sand ^{F,G,I}	
FINE-GRAINED SOILS	Silt and Clays	inorganic	PI > 7 and plots on or above "A" line ^J	CL	Lean clay ^{K,L,M}	
			PI < 4 or plots below "A" line ^J	ML	Silt ^{K,L,M}	
	50 % or more passes the No. 200 sieve	Silt and Clays	inorganic	Liquid limit - oven dried < 0.75	OL	Organic clay ^{K,L,M,N} Organic silt ^{K,L,M,O}
				Liquid limit - not dried < 0.75	OH	Organic clay ^{K,L,M,P} Organic silt ^{K,L,M,O}
		Silt and Clays	inorganic	PI plots on or above "A" line	CH	Fat clay ^{K,L,M}
				PI plots below "A" line	MH	Elastic silt ^{K,L,M}
Liquid limit 50 or more	organic	Liquid limit - oven dried < 0.75	OH	Organic clay ^{K,L,M,P} Organic silt ^{K,L,M,O}		
		Liquid limit - not dried < 0.75	OH	Organic clay ^{K,L,M,P} Organic silt ^{K,L,M,O}		
HIGHLY ORGANIC SOILS	Primarily organic matter, dark in color, and organic odor			PT	Peat	

3.1.2 Additives and admixtures

A range of different additives and admixtures were used in this study to develop both self-healing and self-immune soil-cement systems subjected to freeze-thaw cycles. Their detailed description is given in the following subsections. The microscopic images of the additives and admixtures presented in this chapter were taken using a Leica DM2700 optical microscope.

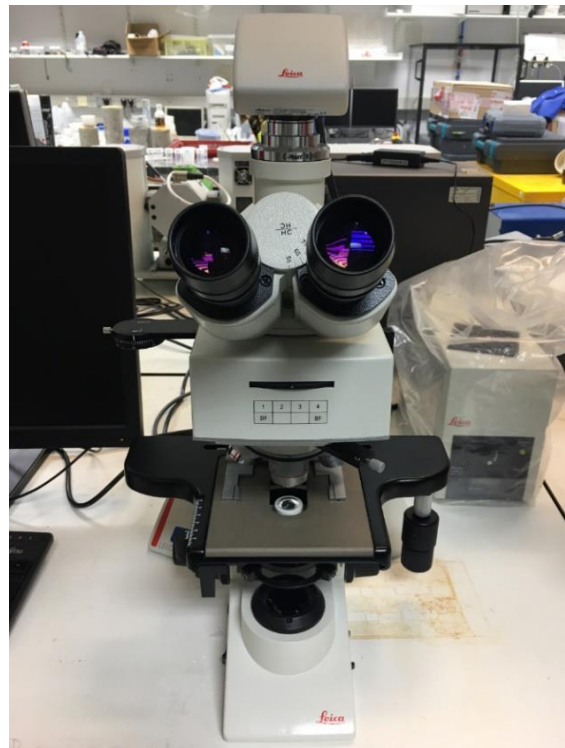
3.1.2.1 Lambson microcapsules

Microcapsules, containing sodium silicate, manufactured by the industrial partner Lambson Limited were used as one of the healing agents for self-healing soil-cement systems in this study (**Figure 3.3**). The microscopic image taken by Leica DM 2700 upright optical microscope (**Figure 3.3c**) is presented in **Figure 3.3a**. The full production procedure as well as microcapsule characterisation is given by Kanellopoulos et al. (2017). The Lambson microcapsules consisted of a gelatine/gum Arabic blend shell materials and encapsulated sodium silicate in an oil emulsion. The encapsulated cargo consisted of 41% sodium silicate, 55% mineral oil and 4% emulsifier. The microcapsules had an average diameter of ~200–300 μm and the shell thickness was 5–20 μm and a density of 0.98 g/cm^3 (Kanellopoulos et al., 2016). Before being added into the soil-cement mixtures, the Lambson microcapsules were first collected from the preserving solution in which they were stored and then extracted and washed by using water, filter paper and a vacuum pump.



(a)

(b)



(c)

Figure 3.3 Images of the Lambson microcapsules used (a) as observed by a Leica DM2700 optical microscope and (b) as observed by the naked eye; and (c) Leica DM 2700 upright optical microscope used.

3.1.2.2 LUVOMAG MgO Pellets

Commercial pellets, LUVOMAG MgO pellets, supplied by Lehmann & Voss, Germany were used in this project to develop self-healing soil-cement systems subjected to freeze-thaw cycles. LUVOMAG MgO pellets were well studied by Alghamri (2017) and used to develop a self-healing concrete, which has shown promising results. An image of the MgO pellets is presented in **Figure 3.4**. The physical properties and chemical compositions of the

LUVOMAG MgO pellets are given in **Table 3.2**. The particle size is 1–2 mm and the density is 3.25 g/cm³.



Figure 3.4 LUVOMAG MgO pellets used in the study.

Table 3.2 Chemical composition and properties of LUVOMAG MgO pellets.

Chemical composition (%)	CaO	SiO ₂	Al ₂ O ₃	Fe ₂ O ₃	MgO	Na ₂ O	TiO ₂	K ₂ O
	3.10	2.47	0.41	1.75	91.76	0.03	0.03	0.04
Loss on ignition LOI (%) = 4.83								
Reactivity* (seconds) = 288±6								
* As measured in laboratory by the chemical reactivity test, detailed in Section 3.1.3 .								

3.1.2.3 SikaAer[®] Solid Microcapsules

SikaAer[®] Solid (SS) microcapsules supplied by Sika Deutschland GmbH were used for developing self-immune soil-cement systems subjected to freeze-thaw cycles. SS microcapsules, with size range of ~5–80 μm, consist of prefabricated air bubbles with an elastic acrylonitril-polymer envelope/shell. Thus, they can provide a controlled air-entrainment. They have a density of 0.2 g/cm³. Optical microscope and scanning electron microscope (SEM) images of SS microcapsules are presented in **Figure 3.5**.

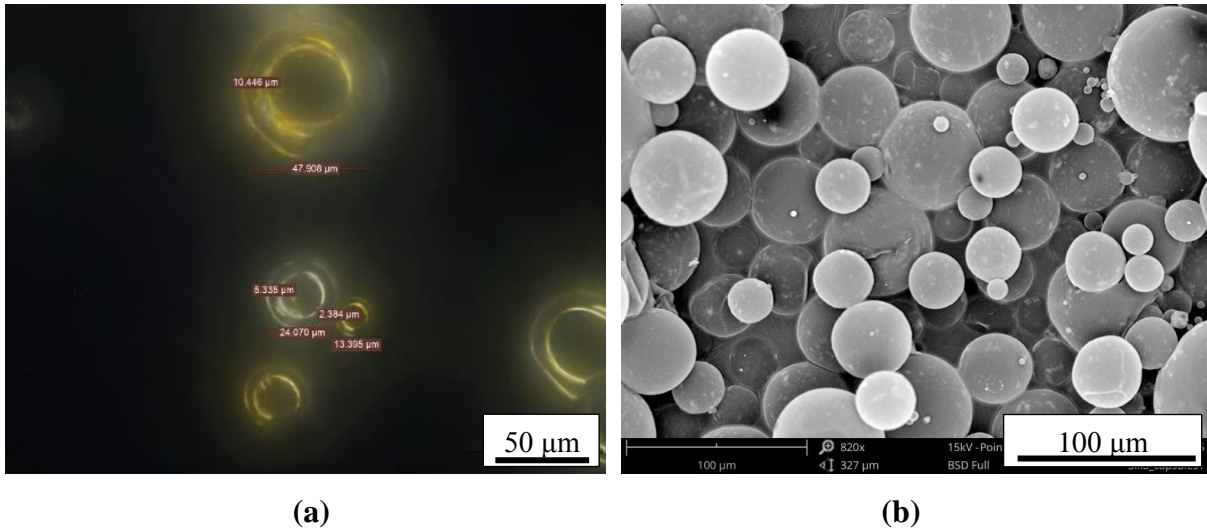


Figure 3.5 Images of the SikaAer[®] Solid microcapsules used in this work (a) an optical microscopic image and (b) a SEM image.

3.1.2.4 Super absorbent polymer (SAP)

SAP A supplied by BASF Chemicals, Germany, a copolymer of acrylamide and sodium acrylate with particle size $\sim 100 \mu\text{m}$, and a density of $\sim 0.75 \text{ g/cm}^3$ was used in this study for the development of self-immune soil-cement system subjected to freeze-thaw cycles. According to the suppliers' information, the polymers have irregular particle shapes as they were produced via the bulk polymerisation technique, followed by crushing into single particles. The images taken with an optical microscope as well as under SEM are presented in **Figure 3.6**.

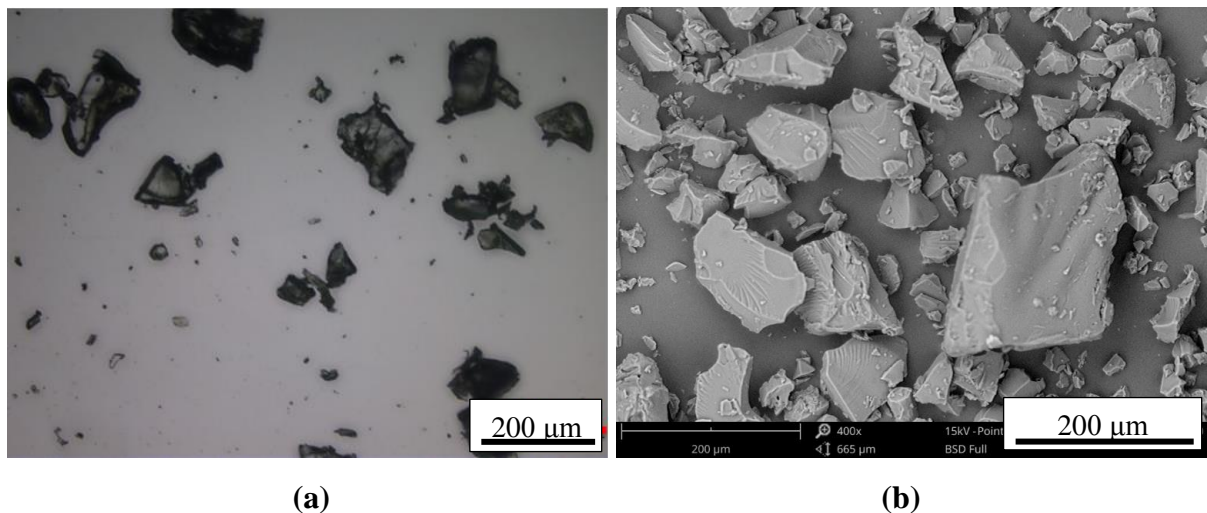


Figure 3.6 Images of the BASF SAP A used in this study (a) observed under an optical microscope and (b) an SEM image.

3.1.3 Chemical reactivity of the MgO pellets

The chemical reactivity of LUVOMAG MgO pellets was measured as the time required for neutralisation of an acidic solution using an accelerated reactivity test as described in Shand (2006) and Jin (2014). A 5 g sample of the LUVOMAG MgO pellets, was reacted with 100 ml of 1 mol/l acetic acid solution in addition to 300 ml of distilled water. The acidic solution with distilled water was kept stirring at a constant speed of 1000 rpm before and after the LUVOMAG MgO pellets were added. A digital pH meter was used to monitor the pH level with time and the reactivity was expressed as the time in seconds required for MgO to completely neutralise the acid (i.e., pH=7).

3.1.4 The tea bag method for the sorptivity of the SAP

The tea bag method (Gruyaert et al., 2016; Mechtcherine and Reinhardt, 2012) was used to measure the absorption characteristics of SAP. Dry SAP powders were placed into a permeable bag, where a known quantity ($M_{\text{sap, dry}}$) was weighed before being submerged in the liquid. The permeable bag with the SAP was then submerged into an excess amount of solution and the weight of the wet SAPs ($M_{\text{sap, wet}}$) was measured every minute for the first 10 minutes. After 10 minutes, $M_{\text{sap, wet}}$ was measured for every 10 minutes until 100 minutes were reached to ensure the equilibrium. The $M_{\text{sap, wet}}$ was measured after the excess solution with the tea bag was removed. The SAP absorption is calculated according to **Eq. 3.1**. It has been suggested by Snoeck et al. (2012) that the fluid held by capillary forces between SAP particles cannot be removed thus leading to a small overestimation of the absorption capacity of SAP. However, SAPs used in this project were all directly mixed with soil-cement mixtures, where capillary forces also exist in this real situation. The method's precision has been suggested to be around $\pm 3.5\%$ (Zohuriaan-Mehr and Kabiri, 2008).

$$\text{SAP}_{\text{absorption}} \text{ (g/g)} = (M_{\text{sap, wet}} - M_{\text{sap, dry}}) / M_{\text{sap, dry}} \quad (3.1)$$

3.1.5 Preparation of cement pore solution

The cement pore solution was produced with a water/cement ratio of 1.67, which is the water/cement ratio of soil-cement system with 25% water content and 15% cement content. As shown in **Figure 3.7**, 300 g of cement and 500 g of water was mixed firstly and then filtrated by using filter paper, filtration funnel, glass flask, and a vacuum pump.



Figure 3.7 Production of cement pore solution.

3.2 Preparation of test specimens

The model soil produced in this study composed of 85% sand and 15% clay. Three cement contents, 10%, 15% and 20% were used and the corresponding water/cement ratio used were 2.5, 1.67 and 1.25, respectively. Samples containing the different agents (e.g. microcapsules, pellets and SAPs) and varying dosages were prepared. Different mix designs were prepared and details of mixing proportions are summarised in **Table 3.3**. Sample identification involves concatenation of the (i) mix cement content; (ii) agent used (L refers to Lambson microcapsules, P refers to LUVOMAG MgO pellets, S refers to SikaAer[®] Solid and SAP refers to SAP A); and (iii) dosage of the agent. For instance, C10L10 represents a 10% cemented soil sample containing Lambson microcapsules that have been added at 10% with respect to the cement mass. Control mixes are identified with its cement content (e.g. C10).

Raw materials including Portland cement, Polwhite E China Clay, sand and agents were mixed in an automatic mixer as shown in **Figure 3.8a**. A constant mixing time of 10 minutes was used to control the degree of mixing. Samples with a height of 100 mm and diameter of 50 mm were prepared using plastic cylindrical moulds (**Figure 3.8c**) while disc samples with a height of 10 mm and diameter of 50 mm were prepared by using silica gel moulds (**Figure 3.8d**). A vertical cut was created on the side of the plastic cylindrical moulds and a thin layer of Vaseline was spread on the inner wall in order to facilitate the demoulding process. The

soil-cement mixture was poured into to the plastic mould in 3 layers and the samples were oscillated for 2 minute for each layer in order to provide a uniform, adequate and similar compaction for each sample as shown in **Figure 3.8b**. As a result, relatively uniform samples with similar density can be made for each series of mix. Control samples and self-healing/self-immune samples with agents were both prepared. All specimens were mixed in a standard laboratory environment with a temperature of 21 °C (± 2 °C) and 50% ($\pm 10\%$) relative humidity (RH). Triplicate samples were prepared for each case to ensure repeatability.

Table 3.3 The compositions of soil-cement mixes prepared.

Mix ID	Mix composition ratios/mass (%)				Agent
	Sand	Clay	Cement	Water	
C10	85	15	10	25	-
C15			15		-
C20			20		-
C10LX*			10		Lambson microcapsules
C15LX*			15		
C20LX*			20		
C15PX*			15		LUVOMAG MgO pellets
C20PX*			20		
C10SX*			10		SikaAer® Solid
C15SX*			15		
C15SAPX*			15		

Note: all the percentage in this table are proportional to the total mass of soil solid; and (*) X represented the dosage of the agent to the cement mass in corresponding mix.



(a)



(b)



(c)



(d)

Figure 3.8 (a) The automatic mixer, (b) samples vibrated on a vibrating table, (c) a plastic mould for the soil-cement samples, and (d) a silica gel mould for the disc samples.

3.3 Curing conditions for sample preparation, freeze-thaw exposure and self-healing

All specimens were placed in a high humidity environment of 97% ($\pm 3\%$) RH and with a temperature of 21 °C (± 2 °C) for curing. Before testing, specimens were generally cured for 7 days. A high humidity was chosen for curing because soil-cement systems under frost attack are generally surrounded by moist soil with high humidity. The high humidity was achieved by placing specimens in plastic box containers, which contained 20 mm gravel at the base,

saturated to 15 mm with water to maintain humidity, as shown in **Figure 3.9a**. A relatively constant and high RH also prevents the potential effect of wet-dry exposure. As for the self-healing curing, self-healing samples were allowed to self-heal for a certain period after a corresponding number of freeze-thaw cycles. The self-healing curing condition is the same with that of sample preparation.

Damage scenarios under different numbers of freeze-thaw cycles were performed to specimens. The freeze-thaw curing was conducted as per ASTM: D560/D560M-15 (2015). During the freeze-thaw curing, each freeze-thaw cycle consisted of 24 hours of all-round freezing at $-25\text{ }^{\circ}\text{C}$ ($\pm 1\text{ }^{\circ}\text{C}$) and 23 hour of thawing in a room temperature of $21\text{ }^{\circ}\text{C}$ ($\pm 2\text{ }^{\circ}\text{C}$). It should be noted that under the thawing process, the samples were treated in an ambience with a moist condition of 97% ($\pm 3\%$) RH so that it can absorb moisture from the atmosphere. During both freezing and thawing, samples were placed on absorbent pads and free potable water was made available under the absorbent pads (open system). The freeze-thaw curing of samples is presented in **Figure 3.9b-c**. Many studies reported that the physical properties of cemented soil stabilise after 8 to 10 freeze-thaw cycles (Wang et al., 2016; Wang et al., 2017). Therefore, most of the samples in this test experienced up to 10 freeze-thaw cycles unless for samples highly durable to freeze-thaw deterioration.



(a)



(b)



(c)

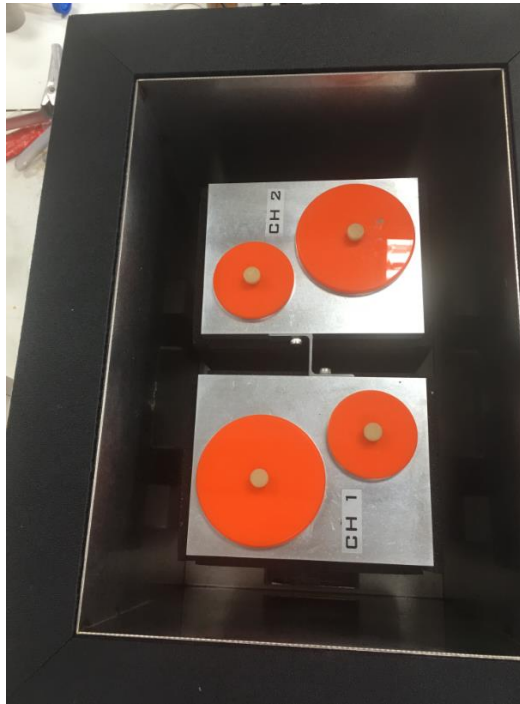
Figure 3.9 (a) The curing tank with 97% ($\pm 3\%$) RH, (b) the freezer used in the experiments, and (c) samples in a thawing tank.

3.4 Fresh properties of soil-cement

3.4.1 Isothermal calorimetry

A Calmetrix I-Cal 2000 HPC High Precision Isothermal Calorimeter (**Figure 3.10a**) compliant with ASTM: C1679-14 (2014) was used to measure the heat of hydration for soil-cement samples incorporating agent additions. Heat evolution associated with endothermic or exothermic reactions can be measured by isothermal calorimeter. Isothermal calorimetry is an excellent technique to investigate the cement hydration process by quantifying the heat transfer. In this study, it was used to evaluate the influence of addition of pellets, microcapsule and SAPs on the hydration process of the soil-cement mixes. The total soil added is 40 g and the quantities of cement, water, and agents used were according to the composition of soil-cement mixtures mentioned in **Section 3.2**. For example, mix C15S1.67 contains 34 g of sand, 6 g of clay, 6 g of cement, 10 g of water, and 0.1 g of SikaAer[®] Solid microcapsules. Testing began by setting the thermostat to 23 °C and left to stabilize for 24 hours. Pre-conditioning of the cement powder and water took place for 2 hours before all ingredients were mixed together for one minute using a plastic spoon. After mixing, the plastic spoon was left inside the sample cup during testing to avoid loss of testing mixtures. Logging of the heat of hydration and the cumulative heat production was carried out for 48 hours. A typical relationship between the thermal power released and the time since mixing is

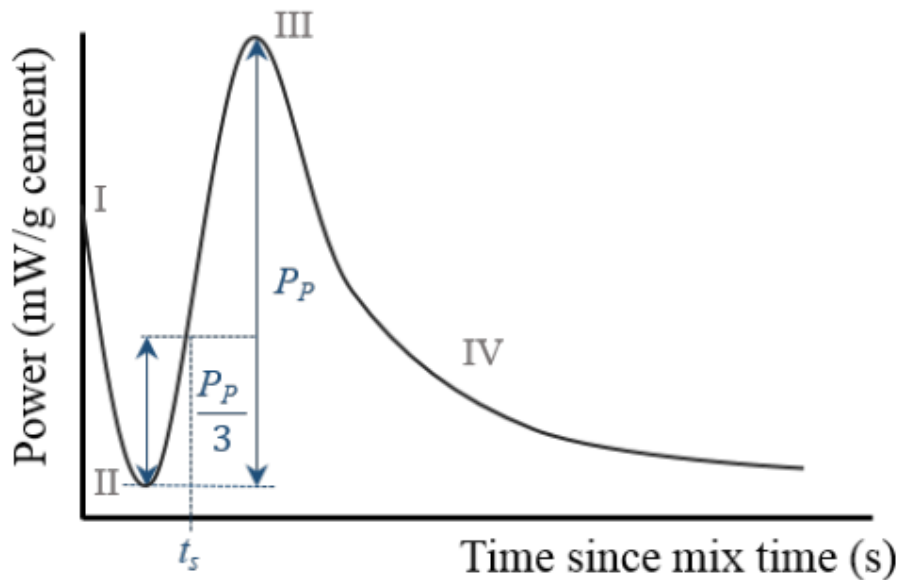
given in **Figure 3.10c**. The peak power P_P was then calculated as the maximum power (first peak) minus the power during the induction period (first trough). The initial setting time was then calculated as the time at one-third of the peak power (**Figure 3.10c**). Duplicate samples were tested for each mix and plots of cumulative energy released were also analysed.



(a)



(b)



(c)

Figure 3.10 (a) the Calmetrix I-Cal 2000 HPC High Precision Isothermal Calorimeter used, (b) a laptop connected for data logging, and (c) typical relationship between thermal power and time for cement hydration samples (Nelson, 1990).

3.4.2 Workability

To determine the effect of adding self-healing and self-immunity agents on the flow characteristics of the fresh soil-cement mixes, flow table tests were conducted according to BS EN 1015-3:1999. The flow table apparatus used was supplied by Controls Group (**Figure 3.11**). The truncated conical mould (larger base at the bottom) with its funnel was set centrally on the disc of the flow table. The soil-cement mix was poured into the mould in two layers, each layer being compacted by 10 short strokes of the tamper to ensure uniform filling of the mould. When the mould was filled with soil-cement mixture, excess soil-cement was skimmed off with a palette knife. The disc was then carefully cleaned of any paste or water. After 15 seconds, the mould was lifted vertically and the disc with fresh soil-cement mixture was jolted 15 times at a constant frequency of one per second to spread out the paste. Finally, the diameter of the paste spread was measured in three directions at each angle of 120° and the average was calculated to the nearest mm. The test was replicated for each mix.



Figure 3.11 The flow table equipment used.



3.5 Experimental methods to verify self-healing and self-immune performance and mechanisms of soil-cement systems subjected to freeze-thaw cycles

After being cured for a specific period (7 days), samples were demoulded and labelled. Laboratory tests were conducted on laboratory modelled soil-cement samples. The experimental programme for the self-healing and self-immunity performance of all soil-cement mixes after freeze-thaw cycles is presented in **Table 3.4** and **Table 3.5**, respectively. To verify the self-healing capabilities, after a certain number of freeze-thaw cycles (e.g. 10 freeze-thaw cycles), the samples were allowed to self-heal for a certain period of time (e.g. 7, 14, 28, and 60 days). The highest number of freeze-thaw cycles carried out depends on the cement content of a mix. For instance, C10, C15 and C20 mixes are subjected to up to 4, 10 and 12 freeze-thaw cycles, respectively. As for the healing period, the Lambson samples were healed for 7 days as its healing rate is relatively fast. On the contrary, the healing rate of MgO pellets samples is relatively slow hence their healing period was prolonged to up to 90 days. Unconfined compressive strength (UCS) was determined for both cylindrical (with 50 mm in diameter \times 100 mm high) samples embedded with Lambson microcapsules and MgO pellets. Hydraulic conductivity test were carried on MgO pellets samples as MgO pellets are anticipated to have the potential to seal cracks. Splitting tensile test, optical microscopic analysis, gas permeability and microstructure analysis of extracted samples were also conducted on disc (with 50 mm in diameter \times 10 mm high) MgO pellets samples to verify the self-healing capabilities.

As for the self-immune soil-cement samples (with SS microcapsules and SAP), their engineering properties were investigated and their performance was compared with the control samples that subjected to a same amount of freeze-thaw cycles (e.g. 0, 1, 5, and 10 freeze-thaw cycles). The self-immunity capability of soil-cement systems were verified by various testing techniques. Volume measurement, moisture content, dry density, porosity, UCS, and hydraulic conductivity were conducted on cylindrical samples. Disc samples were used for tensile splitting and optical microscopy analysis. Small cubes of 3 mm \times 3 mm \times 3 mm were used for high-resolution X-ray computed microtomography (μ CT) to investigate the microstructure of samples.

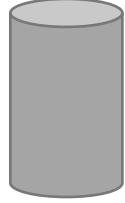


Further details of the experimental programme for different soil-cement systems are presented in the second section of **Chapters 4–6**.

Table 3.4 Experimental programme for investigating the self-healing performance of soil-cement specimens.

Specimen type	Agent	Cement content (% by soil weight)	Number of freeze-thaw cycles	Healing period (days)					
				0	7	14	28	60	90
Cylinder: (Ø50×100) mm 	-	10	0, 1, 2, 3, 4	UCS	UCS	-	-	-	-
		15	0, 1, 5, 10	UCS, HC	UCS, HC	UCS, HC	UCS, HC	UCS, HC	UCS, HC
		20	0, 1, 5, 12	UCS	UCS	-	-	-	-
	Lambson	10	0, 1, 2, 3, 4	UCS	UCS	-	-	-	-
		15	0, 1, 5, 10	UCS	UCS	-	-	-	-
		20	0, 1, 5, 12	UCS	UCS	-	-	-	-
	MgO pellets	15	0, 1, 5, 10	UCS, HC	UCS, HC	UCS, HC	UCS, HC	UCS, HC	UCS, HC
		20	0, 1, 5, 12	UCS	UCS	-	-	-	-
Disc: (Ø50×10) mm 	-	20	0, 1, 5, 10	ST, OM, MA, GP	ST, OM, MA, GP	ST, OM, MA, GP	ST, OM, MA, GP	ST, OM, MA, GP	ST, OM, MA, GP
	MgO pellets	20	0, 1, 5, 10	ST, OM, MA, GP	ST, OM, MA, GP	ST, OM, MA, GP	ST, OM, MA, GP	ST, OM, MA, GP	ST, OM, MA, GP

Note: The samples are initially cured for 7 days before testing. **UCS**: Uniaxial compressive test; **ST**: Splitting tensile test; **HC**: hydraulic conductivity test; **OM**: Optical microscopic analysis; **GP**: Gas permeability; **MA**: Microstructure analysis of extracted samples.

Table 3.5 Experimental programme for investigating the self-immunity performance of soil-cement specimens.

Specimen type	Agent	Cement content (% by soil weight)	Number of freeze-thaw cycles				
			0	1	5	10	20
Cylinder: (Ø50×100) mm 	-	15	UCS, HC	UCS, HC	UCS, HC	UCS, HC	-
	SikaAer® Solid		UCS, HC	UCS, HC	UCS, HC	UCS, HC	UCS, HC
	SAP		UCS, HC	UCS, HC	UCS, HC	UCS, HC	UCS, HC
Disc: (Ø50×10) mm 	-		ST, OM	ST, OM	ST, OM	ST, OM	-
	SikaAer® Solid		ST, OM	ST, OM	ST, OM	ST, OM	OM
	SAP		ST, OM	ST, OM	ST, OM	ST, OM	OM
Cube: (~3×3×3) mm 	-		μCT	μCT			
	SikaAer® Solid		μCT	μCT			
	SAP		μCT	μCT			

Note: The samples are initially cured for 7 days before testing. **UCS**: Uniaxial compressive test; **ST**: Splitting tensile test; **HC**: hydraulic conductivity test; **OM**: Optical microscopic analysis; **μCT**: high resolution X-ray computed microtomography.

3.5.1 Volume, water content and dry density

The diameter and length of the samples were measured by electronic vernier callipers as shown in **Figure 3.12**. Each dimension was measured in three directions at each angle of 120° to obtain average values at the nearest 0.1 mm. Debris collected from uniaxial compressive strength test was dried in an oven at a temperature of 110°C ($\pm 5^\circ\text{C}$) to a constant mass. The loss of mass due to drying is considered to be water in the soil-cement specimen (ASTM: D2216-10, 2010). The water content was calculated using the mass of water and the mass of the dry specimen. **Figure 3.13** presents the electronic balance and the oven used for water content measurement. The dry density of soil-cement samples was determined by using the direct measurement described in ASTM: D7263-09 (2009).



Figure 3.12 Dimension measurements.



(a)



(b)

Figure 3.13 Water content measurements using (a) electronic balance for weight measurements, and (b) oven for drying the samples.

3.5.2 Porosity test

It is commonly believed that the volume and porosity of the soil increase after experiencing freeze-thaw cycles if the soil does not consolidate (Xie et al., 2015). Many researchers suggested that the freeze-thaw resistance of concrete is highly related to the degree of saturation (Fagerlund, 1975, Li et al., 2011). As a result, the variation in porosity, degree of saturation and air content of self-healing and self-immune soil-cement systems were investigated. In this work, the porosity, degree of saturation, and air content of the specimens were calculated according to ASTM: D7263-09 (2009). The porosity (n) is the ratio of the volume of voids to the total volume of the soil:

$$n = \frac{V_v}{V} = \frac{V - V_s}{V} = 1 - \frac{\rho_d}{1000G_s} \quad (3.2)$$

The degree of saturation (S_r) is the ratio of the volume of water to the total volume of the void space:

$$S_r = \frac{V_w}{V_v} = \frac{wG_s}{e} \times 100\% \quad (3.3)$$

The air content (A) is the ratio of the volume of air to the total volume of the soil-cement:

$$A = \frac{V_a}{V} = (1 - S_r)n \times 100\% \quad (3.4)$$

where,

ρ_d = dry density of the soil-cement specimen, kg/m^3 , as determined by the method described in **Section 3.5.1**,

w = water content of soil-cement specimen, %, as determined by the method described in **Section 3.5.1**,

n = porosity, %,

$e = n/(1-n)$, void ratio,

S_r = degree of saturation, %,

V_v = volume of voids in soil-cement specimen, cm^3 ,

V_s = volume of solids in soil-cement specimen, cm^3 ,

V_w = volume of water in soil-cement specimen, cm^3 ,

V_a = volume of air in soil-cement specimen, cm^3 ,

V = volume of soil-cement specimen, cm^3 ,

A = air content of soil-cement specimen, %.

G_s = specific gravity of soil solids in soil-cement specimen,

The specific gravity of the soil-cement particles (G_s) was determined by the test method in ASTM: D854-10 (2010). The soil-cement debris was collected after UCS tests and was oven dried for at least 24 hours. The debris were then crushed (**Figure 3.14a**) so that all the soil-cement solids pass the 4.75 mm (No. 4) sieve. At the start of the test, the mass of the 250 mL pycnometer and the mass of it containing 250 mL of de-air water were measured. About 50g of the dried and crushed soil-cement solids were weighted to nearest 0.01 g before transferred into the 250 mL dry pycnometer with a funnel. Soil particles remaining on the funnel was rinse into the pycnometer by using a wash/spray squirt bottle. Soil-cement slurry was then formed by adding more water into the pycnometer until the water level is between 1/3 and 1/2 of the depth. After that, the soil-cement slurry was boiling for at least 2 hours after it came to a full boil (**Figure 3.14b**), and agitation was adopted if necessary. Finally, the pycnometer was carefully filled with de-aired water to its 250 mL capacity after the pycnometer and the

soil-cement slurry cooled down to 20°C. The mass of pycnometer with water and soil-cement solids at the test temperature (20°C) were recorded.

The specific gravity of the soil-cement particles (G_s) is calculated by

$$G_s = \frac{\rho_s}{\rho_w} = \frac{M_s}{M_{pw} - (M_{pws} - M_s)} \quad (3.5)$$

where:

M_{pw} = mass of the pycnometer and water at 20°C, g,

M_p = the mass of the dry pycnometer, g,

V_p = the volume of the pycnometer, mL,

ρ_w = the density of water at 20°C = 0.99821 g/mL,

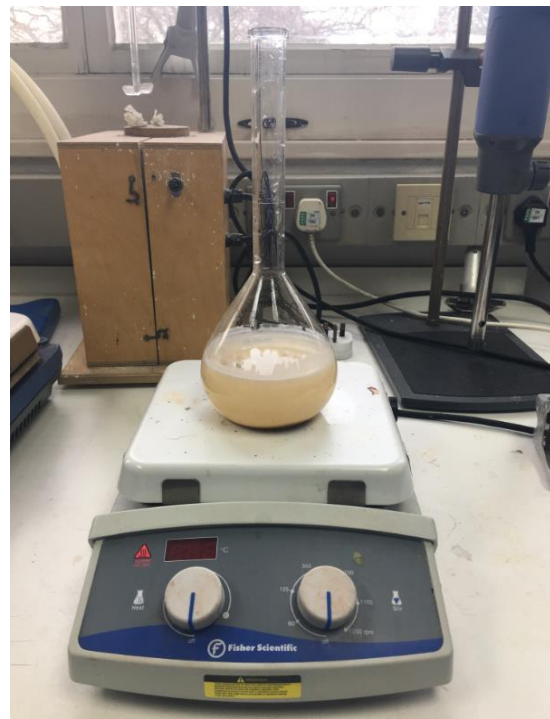
ρ_s = the density of the soil solids g/cm³,

M_s = the mass of the oven dry soil solids (g) and,

M_{pws} = the mass of pycnometer, water, and soil solids at 20°C, g.



(a)



(b)

Figure 3.14 (a) Mortar and pestle and, (b) boiling the soil-cement slurry on a thermometric device.

3.5.3 Strength properties

3.5.3.1 Uniaxial compressive strength (UCS) test

The strength of soil-cement systems may suffer a great degradation due to the freeze-thaw cycles. In this project, the UCS was determined in triplicates based on ASTM: D4219-08 (2008) by using a Controls Testing Uniframe 70-T0108/E loading frame as presented in **Figure 3.15**. Cylindrical samples of diameter 50 mm ×100 mm height were used in this test. A plastic bag was used to surround each sample so as to avoid contaminating the surrounding environment. The UCS test was then started by applying a constant axial strain rate of 1% per minute until failure. The UCS was determined from the axial load at failure in relation to the initial cross sectional area of the test sample as presented in **Eq. 3.6**. The secant modulus E_{50} can also be determined from the stress-strain curve. Regain in mechanical properties including UCS and stiffness of self-healing soil-cement can also be studied.

$$f_c = \frac{P_{max}}{A} \quad (3.6)$$

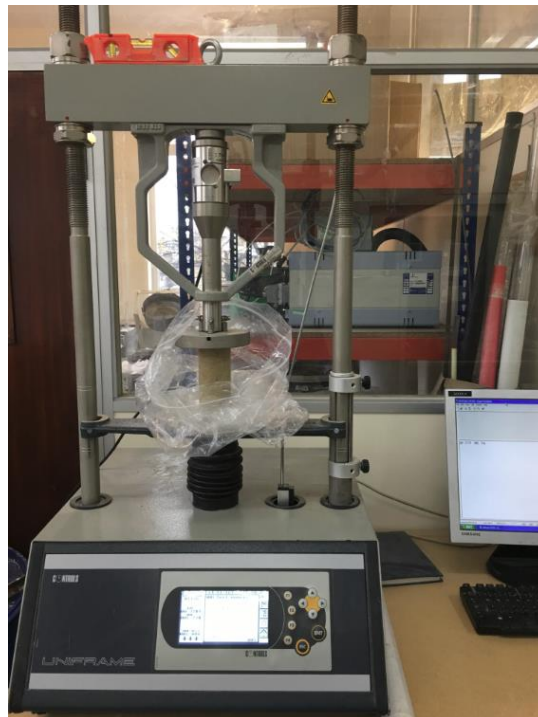


Figure 3.15 Sample tested by Uniframe 70-T0108/E Control Machine.

3.5.3.2 Splitting tensile strength test

The tensile strength of specimen directly reflects the adhesion and bonding between the soil-cement particles. Consequently, this parameter can help to examining the effect of freeze-

thaw cycles on self-immune soil-cement systems and the healing mechanism of self-healing soil-cement samples. Splitting tensile strength tests were carried out following ASTM: C496/C496M-11 (2011). Hardened soil-cement discs of 10 mm depth and 50 mm diameter were used in this test. Triplicate discs were tested for each series of mix. The soil-cement disc was placed in the testing machine as shown in **Figure 3.16**. The loading was applied by using the same machine used for the UCS test. The peak load (F) was recorded in N, and the tensile strength is determined using **Eq. 3.7**:

$$\sigma_t = \frac{2F}{\pi Ld} \quad (3.7)$$

Where, σ_t = tensile splitting strength (N/mm²), L = the length of the contact line of specimen, and d = diameter of the cylindrical specimen.

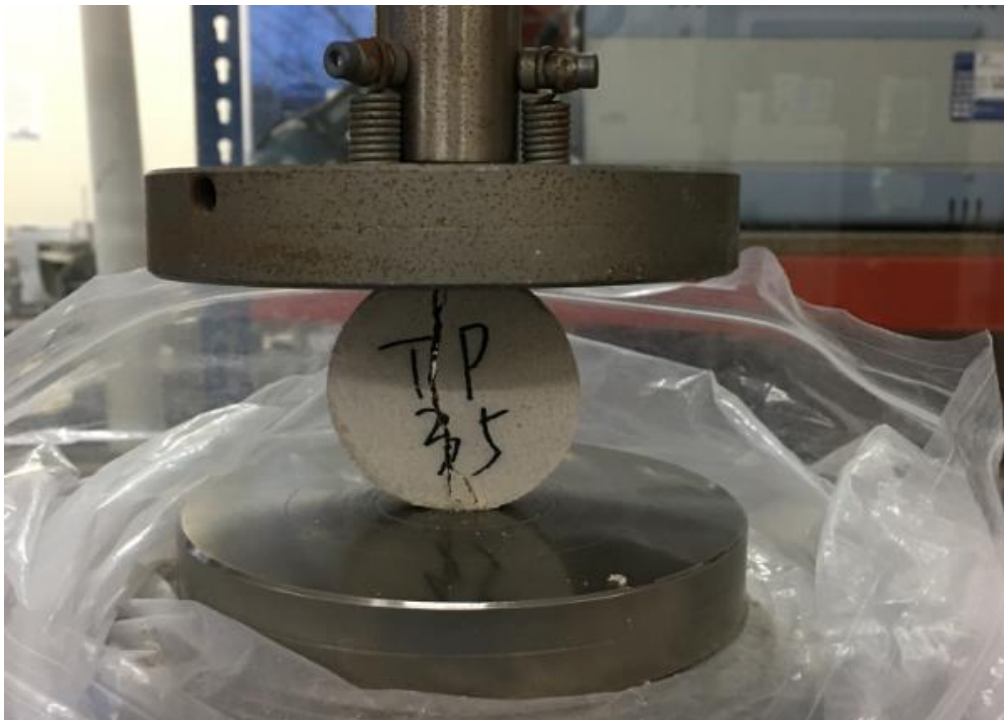


Figure 3.16 Splitting tensile test setup.

3.5.4 Hydraulic conductivity *k*

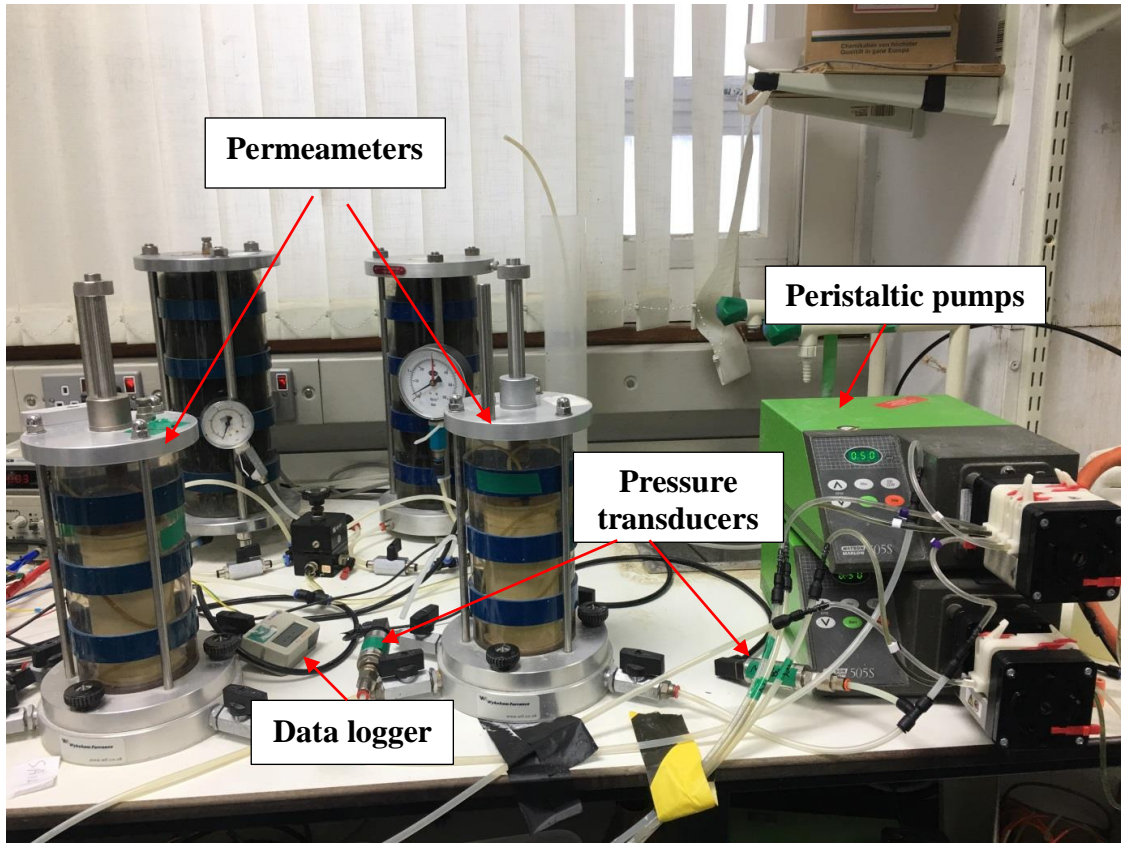
The water permeability depends primarily on the average size of the pores, which in turn is related to the distribution of particle sizes, particle shape and soil structure. As a result, the water permeability reflects the water tightness, cracking status and the change of void ratio of self-healing and self-immune soil-cement systems after freeze-thaw cycles. In this work, the hydraulic conductivity *k* of the specimens was measured according to ASTM: D5084-16 (2016) (Flexible-wall method). Soil-cement cylinders with diameter of 50 mm and height of

100 mm were used in this test. The specimen tested was positioned on the pedestal at the base of a permeameter with a porous stone and paper filter placed at both ends of the sample. A latex rubber membrane was secured over the sample with O-rings and the permeameter was sealed closed and filled with water as shown in **Figure 3.17**. De-air water was used as the permeating liquid and duplicate samples were tested.

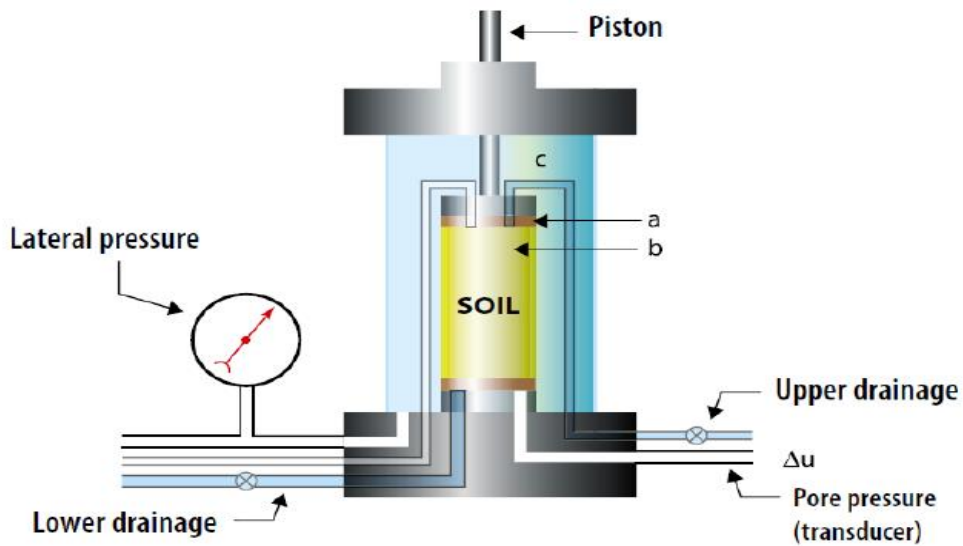
The constant rate of flow method (method D) was adopted as the water permeability of soil-cement sample is relatively low and method D generally requires the shortest period of time. Cell pressure of 400 kPa was used and maintained throughout the test. The samples were left to reach equilibrium at this cell pressure with the inlet and outlet taps open to the atmosphere overnight to allow any consolidation to take place and any build-up of pore water pressure to drop to zero. After that, a constant flow of water was induced using a peristaltic pump connected to the base of the sample flowing to the top of the sample. A transducer was connected to the inflow pipe to measure the pore water pressure generated and the pressure was recorded by a data logger taking readings every five minutes. When a constant flow rate was achieved the volume of water discharged and time interval was recorded. The vertical permeability (k) of the sample is calculated using Darcy's Law:

$$k = \frac{Q \times \gamma_w \times L}{A \times U} \quad (3.8)$$

where: k = coefficient of permeability, Q = quantity of water discharged per unit time, γ_w = unit weight of water, L = length of the sample, A = cross-sectional area of the sample, and U = pore water pressure (as meters of head).



(a)



(b)

Figure 3.17 Permeability testing: (a) the permeameters, peristaltic pumps, pressure transducers and data loggers used, and (b) a schematic set-up for permeability test (courtesy of Controls Group).

3.5.5 Gas permeability test

The gas permeability of soil-cement specimens also reflects the tightness of specimens as the air permeability depends on the distribution and area of cracks as well as volume of voids. The gas permeability test was carried out on disc samples to measure the change in gas permeation performance after freeze-thaw exposure and self-healing. Gas permeability using liquid methanol as the gas source is one of the easiest and fastest way to measure the gas permeability. Cylindrical disk specimen of 10 mm thick and 50 mm diameter was prepared and used in the test. Gas permeability tests were conducted on soil-cement discs after a certain number of freeze-thaw cycles and samples that has been self-healed for a certain period (e.g. 7, 14, 28, and 60 days). The schematic illustration and the experimental setup of the test are shown in **Figure 3.18**.

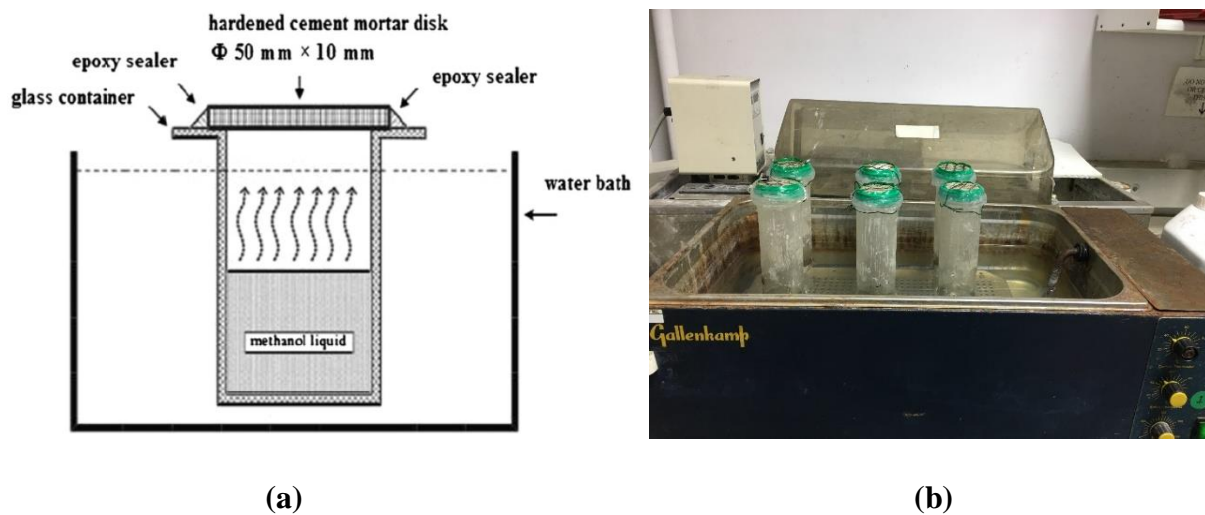


Figure 3.18 The gas permeability tests: (a) a schematic illustration of the experimental setup for the gas permeability test (Yang et al., 2011), and (b) the gas permeability test set-up used.

The liquid methanol gas source based technique was used to evaluate the gas permeability coefficient as described by and (Yang et al., 2011). Discs were fixed with epoxy sealant at the top of the glass pressure cells containing methanol, which were immersed in a 40°C water bath (**Figure 3.18b**). The mass loss with time was recorded in predefined time intervals until a steady-state loss was reached. The air permeability coefficient (k_a) is calculated using the following equations (Yang et al., 2011):

$$k_a = \alpha \frac{L}{A} m^* \quad (3.9)$$

$$\alpha = 2\eta TR_u \frac{P_2}{P_1^2 - P_2^2} \quad (3.10)$$

where L= the length of the sample (m), A = the cross-sectional area perpendicular to the direction of flow (m²), m* = the rate of mass loss (g/hr), and α is a constant for methanol in a particular temperature and pressure difference calculated from η = the dynamic viscosity (Ns/m²), T= the absolute temperature (K), R_u = molecular weight X universal constant (8.3 J/mol K for methanol, P₁ = the inlet pressure (N/m²), and P₂ = the outlet pressure (N/m²).

3.5.6 Optical microscopy and image analysis

Optical microscopy was used in the surface analysis of self-healing and self-immune soil-cement samples. Surface analysis using light optical microscopy can provide insights for the damage formation during freeze-thaw exposure by comparing control and self-immune soil-cement samples. Cylindrical disk specimens with 10 mm thick and 50 mm diameter were prepared for this purpose. A Leica LED2000 optical microscope (**Figure 3.19**) was used to observe crack width induced by the freeze-thaw cycles. Crack healing of self-healing soil-cement samples was also observed by the optical microscopy. Physical crack sealing is an important factor in the self-healing process and is a primary indicator for monitoring its progress. The crack distribution, width, length and area, chemical and mineral admixtures distribution as well as the products of self-healing can be identified. This test also enables visualization of crystal deposition and the determination of healing rate. Images were taken by the microscope in several spots (e.g. 5 spots) on a disc sample and image analysis software was used to analyse the acquired data. The crack formation after freeze-thaw cycles as well as the crack healing was analysed. The crack formation after a certain number of freeze-thaw cycles can be calculated by:

$$CA (\%) = \frac{\sum CA_i}{\sum A_i} \quad (3.11)$$

where,

CA = the crack percentage of soil-cement after subjected to a certain number of freeze-thaw cycles, CA_i = the crack area calculated on the spot i and

A_i = the total area of spot i.

Moreover, the crack-healing efficiency will be evaluated by the percentage of the crack area closure over time, CH (%) using the following equation:

$$CH (\%) = \frac{\sum CA_i - \sum HA_i}{\sum CA_i} \quad (3.12)$$

Where, HA_i = the crack area calculated after a certain healing period.



Figure 3.19 The Leica LED2000 optical microscope used to measure and monitor cracks.

3.5.7 Microstructural analysis

3.5.7.1 Preparation of samples

Thermogravimetric analysis (TGA), scanning electron microscopy (SEM) and energy dispersive X-ray spectroscopy (EDX) tests were employed to characterise the healing products formed as well as the microstructure of self-healing and self-immune soil-cement samples. For TGA, the debris of the samples with different healing period were collected and were ground to the fineness of 75 μm . For SEM and EDX test, small chips of about 5 mm thickness were collected for all the samples. All the samples used in TGA and SEM tests were dried in the oven at 60 $^{\circ}\text{C}$ for at least 24 h and then kept in the vacuum desiccator until the time of testing.

3.5.7.2 Scanning electron microscopy (SEM) and energy dispersive X-ray spectroscopy (EDX)

The scanning electron microscope (SEM) was used to characterise the microstructural surface morphology of the self-healing soil-cement specimens and energy dispersive X-ray spectroscopy (EDX) was used to study the elemental composition. The breakage of embedded capsules was visualised by this test and the healing mechanism and triggering mechanism (freeze-thaw action) can be better understood. Small chipped pieces were carefully collected from the soil-cement specimens that were tested to failure during strength tests. The samples were mounted onto metal stubs using carbon paste and coated with gold film to ensure good conductivity prior to SEM testing. Phenom Pro X Desktop SEM as shown in **Figure 3.20** was used. Samples were scanned and images were captured at different magnifications. EDX was carried out at the same time to determine the chemical composition of the material interested.

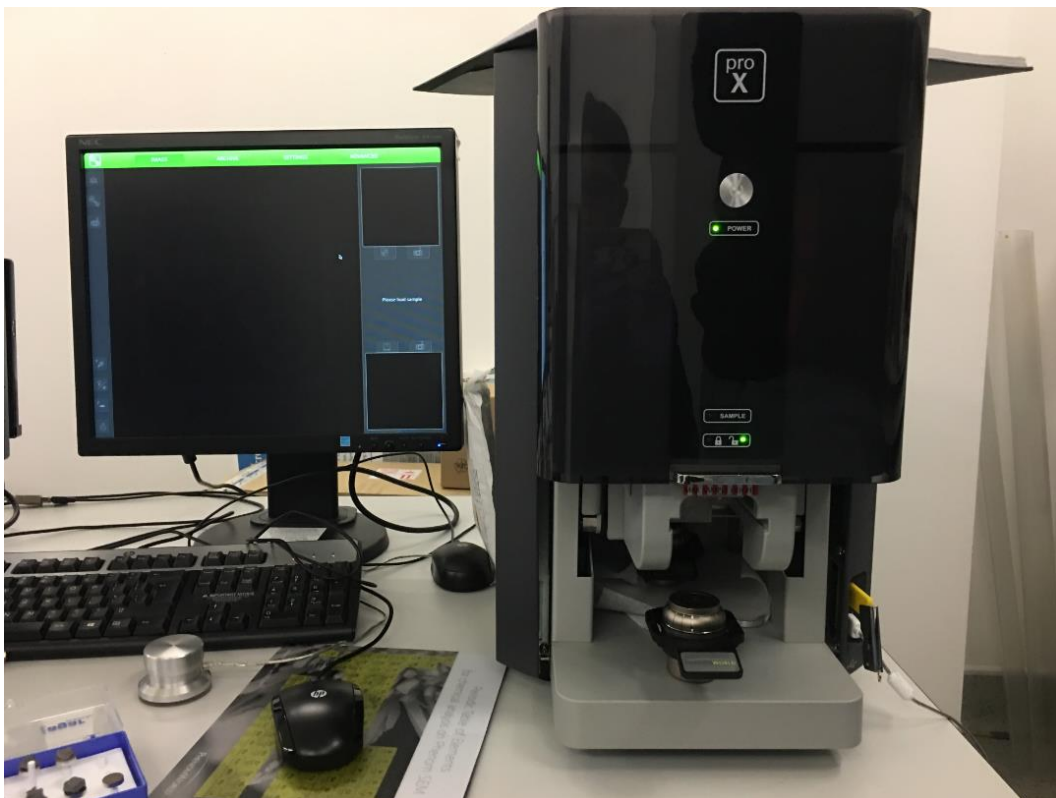


Figure 3.20 The Phenom Pro X Desktop scanning electron microscope (SEM) used.

3.5.7.3 Thermogravimetric analysis (TGA)

TGA of extracted powder was carried out using a Perkin Elmer STA 6000 (**Figure 3.21**). TGA measures weight, temperature, and temperature change with precision while heating the

samples. During the TGA test, small amount of the collected powder (20 ± 2 mg) was introduced into the ceramic crucible. After that, the sample was heated up from 30°C to 1000°C at a constant rate of $10^\circ\text{C}/\text{min}$. Thermogravimetric and DTG (first derivative of the thermogravimetric data) curves were obtained by plotting normalised sample weight (%) with sample temperature ($^\circ\text{C}$). Different materials were identified based on their thermal characteristics in DTG.

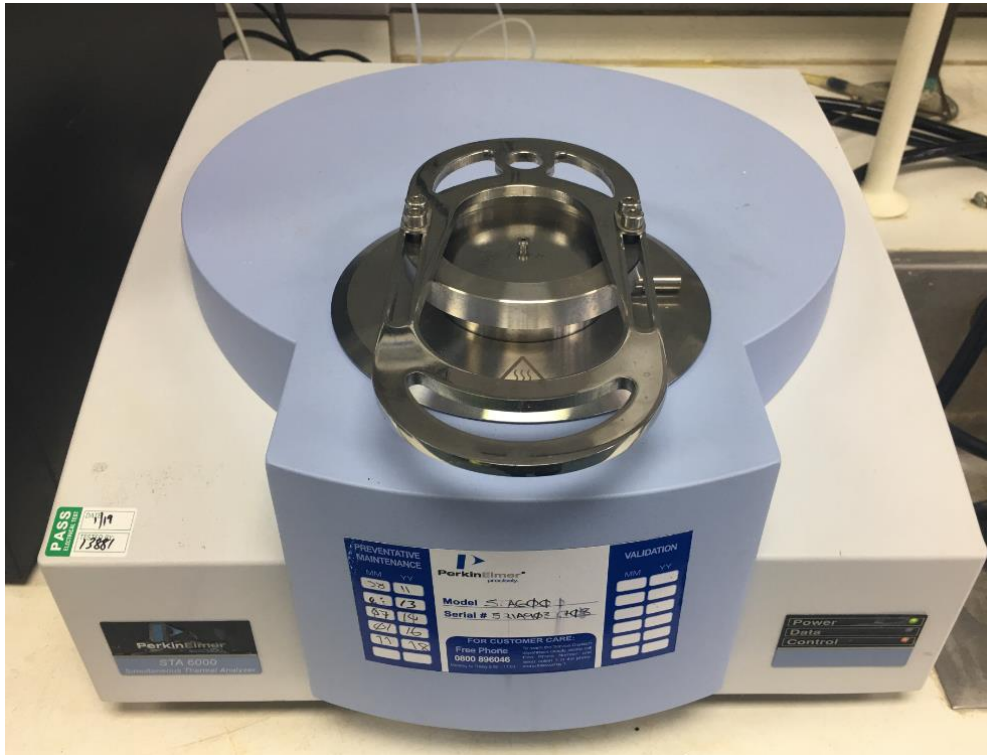


Figure 3.21 The Perkin Elmer STA 6000 thermogravimetric analysis system used.

3.5.8 High-resolution X-ray computed microtomography (μCT)

High-resolution X-ray computed microtomography (μCT) is an experimental method that uses X-rays to create cross-section of a physical object, which can be used to reconstruct a virtual model (3D model) without damaging the original object. High-resolution X-ray μCT provides high-resolution scanning results as the pixel size of the generated cross-sections are in the micrometre range. As a result, the microstructure of the soil-cement samples can be examined and revealed by the μCT . The X-ray CT scanner used in this study was the Nikon XT H 225 ST industrial CT scanning apparatus (**Figure 3.22**). This apparatus had 225 kV microfocus X-ray source with $3\ \mu\text{m}$ focal spot size. Thus, it was able to produce high-resolution cross-sections of the soil-cement samples with 3 micron spot size. The obtained resolution is an important factor to consider and the resolution of the image obtained was

2000×2000 pixels. Larger objects were imaged at a lower magnification and consequently at an inferior resolution than smaller samples. Therefore, the soil-cement samples used in the μ CT scan has a size of 3 mm×3 mm×3 mm as previously presented in **Table 3.5**. Control samples as well as samples embedded with SS microcapsules or SAPs were scanned. Duplicates were tested for each series of mix.



Figure 3.22 Nikon XT H 225 ST industrial CT scanning apparatus used.

Chapter 4 Development and Performance of Self-healing Soil-cement Systems using Microcapsules and Pellets subjected to Freeze-thaw Cycles

4.1 Introduction

This chapter details attempts to develop a self-healing soil-cement system subjected to freeze-thaw cycles. Based on the previous research reviewed in **Chapter 2**, two different materials, microcapsules (produced by Lambson) and LUVOMAG MgO pellets, were added to soil-cement mixes, and their self-healing capability was investigated. These two healing materials were both proven to be effective for applications in cementitious materials such as concrete, mortar, and cement paste (Giannaros et al., 2016; Mao, 2018; Alghamri, 2017). Details of the Lambson microcapsules and MgO pellets were provided in **Section 3.1.2**. As reviewed in Chapter 2, the Lambson microcapsules were selected as a healing agent for soil-cement not only because they can survive the mixing process intact, but also because they break easily in hardened cementitious materials upon their intersection by a crack. Their cargo material, liquid sodium silicate in an oil emulsion, reacts with the cement hydration product calcium hydroxide to form C-S-H gel. LUVOMAG MgO pellets were also selected, as they have a huge potential to provide good sealing capability for the cracks generated by the freeze-thaw cycles. The presence of water in the freeze-thaw-induced cracks can initiate and enhance the healing process for the MgO pellets.

This chapter describes a range of tests (including isothermal calorimetry tests, unconfined compression strength tests, tensile tests, optical microscopy tests, hydraulic conductivity tests, and gas permeability tests) that were performed to verify and quantify the self-healing capability of healing agents. Furthermore, a series of microstructural analysis techniques were used to characterise the healing products formed by the agents in order to reveal their self-healing mechanism. Scanning electron microscopy (SEM), energy-dispersive X-ray spectroscopy (EDX), and thermogravimetric analysis (TGA) were used for this purpose.

4.2 Materials and mix proportions

Soil-cement mixes, with and without healing materials, were prepared and **Table 4.1–4.2** shows the mix constituents and nomenclatures. Details regarding the preparation of the soil-cement samples and curing conditions were given in **Section 3.3**. Soil-cement mixes containing sand, clay, cement, water and varying quantities of the Lambson microcapsules

and LUVOMAG MgO pellets were prepared. The soil-cement specimens were prepared with three cement contents, namely 10%, 15% and 20%, and with corresponding water-to-cement ratios of 2.5, 1.67 and 1.25, respectively. The Lambson microcapsules were added according to the mass fraction of cement because the reaction of sodium silicate with the cement hydration products is the trigger of the autonomic self-healing. Two dosages of 5% and 10% of the Lambson microcapsules were added in the soil-cement systems. As for the MgO pellets, since their diameter and crushing strength are similar to the sand (Alghamri, 2017), the MgO pellets were added into the soil-cement by replacing the sand that with similar particle size therefore minimised the influence of the particle size distribution, density, and mechanical properties of modelled soil-cement system. Alghamri (2017) suggested that 10% replacement of sand by the MgO pellets would enhance the self-healing capability of mortar without significantly compromising the fresh and hardened properties. Thus, in this study, the MgO pellets were added similarly by replacing 10% of the sand particles of the soil-cement mixes. All the control mixes and the self-healing mixes with different types and quantities of healing agents were labelled accordingly as shown in **Table 4.1–4.2**. For a single mix, all samples shared a similar dry density and triplicate samples were prepared for every single test. A critical and comprehensive review of Lambson microcapsules and the MgO pellets was given in **Section 2.3.3** in terms of their properties and applications in cementitious materials. Characteristics of the healing agents including size, density, and morphology under microscope and SEM were presented in **Section 3.1.2**.

The survivability of the Lambson microcapsules and MgO pellets after freeze-thaw cycles or after mixing within the soil-cement mixes was investigated using a light microscope. The hydration of the fresh soil-cement samples containing the healing materials was tested using isothermal calorimetry whilst the workability was measured by the flow table test. To study the characteristics of the volume, dry density, UCS, Young's modulus, and water permeability, cylindrical samples (50mm diameter × 100mm height) were tested while disc samples (50mm diameter × 10mm height) were used for tensile strength, gas permeability, and surface analysis. The experimental programmes for investigating the self-immune performance of the soil-cement specimens were given previously in **Table 3.4**. All the soil-cement specimens were firstly cured for 7 days before being subjected to freeze-thaw cycles. After 0, 1, 5, 10 (or 12) freeze-thaw cycles, the soil-cement samples were cured to regain their durability and mechanical properties. A variety of techniques were used to assess the

physical properties, strength properties, permeability and microstructure of the soil-cement specimens and the healing products.

Table 4.1 Mix composition of soil-cement samples containing Lambson microcapsules.

Mix ID	Mix ingredients Ratios/mass (%)			Admixture	Mass fraction in cement, m_f (%)	Volume fraction in cement, v_f (%)
	Soil	Water	Cement			
C10	100	25	10	-	-	-
C15			15	-	-	-
C20			20	-	-	-
C10L5			10	Lambson microcapsules	5	15
C10L10			10		10	30
C15L5			15		5	15
C15L10			15		10	30
C20L5			15		5	15

Note: all percentages in this table are proportional to the total mass of soil solid unless otherwise specified.

Table 4.2 Mix composition of soil-cement samples containing MgO pellets.

Mix ID	Mix ingredients ratios/mass (%)				Admixture	Mass fraction in sand m_f (%)
	Sand	Clay	Water	Cement		
C15P10	85	15	25	15	LUVOMAG MgO pellets (1–2 mm)	10
C15P10_S	85	15	25	15	LUVOMAG MgO pellets (0.6–1 mm)	10

Note: all percentages in this table are proportional to the total mass of soil solid unless otherwise specified.

4.3 Effect of freeze-thaw cycles on the physical and mechanical properties of soil-cement systems

4.3.1 Effect of freeze-thaw cycles on the UCS of soil-cement systems

Several reports (Davis et al., 2007, Liu et al., 2010) have suggested that the freeze-thaw durability of soil-cement systems can be improved by increasing the system's cement content. Thus, this section discusses the influence of cement content on the freeze-thaw durability of soil-cement systems in terms of unconfined compressive strength (UCS). Three control mixes, C10, C15, and C20, which have cement contents of 10%, 15%, and 20% respectively, were used. As shown in **Figure 4.1**, the 7-day UCS of the soil-cement samples increased with cement content, and the average 7-day UCS values for the C10, C15, and C20 samples were 1.3 MPa, 3.6 MPa, and 5.8 MPa, respectively. This trend was anticipated, as with more cement added, more cement hydration products can be produced. Therefore, the bonds between soil particles were strengthened.

In terms of the effect of freeze-thaw cycles on UCS, **Figure 4.2** shows that higher cement contents not only increased the 7-day UCS values, but also had a positive effect on the UCS values of the soil-cement systems' freeze-thaw samples. A higher cement content improves the freeze-thaw resistance of the soil-cement system because it reduces the amount of freezable water within the soil-cement matrix, thus increasing the strength of the structure. A wide range of changes in UCS were observed for the three different mixes as they were subjected to varying numbers of freeze-thaw cycles. However, their performance appeared to be dependent on the cement content of the soil-cement. For the C10 sample, UCS decreased from 1.3 MPa to 0.3 MPa after only 2 freeze-thaw cycles, while the UCS of the C15 sample decreased from 3.6 MPa to 0.6 MPa after 10 freeze-thaw cycles. The UCS of the C20 sample reduced from 5.8 MPa to 2.5 MPa after 12 freeze-thaw cycles. The observation that freeze-thaw durability increases with increased cement content is consistent with the results of many other researchers (Altun et al., 2009; Liu et al., 2010; Shibi and Kamei, 2014).

However, as shown in **Figure 4.2**, the UCS of C10 decreased by roughly 72% after as few as two freeze-thaw cycles. Similarly, an 84% decrease in UCS was recorded for C15 after 10 freeze-thaw cycles. Despite having 20% cement content, the UCS of C20 reduced by approximately 57% after 12 freeze-thaw cycles. It appears that, while C20 can survive more freeze-thaw cycles due to its higher initial strength, it is still very vulnerable to repeated freeze-thaw action. It is also important to note that increasing the cement content beyond

ordinary levels represents a less economical, less environmentally friendly option. As a result, it appears that adding more cement to the soil-cement system is not an effective method for improving the freeze-thaw durability of soil-cement system. Thus, an alternative is needed.

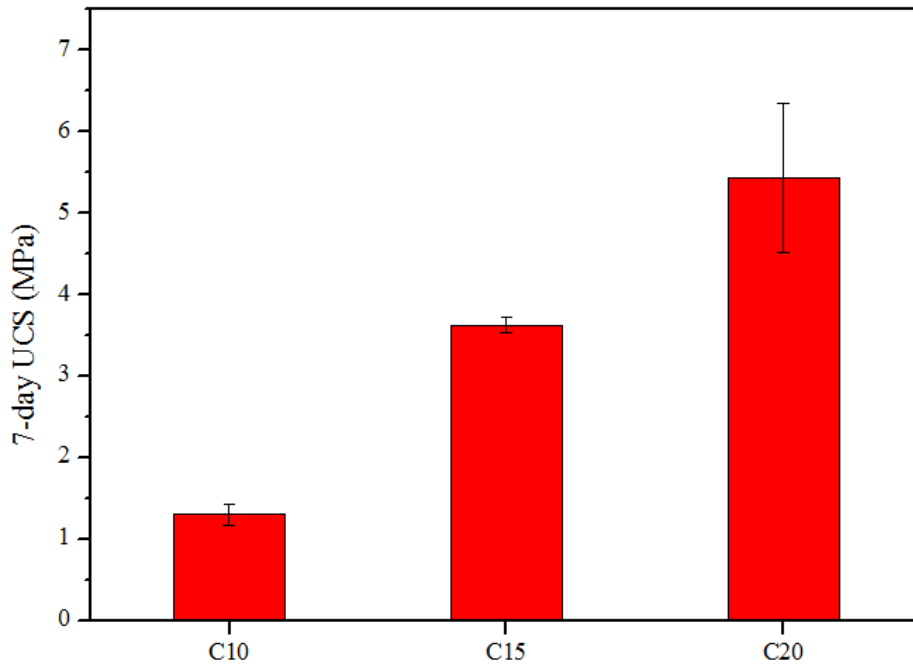


Figure 4.1 7-day UCS values for soil-cement samples with different cement contents.

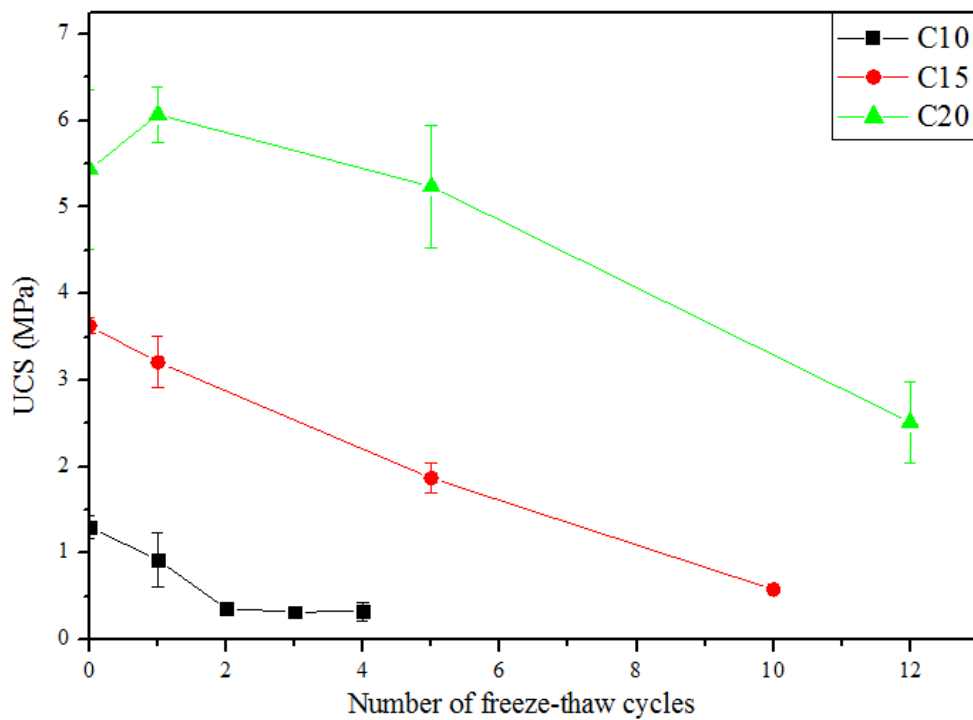


Figure 4.2 UCS values for soil-cement samples with 10%, 15%, and 20% cement content after varying numbers of freeze-thaw cycles.

4.3.2 Mechanisms behind the behaviour of soil-cement systems subject to freeze-thaw cycles

Prior to the development of the self-immune soil-cement systems, the mechanism behind the behaviour of soil-cement systems subjected to freeze-thaw cycles should be understood. As reviewed in **Section 2.1**, even though many studies have examined the behaviour of soil/soil-cement systems under freeze-thaw conditions, there is no general agreement on the precise mechanism by which freeze-thaw damage occurs. Therefore, after summarising the changes that occur in the physical and mechanical properties of control soil-cement samples during freeze-thaw cycles, this section attempts to illuminate the mechanism of the freeze-thaw process.

First, it should be noted that availability of water is a predominant factor that affects the mechanism of the freeze-thaw process for soil-cement systems. In this study, an open system (i.e., a system where the soil-cement system can access water during freeze-thaw curing) was used for freeze-thaw curing, as in-situ soil-cement systems usually have access to water. Soil-cement samples in open systems suffer more freeze-thaw deterioration than similar samples in closed systems, as the freezing of water causes the internal volume expansion within the system that drives the freeze-thaw damage process. For the control mix (C15), water content (**Figure 4.3a**) and the degree of saturation (**Figure 4.3b**) generally increased after freeze-thaw cycles. This is fundamental to the damage the soil-cement system suffers in terms of volume (**Figure 4.3a**), strength, and tightness.

During freezing, the volume of water within the cement increases by 9%. This exerts pressure on the soil-cement matrix, which causes minor pores and fissures to enlarge and become interconnected. When the system thaws, the temperature gradient enables the frozen sample to suck water from the water underneath through the pores and cracks formed during freezing. As more freeze-thaw cycles occur, more and more water is sucked into the soil-cement matrix, and the pores and cracks enlarge further. As a result, the water content, the degree of saturation, and the volume of the soil-cement samples increase with increasing numbers of freeze-thaw cycles. As the pores enlarge and cracks propagate, the volume, porosity (**Figure 4.3c**), and hydraulic conductivity of the soil-cement increase as well. However, the dry density and air content (**Figure 4.3d**) of the soil-cement decreases. Simultaneously, the bonding and cohesion between soil-cement particles weakens. Therefore, the strength and

stiffness of the soil-cement system are reduced. The results presented in **Figure 4.3** support this mechanism.

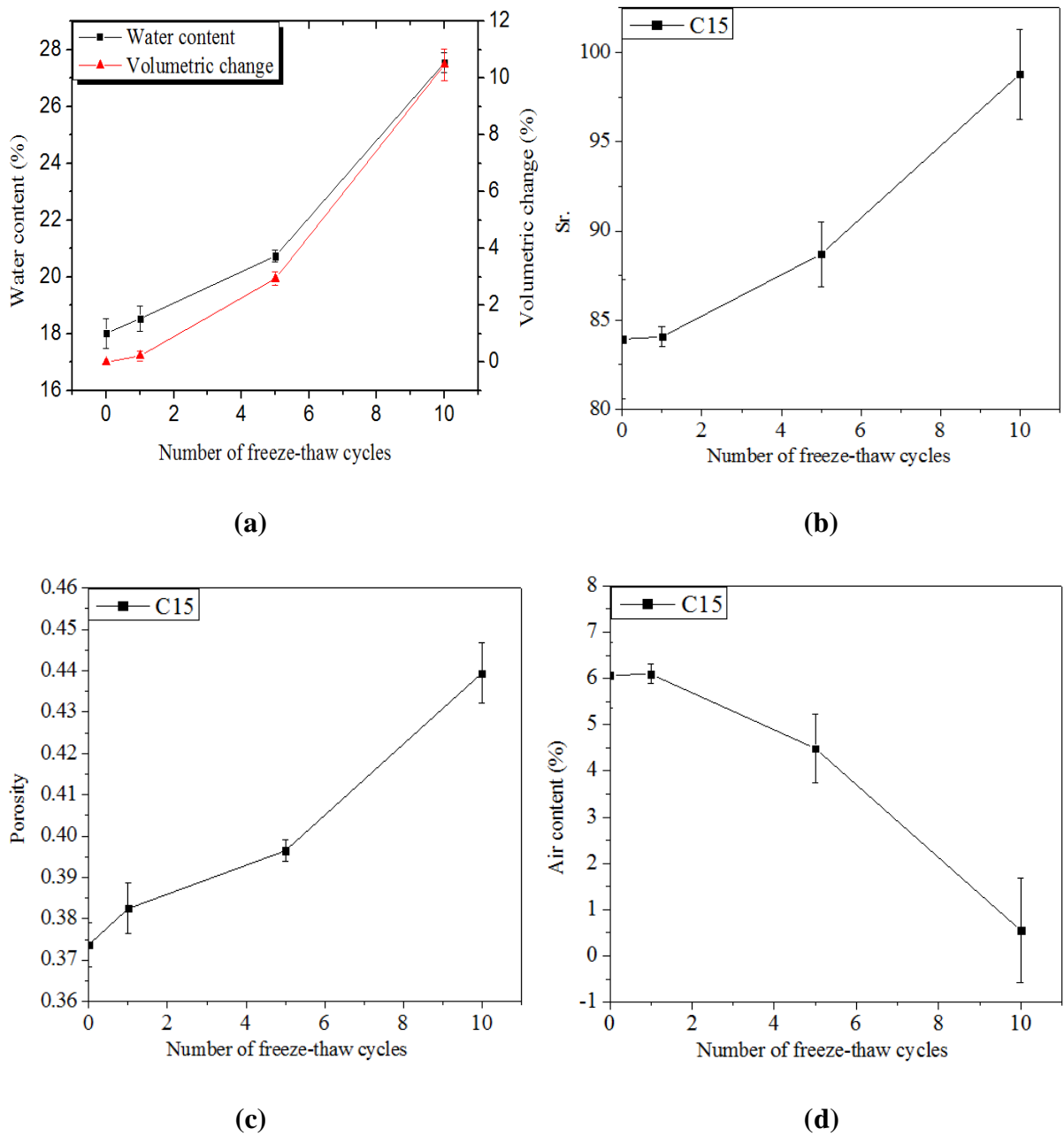


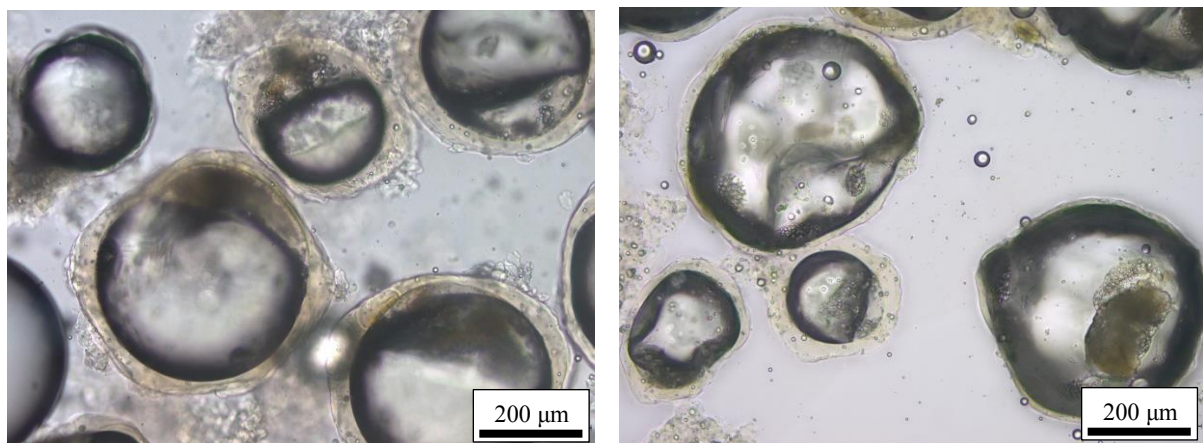
Figure 4.3 Correlations between (a) water content and volumetric change, (b) degree of saturation, (c) porosity, and (d) air content of C15 for increasing numbers of freeze-thaw cycles.

4.4 Development and performance of self-healing soil-cement systems subject to freeze-thaw cycles using Lambson microcapsules

Having been selected as a promising healing agent for soil-cement systems subject to freeze-thaw cycles, Lambson microcapsules were added to soil-cement mixes to provide autonomic self-healing. As described in **Section 3.1.2**, the Lambson microcapsules contained sodium silicate solution, which reacts with calcium hydroxide during the cement hydration process to produce C-S-H gel. The associated chemical reactions are provided in **Eq. 2.6**. The C-S-H gel not only doubles the volume of the original solution, but also provides adhesion between particles in the matrix, filling cracks and restoring the structure's strength. The development of self-healing soil-cement systems using Lambson microcapsules, and their performance subjected to freeze-thaw cycles, are studied in this section.

4.4.1 Survivability of the Lambson microcapsules

The survivability of the Lambson microcapsules was investigated to determine whether the healing agent is able to retain its functionality until damage to the soil-cement system occurs. The Lambson microcapsules themselves were exposed to 5 freeze-thaw cycles and then observed under a microscope. Representative optical microscopy images of the Lambson microcapsules before and after 5 freeze-thaw cycles are presented in **Figure 4.4**. After 5 freeze-thaw cycles, the microcapsules remained intact, which indicates that they do not easily break under the effects of aggressive freeze-thaw cycles.



(a) Before freeze-thaw

(b) after 5 freeze-thaw cycles

Figure 4.4 Lambson microcapsules within soil-cement mix samples (a) before freeze-thaw and (b) after 5 freeze-thaw cycles.

In addition, the survivability of the Lambson microcapsules after mixing with the soil-cement mixture was investigated. **Figure 4.5** presents representative optical microscope images of the Lambson microcapsules in the soil-cement paste after mixing. The microcapsules appear as bulbs in the soil-cement samples, indicating that they are able to survive the mixing forces during the mixing of soil-cement.

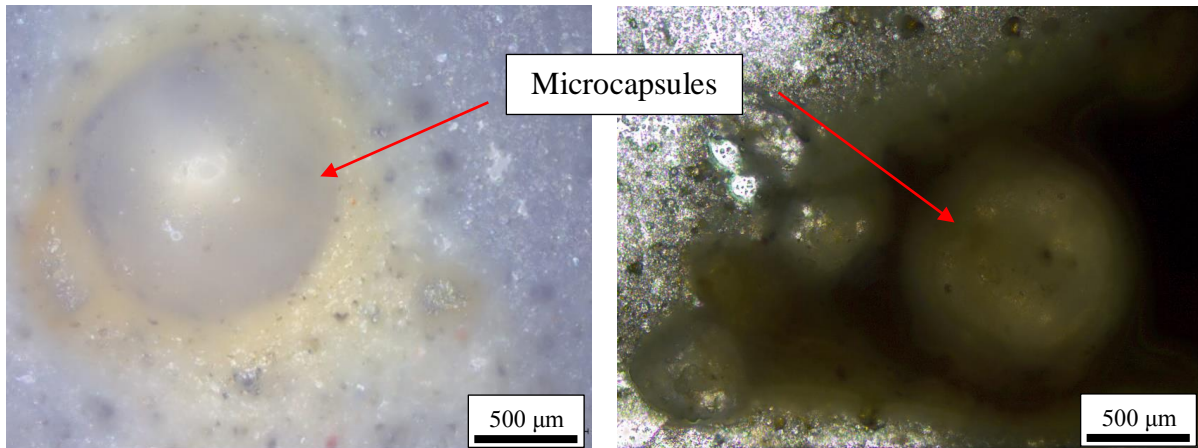


Figure 4.5 Lambson microcapsules in the soil-cement mixes before setting.

4.4.2 SEM

Scanning electron microscopy (SEM) was used to observe the Lambson microcapsules embedded in the C20L5 soil-cement mix matrix. The microcapsules were dispersed evenly throughout the matrix and showed clear signs of breakage in their residual shell material at points of fracture in the matrix (**Figure 4.6**). No shell debris was observed inside of the fractured microcapsules. By contrast, the SEM images reveal that the fractured microcapsules that remained well embedded in the soil-cement matrix formed a dome-like shape. These observations indicate that the microcapsules were not ruptured during the mixing and casting process. If they were, cement hydration products would have formed inside the shells, and the shells would not have retained their spherical shape. SEM images provide further support for the conclusion that Lambson microcapsules survive the mixing process and remain viable in the hardened matrix. Furthermore, the microcapsules were tightly bonded to the soil-cement matrix, and they showed no sign of interfering in the formation of nearby hydration products. These observations are consistent with the results reported by Kanellopoulos et al. (2017) and Giannaros (2017), who argue that Lambson microcapsules are able to survive the mixing process of concrete and mortar.

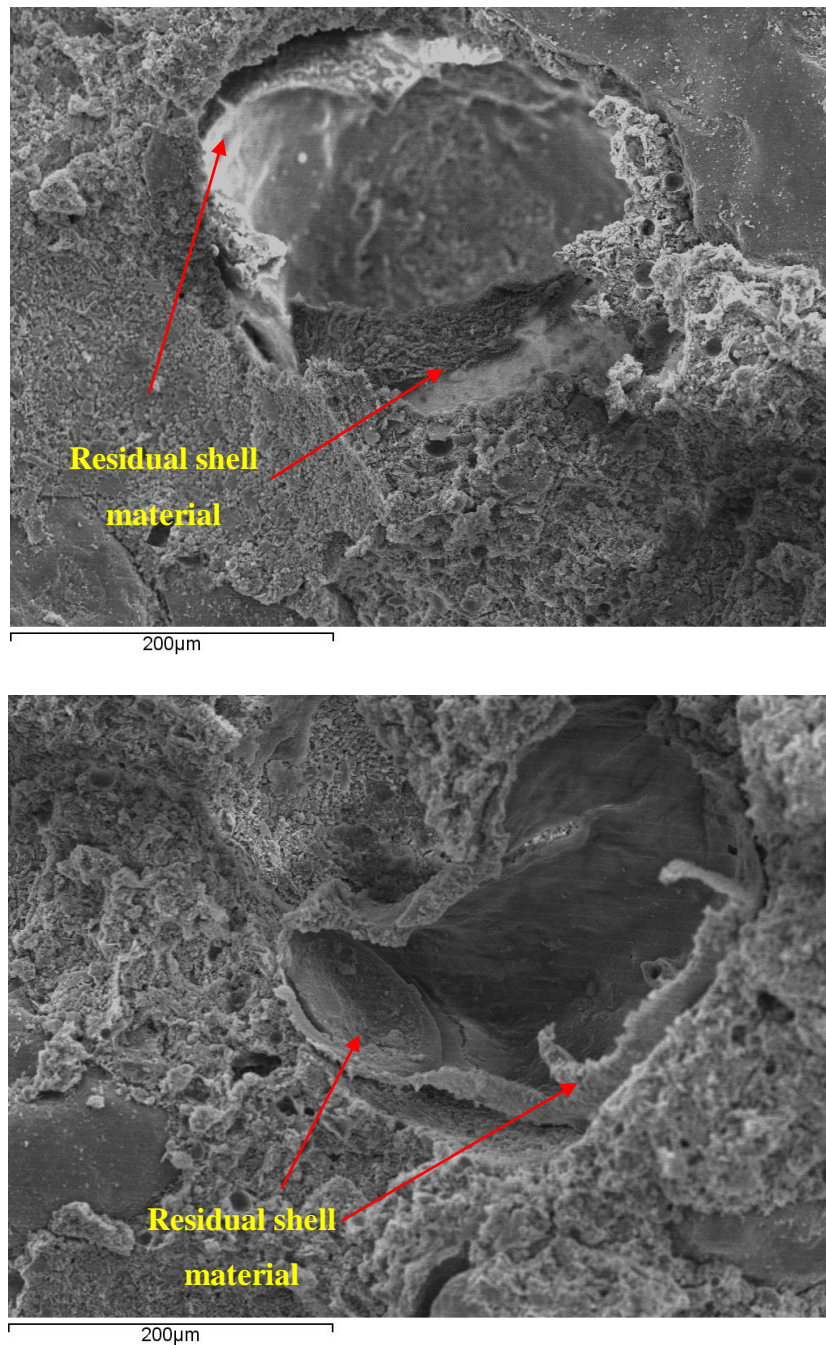


Figure 4.6 SEM images of broken Lambson microcapsules within the soil-cement matrix.

4.4.3 Effect of the microcapsules on the mechanical properties of soil-cement systems

The effect of the Lambson microcapsules on the mechanical properties of the soil-cement mixes was investigated. The Lambson microcapsules were added to soil-cement systems with three different water/cement ratios: 2.5, 1.67, and 1.25 (as detailed in **Section 4.2**). The UCS values of different microcapsule-containing soil-cement mixes are presented in **Figure 4.7**. The error bars in the figures indicate the standard deviation of the means (throughout this

thesis). The results show that the addition of Lambson microcapsules generally decreases the UCS for soil-cement samples. For instance, the UCS values of C10L10 and C15L10 were 22% and 13% lower than their corresponding control mixes, respectively. As discussed in **Section 4.4.1**, the Lambson microcapsules did not break during the mixing process. Therefore, the healing agent was not released in soil-cement system before damage. Thus, because the strength of the Lambson microcapsules is much lower than that of the soil-cement matrix itself, the addition of the microcapsules tended to reduce the strength of soil-cement system. These results are somewhat contrary to a previous study that suggested that the critical value for which the addition of Lambson microcapsules would have a low effect on the compressive strength of the cement was 4% (relative to the weight of the cement) (Giannaros, 2017). Giannaros reported that for a 4% microcapsule dosage, the strength of mortar samples was 17% less than for control samples. For higher dosages, the decrease in UCS plateaued at around 27%. One possible explanation of the contrary result in this study is that the cement content of a soil-cement system is lower than that of mortar or cement paste. Therefore, an equal weight fraction of microcapsules relative to cement in soil-cement systems accounts for a smaller share of the volume of the whole system than for mortar or cement paste.

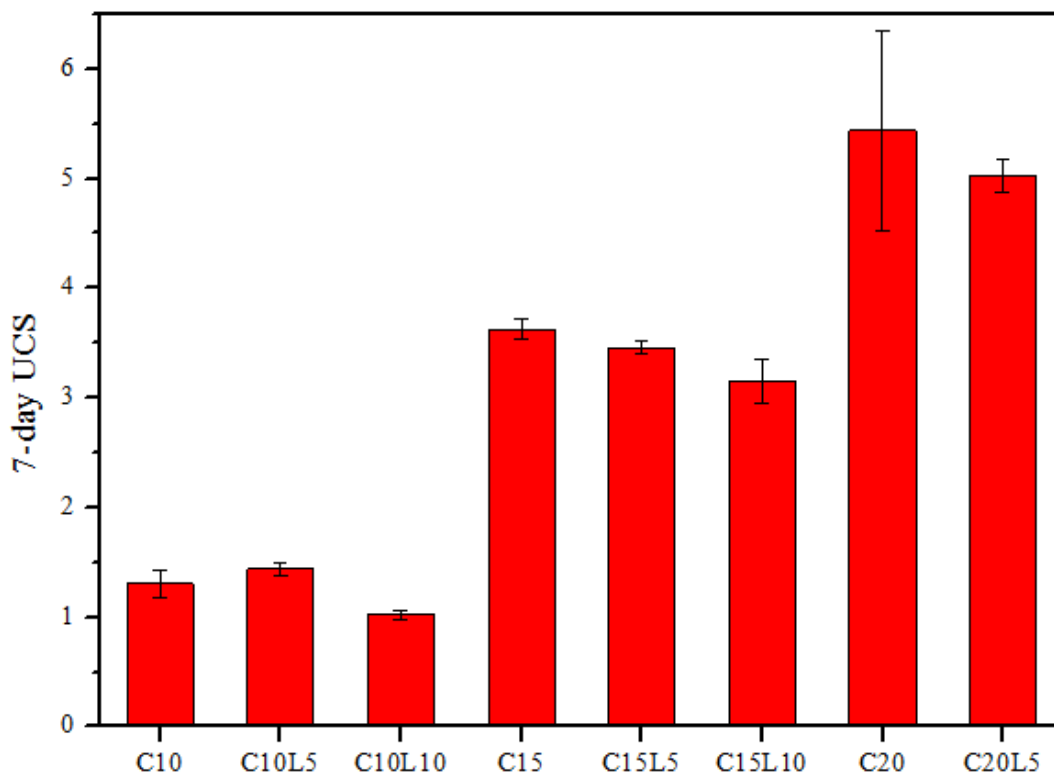


Figure 4.7 Effects of Lambson microcapsules on the 7-day UCS of soil-cement mixes.

4.4.4 Self-healing performance of soil-cement systems embedded with Lambson microcapsules after freeze-thaw cycles

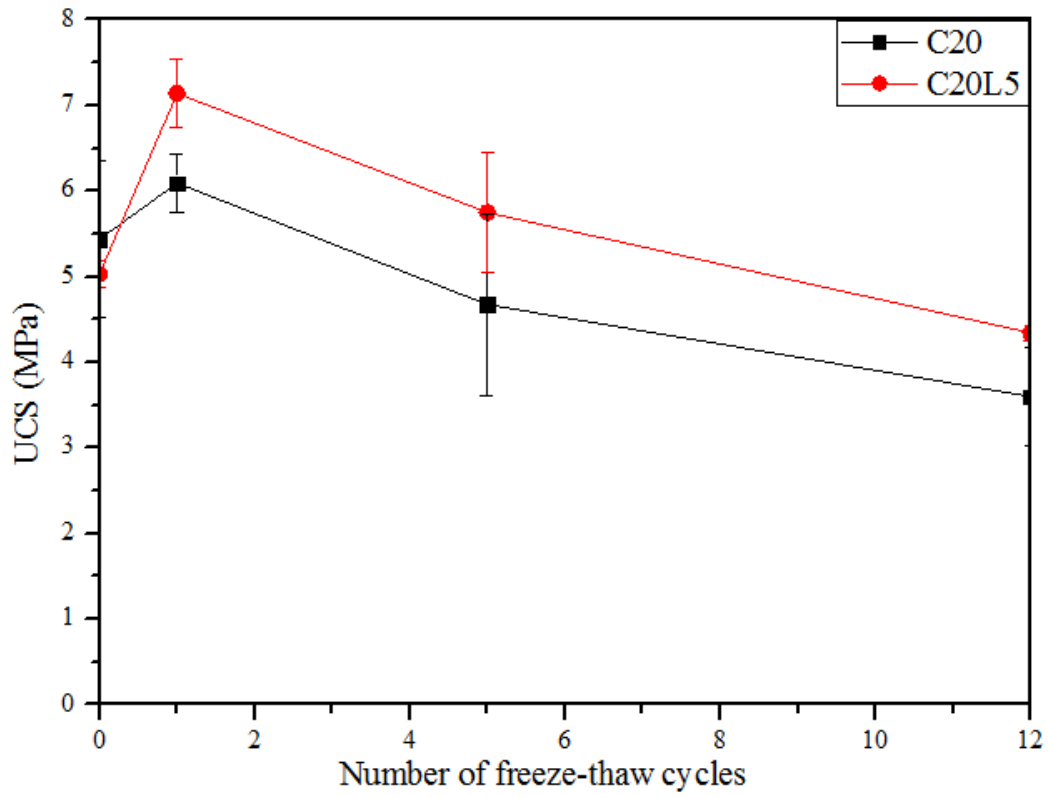
To monitor the self-healing capability of soil-cement systems embedded with Lambson microcapsules after freeze-thaw cycles, UCS tests were carried out on all soil-cement groups. After the control samples and samples embedded with microcapsules were subjected to a number of freeze-thaw cycles, they were cured for 7 days to allow time for the self-healing process to take place. The UCS values of C20L5 and C20 samples are compared in **Figure 4.8a**. Per the graph, the samples containing 5% Lambson microcapsules exhibited slightly lower UCS to the control samples. However, after 1 freeze-thaw cycle and 7 days healing, the UCS of C20L5 samples was 40% higher than their 7-day UCS, whereas this increase of the C20 samples under the same conditions was 12%. This indicates that the Lambson microcapsules did break after freeze-thaw exposure, and the sodium silicate solution within them was released to enhance continuous hydration. More C-S-H gel was produced as the sodium silicate reacted with the calcium hydroxide produced from cement hydration (Kanellopoulos et al., 2015; Pelletier et al., 2010). The UCS values of C20L5 samples after 5 and 12 freeze-thaw cycles (plus the 7-day self-healing period) were 23% and 21% higher than that of C20 samples, respectively. The UCS of control samples gradually reduced with increasing numbers of freeze-thaw cycles, while that of the Lambson microcapsule-embedded samples was higher than its initial UCS even after 5 freeze-thaw cycles. After 12 freeze-thaw cycles, the C20L5 samples retained 86% of their 7-day UCS, while the C15 samples retained only 71%. These results demonstrate that the addition of the Lambson microcapsules provided excellent self-healing capability for C20L5 soil-cement samples. The most effective healing was achieved after the first cycle, though the microcapsules were effective even after 12 cycles.

The UCS values for the soil-cement samples with lower cement content (i.e. 10% and 15%) including mixes C15L5, C15L10, C10L5 and C10L10, after being subjected to freeze-thaw cycles and healing for 7 days are plotted in **Figures 4.8b–c**. However, the addition of Lambson microcapsules did not appear to improve the self-healing capability of these soil-cement mixes. To the contrary: the addition of the Lambson microcapsules tended to slightly reduce the UCS of the soil-cement samples as the number of freeze-thaw cycles increased. For example, the UCS of C15L10 samples after 10 freeze-thaw cycles (7 days of healing) was 65% lower than for control samples. The accelerated deterioration is likely due to the larger pore spaces and higher water content resulting from the addition of the microcapsules

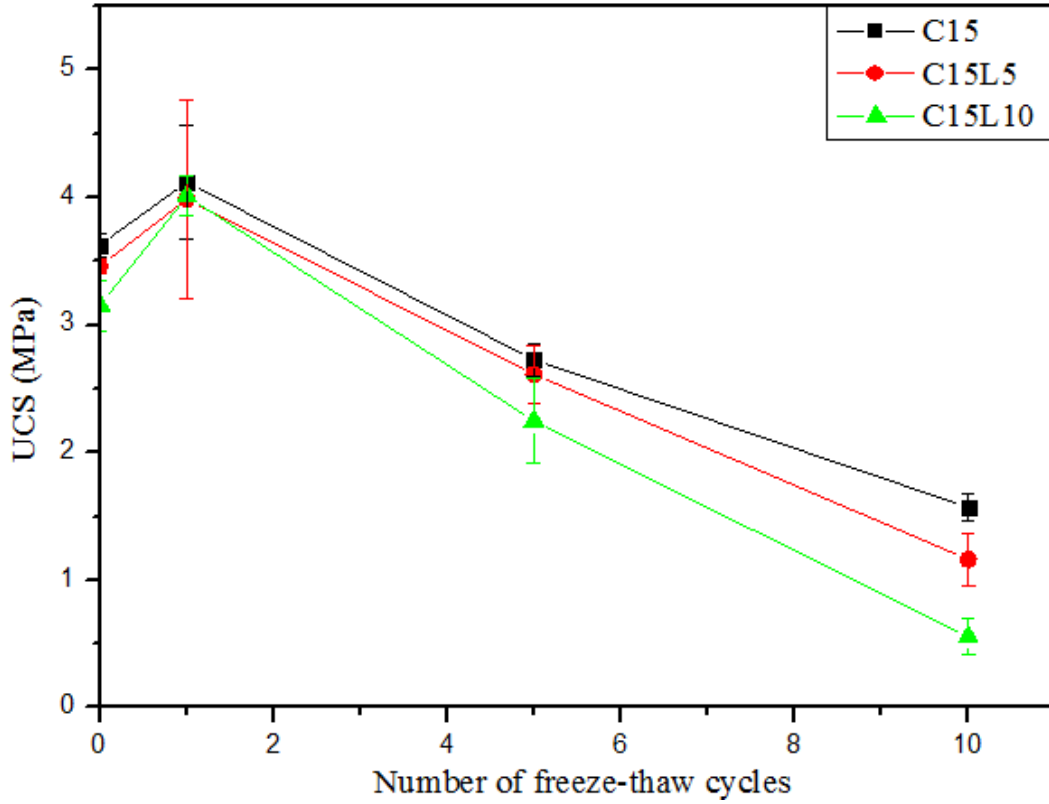
to the soil-cement samples. The Lambson microcapsules may have left voids within the cementitious matrix after breaking, thus increasing the void ratio and leading to higher potential for absorbing water, thereby accelerating the deterioration of the soil-cement system. Another explanation is that the dried residual microcapsule shell material (gelatine) within the soil-cement matrix tended to hydrate, thereby absorbing water from freeze-thaw-induced cracks. Literature, of course, has extensively documented the ways that increased water presence within soil-cement systems accelerates freeze-thaw deterioration.

The change in water content of the different mixes after freeze-thaw cycles is plotted in **Figure 4.9**. These results illustrate that the water content of C15L10 samples after 10 freeze-thaw cycles was 14% higher than that of the C15 samples. Similar findings were also reported by Giannaros et al., (2016), who indicated that the water sorptivity of cement paste after the addition of a 4% volumetric fraction of Lambson microcapsules was slightly higher than for control samples after a 28-day healing period.

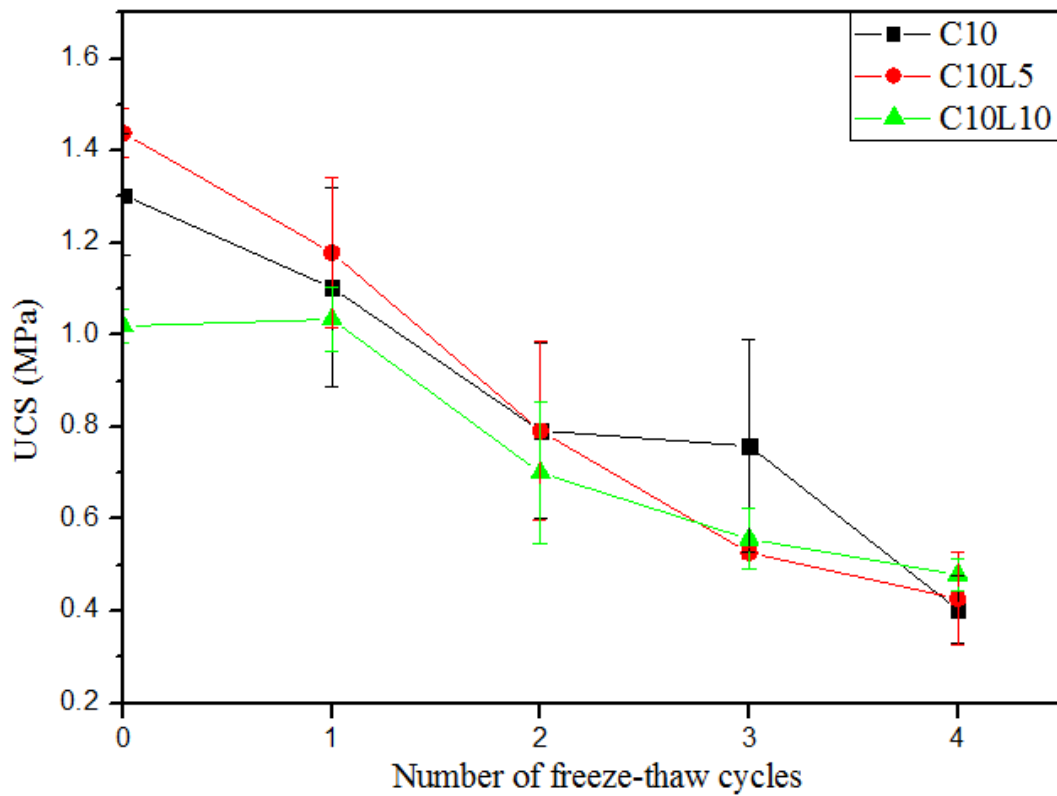
As for Young's modulus, the E_{50} of C20 and C20L5 mixes that were subjected to freeze-thaw cycles and self-healed for 7 days is plotted in **Figure 4.10**. Similar to the UCS results, the E_{50} of C20L5 was found to be considerably higher than for the control mix after the freeze-thaw cycles. After one freeze-thaw cycle, the E_{50} of 7-day healed C20L5 was 52% higher than in the control sample. This difference narrowed to roughly 30% after 5 freeze-thaw cycles and 21% after 12 cycles. Compared to the UCS results, the increase in the E_{50} of the Lambson microcapsules embedded soil-cement samples is more significant. This could be due to the C-S-H gel produced by the healing reaction acting as a binder to bind together the soil-cement matrix into a more cohesive whole. In this scenario, the C-S-H expands outward forms a continuous phase, increasing the stiffness of the soil-cement system. The reason for the reduction in E_{50} at 5 and 12 freeze-thaw cycles is the same as for the UCS results. The healing process requires time to proceed until completion. It is also more difficult to heal and bind the larger cracks that are generated by higher numbers of freeze-thaw cycles. Thus, as the number of cycles increases to 5 and 12, the efficiency of the self-healing could diminish.



(a)



(b)



(c)

Figure 4.8 UCS of the Lambson microcapsule-containing soil-cement samples after different numbers of freeze-thaw cycles and 7 days of healing for cement contents of (a) 20%, (b) 15%, and (c) 10%.

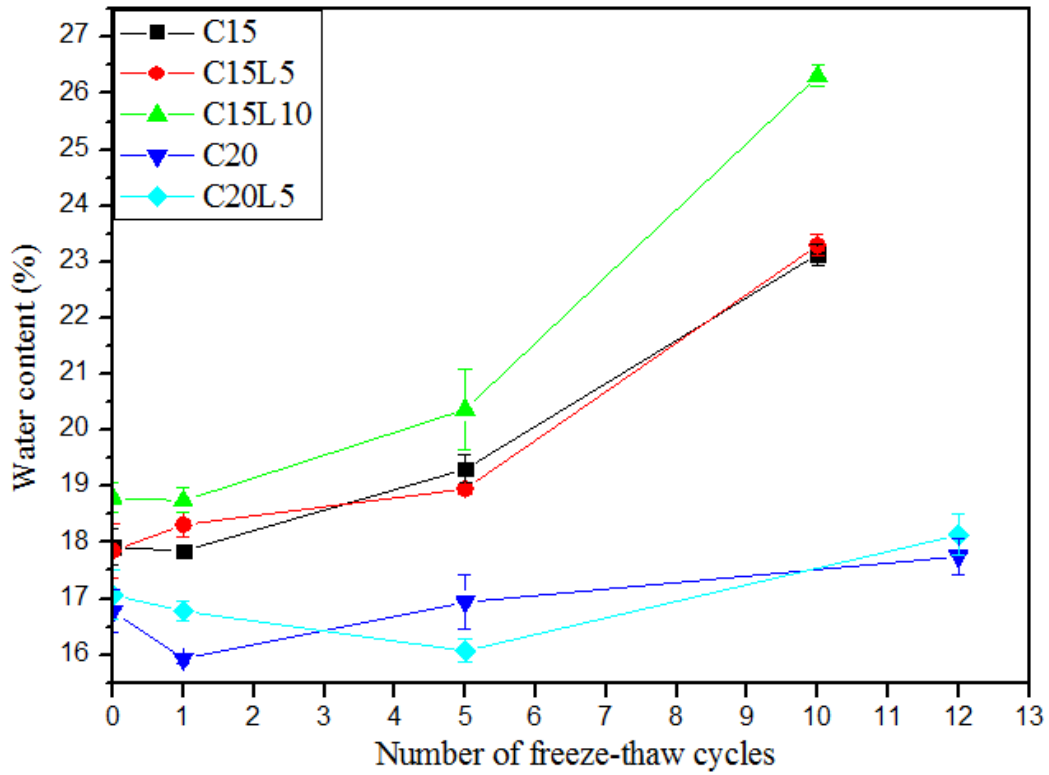


Figure 4.9 Water content of the Lambson microcapsule-containing soil-cement samples after different numbers of freeze-thaw cycles and 7 days of healing.

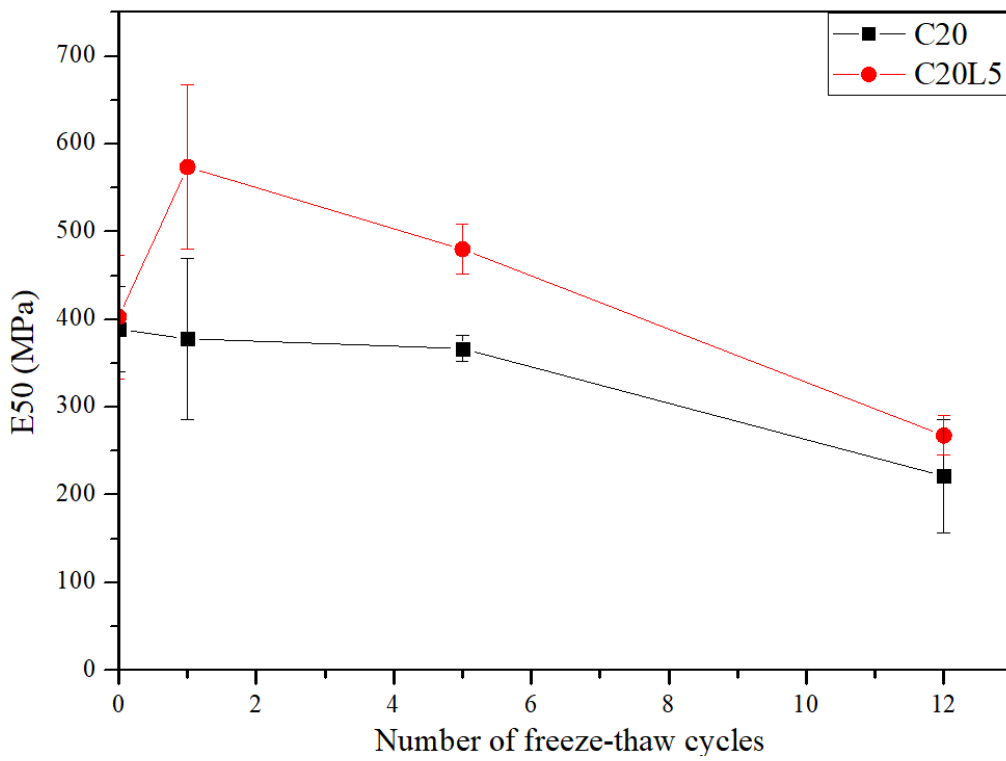


Figure 4.10 E₅₀ of the C20L5 and control mixes after different numbers of freeze-thaw cycles and a 7-day healing period.

4.4.5 Image analysis

The crack sealing capability of the Lambson microcapsules was monitored, and optical microscope images were taken on the C20L5 disc samples at different healing times after 10 freeze-thaw cycles. Representative microscope images are presented in **Figure 4.11**. Very little crack healing was observed on the surfaces of the samples even after 60 days of healing. This is conceivable as the healing product produced was C-S-H gel, which only doubles in volume when it reacts with calcite. In addition, the release of the healing agents from the capsules into nearby empty spaces may have left empty space inside the capsules. Furthermore, as the dosage of the Lambson microcapsules was relatively low, at just 5% of the weight of the cement (equivalent to roughly 15% of the cement's volume), the amount of C-S-H gel produced may not have enough volume to seal the cracks.

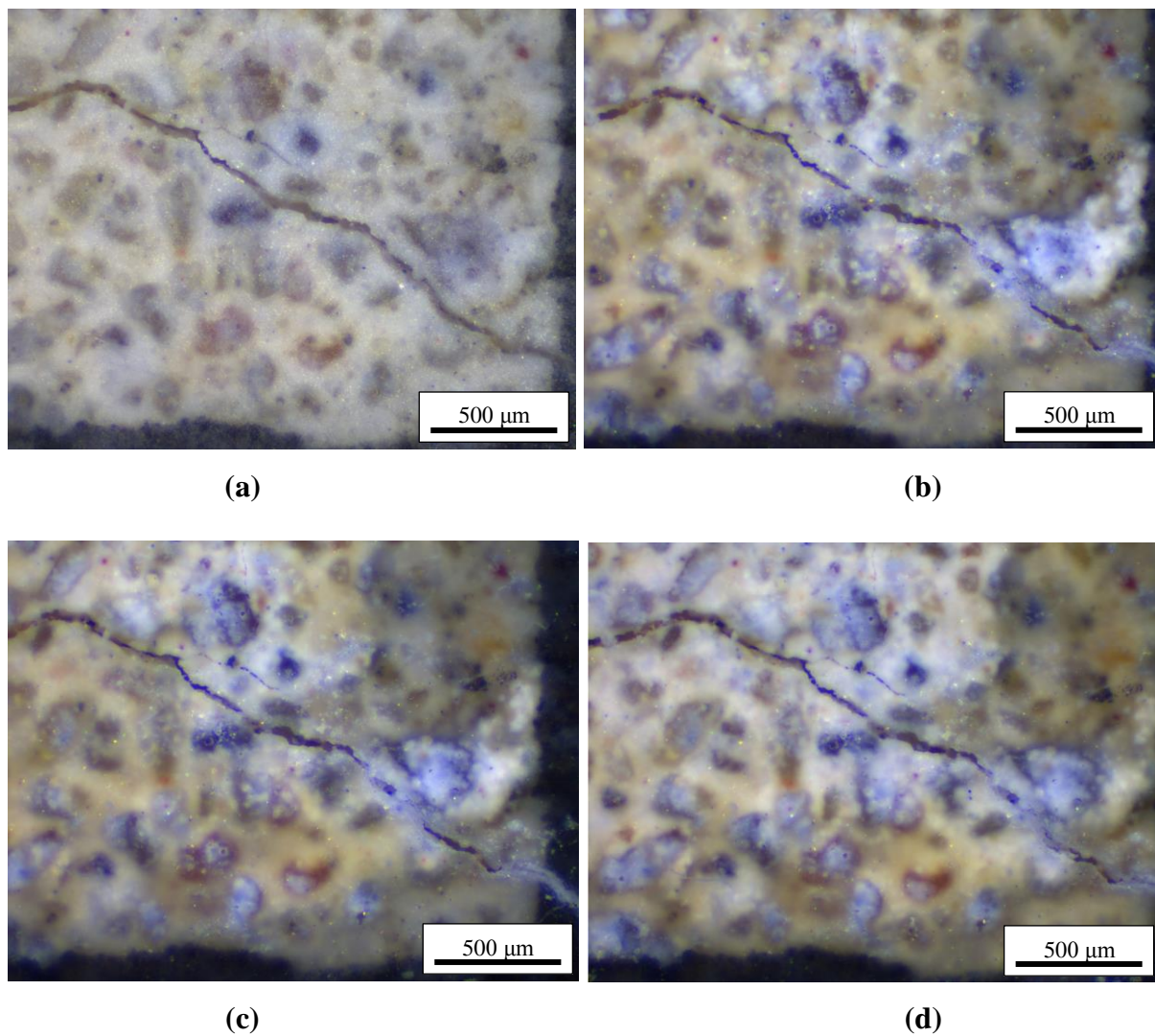


Figure 4.11 Microscopic images of C20L5 samples that were damaged by 10 freeze-thaw cycles and self-healed afterward for (a) 0 days, (b) 7 days, (c) 28 days, and (d) 60 days.

4.4.6 Summary of the performance of self-healing soil-cement systems using Lambson microcapsules

Per results presented above, the addition of Lambson microcapsules equalling up to 10% of the weight of the cement has little effect on the initial strength of the soil-cement system. For the C20L5 mix, the addition of the microcapsules provides good self-healing capability in terms of UCS after freeze-thaw cycles. However, for soil-cement samples with lower cement contents (e.g. 15% and 10%), the addition of the Lambson microcapsules tended to decrease the UCS of the soil-cement rather than increasing it after freeze-thaw cycles. Compared to concrete and cement paste, the water/cement ratio of the soil-cement system is much higher (e.g. water/cement =0.5 vs. water/cement =2.5, 1.67). Therefore, the amount of unhydrated cement and cement hydration products (calcium hydrate) is considerably lower than those of concrete, mortar, and cement paste. In addition, with higher pore space and lower overall strength, the microcapsules may not break as easily after freeze-thaw cycles. Thus, the cargo materials may not be released into the soil-cement system when the system has relatively low cement content. In addition, the use of Lambson microcapsules could increase the potential of soil-cement to absorb water due to the water absorbent nature of the capsules' shell material and the increase in voids ratio in soil-cement systems. Increased water absorption during the freeze-thaw process is, of course, detrimental to overall durability of the soil-cement system.

It can be concluded that the self-healing performance of Lambson microcapsules embedded within a soil-cement system is heavily affected by the cement content of the system. Lambson microcapsules can provide good self-healing ability for soil-cement subjected to freeze-thaw cycles, but this appears limited only to soil-cement systems with relatively high cement content (e.g., 20%). For lower cement contents, the addition of Lambson microcapsules can be detrimental to the freeze-thaw durability of soil-cement system. As a result, LUVOMAG MgO pellets were used as an alternative healing agent for soil-cement systems with lower cement content. The development and performance of these pellets are discussed in the following sections.

4.5 Autonomic self-healing performance of soil-cement systems with LUVOMAG MgO pellets after freeze-thaw cycles

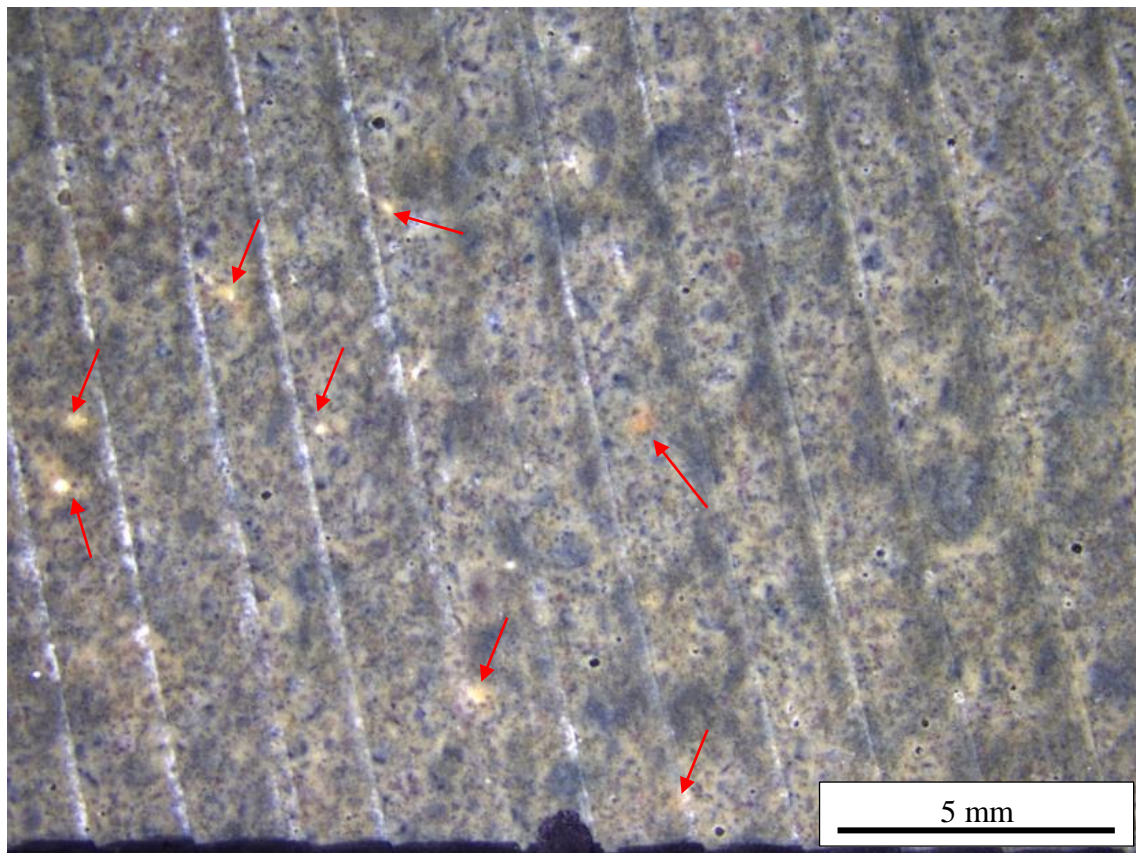
As reviewed in **Chapter 2**, LUVOMAG MgO pellets react with water to yield brucite and hydrated magnesium carbonates (HMC). This section describes how MgO pellets were added

to a soil-cement mixture to develop a self-healing soil-cement system. The self-healing performance of this system after freeze-thaw cycles is also reported.

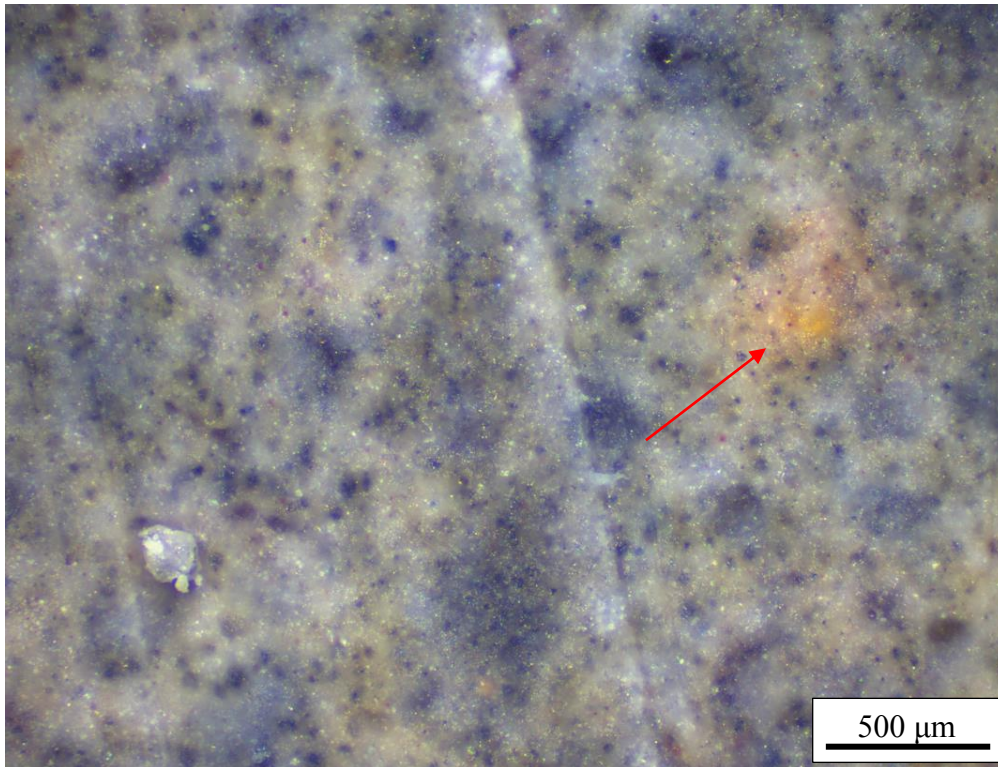
4.5.1 Influence of LUVOMAG MgO pellets on the properties of soil-cement systems

4.5.1.1 Distribution of MgO pellets embedded within a soil-cement matrix

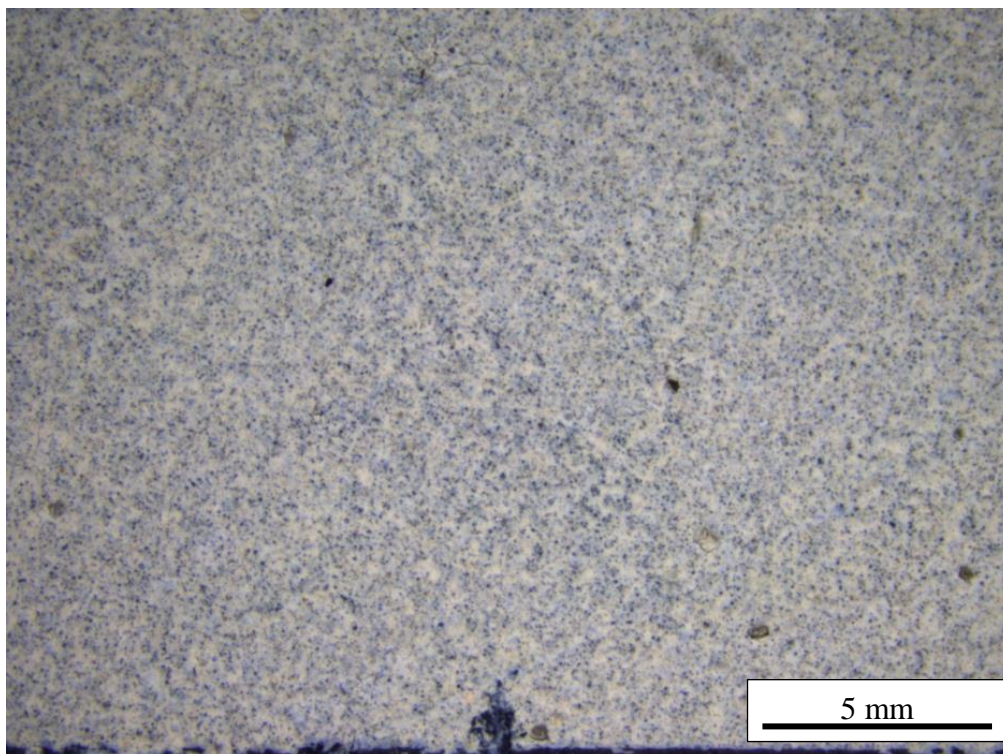
In order to explore the distribution of MgO pellets inside soil-cement specimens, disc specimens were prepared and studied. **Figure 4.12** shows the distribution of MgO pellets across sample sections. The MgO pellets are indicated by the red arrows in **Figure 4.12a**. The pellets are not present in control samples (**Figure 4.12c**). Per **Figure 4.12a**, the MgO pellets in the experimental samples were uniformly distributed throughout the soil-cement matrix, and no segregation was observed. Close inspection revealed that the MgO pellets were well embedded in the soil-cement matrix, and they were strongly bonded to the soil-cement matrix itself, as shown in **Figure 4.12b**. As the particle size and the crushing strength of the MgO pellets were similar to those of the sand particles they replaced, no noticeable change in the structural properties of the soil-cement matrix were anticipated.



(a)



(b)



(c)

Figure 4.12 Image of soil-cement specimens with and without the MgO pellets. Microscopic observation reveals the (a) distribution and (b) embedment of MgO pellets inside the soil-cement samples and the lack thereof within control samples (c).

4.5.1.2 Effect of the MgO pellets on cement hydration

This section primarily focuses on the effects on the hydration process of a soil-cement mix when replacing 10% of sand particles with MgO pellets. It includes a brief study of the survivability of the MgO pellets within the soil-cement matrix. This property is of special interest, as, if the MgO pellets do not survive the mixing and curing of the cement, they may react with and consume the water in the soil-cement mix. This affect the properties of soil-cement systems.

The thermal power produced per gram of cement during the first 48 hours for mixes containing 10% MgO pellets (C15P10) in comparison to the control mix (C15) is presented in **Figure 4.13**. In addition, the peak power values and the setting time calculated for all mixes are summarised in **Table 4.3**.

Generally, the addition of the MgO pellets reduced the setting time and the peak power values compared to the control mix (C15). The initial setting time decreased by 9.4% (from 4.46 to 4.04 hours), while the peak power reduced by 4.9% (from 4.28 to 4.07 mW/g). This result was anticipated, as the added MgO pellets absorb and consume some water, therefore slightly reducing the amount of water available for cement hydration. With less water in the soil-cement mix for cement hydration, the setting time and peak power are reduced. However, the reduction in setting time and peak power is marginal, which suggests that the addition of the MgO pellets has little effect on the hydration process of soil-cement.

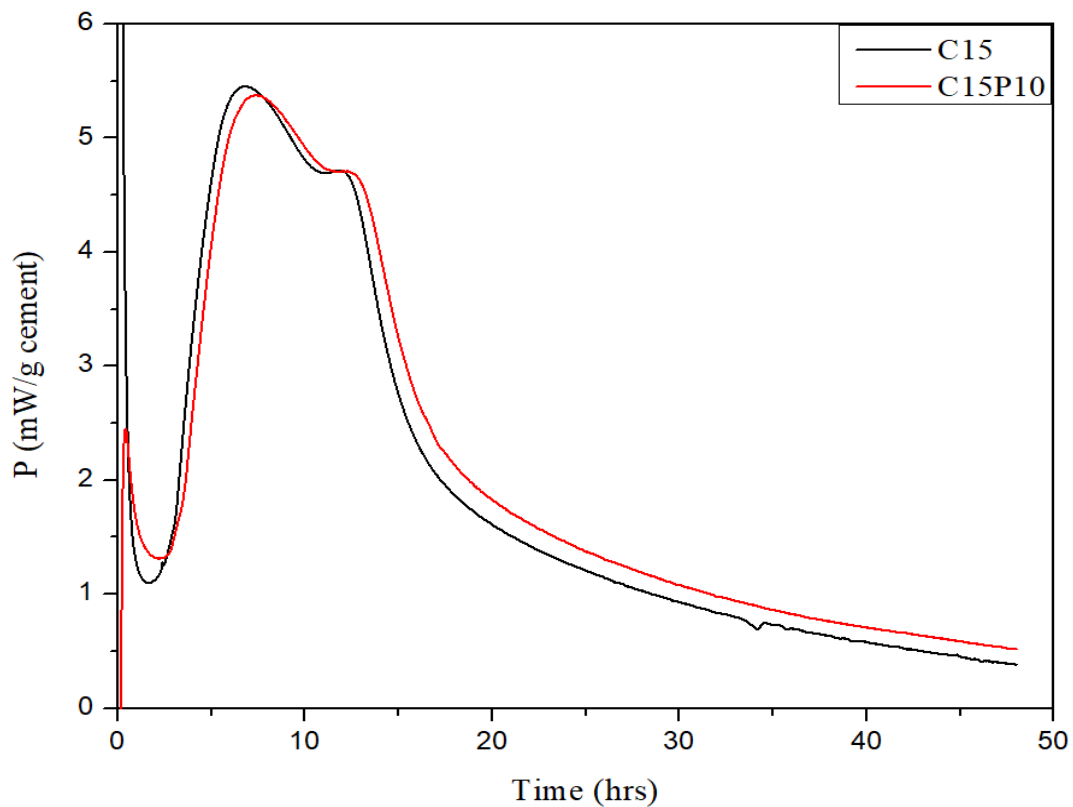


Figure 4.13 Effects of replacing 10% of sand with MgO pellets on the isothermal (23°C) power and energy production of soil-cement mixes.

Table 4.3 Initial setting time and peak power values for soil-cement samples with and without MgO pellets.

Mix	Initial setting time (hrs)	Peak power (mW/g)
C15	4.46±0.08	4.28±0.07
C15P10	4.04±0.10	4.07±0.05

4.5.1.3 Flowability

The flow table values of soil-cement samples containing MgO pellets of various diameters are presented in **Figure 4.14**. The MgO pellets used in C15P10 have a diameter of 1–2 mm, while those used in C15P10_S have a smaller diameter of 0.6–1 mm. In both mixes, the MgO pellets were added by replacing 10% of the sand with particles of the same diameter. The control mix (C15) displayed a flow value of 190 mm, while the flow values of C15P10 and C15P10_S were 171 mm and 162 mm, respectively. The addition of the MgO pellets appeared to lead to a decrease in flow value of 10% and 15% for C15P10 and C15P10_S

mixes, respectively. This reduction in workability may be attributed to two causes. First, as previously described, the MgO pellets were able to physically absorb some water during the mixing stage. Second, the MgO pellets may have become involved in the hydration process and may have consumed some water during mixing. These results are slightly different than those reported by Aghamri (2017). He reported that MgO pellets reduced the workability of mortar mixes by a very small margin, noting that flow value reduced from 156 mm to 152 mm. This is likely because the water/cement ratio in his mortar was 0.5. Therefore, water was mostly consumed by the excess cement, and any reaction with the MgO pellets was minimal. However, the water/cement ratio of the mix presented in **Figure 4.14** was 1.67. Thus, more water could be absorbed and react with the MgO pellets.

The effect of MgO pellet size on the workability of the fresh mix was also investigated. The change in pellet diameter also appeared to affect the workability of the mix. As shown in **Figure 4.14**, the mix with a smaller pellet diameter had lower flow values than that with a larger pellet diameter. A possible explanation for this is that pellets with smaller diameters have a larger surface area to mass ratio than those with larger diameters. The larger surface contact area enhanced the reaction between the MgO pellet and the water and therefore reduced the free water available in the mix. This led to a greater reduction in workability. In addition, (Huang and Ye, 2014) found that the total healing agent released from capsules hit by the crack increased linearly with the capsule's diameter. Thus, to minimise the effect on the workability of the soil-cement mix, and to increase the likelihood of the crack hitting MgO pellets, pellets with diameters of 1–2 mm were selected for the self-healing soil-cement system.

It was found that the incorporation of the MgO pellets reduced the workability of the soil-cement mix. However, the reduction in flow value of only 10% was considered acceptable. These results match those observed by Hung and Kishi (2013), who studied the workability of fresh concrete containing granules of supplementary cementitious materials. They reported that the incorporation of self-healing granules into a concrete mix slightly decreased its workability. They attributed this reduction to water absorption and further reactions between the granules and the mixing water. However, they concluded that granules can be considered an effective means of alleviating the workability reduction caused by direct incorporation of powdered self-healing materials.

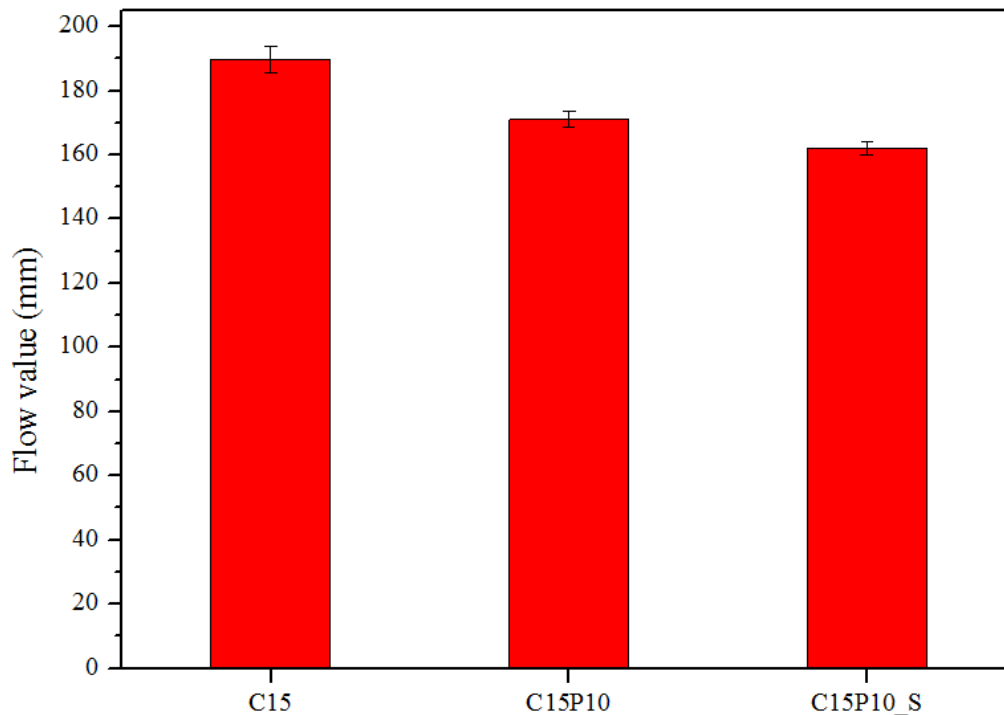


Figure 4.14 Flow values of different soil-cement mixes with embedded MgO pellets.

4.5.1.4 Water content

Figure 4.15 shows that the addition of MgO pellets slightly reduced the water content of the soil-cement system for both water/cement ratios (1.67 and 1.25). The 7-day water content of C15 was 17.9%, which decreased slightly to 17.3% for C15P10. For the sample with a water/cement ratio of 1.25, the 7-day water content of C20 decreased from 16.8% to 16.2% when 10% of the sand was replaced by MgO pellets (C20P10). This indicates that most of the MgO pellets did not react with the water during the mixing of the soil-cement. The difference in the water content of the C15 and C15P10 mixes over multiple freeze-thaw cycles is presented in **Figure 4.16**. A sharp increase in water content was observed in C15 after 10 freeze-thaw cycles. However, the addition of the MgO pellets appeared to reduce the water content increase considerably. For example, the water content of C15 increased from 17.9% to 27.5% after 10 freeze-thaw cycles, while this increase for C15P10 was from 17.3% to 21.6%. A possible explanation for this is that during the freeze-thaw process, some of the cracks generated by freeze-thaw damage were partially self-healed in C15P10 samples. Therefore, the soil-cement system's water uptake was reduced.

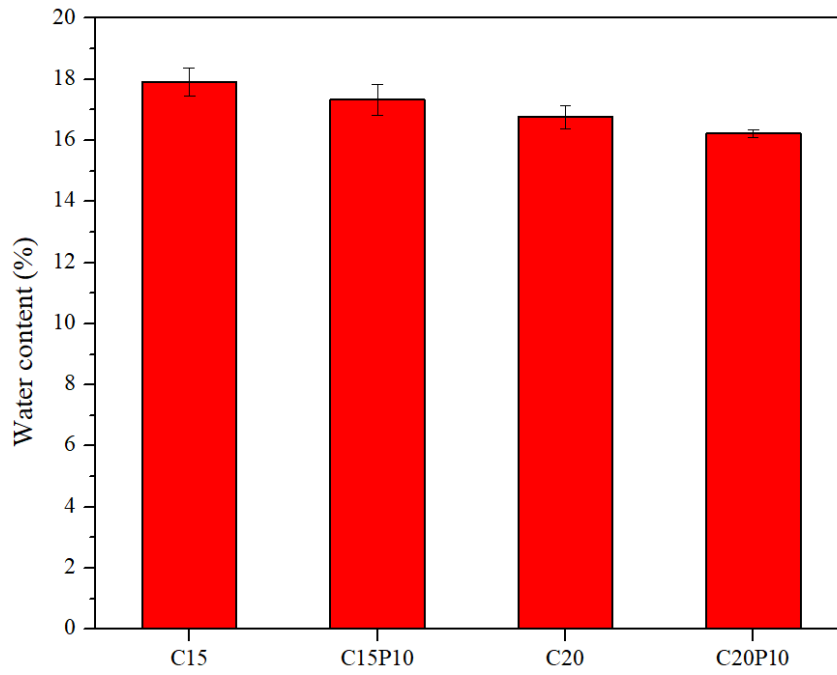


Figure 4.15 The 7-day water content of different soil-cement samples with MgO pellets.

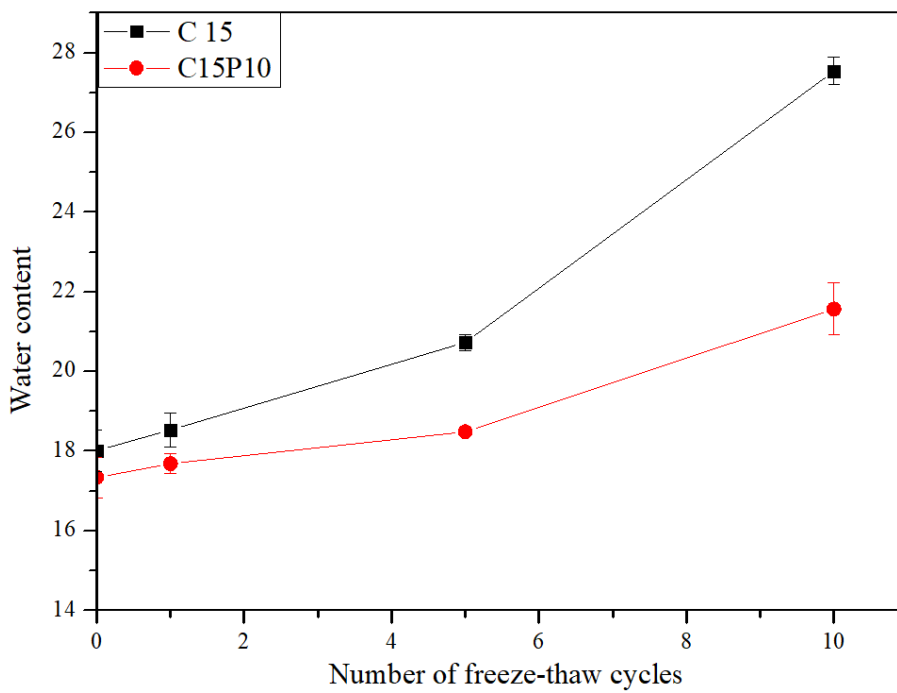
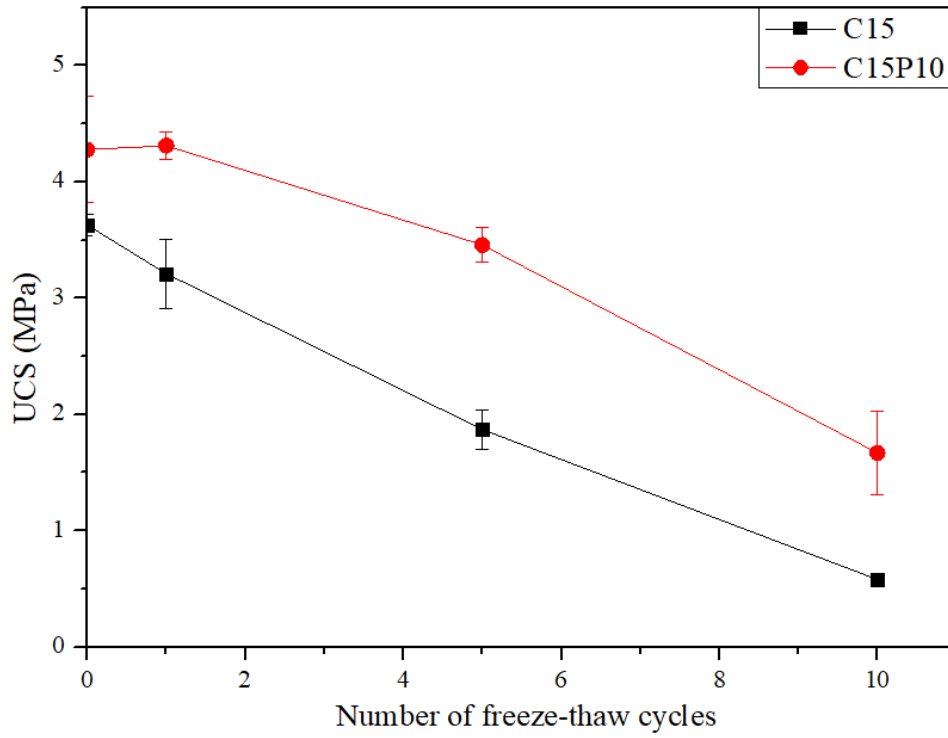


Figure 4.16 The water content of the soil-cement mixes containing MgO pellets subjected to different number of freeze-thaw cycles.

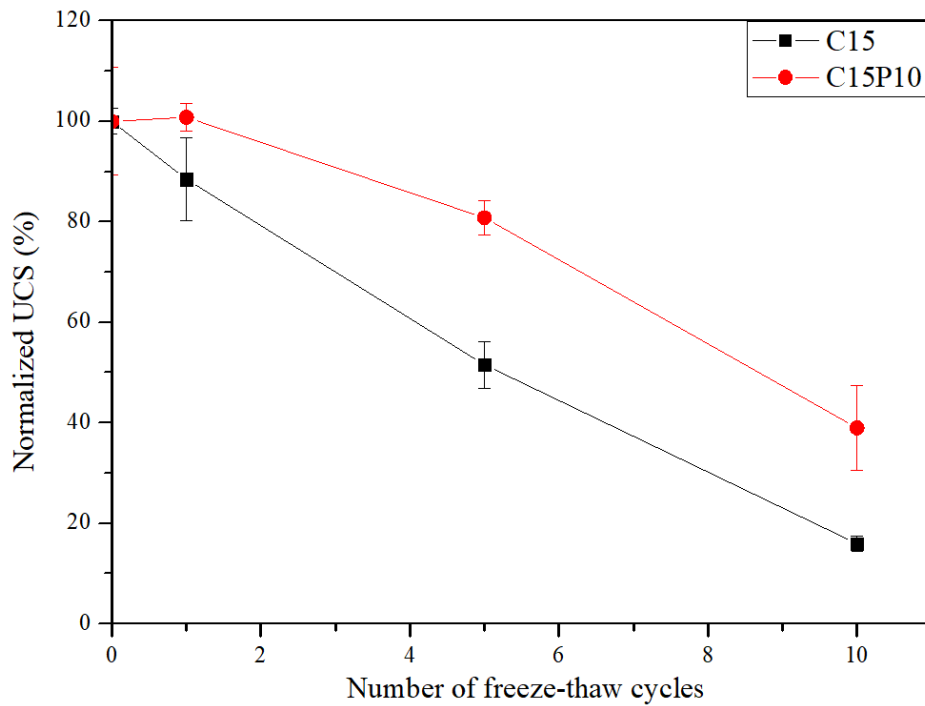
4.5.1.5 Unconfined compressive strength

The UCS of C15, C15P10 and C20P10 mixes were measured after 0, 1, 5, and 10 (or 12) freeze-thaw cycles. These results are presented in **Figure 4.17a**. The addition of MgO pellets generally increased the 7-day UCS of soil-cement systems. The UCS of C15P10 was 18% higher than the UCS of corresponding controls. This increase in 7-day UCS may be attributed to three possible causes. First, the addition of the MgO pellets, to a certain extent, decreased the water/cement ratio of the mixture, which led to a higher strength. Second, the reaction of the MgO pellets with water yielded $\text{Mg}(\text{OH})_2$, MgCO_3 , and hydrated magnesium carbonates, and those products increased the strength of soil-cement. Third, the irregular surfaces and water-absorbing qualities of the MgO pellets could have strengthened the bonds and interlocking between particles.

As shown in **Figure 4.17b**, the addition of MgO pellets generally increased the freeze-thaw resistance of soil-cement mixes in terms of UCS. For example, after 10 freeze-thaw cycles, the residual UCS of C15P10 was 39% while this value of C15 was 16%. The reason for the favourable performance of MgO pellets samples is likely twofold. First, during the freeze-thaw process, the reaction of the MgO pellets with water produced brucite, which swelled, blocking the crack and reducing water uptake into the matrix. This could be vital for the protection of soil-cement systems subject to freeze-thaw cycles, as water expansion during freezing is the predominant reason for freeze-thaw deterioration. Second, as water reacts with MgO to form magnesium hydrates, which can increase the strength of the matrix. The intrusion of water in the vicinity of the MgO pellets facilitates this reaction. To further explore the self-healing performance of MgO pellets embedded in soil-cement systems, their crack sealing capability and their ability to restore the systems' mechanical properties were investigated. The results of these investigations are presented in the following sections.



(a)



(b)

Figure 4.17 The strength behaviour of soil-cement mixes with MgO pellets at different numbers of freeze-thaw cycles: (a) actual UCS values and (b) normalised UCS values.

4.5.1.6 Unconfined compressive strength development

The effect of the MgO pellets on the UCS development of soil-cement over time was also investigated. The UCS values of soil-cement samples containing MgO pellets at curing ages up to 60 days are in **Figure 4.18**. Generally, both the C15 and C15P10 mixes demonstrated constant strength gain over time. Although the 7-day UCS of C15P10 was already higher than that of C15, a more dramatic strength gain was observed for C15P10 than for the control mix between 7 and 14 days. At 7 days, the UCS of C15P10 was roughly 22% higher than for C15 samples, and this difference widened to 42% at 14 days. At 28 days and 60 days, the UCS of C15P10 was approximately 39% higher than that of control samples. However, it should be noted that at 90 days, the difference between the two mixes became neglectable. At this point, both mixes displayed similar strengths of approximately 5.4 MPa.

In sum, the replacement of 10% of the sand in the soil-cement mixture with MgO pellets appeared to significantly enhance the early UCS development of the soil-cement (i.e., UCS development before 60 days). However, it appeared to hamper UCS development at later age (i.e., after 60 days). There may be three possible explanations for this. First, because the MgO pellets react with water, albeit slowly, they may slightly reduce the water/cement ratio of the soil-cement mixture and therefore increase its compressive strength. This explanation is supported by the previous results reported in **Section 4.5.1**, which show that the workability, setting time, and 7-day water content of soil-cement were slightly reduced by the addition of MgO pellets. However, after 60 days, additional hydration of the cement could be hampered by the fact that the MgO pellets have already consumed residual capillary water, impeding further strength gain. It should be noted that the UCS of C15P10 at 90 days was slightly lower than that at 60 days. This reduction may be due to the production of expansive products of MgO, which could generate internal stress and damage the PC-MgO interface, leading to a slight reduction in strength.

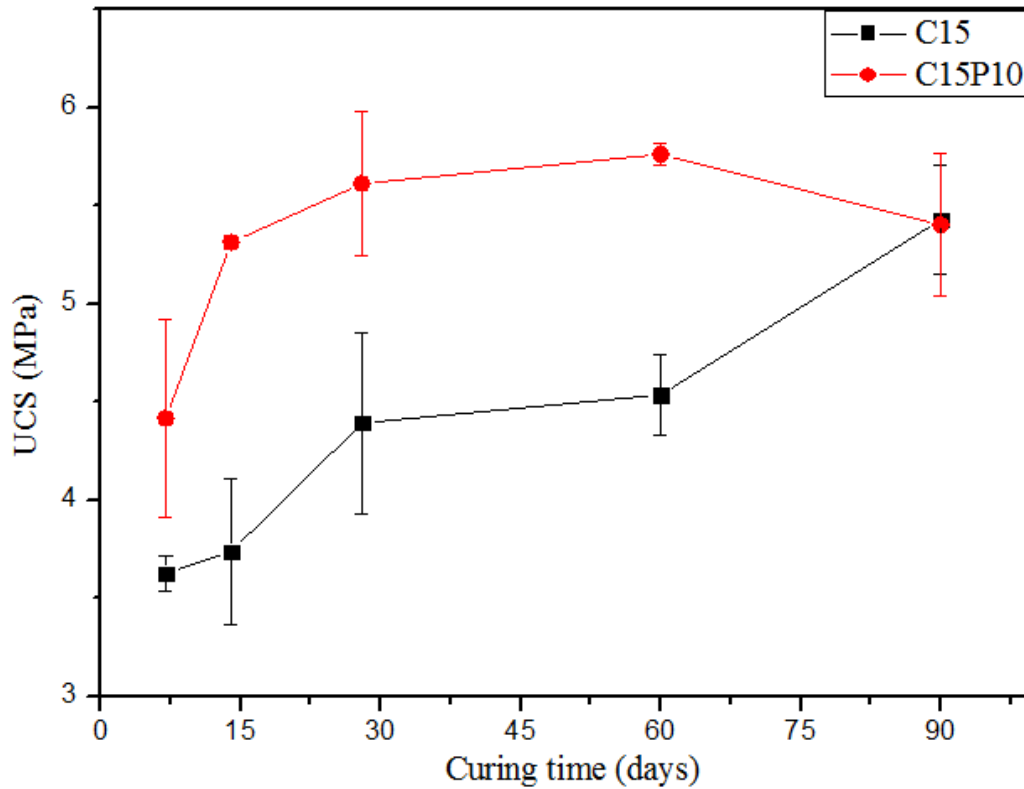


Figure 4.18 The UCS of soil-cement samples containing MgO pellets over time.

On one hand, the replacement of 10% of the mass of sand in the mixture with MgO pellets slightly reduced the workability, setting time, and 7-day water content of the resulting soil-cement. On the other hand, the addition of the MgO pellets considerably increased the 7-day UCS and early strength development (up to 60 days) of soil-cement systems. This finding contradicts a study by Alghamri (2017), which reported that the addition of MgO pellets reduced the UCS of mortar samples by up to 15%. This is understandable, as the water/cement ratio used in that study’s mortar mix was 0.5, while the water/cement ratio used in this study was 1.67 (C15). For mixes with a relatively low water/cement ratio (e.g. 0.5), the consumption of water by MgO pellets is detrimental to the soil-cement’s strength, as not enough water remains late in the curing process for hydration of the cement. However, for mixes with relatively high water content, this water content reduction would increase the hardened strength of cement-related mixes.

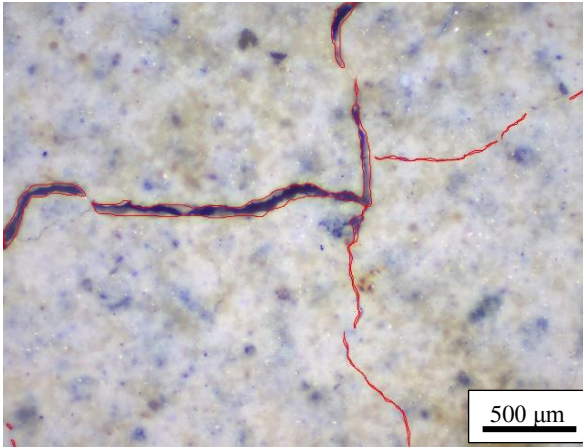
4.5.2 Crack sealing efficiency

To evaluate the crack sealing efficiency of soil-cement samples containing MgO pellets, microscope images were taken of residual cracks in C15P10 soil-cement discs ($\varnothing 10$ mm \times 10 mm) that had been subjected to freeze-thaw cycles and then self-healed for varying numbers

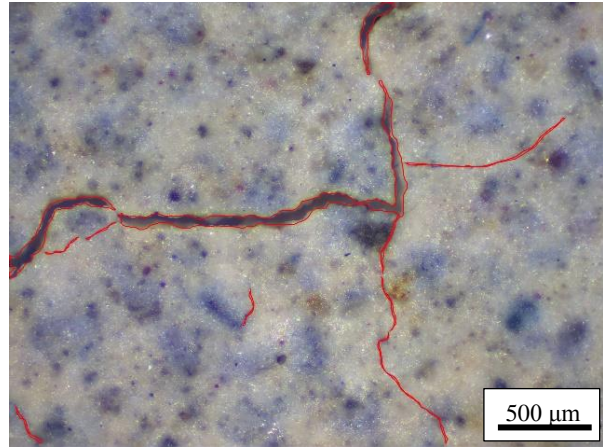
of days. The residual cracks generated after 7 freeze-thaw cycles had crack widths ranging between 0.01 mm and 0.1 mm. As indicated in **Section 3.5.6**, microscope images were taken on samples after 7 freeze-thaw cycles and after varying healing times of up to 60 days. The crack-sealing process is considered to be a good indicator of the efficiency of the self-healing process in cementitious materials (de Rooij et al., 2013).

Microscope images were taken of the soil-cement samples after 7 freeze-thaw cycles and self-healing periods of 0, 7, 28, and 60 days. Some representative images are shown in **Figure 4.19**. It is clear from **Figure 4.19** that soil-cement samples containing MgO pellets had much better crack sealing efficiency than control samples. Autogenic healing was barely observed for control samples (see **Figure 4.19a-b**) after 7 freeze-thaw cycles and self-healed for 60 days. However, as shown in **Figure 4.19c-d**, excellent crack healing (indicated by red arrows) was observed for C15P10 samples. Complete healing of cracks was observed after 60 days of healing. Evidently the addition of the MgO pellets significantly improved the sealing capability of the soil-cement samples. Representative microscopic images showing the development of healing products with times on the surfaces of freeze-thaw damaged soil-cement samples containing MgO pellets are shown in **Figure 4.20**. The cracks were partially healed after 7 days, with further progress observable after 28 and 60 days of healing. Complete closure of the cracks was observed after 28 days of self-healing.

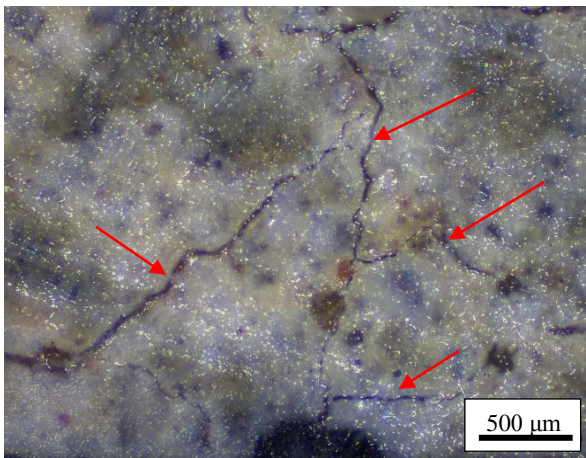
The images were processed to measure crack area via Leica LAS Image Analysis software. Further investigations were conducted to measure the extent of crack generation and crack sealing efficiency (CSE) over time using **Eq. 3.12** presented in **Section 3.5.6**. A summary of the CSE for all samples at different healing times (i.e. 0, 7, 14, 28, and 60 days) is presented in **Figure 4.21**, with error bars indicating standard deviation. The crack healing efficiency of the MgO pellet-containing samples was much higher than the controls, which confirms the microscope observations. The CSE of the C15P10 samples after 7 days of healing was 24%, while the CSE of the control samples was only 0.3%. The crack healing efficiency of the C15P10 samples increased to 81.5% after 14 days of healing, and this value increased to 88.3% after 28 days of healing. In contrast to the control samples, which showed a CSE value of 12.7% after 60 days of healing, a very high CSE of 96.3% was achieved by C15P10 samples that had self-healed for 60 days. There is very little literature concerning the self-healing of soil-cement systems. However, this finding is comparable to Alghamri (2017), which reported that MgO pellet-embedded mortar showed 76–100% crack mouth healing, compared to 40.3% crack mouth healing observed in control samples.



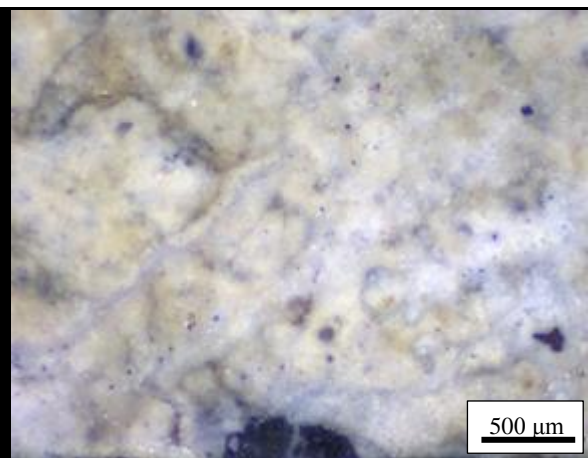
(a) C15 before healing



(b) C15 after 60 days of healing

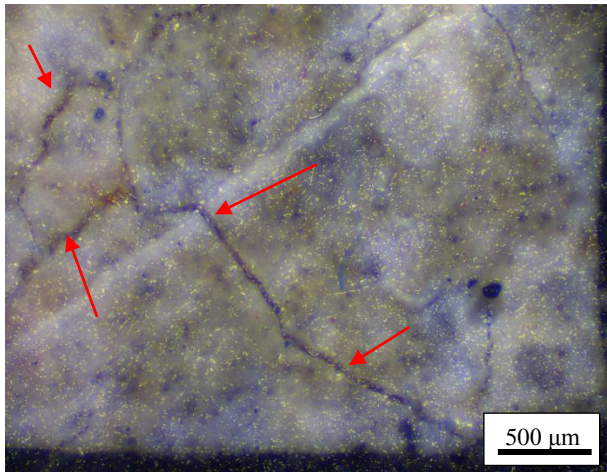


(c) C15P10 before healing

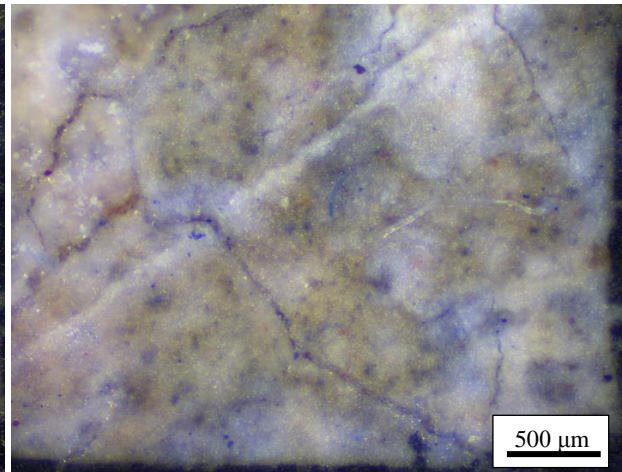


(d) C15P10 after 60 days of healing

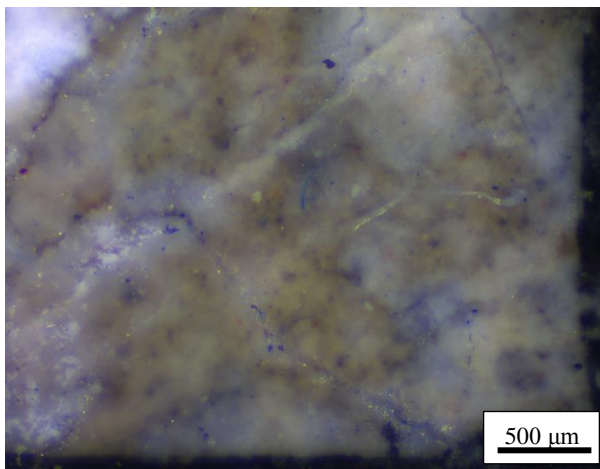
Figure 4.19 Typical optical microscopic images of the crack-sealing patterns of control samples (a-b): (a) damaged by 7 freeze-thaw cycles and (b) self-healed for 60 days; and soil-cement samples containing MgO pellets (c-d): (c) damaged by 7 freeze-thaw cycles and (d) self-healed for 60 days.



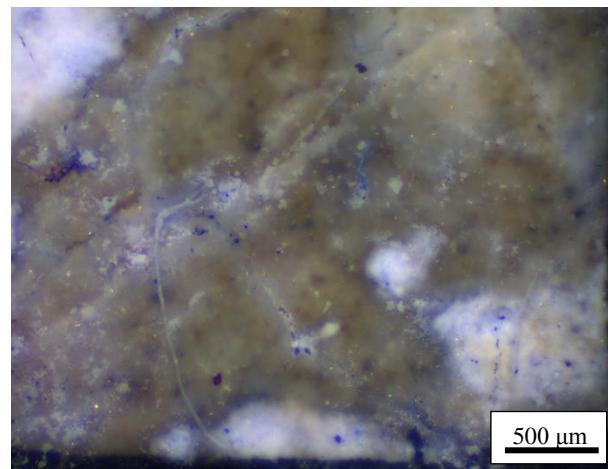
(a) 0 days



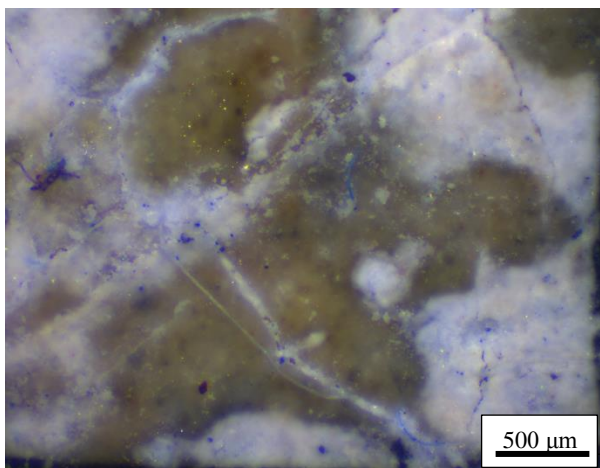
(b) 7 days



(c) 14 days



(d) 28 days



(e) 60 days

Figure 4.20 Typical optical microscopic images showing the development of crack sealing on the surface of C15P10 samples over healing time.

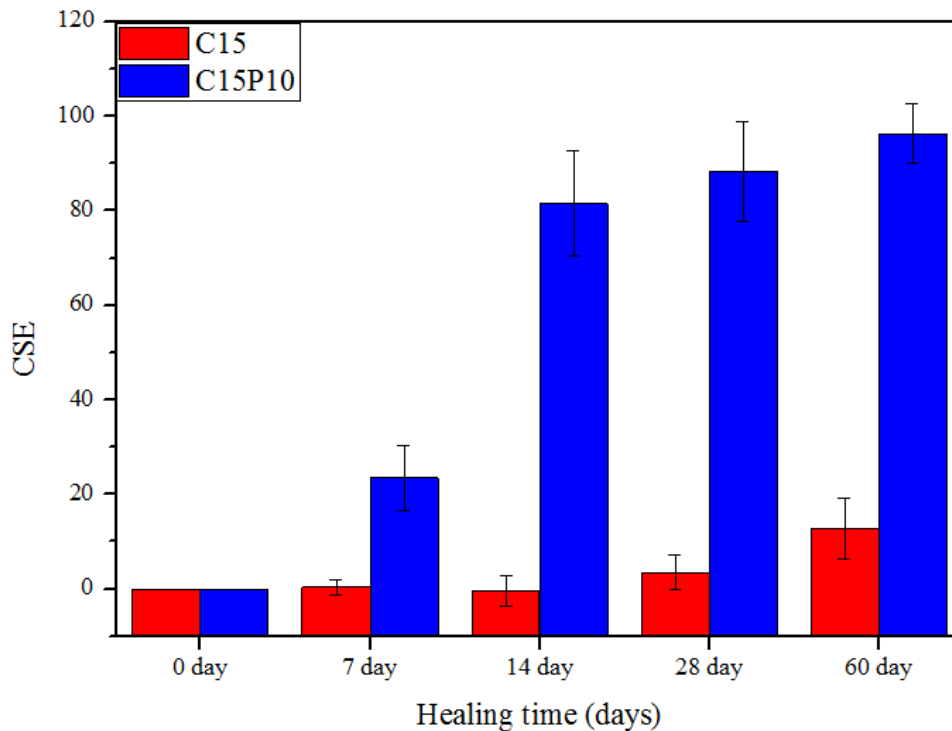


Figure 4.21 Crack sealing efficiency of soil-cement samples, including controls and samples embedded with MgO pellets, both subjected to 7 freeze-thaw cycles, over healing time.

4.5.3 Permeability

4.5.3.1 Water permeability

Ten freeze-thaw cycles were conducted on the C15 and C15P10 mixes before they were healed in ~98% relative humidity (RH) for a variety of healing times. Plots of the water permeability K values of the control and C15P10 specimens are shown in **Figure 4.22**. To highlight the change of K values over the healing period, the permeability ratio is defined as the average of the hydraulic conductivity values of self-healed samples divided by the values of samples after 10 freeze-thaw cycles (K_{healed}/K_{10}). It is plotted against healing time in **Figure 4.23**. The initial point, with $K_{\text{healed}}/K_{10} = 1$ in **Figure 4.23**, represents samples damaged by 10 freeze-thaw cycles without any healing. Per **Figure 4.23**, the water permeability of C15 increased with increasing healing duration. The permeability of soil increases with decreasing moisture content; therefore, the increase in the K values of the control samples (C15) may be due to the desiccation and decomposition of specimens in the early stages of healing in very high relative humidity environments. A slight reduction in the K values was observed for C15 specimens after 60 days of healing. However, for the C15P10

mix, although its permeability ratio was slightly increased after 7 days of healing, a marked reduction in permeability was observed after 28 days of self-healing. The hydraulic conductivity ratio of C15P10 was reduced to 0.27 after 28 days of self-healing, compared to a value of 4.0 for the control specimens.

These results indicate that more healing products were formed in the C15P10 specimens than in the controls, and that these had sealed the cracks that had formed inside the soil-cement samples during the freeze-thaw cycles, reducing permeability. They also indicate that the C15P10 mix has good self-healing capability, and they confirm the crack sealing efficiency results discussed in **Section 4.5.2**. Similar results were reported by Alghamri (2017), which used MgO pellets in mortar samples and found that the sorptivity index decreased by 58% after 28 days of self-healing. Further discussion of the microstructure of the healing products will be presented in **Section 4.5.5**.

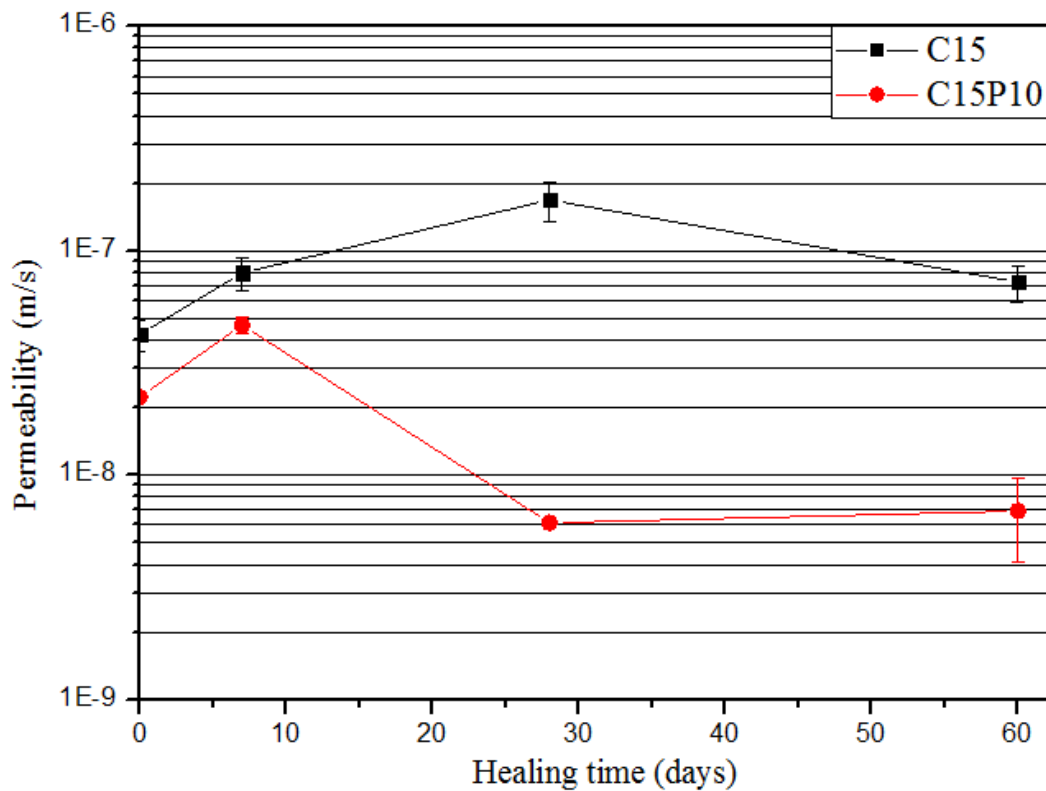


Figure 4.22 Evolution of the permeability values of a soil-cement mix containing MgO pellets and a control sample after 10 freeze-thaw cycles for several healing periods.

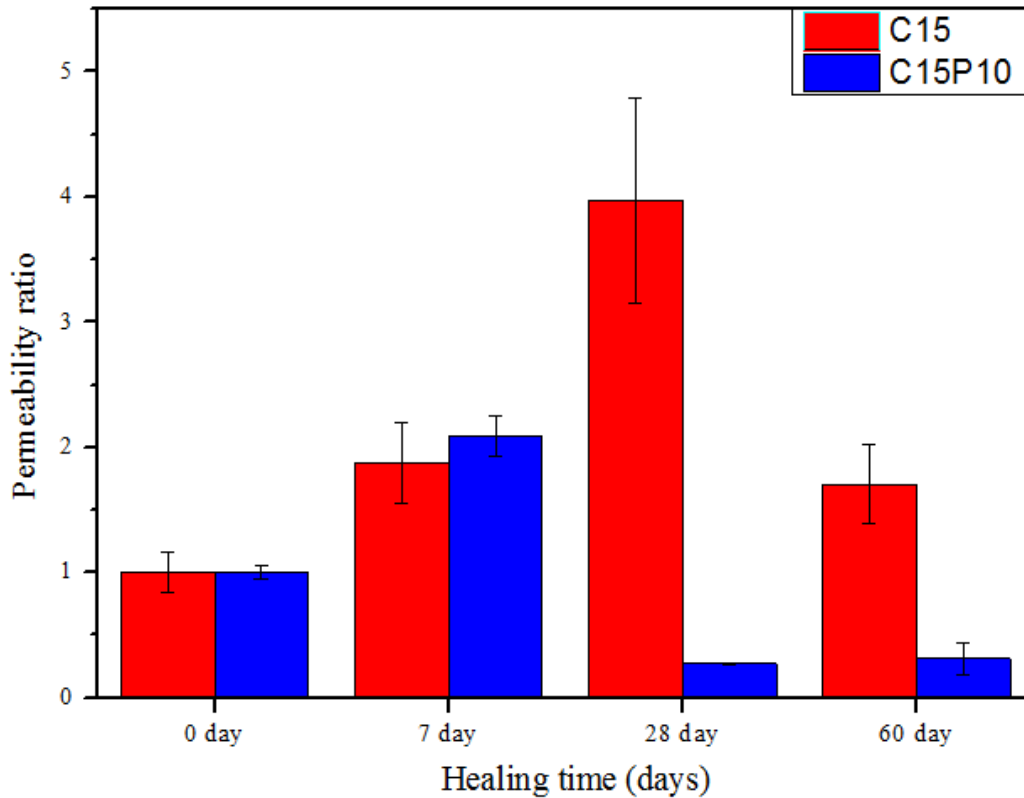


Figure 4.23 Average permeability ratios for several healing periods.

4.5.3.2 Gas permeability

To further examine the self-healing behaviour of soil-cement samples containing MgO pellets, gas permeability tests were conducted on disc samples. As indicated in **Section 3.5.5**, the un-cracked C15P10 disc samples as well as the control samples were tested at an age of 7 days. Other samples were subjected to 7 freeze-thaw cycles and then left to heal in ~98% RH. The gas permeability coefficient was calculated via **Eq. 3.9** and **Eq. 3.10**, both presented in **Section 3.5.5**. The gas permeability coefficient ratio R is defined as the ratio between the gas permeability coefficient of cracked samples after healing and the gas permeability coefficient of un-cracked samples. The coefficient ratio R of the control samples and the samples containing 10% MgO pellets are plotted against healing time in **Figure 4.24**. Similar to the hydraulic conductivity results, the addition of MgO pellets led to a considerable decrease in the gas permeability coefficient ratio R compared to the control samples. The R values of both the C15P10 samples and control samples increased to roughly 2.2 after 7 freeze-thaw cycles. This increase was anticipated, as lots of cracks were generated by the freeze-thaw damage (as previously presented in **Section 4.5.2**). After 3 and 7 days of healing, no noticeable reduction in R was observed for either mix. However, after 14 days of healing, the

R value of C15P10 decreased from 2.2 to 1.4, while the R value of C15 remained unchanged. The R value of C15P10 samples continued to decrease over time, reaching approximately 1 after 60 days of healing. This is a similar gas permeability coefficient as the un-cracked samples. By contrast, the R values of the control samples only decreased to 2.0 after 60 days of healing. These results are in agreement with the crack sealing findings, which showed 85% crack sealing efficiency after 14 days of healing and 96.3% after 60 days of healing.

Overall, these findings strongly indicate that the self-healing capability of soil-cement samples damaged by freeze-thaw cycles can be substantially improved by adding MgO pellets. The effects of the pellets' crack sealing capabilities on the mechanical properties of soil-cement are of significant interest because of their relevance to engineering applications, so they are presented in the next section.

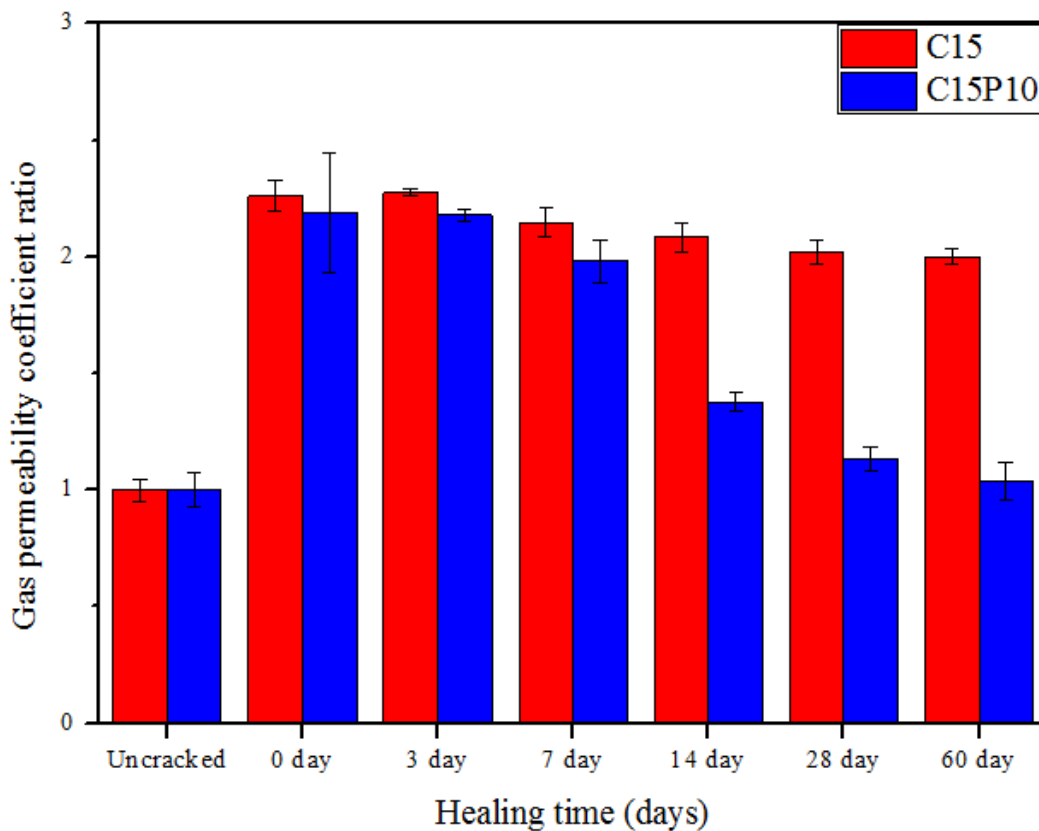


Figure 4.24 Gas permeability coefficient ratios over time for un-cracked and self-healed soil-cement samples after 7 freeze-thaw cycles.

4.5.4 Recovery of mechanical properties

4.5.4.1 UCS and Young's modulus

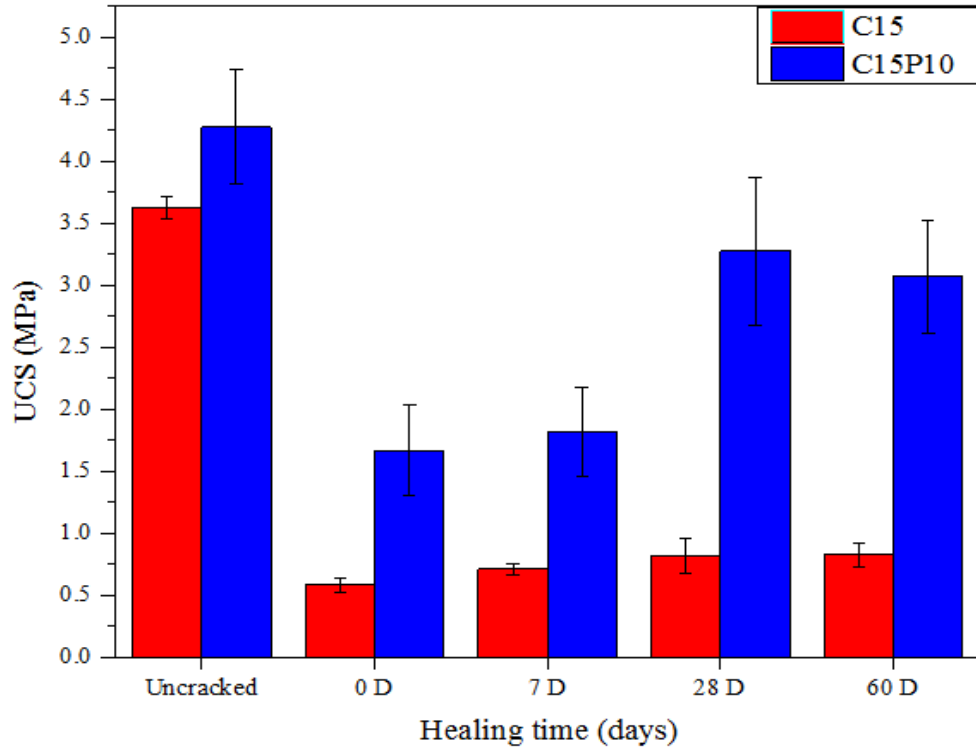
The effect of pellet addition on soil-cement UCS values was discussed in **Section 4.5.1**. It is clear from **Figure 4.17** that although the freeze-thaw resistance of C15P10 is higher than that of C15, both mixes experienced a substantial decrease in UCS after being subjected to freeze-thaw cycles. The UCS of C15P10 decreased from 4.3 MPa to 1.7 MPa, while the UCS of C15 decreased from 3.6 MPa to 0.6 MPa. In order to assess the degree to which they were able to recover their strength, the soil-cement samples were subjected to 10 freeze-thaw cycles before they were self-healed for a predetermined number of days. The UCS and stiffness recovery are the ratio between the increased value after healing and the 7-day UCS and stiffness, respectively.

The UCS values of C15 and C15P10 samples over time are presented in **Figure 4.25**. The UCS values of C15 and C15P10 after 10 freeze-thaw cycles are 0.6 MPa and 1.7 MPa, respectively. After 60 days of healing, the UCS of C15 increased from 0.6 MPa to 0.8 MPa, while the UCS of C15P10 increased from 1.7 MPa to 3.1 MPa. **Figure 4.25b** demonstrates that, in terms of UCS recovery, after 7 days of healing, the C15 samples and MgO pellet-containing samples only achieved marginal strength recovery, with increases of 1.5% and 3.5%, respectively. However, after 28 days healing, the strength recovery of the C15P10 samples increased to 37%, while the strength recovery of control mix was only approximately 4%. Strength recovery appeared to remain constant prior to 28 days of healing for both mixes. At 28 days, however, strength recoveries of 3% and 33% were recorded for the C15 and C15P10 mixes, respectively. An important note is that the strength recovery of the C15P10 samples appeared to reach its maximum at 28 days. For healing times longer than 28 days, additional strength recovery was not reported.

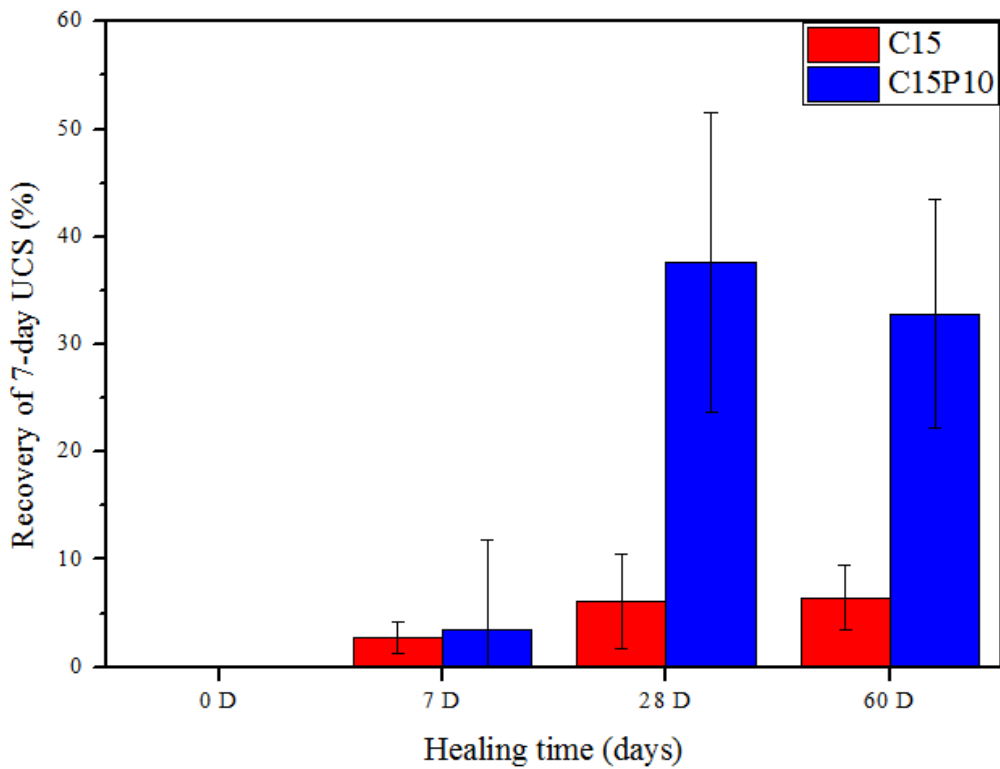
These strength recovery results are slightly higher than those reported by Alghamri (2017), which showed 14–28% flexural strength recovery for mortar samples embedded with MgO pellets. In addition, only 8% and 17% flexural strength recoveries for mortar samples embedded with soda glass capsules containing MgO were recorded in Kanellopoulos et al. (2015) and Qureshi et al. (2016), respectively. The superior strength recovery achieved in this study may be due to the nature of the damage caused in the soil-cement samples by the freeze-thaw cycles. When the soil-cement samples were damaged, cracks were generated within the samples, and water was drawn into the cracks. Rather than producing the single

crack that usually develops in other cementitious materials, freeze-thaw cycles cause soil-cement to develop a network of cracks through which water can permeate, thereby exposing nearby MgO pellets to water. Water is crucial for the healing reactions of MgO-related healing agents (Alghamri, 2017). Thus, since more water was available for the MgO pellets to react with, more healing products were produced. This indicates that MgO pellets represent a promising technique for the development of self-healing soil-cement system subjected to freeze-thaw cycles.

As shown in **Figure 4.26a**, the specimens containing MgO pellets displayed a significantly higher stiffness recovery than the controls. The stiffness recovery values followed similar trends as the UCS recovery values. The stiffness of the C15 mix increased from 18 MPa to 36 MPa after 60 days of healing, while that of C15P10 increased from 78 MPa to 235 MPa. In terms of stiffness recovery, the C15P10 samples showed a recovery rate of 30%, while this figure was just 6% for the C15 samples (**Figure 4.26b**). The UCS and stiffness recovery results are consistent with the crack sealing efficiency and permeability findings presented in **Sections 4.5.2 and 4.5.3**.

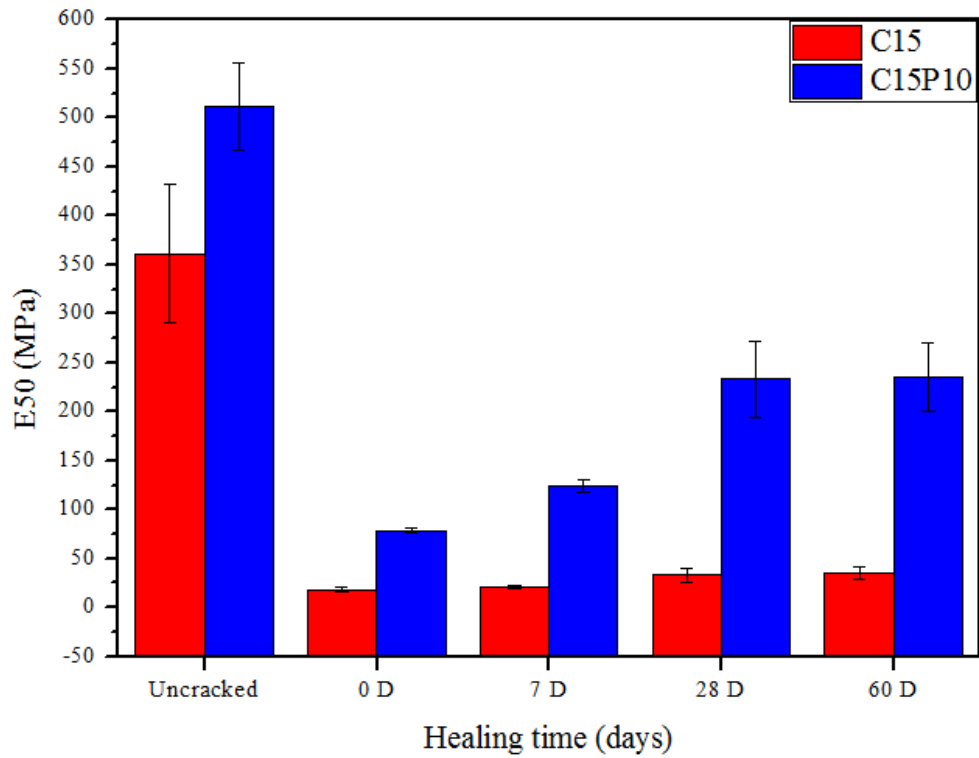


(a)

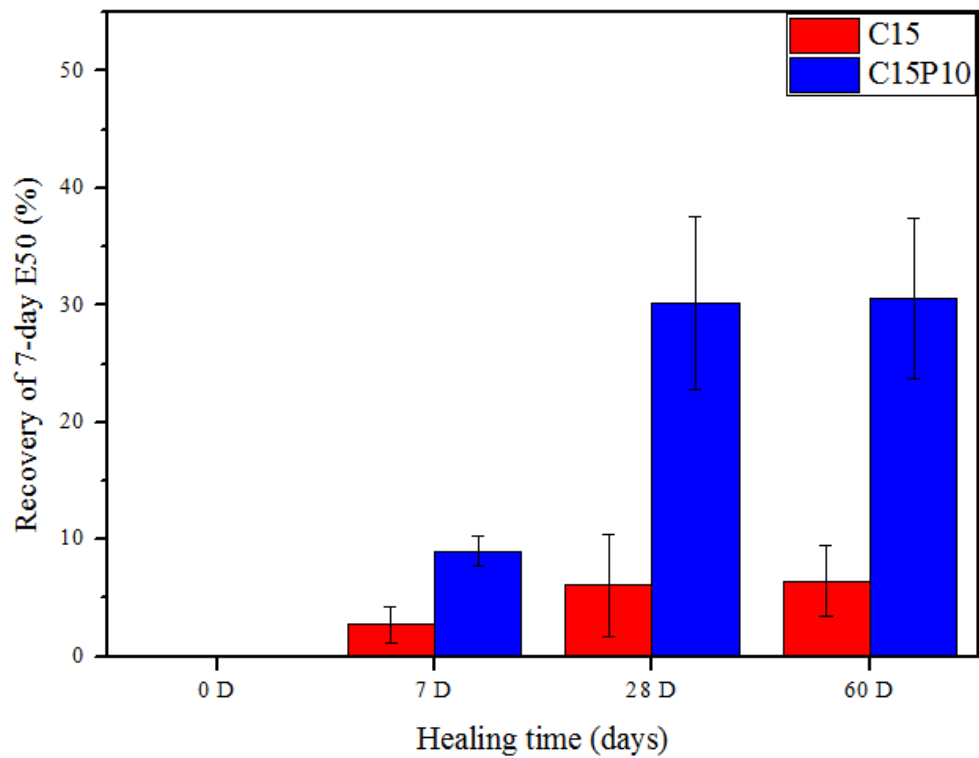


(b)

Figure 4.25 Results for C15P10 samples over time following 10 freeze-thaw cycles in terms of (a) UCS values and (b) UCS recovery (ratio between the increased value after healing and the un-cracked 7-day UCS value).



(a)



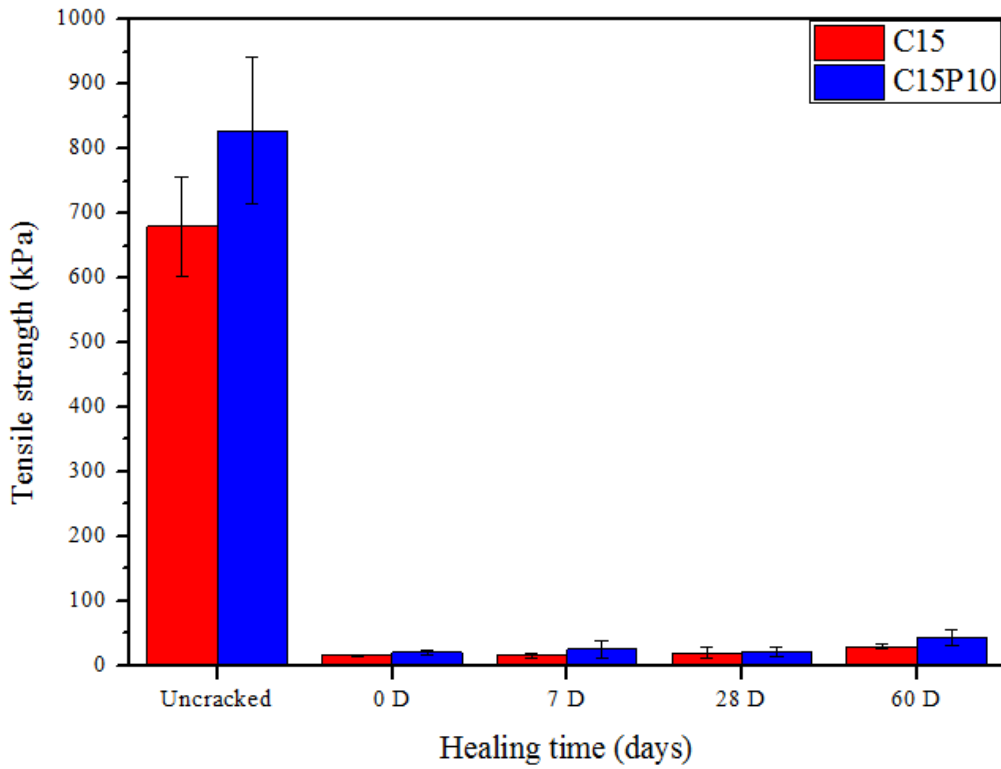
(b)

Figure 4.26 E₅₀ of C15P10 samples over time following 10 freeze-thaw cycles in terms of (a) E₅₀ value and (b) E₅₀ recovery (ratio between the increased value after healing and the uncracked 7-day E₅₀ value).

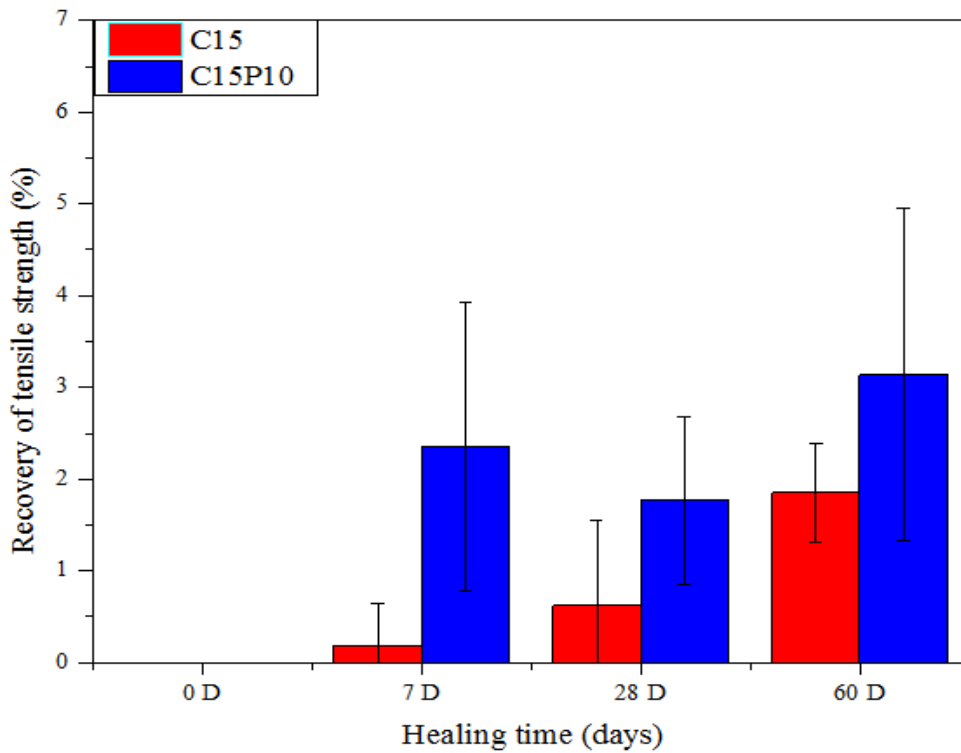
4.5.4.2 Tensile strength

Data from disc specimens subjected to axial splitting tests (detailed in **Section 3.5.3**) were used to obtain tensile strength values for the soil-cement samples. To assess strength recovery, the C15P10 mix and the control samples were subjected to 7 freeze-thaw cycles before they were self-healed for a predetermined number of days. The tensile strength and tensile strength recovery values for the C15P10 samples containing 10% MgO pellets were compared with those of the controls. The results are shown in **Figure 4.27** along with error bars indicating one standard deviation.

As shown in **Figure 4.27a**, tensile strength decreased dramatically after 7 freeze-thaw cycles, with residual tensile strength equalling only 1.7% and 1.2% of the normal 7-day tensile strength for the C15 and C15P10 mixes, respectively. **Figure 4.27b** shows that tensile strength recovered by 1.8% and 3.1% for C15 and C15P10 samples (respectively) after a self-healing period of 60 days. Although a 1.3% higher tensile strength recovery was achieved by the pellet-containing specimens, this recovery is minimal. These results contradict those obtained for UCS and stiffness in the previous section, which suggested strength recovery of up to 38% after 60 days of healing. This contradiction could be due to the chemical nature of healing products. As the healing products of MgO are brucite, hydromagnesite, dypingite, and Mg-bearing carbonates, none of which are adhesive materials, the bonds between soil-cement particles are not strengthened as they come into contact with these chemicals. However, the presence of these Mg-bearing healing products can reduce the void space and improve the interactions between soil-cement particles, therefore increase the compressive strength of soil-cement. This explains the UCS test results. In addition, although nearly complete crack sealing was observed for the C15P10 mix after 60 days in **Section 4.5.2**, this only resulted in approximately 72% residual UCS and 45% residual E_{50} , compared to the 7-day strength values.



(a)



(b)

Figure 4.27 Tensile strength over time for C15P10 samples after 10 freeze-thaw cycles in terms of (a) tensile strength values and (b) tensile strength recovery (ratio between the increased value after healing and the uncracked 7-day tensile strength value).

4.5.5 Characterisation of the healing products

4.5.5.1 Thermogravimetric analysis of the healing products

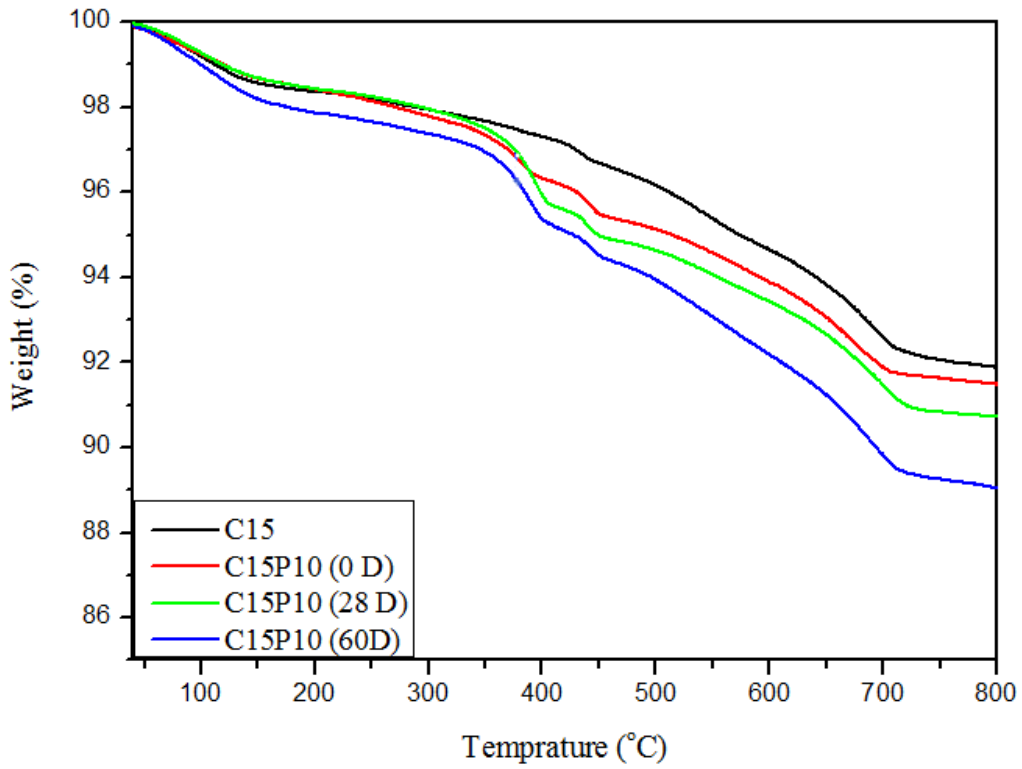
The previous sections reported that the healing products produced by MgO pellets were responsible for the significant improvements in strength recovery and crack sealing efficiency in the experimental samples. Microstructural analysis was carried out to identify these healing products. In order to characterise the healing products, thermogravimetric analysis (TGA) was conducted for all mixes. TGA data and the first derivative of the thermogravimetric data (DTG) curves for all the samples extracted from pellet-containing samples were compared to those for the control samples at various healing times. These comparisons are shown in **Figure 4.28**. The DTG values for the materials that decomposed in different peaks are shown in **Figure 4.28b**. The peak temperatures, temperature ranges, and corresponding weight losses at each step are presented in **Table 4.4**. Peaks related to the decomposition of C-S-H and $\text{Ca}(\text{OH})_2$ at temperatures of approximately 100°C and 450°C (respectively) were observed in all samples. Clear endothermic peaks at 370°C–380°C were detected for all C15P10 samples at a range of healing times. These peaks are attributed to the dehydration of brucite. The weight loss resulting from brucite decomposition increased from 1.7% to 2.4% as the healing time of C15P10 samples increased from 0 to 60 days. These values were much higher than the 0.64% weight loss of the control mix at the same temperature range (200–400°C). Note, however, that the brucite decomposition of C15P10 after 10 freeze-thaw cycles without healing was already 1.72%, which was higher than the 0.64% value obtained for the control sample after 60 days of healing. A possible explanation for this is that the healing process had already occurred during the freeze-thaw process. One final point of interest is that all C15P10 samples showed very weak peaks for portlandite compared to the control sample.

Furthermore, all samples displayed two weight loss peaks at 540°C–580°C and 670–690°C. Mo and Panesar (2012) and Thiery et al. (2007) suggest that these peaks correspond to the decomposition of different types of CaCO_3 and HMCs. As shown in **Table 4.4**, the weight loss between 500°C and 800°C for C15 samples after 60 days of healing was 4.45%. For C15P10 samples after 0, 28, and 60 days of healing, weight losses were 3.92%, 4.16%, and 5.32%, respectively. This confirms that the addition of MgO pellets increased the production of magnesium and calcite materials and that the production of these materials increased over time. Note, however, that while the brucite content increased from 1.72% to 2.34% over the

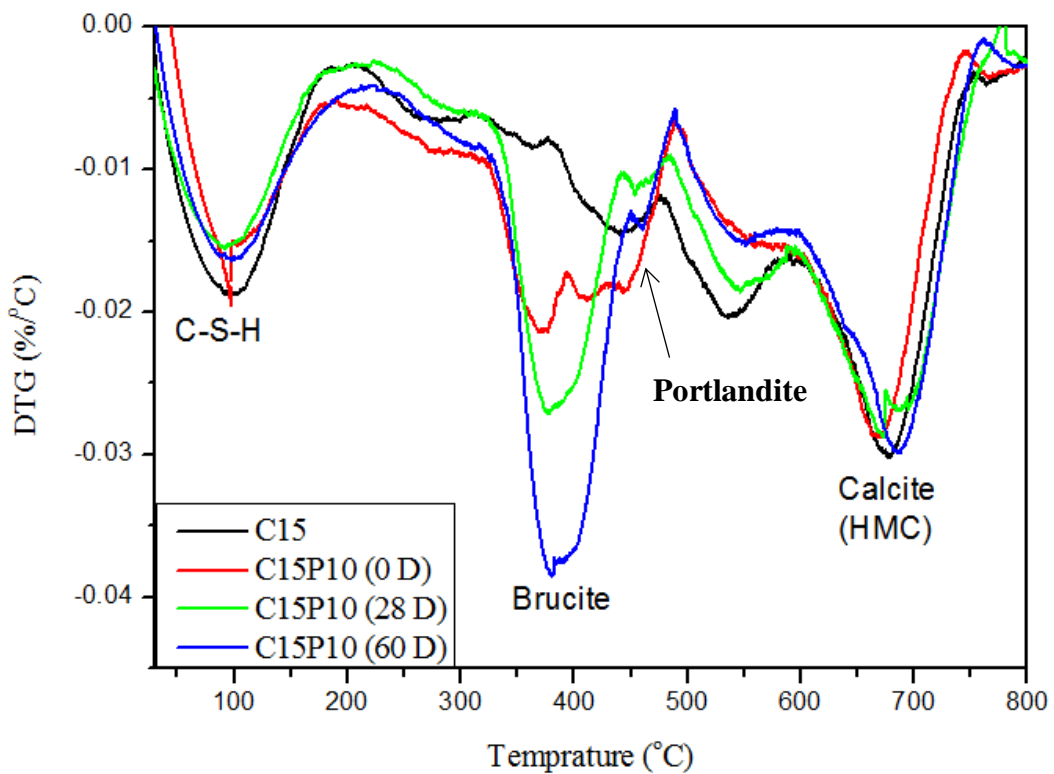
first 28 days, this value only increased to 2.40% from days 28–60. By contrast, over the first 28 days, the CaCO₃ and HMC content increased from 3.92% to 4.16%. This value further increased to 5.32% at 60 days. These results indicate that, during the early stages of the healing process, brucite is the dominant healing product, while CaCO₃ and HMCs are produced in greater quantities later in the healing process.

Table 4.4 Thermal decomposition of the samples collected from all mixes.

Mix	Healing time (days)	Temperature range (°C)	Peak temperature (°C)	Weight loss (%)	Total weight loss (%)
C15	60	40–200	108	2.01	8.23
		200–400	NA	0.64	
		400–500	439	1.77	
		500–600	537	4.45	
		600–800	677		
C15P10	0	40–200	97	1.41	8.75
		200–400	370	1.72	
		400–500	440	1.12	
		500–600	575	3.92	
		600–800	670		
	28	40–200	102	1.52	9.48
		200–400	378	2.34	
		400–500	452	1.46	
		500–600	581	4.16	
		600–800	675		
	60	40–200	98	2.08	11.30
		200–400	380	2.40	
		400–500	455	1.49	
		500–600	552	5.32	
		600–800	688		



(a)



(b)

Figure 4.28 Thermogravimetric analysis results for samples containing MgO pellets and controls at various healing times in terms of (a) TGA and (b) DTG curves.

4.5.5.2 SEM/EDX

Soil-cement samples containing MgO pellets that were self-healed for 28 days after being subjected to 10 freeze-thaw cycles were cracked, and small chips were extracted for analysis. SEM images of these solid pieces were subsequently taken. The minerals (determined by SEM/EDX) on the surface of the soil-cement chips are displayed in **Figure 4.29**. Ettringite and calcite were detected at several spots. Considerable quantities of Mg-rich products such as brucite, hydromagnesite, and dypingite were also observed in the SEM images. These observations confirm the TGA results showing that brucite and HMCs were the major healing products of the pellet-containing samples. Overall, these observations verify the TGA results and confirm that the MgO pellets produce the expected products during the healing process.

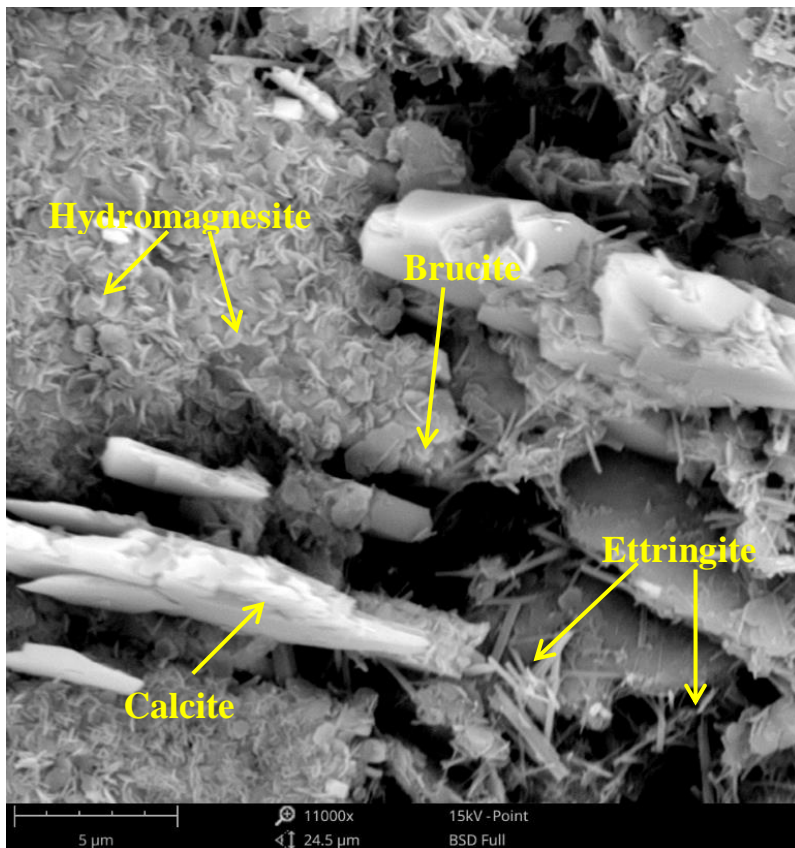
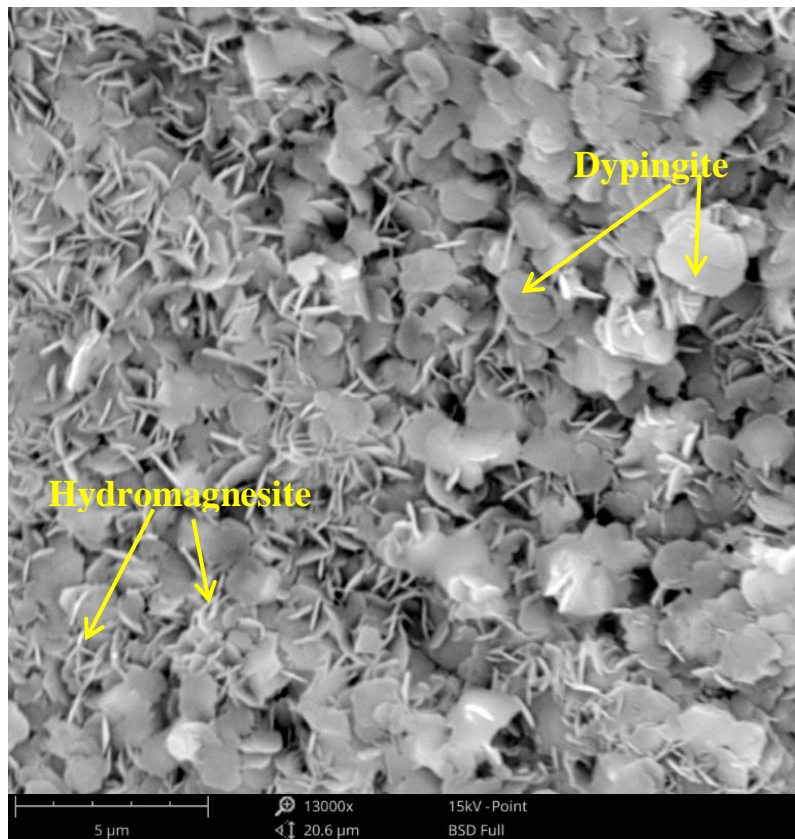


Figure 4.29 SEM images of C15P10 samples subjected to 10 freeze-thaw cycles and self-healed for 28 days.

4.6 Mechanisms of the self-healing processes

Two different healing agents were investigated in this study to provide self-healing capability for soil-cement systems that damaged by freeze-thaw cycles. Self-healing soil-cement systems were developed by adding new healing agents that can diffuse into cracks and subsequently react to form new healing products that plug the cracked section (White et al., 2001). The mechanisms that lead to self-healing in soil-cement systems containing Lambson microcapsule and MgO pellets are not entirely understood. This section, however, attempts to provide insights into these processes.

The mechanisms associated with the Lambson microcapsules and the MgO pellets are slightly different. A schematic representation of the self-healing mechanism that takes place when Lambson microcapsules are used is presented in **Figure 4.31**. When the microcapsule-embedded soil-cement sample is frozen, the water inside the soil-cement matrix expands and produces internal pressure. The microcapsules can be easily ruptured by this pressure, as they are well-bonded with the soil-cement matrix and the material that forms their shells (dried gelatine) is brittle. When the capsules rupture, the cargo material, sodium silicate solution, is released and reacts with $\text{Ca}(\text{OH})_2$ to form C-S-H gel (Giannaros, 2017; Huang and Ye, 2011) as shown in **Figure 4.31b**. The C-S-H gel acts as a binding agent within minor cracks, increasing the strength of soil-cement matrix as a whole. This explanation is supported by the results in **Section 4.4.4**, which show a UCS increase of 40% for C20L5 subjected to 1 freeze-thaw cycle and self-healed for 7 days. The UCS recovery decreased for C20L5 samples subjected to higher number of freeze-thaw cycles, however, implying that self-healing efficiency depends on the width of the cracks. As a result, when the samples with lower cement contents (C15L5 and C15L10) subjected to 10 freeze-thaw cycles, the opened cracks were too significant and negligible self-healing was observed.

The self-healing mechanism that occurs in soil-cement samples embedded with MgO pellets differs from the Lambson microcapsule mechanisms. **Figure 4.30** displays samples containing MgO pellets hit by cracks induced by freeze-thaw cycles. If the strength of the MgO pellets is lower than that of the surrounding soil-cement matrix, the MgO pellets tend to rupture in the presence of these cracks. If the strength of the MgO pellet is higher than that of the matrix, the cracks may propagate along the MgO pellet or intersect with the pellet. In both cases, the pellets can be exposed to water, which causes the MgO material to diffuse into the cracks. The reaction between MgO and water produces new healing products that are able to seal the crack. A conceptual illustration of this healing process taking place within a crack is

shown in **Figure 4.32**. Once a crack is created, the pellets are exposed to water, as water is sucked into the crack during the freeze-thaw process. Subsequently, the water dissolves and diffuses grains of the MgO into the crack (**Figure 4.32a**). The MgO reacts with water, yielding brucite. Hydrated magnesium carbonates are also formed in CO₂-rich environments. Finally, the brucite and hydrated magnesium carbonate products precipitate into the crack and begin to fill the crack over time (**Figure 4.32b**).

These healing processes depend on a variety of parameters. These include the number and location of Lambson microcapsules or the MgO pellets intersected by the crack, the amount of the healing agent diffused into the crack, the crack's geometry, the curing conditions (Huang et al., 2016), the reactivity of the healing agent, the availability of water, and the rate of precipitation of the healing products. The probability that a given crack hits a Lambson microcapsule or MgO pellet depends on the shape, size, number, and dosage of the capsules/pellets (Huang and Ye, 2014). Examples of cracks intercepting/rapturing MgO pellets in soil-cement specimens can be seen in **Figure 4.30**. As the microcapsules and MgO pellets are well-dispersed within the matrix, and as large amount of cracks tend to be generated in soil-cement samples by freeze-thaw cycles, it is very likely that many of the Lambson microcapsules or MgO pellets will be ruptured by the cracks. In addition, as the cracks generated by freeze-thaw cycles are often interconnected, it is likely that any healing materials released are able to diffuse into the water in the interconnected crack network. It is important to note, however, that the availability of water is essential to the healing process. In this study, water not only acts as a reactant, but also provides a medium for the diffusion of ions. Fortunately, due to the water-absorbing nature of soil-cement systems subjected to the freeze-thaw process, the presence of water in the cracks can safely be assumed.

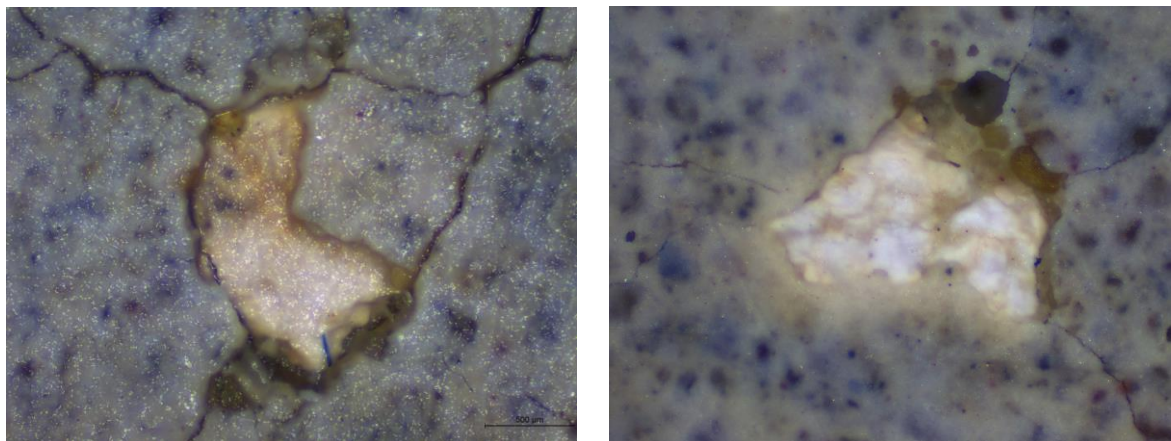
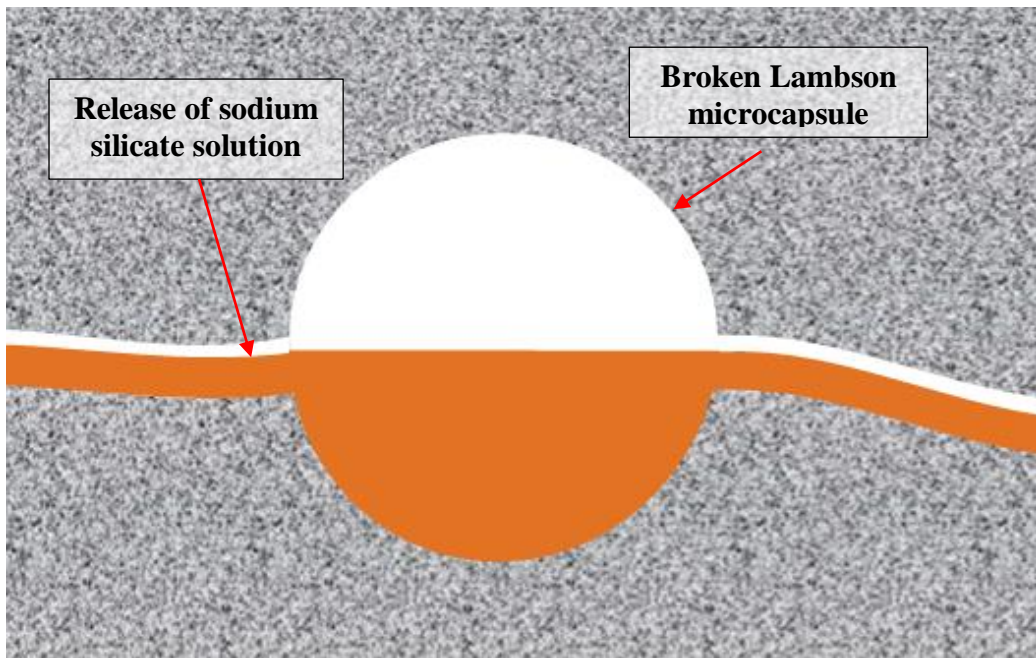
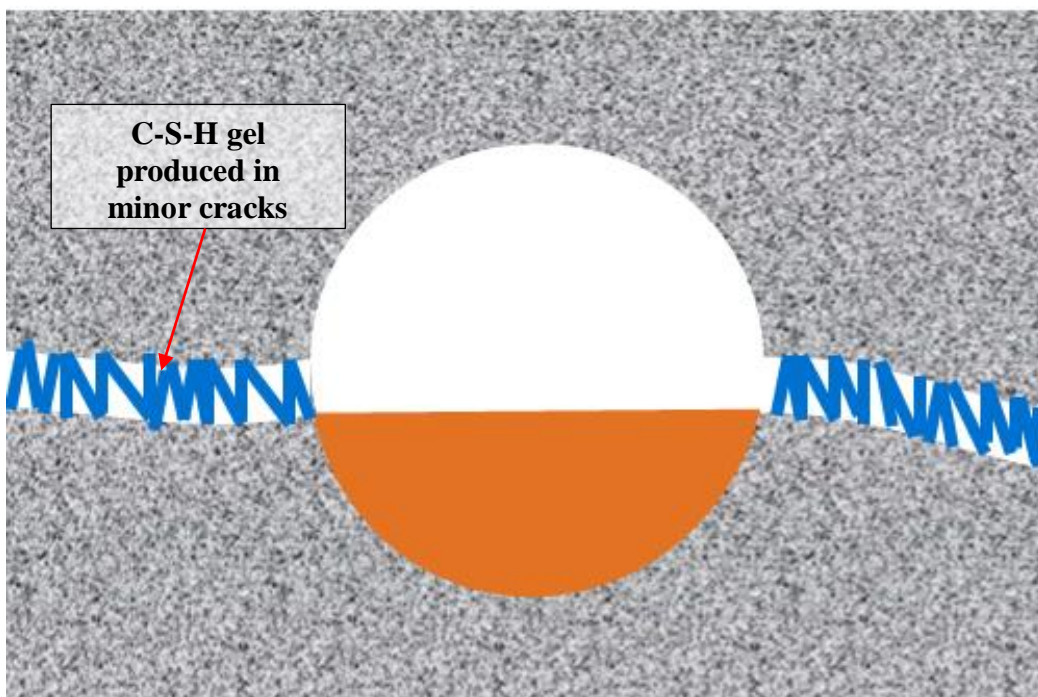


Figure 4.30 Examples of cracks induced by freeze-thaw cycles hitting an MgO pellet in soil-cement specimens.

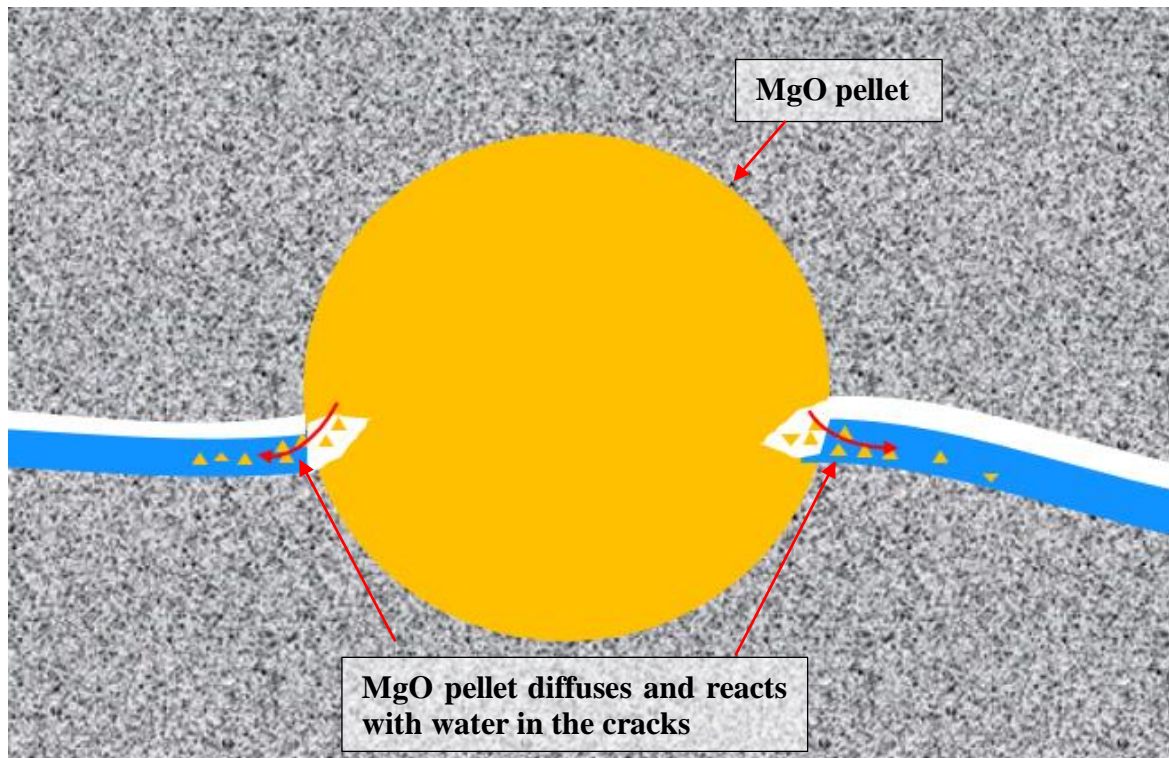


(a)

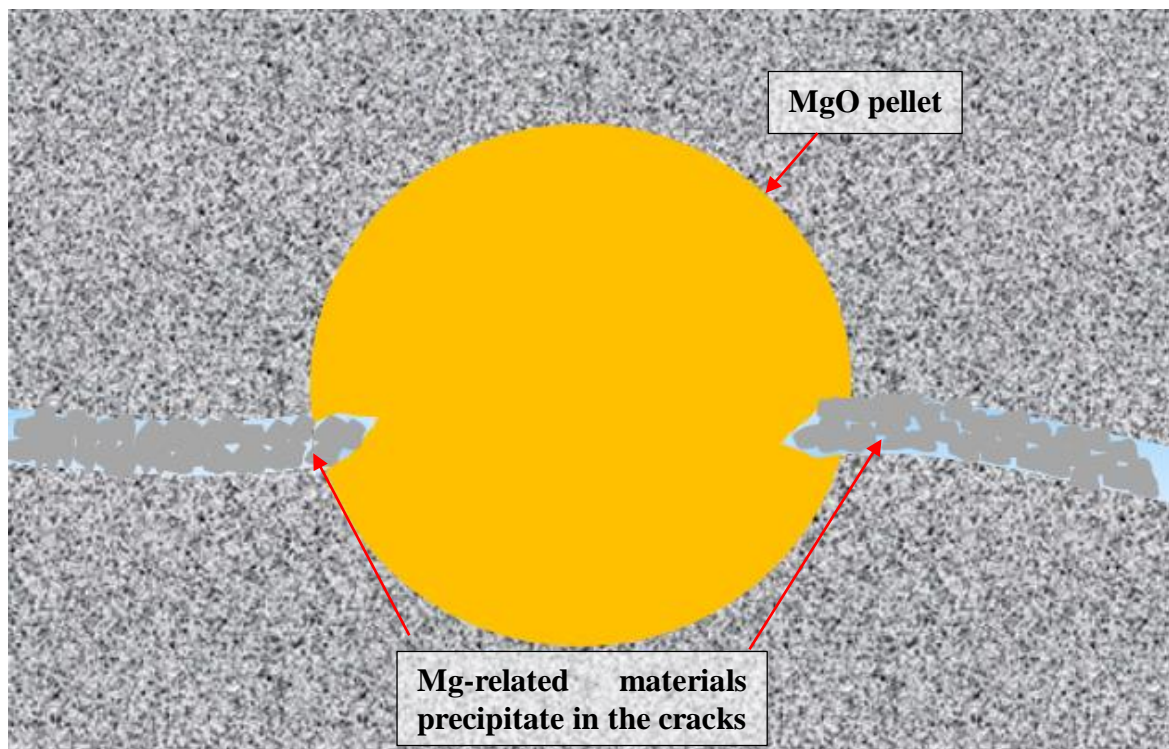


(b)

Figure 4.31 Schematic representation of the hypothesised self-healing mechanism associated with Lambson microcapsules during (a) the initial triggering process and (b) after freeze-thaw damage has been healed.



(a)



(b)

Figure 4.32 Schematic representation of the hypothesised self-healing mechanism associated with the use of MgO pellets during (a) the initial triggering process and (b) after freeze-thaw damage has been healed.

4.7 Concluding remarks

This chapter investigated the development and performance of self-healing soil-cement systems subjected to freeze-thaw cycles. Two types of healing agents were used for this purpose: Lambson microcapsules and LUVOMAG MgO pellets. It was found that a 5% addition of Lambson microcapsules (relative to the weight of the cement) had little effect on the 7-day UCS and E_{50} of soil-cement systems. However, the C20L5 mix that containing a 5% addition of Lambson microcapsules improved the self-healing capability of soil-cement considerably, with a UCS increase of 21–40% after 7 days of healing following 12 freeze-thaw cycles. It was found that the biggest improvement was observed after the first freeze-thaw cycle. However, for soil-cement systems with low cement content, the addition of Lambson microcapsules tended to slightly decrease the UCS value after several freeze-thaw cycles rather than increase the self-healing capability of soil-cement systems. As a result, the use of Lambson microcapsules as a healing agent should be limited to soil-cement systems with relatively high cement contents (e.g., 20%).

The use of MgO pellets was considered an effective technique for the development of soil-cement systems that can self-heal damage caused by freeze-thaw cycles. It was found that the addition of MgO pellets not only increased freeze-thaw resistance, but also significantly improved the self-healing capability of the soil-cement systems following freeze-thaw damage. A crack sealing efficiency of 96% was recorded for freeze-thaw-damaged C15P10 samples after 60 days of healing, while a rate of only 12% was observed for the control mix. Furthermore, a regain of durability in terms of both water permeability and gas permeability was demonstrated by the MgO pellet-containing samples after multiple freeze-thaw cycles. The pellet-containing samples also recovered 30–40% of their UCS and stiffness after 28 days of healing following the freeze-thaw cycles. However, tensile strength recovery was minimal for the pellet-containing samples, which indicates that the healing products do not function as adhesive materials. Microstructure investigations (including TGA and SEM/EDX) revealed that brucite and various hydrated magnesium carbonates (like hydromagnesite and dypingite) were produced in the pellet-containing samples. Overall, these qualitative and quantitative investigations support the notion that MgO pellets show significant potential as self-healing additives for soil-cement systems that experience freeze-thaw cycles.

A few key points of contrast between the different self-healing soil-cement systems subjected to freeze-thaw cycles using the Lambson microcapsules and MgO pellets are apparent following these analyses. First, the Lambson microcapsules appeared only to be effective for

soil-cement systems with relatively high cement content, while the MgO pellets also worked for systems with lower cement content. Second, the healing mechanism of the Lambson microcapsule-embedded samples was primarily due to further hydration that produce C-S-H, while the healing that resulted from the MgO pellets samples was due to the reaction of MgO with water, which yielded magnesium-related materials. More time was needed for the MgO pellets to react and yield their hydration products, compared to the healing mechanism of the Lambson microcapsules. Finally, the Lambson microcapsule-containing samples appeared to have better performance in terms of the recovery of their mechanical properties, while the MgO pellet-containing samples had better performance in terms of crack sealing.

However, freeze-thaw cycles can create large numbers of cracks and substantially deteriorate the engineering properties of the soil-cement system even in the presence of these additives. Although the self-healing capability of soil-cement was greatly improved by the addition of both Lambson microcapsules and MgO pellets, it was found that it is difficult to fully recover the engineering properties of the system regardless of the healing agent used. For this reason, attempts were also made to prevent the damage cause by freeze-thaw cycles.

Chapter 5 Optimisation of Self-immune Soil-cement Systems Subjected to Freeze-thaw Cycles Using SikaAer[®] Solid Microcapsules

5.1 Introduction

Taking inspiration from successful efforts to develop self-healing cementitious materials to date, **Chapter 4** described an investigation of the self-healing performance of soil-cement systems subjected to freeze-thaw cycles. Magnesia pellets and sodium silicate microcapsules were used as healing agents in a variety of experimental analyses. However, as the self-healing process these agents facilitate is only triggered once damage occurs, these methods can fail if the initial damage is sufficient to compromise the entire system. Furthermore, although self-healing soil-cement systems exhibited marked recovery in terms of many important engineering properties, it was not possible to restore full performance after severe freeze-thaw damage.

As a result, another system tailored for soil-cements expected to undergo freeze-thaw cycles was developed. Biological systems, especially the immune system of the human body, provided inspiration for a “self-immune” soil-cement system that can protect itself from the effects of freeze-thaw cycles before damage occurs, thus avoiding the damage partially or entirely.

This chapter describes how a special admixture, named SikaAer[®] Solid (SS) air entraining microcapsules, was used to develop such self-immune soil-cement systems. The performance and mechanism of this mixture’s behaviour was investigated in detail. Thus, the aims of the work presented in this chapter is to quantify the effect of SS microcapsules on the self-immune capability of soil-cement systems experiencing freeze-thaw cycles and to examine the mechanism by which self-immune effects occur. A number of material variables were considered, and a variety of techniques were used. The latter include isothermal calorimetry, flow table tests, uniaxial compression tests, splitting tensile tests, optical microscopy, hydraulic conductivity tests, porosity tests and high-resolution X-ray computed microtomography (μ CT).

This chapter is mainly divided into four parts. The first discusses the effects of freeze-thaw cycles on the physical and mechanical properties of soil-cement systems. In the second part, the influence of SS microcapsules on the initial fresh properties, physical properties, and

mechanical properties of soil-cement systems are investigated. In the third part, the freeze-thaw durability of SS microcapsule-embedded soil-cement systems is assessed in terms of the systems' physical properties, including volume, water content, and dry density, and mechanical properties including unconfined compressive strength (UCS), tensile strength, and stiffness. Finally, durability is assessed in terms of cracking ratio and hydraulic conductivity. The results suggest a relationship between the proportion of SS microcapsules added to the soil-cement system and the self-immune capability of the system under freeze-thaw conditions. This information combined with the effect of microcapsule addition on the intrinsic properties of the soil-cements supports arguments about the best dosage of SS microcapsules for soil-cement applications. In the fourth and final part of the chapter, the mechanism of the freeze-thaw process and the corresponding self-immune mechanism of soil-cement systems using SS microcapsules are discussed.

5.2 Mix design of the soil-cements

Details of the preparation of soil-cement samples were given in **Section 3.2**. A list of mix names and compositions is presented in **Table 5.1**. The control soil-cement specimens were prepared with three cement contents of 10%, 15% and 20%, and with corresponding water/cement ratios of 2.5, 1.67 and 0.8, respectively. The 15% cement content soil-cement was then mixed with varying quantities of SS microcapsules of between 0.67% and 6.66% by mass of the cement and labelled accordingly as shown in **Table 5.1**. The volume fraction, of 0.8% to 7.5% is also included in the table. The dosage of the admixture is given in mass fraction (m_f) of cement because air entraining agents are commonly believed to function during cement hydration. Moreover, the influence of air entraining agent on improving freeze-thaw durability is commonly believed to be related to the air space they create in the matrix therefore the volume fraction (v_f) was also calculated and given. For a single mix, all the samples share a similar dry density and triplicate samples were prepared for every single test.

The SS microcapsules, which are small prefabricated air bubbles with an elastic plastic envelope, were selected following a critical review of air entraining mechanism in **Section 2.2** for building self-immune soil-cement systems that subjected to freeze-thaw cycles. Characteristics of the SS microcapsules including size, density and morphology under microscope and SEM were presented in **Section 3.1.2.3**.

The hydration of fresh soil-cement samples containing a varying proportion of SS microcapsules was tested using isothermal calorimetry whilst the workability was measured by the flow table test. For volume, dry density, UCS, Young’s modulus, and hydraulic conductivity, cylindrical samples (50 mm diameter × 100 mm height) were tested while disc samples (50 mm diameter × 10 mm height) were used for flexural strength and surface analysis. In addition, small cubes of 3 mm×3 mm×3 mm were used for high-resolution X-ray computed microtomography (μ CT). The experimental programmes for investigating the self-immune performance of soil-cement specimens were given previously in **Table 3.5**. All the soil-cement specimens were firstly cured for 7 days before being subjected to freeze-thaw cycles. After 0, 1, 5, 10 and 20 (if necessary) freeze-thaw cycles, a variety of techniques were used to assess the physical properties, strength properties, tightness and microstructure of the soil-cement specimens.

Table 5.1 Mix composition of soil-cement samples containing SikaAer® Solid microcapsules.

Mix ID	Mix ingredients Ratios/mass (%)			Admixture	Mass fraction in cement, m_f (%)	Volume fraction in soil-cement, v_f (%)
	Soil	Water	Cement			
C10	100	25	10	-	-	-
C15			15	-	-	-
C20			20	-	-	-
C15S0.67			15	SikaAer® Solid microcapsules	0.67	~0.8
C15S1.67			15		1.67	~1.8
C15S3.33			15		3.33	~3.8
C15S6.67			15		6.67	~7.5

5.3 Influence of SikaAer[®] Solid microcapsules on the properties of soil-cement systems

5.3.1 Survivability and distribution of SikaAer[®] Solid microcapsules within soil-cement matrices

To develop a system that could confer self-immune qualities to soil-cement during freeze-thaw cycles, SS microcapsules were added to soil-cement systems. Unlike the conventional air-entraining agents commonly used in concrete, SS microcapsules are solids and do not dissolve in water. Therefore, they have excellent survivability during soil-cement mixing, compaction, and hydration. The addition of the SS microcapsules aims to build a self-immune soil-cement system via controlled air entrainment. The microcapsules' elastic, compressible shells (containing air) do not break during freeze-thaw cycles; thus, they create space for water within the system to expand and contract, thereby relieving the excess pressure generated within the soil-cement matrix.

This section investigates the survivability of SS microcapsules within soil-cement systems after mixing and during freeze-thaw cycles. SS microcapsules have diameters of 5–80 μm . This makes them difficult to observe within soil-cement systems using the naked eyes. Therefore, in order to examine the survivability and distribution of SS microcapsules inside the soil-cement matrix, samples were observed using an optical light microscope and scanning electron microscope (SEM). Representative optical microscopic and SEM images are presented in **Figure 5.1**. Favourable results for embedment, distribution, and survivability of SS microcapsules were observed for several different dosages (e.g., 1.67 and 3.33%). **Figure 5.1 (a-c)** presents a typical distribution of SS microcapsules within the soil-cement samples. The SS microcapsules are indicated by the red arrows. Debonding was observed between the microcapsules and the soil-cement matrix, which allows water to enter the space between them. This debonding is probably due to the tendency of the capsules to act as surfactants during cement hydration. They were observed throughout the soil-cement matrix, suggesting good distribution. However, the optical microscope can only observe a very small region of the sample surface. Thus, the distribution of SS microcapsules inside the sample cannot be known with certainty using optical microscopic or SEM images alone. A more detailed sense of the distribution of SS microcapsules inside the soil-cement system can be obtained via High resolution X-ray computed microtomography (μCT). This is discussed in **Section 5.5.4**.

To function properly, the SS microcapsules are required to not only survive the mixing process, but also to survive cyclic freeze-thaw exposure. Therefore, the survivability of SS microcapsules after multiple freeze-thaw cycles was also investigated. Microscopic images of samples embedded with microcapsules that have been subjected to 10 freeze-thaw cycles are presented in **Figure 5.1b** and **Figure 5.1d**. The microcapsules appear to have very good survivability, as, after 10 freeze-thaw cycles, all observed microcapsules remained intact within the soil-cement matrix.

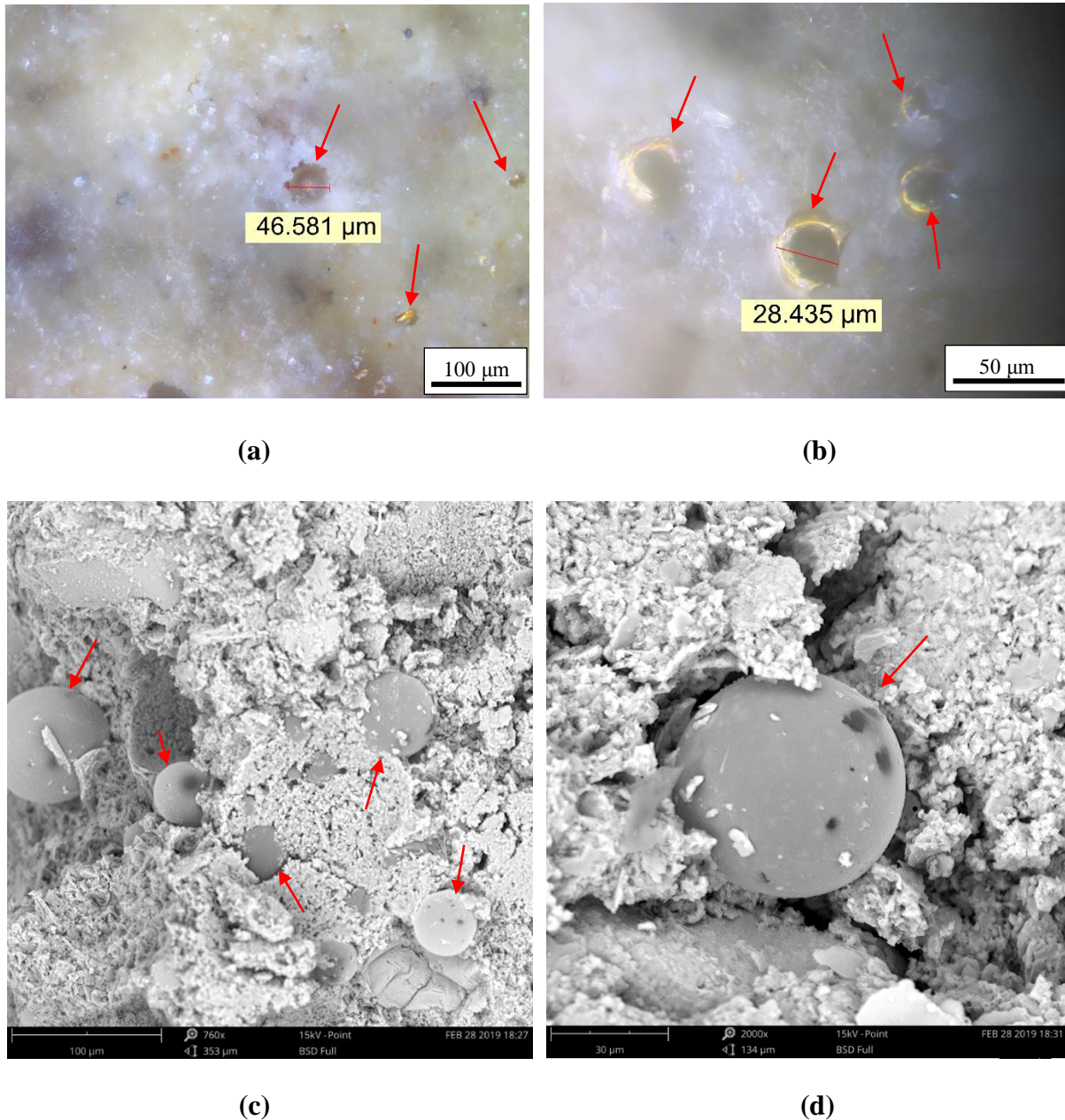


Figure 5.1 Microscopic images and SEM images of SikaAer® Solid microcapsules within the soil-cement matrix. Images depict microcapsules before freeze-thaw cycles (a and c) and after 10 freeze-thaw cycles (b and d).

5.3.2 Fresh properties of the SikaAer[®] soil-cement mixes

5.3.2.1 Calorimetry

This section primarily focuses on the effects of SS microcapsules on the hydration processes of Portland cement within soil-cement mixes. This was considered necessary, as the addition of SS microcapsules may affect the hydration process as they increase the void ratio within the mix, potentially impeding heat transfer. The thermal power produced per gram of cement for mixes containing $m_f = 1.67\%$ (C15S1.67), 3.33% (C15S3.33) and 6.67% (C15S6.67) SS microcapsules relative to the control mix (C15) are presented in **Figure 5.2**. In addition, calculated values of the setting time and peak power values for all mixes are summarised in **Table 5.2**.

Generally, it can be seen from **Figure 5.2** and **Table 5.2** that the addition of SS microcapsules up to 6.67% had little effect on the setting time, and that the capsules slightly increased the peak power values of the cement compared to the control mix. This is a coherent result, as the capsules do not react with materials of the soil-cement mix. C15S1.67 exhibited a similar setting time (4.46 hours) as that of the control mix (4.44 hours). However, a slight change in the calorimetry results was observed for mixes with a higher microcapsule content. Additionally, the peak power values were slightly increased for all mixes following the addition of SS microcapsules. An explanation for this might be that SS microcapsules act as lubricants and surfactants, thereby facilitating the hydration of cement, reducing the setting time, and increasing the peak power values. However, the increased addition of SS microcapsules, coincides with an increase in the void ratio of the soil-cement system. This increased void ratio would disturb the hydration of the cement by disrupting the connections between cement particles. In addition, the increased void ratio could provide a greater volume of mass to dissipate exothermic heat. At dosages higher than 1.67%, the setting time of the mixes increased with the addition of SS microcapsules, which indicates that the effects of the excess void ratio became more dominant than other effects. The setting time for C15S6.67 was roughly 4.8 hours. This represents an increase of approximately 7.8% relative to the 4.5 hours observed for the control mix. Based on these results, a recommended microcapsule dosage of 3.33% relative to the weight of the cement can be added to the soil-cement mix to ensure only a negligible delay in the hydration process.

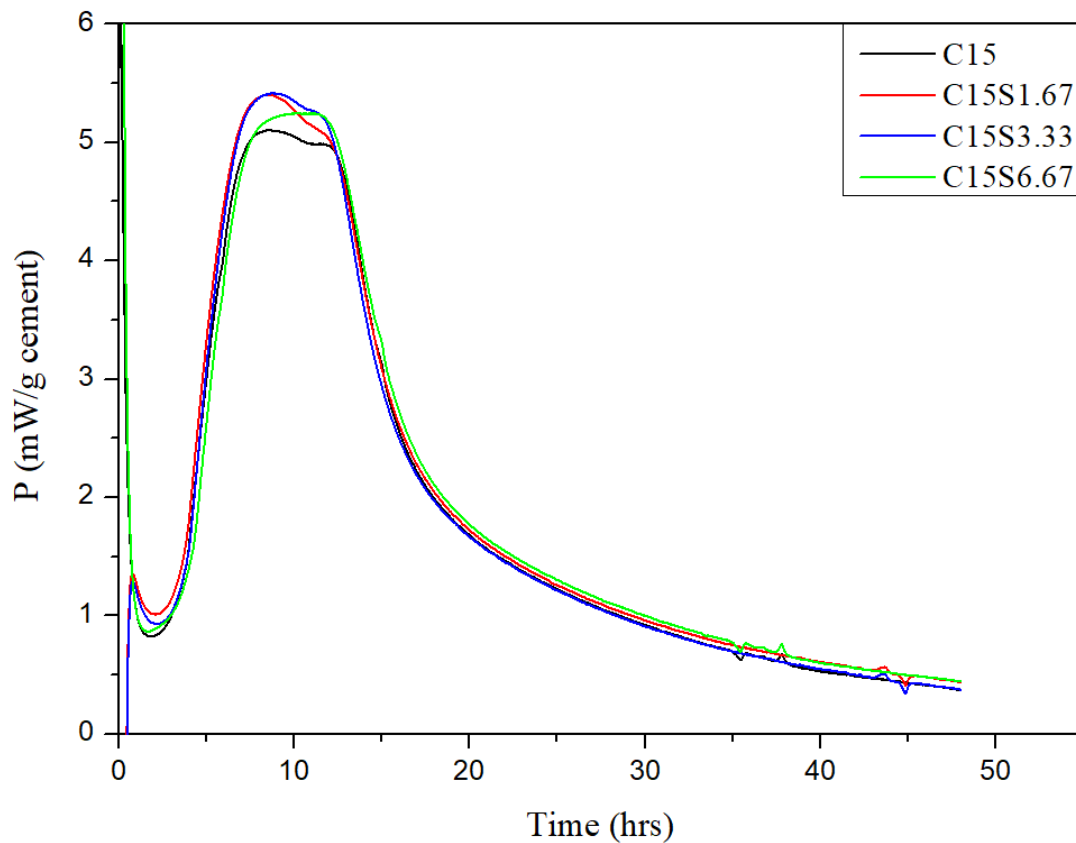


Figure 5.2 Effects of SikaAer® Solid addition on isothermal (23°C) power and energy production of soil-cement mixes.

Table 5.2 Initial setting time and peak power values for soil-cement mixes containing different dosage of SikaAer® Solid microcapsules compared to the control.

Mix	Initial setting time (hrs)	Peak power (mW/g)
C15	4.46±0.08	4.28±0.07
C15S1.67	4.44±0.06	4.39±0.05
C15S3.33	4.57±0.04	4.49±0.04
C15S6.67	4.81±0.08	4.39±0.08

5.3.2.2 Flowability

The flowability of soil-cement mixes embedded with different dosages of SS microcapsules was measured via the flow table tests described in **Section 3.4.2**. **Figure 5.3** illustrates the effects of the addition of different dosages of SS microcapsules on the flow values. Flowability is considered an important parameter in this study, as it affects not only the distribution of SS microcapsules within soil-cement mixtures, but also the workability of

those mixtures. The control mix (C15) showed a flow value of 190 mm. The flow values of mixes C15S1.67, C15S3.33, and C15S6.67 were 187 mm, 193 mm, and 186 mm, respectively. These values indicate that the addition of SS microcapsules does not reduce the workability of the soil-cement mix. This corroborates the manufacturer’s claim that addition of SS microcapsules can improve the workability of cementitious materials (Sika Deutschland GmbH, 2014). Moreover, this result is predictable, as the SS microcapsules do not react with the materials in soil-cement. Therefore, the water/cement ratio within the mix remains unchanged. SS microcapsules may even have positive effects on the workability of soil-cement. By performing a lubricating function, they can reduce friction between aggregates. However, the water/cement ratio for the mix studied is 1.67, which is relatively high. Therefore any lubricating function the microcapsules perform will be minimal. These results are considered favourable as high flowability not only makes the soil-cement easy to mix, but also helps the SS microcapsules to disperse in soil-cement systems.

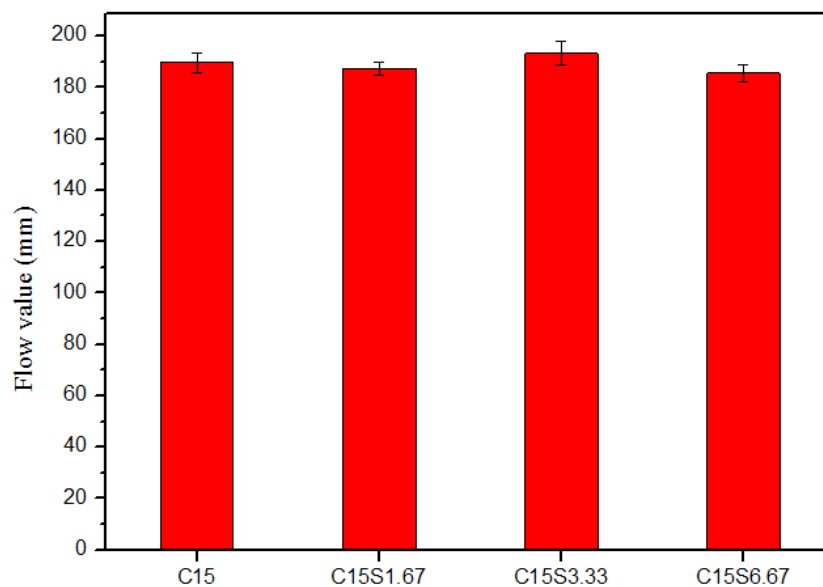


Figure 5.3 Flow table values for soil-cement mixes with different dosages of SikaAer® Solid microcapsules compared to the control mix.

5.3.3 Physical properties

5.3.3.1 Water content

The water content of soil-cement systems embedded with SS microcapsules was measured after 7 days of curing. These data are presented in **Figure 5.4**. **Figure 5.4** shows that the addition of SS microcapsules generally has little effect on the water content of soil-cement systems. This result was anticipated, as the microcapsules, prefabricated air bubbles with an

elastic acrylonitril-polymer envelope, react with neither cement nor water. As discussed in **Section 5.3.2.1**, the addition of SS microcapsules was revealed to have little effect on the calorimetry of the soil-cement systems. However, C15S1.67 showed a lower water content than the control. This decrease may be due to the lubricant effect of SS microcapsules in the soil-cement matrix, which accelerates the hydration process, thus consuming more water. This would corroborate the calorimetry results previously discussed in **Section 5.3.2.1**, which showed that setting time decreased and peak power increased for C15S1.67. For microcapsule dosages of 3.3% and 6.67%, the water content increases slightly from 17.9% (the control result) to 18.4% and 18.6%, respectively. An explanation for this result may be that the higher volume of SS microcapsules and increased air content slightly delay the hydration of cement, therefore causing less water to be consumed after 7 days. These results are also consistent with the calorimetry analysis results for mixes C15S3.33 and C15S6.67.

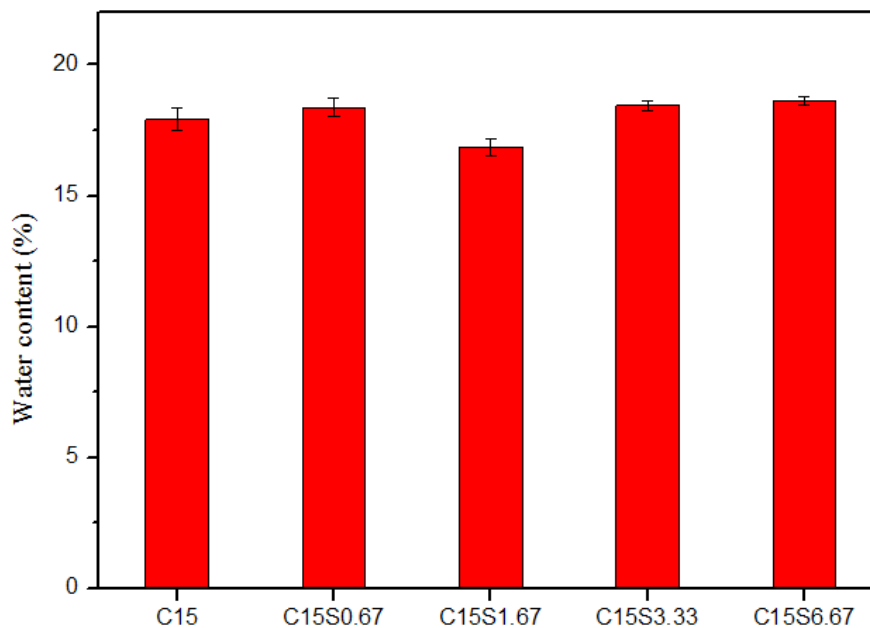


Figure 5.4 Water content of soil-cement mixes with different dosages of SikaAer® Solid.

5.3.3.2 Dry density

Dry density values were calculated from the mass, moisture content, and volume of the specimens. As expected, a gradual decrease in the soil-cement samples' dry density was observed for increasing quantities of microcapsules. The mean and normalised dry density values of all mixes are given in **Figure 5.5**. The 7-day dry density of soil-cement decreased by 1.9%, 3.5%, 8.2%, and 12% for C15S0.67, C15S1.67, C15S3.33 and C15S6.67, respectively. There are several possible explanations for these results. First, SS microcapsules

have a relatively low density, so their addition directly reduces the dry density of soil-cement. In addition, SS microcapsules can act as air-entraining agents when mixed with cement and water therefore air-voids are generated around them. Consequently, the air content of the soil-cement systems embedded with SS microcapsules increased considerably, reducing the systems' dry density. However, this reduction in dry density is not significant unless a large amount of SS microcapsules is added. Considering that a large decrease in dry density is not favourable, a microcapsules dosage of less than 3.33% is recommended.

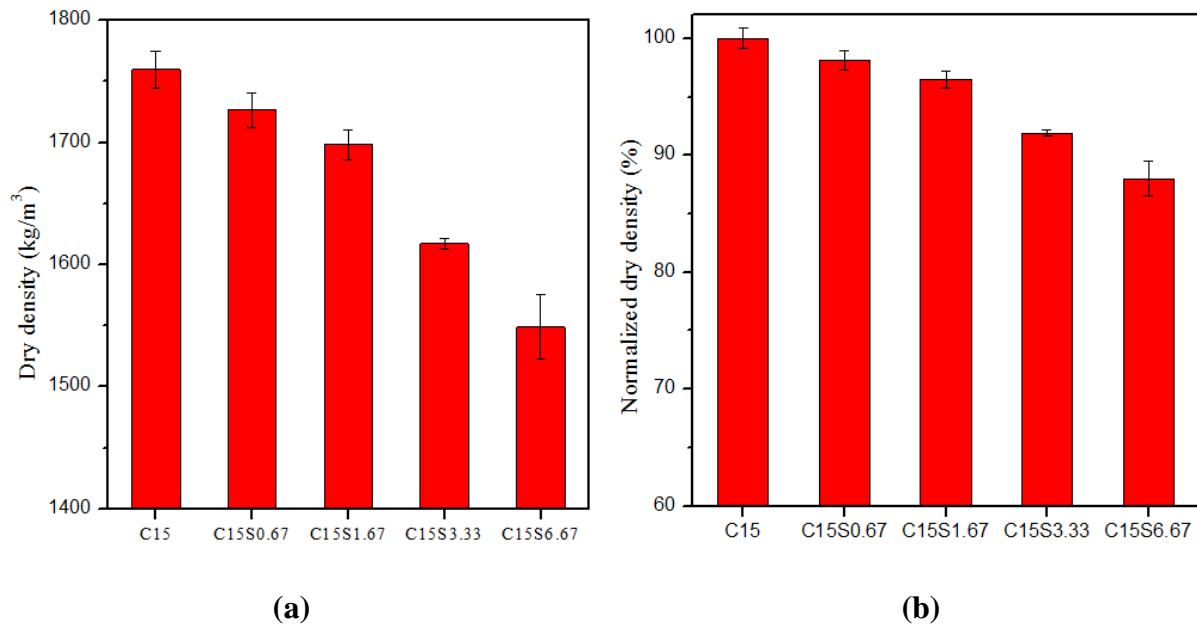


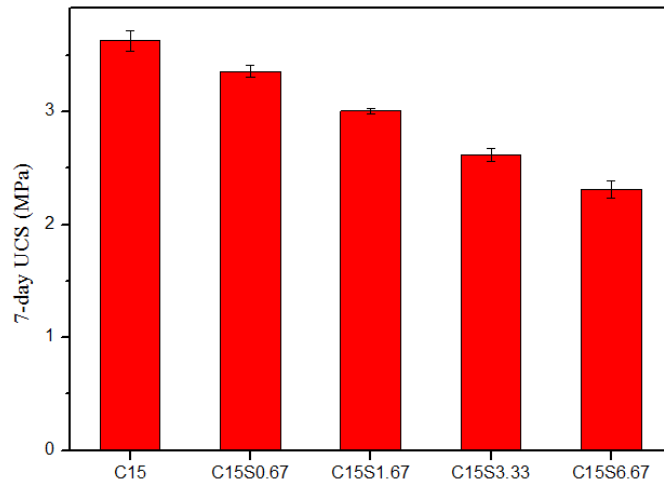
Figure 5.5 (a) Dry density and (b) normalised dry density for soil-cement mixes with different dosages of SikaAer® Solid.

5.3.4 UCS and Young's modulus

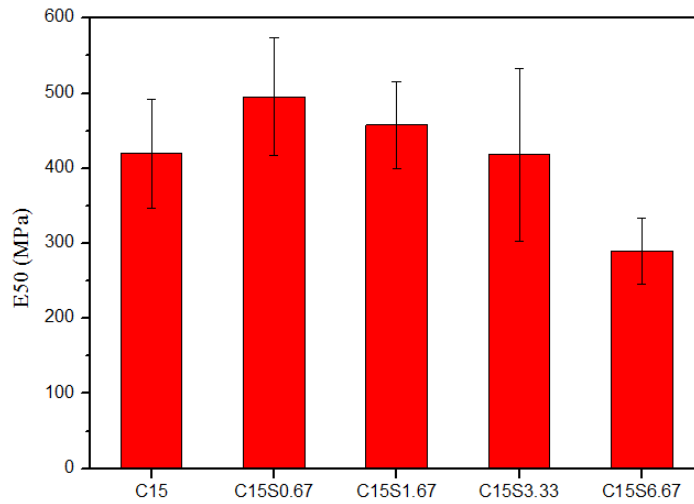
The effects of the addition of SS microcapsules on strength properties like UCS and Young's modulus were also investigated. The mean 7-day UCS for all mixes is shown in **Figure 5.6a**. Generally, the addition of SS microcapsules reduced the 7-day UCS of soil-cement samples. The reduction had a mostly linear relationship with increasing dosage. For example, only a 7% reduction was observed at $m_f = 0.67\%$, while the strength reduction was 27% and 36% after adding 3.33% and 6.67% dosages of microcapsules, respectively. This was anticipated, as the addition of SS microcapsules increases the void ratio of the system, therefore reducing its compactness. Similar results were also reported by Giannaros (2017), which found 13% and 28% UCS reductions for mortar specimens embedded with $m_f = 2.5\%$ and 5% dosages of SS microcapsules, respectively. These results are consistent with the results highlighted in

Section 5.3.3.2, which found a noticeable reduction in dry density when SS microcapsules were added to the soil-cement system.

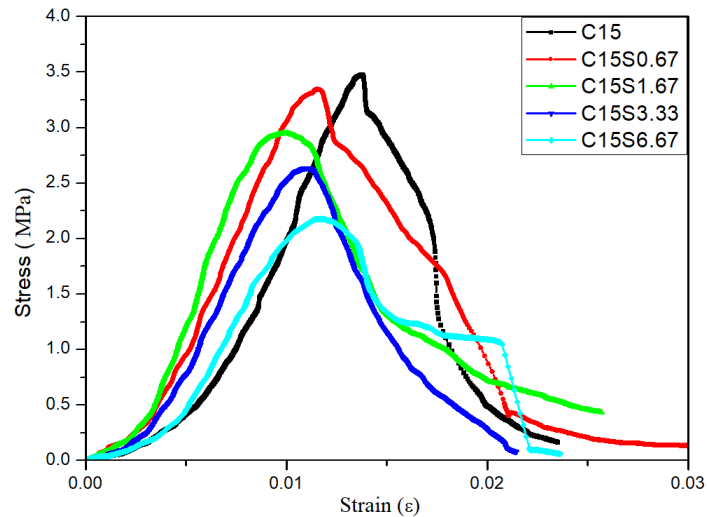
The effects of the addition of SS microcapsules on the stiffness and stress-strain curves for all mixes are presented in **Figure 5.6b** and **Figure 5.6c**, respectively. Unlike the 7-day UCS results, the Young's modulus of the SS microcapsule-containing samples was observed to slightly increase. For example, compared to the control, the E_{50} values of C15S0.67 and C15S1.67 increased by 18% and 9%, respectively. The E_{50} increase contradicts the decrease observed in the 7-day UCS. This result may be explained by the fact that the addition of SS microcapsule facilitates the early hydration of cement, as discussed in **Section 5.3.2.1**. Therefore, as more hydration products were produced in the C15S0.67 and C15S1.67 mixes over 7 days, their stiffness increased relative to the control. However, although more hydration products were produced, the increased void ratio caused by the SS microcapsules would eventually lead to overall reductions in strength and stiffness. As shown in **Figure 5.6c**, C15S6.67 samples were much more ductile than controls, and their E_{50} was 30% lower. With the addition of excess SS microcapsules, the positive effects of enhanced cement hydration become less important and the negative effects of higher void ratio begin to dominate. A significant reduction in strength and stiffness is undesirable for soil-cement systems in engineering practice. Thus, it is recommended that the dosage of SS microcapsules be kept as low as possible once the soil-cement samples demonstrate self-immunity to freeze-thaw deterioration.



(a)



(b)



(c)

Figure 5.6 Mechanical properties of soil-cement samples containing varying dosages of SikaAer® Solid microcapsules: (a) 7-day UCS, (b) Young’s modulus, and (c) stress-stain curves.

5.3.5 Unconfined compressive strength development

The effects of the addition of SS microcapsule on UCS development were also investigated. The UCS values of soil-cement samples containing SS microcapsules at curing times of up to 90 days are presented in **Figure 5.7**. Results show that the addition of 1.67 % of microcapsules reduces the 7-day UCS of soil-cement but accelerates UCS development between 7 and 14 days. At 14 days, the UCS of C15S1.67 was 13% higher than for C15 samples of the same age. However, the difference became negligible at the age of 28 and 60 days. At 90 days, the C15 samples displayed higher strength (namely, 5.4 MPa compared to 4.5 MPa observed for C15S1.67 samples). This is likely caused by the air voids created by the SS microcapsules, as air voids within the cement matrix hamper hydration at later ages (e.g., after 60 days). In sum, the addition of 1.67% SS microcapsules appears to slightly enhance the early UCS development of soil-cement (before 14 days) while hampering UCS development at later age (after 60 days).

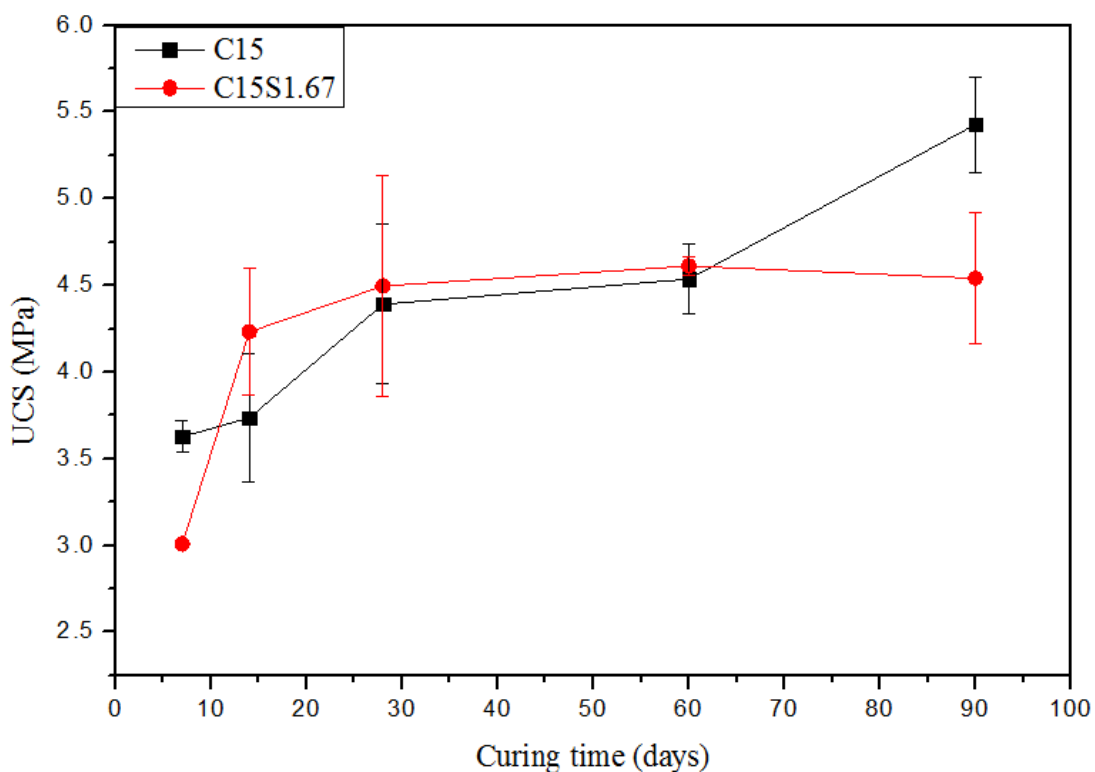


Figure 5.7 UCS of soil-cement samples containing different proportions of SikaAer[®] Solid microcapsules over time.

5.4 Evaluation of the self-immune capability of SikaAer[®] Solid microcapsules embedded soil-cement systems subjected to freeze-thaw cycles

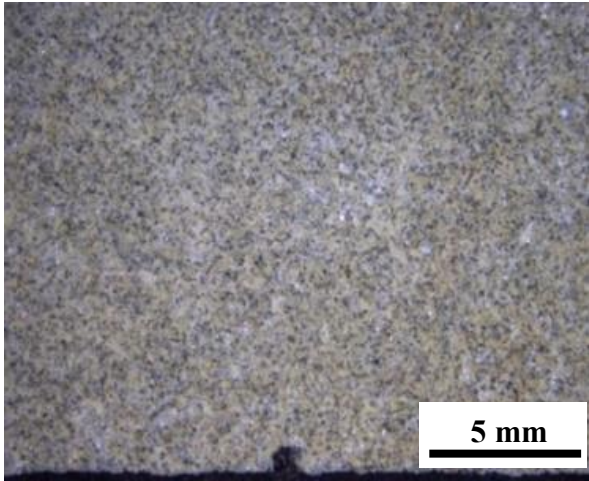
In this section, the freeze-thaw durability of the soil-cement systems embedded with SS microcapsules was evaluated in terms of physical properties, mechanical properties and permeability.

5.4.1 Physical properties

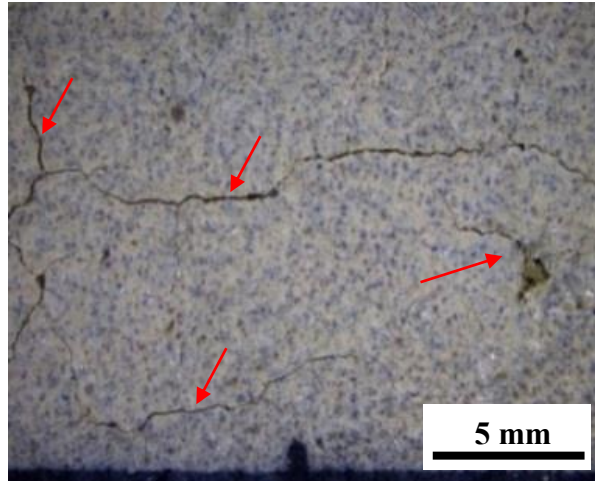
5.4.1.1 Surface crack characterisation

The crack characteristics of the soil-cement systems were observed using a light microscope to examine disc samples. The light microscope was used to investigate the extent of the disruption in the soil-cement specimens after different numbers of freeze-thaw cycles (e.g. 0, 5, 8, and 10). Representative optical microscopic images of the samples, with cracks indicated by red arrows, are presented in **Figure 5.8**. Images were taken with the Leica LED2000 optical microscope. A location on the surface of the soil-cement specimen was marked so that the changes after repeated freeze-thaw cycles could be compared consistently. Thus, the images presented in **Figure 5.8** show only small, specific regions of the sample surface.

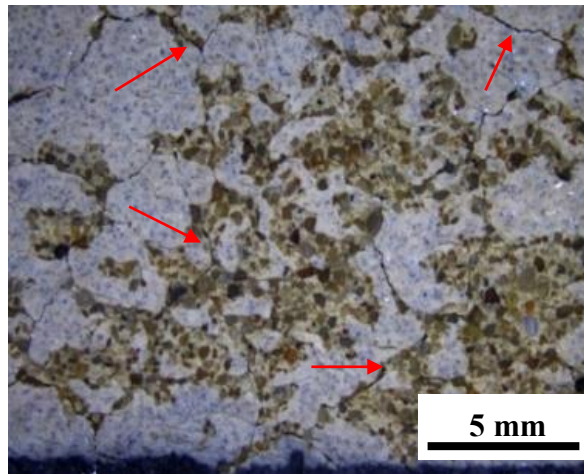
Damage and cracking can be clearly observed on the surfaces of the C15 samples (**Figure 5.8a**) after 5 freeze-thaw cycles. Significant damage was observed after 8 cycles—disc samples were too weak to handle more than 8 freeze-thaw cycles. For the C15S1.67 sample (**Figure 5.8b**), cracks were barely observable after 5 freeze-thaw cycles, but minor cracks were observed after 10 freeze-thaw cycles. However, for C15S3.33 mixes (**Figure 5.8c**), no cracks were observed at all, even after 20 freeze-thaw cycles. Based on these observations, SS microcapsules embedded in the soil-cement systems seem to provide self-immunity to crack formation caused by freeze-thaw cycles. The results of the microscopic analysis and the crack area ratio values revealed that the addition of SS microcapsules significantly improved the freeze-thaw resistance of the soil-cement systems in terms of preventing crack initiation. For microcapsule dosages of 3.33%, the soil-cement systems appeared to be entirely self-immune to up to 20 freeze-thaw cycles, and crack formation was completely eliminated.



No freeze-thaw cycles

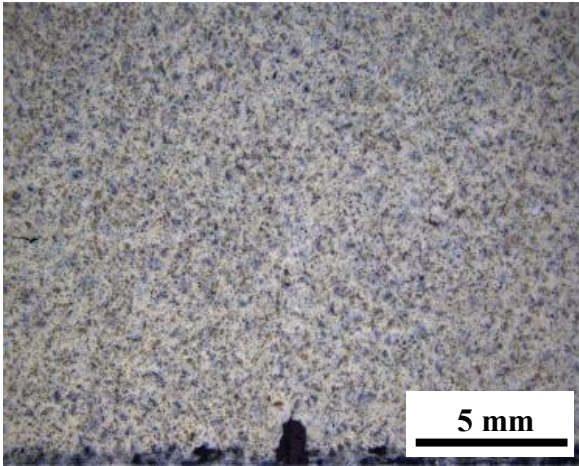


5 freeze-thaw cycles

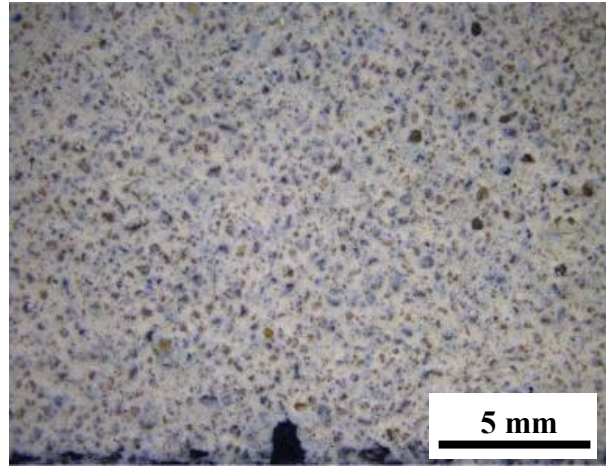


8 freeze-thaw cycles

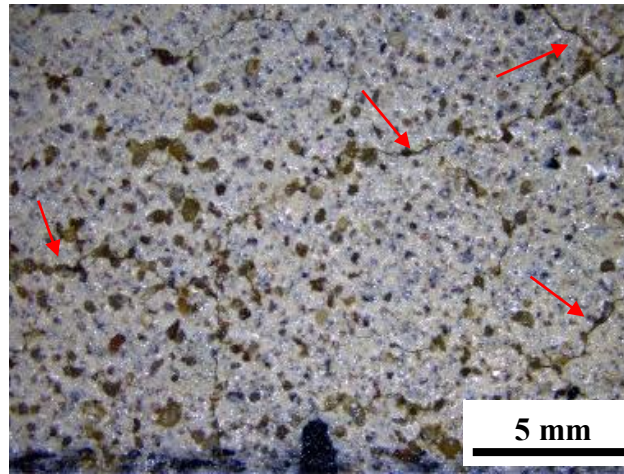
(a)



No freeze-thaw cycles



5 freeze-thaw cycles



10 freeze-thaw cycles

(b)

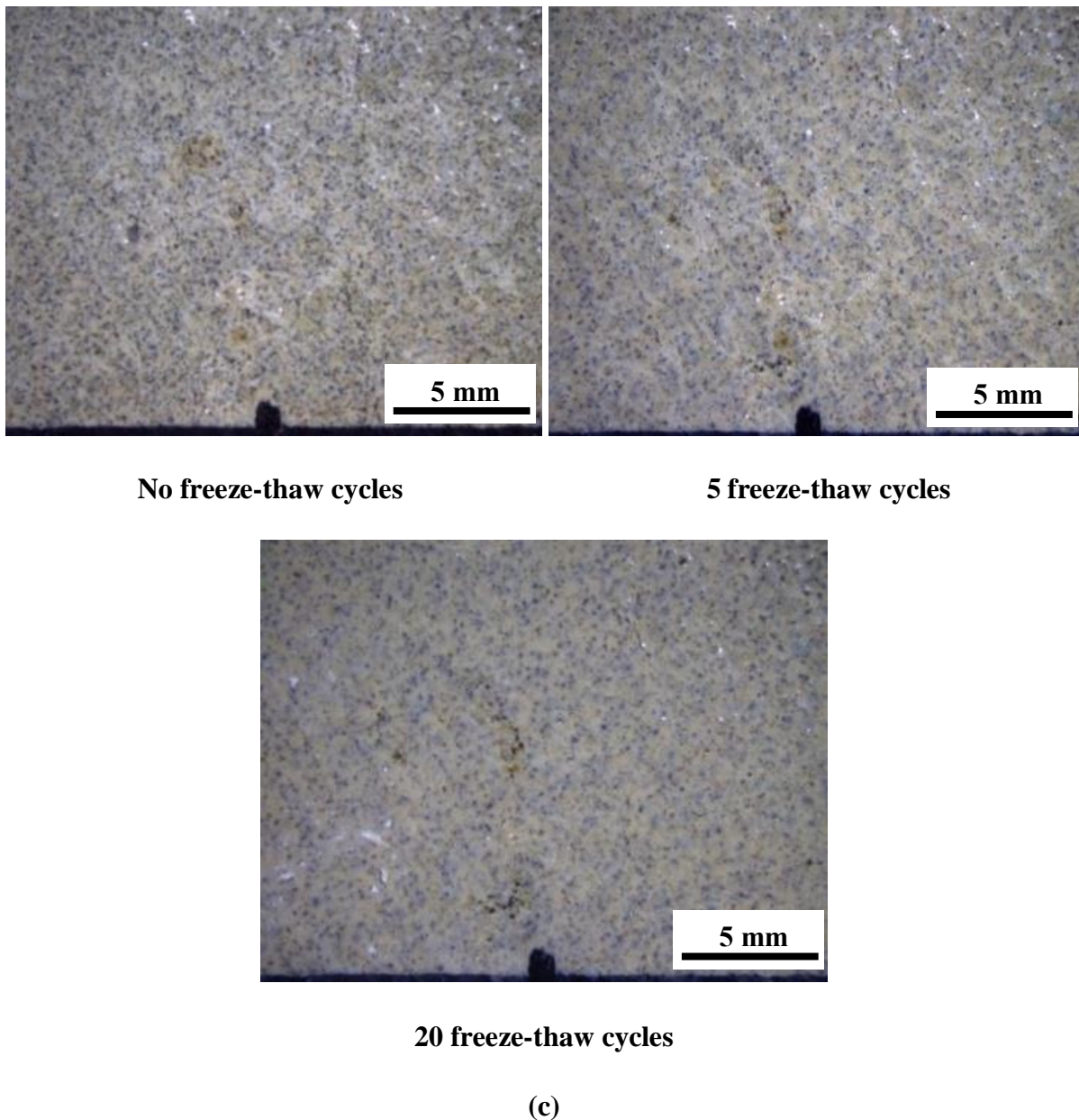


Figure 5.8 Typical microscopic images of cracking patterns in (a) control samples and self-immune samples embedded with (b) 1.67% and (c) 3.33% microcapsule dosages after repeated freeze-thaw cycles.

5.4.1.2 Porosity, degree of saturation (S_r) and air content

The specific gravity (G_s) of the soil-cement particles was determined according to ASTM: D854-10 (2010), and the porosity, degree of saturation, and air content of the soil-cement samples were calculated according to ASTM: D7263-09 (2009). The porosity directly reflects the number of voids in the soil-cement matrix. Thus, change in porosity can reflect changes in crack generation and opening during the freeze-thaw process. Taken together, the degree of saturation and porosity can give insights on the behaviour of internal water when soil-

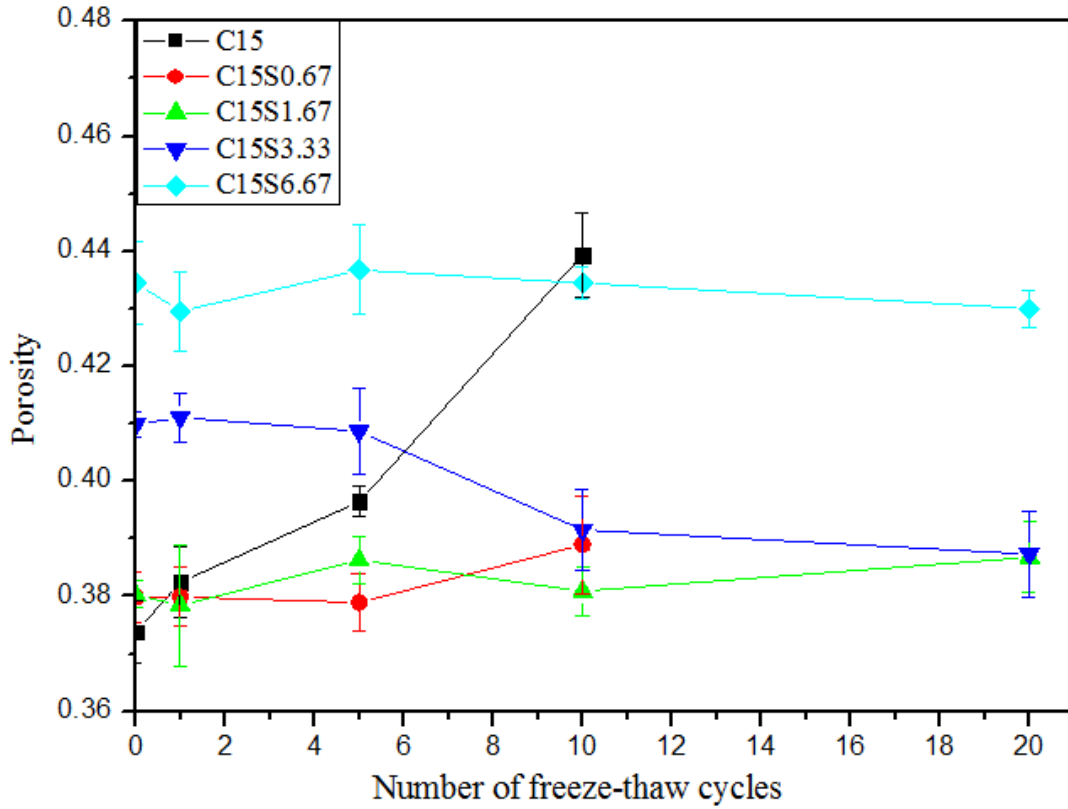
cement samples are subjected to cyclic freeze-thaw action. As presented in **Figure 5.9a**, the porosity of C15 increases with increasing numbers of freeze-thaw cycles: its value changes from 0.37 to 0.44 after 10 cycles, for instance. This increase in the porosity of the soil-cement system is mainly caused by the expansion of ice during freezing, as pores are enlarged and cracks are generated within the system via this process.

While the initial porosity of soil-cement samples in this study did indeed increase with the addition of SS microcapsules, the change in porosity after repeated freeze-thaw cycles was greatly reduced. For example, the porosity of C15S0.67 remained steady for 5 freeze-thaw cycles, and this value only had increased slightly (from 0.38 to 0.39) at 10 freeze-thaw cycles. For other mixes, including C15S1.67, C15S3.33, and C15S6.67, porosity did not increase even after 20 freeze-thaw cycles.

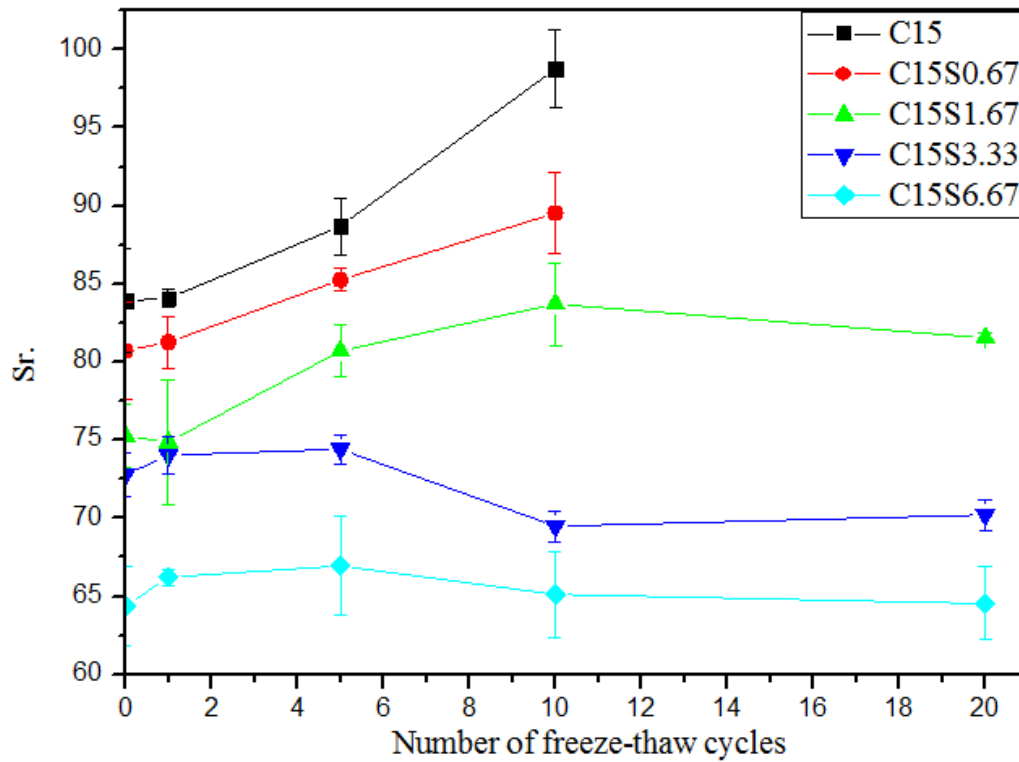
The degree of saturation (Sr.) reflects the saturation status of internal air voids and the degree to which water can enter soil-cement samples during the freeze-thaw process. The degree of saturation was calculated using **Eq. 3.3**. Sr. values for all soil-cement mixes are presented in **Figure 5.9b**. The initial degree of saturation for C15 samples was 84%, and this value increased to 100% after 10 freeze-thaw cycles. This indicates that the C15 specimens were fully saturated after 10 freeze-thaw cycles, which is consistent with the water content trends discussed in **Section 5.4.1.3**. Cyclic freeze-thaw exposure causes a pumping effect that increases the moisture content and degree of saturation of the pore system. If the air void volume is not enough to accommodate a volume expansion of about 9% that occurs when water freezes, or the air pores are situated far apart (over 0.4mm) (Penttala, 2009), hydraulic overpressure occurs. As a result, in the control samples, capillary pores keep opening during freezing, and water migrates into the matrix via the pumping effect that occurs during thawing. After several cycles, internal water content reaches a high level and the soil-cement becomes progressively more vulnerable to freeze-thaw exposure. However, for C15S1.67, C15S3.33, and C15S6.67 samples, the Sr. increase after freeze-thaw cycles was greatly reduced. With dosages of 3.33% or higher, the Sr. of the system did not increase even after 20 freeze-thaw cycles.

Air content is calculated by using **Eq. 3.4**. The values for all the soil-cement mixes are presented in **Figure 5.9c**. The air content of C15 decreased with increasing numbers of freeze-thaw cycles, and this value dropped from 6% to almost zero after 10 freeze-thaw cycles. The addition of SS increased the initial air content of the soil-cement system.

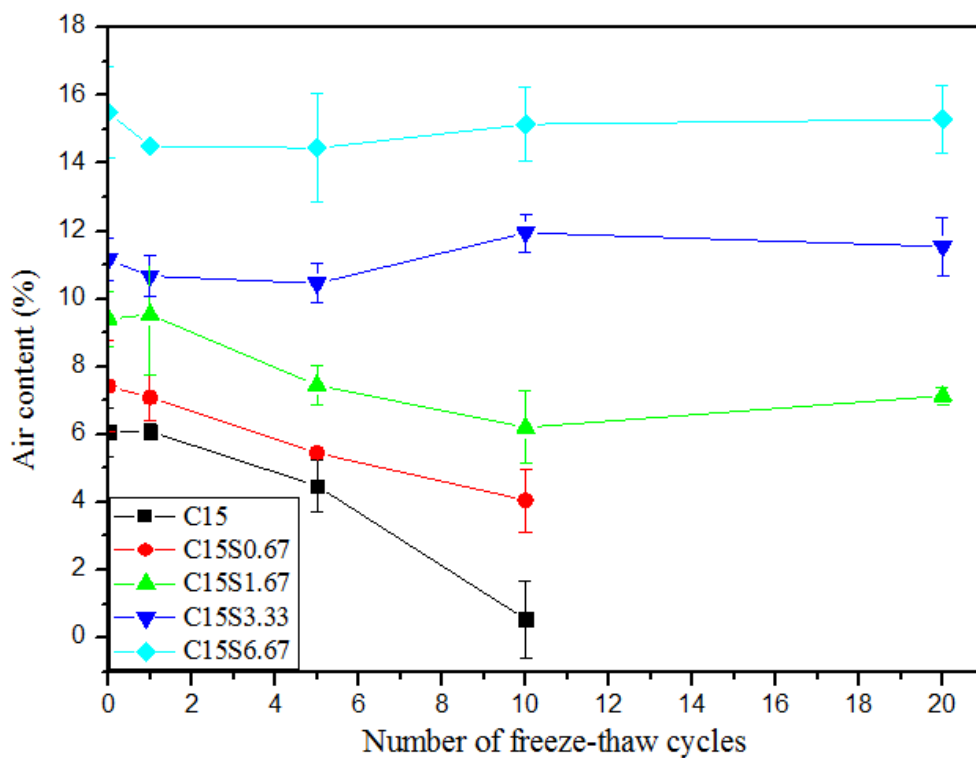
C15S0.67 and C15S1.67 still experienced a decrease in air content, but the decrease was smaller than that of C15. However, mixes C15S3.33 and C15S6.67 exhibited little variation in air content even after experiencing 20 freeze-thaw cycles. As a result, in terms of Sr. and air content, the recommended dosage of SS microcapsule for a soil-cement system that is self-immune to freeze-thaw cycles is 3.33%.



(a)



(b)



(c)

Figure 5.9 (a) Porosity, (b) degree of saturation, and (c) air content of SikaAer microcapsule-embedded soil-cement systems over repeated freeze-thaw cycles.

5.4.1.3 Water content

The water content of each mix was measured by oven-drying the fractured specimens following their uniaxial compressive strength testing. Li et al. (2011) argued that fluid ingress is a primary cause of freeze-thaw damage in concrete. Similarly, water content is also an important parameter of soil-cement systems, and it is an important indicator of the progression of freeze-thaw damage. Water migration plays a key role in freeze-thaw deterioration, as the damage is primarily caused by the freezing of water. The water content of soil-cement mixes with varying dosages of SS microcapsules added over multiple freeze-thaw cycles is shown in **Figure 5.10**. A sharp increase was observed in the moisture content of the control mix (C15) after several freeze-thaw cycles. However, this increase was reduced with the addition of SS microcapsules. After 10 freeze-thaw cycles, the moisture content of C15 was increased by 9.5%, from 18% to 27.5%, but this increase drops to only 2.7% when 0.67% of SS microcapsules are added. With the addition of 1.67% or greater, the moisture content of the soil-cement samples only changes slightly even after 20 cycles.

As discussed in **Section 4.3**, the increased moisture content for the C15 samples was related to water absorption and pore/crack expansion that occurred during the freeze and thaw process. During freezing, the water inside the soil-cement expands by approximately 9%, which enlarges pores and fissures and make them interconnect and forms a flow path within the soil-cement matrix. After this occurs, the temperature difference between the frozen sample and relatively warm water in nearby soil causes a dramatic capillary suction effect. Thus, liquid and vaporous water migrates from warmer to colder areas through the pores and fissures (Guthrie et al., 2006). In this way, the frozen samples tend to suck water from the underlying warm water that is made available during the thawing process, and the soil-cement's water content increases.

However, water content for the four different SS microcapsules dosage mixes (C15S0.67, C15S1.67, C15S3.33, and C15S6.67) was much more stable after the freeze-thaw cycles than in the control mix (C15). An explanation for this might be that the incorporation of SS microcapsules reduces the water migration into soil-cement systems that normally occurs during freeze-thaw cycles. However, the water permeability results in **Section 5.4.3** show that the initial hydraulic conductivity of samples embedded with SS microcapsules is actually higher than that of the control samples. Therefore, the reduced water uptake is likely not due to a change in hydraulic conductivity. Another possible explanation is that the creation of

interlinked cracks during freeze-thaw cycles is prevented by the SS microcapsules, which are able to relieve the pressure generated by water freezing. Moreover, the SS microcapsules themselves are impermeable, so their simple presence may also hinder water ingress. Finally, it bears mentioning that the SS soil-cement system itself could have a sufficiently low hydraulic conductivity to resist the capillary suction generated by the temperature gradient.

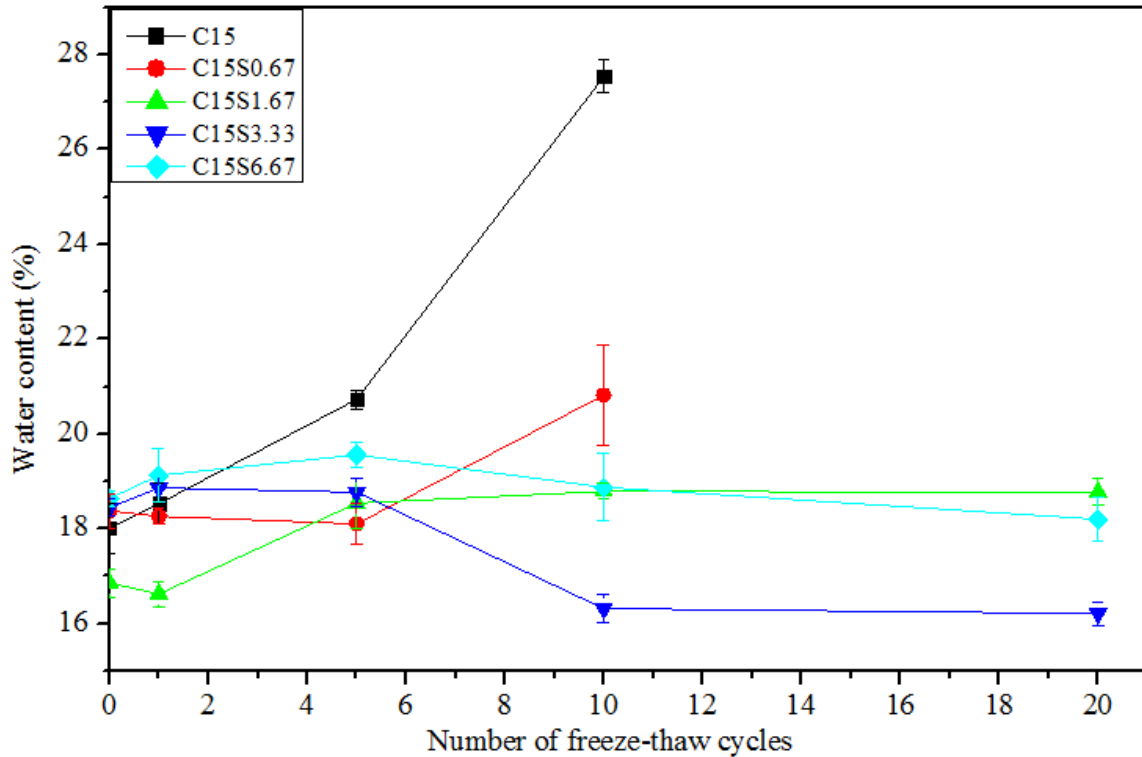


Figure 5.10 Water content of soil-cement samples containing different dosages of SikaAer® Solid microcapsules subjected to repeated freeze-thaw cycles.

5.4.1.4 Volume

The volume of each sample before and after repeated freeze-thaw cycles was recorded, and the resulting volumetric change was calculated. The volumetric change of a sample is defined as the change of volume (dv) compared to its original volume (V_0). Volumetric change is recorded as a percentage. Volume change is a metric that is commonly studied for soil-cement systems, as frost heave presents an important hazard for geotechnical infrastructure projects (e.g. pavement) that undergo freeze-thaw cycles. As shown in **Figure 5.11**, the volume of the C15 samples increased over multiple freeze-thaw cycles. An increase of 11% was observed after 10 cycles. This result is consistent with many studies that have reported that the volume of soil/soil-cement systems increases over repeated freeze-thaw cycles (e.g., Liu et al., 2010; Shibi and Kamei, 2014). The volume increase is likely to be caused by the

ingress of water that occurs during freeze-thaw cycles as well as the expansion of water during freezing. This explanation is corroborated by the strong correlation between volumetric change and water content presented in **Figure 4.3a**.

By adding SS microcapsules, the volumetric change of all soil-cement mixes was greatly reduced. Only <2% volumetric change was measured for C15S0.67 after 10 freeze-thaw cycles. Per **Figure 5.11**, for mixes C15S1.67, C15S3.33, and C15S6.66, volumetric change remains negligible after 20 freeze-thaw cycles. These results indicate that the SS microcapsules greatly reduce the volumetric change caused by the phase change of water. Thus, the addition of at least 1.67% SS microcapsules appears to make the soil-cement system self-immune to the volumetric change caused by freeze-thaw cycles. Frost heave effects can apparently be completely prevented for self-immune soil-cement systems embedded with SS microcapsules. These results further support the results reported in **Section 5.4.1.2**.

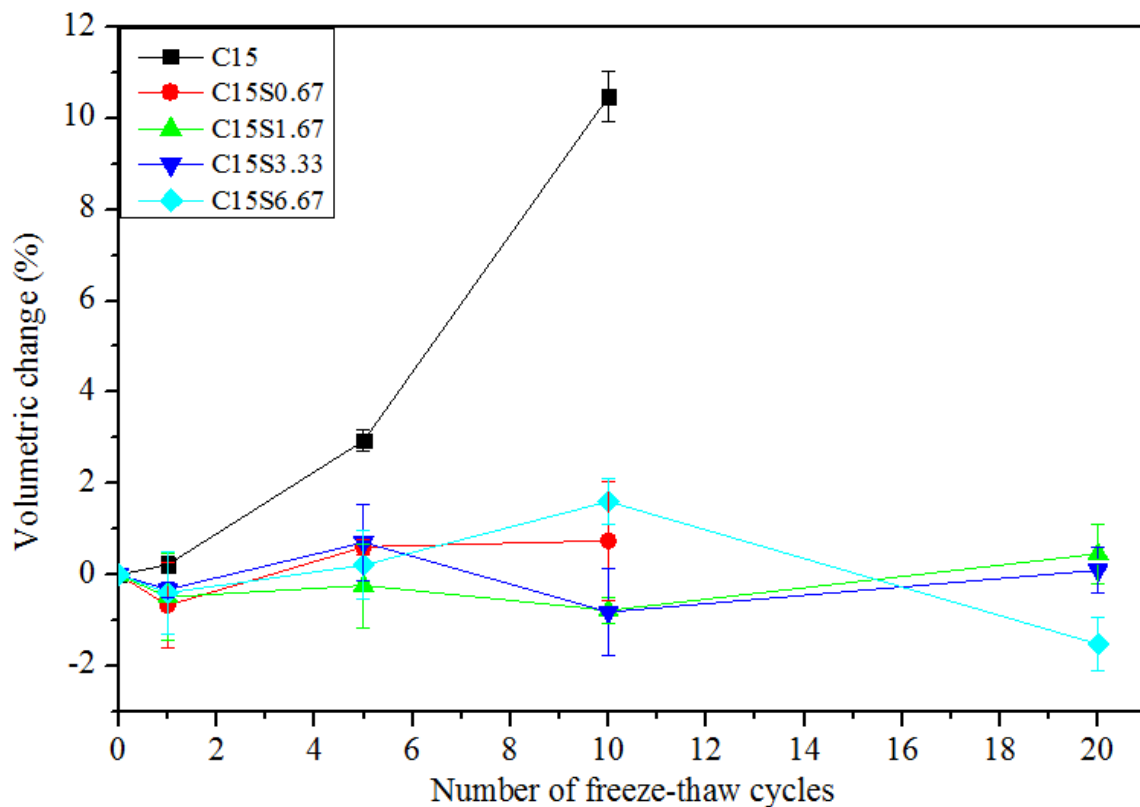


Figure 5.11 Volumetric change of soil-cement samples embedded with different dosages of SikaAer® Solid microcapsules over repeated freeze-thaw cycles.

5.4.1.5 Dry density

Dry density was measured for each soil-cement sample subjected to repeated freeze-thaw cycles, as this metric is an important engineering property for soil-cement systems used in engineering. The change in dry density for all mixes is plotted in **Figure 5.12**. The dry density of C15 was observed to decrease rapidly over increasing numbers of freeze-thaw cycles. The C15 samples' residual dry density was only 89% after 10 freeze-thaw cycles.

As discussed in **Section 5.3.3.2**, the initial dry density of soil-cement is decreased by the addition of SS microcapsules. However, the reduction in dry density that occurs following freeze-thaw cycles greatly decreased for soil-cement systems embedded with SS microcapsules. For C15S0.67, dry density only decreased by 3% after 10 freeze-thaw cycles. For soil-cement mixes embedded with a dosage of 1.67% of SS microcapsules or higher, dry density did not decrease even after 20 cycles. For mix C15S3.33, dry density even increased as the number of freeze-thaw cycles increased: a 4% increase in dry density was observed following 20 freeze-thaw cycles. This increase is likely due to the continuous hydration of cement within the system. These dry density results are consistent with the volume and water content results discussed in previous sections.

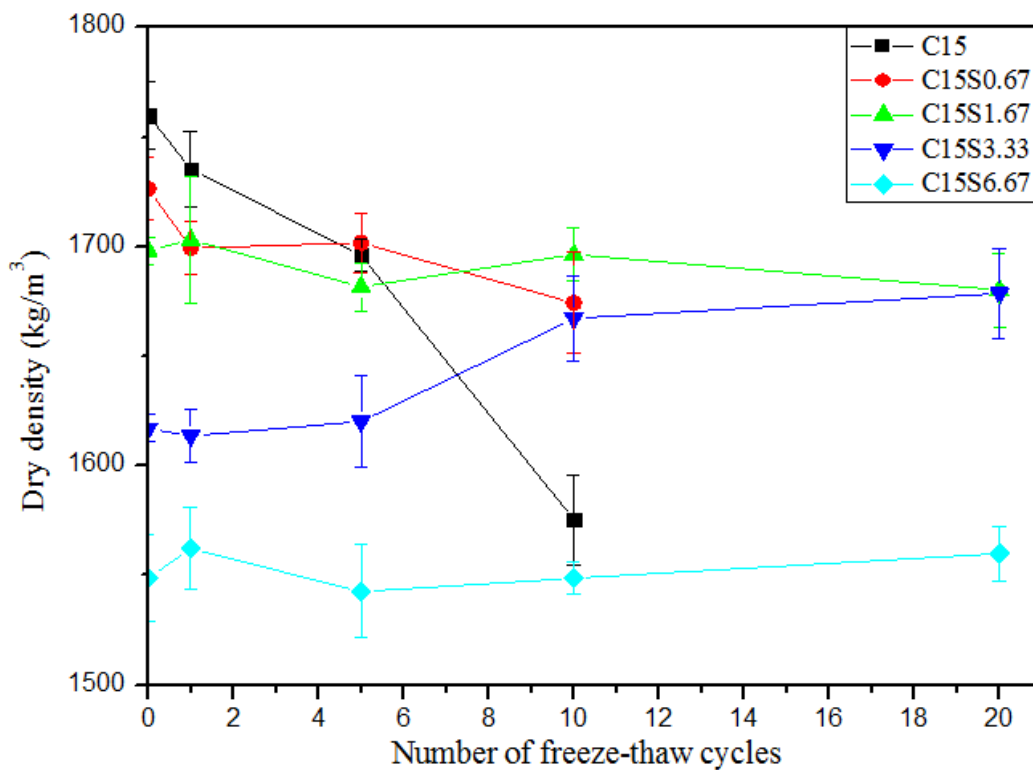


Figure 5.12 Dry density of soil-cement systems embedded with SikaAer[®] Solid subjected to repeated freeze-thaw cycles.

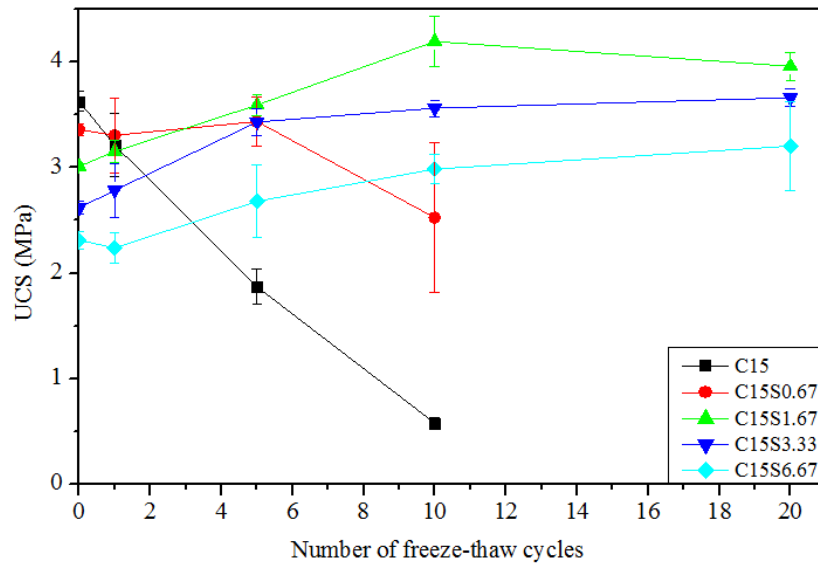
5.4.2 Mechanical properties

5.4.2.1 Unconfined compressive strength and Young's modulus

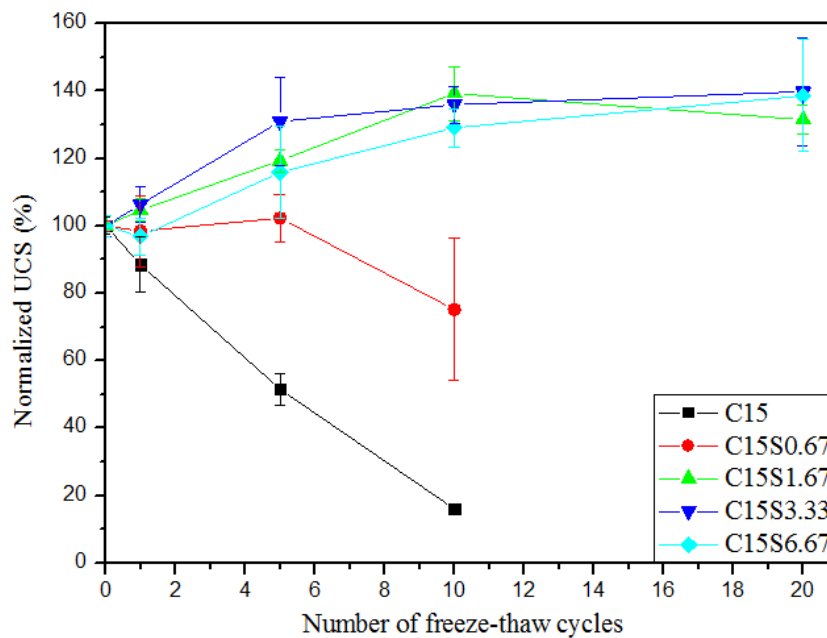
Strength properties are key to determining the overall effectiveness of soil-cement systems. Specimens were initially cured for 7 days before they were subjected to repeated freeze-thaw cycles. Unconfined compressive strength (UCS) testing was performed in triplicate for soil-cement systems exposed to 0, 1, 5, 10, and 20 freeze-thaw cycles. The results are displayed in **Figure 5.13a**. To highlight UCS change in these soil-cement systems, the normalised UCS is plotted over the number of freeze-thaw cycles in **Figure 5.13b**. Demonstrating results consistent with those reported in Jamshidi et al. (2015a), Kamei et al. (2012), and Wang et al. (2017). **Figure 5.13a** shows a general trend of decreasing UCS in control samples (C15) for increasing numbers of freeze-thaw cycles. UCS decreases of approximately 50% and 84% were observed after 5 and 10 freeze-thaw cycles, respectively. However, a remarkable increase in freeze-thaw resistance was observed for soil-cement samples embedded with SS microcapsules, even at dosages as low as 0.67%. The normalised UCS for C15S0.67 was 102% at 5 freeze-thaw cycles and 75% at 10 freeze-thaw cycles, whereas those values for C15 were 55% and 16%, respectively. For 1.67%, 3.33%, and 6.67% microcapsule dosages, remarkably, samples' UCS values increase rather than decreasing over repeated freeze-thaw cycles. The UCS values for C15S3.33 and C15S6.67 even exhibit their highest UCS measurements at 20 freeze-thaw cycles. In any case, the UCS values for C15S1.67, C15S3.33, and C15S6.67 all achieve 130-140% of their 7-day UCS results after 20 freeze-thaw cycles. This strength increase associated with increasing freeze-thaw cycles could be a result of continuous cement hydration, which is consistent with the trends observed for strength development described in **Section 5.3.5**. However, for C15S1.67, UCS began to decrease after 20 freeze-thaw cycles, with a drop from 4.20 MPa to 3.96 MPa observed. This result indicates that the C15S1.67 mix may not be entirely self-immune to freeze-thaw deterioration. As a result, the recommended dosage of SS microcapsules should exceed 1.67% for self-immune soil-cement systems.

Young's modulus, E_{50} values for soil-cement samples with varying SS microcapsule dosages over repeated freeze-thaw cycles are plotted in **Figure 5.14**. Representative stress-strain curves for all mixes are presented in **Figure 5.15**. The stress-strain behaviour of C15 becomes progressively more ductile as the number of freeze-thaw cycles increases. The addition of SS also significantly increases the freeze-thaw durability of soil-cement in terms

of stiffness. The E_{50} trend for all the mixes is very similar to the trend observed for UCS. Yarbaşı et al. (2007) suggested that the more brittle a material is, the more susceptible it is to cracking when frozen. However, for mixes C15S0.67 and C15S1.67, the addition of SS not only increases the stiffness of the soil-cement, but also increases its freeze-thaw resistance. Thus, brittleness appears to have little effect on the freeze-thaw resistance of self-immune soil-cement systems.



(a)



(b)

Figure 5.13 Strength behaviour of soil-cement mixes with various dosages of SikaAer® Solid microcapsules over repeated freeze-thaw cycles in terms of (a) actual UCS values and (b) normalised UCS values.

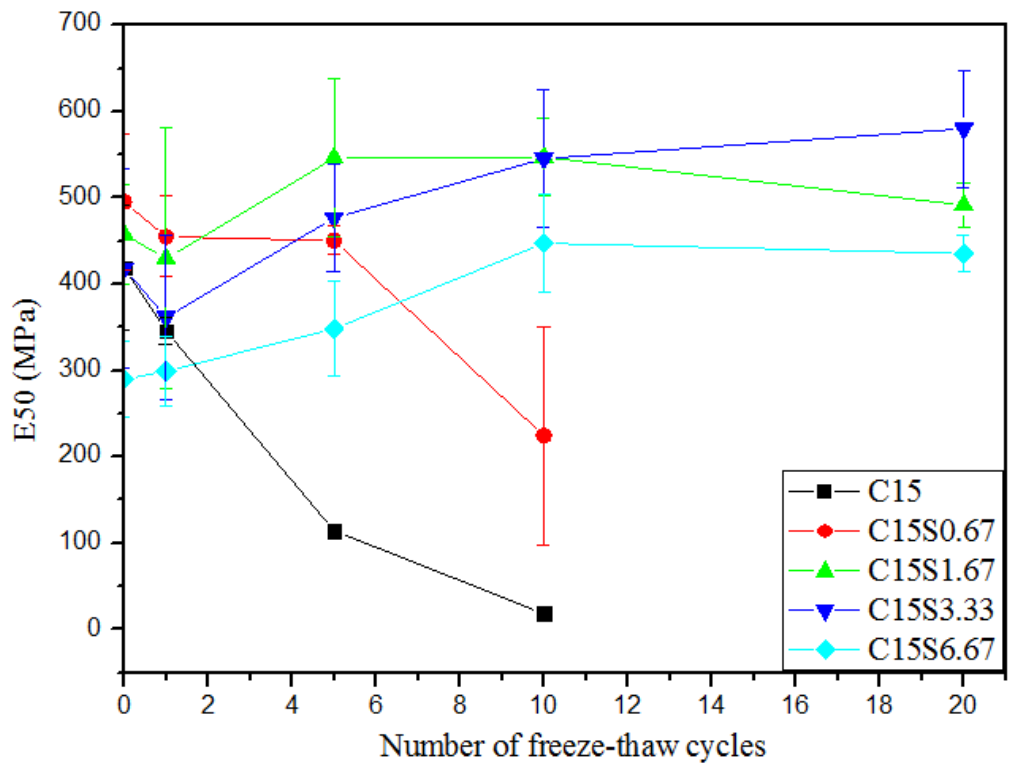


Figure 5.14 E₅₀ values for soil-cement samples over repeated freeze-thaw cycles.

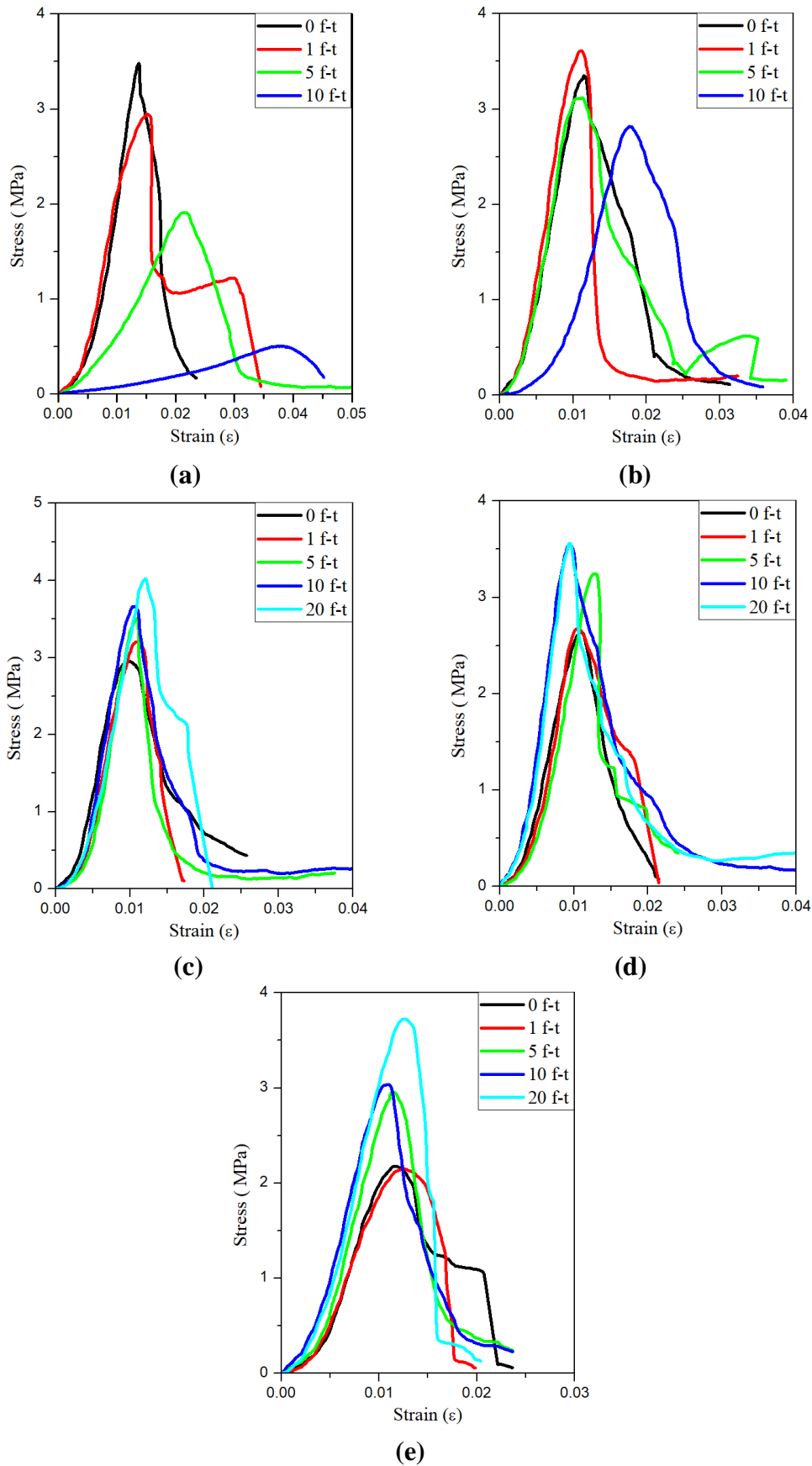


Figure 5.15 Stress-strain behaviour after repeated freeze-thaw cycles for (a) control mix C15, (b) mix C15S0.67, (c) mix C15S1.67, (d) mix C15S3.33, and (e) mix C15S6.67.

5.4.2.2 Tensile strength

The tensile strength of the soil-cement samples was obtained from triplicate disc samples using a splitting tensile test. The mean tensile strength of the samples is given in **Figure 5.16**. Similar to the UCS, the tensile strength of C15 tends to decrease sharply over repeated freeze-thaw cycles. After about 6 cycles, the tensile strength of the C15 disc sample reached nearly zero, indicating a complete loss of tensile strength. Note that the C15 disc samples reached tensile strength failure in fewer freeze-thaw cycles than the cylindrical C15 samples tested for UCS. This is likely due to the smaller height of the disc samples compared to the cylindrical samples (10 mm vs. 100 mm). During freeze-thaw curing, water was sucked from the bottom of the sample. Therefore, thinner samples would be associated with greater water ingress, which would lead to greater overall damage after repeated freeze-thaw cycles.

As shown in **Figure 5.16**, C15S1.67 retained 64% of its original tensile strength after 10 freeze-thaw cycles, while no reduction in tensile strength was observed for C15S3.33. However, these samples' initial tensile strength was slightly lower than that of the controls. These results indicate that the addition of SS microcapsules can significantly improve the freeze-thaw durability of soil-cement system in terms of tensile strength.

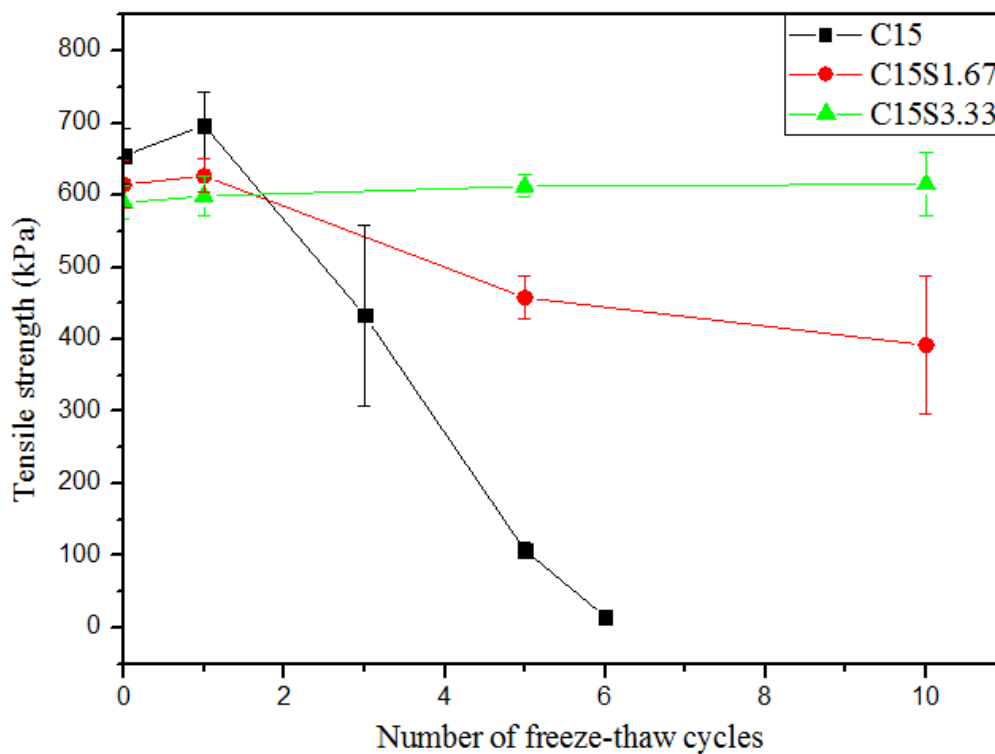


Figure 5.16 Tensile strength of soil-cement samples with different dosages of SikaAer® Solid microcapsules over repeated freeze-thaw cycles.

5.4.3 Permeability

Permeability (k) was measured in duplicate for mixes C15, C15S1.67, and C15S3.33, which were all subjected to 20 freeze-thaw cycles. Permeability measurements were performed in general accordance with method F described in ASTM: D5084-16 (2016) (i.e., using a constant rate of flow method). This method is described in greater detail in **Section 3.5.4**. **Figure 5.17** shows the change in permeability for all mixes after repeated freeze-thaw cycles (i.e. 0, 1, 5, 10, and 20). The figure demonstrates that the permeability of soil-cement systems is very sensitive to freeze-thaw deterioration. The k value of C15 increased by approximately 6 times (or half an order of magnitude) after 1 freeze-thaw cycle. This increase reached 100 times the original value after 5 cycles (approximately 2 orders of magnitude) and finally reached roughly 270 times the original value after 10 cycles (approximately 2.5 orders of magnitude). This increase is likely due to the expansion of voids, crack formation, and subsequent structural degradation caused by the freeze-thaw process. These results also agree with the earlier observations, which showed that the water content, volume, porosity, degree of saturation, and crack area ratio continued to increase for C15 over repeated freeze-thaw cycles. The creation of cracks resulted in a much higher permeability value for the control than in the un-cracked samples, as these cracks were much larger than the pores of the intact specimens. This constant increase in permeability over multiple freeze-thaw cycles is consistent with previous studies of soil-cement systems (Guney et al., 2006, Lake et al., 2016).

Figure 5.17 shows that the addition of SS microcapsules slightly increased the initial permeability of the soil-cement systems. A possible explanation for this might be that the addition of SS increased the porosity of the systems, therefore creating greater space for water to pass through. For a given soil/soil-cement system, permeability is a function of the void ratio. However, the freeze-thaw resistance of soil-cement systems in terms of permeability significantly increased with the addition of SS microcapsules. The permeability increase observed in the control samples amounted to 2.5 orders of magnitudes after 10 freeze-thaw cycles. By contrast, the permeability increased in mixes C15S1.67 and C15S3.33 was negligible. For C15S1.67, permeability increased after 1 and 5 freeze-thaw cycles, but this value decreased afterwards. For the C15S3.33 mix, permeability increased only slightly after the first freeze-thaw cycle and continued to decrease afterwards. After a total of 20 freeze-thaw cycles, the k value of mix C15S3.33 was lower than its original k value. A possible cause for this relates to the progression of the hydration process in soil-cement

systems, which generates more hydration products. The results show that both C15S1.67 and C15S3.33 possessed good self-immunity to freeze-thaw cycles in terms of permeability. They suggest that the water-tightness of self-immune soil-cement systems can be retained even after 20 freeze-thaw cycles.

Another key finding is that, for all the mixes, k values increased after the first freeze-thaw cycle exposure, which is consistent with the literature (Eigenbrod, 1996; Eskişar et al., 2015). This suggests that the first freeze-thaw cycle usually exerts an unavoidable effect on soil-cement samples. One explanation may be that the existing water within some of the saturated pores inevitably expands during the first freezing, causing minor disruption of the soil-cement matrix.

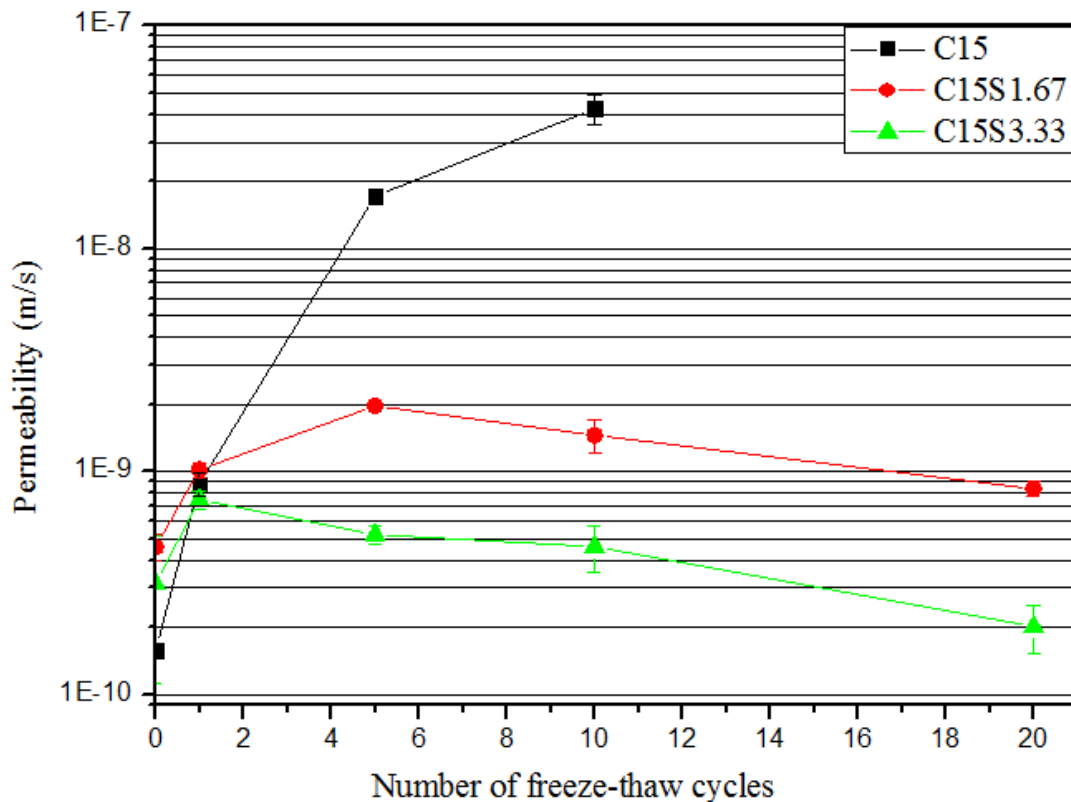


Figure 5.17 Evolution of the permeability values of SikaAer[®] soil-cement samples over repeated freeze-thaw cycles.

Compared with the control mix, the impact of the addition of the SS microcapsules on changes in the behaviour of the soil-cements subjected to freeze-thaw cycles was examined in a number of aspects. Together with the results of physical properties, strength properties and surface analysis, the results of the permeability investigations reveal that the integrity of the structure of the self-immune soil-cement systems can remain undamaged during freeze-thaw

cycles. The addition of SS microcapsules confers a noticeable improvement in terms of the freeze-thaw resistance of soil-cement systems, although their initial engineering properties may slightly deteriorate. In light of these findings, the self-immune mechanisms of soil-cement systems using SS microcapsules are described in the following section.

5.5 Mechanisms of self-immune soil-cement systems using SikaAer[®] Solid microcapsules under freeze-thaw conditions

In this work, the concept of self-immunity is firstly introduced to the soil-cement systems subjected to freeze-thaw deterioration. This section attempts to provide an insight into the mechanisms of self-immunity to freeze-thaw cycles in soil-cement systems embedded with SS microcapsules. The basic principle underlying self-immunity to freeze-thaw exposure is that when water freezes and expands within the soil-cement matrix, the SS microcapsules can respond and act as a buffer against the excess pressure generated, therefore protecting the system from damage. As the pores and fissures inside the matrix thus do not expand during freezing, water ingress is also hindered during the thawing process. In addition, while SS microcapsules increase the void ratio of the system, they do not increase the capillary suction (and thus the potential to absorb water) thanks to their impermeable shells.

5.5.1 Validation of temperature-responsive behaviour

The SS microcapsules are elastic, light, waterproof, and compressible, which allows them to serve as a buffer for the effects of freezing water. Microscopic images were taken of the exact same locations on the soil-cement samples embedded with SS microcapsules in both frozen and thawed states. The typical characteristics and morphology of the SS microcapsules within the soil-cement system in frozen and thawed states are presented in **Figure 5.18**. The SS microcapsule is compressed when the sample is frozen. **Figure 5.18** presents the area measurements of the SS microcapsules in both frozen and thawed states. These show that the SS microcapsules are compressed by roughly 30–40% during freezing in terms of the area measurements.

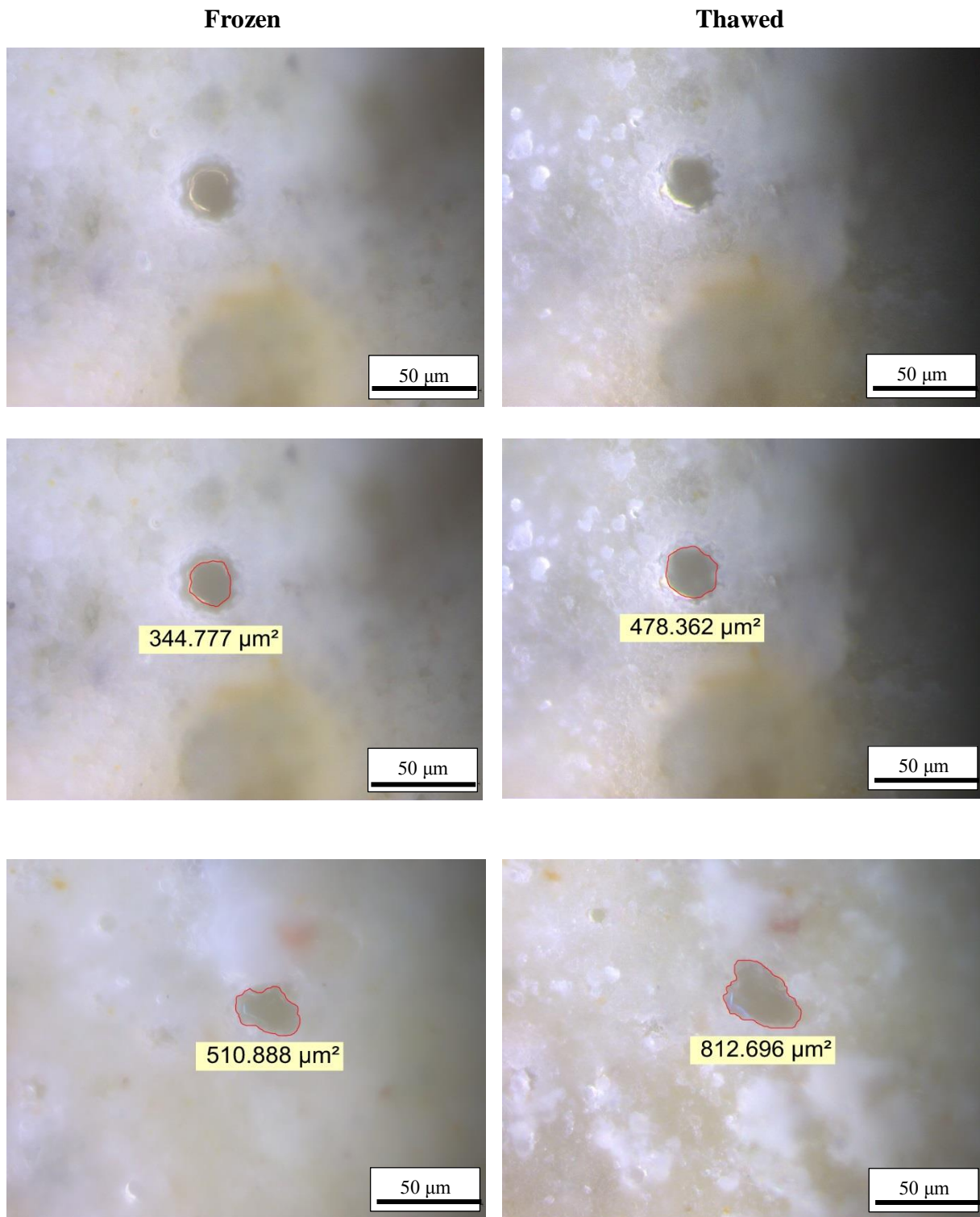


Figure 5.18 Representative microscope images of SikaAer[®] Solid microcapsules in soil-cement in frozen and thawed states with area measurements.

5.5.2 Air content and freeze-thaw resistance

The air content (by volume) of soil-cement samples was calculated. These results, along with the porosity values of soil-cement samples with different dosages of SS microcapsules, are shown in **Figure 5.19**. The porosity and air content of the soil-cement system clearly increase with the addition of SS microcapsules, and this increase is largely linear. This was anticipated, as the SS microcapsules are essentially artificial air bubbles.

The air content values of C15, C15S0.67, C15S1.67, C15S3.33, and C15S6.67 were 6.1%, 7.4%, 9.4%, 11.1%, and 15.5%, respectively. Per the previous sections, the freeze-thaw durability of soil-cement significantly improves with an increasing dosage of SS microcapsules. The previous sections demonstrated that C15S3.33 is the mix with lowest dosage of SS microcapsules that is completely self-immune to freeze-thaw damage. Compared to C15, the air content of C15S3.33 is 5% higher. Thus, to build a soil-cement system that is self-immune against freeze-thaw effects, a 5% greater-than normal level of air pores is recommended.

This outcome contradicts certain past studies (Khoury and Zaman, 2007; Wang et al., 2017) that have suggested that increased pore space makes soil-cement systems more vulnerable to freeze-thaw deterioration. The authors argued that additional pore spaces would facilitate the ingress of water, thus increasing ice formation within the matrix and, consequently, inducing more cracks and fissures. However, entrained air is not identical to entrapped air. The SS microcapsules used in this study are impermeable, have a regular (and small) size and are evenly dispersed. Therefore, they create proper air entraining for soil cement-systems. The reason for this will be further explained in the following sections.

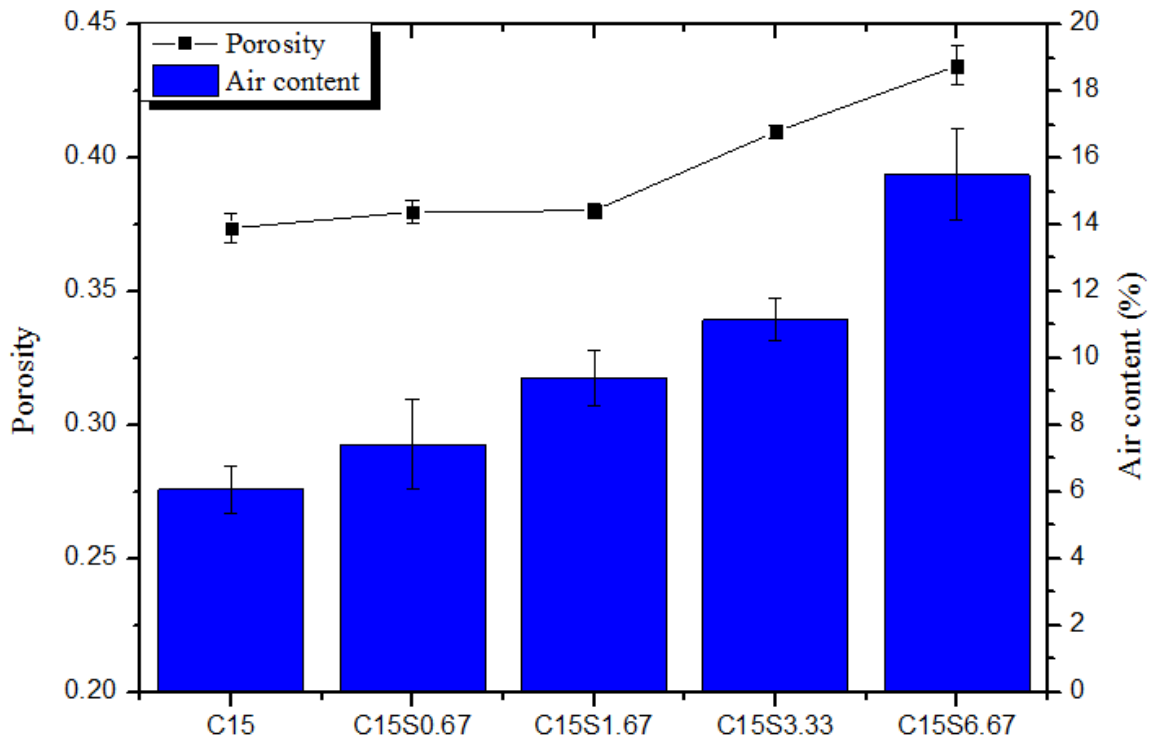


Figure 5.19 Air content and porosity of soil-cement systems with different dosages of SikaAer® Solid microcapsules.

5.5.3 Critical degree of saturation

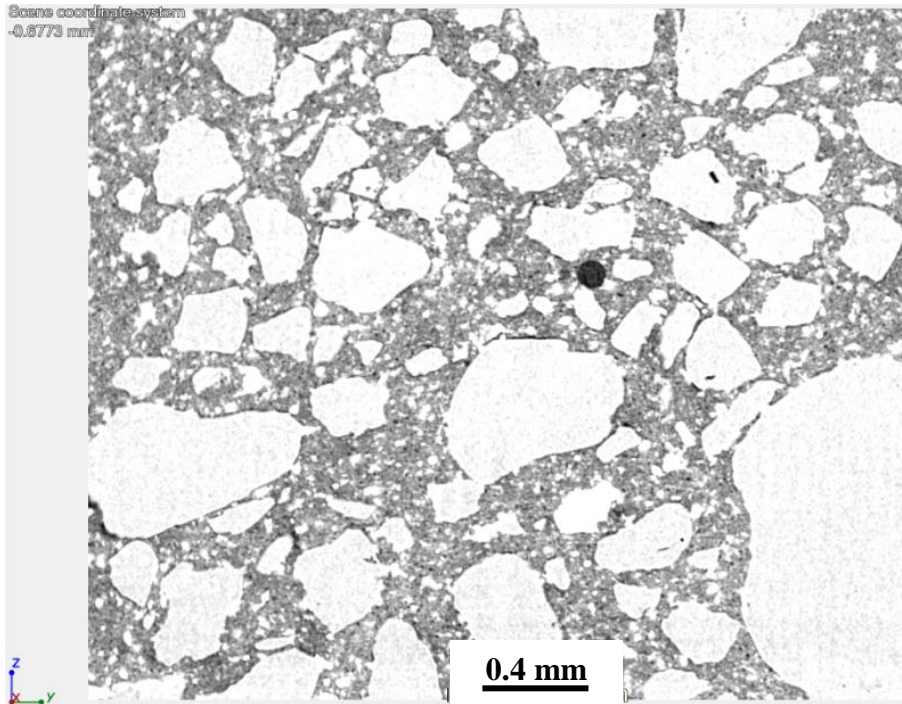
The change in the degree of saturation (S_r) for all mixes under freeze-thaw conditions was discussed in **Section 5.4.1.2**. S_r is another important parameter of self-immunity for soil-cement systems. Another explanation for why increased air content and porosity do not impair the freeze-thaw resistance of soil-cement systems is that increased air content does not necessarily correspond to water ingress. For example, the air content of mix C15S3.33 is 5% higher than that of C15. However, the S_r value of C15S3.33 decreases from 73% to 70% after 20 freeze-thaw cycles, while the S_r value of C15 increases from 84% to 100% after 10 cycles.

According to the results presented in **Figure 5.9b**, the critical degree of saturation for the soil-cement system in this study is 73%. Soil-cement systems are self-immune to freeze-thaw damage if their initial degree of saturation is lower than the critical degree of saturation. For samples (C15S3.33) with an initial degree of saturation less than 73%, S_r values did not increase with increasing numbers of freeze-thaw cycles. Thus, the addition of an adequate amount of SS can reduce the degree of saturation for soil-cement systems. With a S_r value lower than the critical value, the SS microcapsule can provide enough buffer for the water

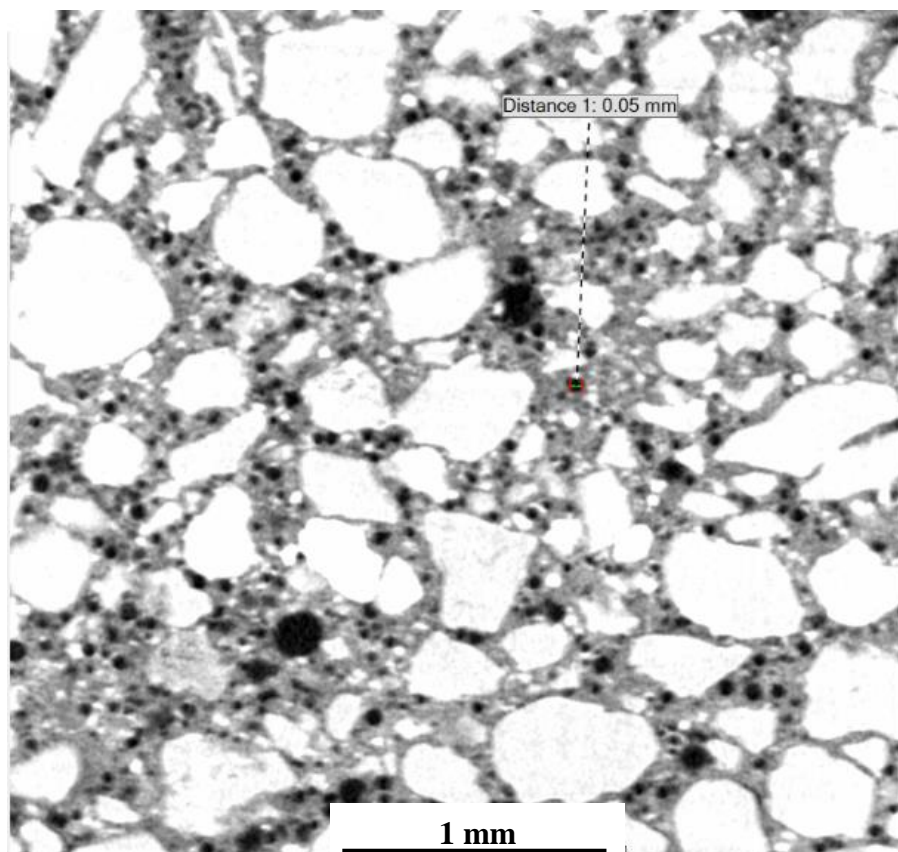
inside the soil-cement system to expand during freezing. However, it should be noted that this value of critical degree of saturation is only applicable to the SS microcapsule-embedded soil-cement system studied.

5.5.4 High resolution X-ray computed microtomography (μ CT)

The self-immune capabilities of soil-cement systems under freeze-thaw conditions depend on several parameters, such as the sizes, the quantity, and distribution of SS microcapsules. The distribution of SS microcapsules is hard to analyse via naked-eye or microscope inspection, the microcapsules have a size of 5-80 μ m. Thus, to investigate the distribution of SS microcapsules within the soil-cement matrix, high resolution X-ray computed microtomography (μ CT) was conducted. **Figure 5.20a** presents a representative cross-section of a C15 specimen. The C15 specimen is close-grained, with only a few air pores and small fissures identifiable in the matrix. However, in the cross section of the C15S3.33 specimen, shown in **Figure 5.20b**, a large number of SS microcapsules can be clearly identified within the matrix. Moreover, the figure shows that the SS microcapsules are uniformly distributed in the soil-cement matrix. As the size of the pores is thus well-regulated, and as the distance between microcapsules is relatively small, the strength reduction caused by the addition of the SS microcapsules is reasonable small.



(a)



(b)

Figure 5.20 Representative μ CT cross-section images of (a) C15 specimens and (b) C15S3.33 specimens with SS microcapsules.

5.5.5 Summary of principles underlying the development of soil-cement systems self-immune to freeze-thaw cycles using SikaAer® Solid microcapsules

Based on the results presented in the previous sections, air entraining using SS microcapsules should be considered an effective technique to increase the freeze-thaw durability of soil-cement systems. However, it should be noted that air entrainment is different from air entrapment. Increasing air content alone cannot directly lead to a higher freeze-thaw resistance. An image of the reconstructed 3-D structure of a C15S3.33 sample using X-ray μ CT is presented in **Figure 5.21**. The figure illustrates three key characteristics of soil-cement systems that use SS microcapsules to become self-immune to freeze-thaw effects.

First, air-entraining pores should have a reasonable size that is neither too big nor too small. Penttala (2009) suggested that the optimal dimensions of air-entraining pores in concrete ranges from 0.02–0.05 mm. SS microcapsules generally have diameters of 5–80 μ m, which makes them similar to the optimal size suggested. If the size of the microcapsules were too big, it would be more difficult for the microcapsule to disperse during mixing. If the microcapsules are not uniformly distributed, they cannot provide as effective a buffer for all parts of the soil-cement system matrix during freeze-thaw action. In addition, big microcapsules may also lead to a greater reduction in important engineering properties (such as structural strength).

Secondly, self-immune soil-cement systems should have enough air volume. In other words, they should incorporate an adequate amount of SS microcapsules to compensate for the volume change water experiences within the system during freezing. In concrete, the air content value depends on the relative volume of the binder paste, as aggregates are considered to be freeze-thaw durable and binder paste is usually considered the vulnerable component (Penttala, 2009). However, in soil-cement systems, there are usually no coarse aggregates used, and the soil is mixed with the cement binder. Therefore, the air content should be taken into consideration relative to the total volume of the soil-cement mixture. Per **Section 5.5.2**, the extra air content of a self-immune soil-cement system is recommended to exceed 5%, and the recommended dosage of SS microcapsule is 3.33%.

Finally, the SS microcapsules should be uniformly distributed in the soil-cement system. **Figure 5.20-5.21** show that SS microcapsules are compatible with the soil-cement composition and that the dispersion of the SS microcapsules within the matrix is sufficiently homogenous. In addition, the distribution of the SS microcapsules can be described in terms

of the critical distance from one SS microcapsule to the nearest neighbour. This distance should be generally small. This is necessary for the pressure generated by freezing water to be relieved evenly throughout the soil-cement system.

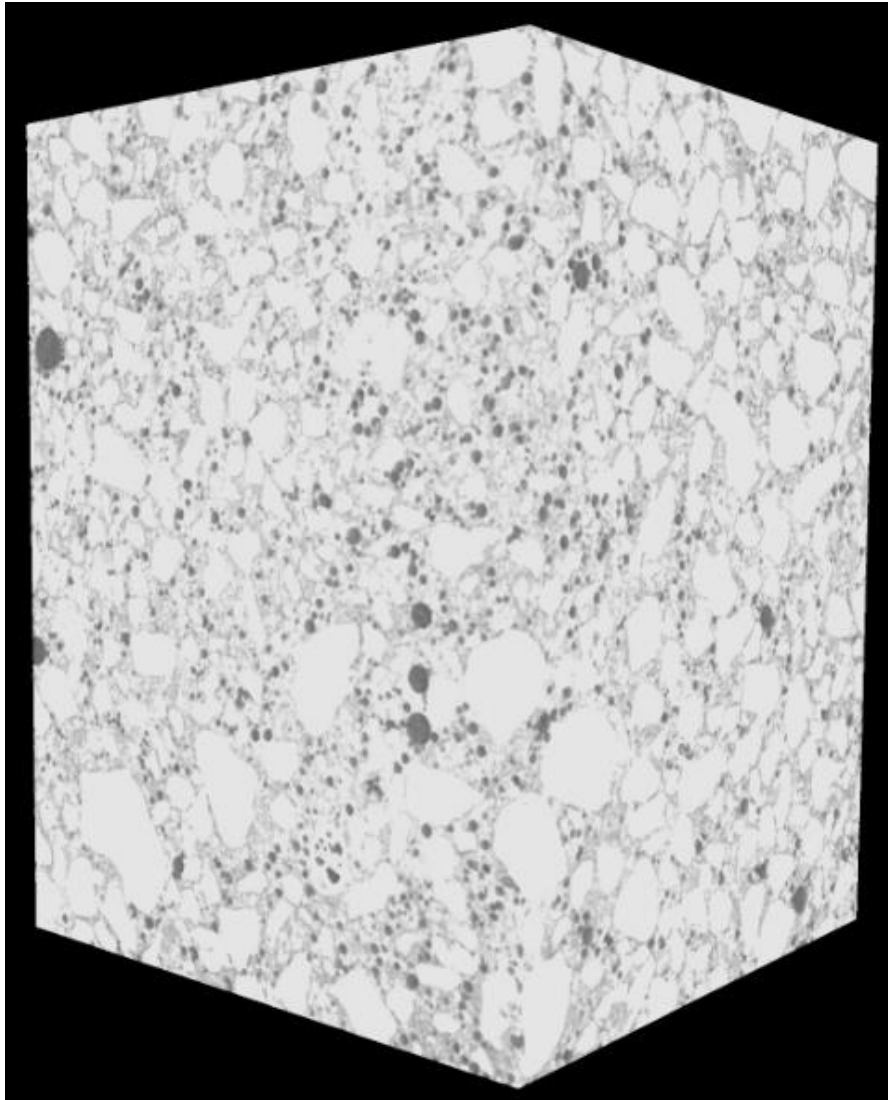


Figure 5.21 3D reconstruction of a typical 7-day C15S3.33 sample using X-ray μ CT.

5.5.6 Overview of the self-immunity mechanism

Based on the preceding investigations of the physical properties of soil-cement after multiple freeze-thaw cycles, the microscopic analyses, and the high-resolution X-ray computed microtomography (μ CT), the self-immune mechanism of soil-cement embedded with SS microcapsule and its behaviour during freeze-thaw action is hypothesised and shown schematically in **Figure 5.22**. The permeability results in **Section 5.4.3** revealed that the addition of SS microcapsules slightly increased the initial permeability of the soil-cement systems. This indicates that the presence of SS microcapsules themselves is less likely to

prevent the movement of liquid water and thus water uptake. However, during the freezing process, ice forms progressively in the porous network within the soil-cement matrix, started with the larger water-filled voids, which are the voids near the SS microcapsules embedded in the matrix. The hydraulic pressure is reduced in these air spaces, so the unfrozen water stored in capillary pores and fissures is sucked into these spaces around the SS microcapsules. When the volume of the water inside the air voids increases by 9% during freezing, the SS microcapsules are compressed, and the excess pressure is relieved. Optical microscopic analysis (**Figure 5.18**) confirmed that SS microcapsules were compressed during the freezing of soil-cement samples. As a result, capillary pores and fissures are not enlarged by ice formation during the freezing process. Here, SS microcapsules and the air-space around them absorb the volume expansion and the excess pressure caused by ice formation. Moreover, to confer comprehensive self-immunity, the combined volume of the SS microcapsules and the air void must be large enough to absorb the extra water volume. They must also be sufficiently distributed throughout the soil-cement matrix to connect to most of the pores and fissures filled with water. As long as the quantity of SS microcapsules is great enough and the capsules are evenly distributed throughout the soil-cement matrix, the soil-cement should be completely self-immune to freeze-thaw deterioration.

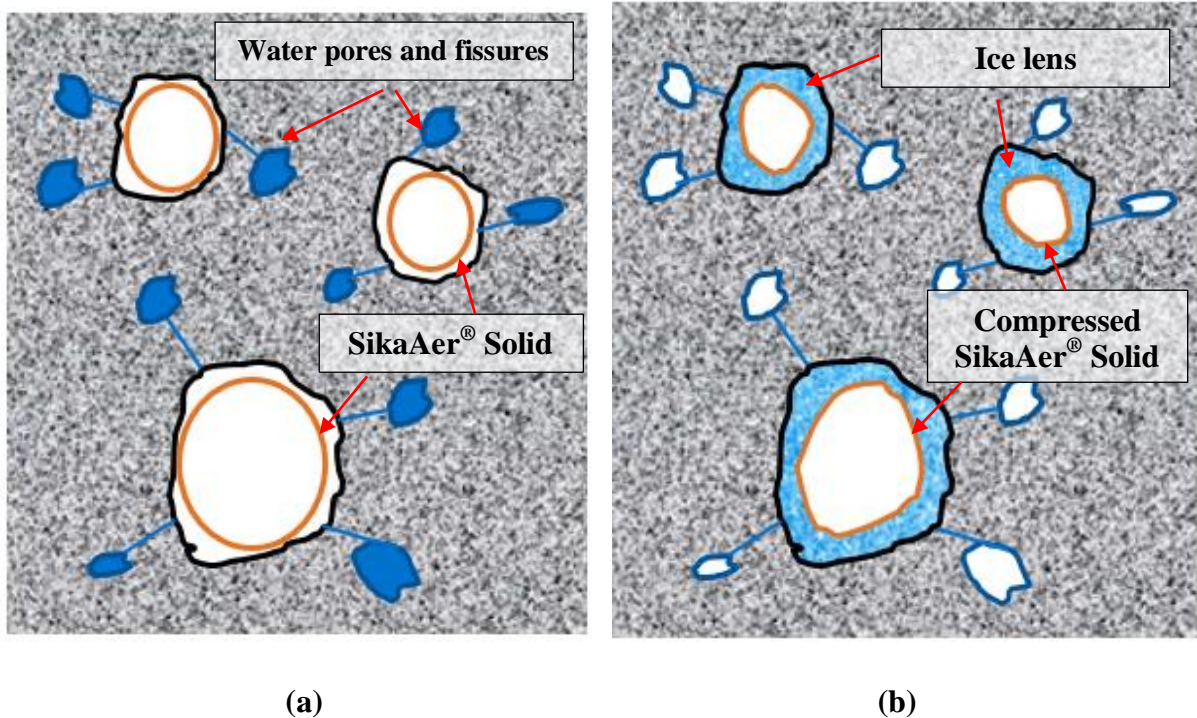


Figure 5.22 Representation of the theorised self-immune mechanism conferred by the use of SikaAer® Solid microcapsules in a soil-cement matrix (a) before freezing and (b) during freezing.

5.6 Concluding remarks

This chapter detailed the development of self-immune soil-cement systems subjected to freeze-thaw cycles by using SS microcapsules and documented those systems' performance. Soil-cement systems embedded different dosages of SS microcapsules were examined. Soil-cement systems are susceptible to freeze-thaw damage, though their initial strength and freeze-thaw durability can be improved by increasing their cement content. However, even with 20% cement content, the UCS of soil-cement systems decreased by 50% after 12 freeze-thaw cycles. In many cases, it can be difficult or almost impossible for soil-cement systems to resist freeze-thaw deterioration over time due to the nature of the freeze-thaw process. When water freezes within soil-cement systems, its volume expands about 9% in the capillary pores and fissures and exert pressure on the soil-cement matrix. This enlarges the pores and fissures. When thawed, the temperature gradient between the frozen sample and the warmer surrounding soil sucks water into the soil-cement system through the pores and cracks widened during freezing. As freeze-thaw cycles repeat, more and more water is absorbed into the soil-cement matrix, and pores and cracks continue to enlarge. Consequently, the volume and water content of the soil-cement system both increase. Simultaneously, the bonding and cohesion between soil-cement particles weakens. Therefore, the strength properties of the soil-cement system deteriorate.

However, in this chapter, adding SS microcapsules to soil-cement samples was proven to be a promising technique for developing soil-cement systems self-immune to freeze-thaw deterioration. The soil-cement's dry density and strength values initially decreased slightly with the addition of SS microcapsules. However, the addition of SS microcapsules significantly increased the freeze-thaw durability of the soil-cement system in terms of UCS, volumetric change, porosity, hydraulic conductivity, and surface cracking ratio after multiple freeze-thaw cycles. The distribution and volume of the SS microcapsules were the two most important factors influencing the self-immune capabilities of the soil-cement systems subjected to freeze-thaw cycles. The distribution of the SS microcapsules is reflected by their critical distance, while the quantity of the SS microcapsules can be quantified in terms of the soil-cement's air content and its critical degree of saturation. The addition of 3.33% SS microcapsules is the lowest dosage in this study that makes a soil-cement system completely self-immune to freeze-thaw damage after 20 cycles. The addition of 3.33% SS microcapsules has little influence on the fresh properties of the soil-cement mix. However, greater additions of SS microcapsules will reduce the dry density, 7-day UCS, and stiffness of the soil-cement,

as well as increasing construction costs. As a result, this study suggests that the optimum dosage of SS microcapsules for the kinds of soil-cement systems this study examines is 3.33% of the cement's mass.

Chapter 6 Development and Performance of Self-immune Soil-cement Systems Subjected to Freeze-thaw Cycles with a Superabsorbent Polymer (SAP)

6.1 Overview

In **Chapter 5**, SikaAer[®] Solid microcapsules were used to develop a self-immune soil-cement system subjected to freeze-thaw cycles, which has presented excellent resistance to freeze-thaw deterioration. However, it was concluded that the addition of SikaAer[®] Solid microcapsules would inevitably reduce the strength properties of soil-cement, which could be unfavourable to soil-cement systems in some engineering practices. It is noteworthy that the biggest disadvantage of the application of SikaAer[®] Solid microcapsules in soil-cement system is the reduction in 7-day UCS, where 27% reduction was observed in C15S3.33 mix (**Section 5.3.4**) compared to that of control mix. Given these findings, subsequent work in this chapter investigated the development of an alternative technique to establish a self-immune soil-cement system subjected to freeze-thaw cycles without deteriorating the strength properties.

To serve this purpose, a superabsorbent polymer (SAP) is used. As reviewed in **Section 2.4.4**, the SAPs have the ability to absorb water during mixing and then gradually release the absorbed water during the soil-cement systems' hardening and hydration processes. The later process creates small cavities inside the soil-cement matrix. It is hypothesised that these cavities can serve as expansion vessels for water to enter and expand during freezing and therefore develop a self-immune system against the freeze-thaw deterioration. The created air space and SAP, is able to enwrap the water and then digest its expansive effects during freezing. The general idea of this self-immune hypothesis is revealed in **Figure 6.1**, where the cavities created by SAPs serve as protective pores in the soil-cement matrix during freeze-thaw actions.

This chapter firstly presents the properties of the BASP SAP A used in the research presented here, and in particular its absorption and desorption characteristics. After that, in the second part, the influence of the SAP A on the initial properties of soil-cement systems, such as the flowability, calorimetry, water content, and strength properties is investigated. In the third part, the freeze-thaw resistance of soil-cement system embedded with different dosages of the SAP is examined. Subsequently, the self-immune mechanism and hypothesis of the SAP-embedded soil-cement system are revealed and validated in the fourth part. Finally, the self-

immune system developed in this chapter is compared with those using SikaAer[®] Solid microcapsules that developed in **Chapter 5**.

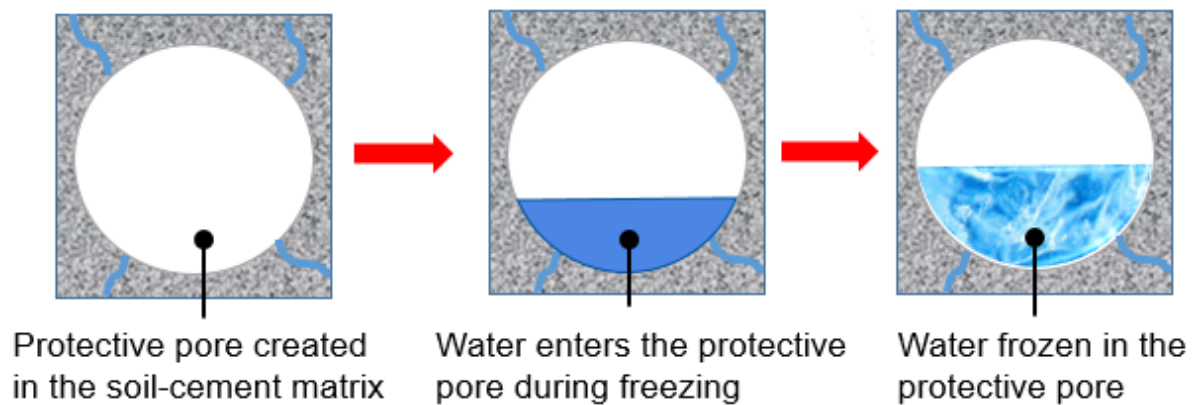


Figure 6.1 Hypothesis of a self-immune soil-cement system during freeze-thaw action.

6.2 Materials and mix proportions

Details of the preparation of the soil-cement samples were given in **Section 3.2** and the list of investigated mix compositions is presented in **Table 6.1**. All the samples prepared in this chapter have a constant cement content of 15% and most of them have a w/c of 1.67. Only mixes C15W31 and C15W31SAP2 were prepared with w/c of 2.07 as additional water was added to pre-soak the SAP. Most of the soil-cement was mixed with varying quantities of dry SAPs, namely 0.25%, 0.5%, 1%, and 2% to the mass of cement, which were labelled accordingly (**Table 6.1**). A critical and comprehensive review of SAPs was given in **Section 2.4** on their properties and applications in cementitious materials. Characteristics of the SAP used in this study including size, density, and morphology under microscope and SEM were presented in **Section 3.1.2.4**. The experimental programmes for investigating the self-immune performance of soil-cement specimens under freeze-thaw conditions were given previously in **Table 3.5**.

Table 6.1 Mix composition of soil-cement samples containing SAPs.

Mix ID	Mix ingredients Ratios/mass (%)			Admixture	Mass fraction in cement, m_f (%)
	Soil	Water	Cement		
C15	100	25	15	-	-
C15SAP0.25				BASF SAP A	0.25
C15SAP0.5				BASF SAP A	0.5
C15SAP1				BASF SAP A	1
C15SAP2				BASF SAP A	2
C15W31	31	-	-	-	-
C15W31SAP2				BASF SAP A	2

6.3 Sorptivity of the BASF SAP A

The properties of the BASF SAP A were first investigated before applying it in the soil-cement systems. The SAP presents an irregular particle shape as shown in **Figure 6.2a**. When encountering water, the SAP absorbs it and swells to form a soft and insoluble gel, as shown in **Figure 6.2b**. It should be noted that this process is reversible and the swelled SAP shrinks when the water stored in it evaporates.

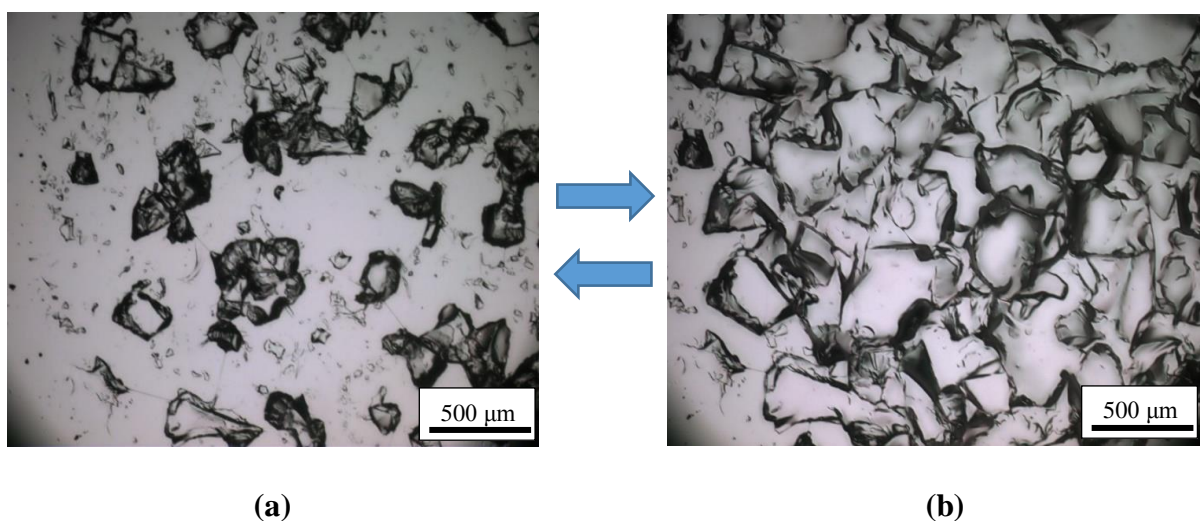


Figure 6.2 Microscopic images showing the (a) dried SAPs and (b) soaked SAPs in the reversible process of the SAP absorption and desorption.

6.3.1 Absorption kinetics

Absorption kinetics is one of the predominant properties of SAPs. As reviewed in **Section 2.5.2**, the SAP absorption is related to many factors among which the SAP, temperature, pH, and ionic concentration of aqueous solution, etc. The Teabag method described in **Section 3.1.4** was used to measure the absorption capacity of the SAP particles. The absorption kinetics of the SAP particles exposed to different aqueous solutions including deionised water, tap water, NaOH solution (0.1 mol/L), NaCl solution (1 mol/L), and a filtrated cement pore solution (**Section 3.1.5**) are presented in **Figure 6.3**. The SAP has different absorption kinetics in different solutions. In all the solutions tested, the absorption of the SAP increased rapidly in the first 10 minutes and then stabilised after approximately 20 minutes. SAP A showed a large absorption of 305g moisture/g SAP in distilled water while this value was much smaller in other aqueous solutions. The absorption value reduced to roughly 50g/g in tap water and 0.1 mol/L NaOH solution while the absorption was only about 20g/g in the 1 mol/L NaCl solution and the simulated cement pore solution. These results are consistent with those reported in Craeye et al. (2018) and Farzalian et al. (2016), where 10–30g/g of SAP absorption is reported in cement pore solution. It has been suggested that the absorption capacity of SAPs is dependent on the pH of the fluid (Craeye et al., 2018). However, **Figure 6.4a** shows the SAP absorption values against pH, where different solutions with different pH values were used: tap water (pH = 7.75), deionised water (pH = 8.0), NaCl solution (1 mol/L, pH = 8.08) and the NaOH solution (0.1 mol/L, pH = 13.1). It is evident from the figure that the absorption capacity of the SAP does not correlate with the pH values. The relationship between the ionic concentration of different solutions and the SAP absorption capacity is plotted in **Figure 6.4b**. It appears that the SAP absorption depends on the ionic concentration of the aqueous solution. This result is in accordance with the literature presented in **Section 2.4.2.3**, which can be explained by the chemical reaction equation suggested in **Figure 2.28**. When the ionic bond in the SAP reacts with water, the ions are released in the water solution. Thus, as a reversible reaction, the ion within the solution will hinder the reaction and hence reduces the SAPs' absorption of water. When cement encountered water, the mix will reach a high pH (~12.5–13) and ionic concentrations (~150–700 mmol/L). The ions released by the cement include Ca^{2+} , K^+ , Na^+ , OH^- , and SO_4^{2-} (Gartner et al., 1985). As the SAPs were added directly into the soil-cement mixture, its absorption capacity in the mix should be approximately 20g/g.

In order to assess the volume of air space that can be created by the SAPs in the soil-cement matrix, the swelling capacity was investigated. This was obtained by the volume increase of the SAP from the dry state to the saturated state. As shown in **Figure 6.5**, the volume expansion ratio calculated for the SAP saturated in deionised water, tap water, and filtered cement pore solution are 264, 44, and 20, respectively.

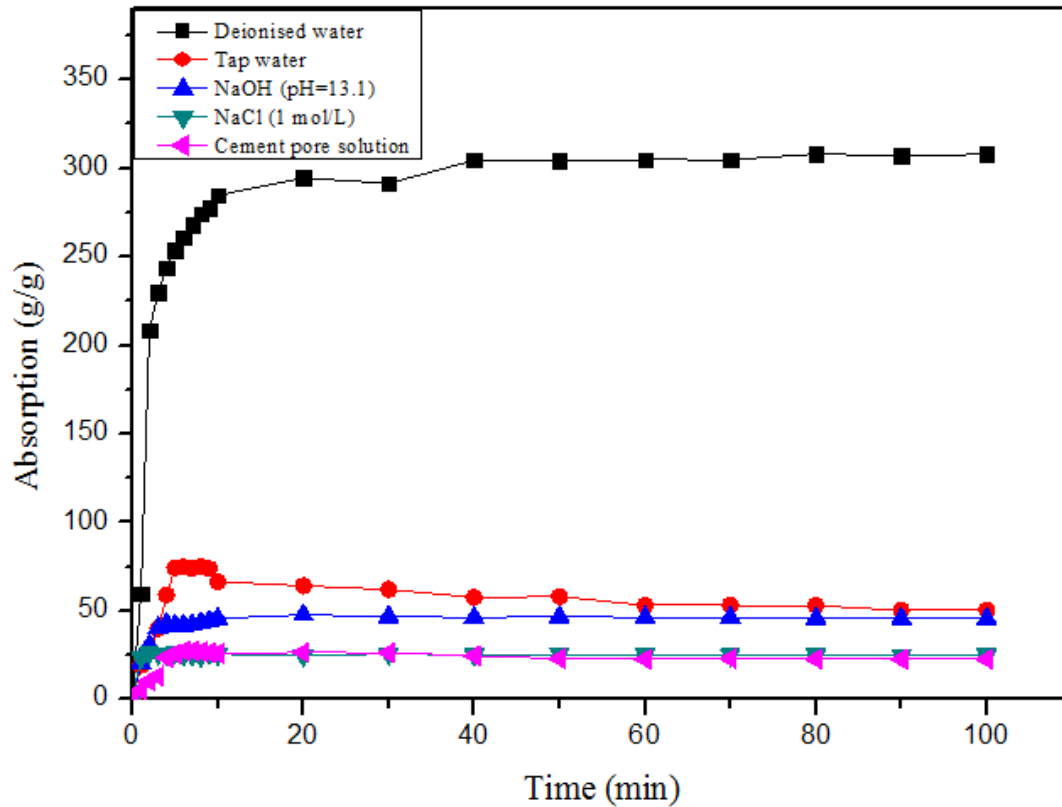
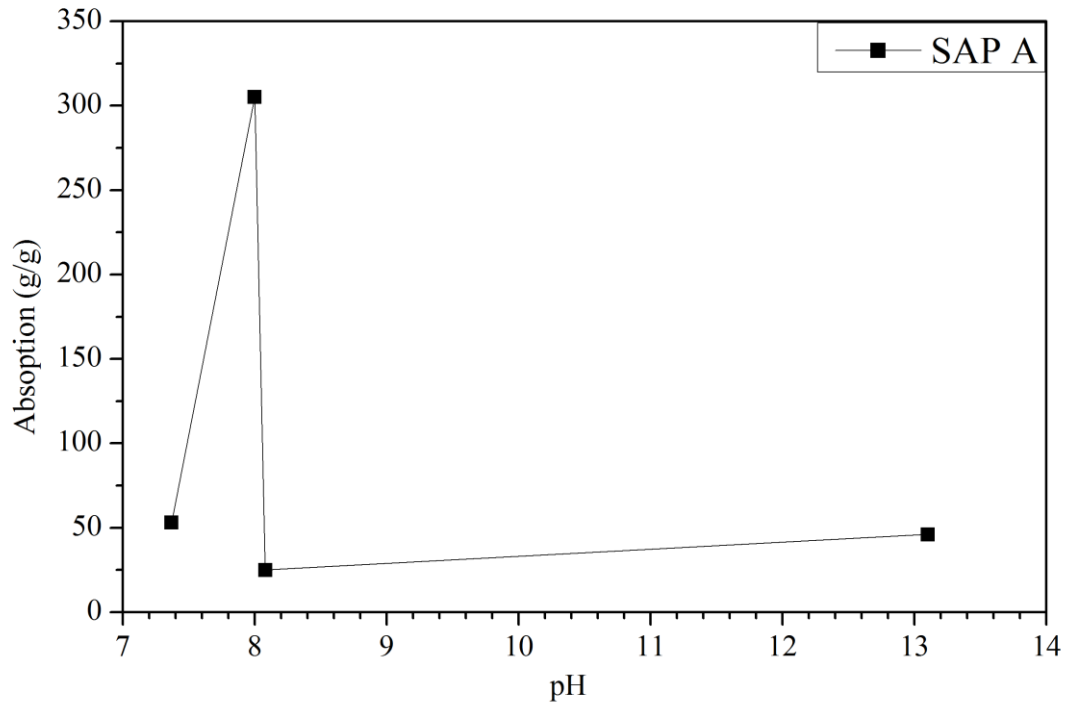
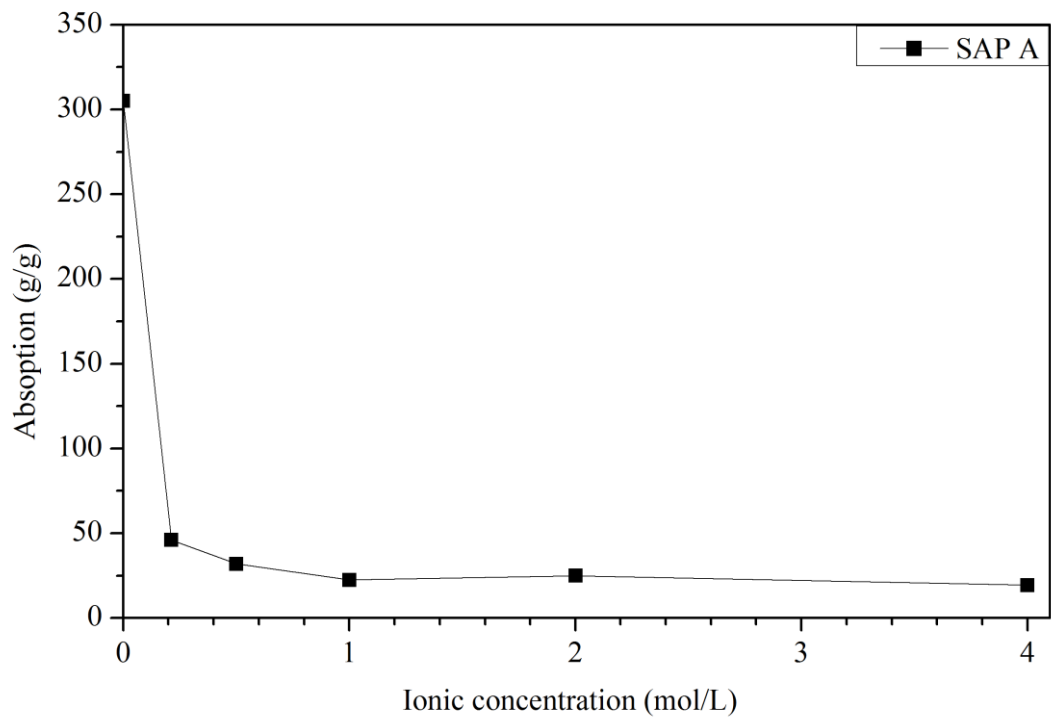


Figure 6.3 Absorption kinetics of SAP A in different types of solutions.



(a)



(b)

Figure 6.4 Absorption capacity of SAP A in different (a) pH values and (b) ionic concentration.

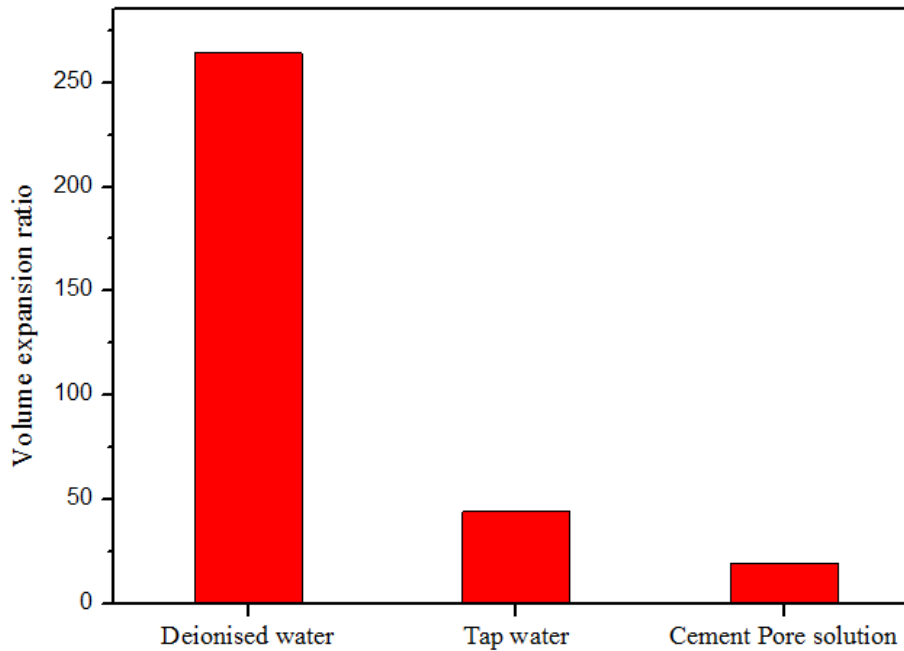


Figure 6.5 Changes in volume of SAP A in deionised water, tap water, and cement pore solution.

6.3.2 Desorption and resorption kinetics

As discussed in **Section 2.4.2.3**, the SAP absorption is reversible. The desorption and resorption behaviour of SAPs was also measured using the Teabag method and the results are presented in **Figure 6.6**. When the SAP were saturated with deionised water and subsequently cured in a 50% ($\pm 10\%$) relative humidity (RH) environment at 20°C during the desorption process, the absorption value reduced to almost 0 after ~57 hours. The rate of reduction was found to decrease with time. This is because the surface water in the SAP is easier to release while the water closer to the core is held by the strong hydrogen bonds formed between the side chains of the polymer (Jensen and Hansen, 2002). However, when the saturated SAP was cured in a 95% ($\pm 2\%$) RH environment at 20°C, only 11% reduction in the absorption value was observed. These results indicate that SAP A can retain more water in the wet environment than in the dry environment.

As shown in **Figure 6.6**, if the SAP dehydrated in 50% ($\pm 10\%$) RH at 20°C was submerged again in deionised water for 100 minutes to reach equilibrium, it was found that the SAP was able to absorb almost the same amount of water as its first saturation level. Two desorption and resorption cycles were conducted and the SAP showed a good resorption capability.

These results suggested that during cement hydration, the water absorbed by the SAP can be gradually donated to the matrix in contact with the SAP during the hydration process.

For a SAP particle with a given diameter and volume expansion capacity, the volume difference between its dry and saturated state can be calculated. For instance, for a SAP particle with a diameter of $100\mu\text{m}$, if it is fully saturated in the cement pore solution, its diameter is expanded to $\sim 270\mu\text{m}$. When the SAP particle releases all the stored water and shrinks to its original diameter, small cavities with equivalent diameter of $\sim 265\mu\text{m}$ will be created in the soil-cement matrix.

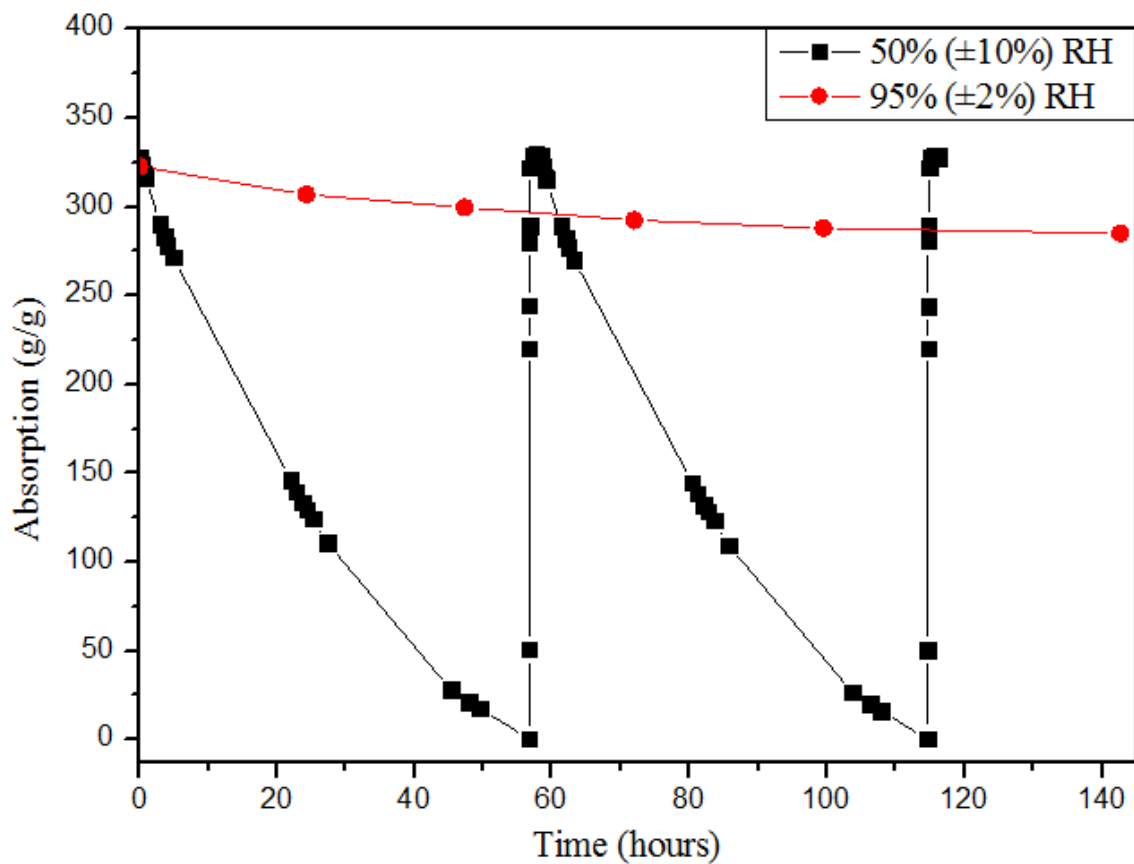


Figure 6.6 Desorption and resorption kinetics of the BASF SAP A in 50% ($\pm 10\%$) and 95% ($\pm 2\%$) RH environment.

6.4 Influence of the BASF SAP A on the fresh, physical, and strength properties of the soil-cement systems

6.4.1 Fresh properties of the SAP-containing soil-cement mixes

6.4.1.1 Calorimetry

The effect of the addition of the BASF SAP A on the hydration processes of Portland cement within the soil-cement mixes was investigated. This property would assess if the added SAP would absorb water and initially alter the water/cement ratio of the soil-cement mix. The thermal power produced per gram of cement for the first 48 hours for mixes containing different SAP content in comparison to the control mix (C15) is presented in **Figure 6.7**. In addition, the calculated values of the setting time and peak power values for all mixes are summarised in **Table 6.2**.

Generally, it can be seen from **Figure 6.7** and **Table 6.2** that the addition of the SAP up to 2% significantly prolonged the setting time and significantly decreased the peak power values of soil-cement compared to control mix. This is understandable as the added SAP absorbed the water from the soil-cement mix during the early stage of mixing therefore changes in the hydration process are inevitable for all SAP mixes. With as little as 0.5% addition of the SAP, the mix C15SAP0.5 exhibited 20% longer setting time (5.36 hours) compared to that of the control mix (4.46 hours). The setting time of mixes C15SAP1 and C15SAP2 was 5.64 hours and 6.48 hours, respectively, which is 26% and 45% longer than the control mix. It is interesting to note that the setting time was increased by the addition of the SAP, given that lower w/c ratio usually leads to reduction in the setting time. A possible explanation for this is that the water absorbed by the SAP during mixing would be gradually released for cement hydration rather than kept stored in the SAP. Consequently, the real w/c ratio of soil-cement was not altered by the addition of the SAP. However, the cement hydration was slowed down as the water stored in the SAP was gradually released. Thus, the setting time of soil-cement mixes was increased by the addition of SAPs.

In addition, the peak power values for all mixes were significantly decreased by the addition of the SAP. Following the increased addition of the SAP, the peak power values of the soil-cement system continued to decrease. The peak power measured for mixes C15SAP0.5, C15SAP1, and C15SAP2 was 24%, 35%, and 53% lower than that of the control mix, respectively. With increased dosage of the SAP, more and more water was absorbed by the SAP initially and therefore the water available in the early stage of the hydration process was

reduced. The gradual release of water by the SAP is a relatively slow process and therefore the reaction between the cement and water is slower than that of the control mix. In addition, the increased void ratio provided greater volume to dissipate the exothermic heat. These characteristics indicate that addition of the SAP could promote the internal curing of soil-cement as water can be stored in the SAP for further hydration.

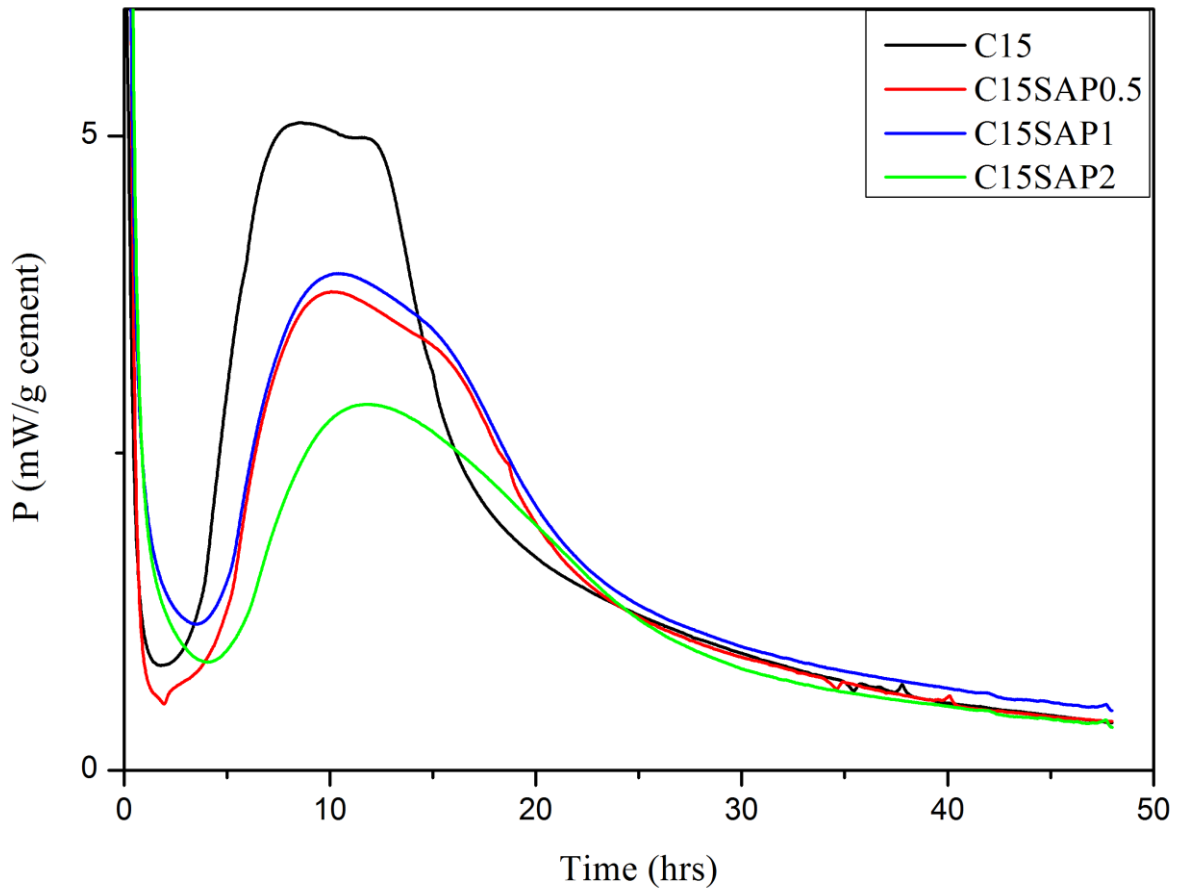


Figure 6.7 The effect of the BASF SAP A addition on the isothermal (23°C) power and energy production of the soil-cement mixes.

Table 6.2 Initial setting time and peak power values for soil-cement mixes containing different dosage of SAP.

Mix	Initial setting time (hrs)	Peak power (mW/g)
C15	4.46±0.08	4.28±0.07
C15SAP0.5	5.36±0.10	3.25±0.05
C15SAP1	5.64±0.07	2.77±0.04
C15SAP2	6.48±0.13	2.03±0.07

6.4.1.2 Flowability of the fresh mixes

The flow table values of all the fresh mixes of the soil-cement with different dosages of the SAP are presented in **Figure 6.8**. Two water/cement ratios of 1.67 and 2.07 were used and the corresponding control mixes are C15 and C15W31. It was noticeable that the addition of the SAP reduced the flow value for all soil-cement mixes. The flow value of mixes C15, C15SAP0.5, C15SAP1, and C15SAP2 were 190 mm, 180 mm, 153 mm, and 126 mm, respectively. **Figure 6.8** illustrates that the addition of the SAP decreased the flowability of soil-cement for both w/c ratio (1.67 and 2.07). With 2% SAP addition, the flow value of mix C15 (25% water) reduced from 190 mm to 126 mm while the flow value of C15W31 (31% water) reduced from 234 mm to 186 mm. It should be pointed out that during the preparation of mix C15W31SAP2, the SAP was firstly saturated with additional 6% of water before being added into the soil-cement mix. Additional 6% of water was added because in the cement pore solution, the absorption capacity of the SAP is $\sim 20\text{g/g}$ ($15\% \times 2\% \times 20 = 6\%$). If the excess 6% of water was completely absorbed by the SAP, then mixes C15W31SAP2 and C15 should have had similar workability. **Figure 6.8** shows that the flow table values of mixes C15 and C15W31SAP2 were 190mm and 186mm, respectively, which are almost the same. This indicates that the SAP was saturated in the fresh soil-cement mix during the mixing if it was added directly into the mix.

These observations on the reduction of workability with the addition of the SAP are reasonable as the SAP was directly added. Thus, it would absorb the water during mixing even though its absorption capacity in cement pore solution is limited. This agrees with the finding of Craeye et al. (2018), which documented that the w/c ratio reduced when SAPs were directly added into concrete. As the amount of free water in the fresh soil-cement mix reduces, reduction in workability is anticipated.

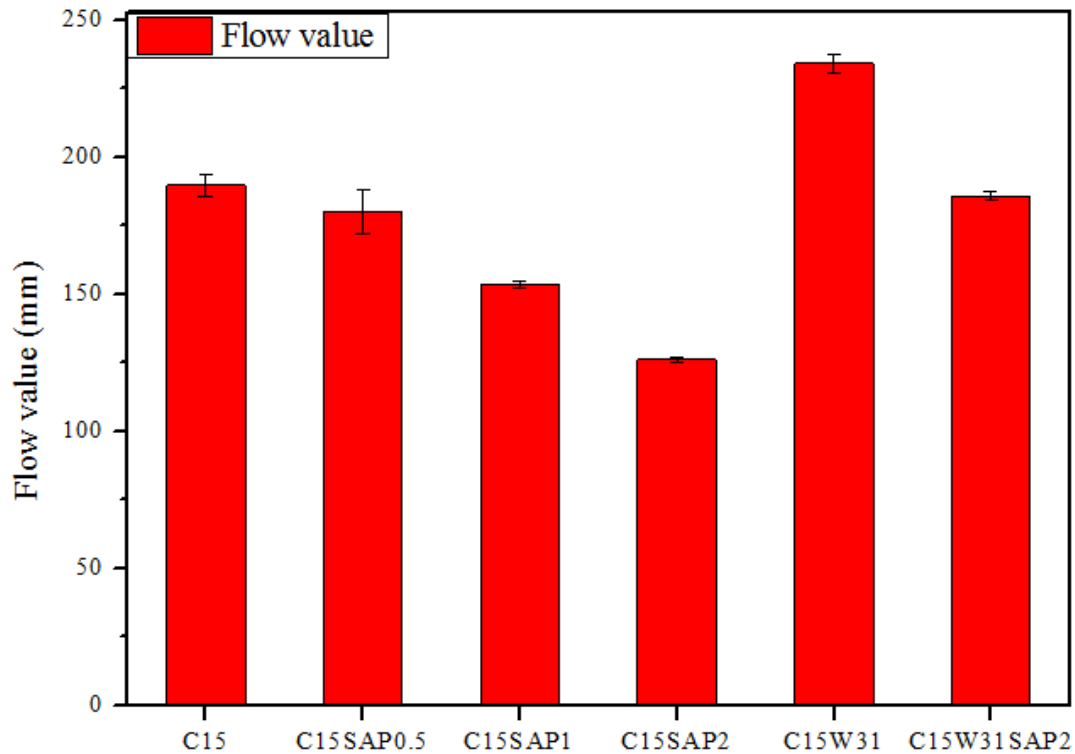


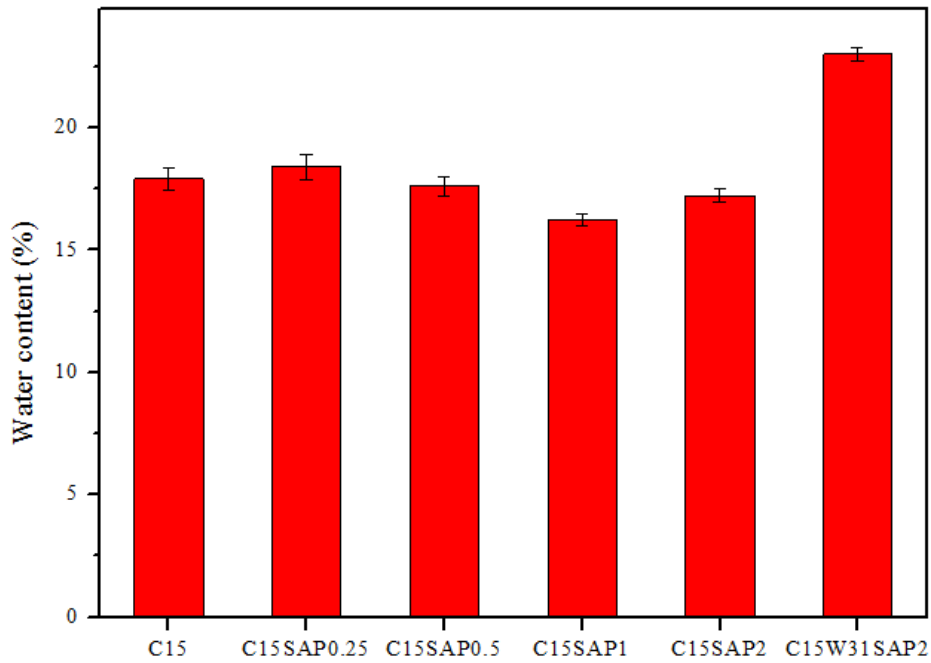
Figure 6.8 Flow values of different soil-cement mixes with different dosages of the BASF SAP A.

6.4.2 Physical properties

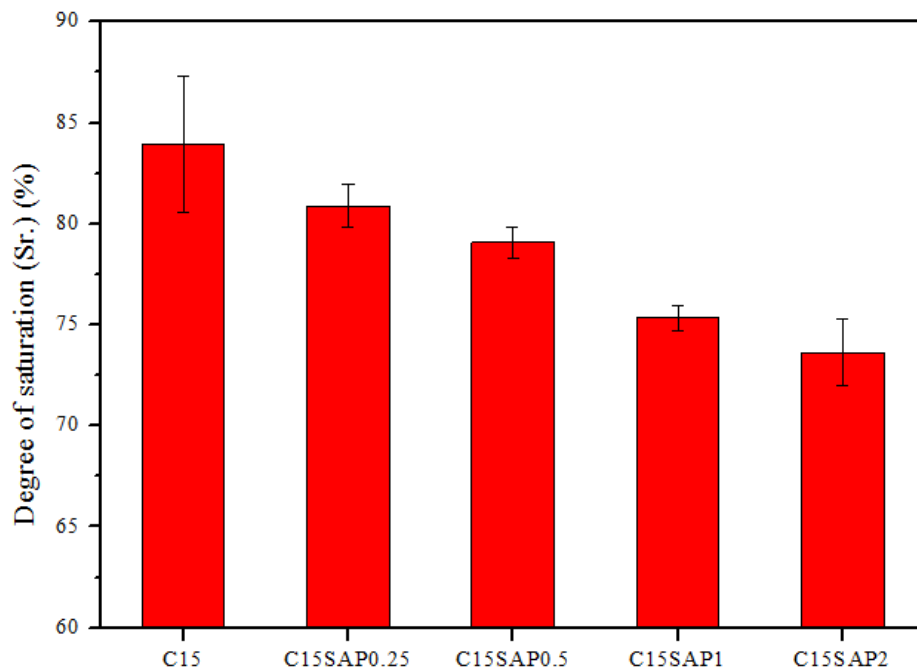
The water content measured for the soil-cement system embedded with different dosages of the SAP after 7 days of curing is presented in **Figure 6.9a**. In general, the addition of the SAP had little effect on the water content of the soil-cement samples for SAP dosages ranging from 0.25% to 2% of the cement. It is interesting to note that the addition of the SAP reduced the workability of the fresh mix but had little influence on the 7-day water content of the soil-cement system. A possible explanation for this observation is that the water was stored in the SAP particles during the mixing process but it was completely released for cement hydration at later stages. If additional water was added to saturate the SAPs before adding them into the soil-cement mix, i.e. mix C15W31SAP2, then the 7-day water content of the soil-cement would have noticeably increased.

The degree of saturation is calculated according to ASTM: D7263-09 (2009) and the 7-day degree of saturation (S_r) value of the soil-cement samples with different dosages of the SAP are presented in **Figure 6.9b**. It can be seen that the S_r value decreased with the increased dosage of the SAP. From mix C15 to C15SAP2, the S_r value reduced from 83.9% to 73.6%. It is noteworthy that the addition of SAP decreased the degree of saturation of the soil-cement

systems, given that the addition of the SAP had little effect on the 7-day water content. This indicates that the addition of the SAP can increase the air content of the soil-cement system without decreasing the water content.



(a)



(b)

Figure 6.9 Effects of the BASF SAP A on the (a) water content, and (b) the degree of saturation of the soil-cement mixes tested.

The mean and normalised dry densities of all the mixes with different SAP dosages are given **Figure 6.10**. It can be seen that the addition of the SAP had little effect on the dry density of the soil-cement systems. For soil-cement mixes embedded with 0–2% of the SAP, their dry density varied in the small range between 1733kg/m³ to 1762kg/m³. It is noteworthy that the addition of the SAP had little effect on the dry density of the soil-cement mixes as it was anticipated that large quantities of air-space would be created. For example, with the 2% SAP addition, the water content of the C15 mix reduced from 17.9% to 17.2% and the dry density reduced from 1760 kg/m³ to 1737 kg/m³, respectively. The slight reduction in the water content could be due to the enhanced cement hydration while the slight reduction in the dry density is caused by the increased air content of the soil-cement by the SAP particles. However, these reductions are minimal. A possible explanation for this is that 2% SAP addition by the weight of the cement only accounted of a very small volume fraction of the system. Another possible explanation is that the addition of the SAP promoted internal curing within the soil-cement system, which reduced the number of capillary pores and fissures to produce a denser soil-cement skeleton.

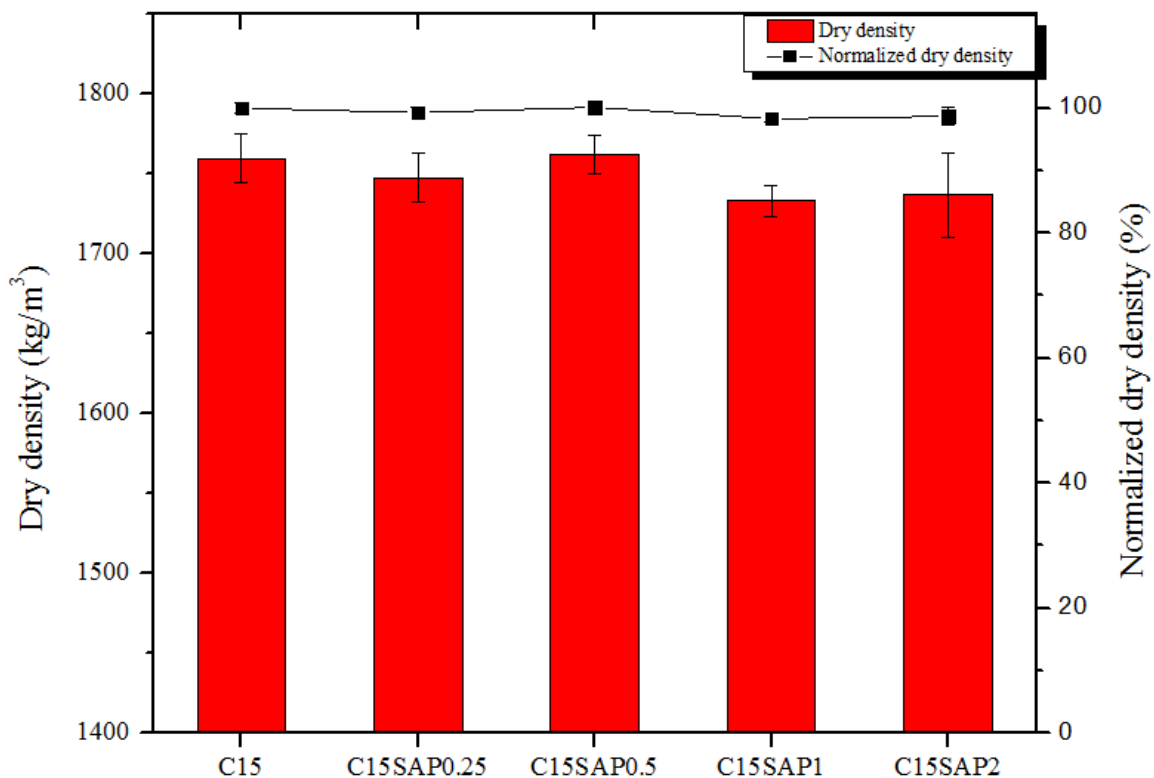


Figure 6.10 Effects of the addition of the BASF SAP A on the dry density of soil-cement mixes tested.

6.4.3 Unconfined compressive strength

The effects of the addition of the SAP on the UCS of soil-cement mixes were investigated. Per **Figure 6.11**, the 7-day UCS of the soil-cement mixes was dependent on the content of the SAP. Generally, the addition of the SAP increased the 7-day UCS of soil-cement mixes, except for the one containing 2%, where a reduction of 8% in the 7-day UCS was recorded. An increase of 12–17% in the UCS values was noticed for the C15SAP0.25, C15SAP0.5, and C15SAP1 mixes compared to the C15 mix. It seems that the 7-day UCS slightly increased with the increased SAP addition but this increase then reduced when the SAP dosage exceeded 0.5%. The increase in UCS is probably due the enhanced internal curing offered by the soaked SAP particles. However, as the dosage increases, the air voids created by SAP are more and more significant and finally become the dominant factor to reduce the UCS of soil-cement. This finding appears to be contradictory with the suggestion that the strength is generally reduced by the addition of SAPs for cementitious materials (Farzarian et al., 2016). However, the w/c ratio used in that study was relatively low for the cement pastes, namely 0.35 and 0.5 respectively. The w/c ratio used in the current study is much higher at 1.67 and 2.07. Thus, a possible explanation for this contradiction is that when the w/c ratio is relatively low, the addition of SAP reduces the UCS of cementitious materials while the addition of SAP may have little effect or increases the UCS for those with relatively high w/c ratio. This also agrees the work by Farzarian et al. (2016) and Mignon et al. (2015), reporting that the reduction in UCS of cement pastes by the addition of SAP is more noticeable at lower w/c ratio than higher w/c ratio.

Soil cement mixes with two w/c ratios (1.67 and 2.07) were tested. Per **Figure 6.11**, the 7-day UCS values of mixes C15 and C15SAP2 were similar, and likewise mixes C15W31 and C15W31SAP2. This indicates that the w/c ratio was not altered by the addition of the SAP in this study. Combining with the workability results in **Section 6.4.1.2**, it can be concluded that the addition of the SAP up to 2% does not decrease the 7-day UCS of soil-cement mixes though reduced the workability significantly. This indicates that the free water was absorbed by the SAP during the mixing but thereafter the water absorbed by the SAP was completely released for cement hydration. Thus, it can be concluded that the addition of SAP has little influence on the w/c ratio for the soil-cement systems used in this study if they were added directly. During mixing, the SAP has priority to absorb water while cement hydration reclaims the priority of water absorption during the cement hydration at later stage.

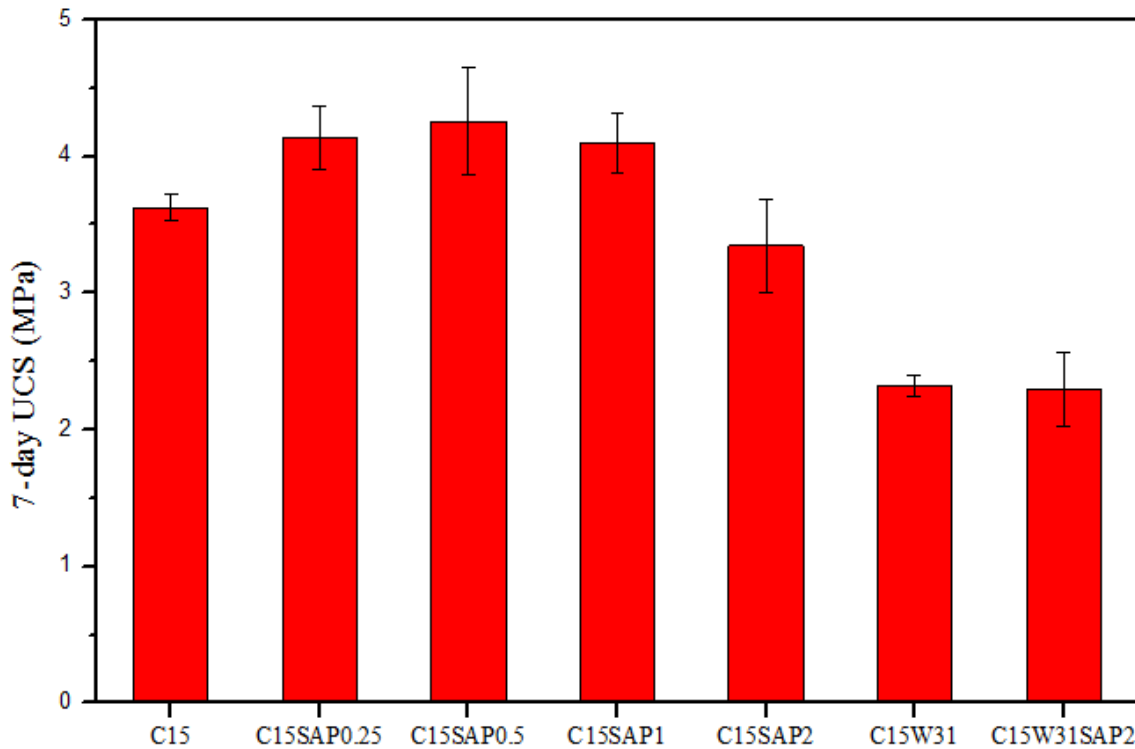


Figure 6.11 Effects of the BASF SAP A on the 7-day UCS of the soil-cement mixes used.

The UCS values of the soil-cement mixes containing the SAP at different curing ages up to 90 days are presented in **Figure 6.12**. Trends in the UCS development for the control soil-cement mix and mixes containing 1% SAP were found to be similar but the UCS of mix C15SAP1 presented noticeably higher UCS values than the control mix at all ages. The results showed that the addition of 1% of the SAP enhanced the UCS values and development over time. At the age of 7, 14, 28, and 60 days, the UCS of mix C15SAP1 was 30–40% higher than that of the control mix (C15) at the same age. However, the difference reduced at 90 days, where the UCS of mix C15SAP1 was only 15% higher than that of mix C15. It is believed that the addition of the SAP improved the internal curing and hydration of the soil-cement mixes at early ages, leading to increase in the UCS at all curing ages (up to 90 days).

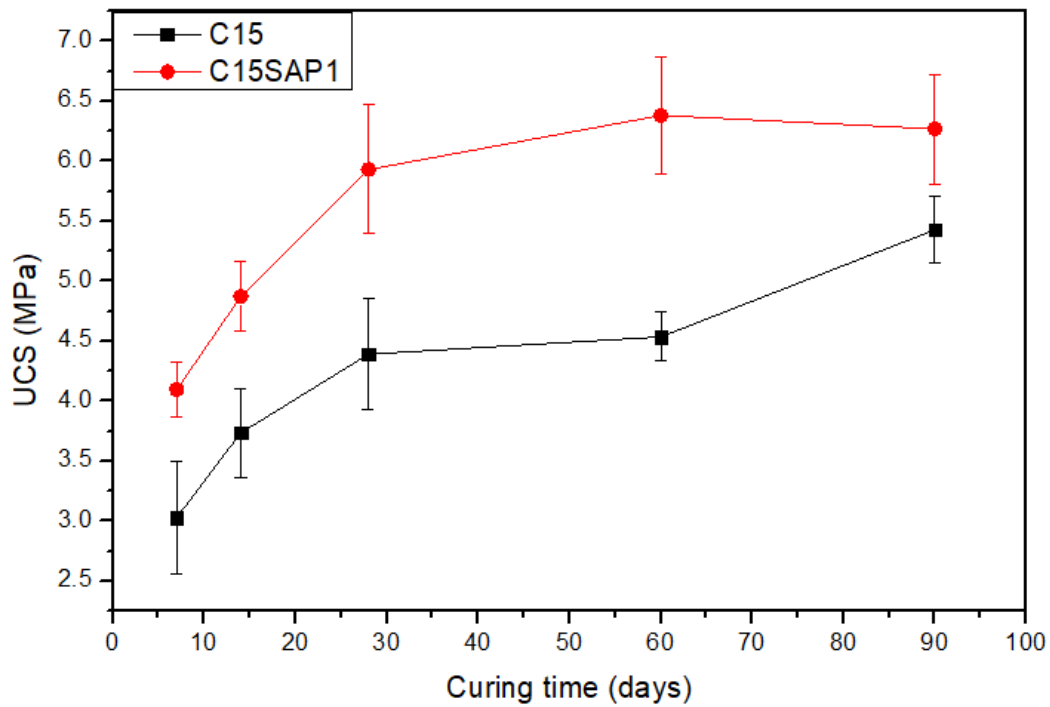


Figure 6.12 The UCS of the SAP-containing soil-cement mixes at different curing times.

6.5 Development and behaviour of self-immune soil-cement systems under freeze-thaw cycles using BASF SAP A

6.5.1 Physical properties

Photos showing the soil-cement mixes subjected to ten freeze-thaw cycles are presented in **Figure 6.13**. From visual inspection, it is found that the addition of the SAP improves the freeze-thaw resistance of the soil-cement mixes. Fewer cracks can be identified on the surface of soil-cement mixes with the increased dosage of the SAP. In general, no cracks were observed on the C15SAP2 mix specimens while various cracks and material spalling can be observed on control samples (C15).



(a) C15



(b) C15SAP0.25



(c) C15SAP1



(d) C15SAP2

Figure 6.13 Photo of the soil-cement specimens after ten freeze-thaw cycles with highlighted cracks and spalling.

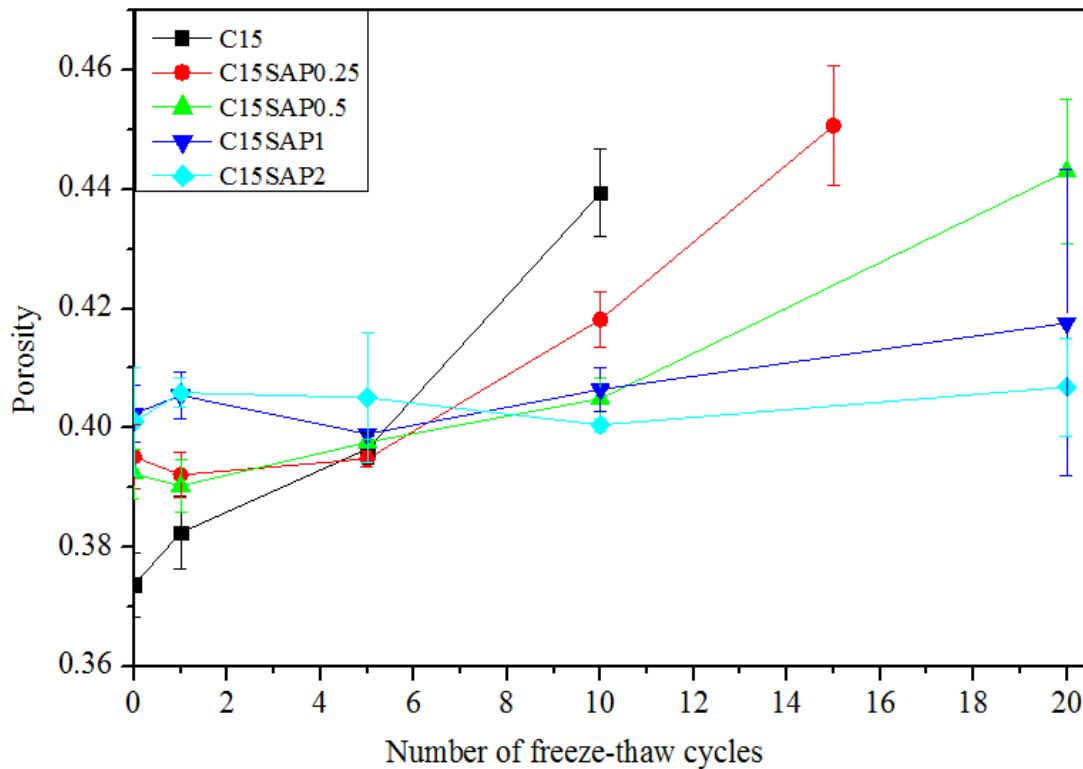
6.5.1.1 Porosity, degree of saturation and air content

The porosity, degree of saturation, and air content of the soil-cement mixes were calculated according to ASTM: D7263-09 (2009) and plotted in **Figure 6.14a**. These parameters are firstly measured to investigate the influence of SAPs addition on the internal structure of soil-cement system. The initial porosities of mixes C15, C15SAP0.25, C15SAP0.5, C15SAP1, and C15SAP2 are 0.374, 0.395, 0.392, 0.402, and 0.401, respectively. The initial porosity of the soil-cement mixes increased with the addition of the SAP and the increase was noticeable with as little as 0.25% of SAP addition. Furthermore, the changes in porosity, degree of saturation, and air content reflected the structural change within the soil-cement matrix during the freeze-thaw process. As discussed in **Chapter 5**, the Sr. and porosity values reflect how the water migrates within soil-cement samples when subjected to freeze-thaw cycles. In general, the porosity of the soil-cement samples increased with the number of freeze-thaw cycles for all mixes. This increase in porosity of the soil-cement mixes was mainly caused by the expansion of ice formation during freezing, where a large number of pores were enlarged and cracks were generated during this process. However, the increase in porosity after freeze-thaw cycles was significantly reduced by SAP addition. For example, after ten freeze-thaw cycles, the porosities of mixes C15SAP0.25, C15SAP0.5, C15SAP1, and C15SAP2 were 0.418, 0.405, 0.406 and 0.400, respectively, which were much lower than the value of 0.439 of the control mix. For mix C15SAP1, the porosity remained constant before ten freeze-thaw cycles but increased by 2.7% after twenty freeze-thaw cycles. For mix C15SAP2, the porosity did not increase with the number of freeze-thaw cycles up to twenty, which indicated that mix C15SAP2 was completely self-immune to the freeze-thaw cycles in terms of porosity change.

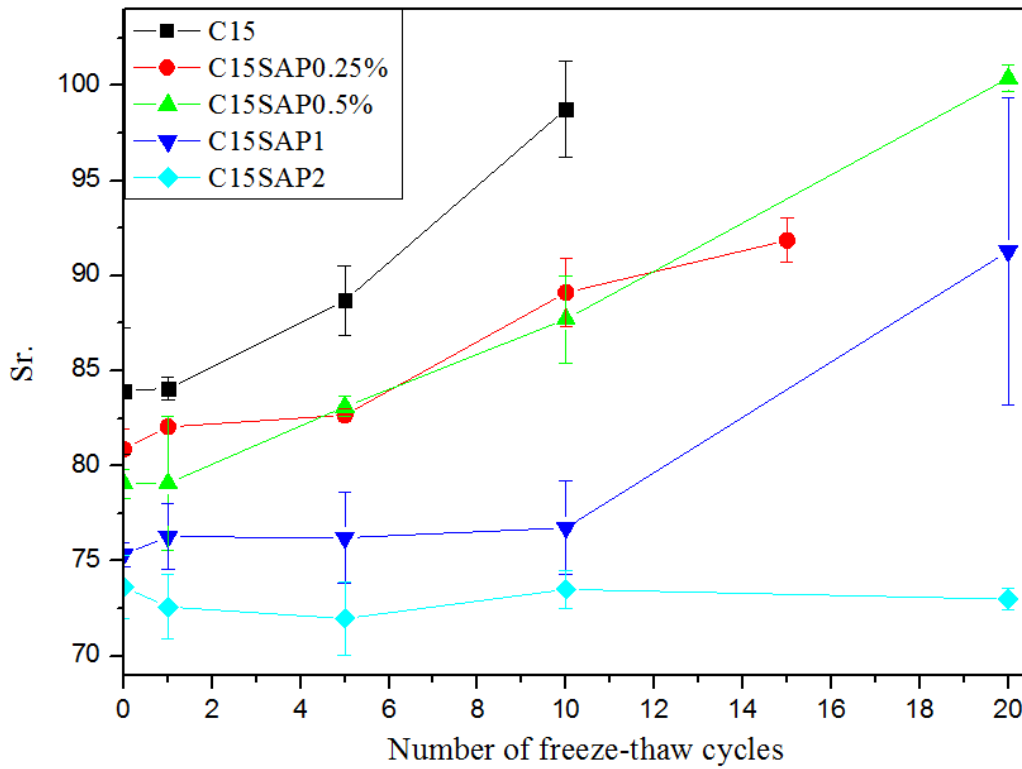
The Sr. values for all the soil-cement mixes with different dosage of the SAP are presented in **Figure 6.14b**. The initial Sr. value of mix C15 samples was 84% and it reached 100% saturation after ten freeze-thaw cycles. With the addition of the SAP, the increase in the Sr. values after the freeze-thaw cycles was significantly reduced. With 2% of SAP addition, the Sr. values of the soil-cement system did not increase even after twenty freeze-thaw cycles.

The air content values of the soil-cement mixes with different dosages of the SAP are presented in **Figure 6.14c**. The air content of mix C15 continued to decrease with the increased number of freeze-thaw cycles and this value dropped from 6% to almost zero after ten freeze-thaw cycles. As shown in **Figure 6.14c**, the initial air content of the soil-cement mixes increased with the addition of the SAP. This indicates that air space was created by the

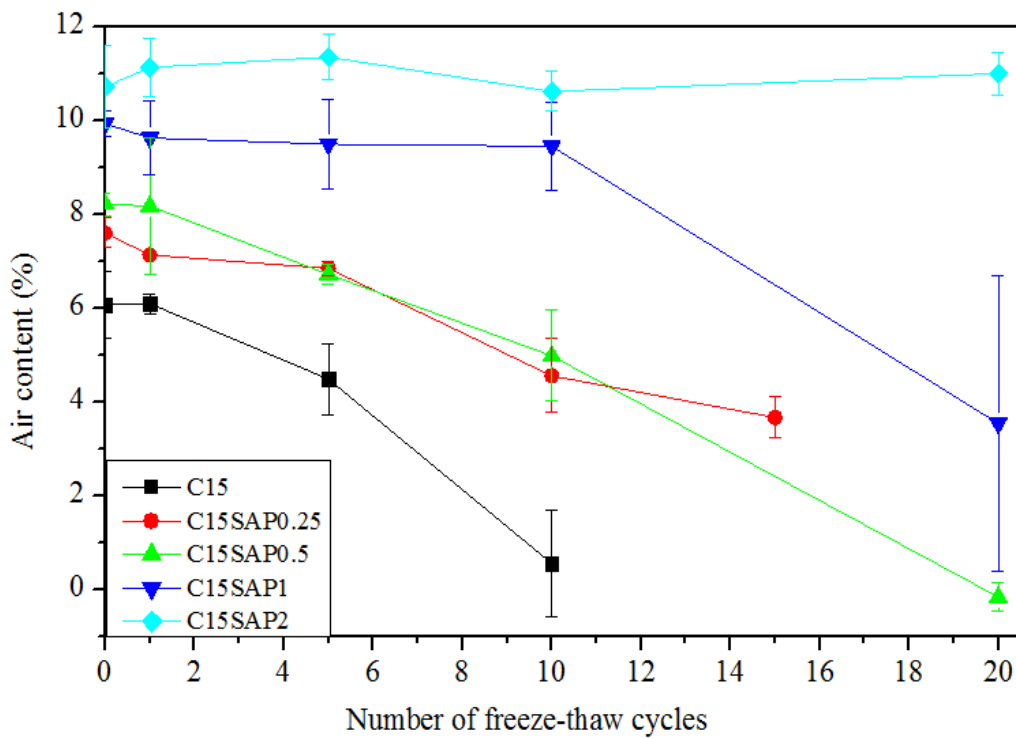
SAP and higher SAP dosages led to higher volume of air spaces. Mixes C15SAP0.25, C15SAP0.5, and C15SAP1 still experienced a considerable decrease in air content after the freeze-thaw cycles but the level of decrease was largely lower than that of the control mix. However, mix C15SAP2 exhibited little variation in air content even after experiencing up to twenty freeze-thaw cycles. Thus, in terms of porosity, degree of saturation and air content, the recommended SAP dosage for building a self-immune soil-cement system subjected to up to 20 freeze-thaw cycles is 2% by weight of the cement.



(a)



(b)



(c)

Figure 6.14 Properties of the soil-cement mixes with different percentages of SAP additions against the number of freeze-thaw cycles in terms of (a) porosity, (b) degree of saturation, and (c) air content.

6.5.1.2 Water content

As explained in **Chapter 5**, the water content is an important parameter of soil-cement systems as it is an indication of the process and damage extent caused by freeze-thaw cycles. Water migration plays a key role in the freeze-thaw deterioration of soil-cement systems and therefore the control of water ingress is considered crucial for the development of self-immune soil-cement system. It was reported in the literature that water can be drawn into the frozen part of the soil from the underlying soil due to the temperature gradient between the frozen part and warmer part (Guthrie et al., 2006). Similarly, as discussed in **Chapter 5**, the increased moisture content in soil-cement samples was caused by the continuous water absorption due to the temperature gradient and the expansion of pores and cracks caused by the ice expansion during the freeze-thaw process. Moreover, increased water content worsens the damage caused by ice expansion in soil-cement and therefore large increase in water content is anticipated after a number of freeze-thaw cycles.

However, for the soil-cement mixes containing the SAP including C15SAP0.25, C15SAP0.5, C15SAP1 and C15SAP2, the increase in water content after freeze-thaw cycles was observed to be slowed down. The water content of the soil-cement with varying additions of the SAP, subjected to different numbers of freeze-thaw cycles, is presented in **Figure 6.15**. The water ingress into the soil-cement systems after freeze-thaw cycles was significantly reduced by the addition of the SAP when compared with the sharp increase observed in the control mix (C15). For example, the initial water content for all the mixes was similar (~18%) but the water content of C15, C15SAP0.25, C15SAP0.5, C15SAP1, and C15SAP2 after 10 freeze-thaw cycles was 27.5%, 22.1%, 20.6%, 18.1%, and 16.9%, respectively. After 10 freeze-thaw cycles, the moisture content of C15 had increased by 9.5% while this increase dropped to 3.7% when 0.25% of the SAP was added. The water content of C15SAP1 remained stable up to ten freeze-thaw cycles before increased considerably after twenty cycles. As for mix C15SAP2, its water content remained steady even after twenty freeze-thaw cycles, which indicates that water ingress was completely inhibited. Results confirm that the incorporation of the SAP can reduce the water movement in soil-cement systems. The water permeability results in **Section 6.5.3** show that the initial permeability of SAP-embedded samples was lower than that of the control mix. Therefore, the lower water uptake could be due to the lower initial permeability. Another possible explanation for this phenomenon is that the addition of the SAP have created air space for the water to expand when frozen, hence prevented the creation and expansion of the interlinked cracks when subjected to freeze-thaw cycles. Moreover, the SAP

particles were able to absorb large amounts of water and swell. Thus, the presence of swollen SAP may have blocked the internal cracks and hindered the water ingress. In addition, it is noteworthy that the soil-cement system itself should have a relatively low permeability to resist the capillary suction generated by the temperature gradient during the freeze-thaw process.

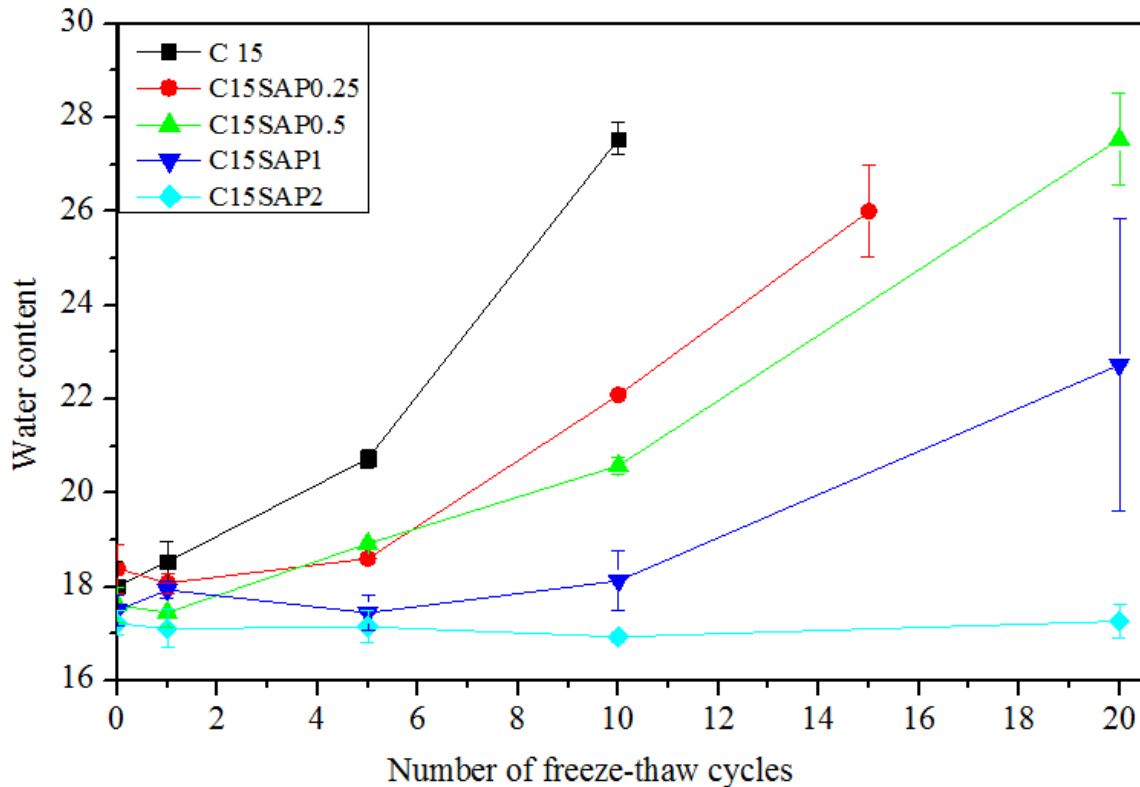


Figure 6.15 The water content of the soil-cement mixes containing different dosages of the BASF SAP A subjected to a number of freeze-thaw cycles.

6.5.1.3 Volumetric change

The volumetric change of all the soil-cement systems with different dosage of the SAP after various numbers of freeze-thaw cycles is shown in **Figure 6.16**. Compared to the control mix, whose volume increased by 11% after ten freeze-thaw cycles, the volumetric change of all soil-cement mixes was significantly reduced with the increased addition of the SAP. Only 1–3% volumetric change was measured for mixes C15SAP0.25, C15SAP0.5, and C15SAP1 after ten freeze-thaw cycles. However, the volumetric change of mix C15SAP0.25 after fifteen freeze-thaw cycles increased to 8.6% and the volumetric changes of mixes C15SAP0.5 and C15SAP1 reached 6.5% and 3.2% after twenty freeze-thaw cycles, respectively. What stands out in **Figure 6.16** is that for mix C15SAP2, its volumetric change

was still negligible even subjected to twenty freeze-thaw cycles. It is evident that 2% SAP addition was able to make the soil-cement systems self-immune to the volumetric change caused by up to 20 freeze-thaw cycles. Thus, in this case, frost heave could be completely prevented.

The increased volume after freeze-thaw cycles is believed to be caused by the ingress of water during freeze-thaw cycles and the volume expansion of water during freezing. As water was absorbed into the soil-cement, the volume of soil-cement also increased with the freeze-thaw cycles. This explanation is strengthened by the good correlation between the volumetric change and the water content presented in **Figure 6.17**, where the trends of increase for volumetric change and water content after freeze-thaw cycles are very similar.

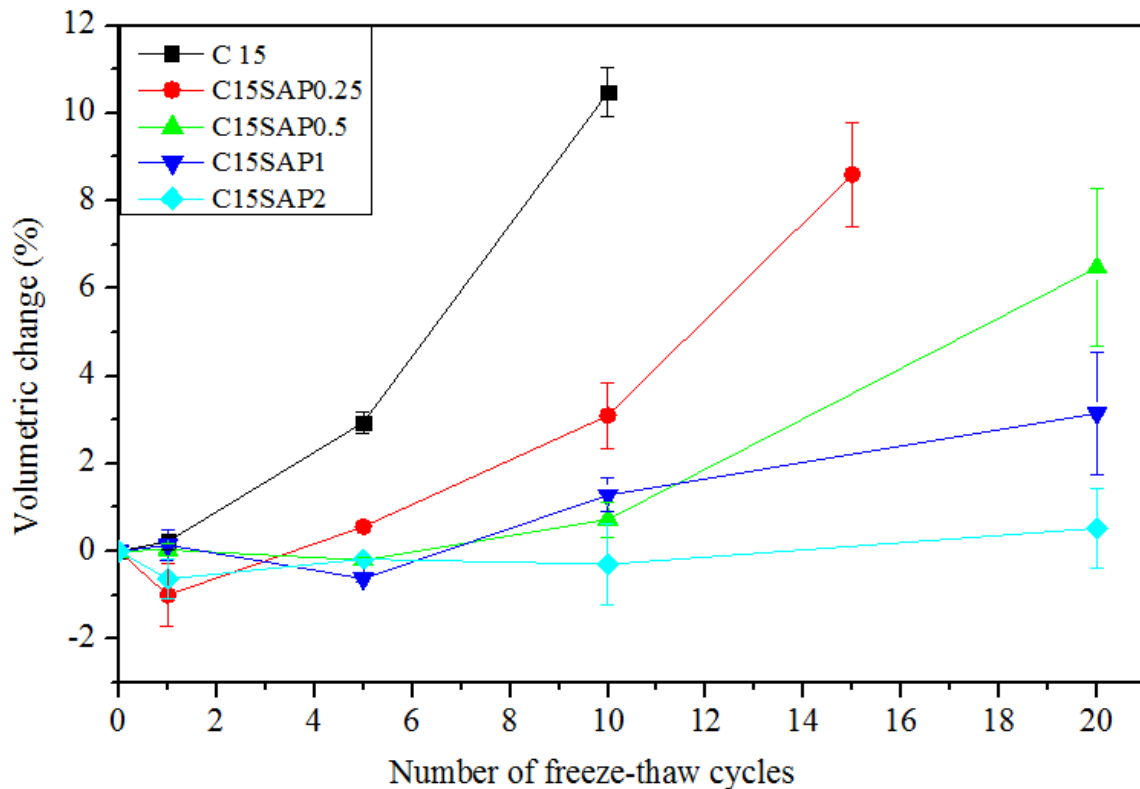


Figure 6.16 The volumetric change of the soil-cement mixes embedded with different dosage of the BASF SAP A under freeze-thaw cycles.

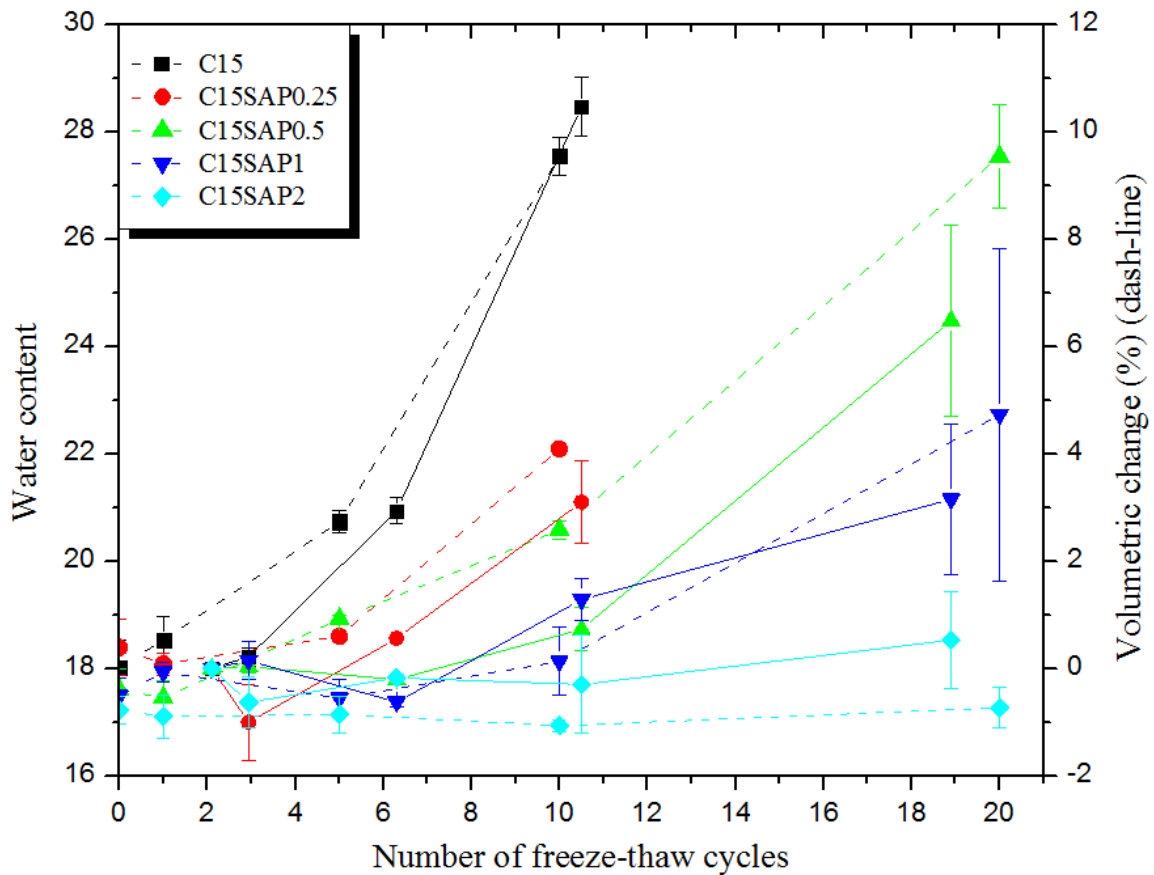


Figure 6.17 The correlation between water content and volumetric change of the soil-cement mixes embedded with different dosage of the BASF SAP A over repeated freeze-thaw cycles.

6.5.1.4 Dry density

Changes in dry density for all the SAP mixes with different numbers of freeze-thaw cycles is plotted in **Figure 6.18**. The dry density of all soil-cement mixes decreased with increased number of freeze-thaw cycles. For the control sample, the dry density decreases from 1760 kg/m³ to 1575 kg/m³ after 10 freeze-thaw cycles. As discussed in **Section 6.4.2**, the addition of the SAP had little influence on the initial dry density of the soil-cement. However, the reduction in dry density due to the freeze-thaw cycles was largely reduced for SAP-containing soil-cement systems. After ten freeze-thaw cycles, the dry density of mix C15SAP0.25 was 1687 kg/m³, which is 7% higher than that of the control samples subjected to a same number of freeze-thaw cycles. The reduction in dry density after freeze-thaw cycles continued to reduce with increased dosage of the SAP. It is interesting to note that for mix C15SAP2, its dry density remained constant after up to twenty freeze-thaw cycles. These

results in dry density are consistent with the results of the volume and water content that were discussed in **Sections 6.5.1.2 and 6.5.1.3**.

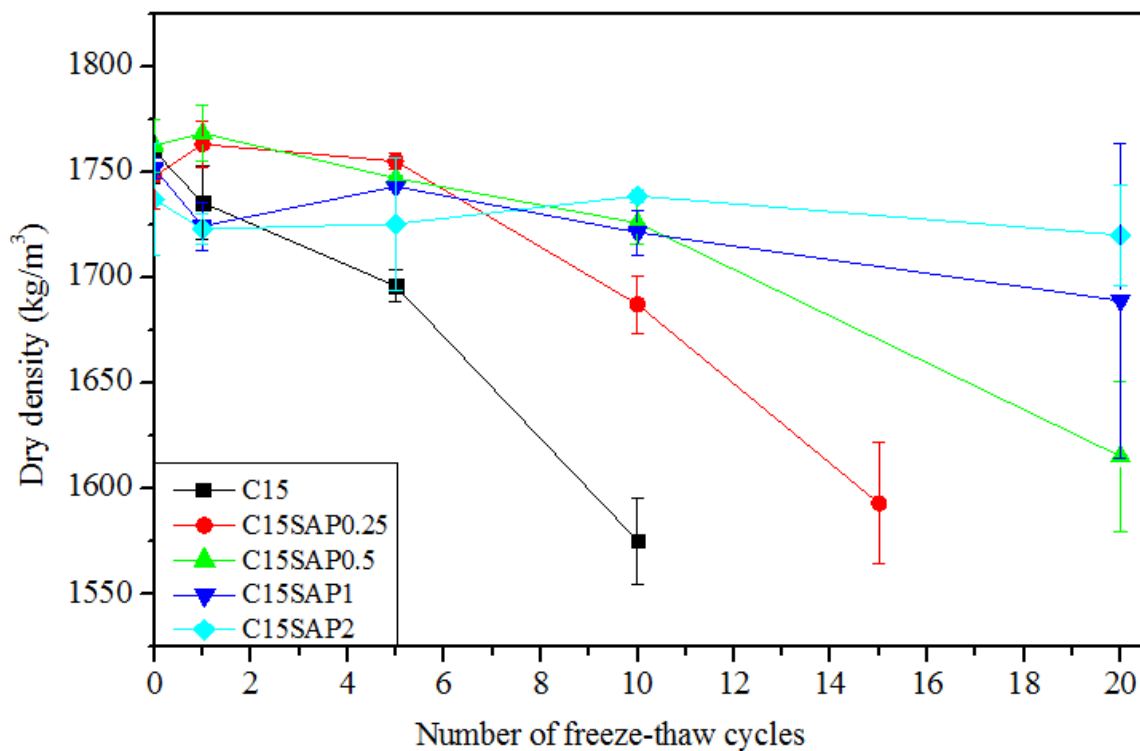


Figure 6.18 The dry density of the SAP-embedded soil-cement systems over repeated freeze-thaw cycles.

6.5.2 Unconfined compressive strength

UCS testing was performed on triplicate samples for all the soil-cement mixes that were exposed to 0, 1, 5, 10, and 20 freeze-thaw cycles and the results are presented in **Figure 6.19**. As shown in **Figure 6.19**, the addition of the SAP has a positive effect on the freeze-thaw resistance of the soil-cement mixes in terms of UCS. In the case of C15SAP0.25 and C15SAP0.5 mixes, the UCS values after 10 freeze-thaw cycles was 1.7 MPa and 2.8 MPa, respectively, already showing a considerable improvement compared to the control mix (0.6 MPa). Results also confirm the superior performance of soil-cement mixes with addition of 2% of the SAP against freeze-thaw damage. The UCS of mix C15SAP2 not only remained unaffected by the freeze-thaw cycles but in fact showed an increase of 33% after 5 freeze-thaw cycles. This increase in UCS is likely to be caused by the continuous hydration of the cement. This implies that mix C15SAP2 became self-immune to deterioration caused by up to 20 freeze-thaw cycles in terms of UCS.

The effect of different w/c ratio on the UCS of soil-cement systems after a number of freeze-thaw cycles is presented in **Figure 6.20**. It can be found that mix C15W31SAP2 also exhibited much higher freeze-thaw resistance than mix C15W31. This indicates that the addition of the SAP is beneficial for the freeze-thaw resistance of soil-cement systems with different w/c ratios. Notwithstanding the considerable increase in freeze-thaw resistance, it was shown that the UCS of mix C15W31SAP2 reduced by 56% after 10 freeze-thaw cycles. Thus, it should be noted that the 2% addition of the SAP should not be considered as the optimum dosage for the soil-cement systems with different w/c ratios.

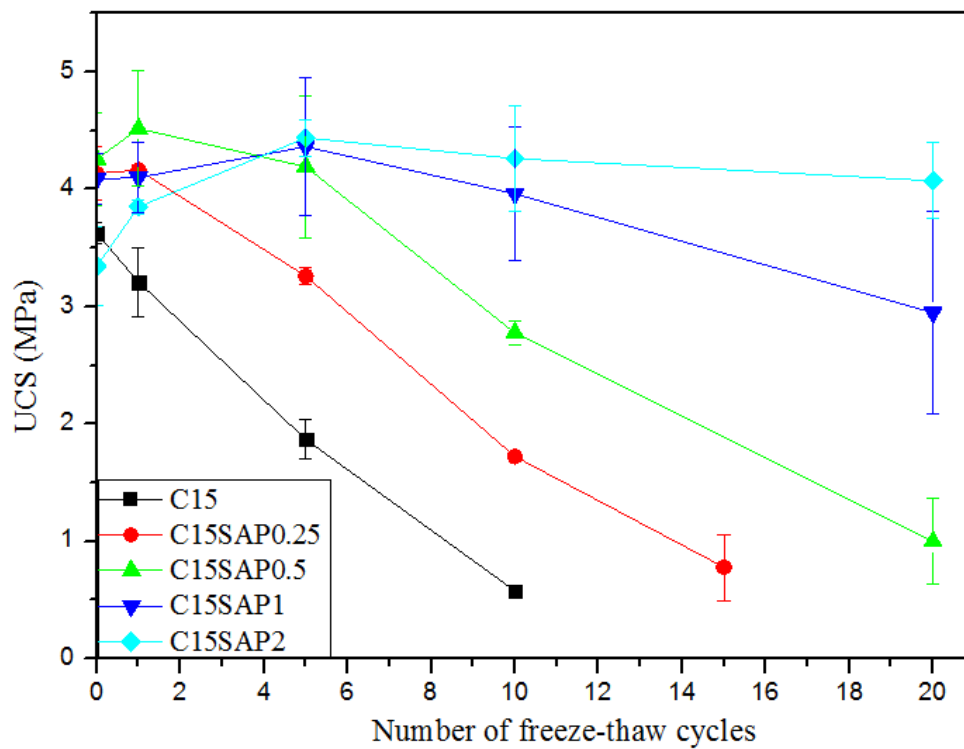


Figure 6.19 The USC of the soil-cement mixes with different dosages of the SAP over repeated freeze-thaw cycles.

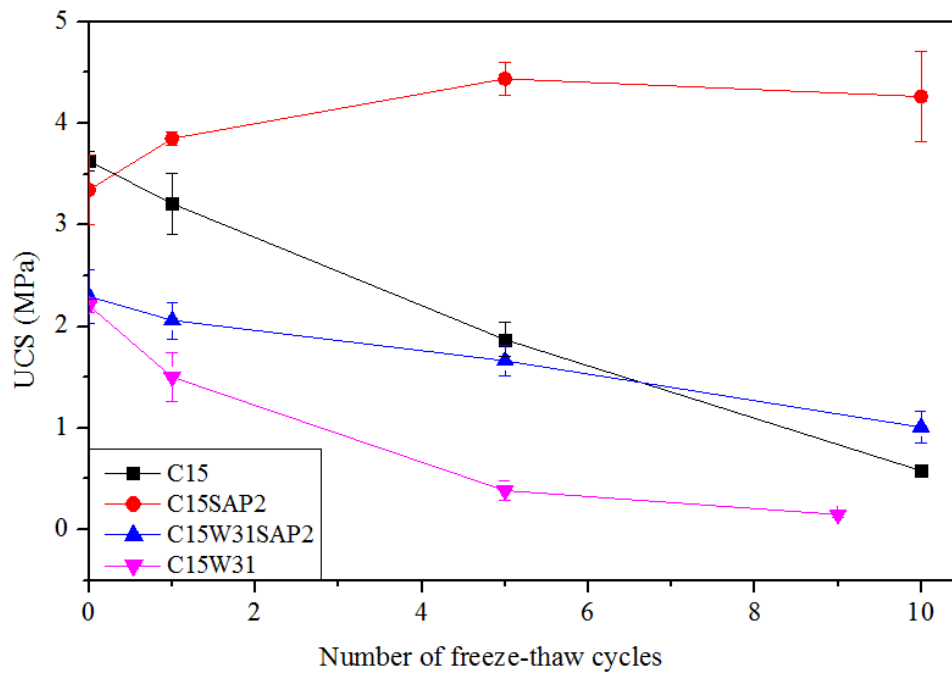


Figure 6.20 The strength behaviour of the soil-cement mixes with two different w/c ratios that are both embedded with 2% SAP over repeated freeze-thaw cycles.

6.5.3 Permeability

The permeability k was measured on duplicate samples for mixes C15, C15SAP1, and C15SAP2 which were subjected to up to 20 freeze-thaw cycles. The change of permeability for all the mixes after different numbers of freeze-thaw cycles (i.e. 0, 1, 5, 10 and 20) is presented in **Figure 6.21**. Results reveal that the addition of the SAP has little effect (C15SAP1) on or slightly decreased (C15SAP2) the initial permeability of the soil-cements compared to that of control mix (C15). It is noteworthy that the addition of the SAP decreased rather than increased the permeability of soil-cement systems, given that the addition of the SAP increased the porosity of the soil-cement system, as was reported in **Section 6.5.1.1**. A possible explanation for this could be that the addition of the SAP enhanced the internal curing of the soil-cement system and therefore reduced the number and width of internal cracks and fissures (Shen et al., 2016). Moreover, when it encountered water, the SAP within the air space may have absorbed water and swelled thereby clogging the flow path of water within the soil-cement matrix.

As discussed in **Section 5.4.3**, the permeability of mix C15 was largely increased due to freeze-thaw deterioration. Similarly with those embedded with SikaAer[®] Solid microcapsules, the addition of the SAP also largely increased the freeze-thaw resistance in terms of

permeability of the soil-cement systems. The permeability of the control samples was up to 2.5 orders of magnitude higher after 10 freeze-thaw cycles, while the measured permeability of mix C15SAP1 was only around half an order of magnitude higher. However, the permeability of mix C15SAP1 did increase by 2 orders of magnitudes after 20 freeze-thaw cycles, which indicates that mix C15SAP1 is not completely self-immune to freeze-thaw deterioration. As for mix C15SAP2, its permeability only slightly increased after the first freeze-thaw cycle but remained constant afterwards. After a total of 20 freeze-thaw cycles, the increase in the permeability of mix C15SAP2 was negligible and the k value was even lower than the 7-day k value of the control mix. The results show that mix C15SAP2 possessed a good self-immune capability against the freeze-thaw cycles in terms of permeability. As is already established, the addition of the SAP generated air-space for water within the soil-cement system to expand and contract. With a sufficient volume of air-space, the soil-cement system could become self-immune to freeze-thaw deterioration and maintain its low permeability. It was also found that the first freeze-thaw cycle exerted an indispensable effect on the permeability of the soil-cement samples. This indicates that the existing water within some of the saturated pores would inevitably expand during first freezing and cause minor disruption on the soil-cement matrix. After the first freeze-thaw cycle, the matrix of mix C15SAP2 could reach an equilibrium and its permeability showed little variation when subjected to further freeze-thaw cycles.

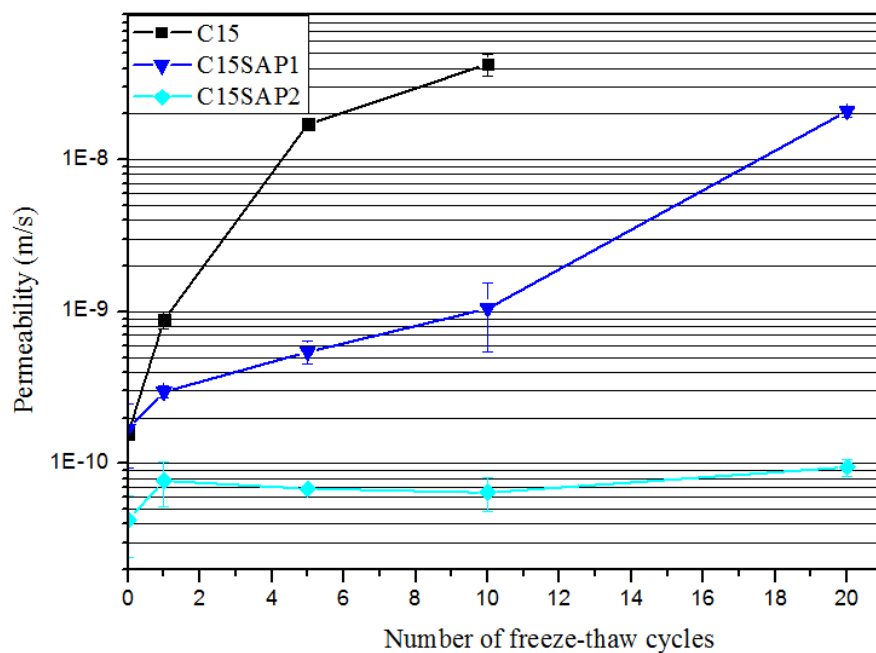
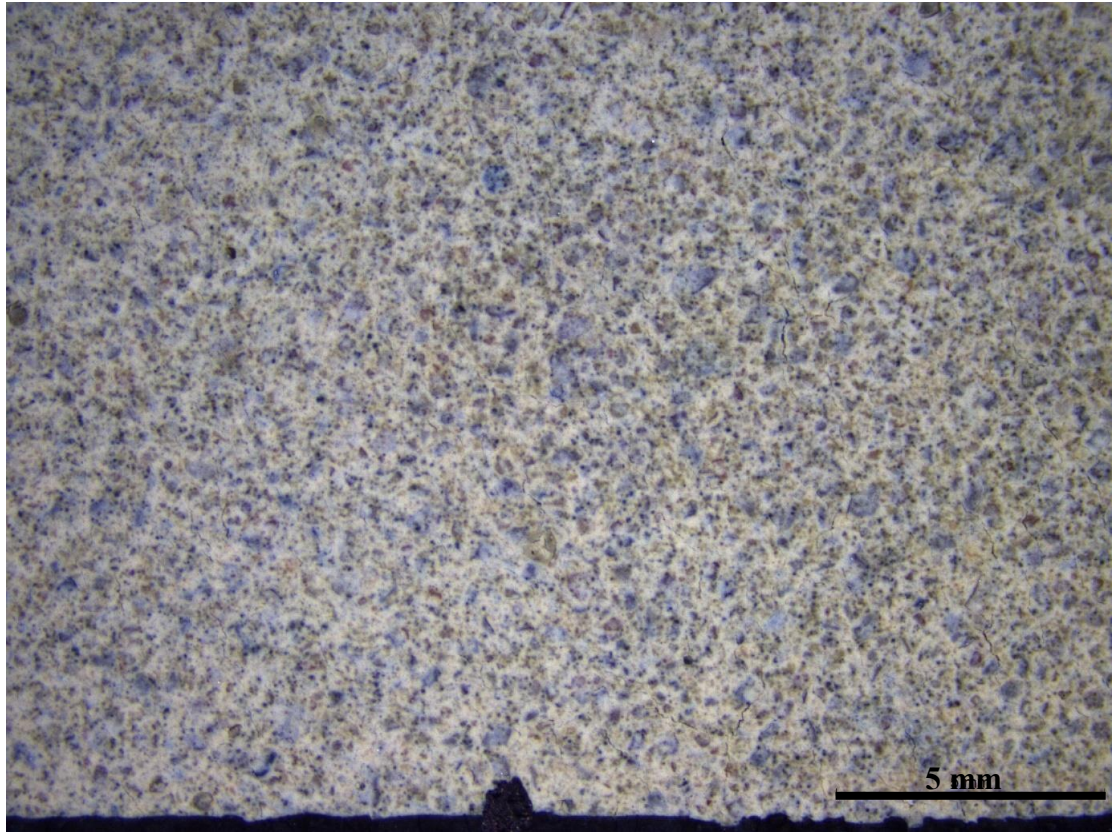


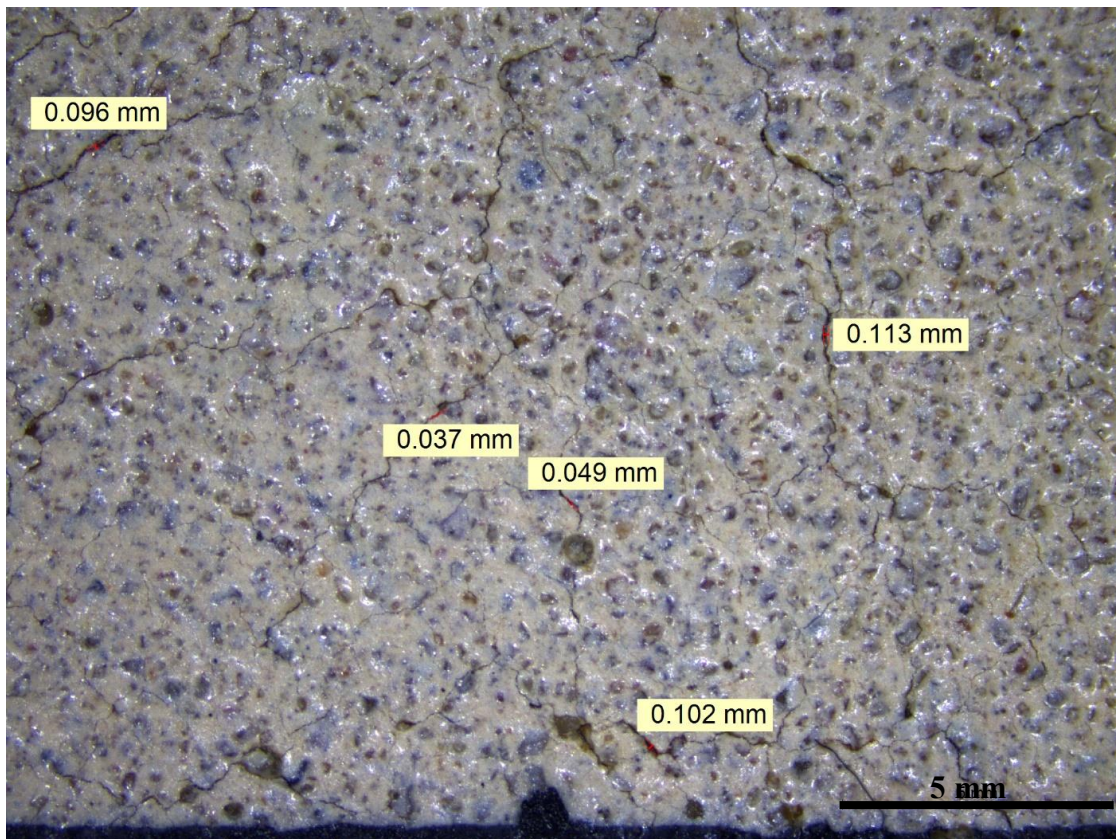
Figure 6.21 The evolution of the permeability values of the SAP-containing soil-cement mixes over repeated freeze-thaw cycles.

6.5.4 Surface crack characterisation

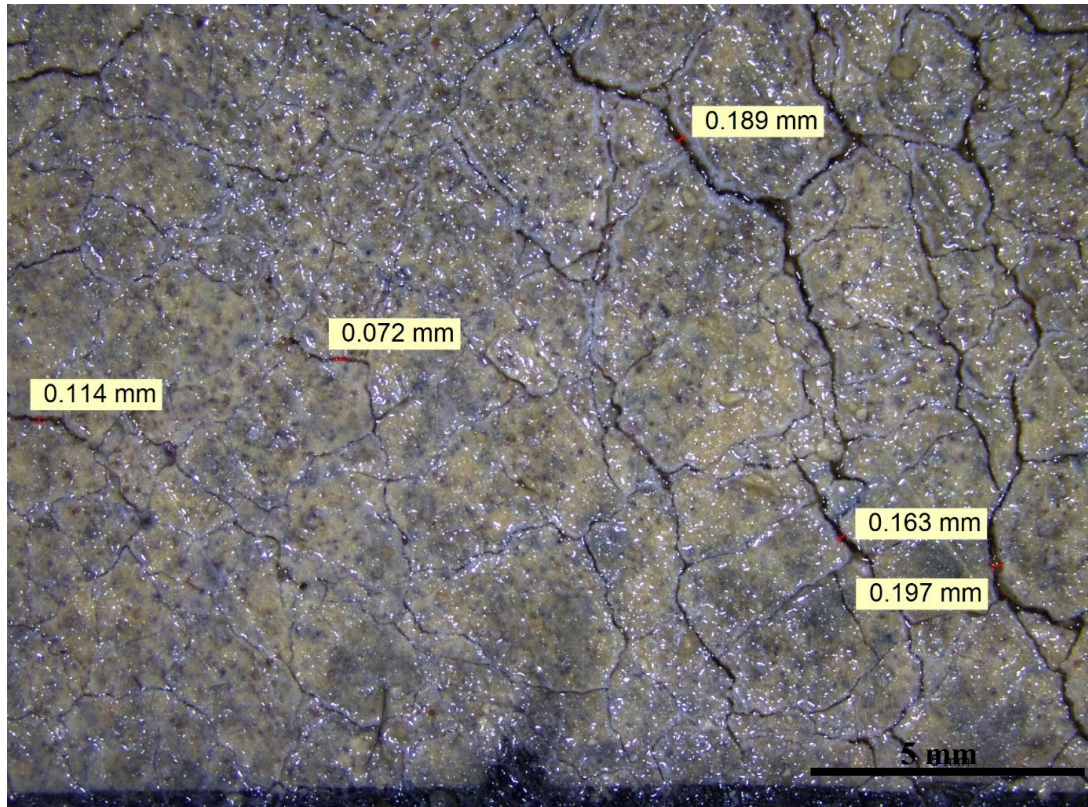
An examination of the microstructure using a light microscope was performed to investigate the extent of disruption of the control and the SAP-embedded soil-cement specimens after a different number (e.g. 0, 5, 8, and 20) of freeze-thaw cycles exposure. Representative optical microscope images of mixes C15 and C15SAP2 after different numbers of freeze-thaw cycles are presented in **Figure 6.22 (a-c)** and **(d-f)**, respectively. Images were taken under the microscope on the surface of the soil-cement disc specimens and their surface characteristics after a different number of freeze-thaw cycles were monitored and compared. Mix C15 samples showed no crack without freeze-thaw cycles (**Figure 6.22a**). Damage and cracks can be easily seen on the surface of mix C15 samples after 5 freeze-thaw cycles, where the cracks had a width up to ~0.1mm (**Figure 6.22b**). Significant damage was observed after 8 freeze-thaw cycles (disc samples were too weak to handle after the 8 freeze-thaw cycles), where cracks with width up to 0.2 mm have propagated across the entire surface of mix C15 samples (**Figure 6.22c**). However, for mix C15SAP2 samples, although the cavities created by the SAP can be easily discerned, no cracks were observed on their surface before freeze-thaw process (**Figure 6.22d**), after 5 freeze-thaw cycles (**Figure 6.22e**) and after 20 freeze-thaw cycles (**Figure 6.22f**). Based on these observations, it is deduced that the 2% SAP-embedded soil-cement systems could possess self-immunity to crack formation caused by up to 20 freeze-thaw cycles and crack formation can be completely eliminated.



(a)



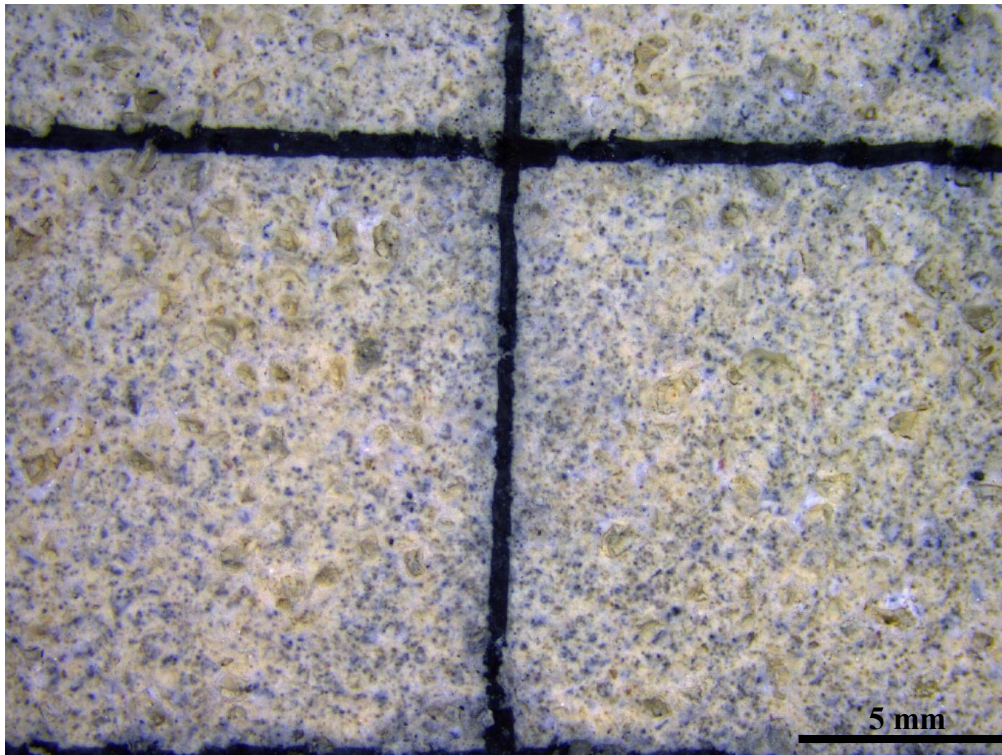
(b)



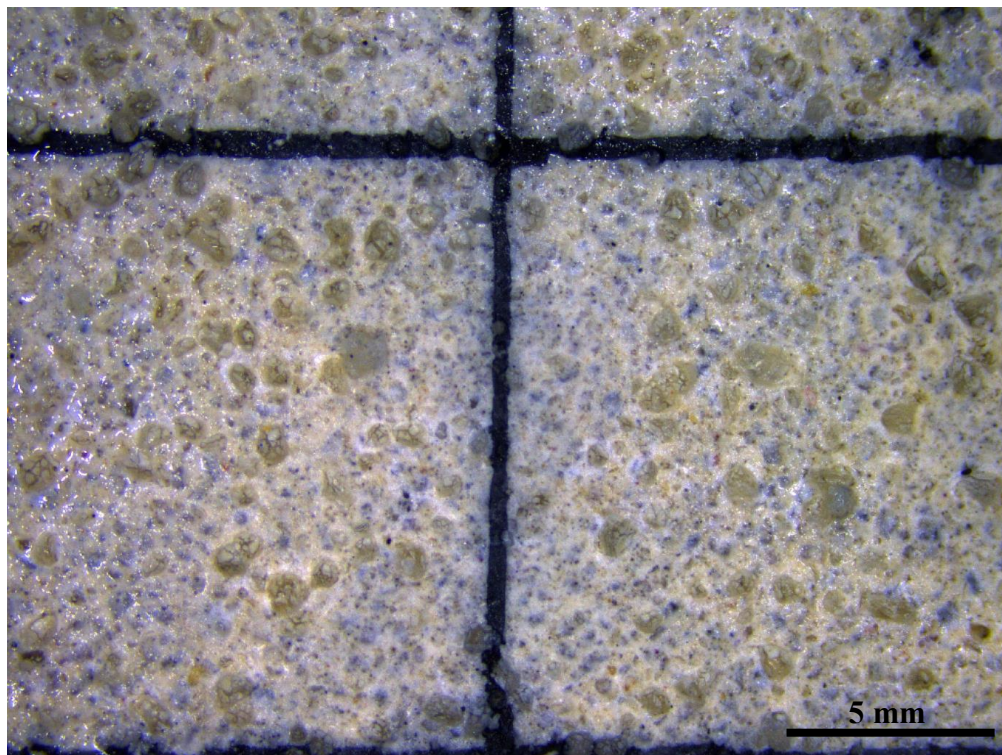
(c)



(d)



(e)



(f)

Figure 6.22 Surface crack identification of mixes C15 (a-c) and C15SAP2 (d-f): (a) C15 with no freeze-thaw cycles, (b) C15 after 5 freeze-thaw cycles and (c) C15 after 8 freeze-thaw cycles, (d) C15SAP2 with no freeze-thaw cycles, (e) C15SAP2 after 5 freeze-thaw cycles, and (f) C15SAP2 after 20 freeze-thaw cycles.

6.5.5 Summary and recommended dosage of SAP addition for building self-immune soil-cement system

The results presented in the previous **Sections 6.5.1-6.5.4** demonstrated that the addition of the SAP improved the freeze-thaw durability of soil-cement systems and the SAP dosage is a decisive factor for this improvement. The resistance of the soil-cement systems against freeze-thaw deterioration increased with the increase of SAP dosage. It should be noted that the freeze-thaw deterioration simulated in this study was very harsh as the samples were frozen at -25°C and thawed at 20°C . The temperature difference is 45°C of sudden change and water is available for soil-cement samples to absorb from underneath them during both freezing and thawing. The results in terms physical properties, UCS, permeability and surface crack characterisation all suggested that for the soil-cements used in this study, an addition of 2% is the optimum SAP dosage for developing a self-immune soil-cement system under freeze-thaw cycles.

6.6 Mechanisms of self-immunity in soil-cement systems under freeze-thaw cycles using SAPs

The damaging mechanisms of the soil-cement systems under cyclic freeze-thaw and the concept of self-immunity were introduced in **Section 4.3** and **5.5**. The basic principle of the self-immunity of soil-cement under freeze-thaw exposure is that when water freezes and expands in the matrix, the self-immune system can respond to this change by dissipating the excess volume/pressure generated by water freezing therefore protecting the system from damage. The results presented in the previous sections reveal that the addition of the SAP could provide good self-immunity to the soil-cement systems under freeze-thaw conditions. However, the self-immunity mechanisms of the SAP-embedded soil-cement systems under freeze-thaw cycles remained unknown and therefore they would be investigated and revealed in the following sections.

6.6.1 Air content and freeze-thaw resistance

As discussed in **Section 2.2**, it is commonly believed that air content is a crucial parameter for air-entraining cementitious materials. The air content and porosity values of the soil-cement samples with different dosages of the SAP are shown in **Figure 6.23**. The air content (by volume) of the soil-cement systems increased with the addition of the SAP and this increase was largely linear, namely the values for mixes C15, C15SAP0.25, C15SAP0.5, C15SAP1, and C15SAP2 was 6.1%, 7.6%, 8.2%, 9.9%, and 10.7%, respectively. This

indicates that the air space was created by the added SAP in the soil-cement systems. The air content of mixes C15SAP1 and C15SAP2 was 4% and 5%, respectively higher than that of mix C15. However, mix C15SAP1 was not self-immune to freeze-thaw damage as its engineering properties, though improved significantly, deteriorated noticeably after 10 freeze-thaw cycles. Conversely, no deterioration was observed for mix C15SAP2 after 20 freeze-thaw cycles. It is found that C15SAP2 was the mix with the lowest dosage of the SAP that was completely self-immune to freeze-thaw damage. As a result, it can be suggested that 5% of additional air pores is needed to build a self-immune soil-cement system against freeze-thaw actions.

Khoury and Zaman (2007) and Wang et al. (2017) suggested that the increased pore space renders a soil-cement system more vulnerable to freeze-thaw deterioration. They argued that additional pore spaces would increase the ingress of water thus increase the ice lens evolutions and, consequently, induce more cracks and fissures during freezing. In this study, it should be noted that the air space created by the SAP was entrained air rather than entrapped air. It is believed that the air space created by the SAP was of regular reasonable size and was well distributed therefore creating appropriate air-entraining for the soil-cement systems. The evidence for this explanation will be further discussed in the following sections.

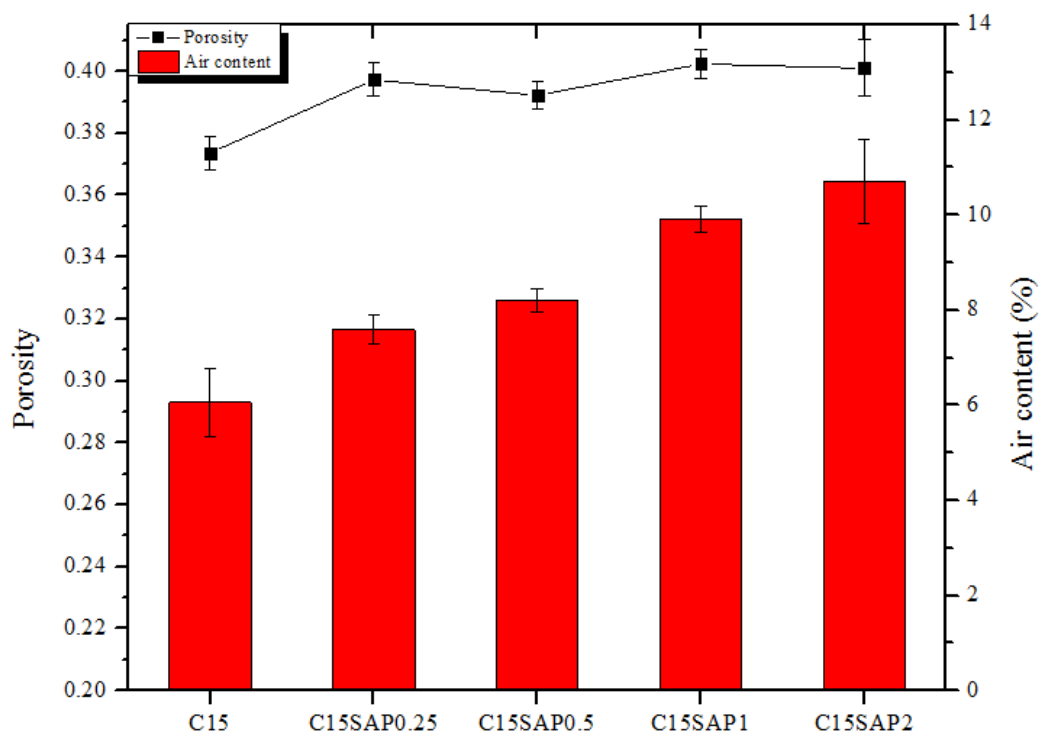


Figure 6.23 Air content and porosity of the soil-cement systems with different dosage of the BASF SAP A.

6.6.2 Critical degree of saturation

The change of degree of saturation for all the mixes with different dosage of the SAP under freeze-thaw cyclic action was discussed in **Section 6.5.1.1**. To define the level of saturation at the point when freeze-thaw damage initiates, a critical degree of saturation (S_{cr}) was suggested in **Section 5.5.3**. It was reported in **Section 6.5.1.1** that increased air content and porosity due to SAP addition do not impair the freeze-thaw resistance of soil-cement systems. A possible explanation is that increased air content does not necessarily increase the water ingress. The air content of mix C15SAP2 was 5% higher than that of the control mix C15. However, the S_r values of mix C15SAP2 remained constant at ~73% even after 20 freeze-thaw cycles while that of mix C15 increased from 84% to 100% after 10 freeze-thaw cycles.

According to the results presented in **Figure 6.14b**, it can be suggested that the critical degree of saturation for the soil-cement systems embedded with the SAP in this study was 73%. It should be highlighted that the critical degree of saturation is also 73% for the self-immune soil-cement embedded with SikaAer[®] Solid microcapsules as discussed in **Chapter 5**. For the soil-cement system studied, their degree of saturation did not increase after up to 20 freeze-thaw cycles if their initial degree of saturation was less than 73%. SAP addition can reduce the degree of saturation of the soil-cement systems. It appears that with a degree of saturation lower than the critical value (~73%), the soil-cement system mixed with the SAP is able to provide sufficient air space for the water inside the pores and fissures to enter and expand during the freezing and thawing processes. However, it should be noted that this critical value is only applicable to the self-immune soil-cement systems studied, which are embedded with either SS or SAP. For other soil-cement systems with S_r value lower than 73%, they may still very susceptible to freeze-thaw damage.

6.6.3 Scanning electron microscopy

SEM images were taken of the soil-cement samples containing the SAP that were cured for 7 days. Representative SEM images showing the SAP particles (indicated by red arrows) in the soil-cement matrix are presented in **Figure 6.24**. The SAP particles can be easily identified in the SEM images. They appeared dry and shrunk in the soil-cement matrix. It can be seen from the images that the SAP particles were all identified within a void in the soil-cement matrix, where the air space was believed to be created by the SAP particles. It is believed that the SAP particles were saturated during the mixing of the soil-cement and the volume of the SAP particles expanded by ~20 times. However, during the hydration process, the water

stored in the SAP particles donated to the cement hydration and the SAP particles gradually shrunk and created air-spaces around them. This behaviour was also reported by other researchers (Craeye et al., 2018, 2013; Hasholt et al., 2015; Mechtcherine et al., 2017). This explanation is supported by the facts that the initial workability of fresh mixes was reduced while the 7-day water content and UCS values of the samples remained almost unchanged for the SAP mixes compared with the control mix.

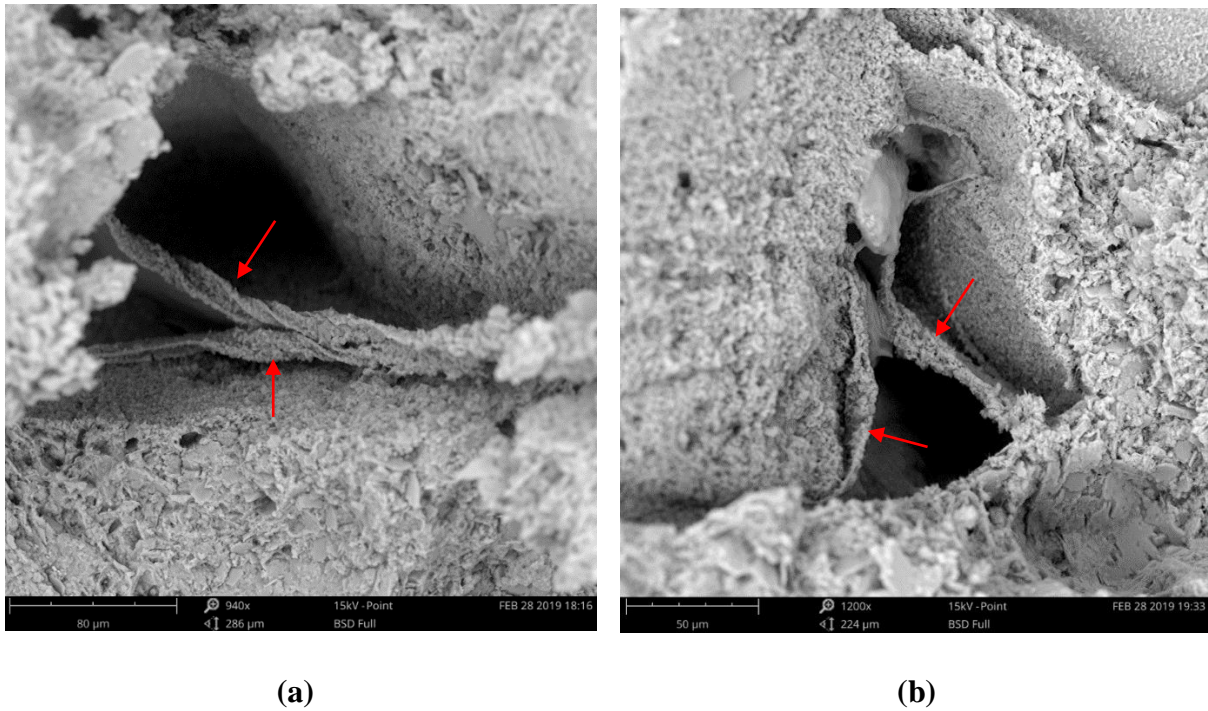


Figure 6.24 SEM images of C15SAP2 soil-cement samples containing SAPs. The scale bars in (a) and (b) are 80 and 50 μm, respectively.

6.6.4 High resolution X-ray computed microtomography (μCT)

6.6.4.1 Microstructure of soil-cement samples containing the BASF SAP A

As discussed in **Section 5.5.5**, the self-immune capability of soil-cement systems under freeze-thaw action depended on several parameters such as the size, quantity and distribution of the air-space. Therefore, high-resolution X-ray computed microtomography (μCT) was conducted to investigate the size and distribution of the air-space that was created by the SAP particles within the soil-cement matrix. The SAP particles and the air space surrounding it could be visualised, which are indicated by the red arrows in **Figure 6.25**, and their structures are very similar to that presented in the SEM images (**Figure 6.24**).

Figure 6.26a presents a representative cross-section showing a close-grained soil-cement matrix where only a few air pores and small fissures could be identified in a typical mix C15 specimen. In the matrix of the control specimen, air bubbles were rarely seen. However, in the cross-section of mix C15SAP2 specimens shown in **Figure 6.26b**, large quantities of air voids containing shrunk SAP particles could be clearly identified within the soil-cement matrix. The shape of these air spaces was irregular and the size of these pores varied from ~100 μm to ~400 μm . It is apparent from the figure that the air-spaces were well distributed in the soil-cement matrix. Moreover, as the SAP particles were well dispersed in the soil-cement matrix, the distance between the air spaces was relatively small. These air voids had scattered, small and irregular structures in the matrix of mix C15SAP2 specimens. As the SAP particles were commonly identified within the cavities, these cavities were believed to be generated by the addition of the SAP particles, which absorbed water during the mixing and then released water during the cement hydration.

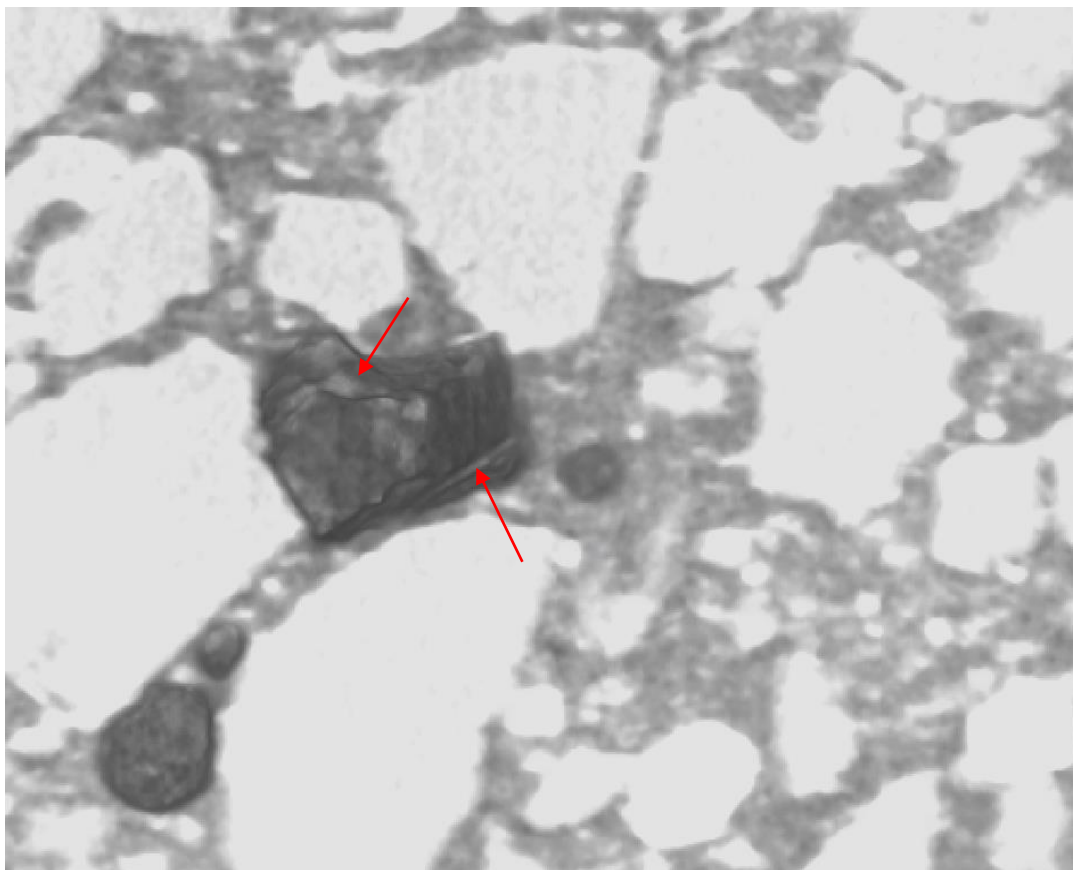
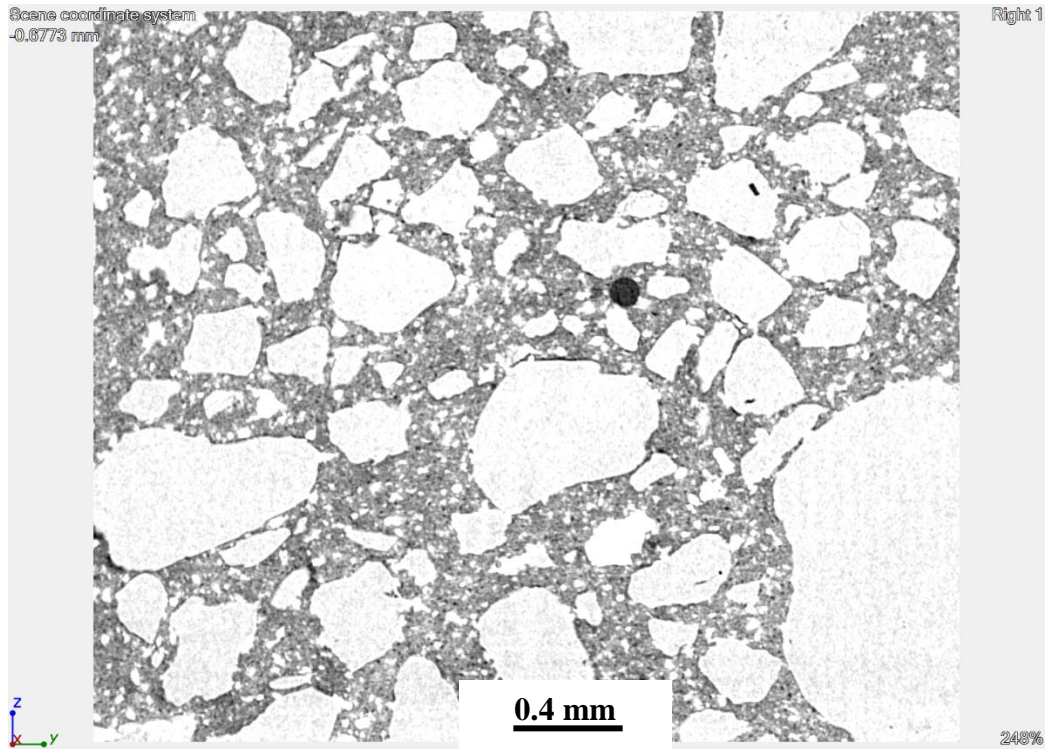
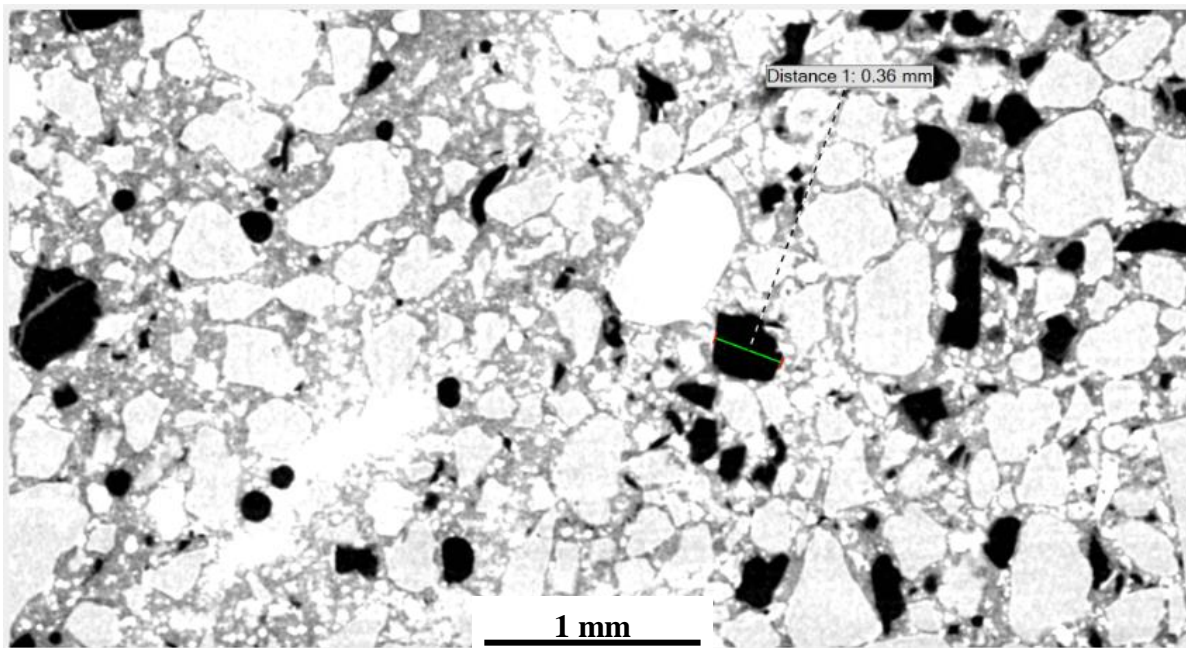


Figure 6.25 The BASF SAP particles identified in the soil-cement matrix using μCT .



(a)



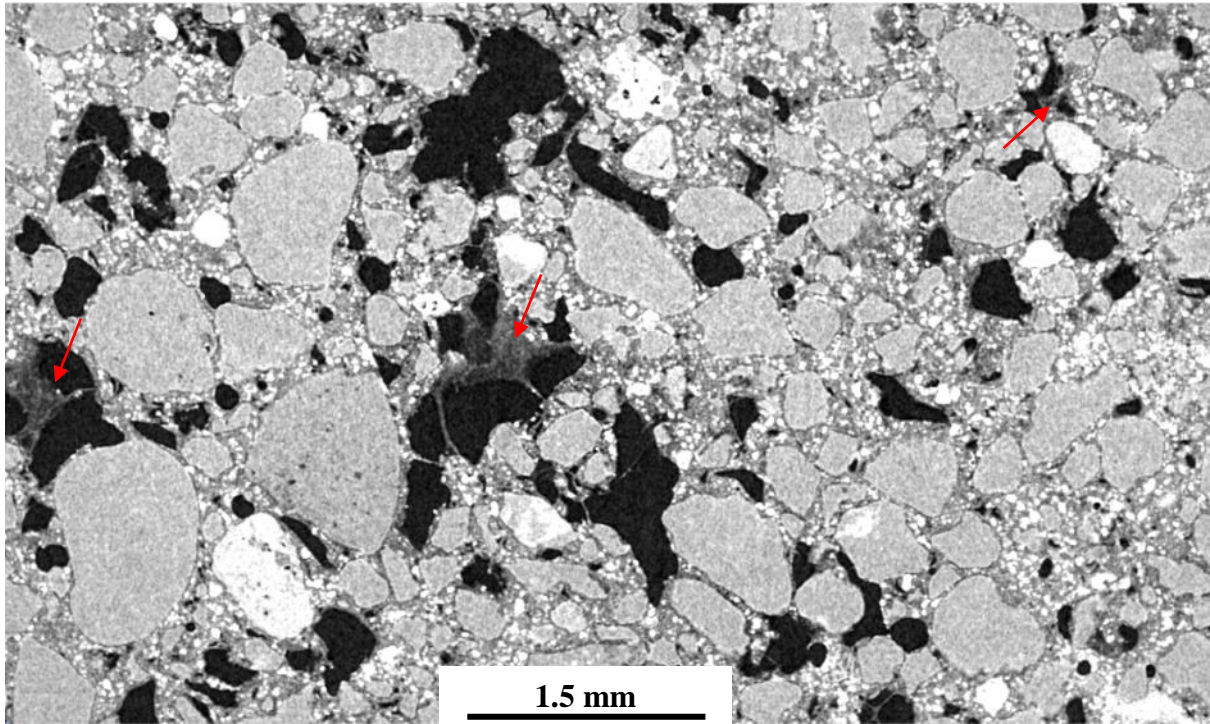
(b)

Figure 6.26 Representative μ CT cross-section images of (a) the C15 control mix specimens and (b) C15SAP2 specimens with 2% SAP content.

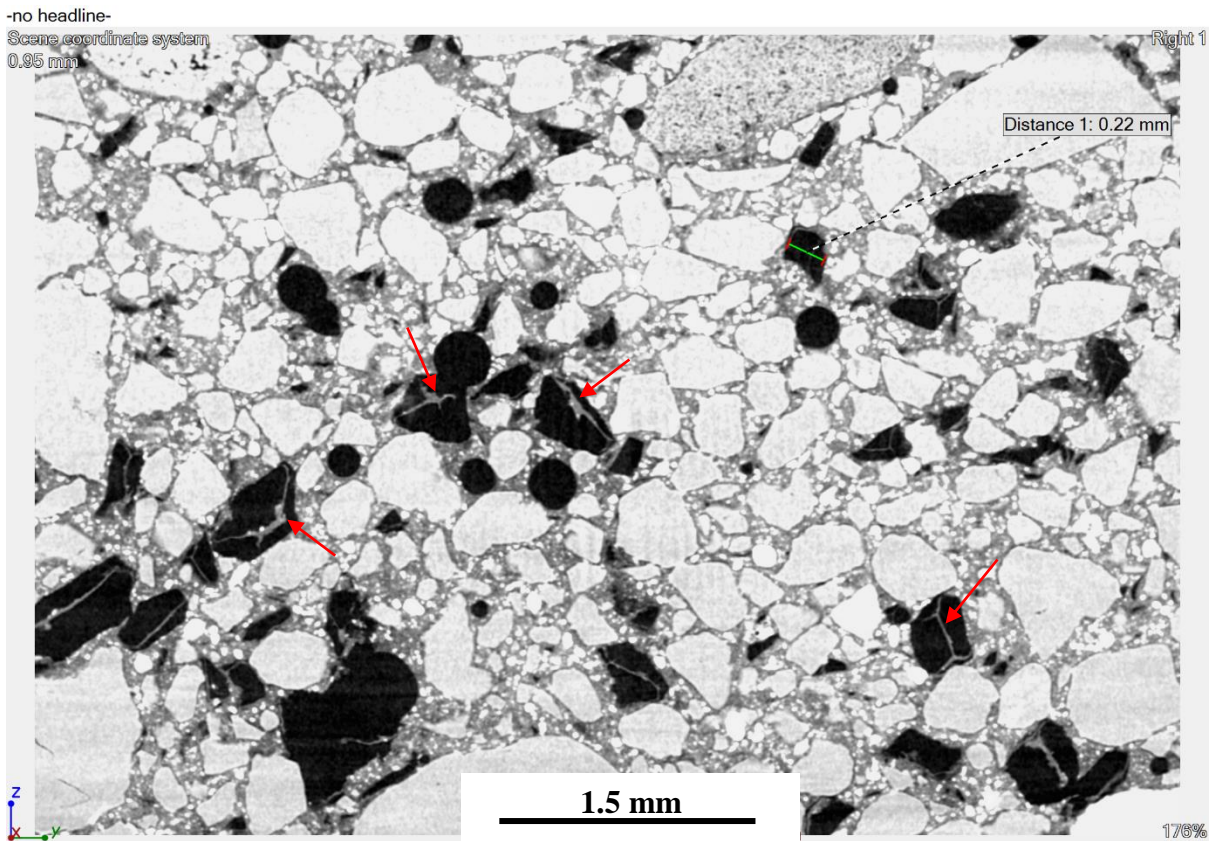
6.6.4.2 Development process of self-immune soil-cement system using SAPs

The air spaces formed by the SAP particles were very recognisable as their shape is more irregular compared to air bubbles. As discussed in **Section 6.3**, the absorption capacity of the SAP particles in the cement pore solution was ~ 20 g/g, which means that 1g of the SAP could absorb 20g of water. With this absorption capacity, the volume of a fully saturated SAP particle could expand approximately 20 times, which means that its diameter would expand ~ 2.7 times in equivalent diameter.

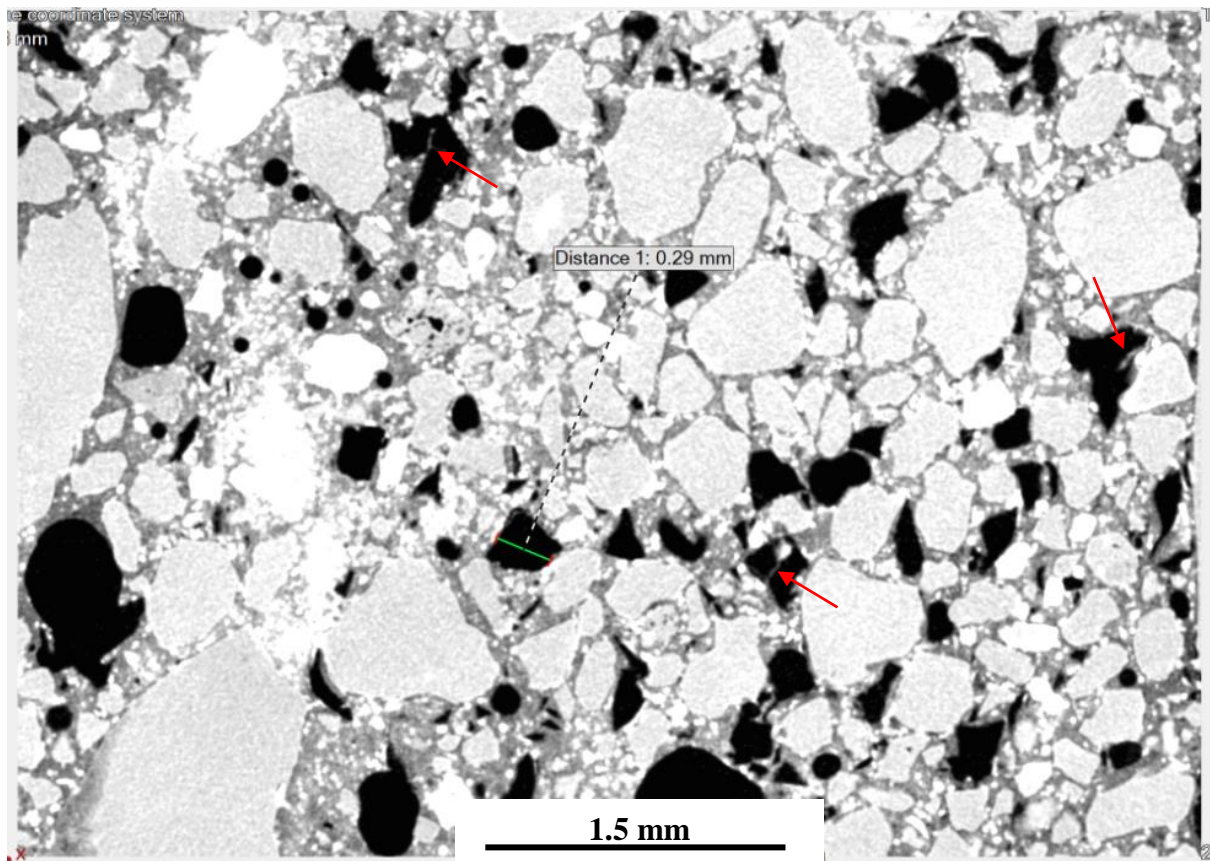
Figure 6.27a-c presents μ CT images that were taken on mix C15SAP2 specimens at different curing ages of 20, 36, and 60 hours respectively. The SAP particles are indicated by the red arrows. At the curing age of 20 hours, some of the SAP particles were still in a liquid gel form, which could be easily identified in the soil-cement matrix (**Figure 6.27a**). At this age, many air voids (dark zone) were already created and could be easily identified in the μ CT images (black area). At the age of 36 hours, the SAP particles in liquid states were hardly found but the shrunk SAP particles could be easily identified in the soil-cement matrix (**Figure 6.27b**). At the age of 60 hours, only a few SAP particles could be visualised in the air-space they created (**Figure 6.27c**), which indicates that the water within the SAP particles was almost all completely released.



(a)



(b)



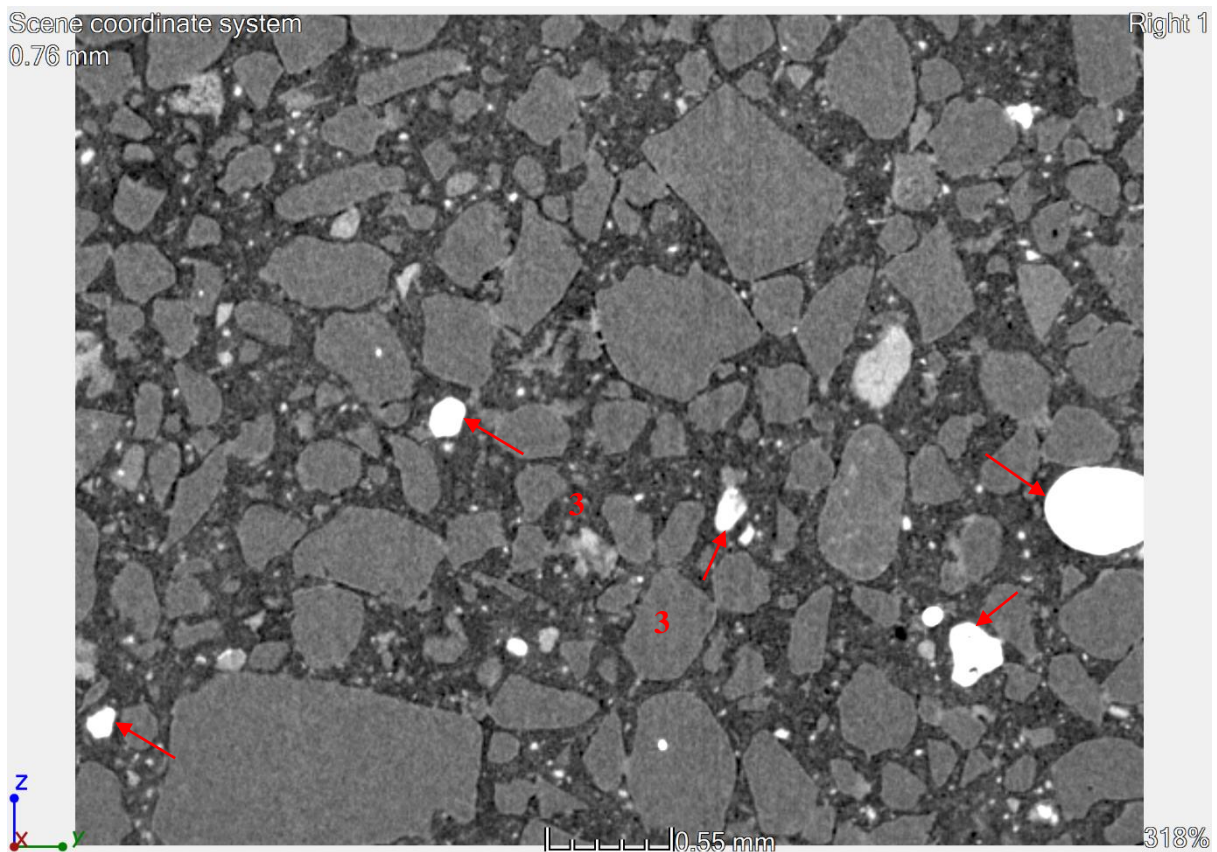
(c)

Figure 6.27 Representative μ CT cross-section images of mix C15SAP2 specimens, highlighting the SAP particles, at the curing age of (a) 20 hours, (b) 36 hours, and (c) 60 hours.

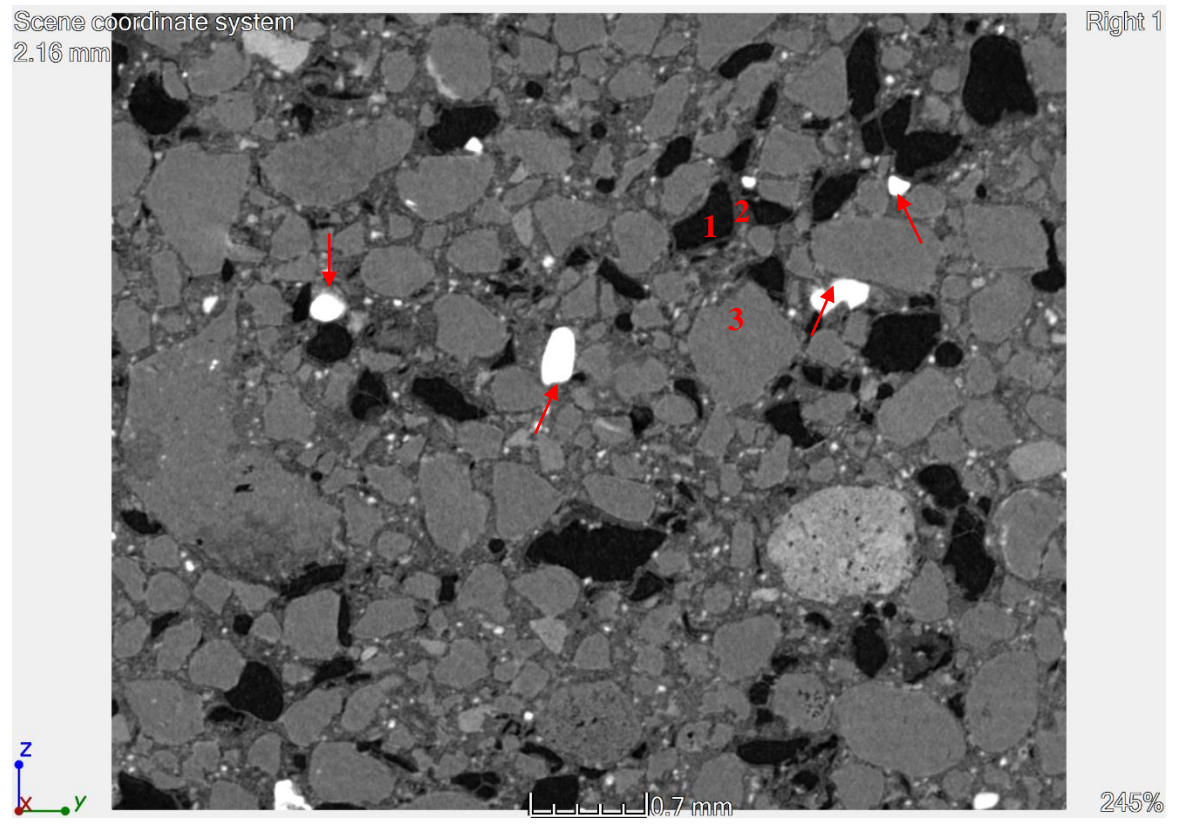
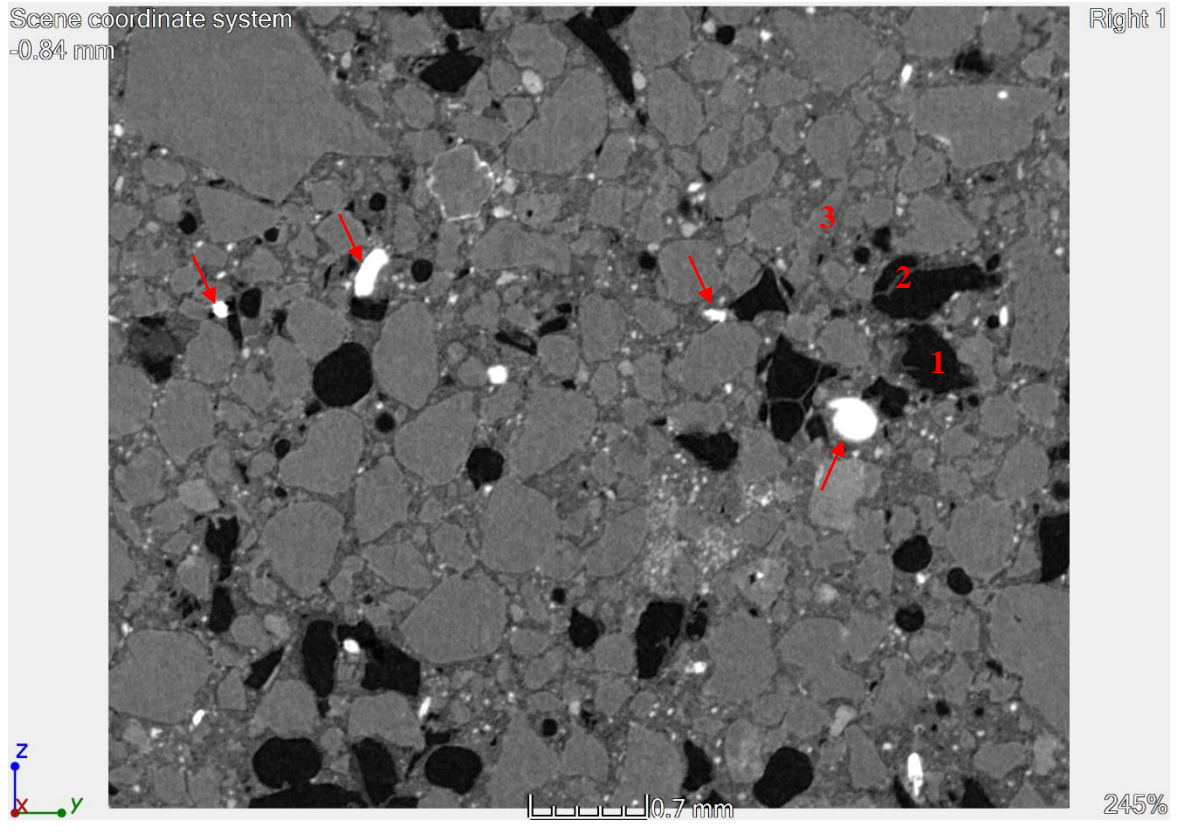
6.6.4.3 Behaviour of self-immune soil-cement systems during the freeze-thaw cyclic action

High-resolution μ CT images were also taken on mix C15SAP2 specimens during the freeze-thaw cyclic process and the behaviour of the SAP particles during the freeze-thaw cycles is revealed. Representative cross-sections of the frozen mixes C15 and C15SAP2 specimens obtained by μ CT are presented in **Figure 6.28a** and **Figure 6.28b**, respectively. Ice lens in **Figure 6.28a**, which are indicated by the red arrows, can be identified in the closely grained soil-cement matrix. Per **Figure 6.28a**, it is obvious that in the closely grained soil-cement matrix, there is no space to compensate for the volume expansion of the ice lens. However, for the frozen mix C15SAP2 samples, ice was identified in the air space (dark zone) created by the SAP particles (**Figure 6.28b**). As a result, the air space created room for ice to expand in the soil-cement system therefore preventing the generation of cracks through excess

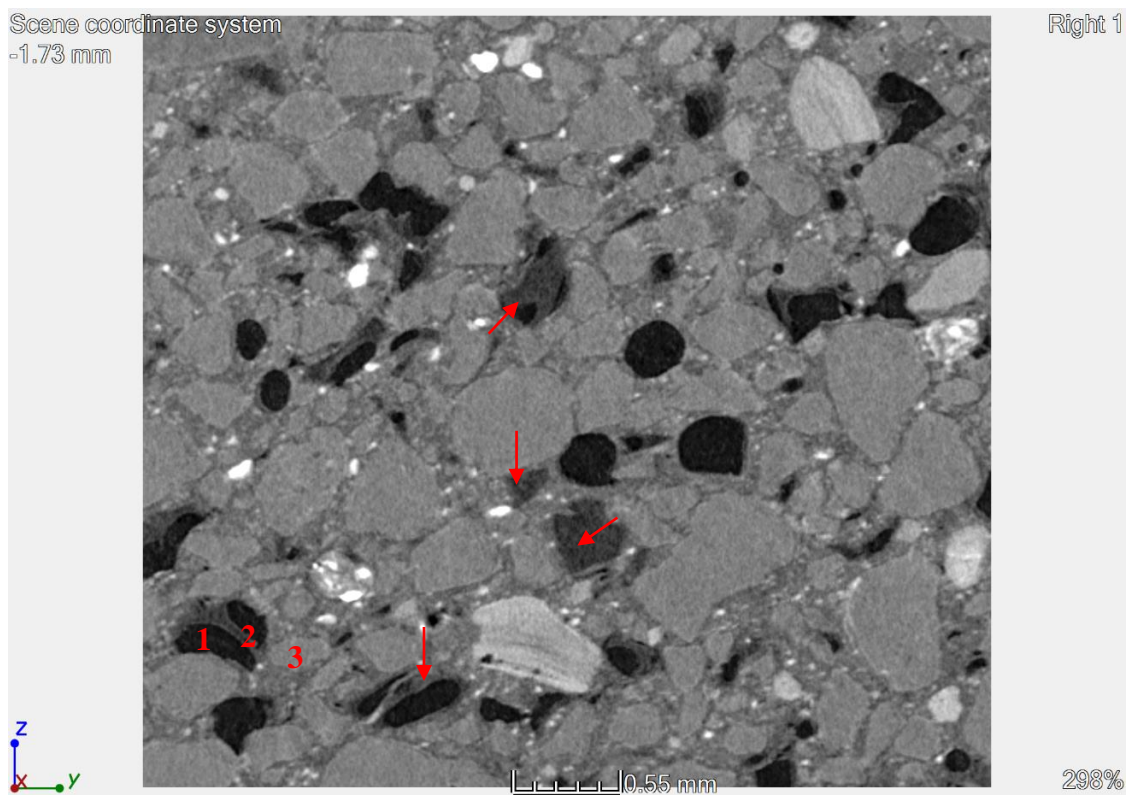
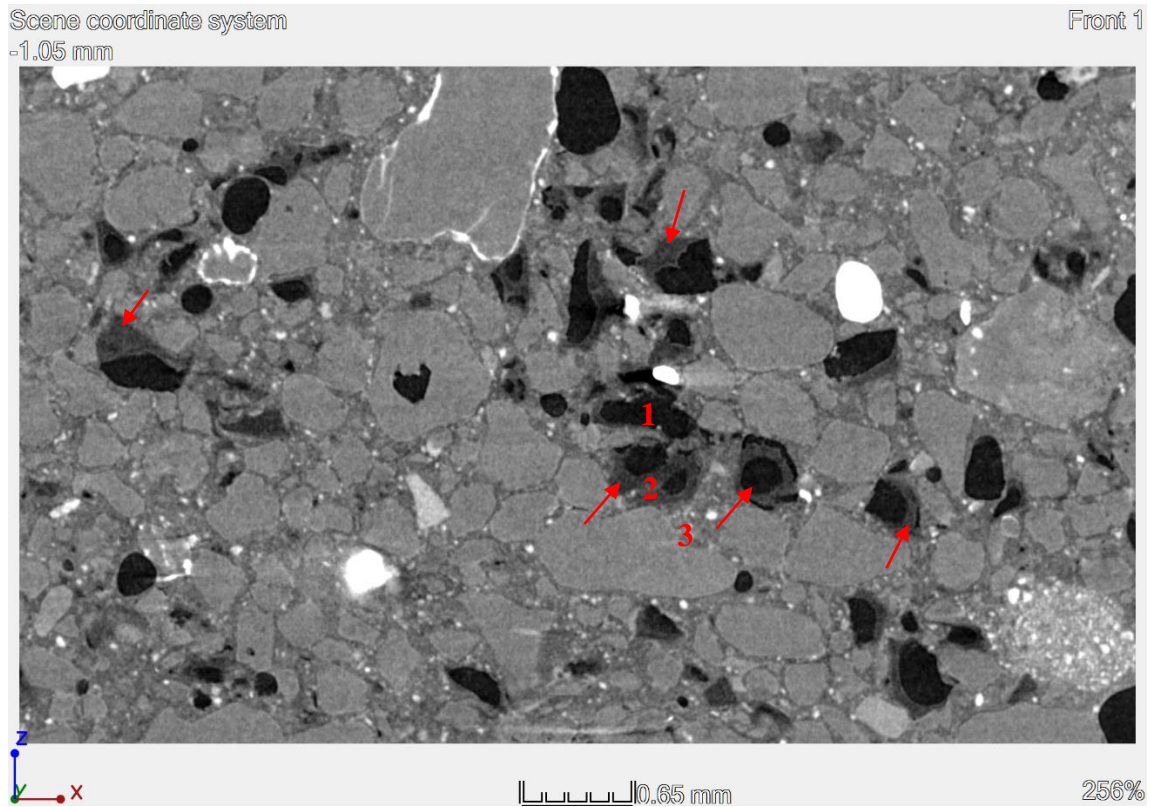
pressure. **Figure 6.28c** presents the μ CT images of partially thawed mix C15SAP2 samples. During the thawing stage, the SAP particles absorbed the water nearby and the swelled SAP particles (indicated by the red arrow) could be easily identified in the air space they created in the soil-cement matrix. During the next freezing cycle, the SAP gel particles would become frozen in the air space and they would not exert excess pressure onto the nearby soil-cement matrix as long as the air space was large enough to accommodate the increased volume. As a result, the SAP-containing soil-cement samples presented much better freeze-thaw resistance than the control mix. With sufficient air space created by the SAP particles, the soil-cement system, like mix C15SAP2, could become completely self-immune to freeze-thaw deteriorations.



(a)



(b)



(c)

Figure 6.28 Representative μ CT cross-section images of (a) frozen C15 control sample, (b) frozen C15SAP2 sample, and (c) partially thawed C15SAP2 sample. The micrographs highlight the SAP voids (1), SAP particles (2), and soil-cement matrix (3).

6.6.5 Summary of principles of the development and mechanisms of self-immune soil-cement system under freeze-thaw cycles using BASF SAP A

Based on the results of the physical properties of the soil-cement mixes after freeze-thaw cycling, microscopic analysis and μ CT, the self-immunity mechanisms of soil-cement with SAPs and its behaviour during freeze-thaw action is hypothesised and shown schematically in **Figure 6.29**.

6.6.5.1 Development of self-immune soil-cement system using SAPs

The addition of BASF SAP A in soil-cement, similar to the SikaAer[®] Solid microcapsules used in **Chapter 5**, provided room for water to expand when frozen, although through a different mechanism. As shown in **Figure 6.29a**, during the mixing, the SAP particles were fully saturated with water and occupied a space within the matrix. However, during the cement hydration process, the SAP particles also had the ability to gradually release their stored water completely during hardening and hydration processes in soil-cement. In this process, the SAP reduced its volume as water was released and small cavities were created (**Figure 6.29b**). For example, as discussed in **Section 6.3.2**, for a SAP particle with a diameter of 100 μ m, its diameter would swell to \sim 270 μ m when saturated in cement pore solution. As most of the water stored in the SAP particle is donated for cement hydration, a space with an equivalent diameter of 265 μ m can be formed. These pores serve as vessels for water to enter and expand when subjected to freeze-thaw cycles. An image of reconstructed 3D structure of a C15SAP2 mix sample using μ CT is presented in **Figure 6.30**.

6.6.5.2 Overview of the self-immune mechanism under freeze-thaw cycles

During the freezing process, the ice was formed progressively in the porous network of soil-cement matrix, started with the larger voids, which are the voids created by the SAP in the soil-cement matrix. As shown in **Figure 6.29c-d**, as the hydraulic pressure was reduced in this air space, the unfrozen water stored in the capillary pores and fissures was sucked into this air space and absorbed by the SAP particles. During freezing, the volume of the SAP particles and water expanded by 9% inside the air voids. μ CT images (**Figure 6.28**) proved that water was absorbed by the SAP particles within the air space as partially saturated SAP particles were identified in the thawing soil-cement matrix. As a result, the capillary pores and the fissures would not be enlarged by the ice formation during freezing. The air-spaces created by the SAP particles digest the volume expansion and excess pressure caused by ice

formation. In order to possess a comprehensive self-immune capability to freeze-thaw deteriorations, the volume of air space created by the SAP should be of sufficient quantity and should be well distributed in the soil-cement matrix so that the formed artificial voids become connected to most of the pores and fissures that contained water.

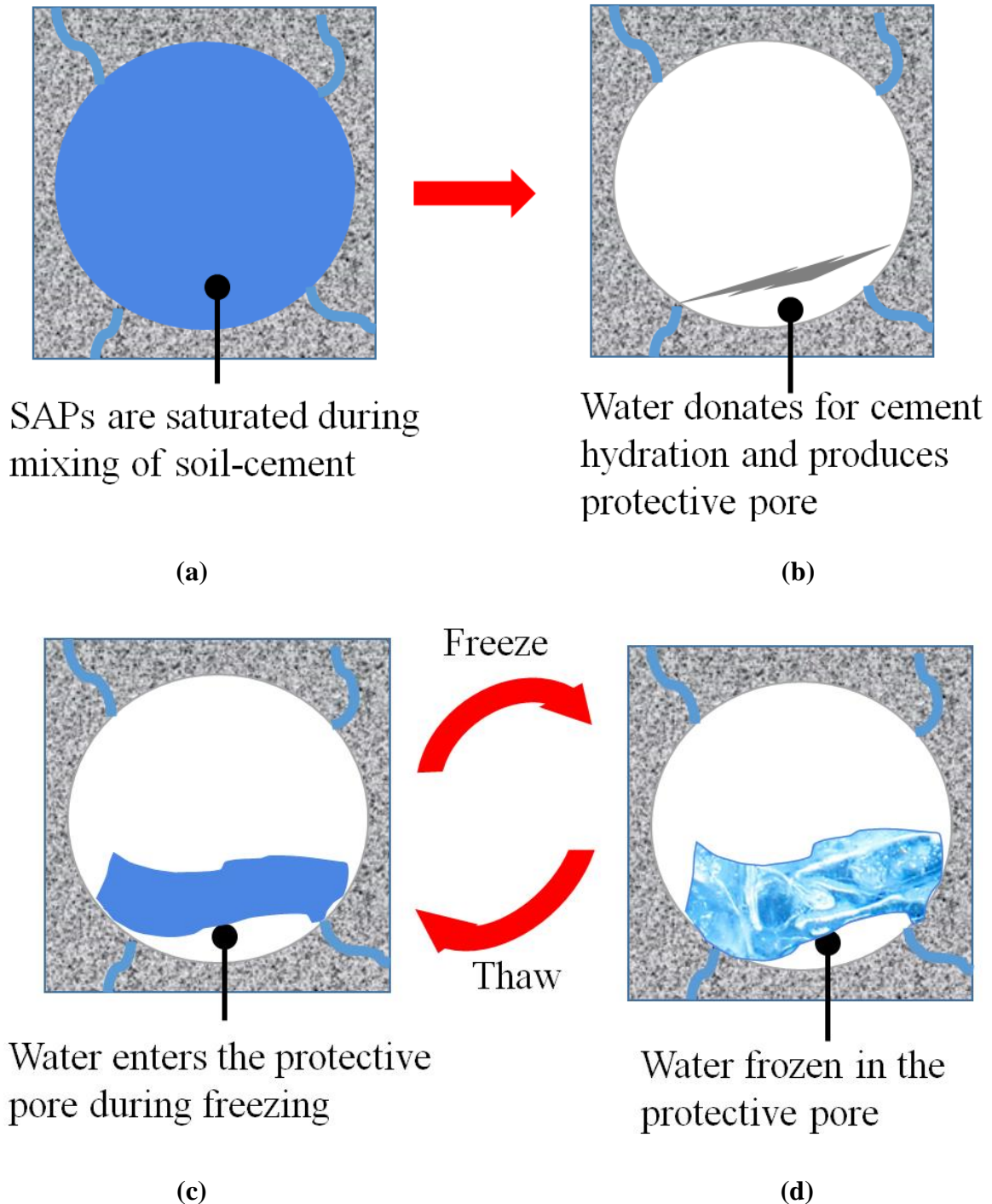


Figure 6.29 A schematic representation of the hypothesised self-immune mechanism taking place based on the use of the BASF SAP A in a soil-cement matrix (a) during mixing, (b) during cement hydration, (c) at room temperature and (d) during freezing.

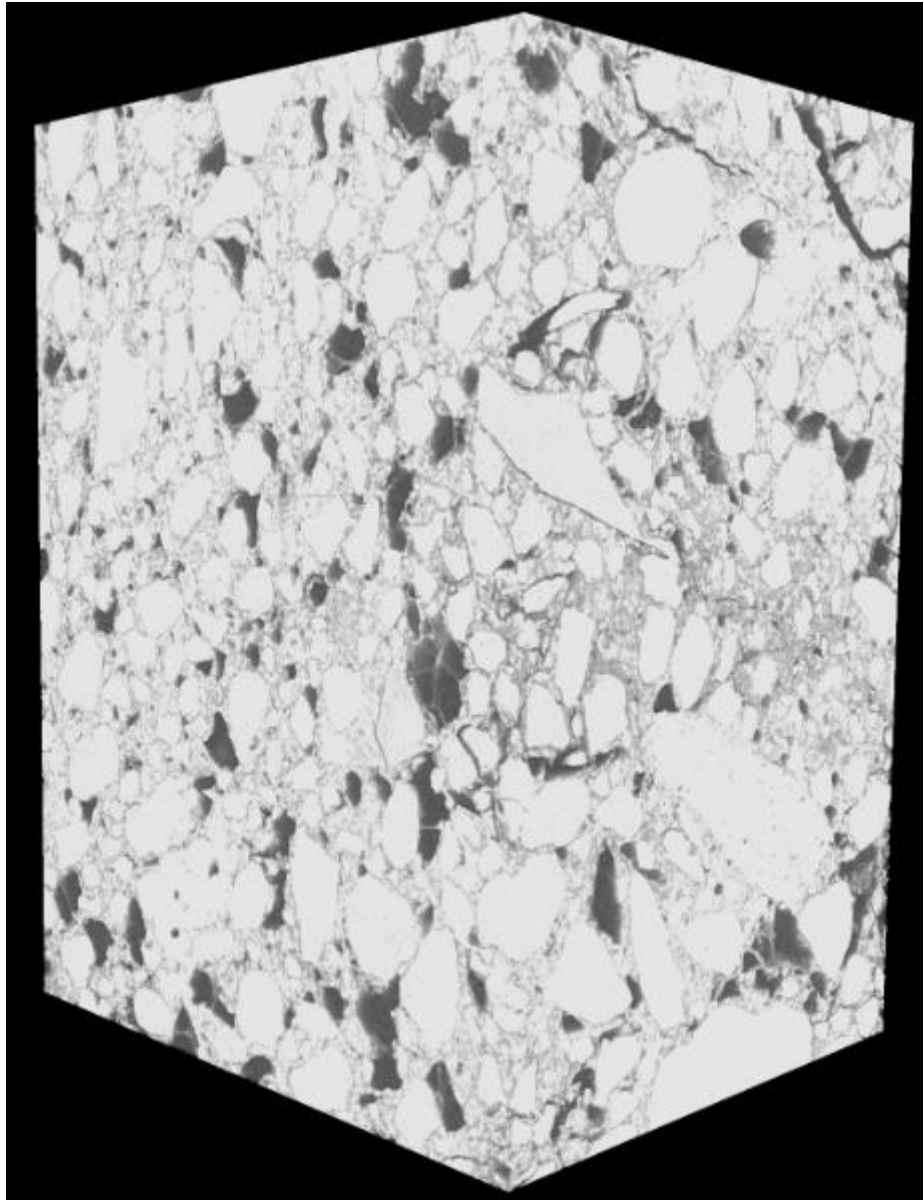


Figure 6.30 3D reconstruction of a representative 7-day C15SAP2 sample before freeze-thaw cycles using μ CT.

6.7 Comparison between the different self-immune soil-cement systems under freeze-thaw cycles

Two different self-immune soil-cement systems under freeze-thaw cycles, one using SikaAer[®] Solid microcapsules and the other using BASF SAP A were developed and their performance was investigated. In this study, the optimum dosage suggested in **Chapter 5** for developing a SikaAer[®] Solid microcapsules-embedded self-immune soil-cement system subjected to freeze-thaw cycles was 3.33% (by weight of cement) while the optimum dosage was 2% using the SAP. These two systems have showed excellent self-immunity capability to

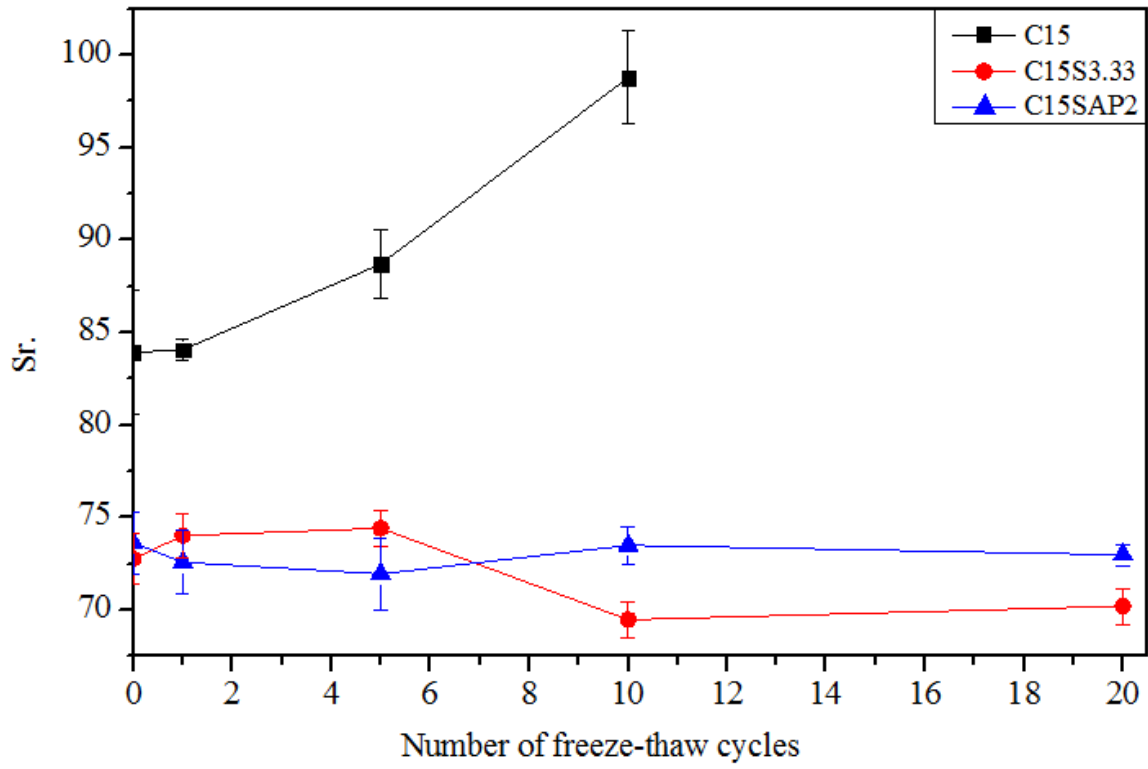
the freeze-thaw cycles imposed, with no deterioration was observed on their various physical and engineering properties even up to 20 cycles.

A comparison between the engineering properties of the soil-cement systems containing 3.33% SikaAer[®] Solid microcapsules and 2% SAPs are plotted in **Figure 6.31a-g**. A comparison summarising some key properties is presented in **Table 6.3**. It can be seen that both systems with SikaAer[®] Solid microcapsules (C15S3.33) and the SAP (C15SAP2) presented excellent freeze-thaw resistance in various aspects including degree of saturation, air content, water content, volumetric change, water content, UCS, dry density, permeability, and workability. The initial degree of saturation for mixes C15S3.33 and C15SAP2 were 72.8% and 73.6%, respectively, which are very similar and much lower than the value of 83.9% for the control mix. The initial air content of mixes C15S3.33 and C15SAP2 were 11.1% and 10.7%; both ~5% higher than that of control. However, it should be highlighted that the self-immune soil-cement systems embedded with the SAP presents better initial engineering properties than that with SikaAer[®] Solid microcapsules. For example, the 7-day UCS of mix C15SAP2 was ~27.4% higher than that of mix C15S3.33 and the dry density was ~7.4% higher. Moreover, the permeability of mix C15SAP2 was 7 times lower than that of mix C15S3.33.

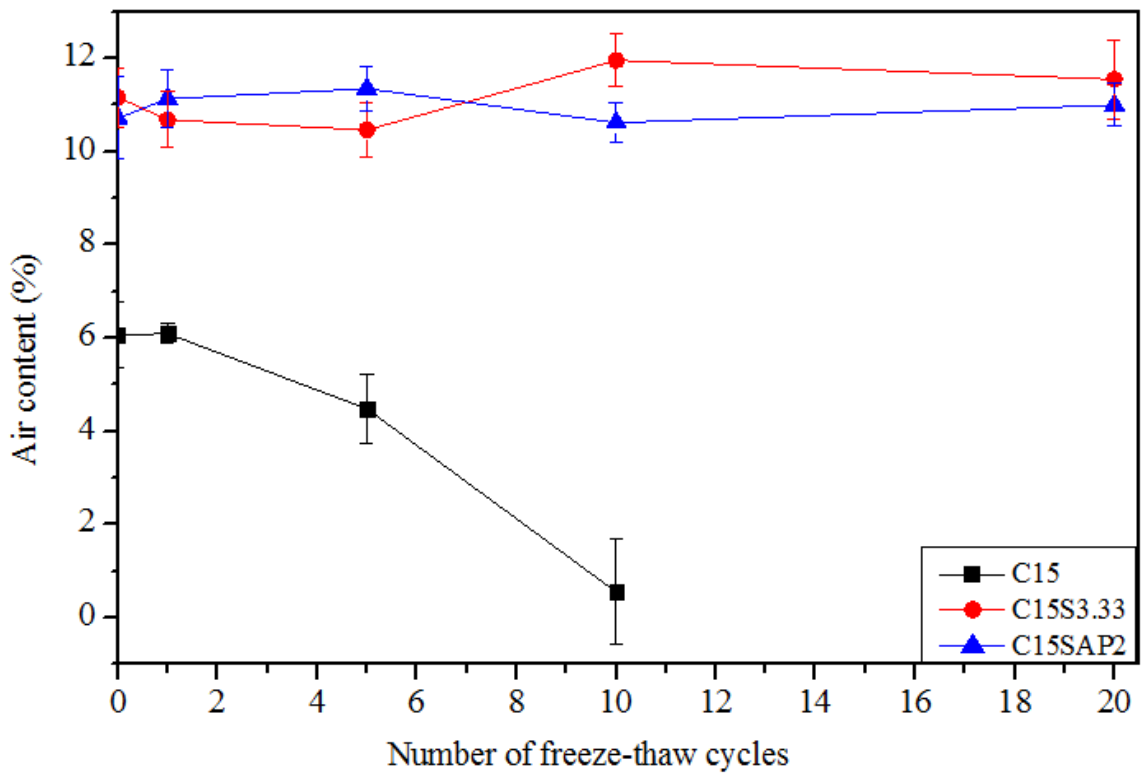
However, the added SAPs increased the setting time and reduced the peak power during cement hydration while the SikaAer[®] Solid microcapsules has little effect on the calorimetry of soil-cement. Another drawback of the self-immune soil-cement system subjected to freeze-thaw cycles developed by using the SAP is the reduction in workability. The addition of SikaAer[®] Solid microcapsules had little effect on the workability of soil-cement while the addition of the SAP reduced the workability of the soil-cement mix. As shown in the **Table 6.3**, mix C15S3.33 had a flow value of 193 mm while the flow value of mix C15SAP2 was only 126 mm. It should be noted that the workability of the SAP containing soil-cement should not be too low to ensure that it does not affect the effective dispersion of the SAP particles within the soil-cement. However, the result revealed by the μ CT images showed that the SAP particles were uniformly distributed in the C15SAP2 samples, which indicated that the reduced workability was not detrimental to the dispersion of the SAP particles in the soil-cement mix studied. In addition, as the soil-cement systems used in the infrastructure are commonly mixed *in-situ*, a lower workability is not considered a major problem.

Table 6.3 Comparison of key properties among C15, C15S3.33, and C15SAP2.

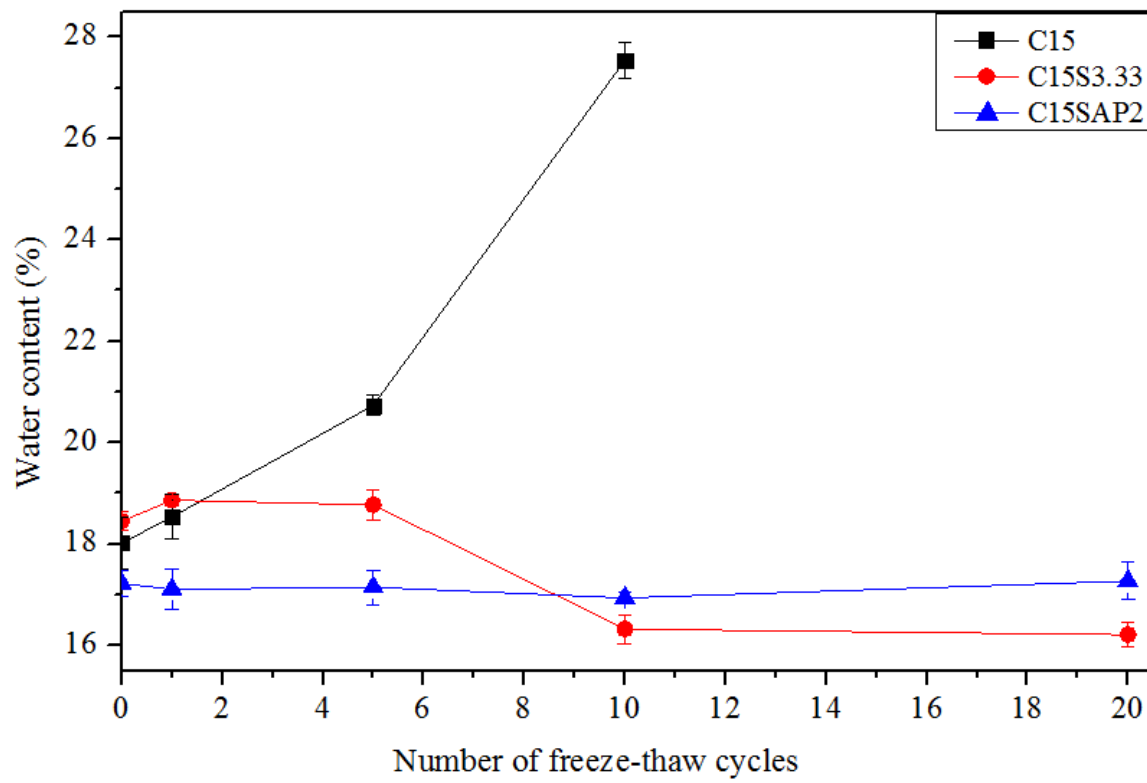
	C15	C15S3.33	C15SAP2
Properties before subjected to freeze-thaw cycles			
Initial setting time (hrs)	4.46	4.57 ↑	6.48 ↑
Flow value (mm)	190	186 ↓	126 ↓
Water content (%)	17.9	18.4 ↑	17.2 ↓
7-day dry density (kg/m ³)	1760	1617 ↓	1737 ↓
Porosity	0.374	0.410 ↑	0.401 ↑
Sr. (%)	83.9	73.6 ↓	73.6 ↓
Air content (%)	6.1	11.1 ↑	10.7 ↑
7-day UCS (MPa)	3.6	2.61 ↓	3.34 ↓
7-day tensile strength (kPa)	654.5	589.5 ↓	809.7 ↑
Permeability <i>k</i> (m/s)	1.57×10 ⁻¹⁰	3.14×10 ⁻¹⁰ ↑	4.26×10 ⁻¹¹ ↓
Properties after subjected to 10 freeze-thaw cycles			
Water content (%)	27.5	16.3 ↓	16.9 ↓
Dry density (kg/m ³)	1575	1667 ↑	1739 ↑
Volumetric change (%)	10.5	-0.8 ↓	-0.3 ↓
Porosity	0.439	0.392 ↓	0.400 ↓
Sr. (%)	98.8	69.5 ↓	73.5 ↓
Air content (%)	0.6	11.9 ↑	10.6 ↑
UCS (MPa)	0.58	3.56 ↑	4.26 ↑
Permeability <i>k</i> (m/s)	4.25×10 ⁻⁸	4.60×10 ⁻¹⁰ ↓	6.45×10 ⁻¹¹ ↓
Note: all the values are the mean test value of triplicate samples; ↑ indicates higher while ↓ indicates lower values than that of control mix.			



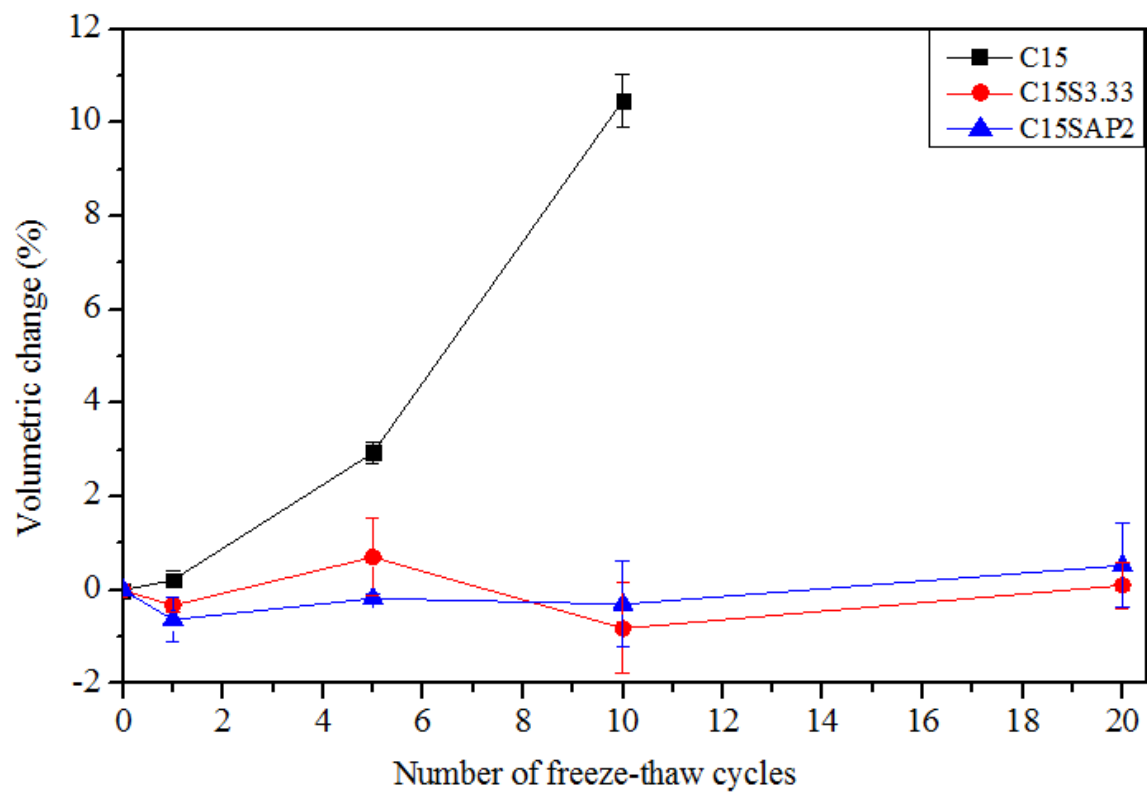
(a)



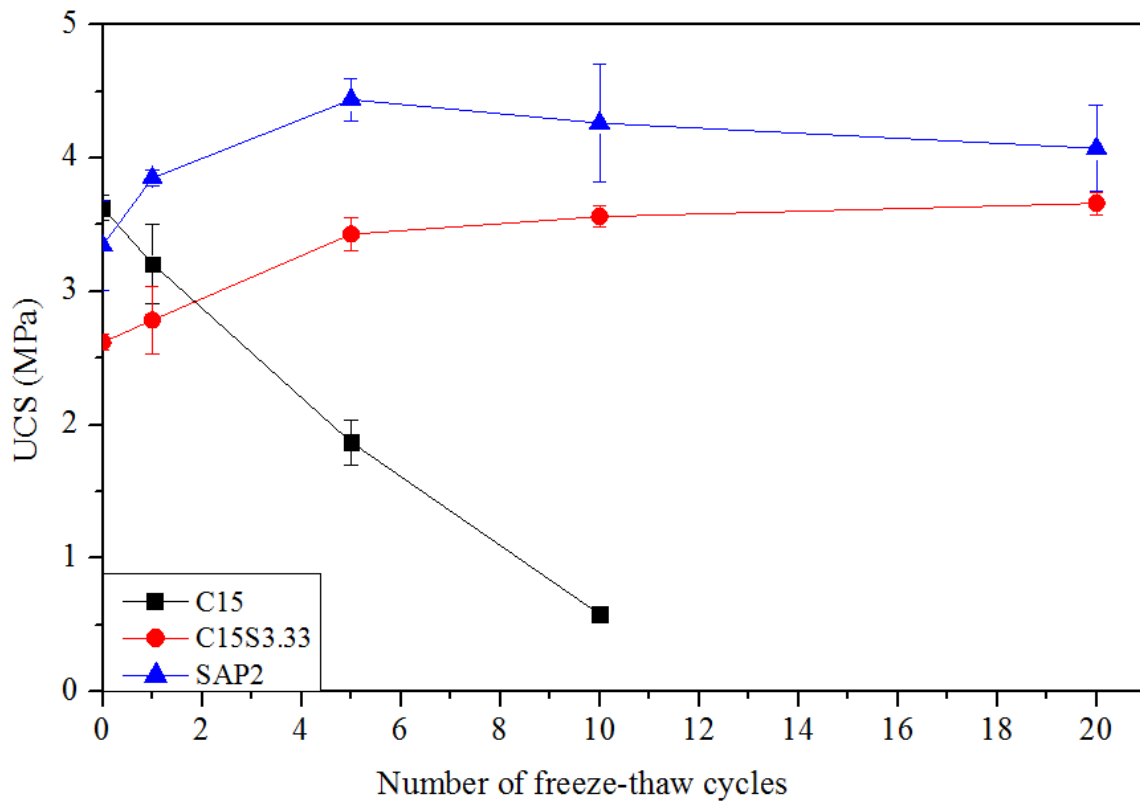
(b)



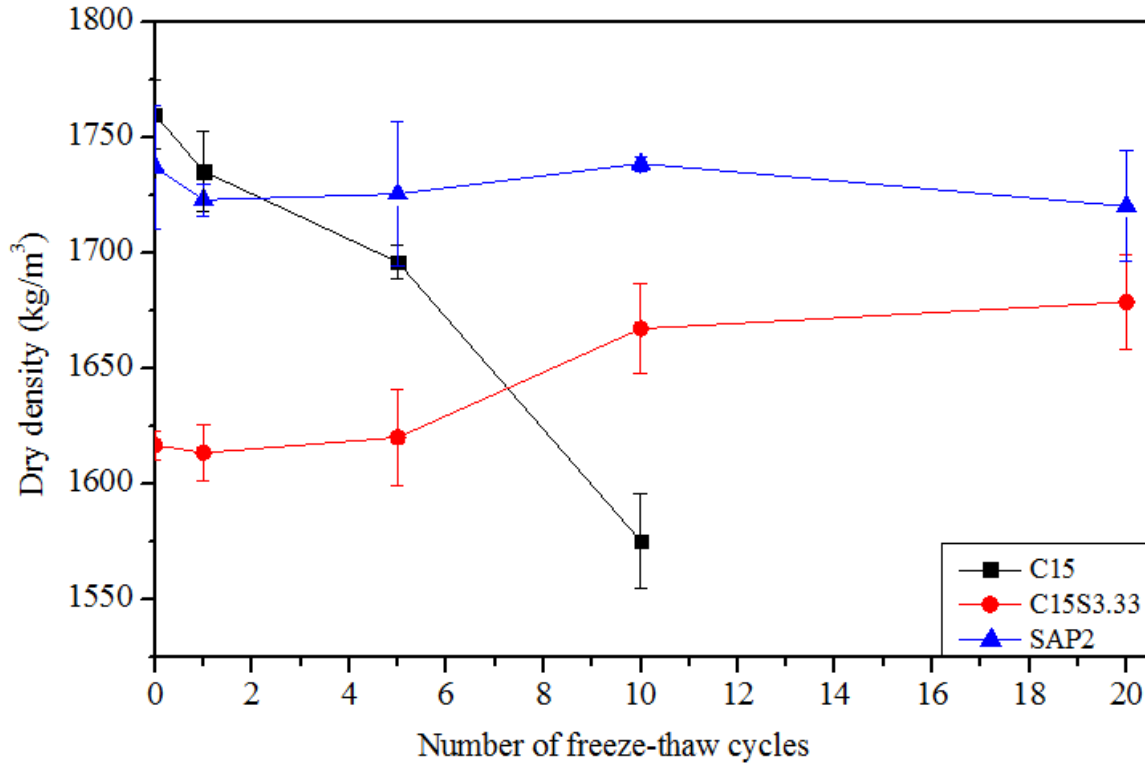
(c)



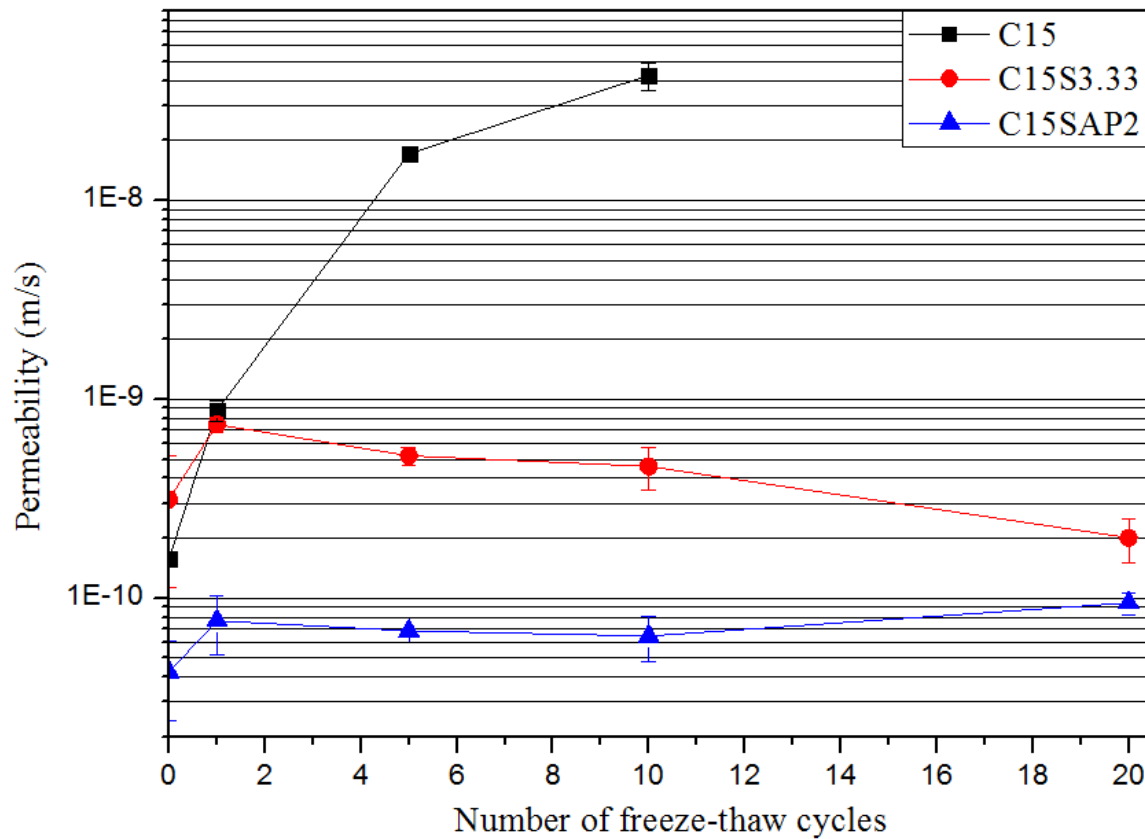
(d)



(e)



(f)



(g)

Figure 6.31 Comparison between self-immune systems embedded with SikaAer® Solid and BASF SAP A in terms of (a) degree of saturation, (b) air content, (c) water content, (d) volumetric change, (e) UCS, (f) dry density, and (g) permeability.

6.8 Concluding remarks

This chapter presented details of the development and performance of self-immune soil-cement systems subjected to freeze-thaw cycles by using BASF SAP A as an alternative to SikaAer® Solid microcapsules. The sorptivity of the SAP revealed that its absorption capacity in the cement pore solution was 20g/g and this absorption process was found to be reversible. Soil-cement systems embedded with different dosages of the SAP were examined. In **Chapter 5**, the initial dry density, strength properties of soil-cement generally decreased with the addition of SikaAer® Solid microcapsules. However, in this chapter, it was found that the addition of the SAP, with a dosage of up to 2%, had little or slight effect on the initial dry density, strength properties and permeability of the soil-cement mixes investigated. Furthermore, the addition of the SAP significantly increased the freeze-thaw resistance of the soil-cement systems in terms of UCS, volumetric change, porosity, permeability, and surface

cracking ratio. It can be concluded that the addition of the SAP is an effective technique to improve the freeze-thaw resistance of soil-cement mixes. In general, the freeze-thaw resistance of soil-cement increased with the addition of the SAP up to 2%. It was found that the addition of 2% SAP enabled the soil-cement systems to be completely self-immune to freeze-thaw damage for up to 20 cycles. However, the dry density and strength of the soil-cement began to decrease with >1% dosage of the SAP, implying that a higher addition of the SAP would impair the engineering properties of the soil-cement as well as increase the construction cost. As a result, it is recommended that the optimum dosage of the SAP for the soil-cement system used in this study should be 2% by weight of the cement mass.

The mechanism of self-immune soil-cement using the BASF SAP A was revealed. The SAP particles were fully saturated during the mixing stage but the water was donated for cement hydration afterwards therefore small cavities were created in the soil-cement matrix. These cavities then served as vessels for water to enter and expand during freeze-thaw cycles therefore damage due to ice expansion was prevented. Compared with SikaAer[®] Solid microcapsules embedded self-immune soil-cement system, the self-immune soil-cement using the BASF SAP A exhibited equivalent excellent freeze-thaw resistance. However, its initial engineering properties including UCS, dry density, and permeability are better than that of the SikaAer[®] Solid microcapsules-embedded mixes. The only limitation for using the SAP is that it absorbs water during the mixing therefore reduces the workability of soil-cement mix.

Chapter 7 Conclusions and Recommendations

7.1 Conclusions

Chapter 1 presents background information regarding the durability challenges that face soil-cement systems subjected to freeze-thaw cycles. Soil-cement systems are widely used in engineering practice to improve the engineering properties of soft or contaminated soils that would otherwise be unsatisfactory for construction. However, they are vulnerable to freeze-thaw cycles. Deterioration due to freeze-thaw cycles can cause civil infrastructure being out of service unpredictably and make future maintenance indispensable and costly. Currently, this issue is addressed through uneconomical and time-consuming overdesign, the implementation of maintenance programs, or both. Considering the large amounts of CO₂ emissions produced from cement production, developing soil-cement systems that can withstand freeze-thaw cycles more effectively represents a chance not only to make construction projects stronger and more efficient, but also to contribute to the well-being of the planet. Recent research has attempted to develop sustainable and resilient systems comprising materials and structures that, like biological systems, can continually adapt to their environment. This research provided insight into how this study might address the aforementioned problems. Therefore, this research focuses on the development and performance of “self-healing” and “self-immune” soil-cement systems that can respond and adapt to freeze-thaw cycles.

The critical review of the literature in **Chapter 2** reveals that the freeze-thaw durability of soil-cement systems can be affected by various factors, including cement content, water content, the intensity of freeze-thaw cycles, and curing conditions. Freeze-thaw cycles cause degradation of many engineering properties important to soil-cement systems, including strength, structure, and permeability. However, although various methods have been used to improve the freeze-thaw resistance of soil-cement systems, no wholly satisfactory technique has yet been proposed. The successful application of air-entraining techniques in concrete provides insight for improving the freeze-thaw resistance of soil-cement systems. Although the precise mechanisms of air entrainment and the freeze-thaw process itself are still under investigation, the entrained air pores are believed to act as reservoirs and cryo-pumps to accommodate the ice crystals and the excess pressure generated during freezing. The effectiveness of air entraining is thought to depend on the volume and distribution of air

pores, which can be attributed to the air content, space factor, and critical degree of saturation of the matrix.

However, to date, there has been no literature covering the use of air entrainment in soil-cement systems. Nonetheless, the proposed mechanisms for air entraining and the freeze-thaw process provide insights for the development of self-immune soil-cement systems that contain protective pores. Various healing agents and techniques for cementitious materials, such as capsule-based self-healing, mineral admixtures and additives, and pellet-based self-healing, were reviewed. A considerable degree of mechanical property recovery and crack closure was reported by many researchers. Capsule-based and pellet-based self-healing techniques appeared to be the most promising for soil-cement systems under freeze-thaw conditions, as their triggering mechanisms can be easily controlled. Furthermore, the properties of SAPs, their applications in terms of self-healing, and their applications in terms of improving the freeze-thaw resistance of cementitious materials revealed that they demonstrate significant potential for soil-cement systems subjected to freeze-thaw cycles.

The materials and techniques used in this study are illustrated in **Chapter 3**. Lambson microcapsules and LUVOMAG MgO pellets were used to develop self-healing soil-cement systems, while SikaAer[®] Solid (SS) microcapsules and BASF SAP A were used to develop self-immune soil-cement systems. The self-healing and self-immune performance and mechanisms of soil-cement systems under freeze-thaw conditions were verified via various experimental methods. Qualities and techniques of interest included UCS, porosity, gas and water permeability, optical microscopy and image analysis, SEM and EDX, TGA, and μ CT tests. The experimental techniques used in this study are proven effective to reveal the properties, behaviours, and mechanisms of self-healing and healing-immune soil-cement systems subjected to freeze-thaw cycles.

Chapter 4 presents the development and performance of self-healing soil-cement systems subjected freeze-thaw cycles using Lambson microcapsules and LUVOMAG MgO pellets. It was found that a C20L5 mix containing 5% Lambson microcapsules improved the self-healing capability of soil-cement considerably. An increase of 21–40% in UCS was observed after 12 freeze-thaw cycles and 7 days of healing. Moreover, the addition of 5% Lambson microcapsules had little effect on the 7-day UCS and E_{50} of the C20L5 mix. However, the results also revealed that for soil-cement systems with lower cement content, the addition of Lambson microcapsules tended to slightly decrease the UCS of soil-cement rather than

increasing the self-healing capability of soil-cement after multiple freeze-thaw cycles. As a result, the use of Lambson microcapsules as a healing agent should be limited to soil-cement systems with relatively high cement content (e.g., 20%).

Another self-healing soil-cement system employs MgO pellets. The addition of MgO pellets not only increased the system's initial strength, and its freeze-thaw resistance, but also significantly improved the self-healing capability of the system following freeze-thaw cycles. 96% crack sealing efficiency was recorded for freeze-thaw damaged C15P10 (i.e., samples with 10% of the sand in the cement mixture replaced with MgO pellets) samples after 60 days of healing. By contrast, 12% crack sealing efficiency was observed in the control mix. Even with a shorter healing time of 14 days, the crack healing efficiency of the C15P10 samples was 81.5%. In addition, strength and stiffness recovery was found to be 30–40% after 28 days of healing. From microstructure investigations involving TGA and SEM/EDX, it was found that brucite and various hydrated magnesium carbonates, such as hydromagnesite and dypingite, were produced in the MgO pellet-embedded samples after freeze-thaw cycles.

The Lambson microcapsules appeared to be only effective for soil-cement systems with relatively high cement content, while the MgO pellets also worked for systems with lower cement content. This may be due to the larger amount of healing agents contained in solid MgO pellets. The healing in the Lambson microcapsule-embedded samples was primarily due to further hydration reactions producing C-S-H, while the healing in the MgO pellet-embedded samples was due to MgO reactions yielding magnesium-related materials. The MgO pellets were not uniformly superior, however. A longer time was required for the MgO pellets to react and yield their healing products, while the Lambson microcapsule acted more quickly. Moreover, the Lambson microcapsule-containing samples had better performance in terms of mechanical property recover, due to the production of C-S-H, while the MgO pellet-containing samples had better performance in terms of crack sealing due to the swelling of MgO when reacted with water. However, in this study, the soil-cement systems were generally severely damaged by the freeze-thaw cycles before healing could begin. Thus, the engineering properties of the systems may not have been fully recoverable. In real applications, healing may occur after each freeze-thaw cycle, which means self-healing soil-cement systems may display better performance.

In **Chapter 5**, a novel self-immune soil-cement system embedded with SS microcapsules is developed. The addition of SS microcapsules slightly reduced the initial UCS, dry density,

and hydraulic conductivity of the soil-cement systems, which is unfavourable. However, the freeze-thaw durability of the soil-cement system in terms of UCS, volumetric change, porosity, hydraulic conductivity, and surface cracking ratio were significantly increased. The distribution and volume of SS microcapsule are two major factors influencing the self-immunity of the system against freeze-thaw action. The distribution of the SS microcapsule is represented by the critical distance between adjacent microcapsules, while the quantity of the microcapsules is expressed in terms of the soil-cement's air content and its critical degree of saturation. It was found that the addition of 3.33% SS microcapsules was the lowest dose that made the soil-cement system in this study completely self-immune to freeze-thaw damage after 20 cycles. Porosity measurements showed that the air content of soil-cement specimens increased from approximately 6% to 11% following the addition of 3.33% SS microcapsules. X-ray μ CT scan results showed that small cavities with diameters of 5–80 μ m were evenly distributed within the soil-cement system. These uniformly distributed, small, compressible microcapsules conferred self-immunity by serving as buffers for the excess pressure generated as water freezes. Even after 20 freeze-thaw cycles, little deterioration in UCS and hydraulic conductivity were observed, and almost no crack formation was identified by optical microscopy. By contrast, control samples showed an 84% reduction in UCS and a 2.5 order of magnitude increase in hydraulic conductivity after 10 freeze-thaw cycles.

The development and performance of self-immune soil-cement systems using BASF SAP A as an alternative to SS microcapsules is presented in **Chapter 6**. SAPs can absorb water about 20 times of their own weight during the mixing of soil-cement, and this absorption process was found to be reversible. As a result, these SAPs can gradually release the absorbed water during the self-desiccation processes that occurs in soil-cement during hardening and hydration. Therefore, the SAPs reduce in volume as they release water, creating small pores. This mechanism was verified by X-ray μ CT scan results showing that small cavities with diameters of roughly 250 μ m were evenly distributed within the soil-cement matrix. These pores serve as reservoirs by allowing water to enter and ice crystals to form, much like the air voids caused by air entraining. Compared to the SS microcapsules, which generally reduced the initial dry density and strength properties of the soil-cement system, the addition of the SAP had little effect on the initial dry density, strength properties and permeability of the soil-cement mixes investigated for dosages of up to 2%. Moreover, compared to SS microcapsule-embedded soil-cement systems, soil-cement systems using BASF SAP A exhibited equivalent excellent freeze-thaw resistance. The addition of 2% SAP

was the optimum dosage recommended in terms of conferring self-immunity, as this produced soil-cement systems self-immune to freeze-thaw damage after 20 cycles. Similar to the soil-cement systems containing 3.33% SS microcapsules described in **Chapter 5**, porosity measurements showed that the air content of the 2% SAP-embedded soil-cement system also increased from 6% to 11%. As a result, it can be suggested that 5% additional protective air pores are needed to build a soil-cement system self-immune to freeze-thaw action.

This thesis presents a novel philosophy for improving the freeze-thaw durability of soil-cement systems that incorporates the concepts of “smart” materials, including the concepts of self-healing and self-immunity. The basic design of the self-healing soil-cement systems developed in this thesis has been described above. Lambson microcapsules and MgO pellets were embedded in soil-cement systems as self-healing agents. Both systems showed promising results, leading to good recovery of engineering properties like strength and permeability. However, if severe damage was induced by freeze-thaw actions before healing, the system could not always fully recover its engineering properties.

Furthermore, SS microcapsules and BASF SAP A were suggested as means to achieve soil-cement systems self-immune to freeze-thaw cycles. The soil-cement specimens containing SS microcapsules and BASF SAP A showed remarkable performance under freeze-thaw conditions compared to control specimens. The treated samples fared better in terms of UCS, volumetric change, porosity, hydraulic conductivity, and surface crack analysis. There was, however, a small initial decrease in the mechanical properties of the soil-cement specimens when SS microcapsules were used. BASF SAP A had a smaller effect on the mechanical properties of the soil-cement specimens than the SS microcapsules. However, using BASF SAP A reduced the workability of the soil-cement mixes, as it absorbed water during mixing, while the SS microcapsules had little effect on the workability.

7.2 Recommendations for practice and future research

This thesis has investigated various possibilities for improving the freeze-thaw durability of soil-cement systems. It found that this can be achieved by either developing self-healing soil-cement systems using Lambson microcapsules and MgO pellets or by developing self-immune soil-cement systems using SS microcapsules and BASF SAP A. For soil-cement systems with 20% cement content or greater, the addition of Lambson microcapsules can significantly improve self-healing after freeze-thaw cycles. However, for soil-cement systems

with cement content less than 20%, the use of Lambson microcapsule is not recommended. For soil-cement systems with lower cement content (e.g., 15%), it is better to use MgO pellets to develop a self-healing soil-cement system.

For self-immune soil-cement systems, SS microcapsules or BASF SAP A is recommended. Soil-cement systems using either additive can self-immune to up to 20 freeze-thaw cycles. It should be noted that the freeze-thaw process conducted in this study was extremely severe, so the self-immune soil-cement systems described in this study would likely be able to survive more freeze-thaw cycles under milder freeze-thaw conditions.

Further research is also recommended. For the self-healing soil-cement systems in this study, healing was permitted only after they were subjected to a certain number of freeze-thaw cycles (e.g., 12). As a result, the damage induced by a large number of freeze-thaw cycles may have been too significant to heal completely. In a future study, it would be worthwhile to investigate the performance of soil-cement systems allowed to heal themselves after each cycle. It is anticipated that, for self-healing soil-cement systems using MgO pellets, healing could initiate after every freeze-thaw cycle. In such circumstances, the freeze-thaw durability and sustainability of MgO pellet-embedded self-healing soil-cement systems could improve. Furthermore, it would also be productive to evaluate the self-healing performance of soil-cement systems incorporating both Lambson microcapsules and MgO pellets. Finally, further investigations could be carried out for soil-cement systems incorporating other kinds of healing agents.

It also should be noted that only one kind of soil-cement system was modelled in this study. Investigations could be conducted on the applicability of these self-healing and self-immune agents on other kinds of soil-cement systems. It would be useful, for instance, to study SS microcapsules and BASF SAP A in soil-cement systems using different cement contents and different types of soils. Furthermore, the properties of SS microcapsules and BASF SAP A suggest that they have potential to provide self-immune capabilities for soil-cement systems that are heavily compacted. As discussed in **Chapter 6**, the only limitation documented for the SAP was that it reduced the workability of the soil-cement. Therefore, superplasticisers could potentially be added along with the SAP to improve the workability of the ensuing soil-cement mix. In addition, incorporating both SS microcapsules and BASF SAP A together in soil-cement systems could yield unexpected results. It is possible that the reduction in mechanical properties like dry density due to the addition of SS microcapsules and the

reduction of workability due to the addition of SAP could be minimised in some optimum combination.

Finally, this research was carried out at a laboratory scale. Thus, future studies should investigate the application and performance of these self-healing and self-immune soil-cement systems in field tests. Given that the Lambson microcapsules, the MgO pellets, the SS microcapsules, and the SAPs used in this study's soil-cement systems are all produced commercially, it should be easy to test these systems at a larger scale. Similarly, a life cycle analysis could be carried out to evaluate the benefits these self-healing and self-immune soil-cement systems convey in real engineering applications.

References

- Ahmed, A., Ugai, K., Kamei, T., 2011. Laboratory and field evaluations of recycled gypsum as a stabilizer agent in embankment construction. *Soils Found.* 51, 975–990.
<https://doi.org/10.3208/sandf.51.975>
- Ahn, T.-H., Kishi, T., 2010. Crack Self-healing Behavior of Cementitious Composites Incorporating Various Mineral Admixtures. *J. Adv. Concr. Technol.* 8, 171–186.
<https://doi.org/10.3151/jact.8.171>
- Al-Tabbaa, A., 2013. Reactive magnesia cement, in: *Eco-Efficient Concrete*. Elsevier, pp. 523–543. <https://doi.org/10.1533/9780857098993.4.523>
- Al-Tabbaa, A., Evans, C.W., 1998. Pilot in situ auger mixing treatment of a contaminated site. Part 1: treatability study. *Proc. ICE - Geotech. Eng.* 52–59.
<https://doi.org/10.1680/geng.2002.155.3.187>
- Al-Tabbaa, A., Harbottle, M.J., 2015. Self-healing materials and structures for geotechnical and geo-environmental applications. *Proc. XVI ECSMGE Geotech. Eng. Infrastruct. Dev.* 589–594. <https://doi.org/10.1680/ecsmge.60678>
- Al-Tabbaa, A., Kanellopoulos, A., 2014. Nano/Micro-scale chemical and biological healing via MICROENCAPSULATION. CH2M Hill workshop.
- Alghamri, R., 2017. Development and performance of smart aggregates for self-healing of cement based materials. University of Cambridge.
- Alghamri, R., Kanellopoulos, A., Litina, C., Al-Tabbaa, A., 2018. Preparation and polymeric encapsulation of powder mineral pellets for self-healing cement based materials. *Constr. Build. Mater.* 186, 247–262. <https://doi.org/10.1016/j.conbuildmat.2018.07.128>
- Altun, S., Sezer, A., Erol, A., 2009. The effects of additives and curing conditions on the mechanical behavior of a silty soil. *Cold Reg. Sci. Technol.* 56, 135–140.
<https://doi.org/10.1016/j.coldregions.2008.11.007>
- Anderson, K., Bows, A., Mander, S., 2008. From long-term targets to cumulative emission pathways: Reframing UK climate policy. *Energy Policy* 36, 3714–3722.
<https://doi.org/10.1016/j.enpol.2008.07.003>

- ASTM: C1679-14, 2014. Standard Practice for Measuring Hydration Kinetics of Hydraulic Cementitious Mixtures Using Isothermal Calorimetry. ASTM Int. 04, 1–15.
<https://doi.org/10.1520/C1679-14>
- ASTM: C496/C496M-11, 2011. Standard Test Method for Splitting Tensile Strength of Cylindrical Concrete Specimens. ASTM Int. <https://doi.org/10.1520/C0496>
- ASTM: D2216-10, 2010. Standard Test Methods for Laboratory Determination of Water (Moisture) Content of Soil and Rock by Mass. ASTM Int.
<https://doi.org/10.1520/D2216-10.N>
- ASTM: D2487-17, 2017. Standard Practice for Classification of Soils for Engineering Purposes (Unified Soil Classification System). ASTM Int. 1–10.
<https://doi.org/10.1520/D2487-17>
- ASTM: D4219-08, 2008. Standard Test Method for Unconfined Compressive Strength Index of Chemical- Grouted Soils. ASTM Int. <https://doi.org/10.1520/D4219-08.2>
- ASTM: D5084-16, 2016. Standard Test Methods for Measurement of Hydraulic Conductivity of Saturated Porous Materials Using a Flexible Wall Permeameter. ASTM Int.
<https://doi.org/10.1520/D5084-10>.
- ASTM: D560/D560M-15, 2015. Standard Test Methods for Freezing and Thawing Compacted Soil-Cement Mixtures. ASTM Int. <https://doi.org/10.1520/D0560-03>.
- ASTM: D7263-09, 2009. Standard Test Methods for Laboratory Determination of Density (Unit Weight) of Soil Specimens. ASTM Int. <https://doi.org/10.1520/D7263-09.2>
- ASTM: D854-10, 2010. Standard Test Methods for Specific Gravity of Soil Solids by Water Pycnometer. ASTM Int. 1–8. <https://doi.org/10.1520/D0854-10>.
- ASTM C457/C457M-16, 2016. Standard Test Method for Microscopical Determination of Parameters of the Air-Void System in Hardened Concrete. ASTM Int.
https://doi.org/10.1520/C0457_C0457M-16
- ASTM D559/D559M-15, 2015. Standard Test Methods for Wetting and Drying Compacted Soil-Cement Mixtures. ASTM Int. <https://doi.org/10.1520/D0559-03>
- ASTM D560/D560M-16, 2016. Standard Test Methods for Freezing and Thawing Compacted Soil-Cement Mixtures. ASTM Int. <https://doi.org/10.1520/D0560>

- Baquerizo Ibarra, L.G., 2015. Impact of water activity on the mineralogy of hydrated cement. *École polytechnique fédérale de Lausanne.*
- Baykal, G., Döven, A.G., 2000. Utilization of fly ash by pelletization process; theory, application areas and research results. *Resour. Conserv. Recycl.* 30, 59–77. [https://doi.org/10.1016/S0921-3449\(00\)00042-2](https://doi.org/10.1016/S0921-3449(00)00042-2)
- Bin-Shafique, S., Rahman, K., Yaykiran, M., Azfar, I., 2010. The long-term performance of two fly ash stabilized fine-grained soil subbases. *Resour. Conserv. Recycl.* 54, 666–672. <https://doi.org/10.1016/j.resconrec.2009.11.007>
- Breugel, K. Van, 2007. Is there a market for self-healing cement-based materials. *Proc. First Int. Conf. Self Heal. Mater.* 1–9. <https://doi.org/10.1016/j.conbuildmat.2015.10.146>
- Chai, M., Zhang, H., Zhang, J., Zhang, Z., 2017. Effect of cement additives on unconfined compressive strength of warm and ice-rich frozen soil. *Constr. Build. Mater.* 149, 861–868. <https://doi.org/10.1016/j.conbuildmat.2017.05.202>
- Chamberlain, E. J., Iskandar, I., and Hunsicker, S.E., 1990. Effect of freeze-thaw cycles on the permeability and macrostructure of soils. *Proc, Int. Symp. Frozen Soil Impacts Agric., Range, For. Lands, CRREL Spec. Rep. 90-1, U. S. Army Corps Eng. Cold Reg. Res. Eng. Lab. Hanover, N.H.,* 145–155.
- Chamberlain, E.J., Gow, A.J., 1979. Effect of freezing and thawing on the permeability and structure of soils. *Eng. Geol.* 13, 73–92. [https://doi.org/10.1016/0013-7952\(79\)90022-X](https://doi.org/10.1016/0013-7952(79)90022-X)
- Cordon W A, 1967. *Freezing and Thawing of Concrete – Mechanisms and Control*, ACI Monograph NR 3, Farmington Hills, MI, American Concrete Institute.
- Coussy, O., 2005. Poromechanics of freezing materials. *J. Mech. Phys. Solids* 53, 1689–1718. <https://doi.org/10.1016/j.jmps.2005.04.001>
- Craeye, B., Cockaerts, G., Kara De Maeijer, P., 2018. Improving Freeze–Thaw Resistance of Concrete Road Infrastructure by Means of Superabsorbent Polymers. *Infrastructures* 3, 1–14. <https://doi.org/10.3390/infrastructures3010004>
- Craeye, B., Tielemans, T., Lauwereijssens, G., Stoop, J., 2013. Effect of super absorbing polymers on the freeze-thaw resistance of coloured concrete roads. *Road Mater. Pavement Des.* 14, 92–106. <https://doi.org/10.1080/14680629.2012.743670>

- Dash, J.G., Rempel, A.W., Wettlaufer, J.S., 2006. The physics of premelted ice and its geophysical consequences. *Rev. Mod. Phys.* 78, 695–741.
<https://doi.org/10.1103/RevModPhys.78.695>
- Davis, K., Warr, L., Burns, S., Hoppe, E.J., 2007. Physical and chemical behavior of four cement-treated aggregates. *J. Mater. Civ. Eng.* 19, 891–897.
[https://doi.org/10.1061/\(ASCE\)0899-1561\(2007\)19:10\(891\)](https://doi.org/10.1061/(ASCE)0899-1561(2007)19:10(891))
- de Rooij, M., Van Tittelboom, K., De Belie, N., Schlangen, E., 2013. Introduction, in: *State-of-the-Art Report of RILEM Technical Committee 221-SHC: Self-Healing Phenomena in Cement-Based Materials*. pp. 1–17. https://doi.org/10.1007/978-94-007-6624-2_1
- Dempsey, B.J., Thompson, M.R., 1968. Durability properties of lime-soil Mixtures. *Highw. Res. Board* 235, 61–75.
- Dry, C., Corsaw, M., Bayer, E., 2003. A comparison of internal self-repair with resin injection in repair of concrete. *J. Adhes. Sci. Technol.* 17, 79–89.
<https://doi.org/10.1163/15685610360472457>
- Dry, C.M., Corsaw, M.J.T., 1998. A time-release technique for corrosion prevention. *Cem. Concr. Res.* 28, 1133–1140. [https://doi.org/10.1016/S0008-8846\(98\)00087-8](https://doi.org/10.1016/S0008-8846(98)00087-8)
- Du, L., Folliard, K.J., 2005. Mechanisms of air entrainment in concrete. *Cem. Concr. Res.* 35, 1463–1471. <https://doi.org/10.1016/j.cemconres.2004.07.026>
- Ebrahimi, A., Edil, T.B., Son, Y.-H., 2012. Effectiveness of Cement Kiln Dust in Stabilizing Recycled Base Materials. *J. Mater. Civ. Eng.* 24, 1059–1066.
[https://doi.org/10.1061/\(asce\)mt.1943-5533.0000472](https://doi.org/10.1061/(asce)mt.1943-5533.0000472)
- Eigenbrod, K.D., 2003. Self-healing in fractured fine-grained soils. *Can. Geotech. J.*
<https://doi.org/10.1139/t02-110>
- Eigenbrod K.D., 1996. Effects of cyclic freezing and thawing on volume changes and permeabilities of soft fine-grained soils. *Can. Geotech. J.* 33, 529–537.
- Endo M., 1976. Recent development in dredged material stabilization and deep chemical mixing in Japan. *Soils and Site Improvement*. University of California, Berkeley, lifelong learning seminar.

- Eriksson, D., Gasch, T., Malm, R., Ansell, A., 2018. Freezing of partially saturated air-entrained concrete: A multiphase description of the hygro-thermo-mechanical behaviour. *Int. J. Solids Struct.* 152–153, 294–304. <https://doi.org/10.1016/j.ijsolstr.2018.07.004>
- Eskişar, T., Altun, S., Kalipcilar, I., 2015. Assessment of strength development and freeze-thaw performance of cement treated clays at different water contents. *Cold Reg. Sci. Technol.* 111, 50–59. <https://doi.org/10.1016/j.coldregions.2014.12.008>
- F. Buchholz and A. Graham, 1998. *Modern Superabsorbent Polymer Technology*. Wiley-VCH, New York 154–157, 194–197.
- Fagerlund, G., 1977. The international cooperative test of the critical degree of saturation method of assessing the freeze/thaw resistance of concrete. *Matériaux Constr.* 10, 231–253. <https://doi.org/10.1007/BF02478694>
- Fagerlund, G., 1973. Critical degrees of saturation at freezing of porous and brittle materials. *Tid. Institutionen för byggnadsteknik, Tek. högskolan i Lund*. <https://doi.org/10.14359/17604>
- Farzarian, K., Pimenta Teixeira, K., Perdigão Rocha, I., De Sa Carneiro, L., Ghahremaninezhad, A., 2016. The mechanical strength, degree of hydration, and electrical resistivity of cement pastes modified with superabsorbent polymers. *Constr. Build. Mater.* 109, 156–165. <https://doi.org/10.1016/j.conbuildmat.2015.12.082>
- Freyermuth, C.L., 2001. Life-cycle cost analysis for large segmental bridges. *Concrete Int.* 23(2), 89–95.
- Garber, S., Rasmussen, R.O., Harrington, D., 2011. *Guide to Cement-Based Integrated Pavement Solutions*.
- Gartner, E.M., Tang, F.J., Wwiss, S.J., 1985. Saturation Factors for Calcium Hydroxide and Calcium Sulfates in Fresh Portland Cement Pastes. *J. Am. Ceram. Soc.* 68, 667–673. <https://doi.org/10.1111/j.1151-2916.1985.tb10122.x>
- Giannaros, P., 2017. *Laboratory and Field Investigation of the Performance of Novel Microcapsule-Based Self-Healing Concrete*. University of Cambridge.
- Giannaros, P., Kanellopoulos, A., Al-Tabbaa, A., 2016. Sealing of cracks in cement using microencapsulated sodium silicate. *Smart Mater. Struct.* 25, 1–12. <https://doi.org/10.1088/0964-1726/25/8/084005>

- Glatt GmbH Binzen, 2005. Fluid bed systems, USA .
- Gokce, A., Nagataki, S., Saeki, T., Hisada, M., 2004. Freezing and thawing resistance of air-entrained concrete incorporating recycled coarse aggregate: The role of air content in demolished concrete. *Cem. Concr. Res.* 34, 799–806.
<https://doi.org/10.1016/j.cemconres.2003.09.014>
- Granger, S., Loukili, A., Pijaudier-Cabot, G., Chanvillard, G., 2007. Experimental characterization of the self-healing of cracks in an ultra high performance cementitious material: Mechanical tests and acoustic emission analysis. *Cem. Concr. Res.* 37, 519–527. <https://doi.org/10.1016/j.cemconres.2006.12.005>
- Gruyaert, E., Debbaut, B., Snoeck, D., D áz, P., Arizo, A., Tziviloglou, E., Schlangen, E., De Belie, N., 2016. Self-healing mortar with pH-sensitive superabsorbent polymers: testing of the sealing efficiency by water flow tests. *Smart Mater. Struct.* 25, 084007.
<https://doi.org/10.1088/0964-1726/25/8/084007>
- Guney, Y., Aydilek, A.H., Demirkan, M.M., 2006. Geoenvironmental behavior of foundry sand amended mixtures for highway subbases. *Waste Manag.* 26, 932–945.
<https://doi.org/10.1016/j.wasman.2005.06.007>
- Guthrie, W.S., Hermansson, Å., Woffinden, K.H., 2006. Saturation of Granular Base Material Due to Water Vapor Flow during Freezing: Laboratory Experimentation and Numerical Modeling, in: *Current Practices in Cold Regions Engineering*. American Society of Civil Engineers, Reston, VA, pp. 1–12. [https://doi.org/10.1061/40836\(210\)66](https://doi.org/10.1061/40836(210)66)
- Guthrie, W.S., Lay, R.D., 2007. Effect of Reduced Cement Contents on Frost Heave of Silty Soil: Laboratory Testing and Numerical Modeling. *Transp. Res. Board 86th Annu. Meet.* January 21-25, 2007 Washington, D.C.
- Harbottle, M.J., Lam, M., Botusharova, S.P., Gardner, D.R., 2014. Self-healing soil : Biomimetic engineering of geotechnical structures to respond to damage. *7th Int. Congr. Environ. Geotech.*
- Hasholt, M.T., Jensen, O.M., Laustsen, S., 2015. Superabsorbent Polymers as a Means of Improving Frost Resistance of Concrete. *Adv. Civ. Eng. Mater.* 4, 20150012.
<https://doi.org/10.1520/ACEM20150012>

- Hayward Baker. Dry Soil Mixing. <https://www.haywardbaker.com/solutions/techniques/dry-soil-mixing>, accessed 2019.
- Hearn, N., Morley, C.T., 1997. Self-sealing property of concrete - Experimental evidence. *Mater. Struct.* 30, 404–411. <https://doi.org/10.1007/BF02498563>
- Hong, G., Choi, S., 2017. Rapid self-sealing of cracks in cementitious materials incorporating superabsorbent polymers. *Constr. Build. Mater.* 143, 1–9. <https://doi.org/10.1016/j.conbuildmat.2017.03.133>
- Hua, X., 2010. Self-healing of Engineered Cementitious Composites (ECC) in Concrete Repair System. Master thesis, Delft Univ. Technol.
- Huang, H., Ye, G., 2014. A Review on Self-Healing in Reinforced Concrete Structures in View of Serving Conditions. 3rd Int. Conf. Serv. Life Des. Infrastructure, Zhuhai, China 1–14.
- Huang, H., Ye, G., 2011. Application of sodium silicate solution as self-healing agent in cementitious materials. *Int. RILEM Conf. Adv. Constr. Mater. Through Sci. Eng.* 530–536. <https://doi.org/978-2-35158-116-9>
- Huang, H., Ye, G., Qian, C., Schlangen, E., 2016. Self-healing in cementitious materials: Materials, methods and service conditions. *Mater. Des.* 92, 499–511. <https://doi.org/10.1016/j.matdes.2015.12.091>
- Huber, K., 1993. Calcium-induced shrinking of polyacrylate chains in aqueous solution. *J. Phys. Chem.* 97, 9825–9830. <https://doi.org/10.1021/j100140a046>
- Hung, V. V, Kishi, T., Ahn, T.H., 2013. Development of Self-Healing Granules Having Semi- Capsulation Effect By Using Cement Compound , Chemical / Mineral Admixtures & Its Watertight Performance Through Crack. *Proc. 4th Int. Conf. Self-Healing Mater.* 418–421.
- Hwang, D., Damodaran, S., 1996. Equilibrium swelling properties of a novel ethylenediaminetetraacetic dianhydride (EDTAD) - modified soy protein hydrogel. *J. Appl. Polym. Sci.* 62, 1285–1293. [https://doi.org/10.1002/\(SICI\)1097-4628\(19961121\)62:8<1285::AID-APP19>3.3.CO;2-5](https://doi.org/10.1002/(SICI)1097-4628(19961121)62:8<1285::AID-APP19>3.3.CO;2-5)

- Jacobsen, S., Marchand, J., Boisvert, L., 1996. Effect of cracking and healing on chloride transport in OPC concrete. *Cem. Concr. Res.* 26, 869–881. [https://doi.org/10.1016/0008-8846\(96\)00072-5](https://doi.org/10.1016/0008-8846(96)00072-5)
- Jacobsen, S., Sellevold, E.J., 1996. Self healing of high strength concrete after deterioration by freeze/thaw. *Cem. Concr. Res.* 26, 55–62. [https://doi.org/10.1016/0008-8846\(95\)00179-4](https://doi.org/10.1016/0008-8846(95)00179-4)
- Jamshidi, R.J., Lake, C.B., 2014. Hydraulic and strength properties of unexposed and freeze–thaw exposed cement-stabilized soils. *Can. Geotech. J.* 52, 283–294. <https://doi.org/10.1139/cgj-2014-0100>
- Jamshidi, R.J., Lake, C.B., Barnes, C.L., 2015a. Examining Freeze/Thaw Cycling and Its Impact on the Hydraulic Performance of Cement-Treated Silty Sand. *J. Cold Reg. Eng.* 29, 04014014. [https://doi.org/10.1061/\(ASCE\)CR.1943-5495.0000081](https://doi.org/10.1061/(ASCE)CR.1943-5495.0000081)
- Jamshidi, R.J., Lake, C.B., Barnes, C.L., 2015b. Evaluating Impact Resonance Testing As a Tool for Predicting Hydraulic Conductivity and Strength Changes in Cement-Stabilized Soils. *J. Mater. Civ. Eng. ASCE* 27. [https://doi.org/10.1061/\(ASCE\)MT.1943-5533.0001318](https://doi.org/10.1061/(ASCE)MT.1943-5533.0001318).
- Jamshidi, R.J., Lake, C.B., Barnes, C.L., Hills, C.D., Gunning, P., 2011. Physical performance of cement-treated silty sand soil under cycles of freezing/thawing. 14th Pan-American Conf. Soil Mech. Geotech. Eng. (PCSMGE), 64th Can. Geotech. Conf.
- Jamshidi, R.J., Lake, C.B., Gunning, P., Hills, C.D., 2016. Effect of Freeze/Thaw Cycles on the Performance and Microstructure of Cement-Treated Soils. *J. Mater. Civ. Eng.* 28, 04016162. [https://doi.org/10.1061/\(ASCE\)MT.1943-5533.0001677](https://doi.org/10.1061/(ASCE)MT.1943-5533.0001677)
- Janoo, V.C., Firicano, A.J., Barna, L.A., Orchino, S.A., 1999. Field Testing of Stabilized Soil. *J. Cold Reg. Eng.* 13, 37–53. [https://doi.org/10.1061/\(ASCE\)0887-381X\(1999\)13:1\(37\)](https://doi.org/10.1061/(ASCE)0887-381X(1999)13:1(37))
- Jensen, O.M., Hansen, P.F., 2002. Water-entrained cement-based materials: II. Experimental observations. *Cem. Concr. Res.* 32, 973–978. [https://doi.org/10.1016/S0008-8846\(02\)00737-8](https://doi.org/10.1016/S0008-8846(02)00737-8)
- Jiang, Z., Li, W., Yuan, Z., 2015. Influence of mineral additives and environmental conditions on the self-healing capabilities of cementitious materials. *Cem. Concr. Compos.* 57, 116–127. <https://doi.org/10.1016/j.cemconcomp.2014.11.014>

- Jin, F., 2014. Characterisation and Performance of Reactive MgO-based Cements with Supplementary Cementitious Materials. University of Cambridge.
- Jones, W., Weiss, W.J., 2014. Freeze Thaw Durability of Internally Cured Concrete Made Using Superabsorbent Polymers. Proc. 4th Int. Conf. Durab. Concr. Struct. 3–11. <https://doi.org/10.5703/1288284315376>
- Joseph, C., Jefferson, A.D., Isaacs, B., Lark, R.J., Gardner, D.R., 2010. Experimental investigation of adhesive-based self-healing of cementitious materials. Mag. Concr. Res. 62, 831–843. <https://doi.org/10.1680/macr.2010.62.11.831>
- Justs, J., Wyrzykowski, M., Bajare, D., Lura, P., 2015. Internal curing by superabsorbent polymers in ultra-high performance concrete. Cem. Concr. Res. 76, 82–90. <https://doi.org/10.1016/j.cemconres.2015.05.005>
- Kamei, T., Ahmed, A., Shibi, T., 2012. Effect of freeze–thaw cycles on durability and strength of very soft clay soil stabilised with recycled Bassanite. Cold Reg. Sci. Technol. 82, 124–129. <https://doi.org/10.1016/j.coldregions.2012.05.016>
- Kanellopoulos, A., Giannaros, P., Al-Tabbaa, A., 2016. The effect of varying volume fraction of microcapsules on fresh, mechanical and self-healing properties of mortars. Constr. Build. Mater. 122, 577–593. <https://doi.org/10.1016/j.conbuildmat.2016.06.119>
- Kanellopoulos, A., Giannaros, P., Palmer, D., Kerr, A., Al-Tabbaa, A., 2017. Polymeric microcapsules with switchable mechanical properties for self-healing concrete: Synthesis, characterisation and proof of concept. Smart Mater. Struct. 26. <https://doi.org/10.1088/1361-665X/aa516c>
- Kanellopoulos, A., Qureshi, T.S., Al-Tabbaa, A., 2015. Glass encapsulated minerals for self-healing in cement based composites. Constr. Build. Mater. 98, 780–791. <https://doi.org/10.1016/j.conbuildmat.2015.08.127>
- Kessler, M.R., Sottos, N.R., White, S.R., 2003. Self-healing structural composite materials. Compos. Part A Appl. Sci. Manuf. 34, 743–753. [https://doi.org/10.1016/S1359-835X\(03\)00138-6](https://doi.org/10.1016/S1359-835X(03)00138-6)
- Khoury, N.N., Zaman, M.M., 2007. Environmental Effects on Durability of Aggregates Stabilized with Cementitious Materials. J. Mater. Civ. Eng. 19, 41–48. [https://doi.org/10.1061/\(ASCE\)0899-1561\(2007\)19:1\(41\)](https://doi.org/10.1061/(ASCE)0899-1561(2007)19:1(41))

- Kiatkamjornwong, S., Phunchareon, P., 1999. Influence of reaction parameters on water absorption of neutralized poly(acrylic acid-co-acrylamide) synthesized by inverse suspension polymerization. *J. Appl. Polym. Sci.* 72, 1349–1366.
[https://doi.org/10.1002/\(SICI\)1097-4628\(19990606\)72:10<1349::AID-APP16>3.0.CO;2-K](https://doi.org/10.1002/(SICI)1097-4628(19990606)72:10<1349::AID-APP16>3.0.CO;2-K)
- Kim, W., Daniel, D.E., 1992. Effects of Freezing on Hydraulic Conductivity of Compacted Clay. *J. Geotech. Eng.* 118, 1083–1097. [https://doi.org/10.1061/\(ASCE\)0733-9410\(1992\)118:7\(1083\)](https://doi.org/10.1061/(ASCE)0733-9410(1992)118:7(1083))
- Kishi, T., 2013. Development of crack self-healing concrete by cost beneficial semi-capsulation technique. *Sustain. Constr. Mater. Technol.* 2013-Augus, 1–9.
- Klich, I., Wilding, L.P., Drees, L.R., Landa, E.R., 1999. Importance of Microscopy in Durability Studies of Solidified and Stabilized Contaminated Soils. *Soil Sci. Soc. Am. J.* 63, 1274–1283.
- Lake, C.B., Yousif, M.A.-M., Jamshidi, R.J., 2016. Examining freeze/thaw effects on performance and morphology of a lightly cemented soil. *Cold Reg. Sci. Technol.* 134, 33–44. <https://doi.org/10.1016/j.coldregions.2016.11.006>
- Lavanya, K., 2011. Pelletization Technology : a Quick Review. *Ijpsr* 2, 1337–1355.
[https://doi.org/http://dx.doi.org/10.13040/IJPSR.0975-8232.2\(6\).1337-55](https://doi.org/http://dx.doi.org/10.13040/IJPSR.0975-8232.2(6).1337-55)
- Lee, H.X.D., Wong, H.S., Buenfeld, N.R., 2016. Self-sealing of cracks in concrete using superabsorbent polymers. *Cem. Concr. Res.* 79, 194–208.
<https://doi.org/10.1016/j.cemconres.2015.09.008>
- Lee, H.X.D., Wong, H.S., Buenfeld, N.R., 2010. Potential of superabsorbent polymer for self-sealing cracks in concrete. *Adv. Appl. Ceram.* 109, 296–302.
<https://doi.org/10.1179/174367609X459559>
- Lee, Y.S., Ryou, J.S., 2016. Crack healing performance of PVA-coated granules made of cement, CSA, and Na₂CO₃ in the cement matrix. *Materials (Basel)*. 9.
<https://doi.org/10.3390/MA9070555>
- Lee, Y.S., Ryou, J.S., 2014. Self healing behavior for crack closing of expansive agent via granulation/film coating method. *Constr. Build. Mater.* 71, 188–193.
<https://doi.org/10.1016/j.conbuildmat.2014.08.045>

- Lejcuś, K., Śpitalniak, M., Dabrowska, J., 2018. Swelling behaviour of superabsorbent polymers for soil amendment under different loads. *Polymers (Basel)*. 10. <https://doi.org/10.3390/polym10030271>
- Li, G., Ma, W., Mu, Y., Wang, F., Fan, S., Wu, Y., 2017. Effects of freeze-thaw cycle on engineering properties of loess used as road fills in seasonally frozen ground regions, North China. *J. Mt. Sci.* 14, 356–368. <https://doi.org/10.1007/s11629-016-4005-4>
- Li, V.C., Herbert, E., 2012. Robust Self-Healing Concrete for Sustainable Infrastructure. *J. Adv. Concr. Technol.* 10, 207–218. <https://doi.org/10.3151/jact.10.207>
- Li, V.C., Lim, Y.M., Chan, Y.-W., 1998. Feasibility study of a passive smart self-healing cementitious composite. *Compos. Part B Eng.* 29, 819–827. [https://doi.org/10.1016/S1359-8368\(98\)00034-1](https://doi.org/10.1016/S1359-8368(98)00034-1)
- Li, W., Pour-Ghaz, M., Castro, J., Weiss, J., 2012. Water Absorption and Critical Degree of Saturation Relating to Freeze-Thaw Damage in Concrete Pavement Joints. *J. Mater. Civ. Eng.* 24, 299–307. [https://doi.org/10.1061/\(ASCE\)MT.1943-5533.0000383](https://doi.org/10.1061/(ASCE)MT.1943-5533.0000383)
- Litina, C., 2016. Development and Performance of Self-Healing Blended Cement Grouts with Microencapsulated Mineral Agents. University of Cambridge.
- Litina, C., Kanellopoulos, A., Al-Tabbaa, A., 2014. Alternative repair system for concrete using microencapsulated healing agents. *Concr. Solut. - Proc. Concr. Solut. 5th Int. Conf. Concr. Repair* 97–103.
- Litina, C., Al-Tabbaa, A., 2013. Self-healing capacity of hardened cement suspensions with high levels of cement substitution. *ICSHM 2013 Proc. 4th Int. Conf. Self-Healing Mater.* 201–205.
- Litvan, G.G., 1988. The mechanism of frost action in concrete - theory and practical implications. *Proc. Work. Low Temp. Eff. Concr. Natl. Res. Counc. Canada, Montr. Canada* 115–134.
- Liu, J., Wang, T., Tian, Y., 2010. Experimental study of the dynamic properties of cement- and lime-modified clay soils subjected to freeze-thaw cycles. *Cold Reg. Sci. Technol.* 61, 29–33. <https://doi.org/10.1016/j.coldregions.2010.01.002>

- Ma, X., Liu, J., Wu, Z., Shi, C., 2017. Effects of SAP on the properties and pore structure of high performance cement-based materials. *Constr. Build. Mater.* 131, 476–484. <https://doi.org/10.1016/j.conbuildmat.2016.11.090>
- Mao, S., Islam, M.R., Xue, X., Yang, X., Zhao, X., Hu, Y., 2011. Evaluation of a water-saving superabsorbent polymer for corn (*Zea mays* L.) production in arid regions of Northern China. *African J. Biotechnol.* 6, 4108–4115. <https://doi.org/10.5897/AJAR11.395>
- Mao, W., 2018. Reactive MgO and Self-healing Microcapsules for Enhanced Well Cement System Performance. University of Cambridge.
- Mardani-Aghabaglou, A., Kalıpcılar, İ., İnan Sezer, G., Sezer, A., Altun, S., 2015. Freeze–thaw resistance and chloride-ion penetration of cement-stabilized clay exposed to sulfate attack. *Appl. Clay Sci.* 115, 179–188. <https://doi.org/10.1016/j.clay.2015.07.041>
- Mechtcherine, V., Reinhardt, H.-W., 2012. Application of Super Absorbent Polymers (SAP) in Concrete Construction. Springer Netherlands, Dordrecht. <https://doi.org/10.1007/978-94-007-2733-5>
- Mechtcherine, V., Schröfl, C., Wyrzykowski, M., Gorges, M., Lura, P., Cusson, D., Margeson, J., De Belie, N., Snoeck, D., Ichimiya, K., Igarashi, S.I., Falikman, V., Friedrich, S., Bokern, J., Kara, P., Marciniak, A., Reinhardt, H.W., Sippel, S., Bettencourt Ribeiro, A., Custódio, J., Ye, G., Dong, H., Weiss, J., 2017. Effect of superabsorbent polymers (SAP) on the freeze–thaw resistance of concrete: results of a RILEM interlaboratory study. *Mater. Struct. Constr.* 50. <https://doi.org/10.1617/s11527-016-0868-7>
- Meissner, H.P., Michaels, A.S., Kaiser, R., 1964. Spontaneous Pelletization in Fine Powders. *Ind. Eng. Chem. Process Des. Dev.* 3, 197–201. <https://doi.org/10.1021/i260011a002>
- Mignon, A., Snoeck, D., Dubruel, P., Vlierberghe, S. Van, De Belie, N., 2017. Crack mitigation in concrete: Superabsorbent polymers as key to success? *Materials (Basel)*. 10. <https://doi.org/10.3390/ma10030237>
- Mignon, A., Snoeck, D., Schaubroeck, D., Luickx, N., Dubruel, P., Van Vlierberghe, S., De Belie, N., 2015. pH-responsive superabsorbent polymers: A pathway to self-healing of

- mortar. *React. Funct. Polym.* 93, 68–76.
<https://doi.org/10.1016/j.reactfunctpolym.2015.06.003>
- Mills, J., Shilson, S., Woodley, Q., Woodwark, A., 2011. Keeping Britain moving. United Kingdom 's Transp. Infrastruct. needs.
- Mo, L., Deng, M., Tang, M., 2010. Effects of calcination condition on expansion property of MgO-type expansive agent used in cement-based materials. *Cem. Concr. Res.* 40, 437–446. <https://doi.org/10.1016/j.cemconres.2009.09.025>
- Mo, L., Panesar, D.K., 2012. Effects of accelerated carbonation on the microstructure of Portland cement pastes containing reactive MgO. *Cem. Concr. Res.* 42, 769–777.
<https://doi.org/10.1016/j.cemconres.2012.02.017>
- Mohammed, A.A.S., Pandey, R.K., 2015. Effect of Air Entrainment on Compressive Strength , Density , and Ingredients of Concrete. *Int. J. Mod. Eng. Res.* 5, 77–81.
- Musharraf, M., Khoury, N., 2003. Effect of Freeze-Thaw Cycles on Class C Fly Ash Stabilized Aggregate Base. *Proc. 82nd Annu. Meet. Transp. Res. Board.*
- Natale, P.J., 2010. Failing Infrastructure — Threatening our Economy and Way of Life. *NJIT Mag.*
- Nelson, E.B. 1990. *Well Cementing*. Vol. 28. Newnes.
- Nicholson, P.G., 2015. Admixture Soil Improvement. *Soil Improv. Gr. Modif. Methods* 231–288. <https://doi.org/10.1016/b978-0-12-408076-8.00011-x>
- OECD/ITF, 2013. Spending on Transport Infrastructure 1995-2011. *Int. Transp. Forum.*
- Othman, M. a., Benson, C.H., 1993. Effect of freeze–thaw on the hydraulic conductivity and morphology of compacted clay. *Can. Geotech. J.* 30, 236–246.
<https://doi.org/10.1139/t93-020>
- Pamukcu, S., Topcu, I.B., Guven, C., 1994. Hydraulic conductivity of solidified residue mixtures used as a hydraulic barrier. *Hydraul. Conduct. Waste Contam. Transp. Soil (STP 1142)* 505–520. <https://doi.org/10.1520/STP23905S>
- PCA, 2005. *Soil-Cement Technology for Pavements : Different Products for Different Applications*. Pavements 4.

- Pelletier, M.M., Brown, R., Shukla, A., Bose, A., 2010. Self-healing concrete with a microencapsulated healing agent. Univ. Rhode Island, Kingston, USA.
- Pelto, J., Leivo, M., Gruyaert, E., Debbaut, B., Snoeck, D., De Belie, N., 2017. Application of encapsulated superabsorbent polymers in cementitious materials for stimulated autogenous healing. *Smart Mater. Struct.* 26, 105043. <https://doi.org/10.1088/1361-665X/aa8497>
- Penttala, V., 2009. Causes and mechanisms of deterioration in reinforced concrete, in: *Failure, Distress and Repair of Concrete Structures*. Elsevier, pp. 3–31. <https://doi.org/10.1533/9781845697037.1.3>
- Peppas, N.A., Bures, P., Leobandung, W., Ichikawa, H., 2000. Hydrogels in pharmaceutical formulations. *Eur. J. Pharm. Biopharm.* 50, 27–46. [https://doi.org/10.1016/S0939-6411\(00\)00090-4](https://doi.org/10.1016/S0939-6411(00)00090-4)
- Peppin, S.S.L., Style, R.W., 2013. The physics of frost heave and ice-lens growth. *Vadose Zo. J.* 12, 1–12. <https://doi.org/10.2136/vzj2012.0049>
- Popovics S., 1998. *Strength and related properties of concrete*. New York, Wiley. 309–311, 373–375.
- Porbaha, A., 1998. State of the art in deep mixing technology: part I. Basic concepts and overview. *Proc. Inst. Civ. Eng. - Gr. Improv.* 2, 81–92. <https://doi.org/10.1680/gi.1998.020204>
- Porbaha, A., Shibuya, S., Kishida, T., 2000. State of the art in deep mixing technology. Part III: geomaterial characterization. *Proc. Inst. Civ. Eng. - Gr. Improv.* 4, 91–110. <https://doi.org/10.1680/grim.2000.4.3.91>
- Porbaha, A., Tanaka, H., Kobayashi, M., 1998. State of the art in deep mixing technology: part II. Applications. *Proc. Inst. Civ. Eng. - Gr. Improv.* 2, 125–139. <https://doi.org/10.1680/gi.1998.020303>
- Portland Cement Association, 2001. *Soil-cement inspector's manual*.
- Powers, T.C., 1945. A working hypothesis for further studies of frost resistance of concrete. *J. Am. Concr. Inst.* 16 (4), 245–272. doi: 10.14359/8684.

- Powers, T.C. , 1949. The air requirement of frost-resistant concrete. In: Proceedings of the Highway Research Board, 29. Portland Cement Association, pp. 184–211.
- Powers, T.C. , Helmuth, R.A. , 1953. Theory of volume changes in hardened Portland cement paste during freezing. In: Proceedings of the Highway Research Board. Portland Cement Association, pp. 285–297.
- Qi, J., Ma, W., Song, C., 2008. Influence of freeze-thaw on engineering properties of a silty soil. *Cold Reg. Sci. Technol.* 53, 397–404.
<https://doi.org/10.1016/j.coldregions.2007.05.010>
- Quadrelli, R., Peterson, S., 2007. The energy–climate challenge: Recent trends in CO₂ emissions from fuel combustion. *Energy Policy* 35, 5938–5952.
<https://doi.org/10.1016/j.enpol.2007.07.001>
- Qureshi, T., Al-Tabbaa, A., 2014. The effect of magnesia on the self-healing performance of Portland cement with increased curing time. *1st Int. Conf. Ageing Mater. Struct.* 635–642. <https://doi.org/DOI: 10.13140/RG.2.1.4458.4804>
- Qureshi, T.S., Al-Tabbaa, A., 2016. Self-healing of drying shrinkage cracks in cement-based materials incorporating reactive MgO. *Smart Mater. Struct.* 25.
<https://doi.org/10.1088/0964-1726/25/8/084004>
- Qureshi, T.S., Kanellopoulos, A., Al-Tabbaa, A., 2016. Encapsulation of expansive powder minerals within a concentric glass capsule system for self-healing concrete. *Constr. Build. Mater.* 121, 629–643. <https://doi.org/10.1016/j.conbuildmat.2016.06.030>
- Ramm, W., Biscop, M., 1998. Autogenous healing and reinforcement corrosion of water-penetrated separation cracks in reinforced concrete. *Nucl. Eng. Des.* 179, 191–200.
[https://doi.org/10.1016/S0029-5493\(97\)00266-5](https://doi.org/10.1016/S0029-5493(97)00266-5)
- Reinhardt, H.W., Assmann, a, Mönnig, S., 2008. Superabsorbent polymers (SAP) - An admixture to increase the durability of concrete. *1st Int. Conf. Microstruct. Relat. Durab. Cem. Compos.* 13-15 Oct. 313–322.
- Research In China, 2015. Global and China Superabsorbent Polymers (SAP) Industry Report, 2014-2018.

- Rha, C.Y., Seong, J.W., Kim, C.E., Lee, S.K., Kim, W.K., 1999. Properties and interaction of cement with polymer in the hardened cement pastes added absorbent polymer. *J. Mater. Sci.* 34, 4653–4659. <https://doi.org/10.1023/A:1004689711139>
- Richard Baker Harrison Ltd, 2011. Data sheet: Polwhite E China Clay.
- Riyazi, S., Keavern, J.T., Mulheron, M., 2017. Super absorbent polymers (SAPs) as physical air entrainment in cement mortars. *Constr. Build. Mater.* 147, 669–676. <https://doi.org/10.1016/j.conbuildmat.2017.05.001>
- Sayyari, M., Ghanbari, F., 2012. Effects of Super Absorbent Polymer A 200 on the Growth , Yield and Some Physiological Responses in Sweet Pepper (*Capsicum Annum L .*) Under Various Irrigation Regimes. *Int. J. Agric. Food Res.* 1, 1–11. <https://doi.org/10.24102/ijafr.v1i1.123>
- Scherer, G.W., 1999. Crystallization in pores. *Cem. Concr. Res.* 29, 1347–1358. [https://doi.org/10.1016/S0008-8846\(99\)00002-2](https://doi.org/10.1016/S0008-8846(99)00002-2)
- Scherer, G.W., 1993. Freezing gels. *J. Non. Cryst. Solids* 155, 1–25. [https://doi.org/10.1016/0022-3093\(93\)90467-C](https://doi.org/10.1016/0022-3093(93)90467-C)
- Schweins, R., Huber, K., 2001. Collapse of sodium polyacrylate chains in calcium salt solutions. *Eur. Phys. J. E* 5, 117–126. <https://doi.org/10.1007/s101890170093>
- Selezneva, O.I., Jiang, Y.J., Larson, G., Puzin, T., 2008. Long Term Pavement Performance Computed Parameter : Frost Penetration, FHWA-HRT-08-057.
- Shand, M.A., 2006. *The chemistry and technology of magnesia.* John Wiley & Sons.
- Shang, H., Yi, T., 2013. Freeze-Thaw Durability of Air-Entrained Concrete. *Sci. World J.* 2013, 1–6. <https://doi.org/10.1155/2013/650791>
- Shen, D., Shi, H., Tang, X., Ji, Y., Jiang, G., 2016. Effect of internal curing with super absorbent polymers on residual stress development and stress relaxation in restrained concrete ring specimens. *Constr. Build. Mater.* 120, 309–320. <https://doi.org/10.1016/j.conbuildmat.2016.05.048>
- Shibi, T., Kamei, T., 2014. Effect of freeze–thaw cycles on the strength and physical properties of cement-stabilised soil containing recycled bassanite and coal ash. *Cold Reg. Sci. Technol.* 106–107, 36–45. <https://doi.org/10.1016/j.coldregions.2014.06.005>

- Shihata, S.A., Baghdadi, Z.A., 2001. Simplified method to assess freeze-thaw durability of soil cement. *J. Mater. Civ. Eng.* 4, 243–247.
- Sika Deutschland GmbH, 2014. Product Data Sheet-SikaAer® Solid 1–2.
- Sikora, K.S., Klemm, A.J., 2015. Effect of Superabsorbent Polymers on Workability and Hydration Process in Fly Ash Cementitious Composites. *J. Mater. Civ. Eng.* 27, 04014170. [https://doi.org/10.1061/\(ASCE\)MT.1943-5533.0001122](https://doi.org/10.1061/(ASCE)MT.1943-5533.0001122)
- Sisomphon, K., Copuroglu, O., Fraaij, A., 2011. Application of encapsulated lightweight aggregate impregnated with sodium monofluorophosphate as a self-healing agent in blast furnace slag mortar. *Heron* 56, 17–36.
- Sisomphon, K., Copuroglu, O., Koenders, E.A.B., 2013. Effect of exposure conditions on self healing behavior of strain hardening cementitious composites incorporating various cementitious materials. *Constr. Build. Mater.* 42, 217–224. <https://doi.org/10.1016/j.conbuildmat.2013.01.012>
- Sisomphon, K., Copuroglu, O., Koenders, E.A.B., 2012. Self-healing of surface cracks in mortars with expansive additive and crystalline additive. *Cem. Concr. Compos.* 34, 566–574. <https://doi.org/10.1016/j.cemconcomp.2012.01.005>
- Sivakumar Babu, G.L., Sporer, H., Zanzinger, H., Gartung, E., 2001. Self-Healing Properties of Geosynthetic Clay Liners. *Geosynth. Int.* 8, 461–470. <https://doi.org/10.1680/gein.8.0203>
- Snoeck, D., Dewanckele, J., Cnudde, V., De Belie, N., 2016. X-ray computed microtomography to study autogenous healing of cementitious materials promoted by superabsorbent polymers. *Cem. Concr. Compos.* 65, 83–93. <https://doi.org/10.1016/j.cemconcomp.2015.10.016>
- Snoeck, D., Jensen, O.M., De Belie, N., 2015. The influence of superabsorbent polymers on the autogenous shrinkage properties of cement pastes with supplementary cementitious materials. *Cem. Concr. Res.* 74, 59–67. <https://doi.org/10.1016/j.cemconres.2015.03.020>
- Snoeck, D., Steuperaert, S., Van Tittelboom, K., Dubruel, P., De Belie, N., 2012. Visualization of water penetration in cementitious materials with superabsorbent polymers by means of neutron radiography. *Cem. Concr. Res.* 42, 1113–1121. <https://doi.org/10.1016/j.cemconres.2012.05.005>

- Snoeck, D., Van Tittelboom, K., Steuperaert, S., Dubruel, P., De Belie, N., 2014. Self-healing cementitious materials by the combination of microfibres and superabsorbent polymers. *J. Intell. Mater. Syst. Struct.* 25, 13–24. <https://doi.org/10.1177/1045389X12438623>
- Souza, L.R. de, 2017. Design and synthesis of microcapsules using microfluidics for autonomic self-healing in cementitious materials. University of Cambridge. <https://doi.org/https://doi.org/10.17863/CAM.16673>
- Suhendro, B., 2014. Toward green concrete for better sustainable environment. *Procedia Eng.* 95, 305–320. <https://doi.org/10.1016/j.proeng.2014.12.190>
- Taki O. and Yang D., 1991. Soil cement mixed wall technique. *Geotechnical Engineering Congress*. American Society of Civil Engineers, New York, Special Publication 27, pp. 298-309.
- Tennis, P.D., Jennings, H.M., 2000. A model for two types of calcium silicate hydrate in the microstructure of Portland cement pastes. *Cem. Concr. Res.* 30, 855–863. [https://doi.org/10.1016/S0008-8846\(00\)00257-X](https://doi.org/10.1016/S0008-8846(00)00257-X)
- Thiery, M., Villain, G., Dangla, P., Platret, G., 2007. Investigation of the carbonation front shape on cementitious materials: Effects of the chemical kinetics. *Cem. Concr. Res.* 37, 1047–1058. <https://doi.org/10.1016/j.cemconres.2007.04.002>
- Thomas, J.J., Jennings, H.M., 2006. A colloidal interpretation of chemical aging of the C-S-H gel and its effects on the properties of cement paste. *Cem. Concr. Res.* 36, 30–38. <https://doi.org/10.1016/j.cemconres.2004.10.022>
- Uddin, K., Balasubramaniam, A.S., Bergado, D.T., 1997. *Engineering_Behavior_of_Cement-Treated_B.pdf*. *Geotech. Eng. No. 1*, 89–119.
- USEPA, 1997. Update to Exposure Factors Handbook. *Environ. Prot. I.*
- USGS, 2019. Mineral Commodity Summaries, U.S. Geological Survey. <https://doi.org/10.3133/70202434>
- V. Mechtcherine, H.-W.R., 2012. Application of Superabsorbent Polymers (SAP) in Concrete Construction. Springer.

- Van Tittelboom, K., Adesanya, K., Dubruel, P., Van Puyvelde, P., De Belie, N., 2011. Methyl methacrylate as a healing agent for self-healing cementitious materials. *Smart Mater. Struct.* 20, 125016. <https://doi.org/10.1088/0964-1726/20/12/125016>
- Van Tittelboom, K. and de Belie, N., 2010. Self-healing concrete: Suitability of different healing agents. *Int. J. 3R's*, 1, 12–21.
- Van Tittelboom, K., De Belie, N., 2013. Self-healing in cementitious materials-a review, *Materials*. <https://doi.org/10.3390/ma6062182>
- Viklander, P., 1998. Permeability and volume changes in till due to cyclic freeze / thaw. *Can. Geotech. J.* 35, 471–477. <https://doi.org/10.1139/t98-015>
- Wang, D. yan, Ma, W., Niu, Y. hong, Chang, X. xiao, Wen, Z., 2007. Effects of cyclic freezing and thawing on mechanical properties of Qinghai-Tibet clay. *Cold Reg. Sci. Technol.* 48, 34–43. <https://doi.org/10.1016/j.coldregions.2006.09.008>
- Wang, F., Ping, X., Zhou, J., Kang, T., 2019. Effects of crumb rubber on the frost resistance of cement-soil. *Constr. Build. Mater.* 223, 120–132. <https://doi.org/10.1016/j.conbuildmat.2019.06.208>
- Wang, H., Deng, A., Yang, P., 2017. Strength and Stiffness of Stabilized Alluvial Silt under Frost Actions. *Adv. Mater. Sci. Eng.* 2017, 1–13. <https://doi.org/10.1155/2017/5605471>
- Wang, S., Lv, Q., Baaj, H., Li, X., Zhao, Y., 2016. Volume change behaviour and microstructure of stabilized loess under cyclic freeze–thaw conditions. *Can. J. Civ. Eng.* 43, 865–874. <https://doi.org/10.1139/cjce-2016-0052>
- Wang, X., Xing, F., Zhang, M., Han, N., Qian, Z., 2013. Experimental study on cementitious composites embedded with organic microcapsules. *Materials (Basel)*. 6, 4064–4081. <https://doi.org/10.3390/ma6094064>
- Wei, H., Jiao, Y., Liu, H., 2015. Effect of freeze-thaw cycles on mechanical property of silty clay modified by fly ash and crumb rubber. *Cold Reg. Sci. Technol.* 116, 70–77. <https://doi.org/10.1016/j.coldregions.2015.04.004>
- White, S.R., Sottos, N.R., Geubelle, P.H., Moore, J.S., Kessler, M.R., Sriram, S.R., Brown, E.N., Viswanathan, S., 2001. Autonomic healing of polymer composites. *Nature* 409, 794–797. <https://doi.org/10.1038/35057232>

- Wong, L.C., Haug, M.D., 1991. Cyclical closed-system freeze–thaw permeability testing of soil liner and cover materials. *Can. Geotech. J.* 28, 784–793. <https://doi.org/10.1139/t91-095>
- World Commission on Environment and Development, 1983. *World commission on environment and development : our common future.*
- Wu, M., Johannesson, B., Geiker, M., 2012. A review: Self-healing in cementitious materials and engineered cementitious composite as a self-healing material. *Constr. Build. Mater.* 28, 571–583. <https://doi.org/10.1016/j.conbuildmat.2011.08.086>
- Xie, S., Qu, J., Lai, Y., Zhou, Z., Xu, X., 2015. Effects of freeze-thaw cycles on soil mechanical and physical properties in the Qinghai-Tibet Plateau. *J. Mt. Sci.* 12, 999–1009. <https://doi.org/10.1007/s11629-014-3384-7>
- Yang, Z., Hollar, J., He, X., Shi, X., 2011. A self-healing cementitious composite using oil core/silica gel shell microcapsules. *Cem. Concr. Compos.* 33, 506–512. <https://doi.org/10.1016/j.cemconcomp.2011.01.010>
- Yarbaşı, N., Kalkan, E., Akbulut, S., 2007. Modification of the geotechnical properties, as influenced by freeze-thaw, of granular soils with waste additives. *Cold Reg. Sci. Technol.* 48, 44–54. <https://doi.org/10.1016/j.coldregions.2006.09.009>
- Yun, K.-K., Kim, K.-K., Choi, W., Yeon, J., 2017. Hygral Behavior of Superabsorbent Polymers with Various Particle Sizes and Cross-Linking Densities. *Polymers (Basel)*. 9, 600. <https://doi.org/10.3390/polym9110600>
- Zeng, Q., Li, K., Fen-Chong, T., 2016. Effect of supercooling on the instantaneous freezing dilation of cement-based porous materials. *J. Build. Phys.* 40, 101–124. <https://doi.org/10.1177/1744259116649321>
- Zhang, Y., Johnson, A.E., White, D.J., 2016. Laboratory freeze-thaw assessment of cement, fly ash, and fiber stabilized pavement foundation materials. *Cold Reg. Sci. Technol.* 122, 50–57. <https://doi.org/10.1016/j.coldregions.2015.11.005>
- Zohuriaan-Mehr, M.J., Kabiri, K., 2008. Superabsorbent polymer materials: A review. *Iran. Polym. J.* 17, 451–477. <https://doi.org/http://journal.ippi.ac.ir>

Zohuriaan-Mehr, M.J., Omidian, H., Doroudiani, S., Kabiri, K., 2010. Advances in non-hygienic applications of superabsorbent hydrogel materials. *J. Mater. Sci.* 45, 5711–5735. <https://doi.org/10.1007/s10853-010-4780-1>

Zuber, B., Marchand, J., Delagrave, A., Bournazel, J.P., 2000. Ice formation mechanisms in normal and high-performance concrete mixtures. *J. Mater. Civ. Eng.* 12, 16–23. [https://doi.org/10.1061/\(ASCE\)0899-1561\(2000\)12:1\(16\)](https://doi.org/10.1061/(ASCE)0899-1561(2000)12:1(16))